



Sustainable Civil Engineering Structures and Construction Materials, SCESCM 2016

## Resistance of concrete with calcium stearate due to chloride attack tested by accelerated corrosion

Agus Maryoto<sup>a,\*</sup>

<sup>a</sup>Jenderal Soedirman University, Civil Engineering Department, Jl. Mayjend. Sungkono KM 5, Purbalingga, Central Java, Indonesia, 53371

---

### Abstract

Water tightness of concrete is usually specified by how much water penetrates or infiltrates into concrete. This indication is applied to detect the possibility of corrosion attack due to aggressive ions such as chloride into reinforced concrete. Since the corrosion occurs on the steel bar of concrete, corrosion level is another methods to express impermeability of concrete. Unfortunately, corrosion process due to chloride attack in the real environment needs several decades. One of the methods which is used to measure corrosion process rapidly is an accelerated corrosion test. This study investigates water tightness and corrosion resistance due to chloride ion in the concrete with calcium stearate by using absorption and electrolytic corrosion test. Two types of concrete mixture i.e. CS-0 and CS-1 are considered in the experiment. Each type of concrete mixture comprises three groups of testing, which are compressive strength, absorption, and electrolytic corrosion test. The dimension of the specimen for compressive strength is 100 mm of diameter and 200 mm in height, and for absorption is 75 mm of diameter and 150 mm in height. Meanwhile, dimension of the electrolytic corrosion specimen is a cube with a size of 100 cm x 100 cm x 200 mm. The result shows that concrete with calcium stearate 1 kg per cubic meter of concrete has a better water tightness property than concrete without calcium stearate. Furthermore, the tendency is also being supported by corrosion resistance result. It can be observed that concrete with calcium stearate is also more resistant to corrosion attack.

© 2017 The Authors. Published by Elsevier Ltd.

Peer-review under responsibility of the organizing committee of SCESCM 2016.

*Keywords:* water tightness; corrosion attack; corrosion resistance; calcium stearate.

---

---

\* Corresponding author. Tel.: + 62-281-6596700; fax: + 62-281-6596801

E-mail address: [agus\\_maryoto1971@yahoo.co.id](mailto:agus_maryoto1971@yahoo.co.id)

## 1. Introduction

Indonesia is the largest archipelago country in the world with a length of the 99.000 km coastline reached [1]. The geographical condition generates thousand of buildings made of reinforced concrete structure located in an aggressive environment. High chloride ion content in sea water is one of the main cause of the degradation of the carrying capacity of reinforced concrete [2]. Fig. 1 shows the effect of chloride ions on the degradation of reinforced concrete structures [3].

Concrete is an artificial rock that is not watertight. Millions of capillaries and pores are formed shortly after the occurring of hydration reaction between cement and water occurs [4]. Water that is not used for cement hydration reaction evaporates and leaves lanes in the form of capillary evaporation. Gas and chloride ions dissolved in water to penetrate into the concrete through the capillaries are formed and eventually lead the rust formation on concrete reinforcement. There are four cause fluid and ion transport mechanisms into the concrete [5], namely capillary suction, seepage due to the pressure difference, the diffusion due to differences in the concentration of the liquid and the difference in electric potential.



Fig. 1. Corroded rebar in piling.

Calcium stearate in concrete was investigated [6] in order to discover its influence in the microstructure of concrete. Permeability and macro cell corrosion test was conducted by using 30 specimens. The results indicate that calcium stearate reduces level of concrete permeability and possibility of corrosion attack. Even though it improves the properties of concrete, its resistance against corrosion attack is not well remarkable yet. This study investigates then the contribution of calcium stearate in reinforced concrete due to corrosion attack led by chloride ion.

## 2. Experimental work

Corrosion of steel bar in concrete led by natural processes requires decades. It is a problem associated with the time when the effect of materials should be analyzed in accordance with corrosion in short time. In order to speed up the process of corrosion, then accelerated corrosion is carried out in the laboratory. Artificial corrosion is induced by electrolytic processes which is combined with three percent of sodium chloride solution.

Before the main specimens are performed, preliminary testing of the aggregate for the concrete consist of crushed stone and sand is done. Analysing of the aggregate in this regard involves the density, specific gravity, clay content, and gradation. According to the result of the material testing, hereinafter mix proportion of concrete is then composed.

The compressive strength designed is 30 MPa. Table 1 shows the mix proportion of concrete in kilogram per cubic meter.

Table 1. Mix proportion of concrete.

Cement (kg)	Crushed stone (kg)	Sand (kg)	Water (liter)
530	1085	495	235

### 2.1. Specimens

There are two types specimen dimension. The dimension of absorption specimen is a cylinder with 75 mm of diameter and 150 mm in height. Meanwhile, a cube with the size 100 mm x 100 mm and 200 mm with steel bar diameter 12 mm inserted inside of concrete is utilized to investigate the corrosion process. Amount of specimen is shown in Table 2.

Table 2. Number of specimen.

Code	Absorption test	Corrosion test	Compressive strength
CS-0	3	3	3
CS-1	3	3	3

where CS is a symbol for calcium stearate and 0 (zero) and 1 (one) is a content of calcium stearate which is 0 kg and 1 kg per cubic meter of concrete.

### 2.2. Procedures of absorption test

Absorption test is conducted after the specimen has been treated by soaking it into fresh water for 28 days and referring to Indonesia Standard SKSNI S-36-1990-03 [7]. Hereafter, the cylinders are dried in the oven with a temperature of  $100 \pm 5$  degrees Celsius for 3 x 24 hours. The next step is removing the specimens from the oven and placing them on the open space for a day. The further stage is weighing them in the dry condition (a). Soaking the specimens in the fresh water for 30 minutes, then lifting the fresh water out and removing the water from the surface of the concrete specimen. The final step is weighing the specimen in saturated surface dry (b). Absorption of water by the concrete is measured using a below formula.

$$\text{Absorption (\%)} = \frac{b-a}{a} \times 100\% \quad (1)$$

### 2.3. Procedure of electrolytic corrosion test

The curing process of the electrolytic corrosion specimen test as a representation of accelerated corrosion test has been conducted by covering them using wet mattress for 28 days. Installation of the cables to generate the artificial corrosion is shown as Fig. 2. Since the installation of cables is completed, the specimen is immersed in a solution containing 3% sodium chloride as the electrolyte. Direct current electricity is then applied to produce the corrosion on the steel bar in concrete. Testing is ended when the cracks appear on concrete surface due to expansion of rust. Therefore, the corroded steel bar is taken out by breaking the concrete specimen. In order to evaluate the level of corrosion, the corroded steel bar is cleaned with a wire brush. Then, the specimens are soaked in a solution of ammonium citrate 10% to assure that the rust is all removed from steel bar surface. Percentage of corrosion is measured based on the ratio between the amount of corrosion and the initial weight of steel bar.

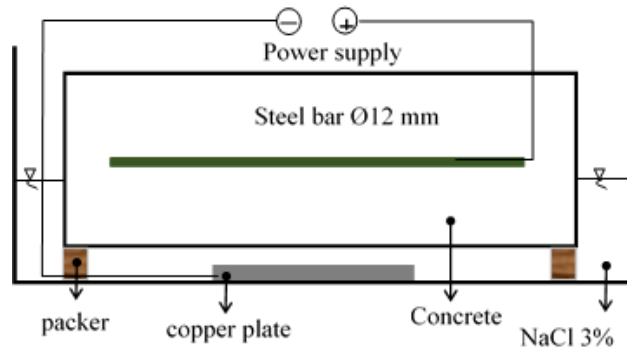


Fig. 2. Scheme of electrolytic corrosion test.

### 3. Results and discussions

#### 3.1. Raw materials of concrete

Analysis of raw materials of concrete shows that specific gravity, density, clay content, and fineness modulus of crushed stone are 2.8, 1.39 gram/cm<sup>3</sup>, 1.75% and 5.68 consecutively. Furthermore, the result of sand analysis is 1.34 gram/cm<sup>3</sup>, 2.81, 1.13% and 2.20 for density, specific gravity, clay content and fineness modulus serially. These results meet with the Indonesia Standard for coarse and fine aggregate, except the clay content of coarse aggregate. However, clay content specified standard does not exceed 1%. At that moment, coarse aggregate should be treated to reduce the clay content. After the treatment, the mix proportion of concrete is tested. At the end of this stage, the compressive strength average of the three specimens is 53.3 MPa. It shows that the mix proportion of concrete matches with the initial planning.

The average of compressive strengths for specimens CS-0 and CS-1 is 37.4 MPa and 38.75 MPa. This result shows that calcium stearate does not significantly affect on the compressive strength. This increasing can be neglected since deviation of compressive strength between specimen CS-0 and specimen CS-1 is very small. Based on the result, it can be summarised that calcium stearate content 1 kg per cubic of concrete has no negative effect on compressive strength.

#### 3.2. Absorption results

The absorption of concrete is shown on Table 3 below. According to the table, concrete with calcium stearate 1 kg/m<sup>3</sup> absorb water less than concrete without calcium stearate. The absorption decreases around 100% from 2.00% to 0.94%. This result agrees with Maryoto [8] investigation. The result shows clearly that by the addition of calcium stearate in the concrete, water and cementitious ratio of concrete is a bit reduced. When the evaporation in the concrete is under processing, capillaries formed has a smaller diameter. It needs more energy to press water penetrate into concrete. With smaller diameter of capillaries, it means that concrete is more solid. Another influence due to the diminution diameter of capillaries in concrete is increasing of the compressive strength.

Fig. 3 shows the process of absorption test. Dry weight appears in Fig. 3(a) and then the specimens are soaked in the water for 30 minutes as seen on Fig. 3(b) after that weigh them to obtain the saturated surface density weight.



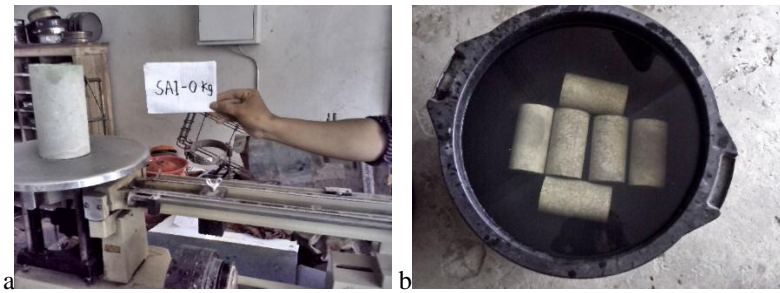


Fig. 3. Absorption test, (a) dry weight; (b) soaking the specimens in the fresh water.

Table 3. Number of specimen.

Code	Number of specimen	Dry weight (kg)	Wet weight (kg)	Absorption (%)	Average absorption (%)
CS-0	1	1.808	1.845	2.00	2.00
	2	1.792	1.831	2.13	
	3	1.786	1.820	1.87	
CS-1	1	1.838	1.859	1.13	0.94
	2	1.818	1.835	0.93	
	3	1.841	1.855	0.74	

### 3.3. Corrosion results

Process of electrolytic corrosion is applied on the specimens for 14 days. During the process, appearance of cracks on the surface of concrete due to corrosion expansion is controlled every day. The process will be ended if the corrosion has already occurred in all of the specimens. In order to analyse levels of corrosion on the steel bar, the specimens are broken to remove the reinforcement from concrete. Fig. 4 shows the steel bar after they are induced by artificial corrosion. Based on the figure, it can be observed visually that more rust is produced in the specimen without calcium stearate CS-0. Visual observation is only simple analysis to compare the specimens CS-0 and CS-1 to resist chloride attack.

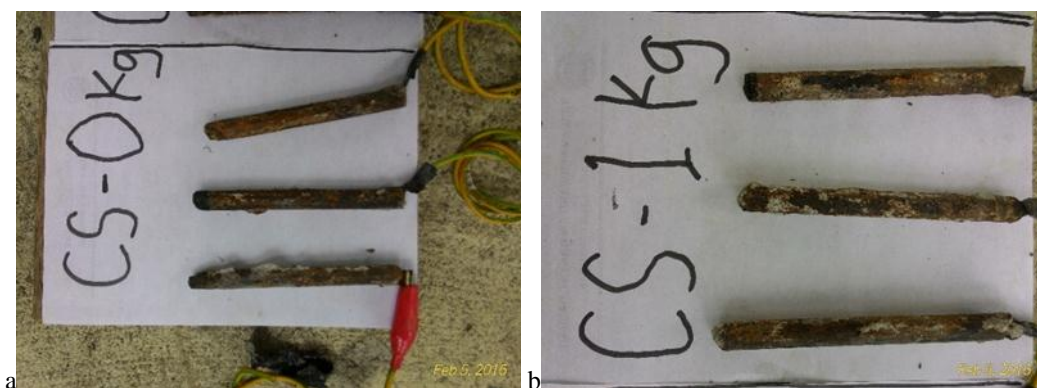


Fig. 4. Corrosion of steel bar, (a) specimens CS-0; (b) specimens CS-1.

In order to obtain the real percentage of the rust, surface of the corroded steel bar is eradicated using wire brush and ammonium citrate solution. By evaluating the steel bar after cleaning them from the rust, percentage of corrosion is obtained as shown in Table 4. The corrosion level of concrete without calcium stearate CS-0 is around 11.79%. On the other hand, concrete with calcium stearate CS-1 is only attacked by corrosion 4.18%. It proves that calcium stearate

significantly protects the concrete from corrosion attack due to chloride ion penetration. This result has a similar tendency to Maryoto [8] study. In his study, Maryoto examined the effect of calcium stearate in concrete using the half-cell potential and macro cell current testing. The result indicates that concrete with calcium stearate has a less possibility of corrosion due to chloride attack. The newest result currently demonstrates the reliability of calcium stearate application in concrete. It improves the microstructure of concrete to decrease the infiltration of chloride ions.

Table 4. Percentage of steel bar corrosion.

Code	Number of specimen	Initial weight (gram)	Final weight (gram)	Percentage of corrosion (%)	Average of corrosion (%)
CS-0	1	87.50	77.50	11.43	11.79
	2	90.50	78.00	13.81	
	3	87.00	78.20	10.11	
CS-1	1	87.90	84.40	3.98	4.18
	2	87.50	84.50	3.43	
	3	87.50	83.00	5.14	

#### 4. Conclusions

According to the above discussions, the following conclusions are summarized.

- Additional of calcium stearate in concrete reduces the water absorption. Consequently, the water tightness of the concrete with calcium stearate is also improved.
- Corrosion on the steel bar due to chloride ion attack can be minimized by adding calcium stearate in concrete as well.

#### Acknowledgements

Author acknowledged for a financial support to publish this research from Jenderal Soedirman University, Indonesia.

#### References

- [1]. <http://nationalgeographic.co.id>, accessed April, 2<sup>nd</sup> 2015.
- [2]. Sosa, M., Lopez, T.P., Reyes, J., Corvo, F., Chab, R.C., Quintana, P. dan Aguilar, D., Influence of the marine environment on reinforced concrete degradation depending on exposure conditions, *International Journal Electrochemical Science*, 6, (2011), pp. 6300-6318.
- [3]. <http://fibertyfo.blogspot.com/2009/04/01/archive.html>.
- [4]. Neville, A.M, *Properties of Concrete*, Longman, USA, 1996.
- [5]. Bertolini, L, Elsener, B., Pedferri, P., dan Polder, R.P, *Corrosion of steel in concrete*, Verlag GmbH & Co. KGaA, Weinheim, 2004.
- [6]. Maryoto, A, Sinergi penggunaan calcium stearate dan fly ash untuk mengurangi penetrasi air di beton, *Jurnal Teknik Sipil dan Perencanaan*, Unnes, Vol. 16 No. 2, (2014), pp. 135-140.
- [7]. DPU. Standar SK SNI S-36-1990-03. 1990. *Spesifikasi Beton Bertulang Kedap Air*. Bandung, Indonesia.
- [8]. Maryoto, A., Improving microstructures of concrete using  $\text{Ca}(\text{C}_{18}\text{H}_{35}\text{O}_2)_2$ , *Procedia Engineering* 125, (2015), pp. 631-637.



Sustainable Civil Engineering Structures and Construction Materials, SCESCM 2016

## Study of pitting resistance of rebar steels in jakarta coastal using simulated concrete pore solution

Moch. Syaiful Anwar<sup>a,\*</sup>, Bobby Fadillah<sup>b</sup>, Arini Nikitasari<sup>a</sup>, Soesaptri Oediyani<sup>b</sup>, Efendi Mabruri<sup>a</sup>

<sup>a</sup>Research Center for Metallurgy and Material, Indonesian Institute of Sciences (LIPI), South Tangerang 15314, Banten, Indonesia

<sup>b</sup>Departement of Metallurgical Engineering, Faculty of Engineering, University of Sultan Ageng Tirtayasa, Cilegon 42435, Banten, Indonesia

---

### Abstract

Carbon steels are generally used to a reinforcement in the concrete constructions, such as bridges, piling, etc. These constructions are not a bit placed in the coastal areas, especially the coastal area of Jakarta. The industrial activities and urban development were a source of sediment loads and pollutants in coastal sea water Jakarta. The presence of chloride content and pollutants in sea water could affect the process of corrosion of reinforcement steel in concrete especially pitting corrosion. In this paper, the behavior of pitting corrosion of reinforcement steel in sea water of Jakarta coastal using simulated concrete pore solution has been studied. The sea waters were taken from two different locations of Jakarta coastal, Ancol beach and Muara Baru fishing port. Each of the sea water was used as a solvent in the simulated concrete pore solution with or without carbonates. The simulated concrete pore solution with chloride was also utilized for comparison test. The cyclic and potentiostatic electrochemical polarization were conducted to evaluate the behavior of pitting corrosion of reinforcing steel. The experimental results showed that the reinforcing steel was susceptible to pitting corrosion in the simulated concrete pore solutions (SPS) of sea water with or without carbonates and in the simulated concrete pore solutions containing 3.5% NaCl. The addition of sodium carbonate and sodium bicarbonate in SPS of sea water increased the breakdown potential value and the total time for the metastable pitting decreased slightly.

© 2017 The Authors. Published by Elsevier Ltd.

Peer-review under responsibility of the organizing committee of SCESCM 2016.

*Keywords:* Reinforcing steel; pitting corrosion; jakarta coastal sea water; simulated concrete pore solution; carbonates.

---

---

\* Corresponding author. Tel.: +0-000-000-0000 ; fax: +0-000-000-0000 .

E-mail address: [tcaco.ama@gmail.com](mailto:tcaco.ama@gmail.com)

## 1. Introduction

Corrosion of reinforcement bar (rebar) steel in concrete is the main factor causing premature damage to the concrete construction, especially the concrete structure of the coast [1]. It could initiate cracks and accelerate the corrosion process in concrete. The delamination and spall also affect decreased durability, rigidity and the service life of concrete structures [2-4]. In addition, the carbonation is another important phenomenon which caused corrosion of reinforcement steel in concrete and reduces the durability of concrete structures [5] caused by the diffusion of CO<sub>2</sub> into the concrete. If it reacts with the hydrated cement compound, the pH of concrete reduces from pH 13 to pH 9 causing to the passive film of steel and accelerated the corrosion process [6]. Additionally, the environmental climate conditions and climate change also contributed directly or indirectly to the corrosion rate of reinforced concrete structures [7-10]. Experimental evidence indicated that the intrusion of chloride and carbonation were strongly influenced by climate conditions and the surrounding environment, the atmospheric CO<sub>2</sub> concentration, temperature and humidity [11].

The penetration of chloride from sea water into concrete and the associated risk for reinforcement corrosion were divided into an initiation phase and a propagation phase. The initiation phase describes the ingress of chloride during the wetting/drying concrete and terminated by depassivation of the reinforcement. Then, the increasing of chloride content is required to prevent repassivation and to enable stable pit growth [12]. The stable pit growth called by pitting corrosion of steel in concrete is also affected by the pH, temperature, microstructure and composition of the concrete-steel interface, and composition and surface of the steel in concrete [13].

According to the World Resources Institute, in 2011, the greenhouse gas emitter of 2,053 billion tonnes produced by Indonesia was ranked sixth after India and Russia [14]. The higher greenhouse gas emitter in Indonesia's air reduced sustainability of reinforcement concrete (RC) structure. For achieving environmental friendly sustainable RC structure, Rajit et al [15] used photo catalytic materials to the RC structure during its construction phase that could reduce the corrosion problem of RC materials.

The present paper reports the pitting resistance of rebar steels exposed in the simulated concrete pore solution (SPS) containing the Jakarta coastal sea water with or without carbonates. For comparison, the distilled water SPS with chloride also utilized in this study. The results of the study may be used to assess the sustainability of RC structure in the Jakarta's coastal.

## 2. Experimental

### 2.1. Specimen Preparation

The specimens with a surface area of 1.13 cm<sup>2</sup> for the polarisation measurements were cut from the rebar steel using cutting machine, connected with copper wire as an electrical contact and mounted with resin to cover the unexposed area. The specimens were polished with SiC paper from grit 400 to 1200 grit. The specimens were then washed in distilled water. The chemical composition of rebar steel is shown in Table 1.

Table 1. Chemical composition of reinforcing steel

Chemical composition (wt%)									
C	Si	Mn	P	S	Cu	Ni	Cr	Mo	Fe
0.37	0.23	0.54	0.03	0.04	0.14	0.06	0.15	0.013	Bal.

The polarisation measurement used three electrodes, the specimens as working electrode, graphite rod auxiliary electrode and saturated calomel electrode (SCE) as reference electrode.

\* Corresponding author. Tel.: +62-813-5730-8827; fax: +62-21-756-0553.  
E-mail address: moch026@lipi.go.id

## 2.2. The test solutions

The polarisation measurement of specimens was conducted in the simulated concrete pore solution (SPS) which the distilled water and Jakarta coastal sea water as the solvent with pH 13 at room temperature using a Gamry G750 system. The two Jakarta coastal sea water were taken from Ancol beach (sea water A) and Muara Baru fishing port (sea water B). The composition of sea water A and B, the chemical composition of simulated concrete pore solution and the SPS composition of test solution are listed in Table 2, Table 3 and Table 4, respectively.

Table 2. Composition of sea water

Parameters	Sea water A	Sea water B	Method Specification
Physical:			
Total Suspended Solids (TSS) *	8.3 mg/L	8.1 mg/L	APHA Section 2540 D, Edition 21 <sup>st</sup> , 2005
Chemical:			
pH	7.7	7.8	APHA Section 4500 H <sup>+</sup> , Edition 21 <sup>st</sup> , 2005
Salinity	32.2 ‰	32.2 ‰	APHA Section 2520 B, Edition 21 <sup>st</sup> , 2005
Chloride (Cl <sup>-</sup> )	19,090 mg/L	20,094 mg/L	APHA Section 4500 Cl <sup>-</sup> , Edition 21 <sup>st</sup> , 2005
COD	104.7 mg/L	53.9 mg/L	SNI 6989.73.2009
BOD	34 mg/L	17 mg/L	APHA Section 5210– B 2005
Magnesium (Mg)	830 mg/L	1080 mg/L	APHA Section 3111 - B 2005 (AAS)
Sulphate (SO <sub>4</sub> )	496 mg/L	492.5 mg/L	JIS K 0101: 2002
Dissolved Oxygen (DO)	7.1 mg/L	7.4 mg/L	IKM/5.4.97/MB
Nitrate (NO <sub>3</sub> -N)	<2 mg/L	<2 mg/L	APHA Section 4500 NO <sub>3</sub> <sup>-</sup> - B 2005
Oil and Fats	<1.41 mg/L	<1.41 mg/L	APHA Section 5520 B Oil & Grease 2005
Natrium (Na)	<0.002 mg/L	<0.002 mg/L	APHA Section 3111 - B 2005 (AAS)

Table 3. Chemical composition of simulated concrete pore solution (SPS)

Chemical composition (mol/liter)			
NaOH	KOH	Ca(OH) <sub>2</sub>	CaSO <sub>4</sub> ·H <sub>2</sub> O
0.1	0.3	0.03	0.02

Table 4. SPS composition of test solution

Solution	SPS solvent + additive
1	Sea water A
2	Sea water B
3	Sea water A + Carbonate (0.03M NaHCO <sub>3</sub> + 0.0015M Na <sub>2</sub> CO <sub>3</sub> )
4	Sea water B + Carbonate (0.03M NaHCO <sub>3</sub> + 0.0015M Na <sub>2</sub> CO <sub>3</sub> )
5	Distilled water
6	Distilled water + 1.5% NaCl
7	Distilled water + 3.5% NaCl

The specimens were immersed in the 500 ml of test solution and allowed to corroded freely for 1 h in the solution before beginning the measurements. At the end of this period, the open circuit potential ( $E_{oc}$ ) was recorded and started from the value of  $E_{oc}$ .

### 2.3. Cyclic polarisation measurement

The cyclic polarisation was applied to measure the breakdown ( $E_b$ ) and protection ( $E_{prot}$ ) potential of the specimens. The measurement of cyclic polarisation referred to ASTM G-61. The potential of the sample was swept from the  $-200$  mV to  $+2500$  mV where a current density limit of  $10$  mA/cm<sup>2</sup> was applied in the specimen. After reaching current density limit, reverse polarisation was started to find susceptibility to pitting corrosion on the specimens. The scan rate of forward and reverse scan was  $5$  and  $1.5$  mV/s, respectively.

### 2.4. Potentiostatic polarisation measurement

To know the peak current density ( $i_{peak}$ ) and the total time for a metastable pitting events ( $t_{pit}$ ) on the specimens, the potentiostatic polarisation was carried out where the current flowing as a result of the applied potential was plotted as a function of time. The parameters were defined in Fig. 1. Peak current density ( $i_{peak}$ ) was defined as,  $i_{peak} = i_{max} - i_{bc}$ . The total time for a metastable pitting event was given by  $t_{pit} = t_g + t_{rp}$ . Where  $i_{max}$ : a maximum current density,  $i_{bc}$ : a base current density,  $t_g$ : a pit growth time and  $t_{rp}$ : a repassivation time [16].

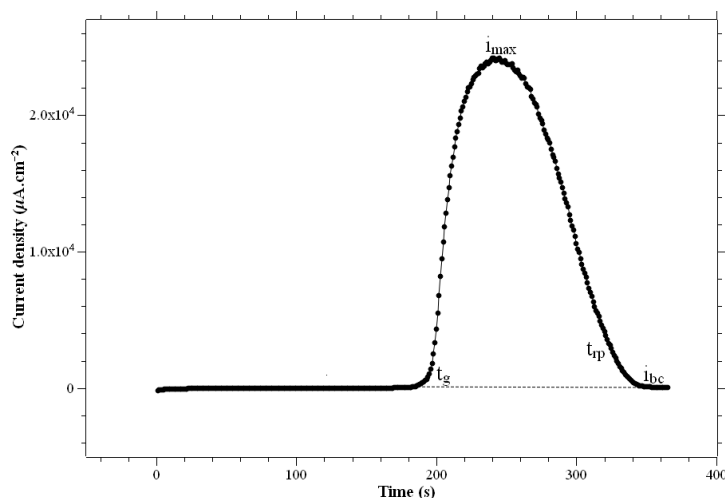


Fig. 1. Potentiostatic polarisation curve

## 3. Results and Discussion

### 3.1. Sea water SPS with or without carbonates ( $0.03M NaHCO_3 + 0.0015M Na_2CO_3$ )

#### 3.1.1. Cyclic polarisation analysis

The cyclic polarisation of rebar steel in the SPS where sea water as solvent with or without carbonate is shown in Fig. 2. In this figure, the hysteresis loop is found in the rebar steel immersed in the SPS sea water with or without carbonate.

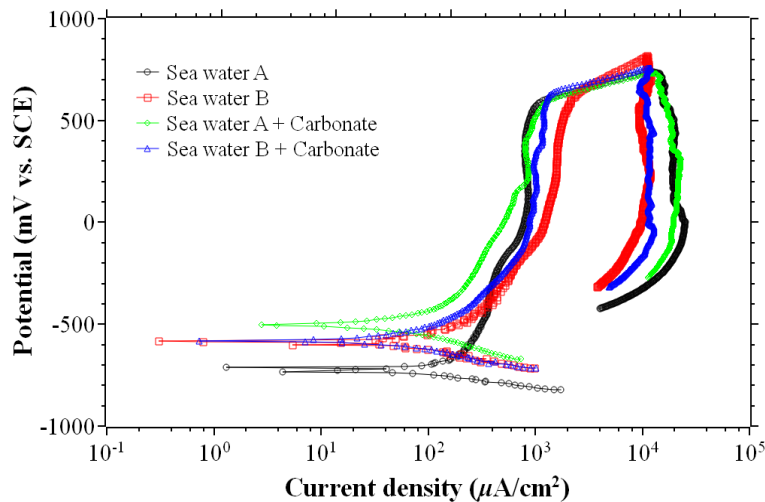


Fig. 2. Cyclic polarisation of rebar steel in the SPS where sea water as solvent with or without carbonate

The parameters determined from the cyclic polarisation of rebar steel in the SPS where sea water as solvent with or without carbonates, such as open circuit potential,  $E_{oc}$ , breakdown potential,  $E_b$ , protection potential,  $E_{prot}$  of the rebar steel were presented in Table 5.

Table 5. The parameter determined from the cyclic polarisation of rebar steel in the SPS where sea water as solvent with or without carbonate

SPS solvent+additive	$E_{oc}$ (mV vs. SCE)	$E_b$ (mV vs. SCE)	$E_{prot}$ (mV vs. SCE)
Sea water A	-623.8	564.9	-467.1
Sea water B	-516.4	602	-308.6
Sea water A + Carbonate	-473	568.3	-268.1
Sea water B + Carbonate	-516.7	632.4	-335.6

In Table 5, the rebar steel immersed in the all test solutions have higher breakdown potential value than the protection potential value. It means that the rebar steel immersed in the all solution have susceptibility to pitting corrosion. The lowest open circuit potential of  $-623.8$  mV vs. SCE and breakdown potential of  $564.9$  mV vs. SCE are found in the rebar steel immersed in the SPS of sea water A without carbonate. It shows that the rebar steel immersed in the SPS of sea water A without carbonate having lower susceptibility of pitting corrosion resistance. The addition of carbonates ( $0.03M NaHCO_3 + 0.0015M Na_2CO_3$ ) in the SPS of sea water increases the breakdown potential value of 0.6% for SPS of sea water A and 5% for sea water B.

### 3.1.2. Potentiostatic polarisation analysis

The potentiostatic polarisation of rebar steel in the SPS where sea water as solvent with or without carbonate presented in Fig. 3. In this figure, the pit growth occurs after 250 s in the rebar steel in all test solutions.

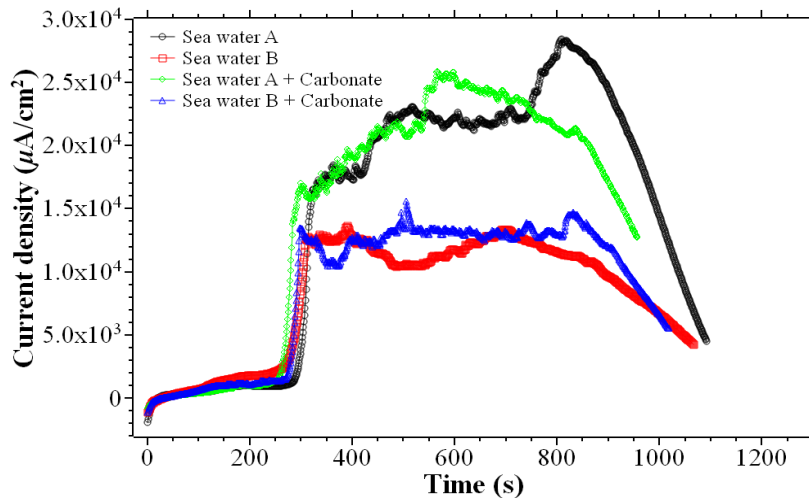


Fig. 3. Potentiostatic polarisation of rebar steel in the SPS where sea water as solvent with or without carbonate

Table 6 shows the parameters value determined from potentiostatic polarisation for rebar steel in the SPS where sea water as solvent with or without carbonate.

Table 6. Parameters determined from potentiostatic polarisation for rebar steel in the SPS where sea water as solvent with or without carbonate

SPS solvent+additive	$i_{\max}$ ( $\mu\text{A}/\text{cm}^2$ )	$i_{bc}$ ( $\mu\text{A}/\text{cm}^2$ )	$i_{\text{peak}}$ ( $\mu\text{A}/\text{cm}^2$ )	$t_g$ (s)	$t_{rp}$ (s)	$t_{\text{pit}}$ (s)
Sea water A	28400	4530	23870	284.9	922.9	1207.8
Sea water B	13700	4020	9680	270	866	1136
Sea water A + Carbonate	25900	12700	13200	254.9	853.9	1108.8
Sea water B + Carbonate	15600	5430	10170	269	857	1126

In Table 6, the highest peak current density of  $23870 \mu\text{A}/\text{cm}^2$  and total time for a metastable pitting event of 1207.8 s are found on the rebar steel immersed in the SPS of sea water A without carbonate. The addition of carbonate ( $0.03\text{M NaHCO}_3 + 0.0015\text{M Na}_2\text{CO}_3$ ) in the SPS of sea water decreases the total time for the metastable pitting event of 8.2% for SPS of sea water A and 0.88% for sea water B. The total time for the metastable pitting of rebar steels immersed in the SPS of sea water is higher when comparing with rebar steels immersed in the SPS of distilled water with or without chloride (Table 6). It may be that the sea water composition was have more aggressive chemical content when compared with sodium chloride solution.

The influence of carbonates ( $\text{NaHCO}_3 + \text{Na}_2\text{CO}_3$ ) in the SPS of sea water increases the breakdown potential ( $E_b$ ) and decreases the total time for the metastable pitting event ( $t_{\text{pit}}$ ). The addition of strong alkaline substance also can be used as an alkaline electrolyte for electrochemical realkalisation treatment of carbonate reinforced concrete [17]. It may enhances durability and sustainability of reinforced concrete structure in the Jakarta's coastal. Even though, addition of sodium carbonate and sodium bicarbonate around 6 and 10 g/L in the concrete decreases compressive strength and tensile strength [18].



### 3.2. Distilled water SPS with or without sodium chloride

#### 3.2.1. Cyclic polarisation analysis

The cyclic polarisation of rebar steel in the SPS where distilled water as solvent with or without chloride is shown in Fig. 4. In this figure, the hysteresis loop is found in the rebar steel immersed in the SPS distilled water with 3.5% NaCl whereas the rebar steel immersed in the SPS distilled water and distilled water with 1.5% NaCl does not show the hysteresis loop.

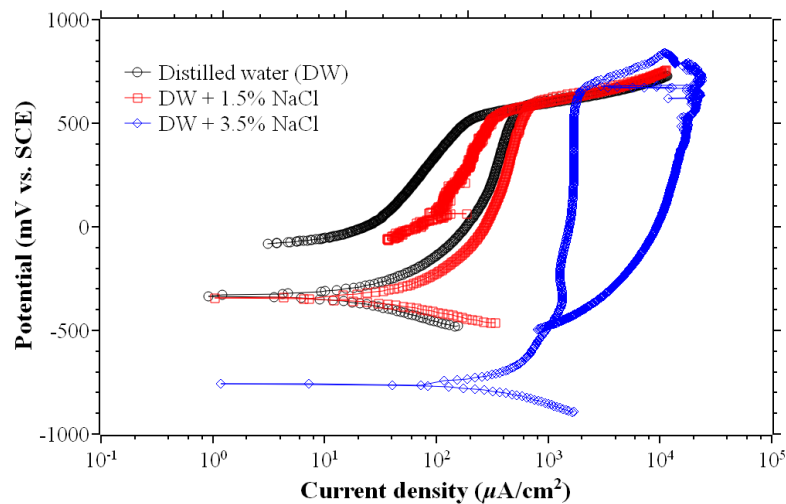


Fig. 4. Cyclic polarisation of rebar steel in the SPS where distilled water as solvent with or without chloride

The parameters determined from the cyclic polarisation of rebar steel in the SPS where distilled water as solvent with or without chloride, such as open circuit potential ( $E_{oc}$ ), breakdown potential ( $E_b$ ), protection potential ( $E_{prot}$ ) of the rebar steel are presented in Table 7. The breakdown potential ( $E_b$ ) could be determined at the inflection point value (in Fig. 4) above the sharp change in slope [19]. The protection potential ( $E_{prot}$ ) could be determined as a cross-over potential (in Fig. 4). Cross over potentials were measured where the hysteresis loop closes [20].

Table 7. The parameter determined from the cyclic polarisation of rebar steel in the SPS where distilled water as solvent with or without chloride

SPS solvent+additive	$E_{oc}$ (mV vs. SCE)	$E_b$ (mV vs. SCE)	$E_{prot}$ (mV vs. SCE)
Distilled water	-280.6	585.2	578.8
Distilled water + 1.5% NaCl	-263.1	605.4	590
Distilled water + 3.5% NaCl	-694.9	662.2	-474.8

In Table 7, the lowest open circuit potential of  $-694.9$  mV vs. SCE is found in the rebar steel immersed in the SPS distilled water with 3.5% NaCl. It indicates that the influence of higher sodium chloride content in the solution decreases potential of rebar steel in the SPS. The highest breakdown potential of  $662.2$  mV vs. SCE and the lowest protection potential of  $-474.8$  mV vs. SCE are found in the rebar steel immersed in the SPS distilled water with 3.5% NaCl. It means that the susceptibility of pitting corrosion resistance of rebar steel immersed in the SPS distilled water with 3.5% NaCl is lower when compared with rebar steel immersed in the distilled water and distilled water with 1.5% NaCl.

### 3.2.2. Potentiostatic polarisation analysis

The potentiostatic polarisation of rebar steel in the SPS where distilled water as solvent with or without chloride is presented in Fig. 5.

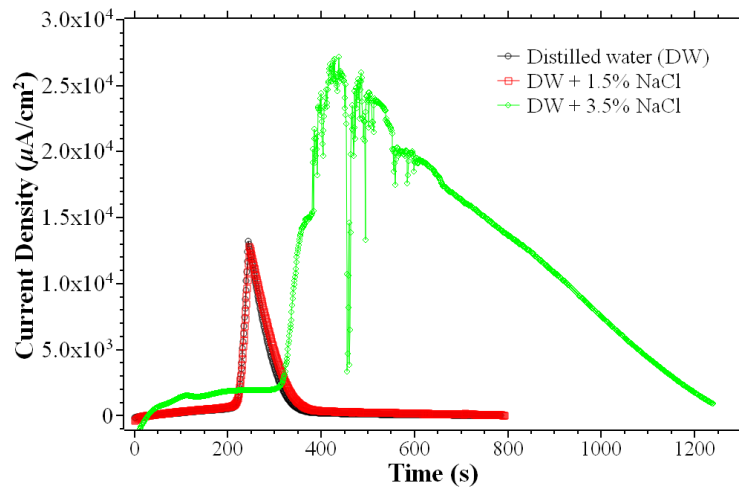


Fig. 5. Potentiostatic polarisation of rebar steel in the SPS where distilled water as solvent with or without chloride

In this figure, the current density of rebar steel in the SPS distilled water and the SPS distilled water with 1.5% NaCl shows constant value until around 200 s. After 200 s, the current density increases sharply until  $13000 \mu\text{A}/\text{cm}^2$  and then decreases sharply until current density reaches constant time of 400 s. At chloride content of 3.5% in the SPS distilled water, the pit growth occurs after 300 s and the maximum current density occurs in the rebar steel at around  $27000 \mu\text{A}/\text{cm}^2$ . Table 8 shows the parameter value determined from potentiostatic polarisation for rebar steel in the SPS where distilled water as solvent with or without chloride. In Table 8, the highest peak current density of  $26480 \mu\text{A}/\text{cm}^2$  and total time for a metastable pitting event of 969 s are found in the rebar steel immersed in the SPS distilled water with 3.5% NaCl.

Table 8. Parameters determined from potentiostatic polarisation for rebar steel in the SPS where distilled water as solvent with or without chloride

SPS solvent+additive	$i_{\text{max}}$ ( $\mu\text{A}/\text{cm}^2$ )	$i_{\text{bc}}$ ( $\mu\text{A}/\text{cm}^2$ )	$i_{\text{peak}}$ ( $\mu\text{A}/\text{cm}^2$ )	$t_{\text{g}}$ (s)	$t_{\text{rp}}$ (s)	$t_{\text{pit}}$ (s)
Distilled water	13200	50	13150	214	350	564
Distilled water + 1.5% NaCl	12800	130	12670	214	360	574
Distilled water + 3.5% NaCl	27400	920	26480	311	658	969

## 4. Conclusions

Refer to this study, the following conclusions can be drawn that the rebar steels immersed in both the SPS of sea water A (Ancol beach sea water) and the SPS of sea water B (Muara Baru fishing port sea water) as well as in the 3.5% NaCl solution have susceptibility to pitting corrosion. The total time for the metastable pitting event of rebar steels immersed in the SPS of sea water A was higher when compared with rebar steel immersed in the SPS of sea water B. While the total time in the metastable pitting event of rebar steels immersed in the 3.5% NaCl solution was lower than rebar steels immersed in the SPS of sea water. Further, the addition of sodium carbonate and sodium bicarbonate in both SPS of sea water A and SPS of sea water B increased the breakdown potential value and

decreased the total time for the metastable pitting event slightly. Therefore the additive carbonates may be used to enhance durability and sustainability of reinforced concrete structure in the Jakarta's coastal.

## Acknowledgements

This research was supported by priority programme of Deputy of Earth Sciences, Indonesian Institute of Sciences (LIPI) Fiscal Year 2015.

## References

- [1] M.Raupach and P.Schic, *NDT and E Int*, 34 (2001) 435.
- [2] E. Kato, M. Iwanami, H. Yokota, Deterioration in ductility of RC beams with corroded reinforcement, *Proceeding of the 1<sup>st</sup> international symposium on life-cycle civil engineering*, Varrena, Italy (2006) 159-164.
- [3] W.Zhu, R. Francois, Corrosion of reinforcement and its influence on the residual structural performance of a26-years-old corroded RC structure, *Constr.Build. mater.* 51 (2014) 461-472.
- [4] J.Rodriguez, L.M. Ortega, J. casal, load carrying capacity of concrete structure with corroded environment, *Constr. Build.Mater* 2 (4) (1997) 239-248.
- [5] J.M.Chi, R. Huang, C.C. yang, Effet of carbonation on mechanical properties nd durability of concrete using accelerated testing method, *J. Marine Sci. and Tech.* (10) (1) (2002) 14-20.
- [6] V.G.Papadakis, M.N. Fardis, C.G. Vayenas, Effect of composition, environmental factor and cement-lime motor coating on concrete carbonation, *Materials and Structure*, (25) (149) (1992) 293-304.
- [7] M.G. Stewart, X.Wang, M.N. Nguyen, Climate change adaptation for corrosion control of concrete infrastructure, *Structural Safety* 35 (2012) 29–39.
- [8] N.S. Trivedi, M.S.Venkrataman, C.Chu, I.S.Cole, Effect of climate change on corrosion rates of structures in Australia, *Climate Change* (124) (2014) 133-146.
- [9] L. Peng and M.G. Stewart , Climate change and corrosion damage risks for reinforced concrete infrastructure in China, *Structure and Infrastructure Engineering*, 2014
- [10] M. N. Nguyen, X. Wang and R. H. Leicester, An assessment of climate change effects on atmospheric corrosion rates of steel structures, *Corrosion Engineering, Science and Technology*, (48) (5) (2013) 359-369.
- [11] Setta A, Scotta R, Vitaliani R, Analysis of chloride diffusion into partially saturated concrete, *ACI Mater J* (90) 1993, 441-451.
- [12] Ueli M. Angst, Bernhard Elsener, Claus K. Larsen, Øystein Vennesland, Chloride induced reinforcement corrosion: Electrochemical monitoring of initiation stage and chloride threshold values, *Corrosion Science* 53 (2011) 1451–1464.
- [13] Nelson Silva, Chloride Induced Corrosion of Reinforcement Steel in Concrete (Threshold Values and Ion Distributions at the Concrete-Steel Interface), Thesis, ISBN 978-91-7385-808-3, Department of Civil and Environmental Engineering, Chalmers University Of Technology, Gothenburg, Sweden, 2013.
- [14] <http://www.wri.org/blog/2014/05/history-carbon-dioxide-emissions>
- [15] Ranjit K. Nath, M. F.M .Zain, Md. Rabiul Alam, Abdul Amir H. Kadhum and A.B.M.A. Kaish, *International Journal of Sustainable Construction Engineering & Technology*, Vol 3, Issue 2, 2012.
- [16] R.K. Gupta, N.L. Sukiman, M.K. Cavanaugh, B.R.W. Hinton, C.R. Hutchinson, N. Birbili, *Electrochimica Acta* 66 (2012) 245– 254.
- [17] YunYun Tong, Véronique Bouteiller, Elisabeth Marie-Victoire, Suzanne Joiret, Efficiency investigations of electrochemical realkalisation treatment applied to carbonated reinforced concrete — Part 1: Sacrificial anode process, *Cement and Concrete Research* 42 (2012) 84–94.
- [18] V.V. Reddy, H.S. Rao, K.N.Jayaveera, Influence strong alkaline substances (sodium carbonate and sodium bicarbonate) in mixing water on strength and setting properties of concrete, *Indian Journal of Engineering & Material Sciences*, Vol. 13, April 2006, pp. 123-128.
- [19] G.S. Frankel, “Pitting Corrosion”, *ASM Handbook Vol. 13A*, (ASM International, Metals Park, OH, 2003): p.237.
- [20] R Baboian and G.S. Haynes, “Cyclic Polarization Measurements - Experimental Procedures and Evaluation of Test Data”, *STP 727 Electrochemical Corrosion Testing*, (ASTM, Philadelphia, PA, 1981): p. 274–282.



Sustainable Civil Engineering Structures and Construction Materials, SCESCM 2016

## Effect of pit distance on failure probability of a corroded RC beam

Mahdi Kioumarsi<sup>a\*</sup>, Gro Markeset<sup>a</sup>

<sup>a</sup>*Oslo and Akershus University College, Oslo, Norway*

---

### Abstract

The present paper studies effect of the variation of pit distance on structural reliability of a reinforced concrete (RC) beam, with particular emphasis on the interference of localized corrosion on adjacent tensile rebars. The research question leading the inquiry of this article is how does average distance between corrosion pits in rebars affect the probability of failure in RC beams. In this paper, by using Monte Carlo Simulation (MCS), probabilities of failure in a corroded RC beam with different pit distances are quantified. Uncertainties in material properties, geometry, loads, corrosion modelling, pit distances and pit interference are taken into account. Statistical data reported in literature regarding the extent and location of corrosion is utilized to undertake a parametric study of corresponding probability distribution functions. According to results, variation of pit distance has significant influence on probabilities of failure. This influence increases if the effect of interference of localized corrosion is taking into account.

© 2017 The Authors. Published by Elsevier Ltd.

Peer-review under responsibility of the organizing committee of SCESCM 2016.

*Keywords:* Concrete structure; localized corrosion; pitting; pit distance; probability of failure; interference of pits

---

### 1. Introduction

Corrosion of steel rebars embedded in reinforced concrete (RC) members, causes deterioration of concrete structures, diminishing their capacity and serviceability. There are two types of corrosion: uniform and localized (pitting) corrosion. A typical deterioration of RC structures exposed to aggressive chloride environments is localized corrosion of rebar. Pitting corrosion can lead to high degrees of cross-section area loss along the rebar [1].

Assessing reliability of RC members with corroding rebars has received increasing attention in recent years [2-9]. Early studies accounted only for uniform corrosion in rebars. However, this approach requires additional measures to take into account spatial variability of cross-section along the bar and the reduction of mechanical properties of the bar due to local stress localizations [10-12].

---

\* Corresponding author. Tel.: +47-67238745.

E-mail address: [Mahdi.kioumarsi@hioa.no](mailto:Mahdi.kioumarsi@hioa.no)

Later studies have become more realistic by developing reliability assessments of RC beams by considering the effect of spatial variability of the localized corrosion on rebars. Kioumars et al. [13] studied the effect of interference of corrosion pits on adjacent rebars on the probability of bending failure of a corroded reinforced concrete beam. Spatial distribution of localized corrosion along a beam is considered in the analyses. These authors considered the appearance of corrosion pits as a Poisson process, i.e. a process in which pits occur continuously and independently.

Different rebars, exposed to different environmental conditions would present different average values of pit distance, which in turn may affect the probability of failure of RC beams. In the present article, we follow up the work by Kioumars et al, drawing attention to the influence of average pit distance on reliability of corroded RC beams. The research objective leading the inquiry of this article is thus: Quantifying effect of average distance between corrosion pits in rebars on the probability of failure in RC beams. To answer the research question, we consider a case study and estimate failure probability using Monte Carlo Simulation (MCS). Uncertainties in material properties, geometry, loads, corrosion modelling, pit distances and pit interference are taken into account. Statistical data reported in literature regarding the extent and location of corrosion is utilized to undertake a parametric study of corresponding probability distribution functions.

## 2. Interference of localized corrosion on adjacent rebars

It is shown that the cross-section reduction varies along the tensile rebars and that the cross-section reduction differs between rebars [14]. The disparities of localized cross-section reduction between rebars may result in interference between the pits (see Fig. 1) [15].



Fig. 1. Plan view of potential pit locations and possible interference of localized corrosion between adjacent tensile rebars [15].

Kioumars et al. [15-17] selected an idealized case to quantify the possible interference of localized corrosion on adjacent rebars in an under-reinforced beam subjected to bending. In the idealized case two adjacent rebars were considered with one corrosion pit each. The two corrosion pits were equal in size. In a series of nonlinear finite element models the combined influence of two variables on the bending ultimate limit state (ULS) was quantified: the ratio of the distance between pits in two adjacent rebars to the distance between tensile rebars,  $l_p/l_r$ , and the ratio of the cross section reduction of the rebar due to localized corrosion to the initial cross section of rebar  $A_{pit}/A_0$ . From the numerical simulations it was found that pits interfere within a critical distance. Interference of localized corrosions reduces gradually for increasing distance between pits in two adjacent rebars ( $l_p$ ). For the investigated beam with 80 mm distance between two adjacent rebars ( $l_r$ ) the critical distance was 100 mm; i.e. for higher ratios of  $l_p/l_r > 100/80 = 1.25$  no interference was observed [15-17].

Current analytical design rules cannot quantify the interference of localized corrosions for intermediate  $l_p/l_r$  ratios ( $0 < l_p/l_r < 1.25$ ) [17]. In order to take into account the possible interference of localized corrosions, Kioumars et al. [15] proposed using a modified total residual cross section of corroded tensile rebars in an analytical analysis of the strength of the cross section:

$$A_{res(mod)} = 2A_0 - (2A_{uni} + A_{pit} + \beta A_{pit}) \quad (1)$$

$$\beta = -0.76(l_p/l_r)^2 + 0.16(l_p/l_r) + 1 \quad (2)$$

where  $A_{res(mod)}$  is the modified total residual cross section of two rebars after uniform and localized corrosion,  $A_0$  is the initial cross section of a rebar,  $A_{uni}$  is the cross section reduction of a rebar due to uniform corrosion,  $A_{pit}$  is the additional cross section reduction of a rebar due to localized corrosion. The interference of localized corrosion is introduced by an interference factor  $\beta$  which is only a function of the ratio of the distance between pits in two adjacent rebars to the distance between tensile rebars.

### 3. Distribution function of localized corrosion

When inspecting naturally corroded rebars it becomes obvious that the distinction between localized and uniform corrosion is not clearly visible, and the explicit modelling of both requires some simplifying assumption. In this paper we used a different geometric description which allows modelling of localized corrosion; the original cross-section ( $A_0$ ), the cross-section reduction due to uniform corrosion ( $A_{uni}$ ), and the cross-section reduction due to localized corrosion ( $A_{pit}$ ). See Fig. 2.

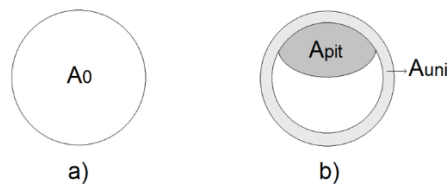


Fig. 2. (a) Original cross-section ( $A_0$ ); (b) uniform ( $A_{uni}$ ) and localized cross-section reduction ( $A_{pit}$ ) [13].

If the uniform corrosion is assumed to be equal to the minimum cross-section loss the number of the pits is high. If the assumed uniform corrosion is increased the number of pits will gradually decrease [13]. This is exemplified in Fig. 3.

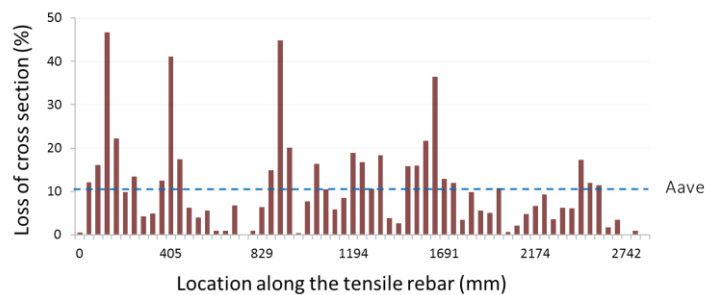


Fig. 3. Cross-section reduction of a corroded rebar. The dashed lines illustrate different assumptions of uniform corrosion, which influences the number of pits.

#### 3.1. Distribution function of pit size ratio ( $A_{pit}/A_0$ )

Maps of steel cross-section losses of the selected corroded rebars were obtained from two recent papers [14, 18]. The average cross-section reduction was measured as mass loss for the rebars, which amounted to approximately 10%.

It is shown that the gamma distribution function represents best variation of the cross-sectional reduction along a rebar [13]. Fig. 4(a) indicates the obtained gamma functions for the selected four naturally corroded rebars. By assuming the four rebars as one long rebar, which is called “composed rebar”, a gamma function is obtained, see Fig. 4(b); this is the one that will be used in this paper. It was assumed that uniform cross section reduction is equal to average cross section reduction (10%).

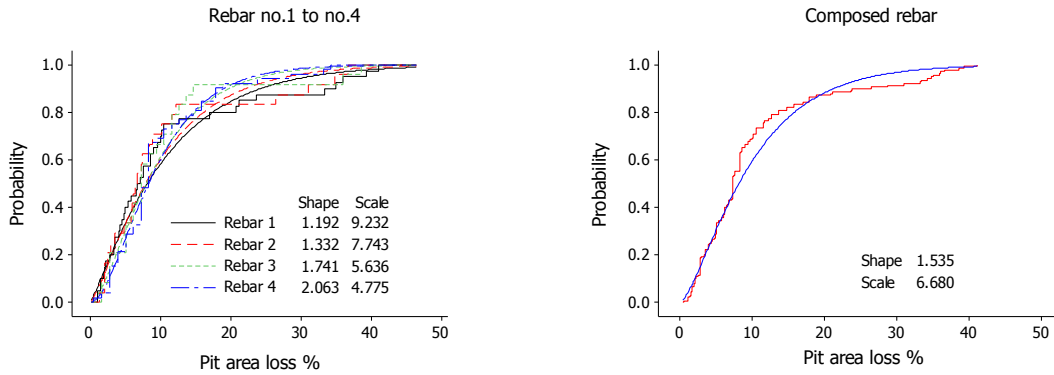


Fig. 4. Empirical and fitted cumulative distributions (using gamma distribution function) of pit size in four naturally corroded rebars, for the assumption of uniform corrosion equal to 10%.

Table 1. Statistics of the ratio of localized cross section reduction to initial cross section of rebar ( $A_{pit}/A_0$ ) based on cross section loss data of four corroded rebars.

Variable	$A_{uni}/A_0$ (%)	Distribution	Shape parameter	Scale parameter	Reference
$A_{pit}/A_0$	10	Gamma	1.16	8.14	Fitted with data from [14, 19]

### 3.2. Distribution function of pit distance ( $l'_p$ )

The occurrence of pits along the tensile rebar can be represented by a Poisson process, i.e. the occurrence of pits is assumed statistically independent [13]. Using measured corrosion data for the same four rebars, the cumulative distribution function of the distance between pits in same rebars were fitted to the exponential probability distribution, see Fig. 5. Similar as for the distributions of pit sizes, pit distance distributions in rebars were fitted for the assumed case where the uniform cross section reduction is equal to average cross section reduction. Table 2 lists the parameters of the fitted distribution functions.

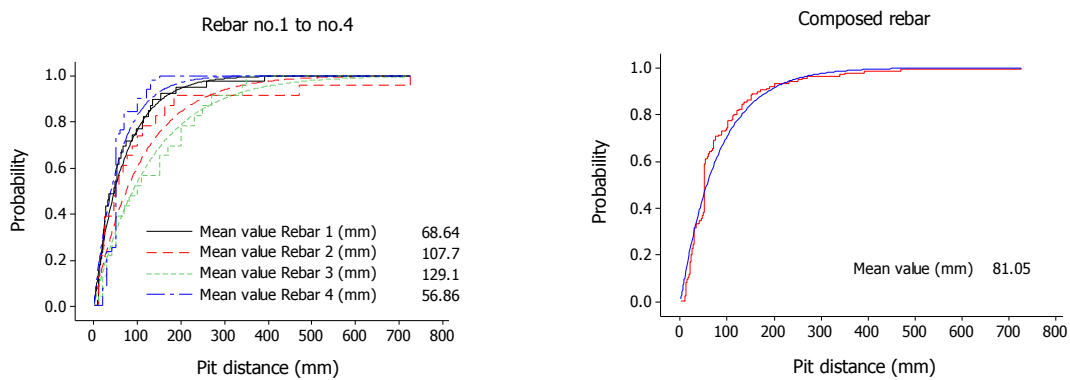


Fig. 5. Empirical and fitted (using exponential distribution function) cumulative distributions of distance between pits in same rebar in four naturally corroded rebars, for the assumption of uniform corrosion equal to 10%.

Table 2. Statistics of the distance between pits in same rebar ( $l'_p$ ) based on cross section loss data of four corroded rebars.

Variable	$A_{uni}/A_0$ (%)	Distribution	Mean Value (mm)	Reference
$l'_p$ (mm)	0	Exponential	47.51	Fitted with data
	10	Exponential	74.48	from [14, 18]

#### 4. Discussion about pit distance and its effect on the distribution functions

Pit distance in corroded rebar is function of the location of the rebar and degree and type of the corrosion. It might be different from lightly to severe corroded condition. In section 3, we obtained the mean value of the pit distance for four corroded rebars. Obtained exponential distribution functions of pit distance in section 3 shows that the mean values of pit distance of the four selected rebars varies from 50 mm to 130 mm when the composed rebar has the mean value of 81 mm, see Fig. 5(a) and Fig. 6. It raises a question that “how variation of the pit distance could influences on failure probability of corroded RC beam”.

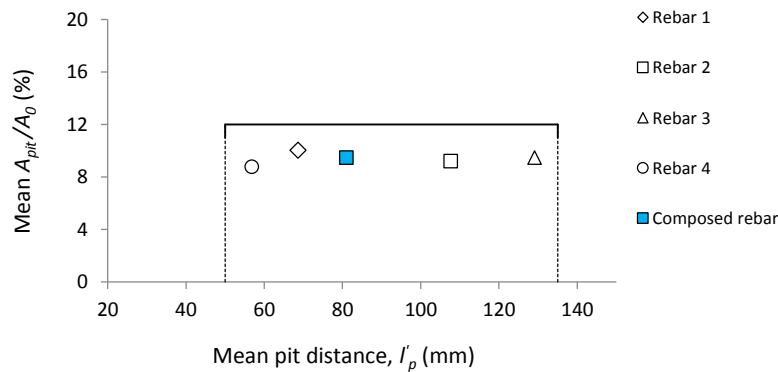


Fig. 6. Relation between mean values of ratio of localized cross section reduction to initial cross section of rebar ( $A_{pit}/A_0$ ) and distance between pits in same rebar ( $l'_p$ ). Uniform cross section reduction equal to (a) zero and (b) 10%.

#### 5. Probabilistic analyses of a RC beam

The purpose of the case study presented in this section is to quantify the effect of pit distance on the probability of failure of a corroded RC beam when the interference effect of localized corrosion is taken into account.

##### 5.1. Case study

Since under-reinforced beams are most common in practice, only this type of beam was considered. Analyses were carried out for a simply supported RC beam. The beam’s dimensions are length 6 m, height 0.35 m and width 0.2 m. The beam included two tensile rebars with diameters of 24 mm and a concrete cover of 36 mm.

##### 5.2. Statistical properties of other random variables

As it discussed earlier, the pit distance ( $l'_p$ ) and ratio of localized cross-section reduction to initial cross section of rebar ( $A_{pit}/A_0$ ) in each tensile rebar are represented by an exponential and gamma distribution functions, respectively. The other statistical variables of the RC beam used in the probabilistic analysis and their distribution functions are given in Table 3.



Table 3. Statistical properties of random variables.

Variable	Symbol	Distribution	Mean ( $\mu$ )	CoV	References
Effective beam depth (mm)	$d$	Log-normal	288	0.03	[2] [19]
Beam section width (mm)	$b$	Normal	200	0.02	[20]
Original rebar diameter (mm)	$d_0$	Normal	24	0.02	[20]
Distance between adjacent tensile rebar (mm)	$l_r$	Normal	80	0.05	-
Self-weight (kN/m)	$Q_w$	Normal	1.5	0.1	[21] [7]
Live load (kN/m)	$Q_L$	Gamma	4.7	0.6	[7] [22]
Concrete compressive strength (MPa)	$f_c$	Log-normal	47.7	0.18	[2] [7, 23]
Steel yield strength (MPa)	$f_y$	Log-normal	592	0.1	[24] [23] [7]

### 5.3. Limit state function and probability of failure

To quantify the failure probability of a corroded beam with interference effect of localized corrosion, the probability of failure was estimated using Monte Carlo Simulation. The limit state function is expressed as:

$$G_M(i) = \frac{f_y A_{res(mod)}^{(i)}}{f_c b d} \left(1 - 0.4 \frac{f_y A_{res(mod)}^{(i)}}{0.8 f_c b d}\right) f_{cd} b d^2 - \frac{(G_L + Q_L) l(i)}{2} (l - l(i)) \quad (3)$$

where  $f_y$  is the steel yield strength,  $f_c$  is the concrete compressive strength,  $b$  is the beam width,  $d$  is the effective height,  $A_{res(mod)}$  is the modified total residual cross-section of two rebars after uniform and localized corrosion, taking into account possible interference,  $G_L$  is self-weight,  $Q_L$  is live load,  $l(i)$  is the location of  $i^{th}$  pit along tensile rebar and  $l$  is length of beam span.

In Monte Carlo Simulation  $A_{res(mod)}$  at the location of each pit on first tensile rebar is calculated following Eq. 1 by pairing it successively with each pit in the adjacent rebar within the critical zone. The respective interference factors  $\beta_i$  are applied for the pits in another tensile rebar. It is assumed that the interference with the pit resulting in the smallest  $A_{res(mod)}$  is dominant. The procedure is repeated by starting with the pits on the second rebar and identifying the potential interference with pits on the first rebar.

Monte Carlo Simulation was used to evaluate the probabilities of failure of the RC beam. At each run using the calculated cross-sectional areas of longitudinal reinforcements and the generated values of the other structural variables, the flexural strengths of the beam at all cross-sections containing pits and at mid-span were evaluated and compared with the corresponding bending moment. At each run, all variables of Table 3 are realised only once per beam. If the limit state function was violated in at least one of the verified cross-sections, the beam is considered as failed. The probability of failure,  $P_f$ , was estimated as the number of runs with a failure of the beam divided by the total number of runs.

## 6. Results

This section presents probabilities of failure ( $P_f$ ) for two cases:

- average cross section loss and localised corrosion are considered *including* the interference of pits,
- average cross section loss and localised corrosion are considered *excluding* the interference of pits.

Moreover, various mean values of the distribution function of pit distance ( $l_p$ ): 20, 40, 60, 80, 100, 120, 140 and 160 mm, were used in the analyses. As it mentioned before, the ratio of average cross-section reduction to original cross section ( $A_{ave}/A_0$ ) is equal to 10%.

Fig. 7 illustrates the failure probability for both cases (a) and (b) with different pit distances. According to obtained results, reducing the pit distance results in increasing  $P_f$ . For the case (b), excluding pit distance, reduction of pit distance from 160 mm to 20 mm leads to 270% increase in increase  $P_f$ . If the effect of interference of localized corrosion is taking into account this influence increases to about 700% (see Fig. 7 case a).

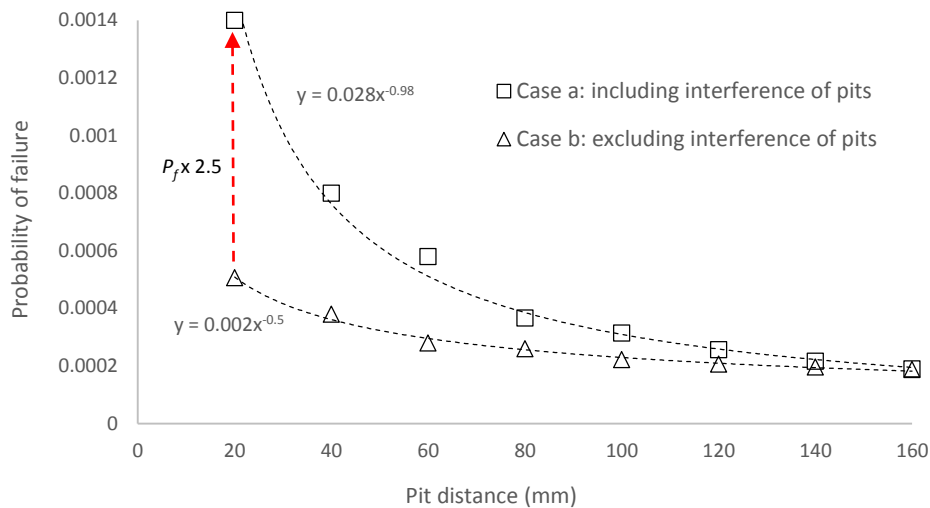


Fig. 7. Effect of the pit distance on probability of failure of the RC beam with and without considering the interference effect of localized corrosion.

The effect of the interference of pits increased by decreasing the pit distance. For example for the model with 20 mm pit distance, the interference effect increases the  $P_f$  up to 2.5 times (See the red arrow in Fig. 7), while for model with 160 mm, there is almost no change in the  $P_f$ . Less number of the pits, due to increase in the pit distance, which reduces the possibility of the interference between pits, could explain this. It could be seen that the effect of interference is substantial when the pit distances are less than 100 mm. This observed value of critical distance (100 mm) obtained by earlier studies [15, 17]. It is shown that, interaction of pits leads to a gradual reduction of the ULS for pit distance less than 100 mm.

Changing the pit distance could also influence on the reliability class suggested by EN90 or ISO13822. When the value of pit distance is larger than critical value the obtained probability of failure is in the normal reliability class with medium consequence of failure. While reducing the pit distance leads to low reliability class with low consequence of failure. Thus, considering the wrong mean value of pit distance could result in the inaccurate reliability assessment of deteriorated structures.

## 7. Conclusion

This paper considered the spatial variation and possible interference of localized corrosion on the reliability of a corroded RC beam. An interference model for the effect of two equal pits in adjacent rebars on the ultimate capacity and the distribution functions of spatial variation of localized corrosion were proposed earlier.

Probability of failure in a corroded RC beam with different pit distances was estimated using Monte Carlo Simulation. Uncertainties in material properties, geometry, loads, corrosion modelling, pit distances and pit interference were taken into account. The occurrence of pits along the tensile rebar was represented by a Poisson process. This assumption was supported by literature data. Based on the above assumption the following conclusions can be drawn:

- Reducing the pit distance leads to increase in the probability of failure. The increase will be intensified when the effect of interference of localized corrosion is taking into account.
- By increasing the mean value of pit distance, the effect of the interference of pits decreases. This is explained by the apparent lower number of pits and the reduced possibility of interference.
- Overestimating the mean value of pit distance in a corroded rebar could result in an underestimation of reliability of deteriorated RC beam.

It is emphasized that the proposed model to consider the pit distance effect on the probability of failure and application of this model was limited to one case study.

## References

- [1] Darmawan, M.S. and M.G. Stewart, Spatial variability of pitting corrosion and its effect on the strength and reliability of prestressed concrete bridge beams. *Struct. Saf.*, 2007. 29(1): p. 16-31.
- [2] Enright, M.P. and D.M. Frangopol, Probabilistic analysis of resistance degradation of reinforced concrete bridge beams under corrosion. *Engineering Structures*, 1998. 20(11): p. 960-971.
- [3] Li, C., Life-cycle modeling of corrosion-affected concrete structures: propagation. *Journal of Structural Engineering*, 2003. 129(6): p. 753-761.
- [4] Stewart, M.G., Spatial variability of pitting corrosion and its influence on structural fragility and reliability of RC beams in flexure. *Structural Safety*, 2004. 26(4): p. 453-470.
- [5] Stewart, M.G., Mechanical behaviour of pitting corrosion of flexural and shear reinforcement and its effect on structural reliability of corroding RC beams. *Structural Safety*, 2009. 31(1): p. 19-30.
- [6] Stewart, M.G. and A. Al-Harthy, Pitting corrosion and structural reliability of corroding RC structures: Experimental data and probabilistic analysis. *Reliability Engineering and System Safety*, 2008. 93(3): p. 373-382.
- [7] Val, D.V., Deterioration of strength of RC beams due to corrosion and its influence on beam reliability. *Journal of Structural Engineering*, 2007. 133(9): p. 1297-1306.
- [8] Val, D.V. and R.E. Melchers, Reliability of deteriorating RC slab bridges. *Journal of Structural Engineering*, 1997. 123(12): p. 1638-1644.
- [9] Val, D.V. and P.A. Trapper, Probabilistic evaluation of initiation time of chloride-induced corrosion. *Reliability Engineering & System Safety*, 2008. 93(3): p. 364-372.
- [10] Cairns, J., et al., Mechanical properties of corrosion-damaged reinforcement. *ACI Materials Journal*, 2005. 102(4): p. 256-264.
- [11] Du, Y., L.A. Clark, and A.H.C. Chan, Impact of reinforcement corrosion on ductile behavior of reinforced concrete beams. *ACI Structural Journal*, 2007. 104(3): p. 285-293.
- [12] Du, Y.G., L.A. Clark, and A.H.C. Chan, Residual capacity of corroded reinforcing bars. *Magazine of Concrete Research*, 2005. 57(3): p. 135-147.
- [13] Kioumarsis, M.M., M. Hendriks, J. Kohler, and M.R. Geiker, The effect of interference of corrosion pits on the failure probability of a reinforced concrete beam. *Engineering Structures*, 2016. 114: p. 113-121.
- [14] Dang, V.H. and R. François, Prediction of ductility factor of corroded reinforced concrete beams exposed to long term aging in chloride environment. *Cement and Concrete Composites*, 2014. 53: p. 136-147.
- [15] Kioumarsis, M.M., M. Hendriks, and M.R. Geiker, Interference of localised corrosion in adjacent reinforcement bar of a beam in bending, in *Concrete innovation conference\_CIC*. 2014: Oslo, Norway.
- [16] Kioumarsis, M.M., M. Hendriks, and M.R. Geiker, Effect of mesh alignment on simulated interference of localised corrosion on adjacent reinforcement rebars in XXII Nordic Concrete Research Symposium. 2014. Reykjavik, Iceland.
- [17] Kioumarsis, M.M., M. Hendriks, and M.R. Geiker, Quantification of the interference of localised corrosion on adjacent reinforcement bars in a concrete beam in bending. *Nordic Concrete Research (NCR)*, 2014. 49: p. 39-57.
- [18] Zhu, W. and R. François, Corrosion of the reinforcement and its influence on the residual structural performance of a 26-year-old corroded RC beam. *Construction and Building Materials*, 2014. 51: p. 461-472.
- [19] Nowak, A.S., A.S. Yamani, and S.W. Tabsh, Probabilistic models for resistance of concrete bridge girders. *ACI Structural Journal*, 1994. 91(3).
- [20] Lu, R., Y. Luo, and J.P. Conte, Reliability evaluation of reinforced concrete beams. *Structural Safety*, 1994. 14(4): p. 277-298.
- [21] Ellingwood, B., Development of a probability based load criterion for American National Standard A58: Building code requirements for minimum design loads in buildings and other structures. Vol. 577. 1980: US Department of Commerce, National Bureau of Standards.
- [22] Chalk, P.L. and R.B. Corotis, Probability model for design live loads. *Journal of the Structural Division*, 1980. 106(10): p. 2017-2033.
- [23] Mirza, S.A. and J.G. MacGregor, Variability of mechanical properties of reinforcing bars. *Journal of the Structural Division*, 1979. 105(5): p. 921-937.
- [24] Zhang, W., et al., Probability Distribution Model for Cross-Sectional Area of Corroded Reinforcing Steel Bars. *Journal of Materials in Civil Engineering*, 2013.



Sustainable Civil Engineering Structures and Construction Materials, SCESCM 2016

## Influence of vacuum mixing on the carbonation resistance and microstructure of reactive powder concrete containing secondary copper slag as supplementary cementitious material (SCM)

Romy Suryaningrat Edwin<sup>a,b</sup>, Elke Gruyaert<sup>a</sup>, Jeroen Dils<sup>a</sup>, Nele De Belie<sup>a,\*</sup>

<sup>a</sup>*Magnel Laboratory for Concrete Research, Faculty of Engineering and Architecture, Department of Structural Engineering, Ghent University, 9052 Ghent, Belgium*

<sup>b</sup>*Faculty of Engineering, Halu Oleo University, Kendari 93132, Indonesia*

---

### Abstract

This study aims to examine the effect of vacuum mixing on the carbonation resistance and microstructure of reactive powder concrete (RPC), made with secondary copper slag as partial cement replacement. In order to obtain a homogenous mixture, a high speed mixer with vacuum was applied. Accelerated carbonation tests (10% CO<sub>2</sub>, 20°C and 60% RH) were performed on RPC, mixed under vacuum conditions, as a comparison to RPC mixed at atmospheric pressure. The evolution of the carbonation depth was determined by spraying phenolphthalein on a freshly split RPC surface at varying ages (1 to 16 weeks). The microstructure of RPC was investigated by a mercury intrusion porosimeter (MIP). The pozzolanic activity of QCS was determined by the Chapelle test, taking into account the carbonation effect on the reference system.

The results obtained, showed that no carbonation was detected after 90 days for the RPC containing copper slag both under vacuum condition and atmospheric pressure. The presence of copper slag in the RPC tends to increase the porosity reduction and decrease the strength enhancement when applying vacuum mixing to the mixture. The result of the Chapelle test indicated that the secondary copper slag did not tend to consume much portlandite.

© 2017 The Authors. Published by Elsevier Ltd.

Peer-review under responsibility of the organizing committee of SCESCM 2016.

*Keywords* : Secondary copper slag; vacuum mixing; carbonation; microstructure; pozzolanic activity.

---

### 1. Introduction

Reactive powder concrete (RPC) is a new breakthrough of concrete technology. The production of this concrete needs a huge amount of cement to improve the concrete strength, which implies high cost. Concrete with higher

---

\* Corresponding author. Tel.: +32 9 264 55 22; fax: +32 9 264 58 45.

*E-mail address*: Nele.Debelie@UGent.be

cement content can cause high heat generation from cement hydration and this phenomenon can lead to the formation of micro cracks, which will allow liquids and gases (e.g. CO<sub>2</sub>) to penetrate into concrete. In the end, ingress of CO<sub>2</sub> will accelerate carbonation in concrete and it will cause the deterioration of reinforced concrete (Song et al. 2006). As a consequence, the service life of the concrete structures will decrease. Although, due to the high cement content, not all of the cement is perfectly hydrated, the large amount of portlandite in the concrete matrix has potency to react with CO<sub>2</sub> to generate CaCO<sub>3</sub>. The process of portlandite carbonation is fast, in which more than 80% carbonation of Ca(OH)<sub>2</sub> is achieved in 2 hours contact with liquid CO<sub>2</sub> in ambient temperature (Vance et al. 2015). In order to overcome this problem, the use of secondary copper slag as cement replacement and vacuum mixing are investigated in this paper, as a means to minimize potential concrete carbonation.

One measure to obtain a void-free mixture is to use an intensive vacuum mixing in which this mixer can remove air content. A void-free mixture contributes to the strength and service life of concrete. This is confirmed by the results of Dils, et al (2012). They concluded that the compressive strength increases when the air content decreases in the UHPC mixture.

Typical by-products that are already widely used in concrete are e.g. fly-ash and blast-furnace slag. Copper slag is one of the by-product materials from the copper smelting. Every year, about 24.6 million tons of copper slag are produced by the copper industry throughout the world (Gorai et al. 2003). In Europe, approximately 5.56 million tons of copper slag are generated by the European copper industry (Gorai et al. 2003), and in Belgium, about 132,240 tons of secondary copper slag are produced in recycling plants annually (FCA 2012, Hagelüken 2006). Since this material needs a large area for landfilling, of which the availability is insufficient, and to avoid problems related to the leaching of heavy metals and other harmful elements, it would be interesting to upgrade these ‘waste’ products in high-value applications. Moreover, the amount of natural resources is declining due to a large consumption in the cement and concrete production. A possible breakthrough can thus be sought in exploiting these by-products within cement and concrete production. This paper presents the influence of vacuum mixing on carbonation and microstructure of RPC containing copper slag as cement replacement. The Chapelle test was chosen to assess the pozzolanic activity of secondary copper slag.

## 2. Material and experimental procedure

### 2.1. Material

The materials used in this study were purchased from Belgian and German companies except for the secondary copper slag, which was obtained from a Belgian Recycling Plant. The secondary slag used in this research was quickly cooled granulated copper slag (QCS). This slag was produced by using primary slag from Cu such as old copper tubes, wires, scraps, cables, alloy coins, plated coins and Cu-Fe (shredded) armatures as raw materials to generate copper blister, copper anodes, and copper cathodes for industry and market. Another binder used in this research was dry undensified silica fume (940U, Elkem), which has a typical bulk density of 200-350 kg/m<sup>3</sup>. As cement, a CEM I 52.5 N HSR/LA was used throughout all experiments. For all concretes, a quartz flour (type M400, Sibelco) with a d<sub>50</sub> of 12 μm was used. An overview of the chemical composition of the powders is given in Table 1.

Table 1. Chemical Composition of the Applied Powders Determined by XRF Analysis [wt.%]

Material	QCS	Cement	Silica fume	Flour (M400)
CaO	7.1	63.4	0.6	0.02
SiO <sub>2</sub>	25.9	21.5	94.2	99.5
Al <sub>2</sub> O <sub>3</sub>	5.9	3.6	1.0	0.2
Fe <sub>2</sub> O <sub>3</sub>	45.5	4.2	0.5	0.03
MgO	0.8	1.6	0.7	n/a
Na <sub>2</sub> O	0.8	0.2	1.0	n/a
K <sub>2</sub> O	0.2	0.6	1.1	0.05
SO <sub>3</sub>	0.4	2.5	0.3	n/a

P2O5	0.8	n/a	0.1	n/a
TiO2	0.3	n/a	n/a	n/a
ZnO	8.8	n/a	n/a	n/a
MnO	0.7	n/a	n/a	n/a
Cr2O3	0.7	n/a	n/a	n/a
CuO	0.4	n/a	n/a	n/a
Pb	0.4	n/a	n/a	n/a

Since the copper slag obtained by the recycling plant was in granulate form, the size of this slag has to be reduced to achieve a product with a higher specific surface area (SSA). The selection of the appropriate method of grinding should be based on the physical properties of the materials. Copper slag has a toughness of 6–7 Mohs hardness and is mainly composed of iron silicate glass (Murari, K et al. 2015; Gorai, B et al. 2003). Therefore, there will be a high energy need to grind this material. In the grinding process, the energy is determined by the time, speed, and number of balls charged. Based on the results obtained by Edwin et al. (2016), the SSA of QCS was 2533 cm<sup>2</sup>/g with the Blaine permeability test. This result can be achieved using the dry method, long duration of grinding (5 times during 12 minutes at 300 rpm) and 5 balls charged. This grinding process was time-consuming and not very productive. In order to reduce the time for the grinding process, the authors now chose a short duration (6 times during 5 minutes at 390 rpm) and 7 balls charged. This method reduced the grinding time with 30 minutes in comparison with that of the long duration method. With the increase in grinding speed and addition of two balls in this method it was expected to achieve a similar fineness as with the grinding method aforementioned. Besides, copper slag tends to be re-compacted when applying a dry method. These are the reasons to choose a wet method instead of dry method. A superplasticizer (Sika Viscocrete-3095x; 0.122 wt%) was chosen to avoid re-compaction. After the grinding process, the particle size distribution (PSD) of copper slag powder was measured by laser diffraction with the size range from 0.1 μm to 1000 μm. The particle size distribution of copper slag, silica fume, and quartz flour obtained by laser diffraction is given in Figure 1. To disperse this material, isopropanol was used since it does not react with copper slag. To avoid agglomeration, the copper slag was put in a sonication bath (5 min) before the measurement. In case of silica fume, distilled water was used as dispersant. In order to obtain well de-agglomerated silica fume, this material was sonicated in two steps. At first, the solution containing silica fume and water was put in an ultrasonic bath for 5 minutes to de-agglomerate the particles. After this, 10% superplasticizer by weight of silica fume was added followed by sonication for 15 minutes prior to measurement. An overview of the parameters used to determine the PSD of the SCMs, cement, and quartz by laser diffraction can be seen in Table 2.

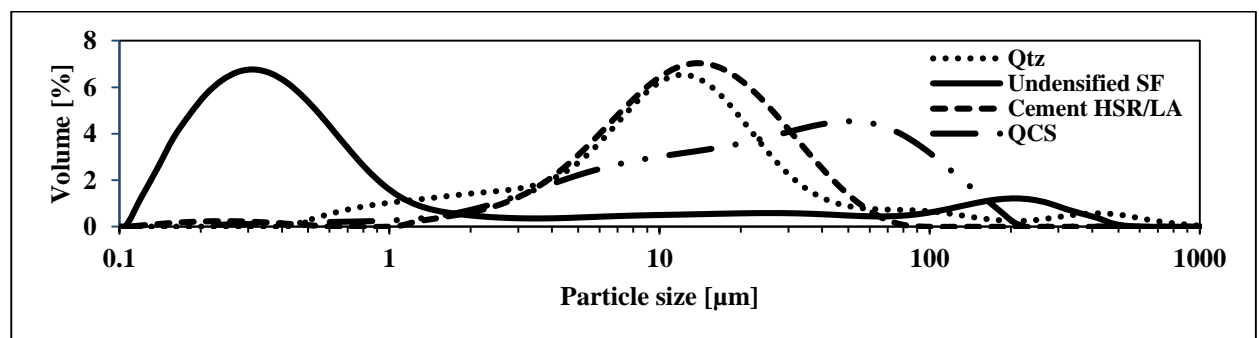


Fig. 1. Particle Size Distribution by Laser Diffraction of the Different Powders

In addition to the PSD by laser diffraction, the fineness of the binders was evaluated by their specific surface area (SSA) using the Blaine air permeability test according to NBN EN 196-6:2010. To start, the pycnometer method was used to measure the density of all powders. Both the density and SSA of the powders are presented in Table 3.

Table 2. Overview of the Parameters Applied to Determine the PSD of the Different Powders by Laser Diffraction

Optical parameters	QCS	Silica fume	CEM I	Quartz flour (Qtz)
Refractive index (RI) [-]	1.731	1.530	1.731	1.55
Absorption coefficient [-]	0.055	0.001	0.003	0.3
Obscuration [%]	10 - 15	5 - 10	5 – 10	5 – 10
Stirrer rate [rpm]	1700	1500	1500	1700
Dispersant RI [-]	1.390	1.390	1.390	1.390
Sonication times [minutes]	5	20	5	5

Table 3. Density and SSA of the Different Powders

Materials	QCS	CEM I	Silica fume	Quartz flour (Qtz)
Density (g/cm <sup>3</sup> )	3.706	3.152	2.017	2.65
SSA (cm <sup>2</sup> /g) :				
Blaine permeability	2277	4955	-	6500
Laser diffraction	2150	5390	56200	5444

## 2.2. Mixing procedure

In this research, the authors used a planetary vacuum mixer with a capacity of 5 liter. The procedure of mixing follows the method shown in Dils, et al. (2013). First the dry materials were poured in the inclined drum. They were mixed during 15 s at 255 rpm. Afterwards, the water and superplasticizer were dosed. After the non-vacuum phase, the maximum speed mixing (910 rpm) was started for 150 s and at the same moment the vacuum phase was applied for 270 s. In the last 120 s of the vacuum phase, the speed was reduced to 255 rpm. In the case of non-vacuum mixing, the same method was applied after dosing the water and superplasticizer, with the mixer set at atmospheric pressure (1013 mbar).

## 2.3. Carbonation depth and mercury intrusion porosimetry (MIP)

After mixing, the fresh concrete was cast in molds with dimensions of 40 mm x 40 mm x 160 mm. Subsequently, they were stored for 2 days at 20 °C and RH > 95%. Afterwards, the specimens were removed from the molds and cured at 20 °C and RH > 95% for 90 days. Before the start of the accelerated carbonation test, a freshly split surface of the samples was sprayed with phenolphthalein to obtain the initial value of the carbonation depth. Five surfaces of the samples were coated with epoxy, leaving one surface exposed in a climate chamber (20 ± 2°C, RH 60 ± 5%) to 10% CO<sub>2</sub>. The carbonation ingress was measured with phenolphthalein after 4, 8 and 16 weeks.

To investigate the influence of vacuum mixing on the porosity, mercury intrusion porosimetry (MIP) was performed on the RPC samples. In order to preserve the pore structure of the specimens, the freeze-drying method was chosen. The specimens for MIP are defined as crushed particles with particle size between 5 and 10 mm. After putting these specimens in the liquid nitrogen for 5 minutes, the temperature of the sample was reduced to -195 0C. Afterwards, the samples were transferred into a freeze-dryer and the temperature changed to -24 0C under vacuum condition and pressure of 0.1 Pa (Zhou, J., 2010). After four weeks, a constant mass was obtained (mass change less than 0.1% in 24 hours). After the period of freeze-drying, a sample of ± 1.40 g was put into a dilatometer (Thermo Scientific corporation) to start the measurement. The mercury was intruded into the specimen and extruded after reaching the maximum pressure. This porosity measurement of the sample was determined using 140 Pascal for the low pressure and 440 Pascal for the high pressure.



### 3. Results and discussions

#### 3.1. Carbonation depth

The carbonation depth for both the samples mixed under vacuum condition (100 mbar) and atmospheric pressure (1013 mbar) which was measured on a freshly split RPC surface using 1% phenolphthalein in 70% ethyl alcohol shows no carbonation up to 16 weeks, as seen in Table 4. Both the reference RPC and the mixtures with copper slag show zero carbonation, as also shown in Table 4. These results confirm that the concrete with low porosity and very dense microstructure has an excellent carbonation resistance (Caijun Shi, et al. 2014). The CSH gel will fill the concrete pores and limit the CO<sub>2</sub> penetration into the concrete. However, the effect of the vacuum mixing and copper slag replacement on the carbonation of RPC is unclear since there is no carbonation detected even in non-vacuum mixing and reference mixture. Therefore, long-term exposure in a climate chamber (e.g. 32 or 64 weeks) is required for RPC to determine the effect of vacuum mixing and copper slag replacement on the carbonation resistance.

Table 4. Results of carbonation test on RPC containing copper slag

Exposure time	Reference		5% CS		10% CS		15% CS		20% CS	
	Vac	N-Vac	Vac	N-Vac	Vac	N-Vac	Vac	N-Vac	Vac	N-Vac
4 weeks	ND	ND	ND	ND	ND	ND	ND	ND	ND	ND
8 weeks	ND	ND	ND	ND	ND	ND	ND	ND	ND	ND
16 weeks	ND	ND	ND	ND	ND	ND	ND	ND	ND	ND

Note. ND = not detected

#### 3.2. Mercury intrusion porosimetry and compressive strength

Figure 2 describes the effect of vacuum mixing on the porosity of RPC containing copper slag as cementitious material. In general, the porosity of RPC mixed under vacuum (100 mbar) and at atmospheric pressure (1013 mbar) decreased with rising copper slag content in RPC mixture at 56 days in comparison with the reference mixture without copper slag. The lowest porosity (4.91%) was achieved for 15% copper slag replacement under vacuum mixing, which decreased about 18.4% compared to the reference specimens. This achievement also occurred for 15% copper slag substitution under non-vacuum condition, which induced a decrease of about 11.4% in porosity compared to control mixtures.

The influence of vacuum mixing on the compressive strength of RPC containing copper slag as cement replacement is shown in Figure 3. It seen that the strength of RPC under vacuum condition increases with rising copper slag substitution in the concrete mixture. The highest compressive strength (158 MPa) is achieved for 10% copper slag. However, this achievement is contradictory with the result of RPC non vacuum, which is similar or (slightly) lower for the RPC with copper slag than for the reference mixture.

Based on the result obtained in Figure 2 and Figure 3, it is necessary to study the influence of vacuum mixing on the porosity reduction and the strength enhancement of RPC containing copper slag.

The influence of vacuum mixing on the reduction of porosity is the highest for the mixtures with 20% copper slag replacement. A decrease of about 22% is seen (Figure 4). Nonetheless, the RPC mixtures with 5% and 10% copper slag replacement showed low porosity reduction, which was less than for the reference mixture. From this result, it can be stated that the effect of vacuum mixing on the porosity of RPC mixtures containing small amounts of copper slag is limited. For higher amount of copper slag replacement, the vacuum mixing contributed more to reduce the porosity of RPC. This achievement is mainly caused by the physical properties of copper slag. Looking into the literature, the angular sharp edges of the copper slag can improve the cohesion of the concrete matrix (Al-Jabri et al. 2011; Shi et al. 2008; Wu et al. 2010; De Schepper et al. 2014). This property has the ability to fill out the air cavities which are removed by vacuum mixing. Nevertheless, due to the differences in homogeneity and complexity of the pore structure, the pore cavities of RPC cannot be successfully filled by copper slag, leaving certain amount of unfilled porosity.



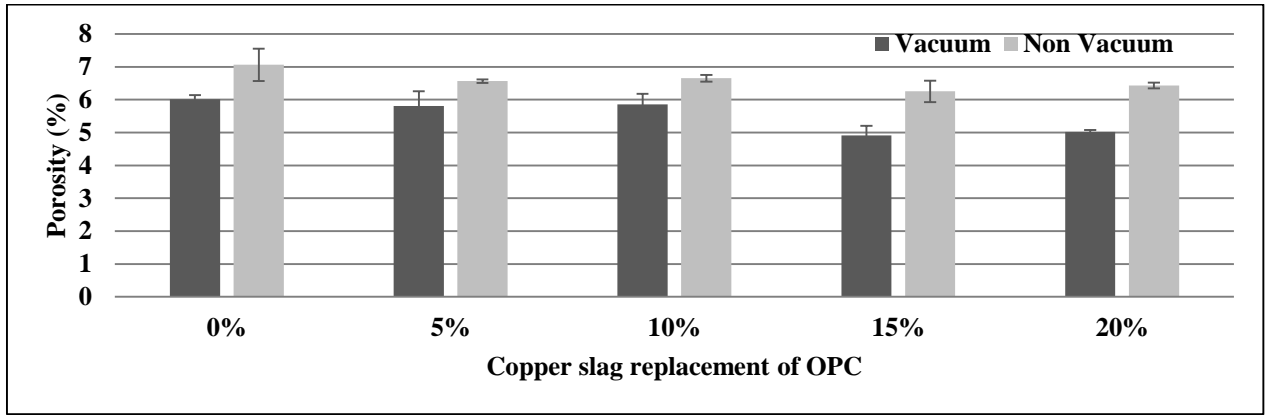


Fig. 2. Influence of mixing procedure (vacuum condition (100 mbar) and atmospheric pressure (1013 mbar)) and copper slag replacement on the porosity of RPC at 56 days (error bars represent standard errors, the average values represent two replicates)

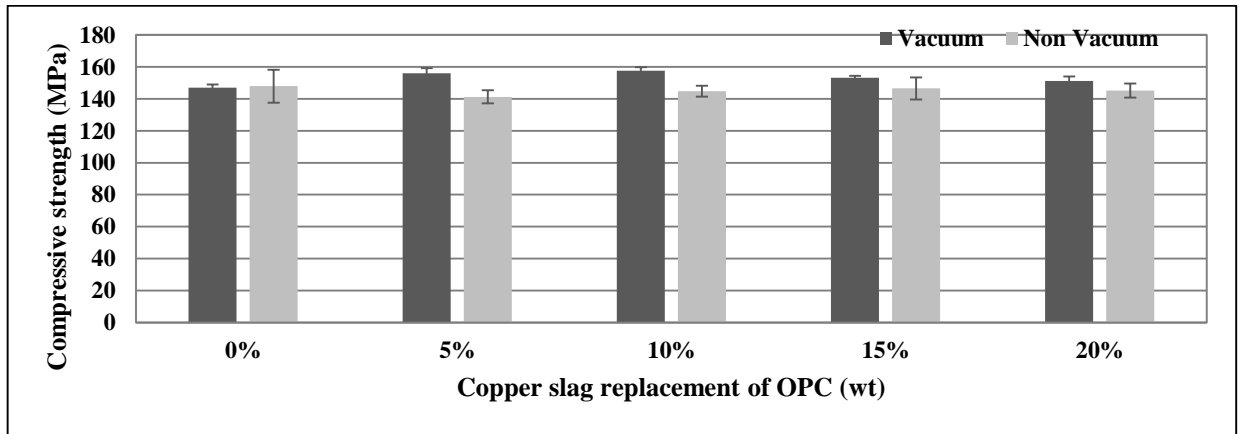


Fig. 3. Strength of RPC mixed under Vacuum (100 mbar) and Atmospheric Pressure (1013) at 56 days (error bars represent standard errors, the average values represent three replicates)

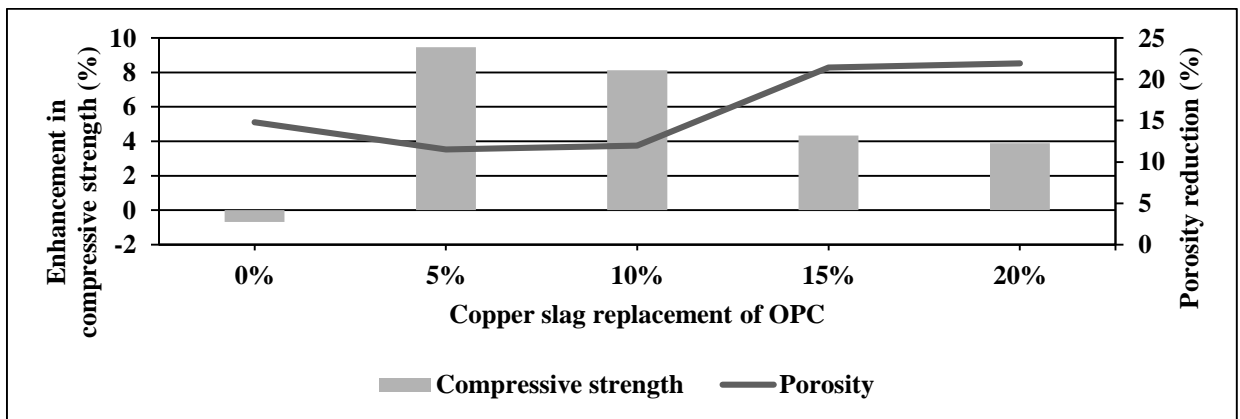


Fig. 4. Relative influence of vacuum mixing versus mixing at atmospheric pressure on the porosity and strength enhancement of RPC at 56 days

The RPC with 0% copper slag showed a compressive strength of 148 MPa when mixed under atmospheric conditions and 147 MPa under vacuum. The strength enhancement for mixes with larger replacement levels (15% and

20%) due to vacuum condition was lower than for mixes with a small quantity of copper slag replacement (5% and 10%), as shown in Figure 4. This result is contradictory with the porosity reduction under vacuum mixing, which was the highest for 15% and 20% copper slag replacement. This finding is in contrast with the result obtained by several researchers (Lian et al. 2011; Bhutta et al. 2012). In their research, they proposed a model relationship between compressive strength and total void ratio. They concluded that the compressive strength of high performance porous concrete (HPPC) was increased with decreasing total void ratio. This current finding can easily be explained by the fact that the increase in compressive strength of concrete is not only caused by porosity reduction, but it is also determined by CSH gel generated during the hydration process. The latter corresponds well to the strong bond in concrete matrix. Moreover, vacuum mixing only contributes to reduce the porosity of RPC. Copper slag reacts with the portlandite to produce CSH gel. Due to the insufficient fineness of this slag, only a small amount of copper slag reacts to generate CSH gel. This can also be explained by the fact that only around 35% of calcium oxide (CaO) is consumed by copper slag in the Chapelle test, as seen below in Figure 5. For larger replacement levels (e.g. 15% and 20%), the amount of CSH gel does not increase, leaving certain amount of unreacted copper slag in concrete matrix. The copper slag shows angular sharp edges, and it will contribute as filler in the concrete matrix. This is the reason for decreasing the porosity of RPC containing higher amount of copper slag.

From Figure 4, it can be stated that the porosity reduction under low air pressure for higher amount of copper slag replacement is double than that of the RPC containing small amount of copper slag. In contrast to the porosity reduction, the strength enhancement for larger replacement levels (15% and 20%) under vacuum mixing is halved compared to low replacement levels.

### 3.3. Chapelle test

The results of the Chapelle test are shown in Figure 5. In this study, the result of the reference indicated that a significant amount of portlandite had reacted although the system was built to avoid carbonation. Based on the amount of portlandite carbonated in the reference system, a formula is used to correct the results of the mixes with copper slag and quartz powder (Snellings et al. 2015) :

$$CH_{corr} = \frac{CH_{calc} - CH_{ref}}{CH_i - CH_{ref}} \quad (4)$$

where

CH<sub>corr</sub> is the corrected consumed calcium hydroxide.

CH<sub>calc</sub> is the calculated consumed calcium hydroxide.

CH<sub>ref</sub> is the consumed calcium hydroxide for the reference.

CH<sub>i</sub> is the initial calcium hydroxide.

Looking into the literature, the amount of portlandite consumed by copper slag in this research was lower than for the three pozzolanic materials (metakaolin, fly ash and natural pozzolans) used in Snellings et al. (2015). This is mainly due to the different chemical composition of the SCMs used by the author and Snellings et al. (2015). The chemical reaction rate to form C-S-H gel is determined by the calcium and siliceous content in SCMs. The calcium-poor and siliceous-rich fractions of pozzolans (metakaolin, fly ash, and natural pozzolans) rapidly consume large amounts of portlandite. Conversely, the calcium-poor and siliceous-moderate secondary copper slag used in the current research tends to consume less portlandite.

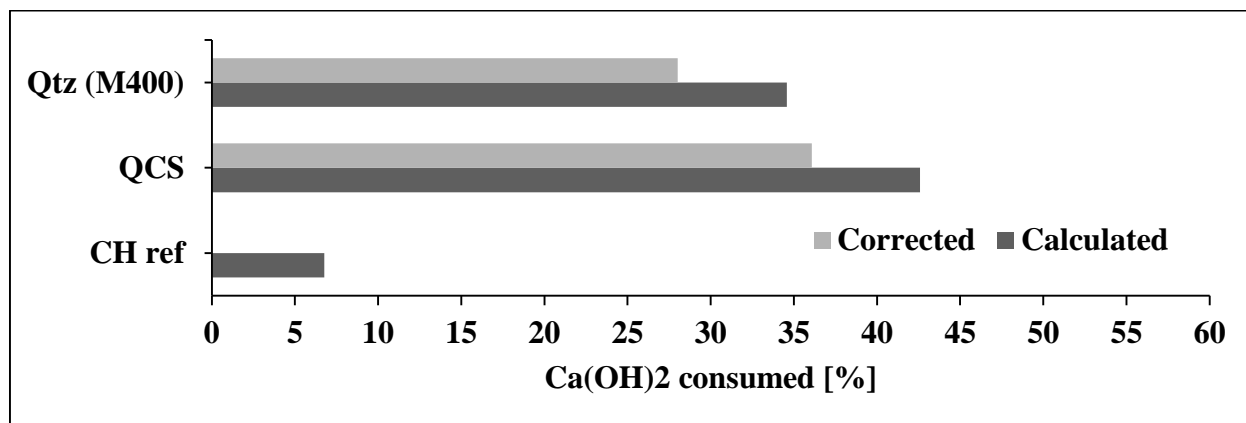


Fig. 5. Amount of  $\text{Ca}(\text{OH})_2$  consumed by 1g of difference types of powder

#### 4. Conclusions

Concerning the effect of vacuum mixing on carbonation and microstructure of RPC containing secondary copper slag as cementitious material, the following conclusions can be drawn:

1. A zero level of carbonation is found for RPC containing copper slag and mixed under vacuum and at atmospheric pressure. This is mainly caused by the low porosity and the very dense microstructure of RPC which increase the resistance against carbonation.
2. By applying vacuum mixing to the RPC mixture, the porosity decreased. The reduction is higher with increasing copper slag content. This result is in contrast with the compressive strength enhancement of RPC, which decreased for larger replacement levels of copper slag.

Assessment of the pozzolanic activity using the Chapelle test indicates low pozzolanic activity of secondary copper slag used in this research. This phenomenon indicates that the amount of CSH gel produced during hydration is limited. However, the porosity reduction of RPC is enhanced by the physical properties of copper slag.

#### Acknowledgements

The author would like to thank the Indonesian Government Scholarship (DIKTI) for providing the financial support to the PhD research project (2013-2016). Special thanks are addressed to the Magnel Laboratory for Concrete Research of Ghent University (staff and researchers) for their contribution to this research.

#### References

- [1] B. Gorai, R.K. Jana, Premchand, Characteristics and utilisation of copper slag - a review, *Resources Conservation and Recycling*. 39(4) (2003) 299-313.
- [2] C. Hagelüken, Recycling of electronic scrap at Umicore precious metals refining, *Acta Metallurgica Slovaca*. (2006) 111-120.
- [3] C. Lian, Y. Zhuge, S. Beecham, The relationship between porosity and strength for porous concrete, *Construction and Building Materials*. 25 (2011) 4294-4298.
- [4] C. Shi, C. Meyer, A. Behnood, Utilization of copper slag in cement and concrete, *Resour. Conserv. Recycl.* 52(10) (2008) 1115–1120.
- [5] C. Shi, Z. Wu, D. Wang, L. Wu, Design and properties of ultra high performance concrete, in: S.O. Ekololu, M. Dundu, X. Gao (Eds.), *Proceedings of the First International Conference on Construction Materials and Structures in Johannesburg*, IOS Press Ebooks, 2014, pp. 86-98.
- [6] J. Dils, V. Boel, G. De Schutter, Influence of intensive vacuum mixing on the compressive strength of cementitious materials, in Alexander et al. (Eds). *Proceedings of the Concrete Repair, Rehabilitation and Retrofitting III in Cape Town*, 2012, pp. 1313-1318.
- [7] J. Dils, V. Boel, G. De Schutter, Influence of cement type and mixing pressure on air content, rheology, and mechanical properties of UHPC, *Construction and Building Materials*. 41 (2013) 455–463.
- [8] F.C. Association, Advance Recycling. From steel slag and  $\text{CO}_2$  to high-grade building material, Interview Recmix Belgium, Metallo Chimique, CHAP-YT bvba, Umicore, D. Fransaeer, Editor, Belgium. (2012).
- [9] H.W. Song, S.J. Kwon, K.J. Byun, C.K. Park, Predicting carbonation in early-aged cracked concrete, *Cement and Concrete Research*. 36 (2006) 979–989.

- [10] J. Zhou, G. Ye, K. Van Breugel, Characterization of pore structure in cement-based materials using pressurization-depressurization cycling mercury intrusion porosimetry (PDC-MIP), *Cement and Concrete Research*. 40 (2010) 1120-1128
- [11] K. Murari, R. Siddique, K.K. Jain, Use of waste copper slag, a sustainable material, *Journal of Material Cycles and Waste Management*. 17(1) (2015) 13-26.
- [12] K.S. Al-Jabri, A.H. Al-Saidy, R. Taha, Effect of copper slag as a fine aggregate on the properties of cement mortars and concrete, *Construction and Building Materials*. 25(2) (2011) 933-938.
- [13] K. Vance, G. Falzone, I. Pignatelli, M. Bauchy, M. Balonis, G. Sant, Direct carbonation of Ca(OH)<sub>2</sub> using liquid and supercritical CO<sub>2</sub>: Implications for carbon-neutral cementation, *Industrial and Engineering Chemistry Research*. 54 (36) (2015) 8908–8918.
- [14] M.A.R. Bhutta, K. Tsuruta, J. Mirza, Evaluation of high-performance porous concrete properties, *Construction and Building Materials*. 31 (2012) 67-73.
- [15] M. De Schepper, P. Verlé, I. Van Driessche, N. De Belie, Use of secondary slags in completely recyclable concrete, *Journal of Materials in Civil Engineering ASCE*. 27 (5) (2014) p. 04014177.
- [16] R. S. Edwin, M. De Schepper, E. Gruyaert, N. De Belie. Effect of secondary copper slag as cementitious material in ultra-high performance mortar, *Construction and Building Materials*. 119 (2016) 31-44.
- [17] R. Snellings and K.L. Scrivener, Rapid screening tests for supplementary cementitious materials: past and future, *Materials and Structures*. (2015) 1-15.
- [18] W. Wu, W. Zhang, G. Ma, Optimum content of copper slag as a fine aggregate in high strength concrete, *Materials & Design*. 31(6) (2010) 2878-2883.



Sustainable Civil Engineering Structures and Construction Materials, SCESCM 2016

## Compressive strength and chloride penetration tests of modified type IP cement concrete with rice ash

Javier, Anna Rose A.<sup>a</sup>, Lopez, Neslyn E.<sup>a</sup>, Juanzon, Joseph Berlin P.<sup>a, \*</sup>

<sup>a</sup>Malayan Colleges Laguna, Cabuayo City, Laguna, Philippines 4026

---

### Abstract

Concrete is one of the most widely used materials in the field of building construction. It is basically composed of aggregates such as gravel and sand, bind together by cement and water. One of the major problems with concrete structures is the corrosion of steel reinforcement. Supplementary Cementitious Materials (SCM) like fly ash, Ground Granulated Blast Furnace Slags (GGBFS), Silica Fume (SF), and rice ash have the characteristics and properties similar to cement. Studies also showed that rice ash can partially replace cement in the concrete mixture. The objective of this study is to conduct a comparative analysis on the compressive strength and chloride penetration depth with 10%, 20% and 30% replacement of the rice ash in the type IP cement. Colorimetric method was used to determine the chloride penetration depth by applying AgNO<sub>3</sub> solution. The results were analyzed using Analysis of Variance (ANOVA). Results show that there are significant differences in each percentage replacement of rice ash in type IP cement. The 10% percent replacement obtained the highest compressive strength and chloride penetration resistance. The improvement of the strength of concrete with rice ash indicated that it was an effective way of improving not only the serviceability of concrete but also preventing chloride penetration that causes corrosion on steel reinforcement.

© 2017 The Authors. Published by Elsevier Ltd.

Peer-review under responsibility of the organizing committee of SCESCM 2016.

*Keywords:* Rice ash; Type IP cement; compressive strength; chloride penetration.

---

### 1. Introduction

One of the major problems with concrete structures is the corrosion of steel reinforcement. A chemical like chloride causes a deleterious problem as it tends to weaken the bonds between steel and concrete. According to [1],

---

\* Corresponding author. Tel.: +0-000-000-0000 ; fax: +0-000-000-0000 .

E-mail address: [jbpjuanzon@mcl.edu.ph](mailto:jbpjuanzon@mcl.edu.ph)

chloride ion diffusion is attributed to the permeability and pore size distribution of concrete. Because of this, the use of blended cement became popular since it has a lower permeability compared to ordinary Portland cement since blended cements use the supplementary cementitious material as partial replacement to cement [2]. Supplementary Cementitious Materials (SCM) like fly ash, Ground Granulated Blast Furnace Slag (GGBFS), Silica Fume (SF), and Rice Ash which are abundant to the environment, have the characteristics and properties similar to cement. Among these SCM, the most commonly known were rice ash and fly ash. More recently, application of rice ash became a popular practice in the construction industry because of its availability.

Rice is a staple food in the Philippines, whereas millions of tons of rice hull are generated after the milling of rice paddy and treated as an agro-waste. Rice hull is either disposed into the environment or burned for fuel. It was found out that burnt rice hull produces ash which has high silica content of about 90-98% after complete combustion. In addition, rice ash produces two colored ash after a period of burning, the white-grey attained at complete combustion or controlled burning and the black ash attained at incomplete combustion or uncontrolled burning [3].

Since white-grey ash underwent complete combustion, it is the most likely to have the highest percentage of silica content as compared to the black ash. In this regard, this study utilized the use of white-grey rice ash to partially replace a percentage of cement, specifically Type IP cement (Portland-Pozzolan cement), in concrete.

## 2. Review of Related Literature

Rice hull is an agricultural waste material which is either disposed as a waste in landfills or burnt as a source of fuel. However, disposing it becomes a threat to the environment because it has a low nutritional value and a lower rate of decomposition [4]. As a solution to this environmental problem, rice ash is utilized as a supplementary cementitious material that is very effective in replacing the partial amount of cement. Rice ash is considered as a natural pozzolan because it does not possess cementitious properties at first, and only after grinding into fine material would it be rich in silica, which is necessary for pozzolanic activity.

Previous Studies showed that the replacement of rice ash to ordinary Portland cement increased the compressive strength of concrete. However, the continuous increase in the percent replacement of rice ash in cement has optimum. From the study of [5] obtained the highest strength at 10% replacement and optimum percent replacement of 20% whereas a study of [6] obtained the highest strength at 30% of rice ash replacement. On the other hand, research conducted by [7] gave a range of 10% to 20% replacement as an optimum percent replacement.

An investigation on rice ash partially replacing the total weight of the Type 1 Portland cement was conducted by [8]. It showed that 20% rice ash replacement obtained the highest strength. However, the 30% rice ash replacement is the optimal value. The tremendous pozzolanic activity and an increase in compressive strength were due to the amorphous silica and fine particle size properties of the rice ash. On the other hand, a reduced chloride penetration of about 28% was found at 30% replacement of type I Portland cement by rice ash. The durability was also improved in a long run because at 90 days of curing time (as opposed to 28 days of curing time), the experiment achieved a lower total charge passed. Thus, it showed the higher sustainability of reinforced concrete design.

## 3. Methodology

### 3.1. Experimental design

Concrete samples used Type-IP cement with varying percentage replacement of rice ash (10%, 20%, and 30%). The rice ash was white-grey color which was obtained after burning the rice ash continuously for two to three days. For the design of concrete mix, special class A mix proportion with a ratio of 1:2:3 was used with water-cement ratio of 0.5. Compression and chloride penetration tests used a cylindrical concrete specimen, with 6 inches diameter by 12 inches height, which complies with [9].

### 3.2. Compressive strength test

Compressive strengths of concrete samples were observed after 28 days and 56 days of curing. The Compression Strength Test was in accordance to [10]. Using the Universal Testing Machine (UTM), a load was applied on the concrete until it reached its failure load. Then the compressive strength was computed using the formula:

$$\text{Compressive strength} = \frac{\text{maximum applied force}}{\text{cross-sectional area}} \quad (1)$$

### 3.3. Chloride penetration test

The concrete specimen was cured for 28 days and ponded in 3% NaCl solution for another 28 days. Afterwards, the specimens were split into half using UTM. The depth of chloride penetration was measured using application of 0.05M Silver Nitrate ( $\text{AgNO}_3$ ) solution onto the sides of concrete samples which was adopted from the study of [11]. Four points on each longitudinal side was measured for a total of eight-point depth measurement for each specimen.

## 4. Data and results

### 4.1. Compressive strength

As shown in Table 1, concrete specimen with 10% replacement of rice ash obtained the highest value of compressive strength, whereas, the concrete specimen with 30% replacement had the lowest capacity for compressive strength for both 28 and 56 days of curing.

Table 1. Compressive Strength of concrete specimens with 0%, 10%, 20%, and 30% replacement

% Rice Ash	Compressive strength after 28 days	Compressive strength after 56 days
0	670.71	772.13
10	805.06	1006.59
20	659.82	946.68
30	372.19	527.03

From 670.71 psi of 0% replacement of rice ash, the compressive strength increased by 17% at 10% replacement but it decreased by 18% at 20% replacement of rice ash and drastically declined at 30% replacement with 44.51% difference as shown in Fig. 1.

The strength increased at 10% rice ash replacement achieved the optimum value for the compressive strength. This is due to the fact that during the process of hydration, C-S-H (Calcium Silicate Hydrate) and C-H (Calcium Hydroxide) were produced and the amorphous silica content of rice ash reacted with the available C-H forming more C-S-H content which gave higher compression strength. However, strength decreases after 20% replacement but no significant difference to the compressive strength of the control mix (0% replacement).

The 10% replacement of rice ash performed the highest compressive strength of concrete as shown in Fig. 2. However, the 20% replacement became the optimum percent replacement after 56 days of curing because it achieved a much higher strength than the concrete without replacement of rice ash.

Fig. 3 shows a similar trend of each percent replacement for both curing days but an increased strength at 56 days of curing. The 10% replacement of rice ash obtained the highest compressive strength among all percent replacement. Comparing the results of compressive strength at 28-day curing with the results of the 56-day curing at each percent replacement, differences in compressive was 13.13%, 20.02%, 30.30% and 29.38% with 0%, 10%, 20% and 30% replacement, respectively.

Longer period of curing gives noticeable enhancement to the strength of concrete because of the pozzolanic reactivity of rice ash. Because pozzolanic reaction takes time to be completed, longer period allows more reaction between C-H and amorphous silicate from rice ash to take place.

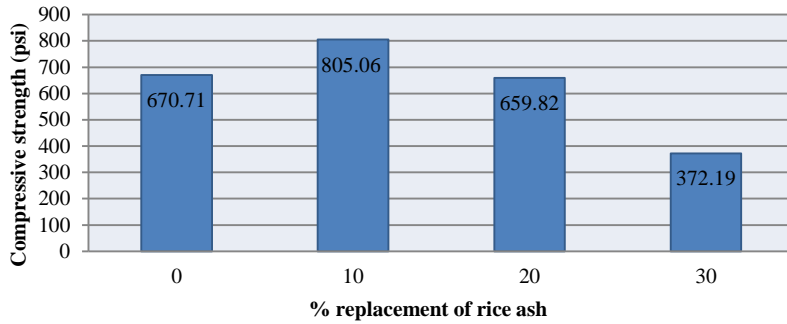


Fig. 1. Compressive strength of concrete after 28 days curing

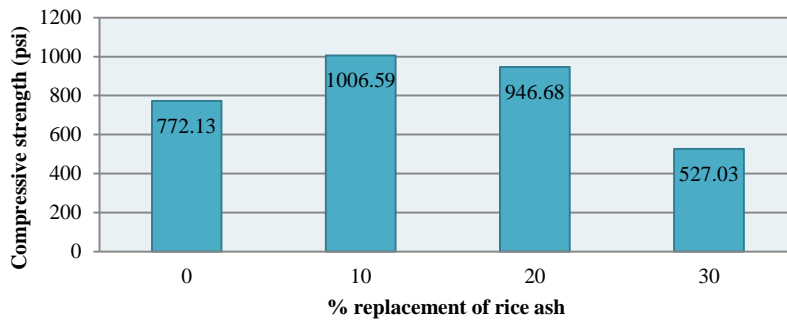


Fig. 2. Compressive strength of concrete after 56 days curing

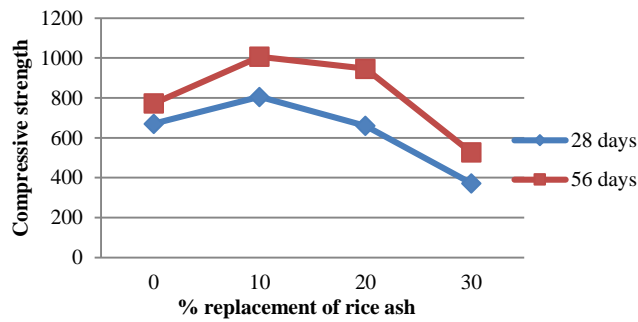


Fig. 3. Compressive strength of concrete after 28 and 56 days curing

#### 4.2. Chloride penetration test

Chloride penetration was determined by using colorimetric method by applying  $\text{AgNO}_3$  solution onto concrete samples. The violet region indicated the depth of penetration of chloride, while the brown and white regions indicated that there were no signs of chloride attack as shown in Fig. 4.





Fig. 4. Measuring chloride penetration depth

Based on the Table 2, 0% replacement of rice ash in type IP cement had the highest average value for depth of penetrating chloride. It means that incorporation of rice ash lessen the diffusion of chloride ion inside the concrete and prevent it from reaching the reinforcing steel. This is attributed to the additional cement gel (C-S-H) produced by rice ash. This gel helps to reduce the voids and blocks capillary inside the concrete making it less permeable to chloride and other chemical attack [2]. However, after 10% replacement of rice ash, the chloride depth with 12.8 mm was increased to 17.71 mm and 17.77 mm at 20% and 30% replacement of rice ash, respectively. This is because cement was reduced and the C-H produced during hydration is not enough to react with the available silica from rice ash thus leaving no chemical reaction.

Table 2. Depth of Chloride Penetration

Specimen	Chloride Penetration Depth (mm)								Average	
	1	2	3	4	5	6	7	8		
CP-0%-1	25.85	21.25	22.41	13.22	17.97	30.49	24.34	26.41	22.74	19.64
CP-0%-2	31.12	15.34	20.32	14.42	14.97	10.65	15.34	10.27	16.55	
CP-0%-3	16.65	16.5	15.24	17.56	31.78	16.19	24.51	18.44	19.61	
CP-10%-1	18.43	14.12	10.95	14.5	16.68	10.29	16.92	15.76	14.71	12.8
CP-10%-2	12.06	9.18	9.6	12.37	14.02	13.58	8.66	11.36	11.35	
CP-10%-3	11.84	18.09	12.67	11.17	9.2	16.6	11.43	7.79	12.35	
CP-20%-1	16.25	17.94	18.43	18.38	17.71	18.57	16.27	18.73	17.79	17.71
CP-20%-2	19.14	20.01	17.42	12.6	19.64	18.51	16.18	17.8	17.66	
CP-20%-3	21.88	17.9	18.5	18.78	17.29	14.17	16.89	16.07	17.69	
CP-30%-1	13.75	16.28	19.46	14.36	16.54	19.13	22.37	18.06	17.49	17.77
CP-30%-2	16.83	17.33	16.19	18.92	18.22	19.22	24.38	21.15	19.03	
CP-30%-3	17.08	15.39	15.4	13.06	18.35	21.54	17.4	15.96	16.77	

At 0% replacement of rice ash, the depth of chloride ingress significantly decreased by 34.76% at 10% replacement, 9.76% at 20% replacement and 9.52% at 30% replacement of rice ash as shown in Fig. 5.

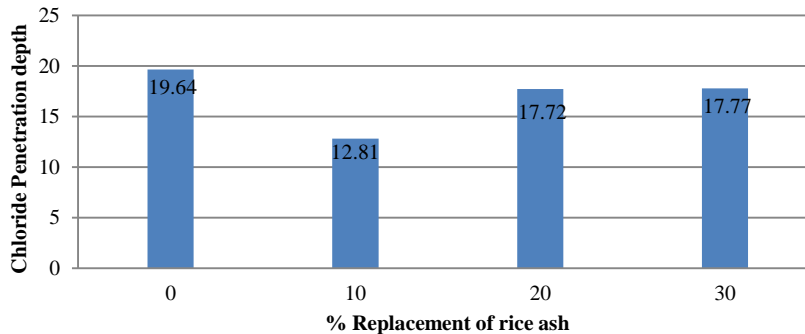


Fig. 5. Depth of chloride penetration in millimeters

## 5. Conclusions

The following conclusions were drawn based on the objectives of the study:

- The 10% replacement of rice ash in type IP cement is the most effective percent replacement for 28 days of curing while 20% replacement becomes the optimum percent replacement after 56 days of curing. Declination of compressive strength after 10% replacement shows that too much silica present in the mixture and the quantity C-H produced after hydration of cement were no longer enough to react with silica of rice ash to produce C-S-H.
- The results indicated that a concrete with 10% replacement of rice ash in type IP cement had the least chloride penetration. Furthermore, results of tests with 20% and 30% replacement of rice ash give lower value of penetrating chloride than concrete without rice ash. It can therefore be concluded that concrete with rice ash reduced the permeability of concrete.
- The test result showed that concrete cured after 56-days of curing gives a much higher strength as compared to specimens tested after 28 days of curing. Longer period of curing improved the compressive strength of concrete.

## 6. Recommendations

It is presented in the results of data that 10% replacement of rice ash in type IP cement obtains the highest compressive strength and chloride penetration resistance among all percent replacement. It is recommended to investigate other properties such as split tensile and flexural test.

Due to limited time, the salt ponding test was performed only for a short period of time. Therefore, it is recommended to perform this test for about 90 days or longer to evaluate more the resistance of concrete to chloride attacks. Alternatively, other test for chloride penetration like Electrical Indication of Concrete's Ability to Resist Chloride Ion Penetration or known as Rapid Chloride Permeability Test (ASTM C1202) can be conducted.

## Acknowledgements

The researchers would like to express her deepest appreciation to Almighty God who is the source of all strength. To Engr. Gingham B. Maranan who gave guidance and useful critiques to this study. To Engr. Hermie M. del Pilar, the Civil Engineering Program Chair who provided supervision throughout of the study. To Dr. Marish Madlangbayan, who helped and gave useful ideas. And to family, colleagues and friend who supported to finish this study.

## References

- [1] Cook, J.D, Rice husk ash. Concrete technology and design, Cement replacement materials, Vol. 3. London: Surrey University Press. pp. 171–95, 1986.

- [2] Givi, A.N., Rashid, S.A., Aziz, F.N., Salleh, M.A.M., Contribution of Rice Husk Ash to the Properties of Mortar and Concrete: A Review, University Putra Malaysia, Malaysia. *Journal of American Science* (2010) 6(3):157-165. ISSN: 1545-1003.
- [3] Mittal, D., “Silica from Ash”, Chemical Technology Dept. Sant Longowal Institute of Engineering and Technology, Sangrur, Punjab, India, 1997.
- [4] Zemke, N., Woods, E., Rice Husk Ash, California Polytechnic Sta. University, 2009.
- [5] Habeeb, G.A., Mahmud, H.B., Study on Properties of Rice Husk Ash and Its Use as Cement Replacement Material, *Material Research*. 2010; 13 (2): 185-190.
- [6] El-Dakroury, A., Gasser, M.S., Rice husk ash (RHA) as cement admixture for immobilization of liquid radioactive waste at different temperatures, *Journals of Nuclear Materials* 381 (2008) 271-277.
- [7] Ismail, M.S., Waliuddint, A. M., Effect of rice husk ash on high strength concrete, *Construction and Building Materials*, Vol. 10 (1996), No. 7, pp. 521-526.
- [8] Ganesan, K., Rajagopal, K., Thangavel, K., Rice husk ash blended cement: Assessment of optimal level of replacement for strength and permeability properties of concrete, *Construction and Building Materials* 22 (2008) 1657-1683.
- [9] American Society of Testing And Materials, ASTM C 31 Standard Practice for Making and Curing Concrete Test Specimens in the Field, *Annual Book of ASTM Standards*, Volume 04.02, ASTM, West Conshohocken, PA.
- [10] American Society of Testing And Materials, ASTM C 39 Standard Test Method for Compressive Strength of Cylindrical Concrete Specimens, *Annual Book of ASTM Standards*, Volume 04.02, ASTM, West Conshohocken, PA.
- [11] He, F., Shi, C., Yuan, Q., Chen, C., Zheng, K., AgNO<sub>3</sub>-based colorimetric methods for measurement of chloride penetration in concrete, *Construction and Building Materials*. Volume 26, Issue 1, January 2012, Pages 1–8.



Sustainable Civil Engineering Structures and Construction Materials, SCESCM 2016

## Need for further development in service life modelling of concrete structures in chloride environment

Gro Markeset<sup>a\*</sup>, Mahdi Kioumarsi<sup>a</sup>

<sup>a</sup>*Oslo and Akershus University Collage of Applied Science, Oslo, Norway*

---

### Abstract

Designing concrete structures for a very long service life may have considerable economic and societal benefits including minimized material consumption over the long term, thus contribute to more sustainable solutions. However, such long service lives require determination and extrapolation of environmental loadings and material durability performance over a long period, as well as reliable and operational models for service life predictions. Codes and standards give deem-to-satisfied recommendations for intended working (service) life up to about 100 years. However, if higher working lives of 200 and 300 years are specified, as for monumental buildings, bridges and other important infrastructures, more in-depth service life predictions are required. This paper focuses on durability and service life predictions for reinforced concrete structures for working (service) life requirements above 100 years.

© 2017 The Authors. Published by Elsevier Ltd.

Peer-review under responsibility of the organizing committee of SCESCM 2016.

*Keywords:* concrete structures; service life; chloride ingress; chloride threshold; probability.

---

### 1. Introduction

Despite the fact that almost all current concrete structural design codes and standards make no allowance for the effects of deterioration during the life of the structure, premature deterioration of concrete buildings and infrastructure due to corrosion of reinforcement is still a severe challenge, both technically and economically. Moreover, repair-work on the public transportation infrastructure are causing significant inconveniences and delays for both the industry and the general public, and are now recognized as a substantial cost for the society.

---

\* Corresponding author. Tel.: +47-67238518

E-mail address: [gro.markeset@hioa.no](mailto:gro.markeset@hioa.no)

The provisions within codes of practice for concrete structural design and the associated materials standards are typical given in tabulated form relating the provision of resistance (e.g. cement type and quality, maximum water/binder ratio, depth of cover, concrete grade, minimum air content, type of curing, control of early cracking, crack width limitation) to the aggressivity of the environment and the length of the design service life.

In general, Eurocode 2 for concrete structures, an a priori assumption is made that 50-year service life will be achieved for structures designed in accordance with the given requirements and provisions. Other national codes and regulations may adopt higher service lives, like in the Norwegian annex to Eurocode 2 [1]; specifying minimum concrete covers for design lives of both 50 and 100 years.

For some important long-life infrastructures and monumental buildings, target service life of 200 and 300 years, or even more, may be specified. Service life modelling, or chloride ingress modelling, based on Fick's second law of diffusion is becoming the common tool for performance-based specifications of such concrete structures.

An interesting long-life infrastructure in this respect is the design and construction of the Second Gateway Bridge in Australia with a service life requirement of 300 years [2]. Chloride induces corrosion was of particular concern for the durability of the main pier pile caps. These elements were designed with a concrete cover to the ordinary black steel of 150 mm. To control surface cracking of such large cover depth, a mat of LDX 2101 stainless steel reinforcement was specified and placed at a distance of 75 mm from the exposed concrete surface. A ternary blend concrete consisting of 30 % fly ash (FA) and 21 % blast furnace slag (BFS) with a water/binder ratio of 0.32 was used in these elements in order to improve concrete durability properties substantially.

Other examples of long service life requirements are the design and construction of concrete foundations for some major residential areas located at the sea front in Norway. In one of those construction projects, the client has specified a target service life (design service life) of 200 years. To meet this design life requirement, a cover of 100 mm to ordinary black steel was specified together with a ternary blend concrete with 6 – 20% FA and 4 % silica fume (SF).

In the above construction projects, the concrete cover specifications were verified through probabilistic service life calculations based on Fick's second law of diffusion. Based on the cover specifications, a conclusion could have been drawn that a cover depth of 100 mm is needed for 200 year design life, whereas 150 mm cover is needed for achieving 300 years. However, this is not the case. This paper discusses the uncertainties associated with the service life model and how the output of the probabilistic model is applied for the prediction and specification of cover depths in the two construction projects

It is worth mentioning that in both projects the service life design included an additional safety margin as electrical continuity was specified for reinforcement in the most aggressive environment, to enable future cathodic protection to be installed.

## 2. Chloride induced corrosion - Service life modelling

Service life of reinforced concrete is often divided into two distinct time periods – the initiation period and the propagation period, respectively. The initiation period is the time when chlorides penetrate through the concrete towards the reinforcement, with negligible concrete deterioration. The propagation period is the time after corrosion initiation of the reinforcement, including concrete cracking, delamination and reduced reinforcement area.

In the design of new structures, the end of service life is often defined at the time when the chloride content at the surface of the reinforcement has exceeded a critical level resulting in depassivation and corrosion initiation of the reinforcement. This critical chloride content, or chloride threshold level, becomes therefore a key parameter in the prediction of the design service life.

For estimation of residual service life and capacity, the corrosion process of the reinforcement (i.e. the propagation period) is important. However, to the authors' knowledge, such operational service life models are lacking.

### 2.1. Initiation period – chloride ingress

The chloride ingress is commonly modelled by Fick's 2nd law of diffusion, [3], assuming all transport of chloride ions in an un-cracked concrete medium will occur by ionic diffusion. The chloride concentration at depth  $x$  at time  $t$

may then be calculated according to equation 1. The time dependency of the diffusion coefficient is further modelled according to equation 2.

$$C(x, t) = C_i + (C_0 - C_i) \cdot \operatorname{erfc} \left( \frac{x}{2 \cdot \sqrt{D_a(t) \cdot t}} \right) \quad (1)$$

$$D_a(t) = D_0 \left( \frac{t_0}{t} \right)^\alpha \quad (2)$$

where:

- C(x, t): chloride concentration at depth x at time t
- C<sub>0</sub>: chloride concentration on the exposed concrete surface
- C<sub>i</sub>: initial chloride concentration in the concrete
- t: exposure time
- x: cover depth
- erfc: the error function complement
- D<sub>a</sub>(t): time dependent apparent (average) chloride diffusion coefficient at time t
- D<sub>0</sub>: chloride diffusion coefficient at the age t<sub>0</sub>.
- α: age factor
- t<sub>0</sub>: time at exposure

The chloride diffusion coefficient will typically decrease as time passes since the capillary pore system will be altered as hydration products continue to form. Further, some chloride ions will become chemically or physically bound as they penetrate the pore system. Other pore blocking mechanisms may also take place in the transition zone between concrete and seawater.

The age factor in equation 2 is modelling how fast the diffusion coefficient is improved over time. Several investigations have been conducted worldwide to stipulate the age factor, α, and many different values may be found in the literature. However, most of the values are based on concrete specimens at relative short exposure periods and from different marine structures with different concrete compositions and under varying exposure conditions.

One of very few systematic long term field investigations suitable for determine reliable data for this ageing effect for relevant concrete recipes are those presented in [4,5] on concrete samples exposed to marine environment in Norway. The main observation from the Norwegian marine field studies was that both the calculated surface chloride concentration C<sub>0</sub> and the apparent chloride diffusion coefficient D<sub>a</sub> are time dependent variables and seem to reach a constant value after about 10-15 years of exposure, as illustrated in Figs. 1 and 2. These studies include concrete recipes with CEM I and fly ash content varying from zero to 20 % by weight of cement, and one series of ternary blend concrete with 4 % silica fume (SF) and 20 % fly ash (FA). The water binder ratio was in the order of 0.40 for all concrete samples. Results from the concrete samples tested in the tidal/splash zone are presented in Table 1. As can be seen, the ternary blend concrete with ordinary Portland cement (OPC), 20 % FA and 4 % SF obtained the lowest diffusion coefficient at early age as well as in the long term.

Table 1. Age factors derived from field measurements on concrete samples over 9 years of marine exposure in the tidal zone. Corresponding diffusion coefficients calculated for 28 days of exposure for different blends of concrete, data from [4].

Type of binders:	Age factor		Calculated diffusion coefficient (m <sup>2</sup> /s)
	Mean value	Variation (%)	Value at 28 days
Ordinary Portland cement (OPC)	0.19	16	7.9·10 <sup>-12</sup>
OPC with 10-20 % silica fume (SF)	0.43	13	7.2·10 <sup>-12</sup>
OPC with 10- 20% fly ash (FA)	0.40	10	8.7·10 <sup>-12</sup>
OPC with 4% SF and 20 % FA	0.46	17	4.1·10 <sup>-12</sup>

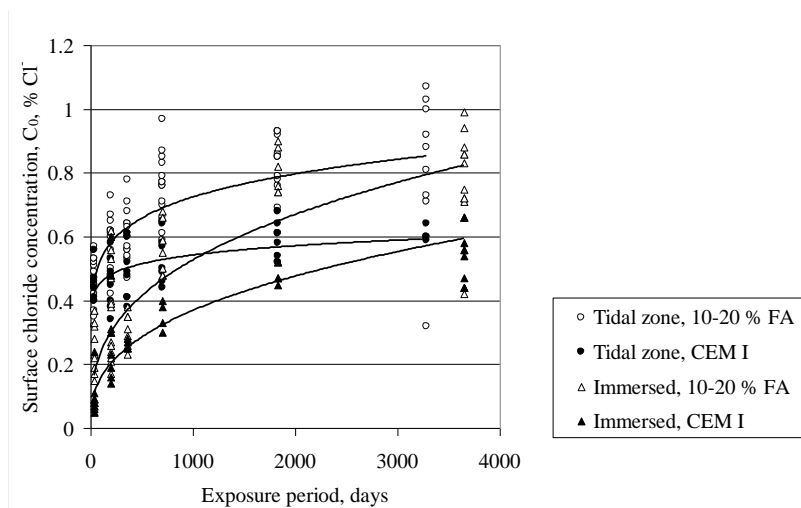


Fig. 1. Surface chloride concentration ( $C_0$ ) in % of concrete weight for concrete with and without fly ash (FA) [5].

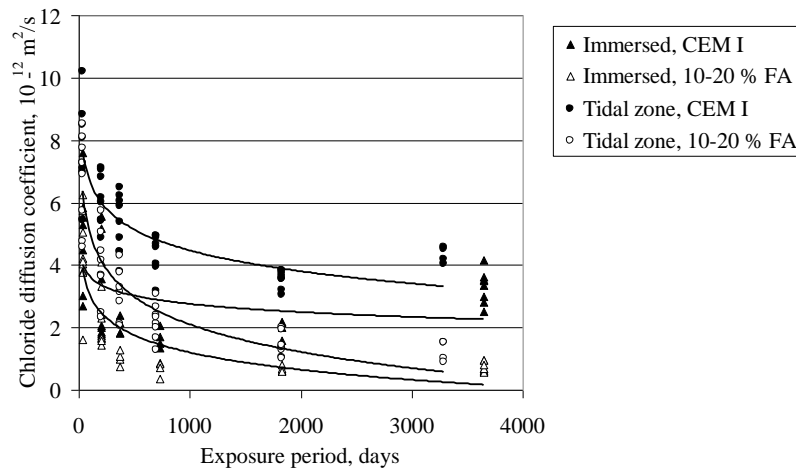


Fig. 2. Apparent diffusion coefficient ( $D_a$ ) for concrete with and without fly ash (FA) [5].

## 2.2. Chloride threshold level – corrosion initiation

When the chloride threshold level is exceeded in a certain small area (pit) on the reinforcement surface, depassivation occurs and corrosion initiation may start. The corrosion in localized small surface pits continues to grow into and along the reinforcing bars. As this corrosion process is of stochastic nature both in its probability of occurrence and in its geometrical distribution and spatial variation, it is necessary to express the threshold value in statistical terms [6-10].

Reliable data for the chloride threshold level are lacking, especially from field exposure of existing structures. Thus, conservative values as often used in service life calculations. In *fib* “Model Code for Service Life Design” [6], a beta distribution with a mean value of 0.60 by weight of cement is suggested. However, higher mean values have been found by Izquierdo et al [10] based on laboratory tests and by Markeset [7] on a real structure. The model proposed by Markeset [7] is based on corrosion sensor measurements on a marine structure in Norway and represented by a lognormal distribution with a mean value for critical chloride content of 0.77 % by weight of cement (or 0.12 % by weight of concrete) and a coefficient of variation of 32%, see Fig. 3.

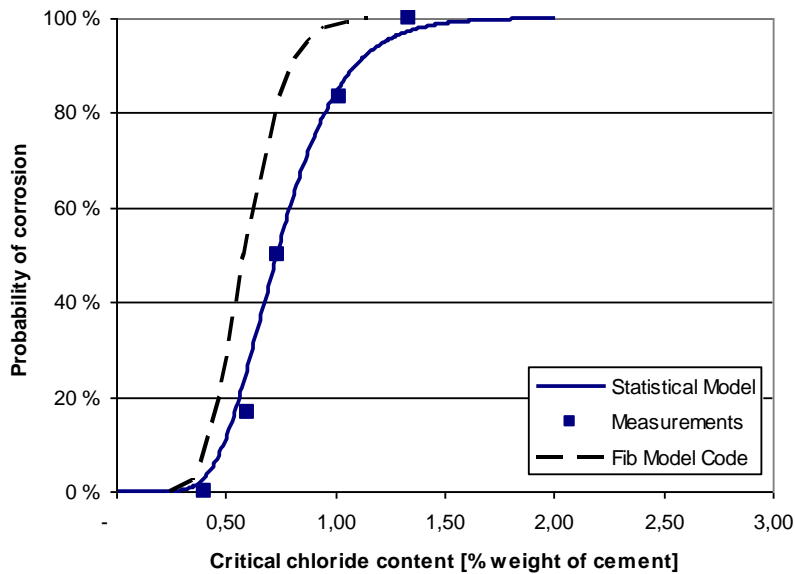


Fig. 3. Probability of corrosion initiation according to Markeset [7] compared to *fib* Model code for service life design [6].

### 3. Probabilistic service life calculations

In the service life calculations, the input parameters in equation 1 and 2 should be considered as stochastic variables characterized by the distribution type, the mean value and the coefficient of variation (COV). The end of service life is defined as the time to onset of corrosion and the limit state function,  $G_{(X)}$ , is defined as the difference between the critical chloride concentration,  $C_{cr}$ , and the calculated chloride concentration,  $C_{(X,t)}$ , at the reinforcement:

$$G_{(X)} = C_{cr} - C_{(X,t)} \quad (3)$$

where  $X$  is a vector of the statistical parameters as diffusion coefficient, surface chloride concentration, concrete cover, etc.

Introducing onset of corrosion as a failure criterion indicates that this criterion must be dealt with as a Serviceability Limit State (SLS). This means that “failure” only leads to economic consequences and that the effect of deterioration will be observable long before risk of collapse is reached. Treating this as a SLS criterion, the acceptance criterion for corrosion initiation may be set as high as 10 % probability (i.e. reliability index  $\beta = 1.28$ ).

#### 3.1. 300 year service life: Pile caps of Second Gateway Bridge

Probabilistic service life calculations are performed for the pile caps of the Second Gateway Bridge in Australia based on the model input parameters given in [2] and summarized in Table 2. Two sets of simulations are conducted; Model 1 with a diffusion coefficient of  $2.0 \cdot 10^{-12} \text{ m}^2/\text{s}$  and age factor  $\alpha=0.56$ , and Model 2 with a constant diffusion coefficient of  $1.1 \cdot 10^{-13} \text{ m}^2/\text{s}$  estimated in [2] as the constant value after 30 years of exposure (i.e.  $\alpha = 0$ ).



Table 2. Input data for the probabilistic time to corrosion initiation predictions, input data from [2].

Variables:	Mean values	Coefficient of variation (COV)	Distributions
Depth of cover (mm):	150	20 %	Normal
Diffusion coefficient, $D_0$ ( $m^2/s$ ):			
Model 1: $D_0$ (for $\alpha = 0.56$ )	$2.0 \cdot 10^{-12}$	25 %	Lognormal
Model 2: $D_0$ (for $\alpha = 0$ )	$1.1 \cdot 10^{-13}$	25 %	Lognormal
Surface chloride content $C_s$ (% by weight of concrete):	0.65	20 %	Normal
Age factors $\alpha$ :			
Model 1	0.56	25 %	Normal
Model 2	0		
Critical chloride content (% by weight of concrete):	0.06	25 %	Lognormal

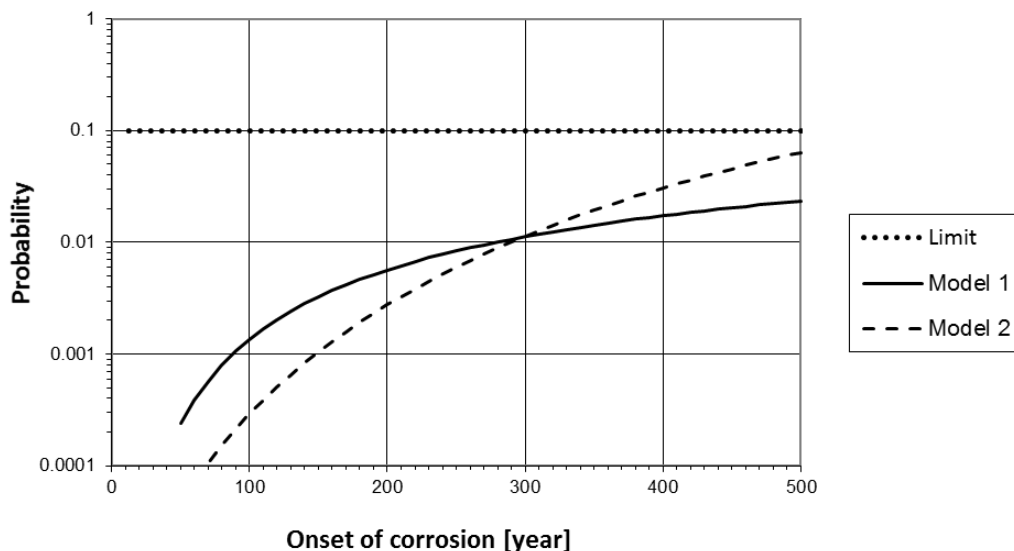


Fig. 4. Probability of corrosion initiation for 150 mm cover depth based on input data given in Table 2.

The probability of corrosion initiation versus service life for the ternary concrete mix and 150 mm depth of cover to the ordinary steel in the pile caps are shown in Fig. 4. As seen, a very low probability of corrosion initiation, about 1 % ( $\beta = 2.32$ ), is obtained for the specified cover of 150 mm. If a probability of 10 % ( $\beta = 1.28$ ) of corrosion initiation is applied, a service life above 500 years may be obtained. The two diffusion models (Model 1 and Model 2) gave about the same result for 300 year of service life.

### 3.2. 200 year service life: Foundation for residential area at sea front

The original calculations leading to the specification of the 100 mm cover depth to ordinary steel, was based on probabilistic calculations using a model denoted “Cover specification model”. The statistical input parameters for this model was developed by calibration towards the cover depth provisions given in the Norwegian annex to Eurocode 2 [1] and the recommendation in [11] for 50- and 100-year design life, respectively. For these cover specification calculations, an acceptance criterion for corrosion initiation of 10 % was applied. The modelling and the statistical parameters are further described in [11].

In this paper the effect of applying the specified ternary blend concrete (20 % fly ash and 4 % silica fume), with the diffusion parameters according to Table 1, as well as applying the statistical distribution for the chloride

threshold given in Fig. 3 [7], has also been studied. The statistical input parameters applied in the probabilistic calculations for all three variations are listed in Table 3.

The probabilistic calculations for the concrete foundation are presented in Fig. 5. The cover specification model calibrated to the Norwegian annex [1] with 10% probability of corrosion initiation corresponds to a cover depth of 100 mm for the target service life of 200 years. By modelling the ternary blend concrete and applying the statistical distribution for threshold level according to Fig. 3, somewhat lower concrete cover, about 80 mm, is found from the probabilistic analysis for 10 % probability of corrosion initiation.

Table 3. Statistical input parameters for the cover depth predictions for target service life of 200 years.

Variables:	Cover specification model	Ternary blend model 1	Ternary blend model 2	Distributions
	Mean values / COV	Mean values / COV	Mean values / COV	
Design Service life (years)	200	200	200	
Diffusion coefficient, $D_0$ ( $m^2/s$ ):	$7.0 \cdot 10^{-12} / 40 \%$	$4.1 \cdot 10^{-12} / 28 \%$	$4.1 \cdot 10^{-12} / 28 \%$	Lognormal
Age factor $\alpha$ :	0.50 / 15 %	0.46 / 17 %	0.46 / 17 %	Normal
Surface chloride concentration $C_s$ (% by weight of concrete)	0.63 / 48 %	0.63 / 48 %	0.63 / 48 %	Normal
Critical chloride content (% by weight of concrete)				
Constant threshold	0.10	0.10	-	Deterministic
Statistical threshold	-	-	0.115 / 32 %	Lognormal

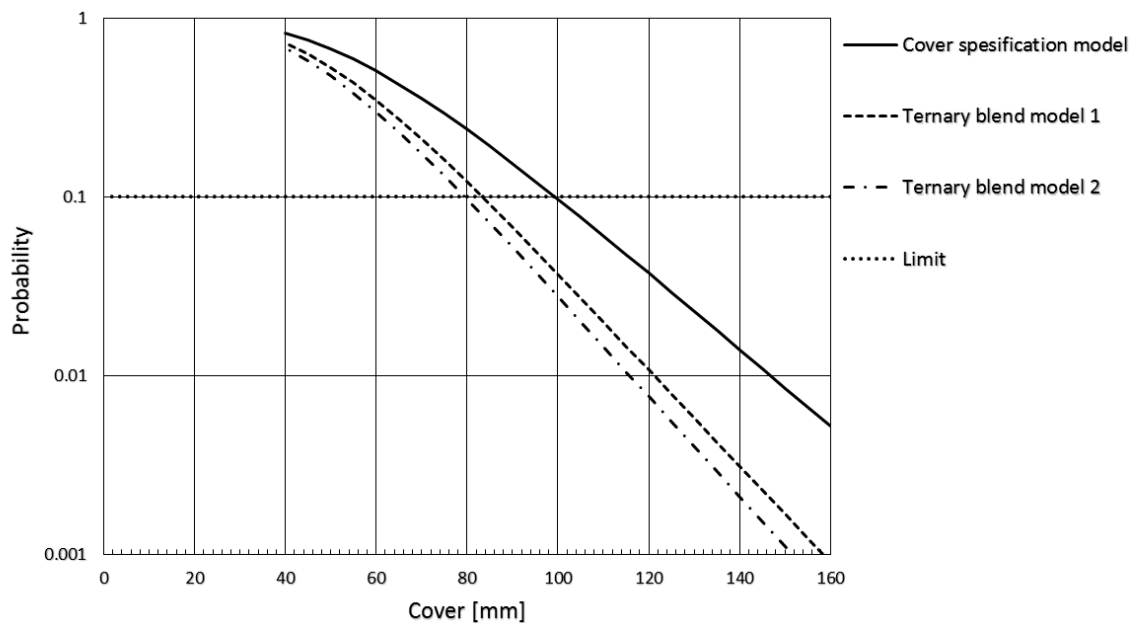


Fig. 5. Probability of corrosion initiation for target service life of 200 years based on input data given in Table 3.

#### 4. Conclusions

The chloride ingress model according to Fick's second law of diffusion is a pure empirical formula verified through test data over the last 20 years. In particular, the modelling of the time dependent diffusion including the age factor has a major impact on the service life prediction. The critical chloride content (chloride threshold) defining the corrosion initiation is another parameter that influences the results significantly. There is a need for more statistical

data for all the model parameters. However, provided good and reliable input parameters the probabilistic approach of service life calculations may be a good decision tool for cover specification for very long service life.

It should also be kept in mind that the model is only applicable for un-cracked concrete. Using very low water binder ratio, i.e. less than 0.4, in order to decrease the chloride diffusion coefficient, the concrete becomes more prone to cracking and may thus give increased chloride ingress.

The two construction projects studied have applied different approaches to the probabilistic calculations of Fick's second law of diffusion as a decision tool for cover specification. Although the statistical input parameters are not identical, the main difference is the definition of end of service life through the actually chosen probability level at corrosion initiation.

## References

- [1] Eurocode 2: Design of concrete structures, National annex NS-EN 1992-1-1:2004/NA:2008.
- [2] J. Connal, M. Berndt, Sustainable Bridges – 300 Year Design Life for Second Gateway Bridge, Proceedings, Austroad Bridges Conference, Auckland, 2009.
- [3] M. Collepardi et. al., Penetration of chloride ions into cement paste and concrete, American Ceramic Society, Vol. 55, USA, 1972.
- [4] O. Skjølsvold, Chloride diffusion into concrete. Evaluation of the ageing effect based on results from field studies', COIN Project Report 11-2009, ISBN 978-82-536-1088-7, (in Norwegian), 2009.
- [5] G. Markeset, O. Skjølsvold, Time dependent chloride diffusion coefficient - field studies of concrete exposed to marine environment in Norway, in: Service Life Design for Infrastructure. Rilem publications, ISBN 978-2-35158-096-7, 2011, pp. 83-90.
- [6] *fib* Bulletin 34, Model Code for Service Life Design, 2006.
- [7] G. Markeset, Critical chloride content and its influence on service life predictions', *MatCorr*, 60 (8) (2009) 593-596.
- [8] C. Andrade, W.R. Whitney Award Lecture: Probabilistic Treatment of the Reinforcement Corrosion, *Corrosion*, 70 (6) (2013) 643-651.
- [9] M. M. Kioumars, M. A.N. Hendriks, J. Kohler, M.R. Geiker, The effect of interference of corrosion pits on the failure probability of a reinforced concrete beam, *Engineering Structures* 114 (2016) 113–121.
- [10] D. Izquierdo, C. Alonso, C. Andrade, M. Castellote, *Electrochimica Acta* 49(17-18), 2731-2739, 2004.
- [11] The Norwegian concrete association Publication No 35, Durability of concrete structures in marine environment (In Norwegian), 2011.



Sustainable Civil Engineering Structures and Construction Materials 2016, SCESCM 2016

## Properties of plain and blended cement concrete immersed in acidic peat water canal

Monita Olivia<sup>a</sup>, Tomy Pradana<sup>a</sup>, Iskandar Romey Sitompul<sup>a,\*</sup>

<sup>a</sup>*Universitas Riau, Kampus Bina Widya Simpang Baru, Pekanbaru Riau 28293, Indonesia*

---

### Abstract

Reinforced concrete structures exposed to the acidic environment, such as acidic soil, agricultural building, industrial acid, are unavoidable in practice. Structures and infrastructures in acidic environment are usually have durability problems related to degradation of concrete cover and corrosion of steel reinforcement. Acidic soil such as peat, contains organic humic acids that can retard cement hydration process, and potentially reduce the concrete integrity after continuous exposed to the environment. This research is aimed to investigate concrete degradation when subjected to peat water by direct field exposure in water canal. The specimens were made from Ordinary Portland Cement (OPC), Portland Composite Cement (PCC) and OPC replaced with 10% (by cement weight) Palm Oil Fuel Ash (OPC POFA). Those plain and blended cement specimens were cast and cured in water pond in laboratory, then immersed in peat water canal up to 120 days. Compressive strength, tensile strength and porosity of specimens were measured at 28, 91 and 120 days. After 120 days of immersion, compressive and tensile strength reduction, and porosity increase were seen for the OPC specimens. The PCC and OPC POFA specimens performed a gradual increase in both compressive and tensile strength, and reduction of porosity with the exposure period. The results indicated that cement type had significant effect on concrete properties exposed to the peat water directly. The test results showed that the PCC samples are more chemically resistant to acid attack in peat water, followed by the OPC POFA samples and finally the OPC samples after subjected to acidic peat water canal.

© 2017 The Authors. Published by Elsevier Ltd.

Peer-review under responsibility of the organizing committee of SCESCM 2016.

*Keywords:* acid, canal, palm oil fuel ash, pozzolanic material, strength

---

---

\* Corresponding author.

*E-mail address:* [monita.olivia@lecturer.unri.ac.id](mailto:monita.olivia@lecturer.unri.ac.id)

## 1. Introduction

Concrete in aggressive environment, such as acid is usually prone early degradation due to harmful ions attack on cement matrix. This is due to calcium binding by the acid ions in the cement matrix that lead to deterioration of concrete. Previous studies confirmed that the acidic resistance of concrete is determined by type, cement composition, pH, aggregate type, and inclusion of pozzolanic materials in cement mixture [1, 2]. There are several methods to improve the concrete properties in aggressive environment such as reducing water to cement ratio, using high performance coatings, using water reducing admixture, improving compaction, producing special mortars, controlling curing and incorporating pozzolan in the cement. Inclusion of pozzolanic materials such as slag, fly ash (FA), rice husk ash, and palm oil ash (POFA) as cement replacement in concrete was reported beneficial to improve the acid resistance of cement at late curing ages by forming CSH through pozzolanic reaction to reduce porosity, refine microstructure and enhance the mechanical properties [3-6].

The effect of acid attack to reinforced concrete structures and infrastructures in peat environment, such as concrete pipes, waterways, foundation piles that are exposed directly to the peat water has recently been of concern due to possible premature reduction of the structures service life. Peat is characterized by its high water and organic matter content from decomposition plants in water logged areas for a very long time. The organic content contains acids that has low pH (3-5). Concrete in that environment usually is vulnerable to acid attack since the pH of medium is extremely acidic and can lead to premature deterioration of concrete, reduction of structural integrity, and high cost for maintenance and repair [7].

Many studies about interaction between cement and humic acid in peat soil were conducted in the last few decades to determine suitable materials for peat soil stabilization. A study about peat stabilization using cement has reported that the organic peat acid could disturb the cement hydration process and delay any strength gain of the stabilized ground [8]. Another study explained that the reaction between cement and water in peat will still produce portlandite or  $\text{Ca}(\text{OH})_2$  and Calcium Silicate Hydrate (CSH) gels at slower rate than normal cement hydration process. This is because the reaction between the humic acids in peat with portlandite or  $\text{Ca}(\text{OH})_2$  in cement matrix forming insoluble products which precipitate out the clay particles. The insoluble products will delay the cement early strength gain, and inhibit the subsequent pozzolanic reactions [9]. This condition reflects on how the humic acid will attack the concrete hydration product for cast in situ concrete. There were two studies about the impact of peat water acidity in mortar and concrete exposed directly to peat water in laboratory condition [10, 11]. In those research, the plain and blended cements were immersed in water from peat swamp. Those initial studies have concluded that the specimens made using blended cements performed better resistance to the peat water than the OPC (Ordinary Portland Cement) control specimens. However, concrete properties that is exposed directly to the peat water has never been reported yet. This research is aimed to study to study the compressive strength, tensile strength, and porosity of the specimens made from plain (OPC) and blended cements (PCC and OPC POFA) binders that were directly exposed to the acidic peat water canal.

## 2. Materials and Method

In this study, the concrete specimens were manufactured using a plain cement (Ordinary Portland Cement-OPC), and blended cements, namely (Portland Composite Cement-PCC) and OPC-Palm Oil Fuel Ash (OPC POFA), aggregates and water. Fine aggregates were river sand with specific gravity of 2.69, fineness modulus of 1.90, and water absorption of 2.24%. Coarse aggregates had specific gravity of 2.72 and water absorption of 2.64%. The type I OPC was used as a control mix, while the PCC is a new type of cement produced to replace the type I cement commercially. The OPC POFA concrete consisted of 10% POFA by cement weight. The palm oil ash was taken from a local incinerator. The ash was dried and sieved using sieve #200. The chemical composition of OPC, PCC and POFA are summarised in Table 1.

The physical and chemical composition of the peat water from Rimbo Panjang, Riau Province are listed in Table 2. The analyzed parameters were color, turbidity, organic content, alkalinity, sulfate and chloride ions, and organic impurities (manganese and iron). From the table, it could be seen that some basic properties of peat water, except manganese, sulfate and chloride ions, were not within tolerable limits of drinking water. Peat water had pH of 3.85, which was acidic than the required pH for drinking water (6.5-8.5). The organic content of peat water was 328 mg/L. This value was considerably higher than the permissible organic content for drinking water. It was reported

that high organic material content is able to disrupt OPC cement hydration process in peat soil stabilization [8].

Table 1. Chemical composition of cement and palm oil fuel ash (POFA)

Oxides (%)	Type of cement/waste		
	Ordinary Portland Cement/ OPC*	Portland Composite Cement/ PCC*	Palm Oil Fuel Ash POFA**
SiO <sub>2</sub>	20.92	23.04	64.36
Al <sub>2</sub> O <sub>3</sub>	5.49	7.40	4.36
Fe <sub>2</sub> O <sub>3</sub>	3.78	3.36	3.41
MgO	-	-	4.58
CaO	65.21	57.38	7.92
Na <sub>2</sub> O	-	-	0.00
K <sub>2</sub> O	-	-	5.57
TiO <sub>2</sub>	-	-	0.87
MnO	-	-	0.1
P <sub>2</sub> O <sub>5</sub>	-	-	3.64
SO <sub>3</sub>	-	-	0.04
Cu (ppm)	-	-	46
Zn (ppm)	-	-	60
H <sub>2</sub> O	-	-	0.59
LOI	-	-	4.97

\*Salain (2009), \*\*PSD Geologi Bandung

Table 2. Physical and chemical composition of peat water

Parameters	Unit	Drinking water qualities*	Results**
Color	TCU	15	500
Turbidity	NTU	5	99.7
pH value	-	6.5-8.5	3.85
Organic content	mg/L	10	328
Alkalinity	mg/L	400	53
Iron (Fe)	mg/L	0.3	0.8
Manganese (Mn)	mg/L	<0.0248	0.1
Sulfate (SO <sub>4</sub> <sup>2-</sup> )	mg/L	400	34
Chloride (Cl)	mg/L	250	31

Source: \*[12], \*\*UPT Laboratorium Kesehatan dan Lingkungan Pekanbaru (2015)

Table 3. Mixture composition of OPC, PCC, and OPC-POFA

Mixes	OPC	PCC	OPC POFA
Cement (kg/m <sup>3</sup> )	507.895	507.895	457.105
Coarse aggregate (kg/m <sup>3</sup> )	987.425	987.425	987.425
Fine aggregate (kg/m <sup>3</sup> )	684.138	684.138	684.138
Water (kg/m <sup>3</sup> )	194.780	194.780	194.780
Palm oil fuel ash- POFA (kg/m <sup>3</sup> )	-	-	50.789

The concrete specimens were designed to have a target strength of  $\pm 35$  MPa and slump values of  $\pm 80$ mm. Table 3 shows the mixture composition for all type of concrete. The samples were cast in 100x200mm mould and cured in water for 28 days. The specimens then were placed in acidic peat water canal, Rimbo Panjang Regency, Riau Province up to 120 days until testing date. Compressive and tensile strength was determined at 28, 91 and 120 days in compliance with SNI 03-1973-1990 and SNI 03-2491-2002. Porosity values was measured at 28, 91 and 150 days after immersed in the water canal. The water canal has 5m width and approximately 1.0-1.50m depth. The pH of the water canal at the age of concrete testing is shown in Table 4. The acidity of the water canal varied between 3.63 to 4.14. The pH values depend on the weather and seasons in Rimbo Panjang Regency, since the concrete exposure was carried out during transition between dry and rainy seasons.

Table 4. pH of peat water canal during testing time

Testing date	pH
age 28	3.6±0.03
age 91	4.3±0.06
age 120	4.1±0.04

### 3. Results and Discussion

#### 3.1. Compressive strength

Fig. 1 shows compressive strength for the specimens in peat water canal after 28, 91 and 120 days of exposures. At 28 days, the compressive strength of the concrete was in the range 33.95-35.23 MPa. All mixes approximately achieved a target strength of  $\pm 35$  MPa, which was designed for rigid pavement concrete in peat environment. It can be seen that the compressive strength of the plain cement concrete (OPC) or control mix decreased gradually with concrete age. A loss in compressive strength of OPC continued until 120 days. The strength reduction for the OPC concrete was 3.77% and 10.33% at 91 and 120 days, respectively. The presence of high CaO content in this mix made the OPC concrete susceptible to acid attack. Acid ions will attack  $\text{Ca}(\text{OH})_2$  and hydration product in OPC, decompose the hydration product, and increase the porosity that followed by reduction of mechanical properties of the concrete [13]. In contrast, an increase in compressive strength was observed for the blended cement concrete specimens (OPC POFA and PCC) after 28 days. Both mixes had significant strength gain by 5.33% and 2.90% after 28 days, respectively, but a slow strength gain was observed after 91 days. Since OPC POFA concrete contains 10% of POFA, the amount of  $\text{Ca}(\text{OH})_2$  was smaller than that of the OPC specimen, therefore acid ion attack could be reduced. Besides, pozzolanic materials such as POFA, slag, fly ash in the blended cements rich in  $\text{SiO}_2$  that react with  $\text{Ca}(\text{OH})_2$  to form Calcium Silicate Hydrate (CSH) to increase densification of the cement matrix. In this research, the effect of pozzolan in OPC POFA and PCC specimens was observed from the slow gradual strength gain for both concrete after 28 days. Hence, addition of pozzolanic materials in blended cement could significantly improved the acid resistance of concrete exposed directly to peat water.

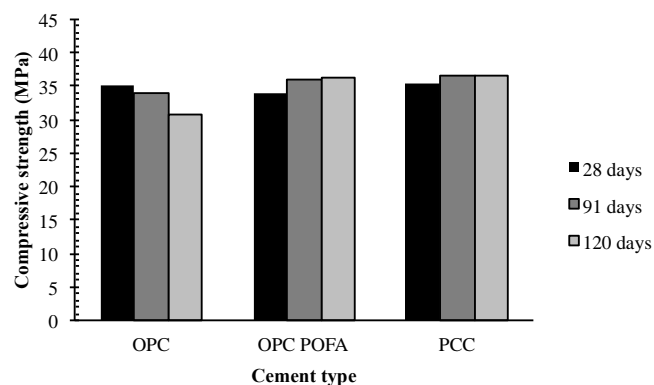


Fig. 1. Variation of compressive strength of specimens after exposed to peat water up to 120 days.

#### 3.2. Tensile strength

Fig. 2 displays the splitting tensile strength of OPC, OPC POFA and PCC at 28, 91 and 120 days. The tensile strength for all concrete at 28 days was in a range of 2.74-2.81 MPa. The highest level of tensile strength was shown by the blended cement PCC at 120 days, while the plain OPC concrete showed the lowest value. Mix OPC lost a tensile strength after 28 days and following a similar trend for the compressive strength. The gradual decrease in

tensile strength of OPC concrete by 2.58% and 8.17% were observed at 91 days and 120 days, respectively. It was suggested that reduction of the tensile strength was assumed from destruction of bonding at the interface of the OPC matrix and aggregates. In reverse, mixes OPC POFA and PCC gained a considerable tensile strength after 91 days by 6.95% and 11.90%, respectively. The bonding between the aggregates and cement matrix was high since the pozzolanic product (CSH gels) improve the concrete microstructure, especially in weak region Interfacial Transition Zone (ITZ). The ITZ is responsible for microstructure improvement that yield better concrete elastic properties. This is in agreement with a previous study which found that mixes using pozzolanic materials (slag) tend to produce a better bonding between the aggregates and cement matrix due to uniform microstructure [14]. In this research, inclusion of pozzolan material through OPC POFA and PCC could enhance better properties and resistance to humic acid in peat water.

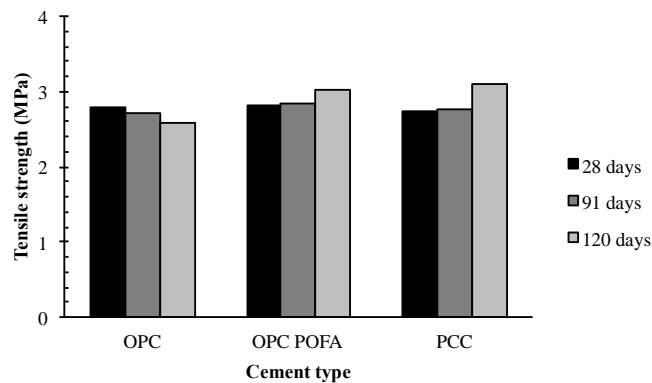


Fig. 2. Variation of tensile strength of specimens after exposed to peat water up to 120 days.

### 3.3. Porosity

The porosity of OPC, OPC POFA and PCC specimens at 28, 91 and 120 days is presented in Fig. 3. The porosity values of all concrete were in the range of 8.79 to 12.52% at 28 days. It can be seen that the porosity of OPC concrete increase gradually by 2.62% and 5.38% at 91 and 120 days, respectively. This clearly shows the acid attack has an influence on the porosity of the plain cement (OPC). An increase in porosity of the OPC concrete under continuous immersion in water canal might be due to the microstructure alteration after CaO and hydration product were decomposed by the acid ion. There was a reverse trend of the blended cement concrete with a considerable decrease of porosity after 91 days. The porosity of OPC POFA and PCC decreased by 24.39% and 15.81%, respectively. The positive improvement could be due to continuous hydration and pozzolanic reaction of the specimens after being subjected in the peat water canal. This clearly shows that the pore development of concrete in peat water canal immersion is more affected by cement composition such as inclusion of pozzolanic material in blended cement.

In general, the field exposure of the plain and blended cement concrete shows that the PCC concrete performed better than the OPC POFA and OPC concretes in the acidic peat environment. After 120 days of exposure to the peat water in water canal, the performance of materials tested ranked in the following order PCC > PC POFA > OPC. PCC cement contains pozzolanic materials (slag, fly ash and silica fume) that provides good chemical resistance against organic acid such as humic acid and will retain the structure for a long period. This is because the chemically resistant particles will be less dissolved and prevent the increase of porosity in cement matrix when it is exposed to the acidic environment. Hence, it is suggested to use blended cement binder for structures in peat environment to reduce acid ion attack to cement matrix and to improve the concrete porosity through pozzolanic reaction.



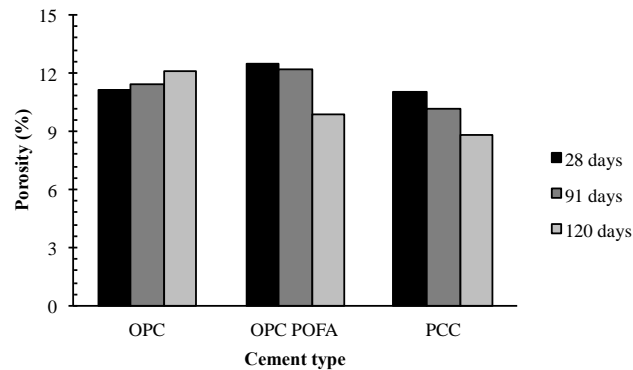


Fig. 3. Variation of porosity of specimens after exposed to peat water up to 120 days.

#### 4. Conclusions

In the present study, the OPC, OPC POFA and PCC concrete properties exposed to peat water were evaluated by immersing the specimens in peat water canal for up to 120 days. The OPC specimens showed quite significant deterioration with a gradual decrease in compressive and tensile strength and an increase of porosity of the plain OPC concrete specimens after subjected to the acidic peat water up to 120 days. The blended cement OPC POFA and PCC concrete showed improved performance than the control mix (OPC) after immersion. This is could be due to the pozzolanic material inclusion in the blended cement that could enhance hydration process, increase strength properties and improve microstructure through Calcium Silicate Hydrate (CSH) formation. In general, results indicated that cement type had significant effect on concrete properties exposed to the peat water directly. The test results showed that the PCC samples are more chemically resistant to acid attack in peat water, followed by the OPC POFA samples and finally the OPC samples after subjected to acidic peat water canal.

#### Acknowledgements

The authors would like to acknowledge all member of Final Year Project Group batch 2 and 3, Structural Engineering Laboratory, and Materials Technology Laboratory, Department of Civil Engineering, Faculty of Engineering, Universitas Riau. This research is funded by Penelitian Unggulan Perguruan Tinggi (PUPT) 2016, No 492/UN.19.5.1.3/LT/2016, Lembaga Penelitian, Universitas Riau, Pekanbaru, Indonesia.

#### References

- [1] V. Zivica, A. Bajza, Acidic attack of cement-based materials- a review Part 2. Factors of rate of acidic attack and protective measures. *Construction and Building Materials*. 16(2002): 215-222.
- [2] R.E. Beddoe, H.W. Doner. Modeling acid attack on concrete: Part 1. The essential mechanisms. *Cement and Concrete Research*. 35(2005): 2333-2339.
- [3] O. Oueslati, J. Duchesne. Resistance of blended cement pastes subjected to organic acids: Quantification of anhydrous and hydrated phases. *Cement & Concrete Composites*. 45(2014): 89-101.
- [4] V. Zivica, M.T. Palou, M. Krizma, L. Bagel. Acidic attack of cement based materials under the common action of high, ambient temperature and pressure. *Construction and Building Materials* 36(2012): 623-629.
- [5] Y. Senhadji, G. Escadeillas, M. Mouli, H. Khelafi, Benosman. Influence of natural pozzolan, silica fume and limestone fine on strength, acid resistance and microstructure of mortar. *Powder Technology*. 254(2014): 314-323.
- [6] Z. Makhloufi, T. Bouziani, M. Hadjoudja, M. Bederina. Durability of limestone mortars based on quarternary binders to sulfuric acid using drying-immersion cycles. *Construction and Building Materials*. 71(2014): 579-588.
- [7] M. Eglinton. Resistance of concrete to destructive agencies. In Hewlett, P.C. (ed). *Lea's Chemistry of Cement and Concrete*. Amsterdam: Elsevier Science and Technology Books.
- [8] S. Kamezian, A. Prasad, B.B.K. Huat, J.B. Bazaz, T.A. Mohammed, F.N. Abdul Aziz. Effect of aggressive pH median on peat treated by cement and sodium silicate grout. *J. Cent. South Univ. Technol.* 18(2011): 840-847.
- [9] M. Janz, S-E. Johansson. 2002. The function of different binding agents in deep stabilization. Research Report. Linköping: Swedish Deep Stabilization Research Centre.

- [10] M. Olivia, U.A. Hutapea, I.R. Sitompul, L. Darmayanti, A. Kamaldi, Z. Djauhari. Resistance of plain and blended cements exposed to sulfuric acid solution and acidic peat water: a preliminary study. The 6th International Conference of Asian Concrete Federation 2014.
- [11] M. Olivia, L. Darmayanti, A. Kamaldi, Z. Djauhari. Kuat tekan beton dengan semen campuran limbah agro-industri di lingkungan asam. 2nd ACE National Conferences 2015.
- [12] Irianto. 1998. Kinetika Penurunan Warna dan Zat Organik Air Gambut menggunakan Tanah Lempung Gambut dengan Sistem Batch. Bandung: Penelitian Puslitbang Pemukiman bekerja sama dengan PAU ITB.
- [13] V. Zivica. Acidic attack of materials based on the novel use of silica fume in concrete. *Construction and Building Materials*. 12(1999): 263-269.
- [14] K. Wu, H. Shi, L. Xu, G. Ye, G.D. Schutter. Microstructural characterization of ITZ in blended cement concretes and its relation to transport properties. *Cement and Concrete Research* 79(2016): 243-256.



Sustainable Civil Engineering Structures and Construction Materials, SCESCM 2016

## Mechanical and durability performance of novel self-activating geopolymer mortars

Cheah Chee Ban<sup>a</sup>, Part Wei Ken<sup>a\*</sup>, Mahyuddin Ramli<sup>a</sup>

<sup>a</sup>*School of Housing, Building & Planning, Universiti Sains Malaysia, 11800 Penang, Malaysia*

---

### Abstract

The research project aimed to explore the feasibility of activating fly-ash based geopolymer by the hybridization of fly-ash (FA) with high calcium wood ash (HCWA), a by-product from timber manufacturing industry, without the addition of conventional alkaline activators and post heat treatment curing regime. The raw materials namely FA and HCWA were characterized in term of their chemical and mineralogical phases by X-ray diffraction (XRD) and X-ray fluorescence (XRF). FA was substituted by HCWA at high replacement level of 50% to 100% at 10% incremental, by binder weight. Hardened geopolymer mortars samples were subjected to water curing and tested on the age of 7, 28 and 7 days + 24 hours hydrothermal treatment. Mechanical performance of the geopolymer mortars were assessed in term of compressive, flexural strength, ultrasonic pulse velocity (UPV) and dynamic modulus. Durability properties namely water absorption, vacuum porosity and capillary absorption were also investigated. Results were positive on the viability of hybridizing FA with HCWA to produce novel self-activating geopolymer mortars as mixtures with PFA replacement level of 50% and 60% showed enhanced mechanical and durability performance at all curing ages in comparison with other HCWA-PFA geopolymer mortar mixtures. Early strength development of HCWA-PFA geopolymer mortars was mainly contributed by the combination of hydraulic reaction of HCWA and geopolymerization of FA. On prolonged curing, strength development was due to the aforementioned reactions, plus pozzolanic reaction between the reactive silica from FA and portlandite formed from HCWA, producing additional secondary C-S-H gels. This experimental program showed positive findings in incorporating highly alkaline materials i.e. HCWA (12% K<sub>2</sub>O) towards activating FA based geopolymers, thus eliminating the needs of external alkaline activator in conventional geopolymers mix design.

© 2017 The Authors. Published by Elsevier Ltd.

Peer-review under responsibility of the organizing committee of SCESCM 2016.

*Keywords:* geopolymer concrete; fly ash; self-activating; waste management; low embodied energy; high-calcium wood ash; low alkalinity

---

---

\* Corresponding author. Tel.: +60 0164871298.

E-mail address: [part.wei.ken@hotmail.com](mailto:part.wei.ken@hotmail.com)

## 1. Introduction

Research in the field of geopolymer technology has gathered pace in the past decades owing to the environmental impact of Ordinary Portland Cement (OPC) production which raised concern amongst the practitioners regarding the sustainability of construction industry [1]. Various source materials have been employed with success such as pulverized fuel ash (PFA) or more commonly known as fly ash, ground granulated blast furnace slag (GGBS), rice husk ash (RHA), palm oil fuel ash (POFA) etc in which the resultant geopolymer mixes exhibited similar or enhanced mechanical and durability performance if compared with OPC concrete [2-5]. However, the transition of geopolymer technology into mass production has not been successful. One of the major drawback of geopolymer system is the over reliance of alkaline activator in order to achieve the desired mechanical and durability performance [6]. The most common alkaline activator used is the synergy mixes of sodium hydroxide (NaOH) and sodium silicate ( $\text{Na}_2\text{SiO}_3$ ). The dosage of alkaline activators ( $\text{NaOH} + \text{Na}_2\text{SiO}_3$ ) in conventional geopolymer mix design ranged from 0.30-0.50 [7, 8] and moreover conventional geopolymeric system most often requires elevated temperature curing ranging from 60-90 °C [9, 10]. The two aforementioned factors have raised doubt on the practicability of geopolymer technology for industrial implementation as it significantly increased the effective cost and also the embodied energy of production of the resultant geopolymer mixes. Current laboratory investigation aims to tackle the aforementioned challenges by incorporating timber manufacturing waste material i.e. high calcium wood ash (HCWA) into fly ash based geopolymer mortar at high PFA replacement level i.e.  $\geq 50\%$  of total binder mass without the need of alkaline activators and elevated curing temperature.

## 2. Materials and methods

### 2.1 Materials

ASTM Class F PFA was sourced from local coal-fired power plant in Manjung, Perak, Malaysia. The specific gravity and specific surface area of PFA were determined to be 2.8 and 3244  $\text{cm}^2/\text{g}$ , respectively.

High Calcium Wood Ash (HCWA) is a by-product from local timber manufacturing industry which utilized wood-waste such as saw dust, woodchips etc in the boiler unit to generate energy for wood drying purposes. Freshly extracted HCWA was sieved through laboratory sieve of 600 $\mu\text{m}$  to remove carbonaceous and large agglomerated particles before being used as constituent materials in the geopolymer mortars fabrication. HCWA was found to have specific gravity of 2.43 and specific surface area of 5671  $\text{cm}^2/\text{g}$ . The detailed chemical composition characterization of PFA and HCWA can be found in author's previous publication [11, 12].

Locally available natural siliceous river sand with specific gravity of 2.65 and maximum aggregate size of 5mm was used as fine aggregate throughout the laboratory investigation. Potable water from local water supply network was used as mixing water.

### 2.2 Methods

#### 2.2.1 Mixture proportioning, mixing and curing

In the experimental program, PFA was replaced by HCWA at 50-100% by binder weight, at 10% step incremental. The sand to binder ratio was held constant at 2.25 throughout the program. The workability of the fresh geopolymer mortars was controlled at between 120-150mm for adequate compaction using the flow table apparatus, thus the water to binder ratio for each mixes varied. The mixture proportioning of HCWA-PFA geopolymer mortars were shown in Table 1.

HCWA-PFA geopolymer mortar mixes were homogenized using epicyclic mixer. The freshly casted mortar samples were left to cured in ambient temperature curing condition i.e. 26°C and 85% RH for 24 h before being subjected to water curing until the designated testing ages. All the hardened HCWA-PFA geopolymer mortar samples were tested at the age of 7, 28 and 7 + 24 h hydrothermal treatment.

Table 1. Mixture proportioning of HCWA-PFA geopolymer mortars.

Batch Designation	HCWA (kg/m <sup>3</sup> )	PFA (kg/m <sup>3</sup> )	Sand (kg/m <sup>3</sup> )	Water (kg/m <sup>3</sup> )	w/b	Flow (mm)
WA50FA50	322	322	1449	219	0.34	145
WA60FA40	386	258	1449	238	0.37	140
WA70FA30	451	193	1449	245	0.38	140
WA80FA20	515	129	1449	258	0.4	140
WA90FA10	580	64	1449	271	0.42	140
WA100FA0	644	0	1449	271	0.42	145

### 2.2.2 Mechanical and durability tests

The mechanical performance of the hardened HCWA-PFA geopolymer mortars was assessed in terms of compressive, flexural, ultrasonic pulse velocity (UPV) and dynamic modulus. Compressive and flexural strength assessment was done in accordance to the testing methods prescribed in BS EN 196-1 and the reported results were based on the average of three representative samples. UPV values of the hardened samples were determined using an electrical pulse generator which measured the propagation velocities of a transmitted ultrasonic pulse and the testing procedure was done in accordance to BS EN 12504-4. Dynamic modulus of the hardened sample was measured by application of non-destructive stress in the longitudinal mode of vibration on the 100 x 100 mm end face of a prism with a path length of 500 mm is done in accordance to the methods prescribed in ASTM C 215.

Three testing parameters were employed to assess the durability performance of HCWA-PFA geopolymer mortars namely water absorption, total porosity and capillary absorption tests. Water absorption test was done based on the testing procedure prescribed in BS 1881-122 while vacuum saturation method recommended by RILEM was employed to measure the total porosity of the hardened mortar samples. Finally, the pore size distribution of the mortar sample was determined using the capillary absorption method prescribed in French Standard NF P 18354.

## 3. Results and discussions

### 3.1 Mechanical properties

#### 3.1.1 Compressive strength

Fig. 1 showed the compressive strength development of HCWA-PFA geopolymer mortars at various curing ages. It can be seen that upon 60% of HCWA replacement level, the compressive strength generally decreased with the increase in HCWA content. During early age of curing i.e. 7 days, strength development of HCWA-PFA geopolymer mortars were mostly governed by geopolymeric reaction resulted from the dissolution of aluminosilicate compounds of PFA, though the hydraulic reaction of HCWA itself is also expected to contribute towards the hardening of the resultant mortar samples. The anticipated geopolymeric gel formation in HCWA-PFA geopolymer mortars is K-A-S-H geopolymer gel since K<sup>+</sup> ions are more reactive than Ca<sup>2+</sup>. When the dry blended materials of HCWA and PFA are in contact with water, the significant amount of Arcanite mineral (12% by weight) inherently present in HCWA dissolved into potassium hydroxide (KOH), this highly alkaline mineral acts as dissolution agent and dissolve the aluminosilicate species of PFA. The dissolved aluminate and silicate ions will undergoes geopolymerization with the reactive K<sup>+</sup> ions to form the geopolymeric framework in the forms of K-A-S-H gel. Upon 28 days of curing age, similar trend was observed with the exception of the compressive strength difference between WA50FA50 and WA60FA40 mixes, where the WA50FA50 mixes exhibited higher compressive strength in comparison with WA60FA40 mixes which is a total contrast in comparison with the 7 days compressive strength results. Similar trend was observed for the accelerated curing series. During prolonged curing, besides geopolymerization and hydraulic reaction of HCWA, the strength development of HCWA-PFA geopolymer mortars is also governed by the formation of secondary C-S-H gels resulted from the pozzolanic reaction between the reactive silica from PFA and portlandite mineral formed from hydration of HCWA [13]. Therefore, higher rate of

long term strength development of HCWA-PFA geopolymer mortars can be anticipated in mixes with higher PFA content.

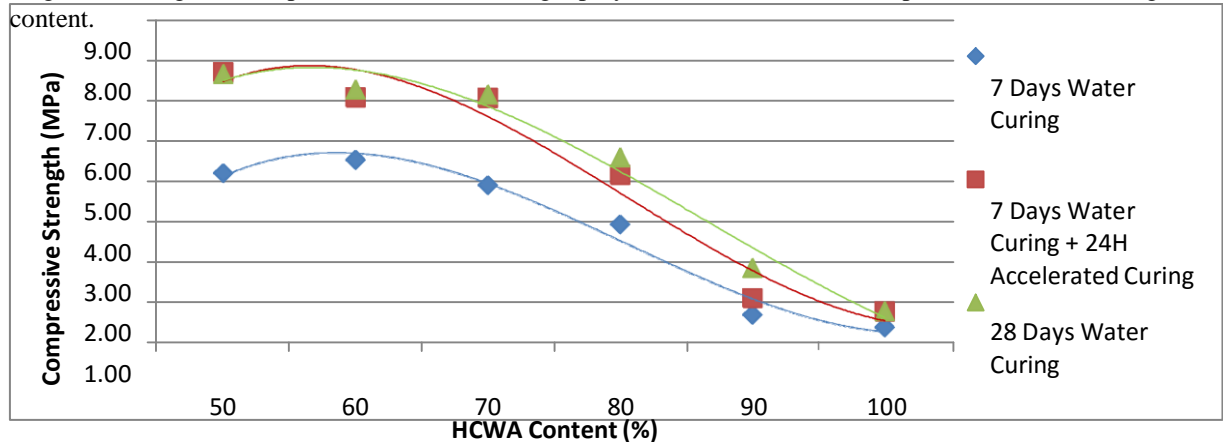


Fig. 1. Compressive strength development of HCWA-PFA geopolymer mortars.

### 3.1.2. Flexural Strength

Flexural strength of HCWA-PFA geopolymer mortars at various HCWA replacement level is shown in Fig. 2. Disregarding the curing ages, upon 60% of HCWA replacement level, flexural strength exhibited a decreasing trend. Also, WA60FA40 mixes showed the highest flexural strength for all the curing ages. At 7 days of curing, the difference in flexural strength for WA60FA40 and WA50FA50 is 29.53%. However, upon 28 days and accelerated curing, the difference is narrowed down significantly, at 4.24% and 13.69%, respectively. The aforementioned phenomenon further suggests that mixes with higher PFA content exhibited higher long term strength development, mainly due to the continuous formation of geopolymeric product and also pozzolanic reaction between the reactive silica from PFA and portlandite from HCWA which resulted in the formation of secondary C-S-H gels. Accelerated curing treatment, on the other hand, was found to have a more pronounce effect with mixes with higher PFA content i.e. WA50FA50, WA60FA40 and WA70FA30, where the flexural strength increment is comparatively higher than other mixes.

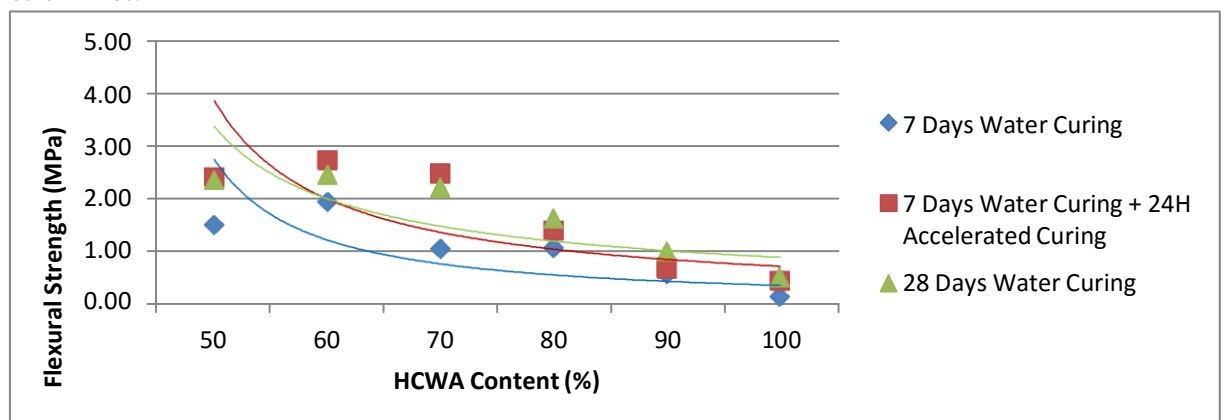


Fig. 2. Flexural strength development of HCWA-PFA geopolymer mortars.

### 3.1.3. Ultrasonic Pulse Velocity (UPV)

Table 2 showed the UPV of HCWA-PFA geopolymer mortars at various HCWA replacement level and curing ages. Consistent with compressive strength result, WA60FA40 mixes exhibited highest UPV value of 3120 m/s at 7 days of curing ages. On the contrary, upon 28 days of curing period, highest UPV value of 3467 m/s was exhibited by WA50FA50 instead. Early age strength development was mostly governed by the hydraulic reaction of HCWA and the formation of geopolymeric products in the form of K-A-S-H gels. Upon 28 days of curing, mixes with higher PFA will trigger higher degree of pozzolanic reaction which yields the formation of secondary C-S-H gels, coupled with the continuous formation of geopolymeric products, resulted in a much denser microstructure hence higher UPV value was obtained.

### 3.1.4. Dynamic Modulus

Dynamic modulus of HCWA-PFA geopolymer mortars are shown in Table 3. For all curing ages, upon 70% of HCWA replacement level, the dynamic modulus of the geopolymer mortars decreased significantly up until 100% HCWA replacement level, indicating a weak internal structure of mixes beyond 70% of HCWA replacement. Similar to compressive strength results, during early curing age, WA60FA40 showed the highest dynamic modulus value of 18.3 GPa, followed by WA70FA30 and WA50FA50 mixes with dynamic modulus value of 17.9 and 16.8 GPa, respectively. Upon 28 days of curing age, WA50FA50 exhibited highest dynamic modulus value of 21.0 GPa, followed by WA60FA40 and WA70FA30, with dynamic modulus value of 20.6 and 19.8 GPa, respectively. Similar trend was observed for accelerated curing mixes, suggesting higher geopolymeric reaction occurred in mixes with higher PFA content due to elevated heat treatment, which resulted in higher formation of K-A-S-H gel within the matrix interface and subsequently higher dynamic modulus was observed.

Table 2. Ultrasonic pulse velocity of HCWA-PFA geopolymer mortars at various curing ages.

Mix Designation	Ultrasonic Pulse Velocity (m/s)		
	7 Days Water Curing	28 Days Water Curing	7 Days Water Curing + 24H Accelerated Curing
WA50FA50	3046	3467	3217
WA60FA40	3120	3394	3276
WA70FA30	3001	3409	3216
WA80FA20	2984	3320	3078
WA90FA10	2907	3162	2908
WA100FA0	2670	3022	2785

Table 3. Dynamic modulus of HCWA-PFA geopolymer mortars at various curing ages.

Mix Designation	Dynamic Modulus (GPa)		
	7 Days Water Curing	28 Days Water Curing	7 Days Water Curing + 24H Accelerated Curing
WA50FA50	16.8	20.97	20.93
WA60FA40	18.3	20.60	19.40
WA70FA30	17.9	19.77	19.82
WA80FA20	15.2	18.10	17.94
WA90FA10	10.2	14.80	11.03
WA100FA0	7.4	10.90	9.50



## 3.2. Durability properties

### 3.2.1. Water Absorption

Water absorption test employed primarily to assess the surface porosity of the hardened HCWA-PFA geopolymer. As can be seen in Fig. 3, at early curing age i.e. 7 days, upon 60% of HCWA replacement level, water absorption of HCWA-PFA geopolymer mortars increased as the HCWA replacement level increased. The higher geopolymeric reaction in mixes with higher PFA content triggered higher amount of K-A-S-H geopolymer gel formation and resulted in a denser geopolymer matrix with lower surface permeability. Similar trend was observed during 28 days of curing and also accelerated curing regime, with the exception WA50FA50 mix exhibited lower water absorption value in comparison with WA60FA40 mix, a total reverse trend if compared with 7 days curing result, suggesting that during prolonged curing, mixes with higher PFA content not only have higher rate of enhancement in mechanical properties, also enhanced durability performance was also observed for HCWA-PFA geopolymer mortars mixes with higher content of PFA. An interesting phenomenon was observed if comparing the water absorption trend in regards with curing ages. Upon 28 days of curing and accelerated curing regime, all the HCWA-PFA geopolymer mortar mixes exhibited an increase of water absorption value if compared to their 7 days cured counterpart. It appeared that prolonged water curing resulted in inferior durability performance of HCWA-PFA geopolymer mortars. During water curing, ions interchange occurred between the water curing medium and also the alkaline pore solution presents in HCWA-PFA geopolymer mortars. As a result, the alkalinity of pore solution of the geopolymer mortars decreased and resulted in disruption of the dissolution rate of the essential geopolymer precursor species i.e. silica and alumina and hence the geopolymerization process in all. Also, it should be noted that during polycondensation reaction, excess water was expelled and it is believed that those expelled water molecules which resided near the surface of the mortar mixes resulted in a higher water penetration and hence the higher water absorption value. Similar observation was reported in author's previous publication [12].

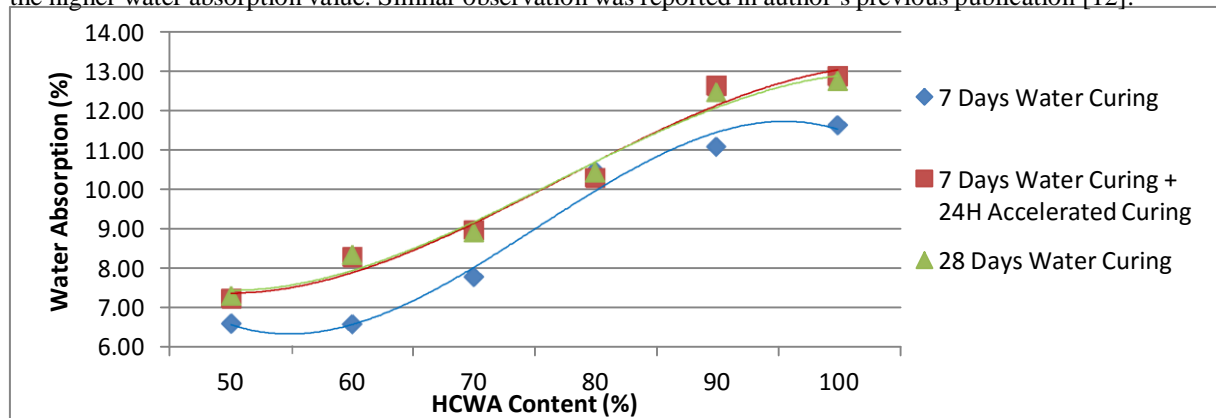


Fig. 3. Water absorption of HCWA-PFA geopolymer mortars at various ages.

### 3.2.2. Total Porosity

Fig. 4 showed the total porosity value of HCWA-PFA geopolymer mortars at various curing ages. At 7 days of curing age, WA60FA40 mix showed a reduction of 1.46% in total porosity value if compared to WA50FA50 mix, mainly due to the geopolymerization reaction and hydraulic reaction of HCWA itself. Upon 60% of HCWA replacement level, the total porosity value of the geopolymer mortars increased with the increasing of HCWA content up to 90% of total binder weight, before a reduction in total porosity value was observed for mortar mix with 100% HCWA content. The higher total porosity value observed for WA80FA20 and WA90FA10 mixes compared with WA100FA0 mix is most probably due to the low amount of PFA content in the mortar mixes which impart a low degree of geopolymerization and hence less dense microstructure. Upon 28 days and accelerated



curing, all the HCWA-PFA geopolymer mortar mixes exhibited an increase in total porosity value, consistent with the results shown in water absorption test earlier. The total porosity results implied that not only does the deleterious water curing method affect the surface porosity of the geopolymer mortars, it also adversely affects the total porosity of the resultant geopolymer mortar mixes. It should be noted that upon 28 days and accelerated curing, WA50FA50 mix showed a lower total porosity value if compared with WA60FA40 mix, a total contrast to 7 days cured mixes. The aforementioned observation further suggests that there is a higher degree of microstructure refinement during long term curing for mortar mixes with higher PFA content, mainly due to the continuous geopolymerization and also formation of secondary C-S-H gels from the pozzolanic reaction between portlandite from HCWA and reactive silica from PFA. The total porosity results were in full agreement with the mechanical properties test discussed earlier.

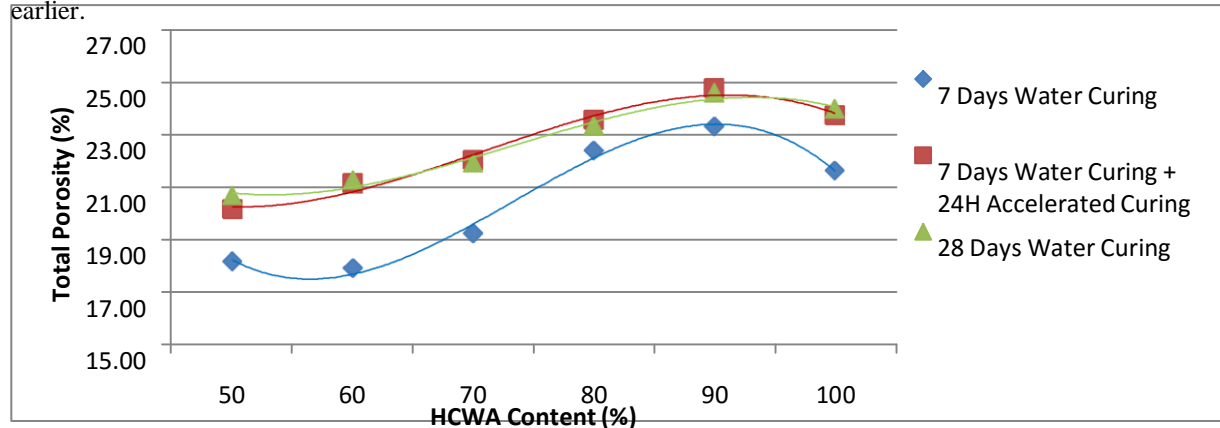


Fig. 4. Total porosity of HCWA-PFA geopolymer mortars at various curing ages.

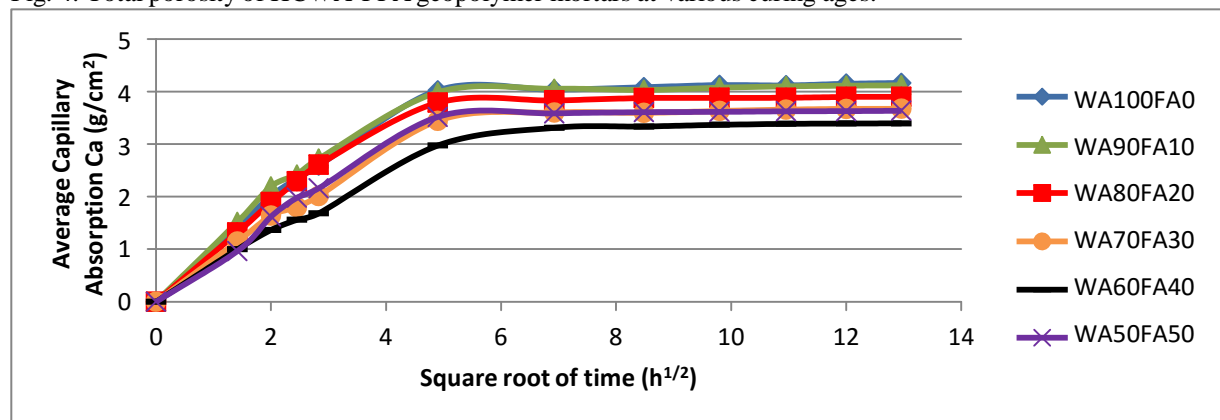


Fig. 5. Capillary absorption of HCWA-PFA geopolymer mortars.

### 3.2.3. Capillary Absorption

The pore size distribution of HCWA-PFA geopolymer mortars is shown in Fig. 5. There are two phases of pore filling phenomena that can be interpreted from the graph i.e. filling of bigger pores during the initial linear phase which lasted up to 2 days and subsequent non-linear phase which lasted up to 7 days of testing period, correspond to the filling of smaller/finer pores. Generally, for the filling of bigger pores, HCWA-PFA geopolymer mortar mixes with 90% of HCWA content showed the highest capillary absorption value, followed by mixes with 100%, 80%, 50%, 70% and 60% of HCWA content. It can be seen that HCWA-PFA geopolymer mortar mixes with small amount of PFA i.e. 10% exhibited higher degree of bigger pores filling, as compared with 0% PFA mortar mix. This

implied that the addition of PFA in small amount brings about negative effect to the pore structure of the resultant matrix, in line with the porosity results which show similar trend. On the other hand, HCWA-PFA geopolymer mortar mixes with 100% HCWA content showed highest capillary absorption value for finer pore filling, followed by mixes with 90%, 80%, 70%, 50% and 60% of HCWA. Thus, it can be said that for the curing period of 7 days, WA60FA40 geopolymer mortar mix exhibited the most desired pore structure amongst all the HCWA-PFA geopolymer mortar mixes, with the lowest capillary absorption value for both the bigger and finer pore filling phases.

#### 4. Conclusions

Following the laboratory investigation, following conclusions can be derived:

- HCWA-PFA geopolymer mortars with HCWA content of 50 and 60% consistently exhibit optimum mechanical and durability performance,
- Strength development of HCWA-PFA geopolymeric system was mainly contributed by geopolymeric reaction which culminated in K-A-S-H geopolymer gels formation during the early ages and pozzolanic reaction in which secondary C-S-H gels were formed during prolonged curing.
- HCWA-PFA geopolymer mortars with higher content of PFA i.e. WA50FA50 mortar mix exhibited enhanced long term mechanical and durability performance, mainly due to the higher degree of pozzolanic reaction.
- Prolonged water curing resulted in inferior durability performance for all HCWA-PFA geopolymer mortars.
- Arcanite mineral inherently presents in HCWA proved crucial in activating PFA by functioning as both dissolution agent for silica and alumina species in PFA and also as binding agent for the formation of geopolymer product i.e. K-A-S-H gels.

#### Acknowledgements

Fundings from Malaysian Ministry of Higher Education (203/PPBGN/6711347) and University Sains Malaysia (1001/PPBGN/814211, 304/PPBGN/6312106) are highly appreciated.

#### References

- [1] J. Davidovits, Geopolymer-chemistry and applications, Saint-Quentin, France:Institut Geopolymere, 2011.
- [2] M.O. Yusuf, M.A.M. Johari, Z.A. Ahmad, M. Maslehuddin, Strength and microstructure of alkali-activated binary blended binder containing palm oil fuel ash and ground blast-furnace slag, *Construction and Building Materials*. 52 (2014) 504-510.
- [3] J. He, Y. Jie, J. Zhang, Y. Yu, G. Zhang, Synthesis and characterization of red mud and rice husk ash based geopolymer composites, *Cem Concr Compos*. 37 (2013) 108-118.
- [4] G. Gorhan, G. Kurklu, The influence of NaOH solution on the properties of the fly ash based geopolymer mortar cured at different temperatures, *Composites B Eng*. 58 (2014) 371-377.
- [5] N. Ranjbar, M. Mehrali, A. Behnia, U. Johnson Alengaram, M.Z. Jumaat, Compressive strength and microstructural analysis of fly ash/palm oil fuel ash based geopolymer mortar, *Mater Des*. 56 (2014) 833-841.
- [6] W.K. Part, M. Ramli, C.B. Cheah, An overview on the influence of various factors on the properties of geopolymer concrete derived from industrial by-products, *Constr Build Mater*. 77 (2015) 370-395.
- [7] P. Chindaprasirt, T. Chareetart, S. Hatanaka, T. Cao, High strength geopolymer using fine high calcium fly ash, *J Mater Civ Eng*. 23 (2010) 264-270.
- [8] M. Olivia, H. Nikraz, Properties of fly ash geopolymer concrete designed by Taguchi method, *Mater Des*. 36 (2012) 191-198.
- [9] D.L.Y. Kong, J.G. Sanjayan, Effect of elevated temperatures on geopolymer paste, mortar and concrete, *Cem Concr Res*. 40 (2010) 334-339.
- [10] U. Rattanasak, P. Chindaprasirt, Influence of NaOH solution on the synthesis of fly ash geopolymer, *Miner Eng*. 22 (2009) 1073-1078.
- [11] C.B. Cheah, M. Ramli, The engineering properties of high performance concrete with HCWA-DSF supplementary binder, *Constr Build Mater*. 40 (2013) 93-103.
- [12] C.B. Cheah, W.K. Part, M. Ramli, The hybridization of coal fly ash and wood ash for the fabrication of low alkalinity geopolymer load bearing block cured at ambient temperature, *Constr Build Mater*. 88 (2015) 41-55.
- [13] C.B. Cheah, A.N. Noor Shazea, W.K. Part, M. Ramli, W.H. Kwan, The high volume reuse of hybrid biomass ash as a primary binder in cementless mortar block, *Am J Appl Sci*. 11 (2014) 1369-1378.



Sustainable Civil Engineering Structures and Construction Materials, SCESCM 2016

## Effect of curing temperature and fiber on metakaolin-based geopolymer

Januarti Jaya Ekaputri<sup>a,c,\*</sup>, Subaer Junaedi<sup>b,c</sup>, Wijaya<sup>c</sup>

<sup>a</sup>*Institut Teknologi Sepuluh Nopember, Surabaya 60111, Indonesia*

<sup>b</sup>*Universitas Negeri Makassar, Indonesia*

<sup>c</sup>*Konsorsim Riset Geopolimer Indonesia, Surabaya 60111, Indonesia*

---

### Abstract

This paper presents mechanical properties of geopolymer mortar with metakaolin as a base material. Cylindrical specimens were prepared with a diameter of 5 cm and 10 cm height. Four compositions of geopolymer paste varied with adding polyvinyl alcohol fiber (PVA) from 0% to 1% by volume of paste. After casting, steam curing method was conducted at 40°C, 60°C and 80°C for 24 hours. A control specimen was cured at room temperature. Some tests were performed for setting time, compressive strength, split-tensile, direct-tensile and porosity. It showed that the strength of fibrous specimens was 67.29 MPa at of 56 days without steam curing. When curing temperature was risen from room temperature 80°C, the strength increased up to 14% at 28 days. Ratio of split to compressive strength was about 10% when 1% fiber was applied. However, an optimum result was shown by specimens containing 0.6% fibers according to direct-tensile test. It is recommended to apply steam curing at 60°C-80°C to increase the tensile strength. © 2017 The Authors. Published by Elsevier Ltd.

Peer-review under responsibility of the organizing committee of SCESCM 2016.

*Keywords:* Metakaolin, geopolymer, PVA, curing temperature

---

### 1. Introduction

Global warming has become a major topic in the wide range of science and engineering research, within the last decade. The problem is related with exhaust emissions such as CO<sub>2</sub> from human activities. It is about 65% of

---

\* Corresponding author. Tel.: +0-000-000-0000 ; fax: +0-000-000-0000 .

E-mail address: [yckim@pknu.ac.kr](mailto:yckim@pknu.ac.kr)

greenhouse gases caused by CO<sub>2</sub> where Portland cement production contributes in a range of 7-8% [1]. Therefore, it is necessary to obtain green concrete materials as an innovative solution. One of the solutions is geopolymer manufacture, which is also known as zero-cement concrete. Most of geopolymer mixtures use by-products in their composition. Fly ash is the most favorable material for making geopolymer concrete [2]. Mud, clay and slag are also utilized as the raw material in geopolymer binders [3-5]. However, in Indonesia, some by products such as fly ash and bottom ash are considered as hazardous materials. It comes to being the application limitation to develop geopolymer products from laboratory to industry scale. In addition, physical characters of by-product vary in some aspects such as origin materials treatment, shape, size, etc. [6-7]. Kaolin is one of the natural pozzolanic materials, which is rich in silica and alumina. With a proper calcination, metakaolin can be produced from 75%-80% by mass of kaolin, which contains soluble silica. Since it consists of reactive oxides, metakaolin requires low concentration of alkali activator [8-9].

In this paper, polyvinyl alcohol fiber (PVA) is introduced to improve tensile strength of metakaolin geopolymer paste. In addition, variations of curing methods were also introduced to investigate the effect of temperature to increase compressive strength. Some influential factors to the mechanical strength of fresh and hardened paste were analyzed and discussed comprehensively. Therefore, this study will be a bench-mark formalization of environmental friendly material using kaolin as one of the alumina-silicate sources.

## 2. Experiment

### 2.1. Materials and Mix Proportions

Kaolin with 2.5 g/cm<sup>3</sup> of density adopted in this study was obtained from Bangka Belitung, Indonesia. Its chemical composition is listed in Table 1.

Table 1 Chemical composition of source materials

Oxides (%)	SiO <sub>2</sub>	Al <sub>2</sub> O <sub>3</sub>	Fe <sub>2</sub> O <sub>3</sub>	CaO	MgO	Na <sub>2</sub> O	K <sub>2</sub> O	TiO <sub>2</sub>	MnO <sub>2</sub>	SO <sub>3</sub>	LOI
	50.26	43.00	0.73	0.04	0.12	0.04	0.57	0.28	0.01	4.72	4.72

Calcination method to activate raw material from kaolin to metakaolin is based on an experimental work developed by Triani [15]. Kaolin with particle size of 75 μm was immersed and stirred in distilled water for 10-15 minutes. It was kept in room temperature for 24 hours until sedimentation occurred. This precipitated materials were not used for making the geopolymer mixture since it may contain unreactive quartz. The top part of silt was collected to be dried in oven. Calcination process is illustrated in Fig. 1 as temperature history of furnace setting. Temperature target of 700°C was set constant for six hours. Metakaolin was then pulverized until its maximum particle size of 75 μm as shown in Fig 2.

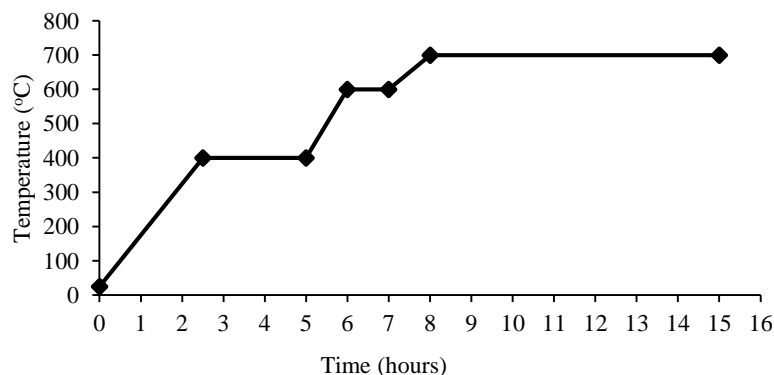


Fig. 1. Temperature History of Kaolin Calcination



Fig. 2. Metakaolin

Alkali activators consisted of sodium hydroxide and sodium silicate. Flake form of sodium hydroxide with 98% purity was prepared for concentration of eight molar. Sodium silicate ( $\text{SiO}_2/\text{Na}_2\text{O} = 2.0$  and solid content 55%) was mixed with sodium hydroxide with a mass ratio of 56:44. Both liquids were mixed together, prepared one day before mixing with metakaolin and kept in environmental control room. Ratio of metakaolin to alkali activators of 1:1 was used for all variations.

PVA-RECS15 as shown in Fig.3 varied with 0%, 0.3%, 0.6% and 1% by paste volume. Fresh paste became more hardened and difficult to cast if it contained more than 1% of PVA. Properties of fibers are listed in Table 2.

All variations of paste were cast in cylindrical molds with 50 mm in diameter and 100 mm in length. Immediately after casting, the specimens were covered with plastic and then cured at a steam chamber with temperature varied at 40°C, 60°C and 80°C for 24 hours. After steam curing, specimens were moist-cured at room temperature until specific age for mechanical and physical testing.

Table 2 Fibers Properties

Physical Properties	Specification
Diameter	38 $\mu\text{m}$
Length	8mm
Density	1.3 gr/cm <sup>3</sup>
Tensile strength	1600 MPa
Bending strength	40 GPa
Melting Point	225°C
Absorption	Less than 1 %



Fig. 3. PVA-RECS 15

Variations of mix proportion and curing temperature are provided in Table 3.

Table 3. Specimen variations

No.	Code	Curing Temperature (°C)	PVA (% Volume)
1	G-0-25		0
2	G-0.3-25	25	0.3
3	G-0.6-25		0.6
4	G-1-25		1
5	G-0-40		0
6	G-0.3-40	40	0.3
7	G-0.6-40		0.6
8	G-1-40		1
9	G-0-60		0
10	G-0.3-60	60	0.3
11	G-0.6-60		0.6
12	G-1-60		1
13	G-0-80		0
14	G-0.3-80	80	0.3
15	G-0.6-80		0.6
16	G-1-80		1

## 2.2. Testings

Setting time for fresh paste was conducted according to ASTM C191 [16]. Compression test to obtain the strength of some specimens at 3, 7, 14, 21, 28 and 56 days was conducted according to ASTM C39 [17]. To obtain the effect of fiber on density of specimens, which the specimens are categorized lightweight concrete, weight and volume of specimens were examined according to ASTM C1693-11 [18]. Splitting test according to ASTM C 496 [19] was conducted for cylindrical specimens at 28 days. Direct tensile test according to CRD-C 260-01 [20] was conducted for dog bone-like shape specimens at 28 days. Porosity test was also performed at 28 days to obtain portions of closed and open porosity as a function of total porosity.

## 3. Results and Discussions

### 3.1. Setting Time

Both initial setting time and final setting time were carried out to observe the effect of fiber to setting time of paste. The result is provided in Fig 4.

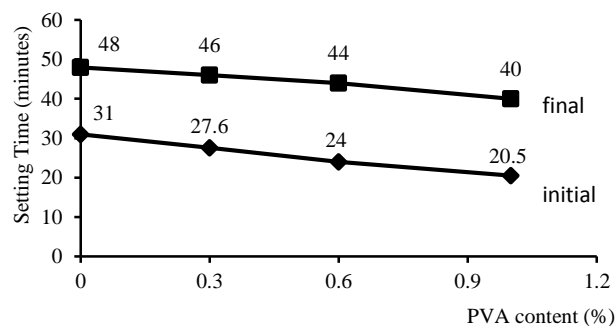


Fig 4. Setting Time

More addition of PVA fibers caused faster initial and final setting time. It is because of more fiber in mixtures turns the mixtures to be more viscous resulting in the decreasing of workability, and the setting becomes quicker. It has a good agreement as a result conducted by Noushini [21]. In this case, for larger scale of application, superplasticizer and retarder are necessary to ensure the mixture workability.

### 3.2. Density

Fig 5. describes the addition of fiber and curing temperature show less effect to density of geopolymer paste. The average density is about 1800 kg/m<sup>3</sup>, which indicates that geopolymer paste is a sort of lightweight concrete. In addition, it was due to the amount of fiber was added at most only 1% by paste volume, and water absorption of fiber is less than 1% of the fiber mass. As a result, thee of PVA does not affect the weight to the volume of mortar geopolymer [22].

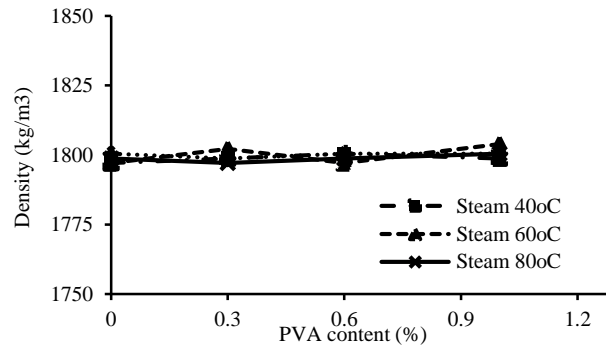


Fig 5. Relation of density and fiber content at different curing

### 3.3. Compressive Strength

Compressive strength test performed at the age of 3,7,14,21,28 and 56 days. An average from three identical specimens was determined for each variation. The results for each variation can be seen in Figure 6 to Figure 9.

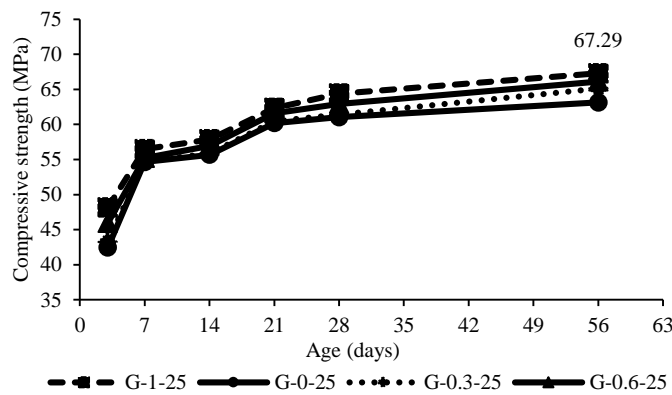


Fig 6. Compressive strength of specimens cured at room temperature

In Fig. 8, it is discovered that adding fiber increases the compressive strength. However, the fiber has less effect to contribute the strength at early age. The strength significantly increases up to seven days. After one week, it increases gradually and still has a tendency to improve until 56 days. Specimens containing 1% of fiber shows the highest compressive strength from the early age until the later age.

An effect of steam curing at 40°C and 60°C with different fiber content is presented in Fig. 7 and Fig 8 respectively. The increase of compressive strength occurred at the early age due to the acceleration of geopolymerization reaction. At 60°C, the strength increased up to 21 days, which was faster than the specimens cured at room temperature and at 40°C. The geopolymeric reaction of metakaolin paste is revealed to be accelerated strongly according to the curing

temperature regardless of the fiber content. Geopolymeric reaction is similar to hydration reaction in cement portland, which occurs rapidly due to heat treatment [23].

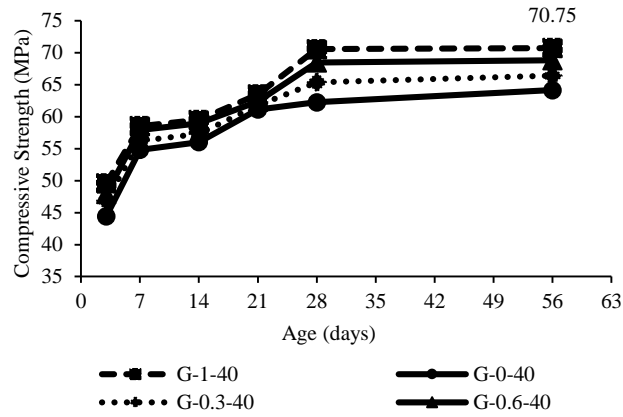


Fig 7. Compressive strength of specimens cured at 40°C

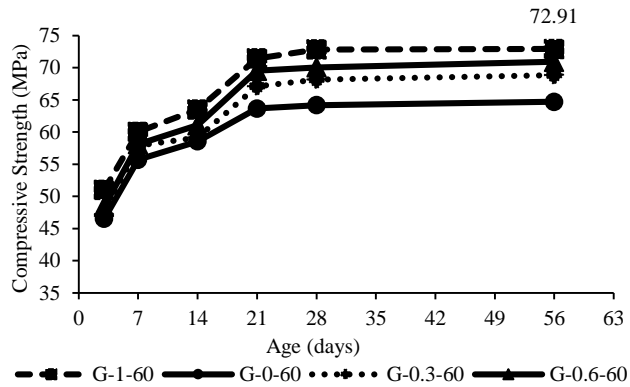


Fig 8. Compressive strength of specimens cured at 60°C

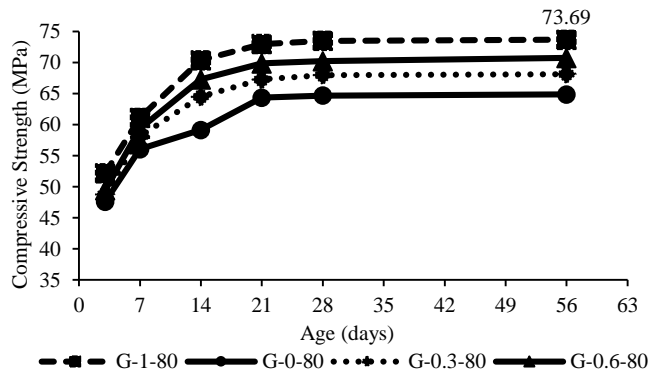


Fig 9. Compressive strength of specimens cured at 80°C



Corresponding to specimens cured at 40°C and 60°C, Fig 9 shows the influence of steam curing at 80°C to the strength. Mechanical strength increased along with fiber content and age of specimens. At 80°C, the strength increased rapidly until 14 days and gradually increased slowly until 21 days. It can be compared with Fig. 6, the compressive strength of specimens at 28 days, which contains 1% of fiber rises up to 14%. It is in accordance with an experimental study conducted by Hardjito [24] using fly ash as the raw material. In his research, the optimum strength of fly ash-based geopolymer concrete was achieved at 75°C.

### 3.4. Splitting Tensile Strength

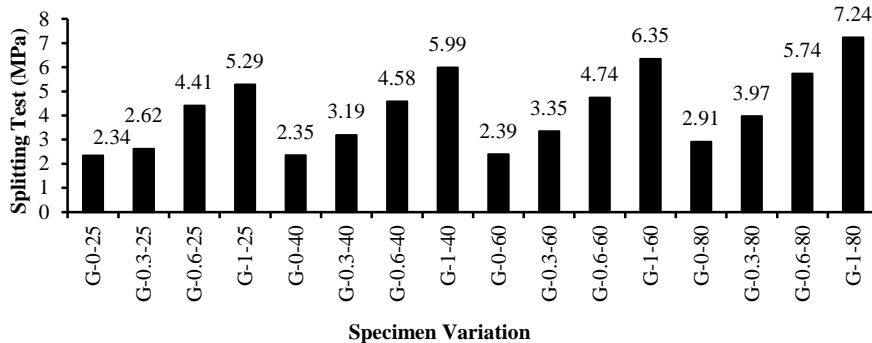


Fig 10. Splitting test of specimens cured at different temperature

Fig. 10 shows the result of splitting test at 28 days. As expected, influence of fiber content indicated more than the heat effect to the strength. It is shown by s G-1-80 containing 1% PVA 80°C. It also implies that fiber has more contributions to tensile strength than compressive strength.

### 3.5. Direct Tensile Strength

Stress-strain relation of dog bone-like specimens is provided in Fig. 11 to Fig. 14. It was predicted that at higher curing temperature, the tensile strength tended to rise. The absence of fiber showed less effect on specimen’s ductility. Fiber content increased the ductility cured at the same condition. However, ductility of specimens containing fiber had a tendency to decrease at higher temperatures. Stress hardening was observed for specimens with 0.6% and 1% of fiber. It indicated that after crack occurred, tensile stresses were transferred to the fiber. Because of fiber, tensile strength is greater than the paste causing hardening phenomenon. This means that the PVA fiber starts to control the crack after paste failure to resist tensile load [26].

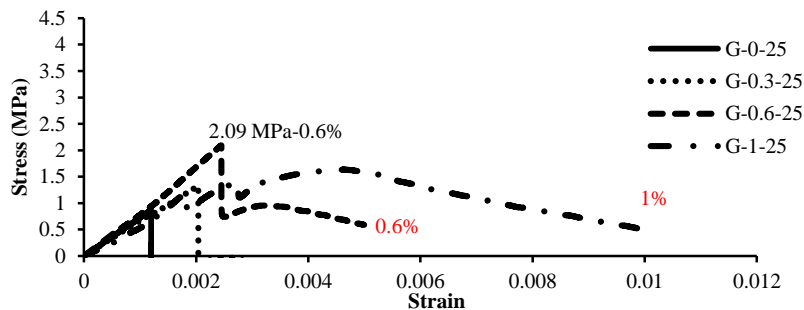


Fig 11. Tensile strength cured at room temperature

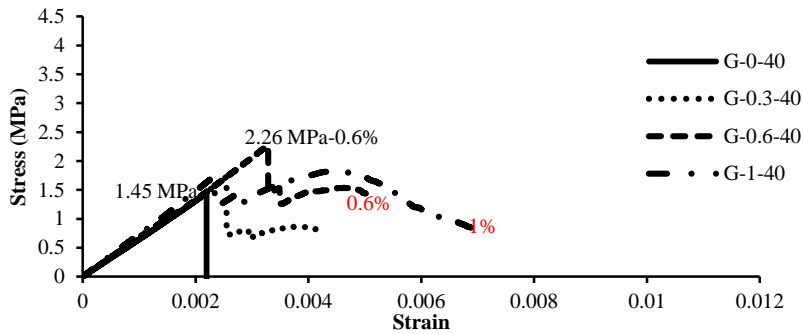


Fig 12. Tensile strength cured at 40°C

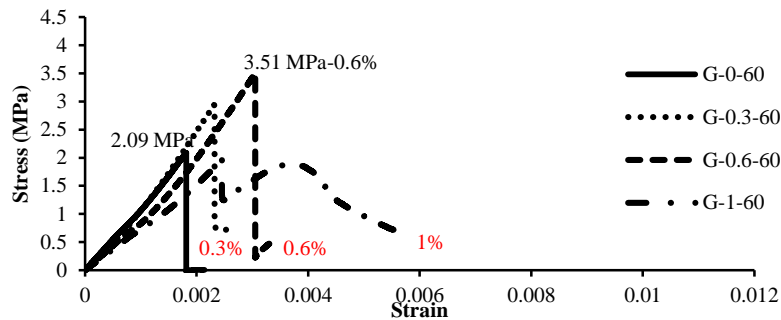


Fig 13. Tensile strength cured at 60°C

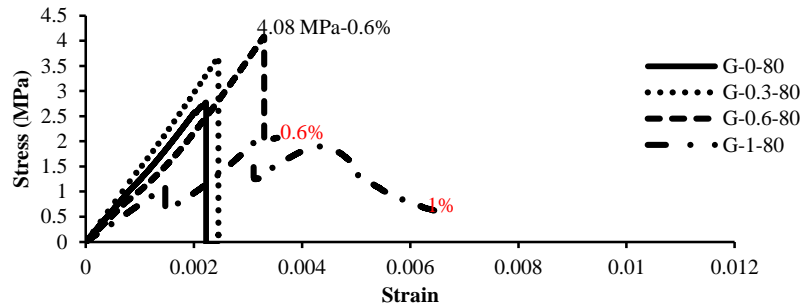


Fig 14. Tensile strength cured at 80°C

A relation of compressive strength and tensile strength at 28 days is represented by some factors. Some relationships such as  $f_{split}/f_c'$ ,  $f_t/f_c'$  and  $\Delta f_t/\Delta \epsilon_t$  are provided in Fig. 15, Fig. 16 and Fig. 17 respectively. Splitting strength,  $f_{split}$ , compressive strength,  $f_c$ , and tensile strength  $f_t$  represents mechanical strength of specimens. Elastic stiffness is corresponded to a ratio of tensile stress ( $\Delta f_t$ ) and tensile strain ( $\Delta \epsilon_t$ ) which is determined before cracks occur.

In Fig. 15, it can be seen that fiber content has more contributions to increasing the ratio of tensile strength to compressive strength. Less influence to this ratio was exhibited by heat effect. This indicated that the increase of split tensile strength had a linear correlation to the increase of compressive strength. At room temperature, this ratio rose from 3% to 9%. At 60°C, it increased up to 9.9%. However, in Fig. 16, there is an optimum point where addition of fiber at 0.6% shows the highest ratio of tensile to compressive strength. Since 1% of fiber resulted in difficulty of

casting, direction of fiber in the paste caused the specimens became less uniform. Fig. 17 shows that the ratio of  $\Delta f_t$  to  $\Delta \epsilon_t$  tends to descend along the increasing of fiber content and curing temperature. It reveals that greater stiffness generates brittleness of geopolymer paste.

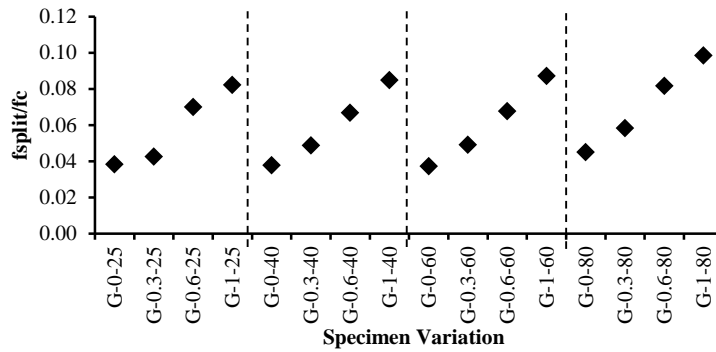


Fig 15. Ratio of splitting strength to compressive strength

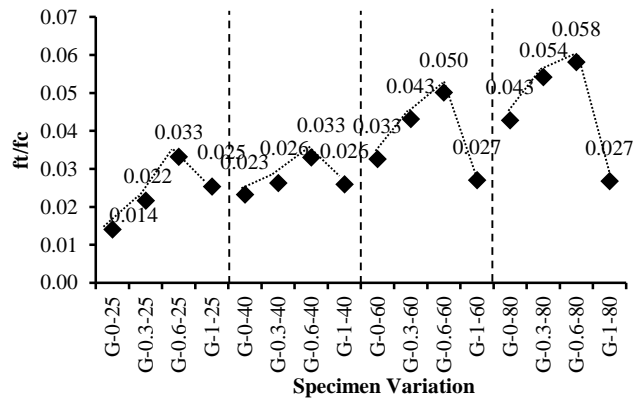


Fig 16. Ratio of tensile strength to compressive strength

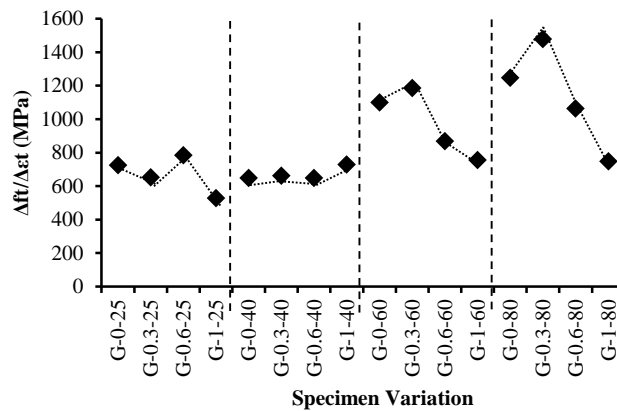


Fig 17. Ratio of tensile strength to tensile strain in elastic condition

### 3.6. Porosity

Fig.18 shows some relations of porosity of specimens containing 0% and 1% fiber. Curing temperature tended to decrease the total pores, which generated more strength. Surprisingly, fiber content showed less effect to the open porosity. In general, fiber increases the open porosity, resulted in denser of mixture and decreasing strength in certain proportion. Results in Fig. 18 reveal that PVA fiber contributes to decreasing of total porosity without affecting density of geopolymer paste.

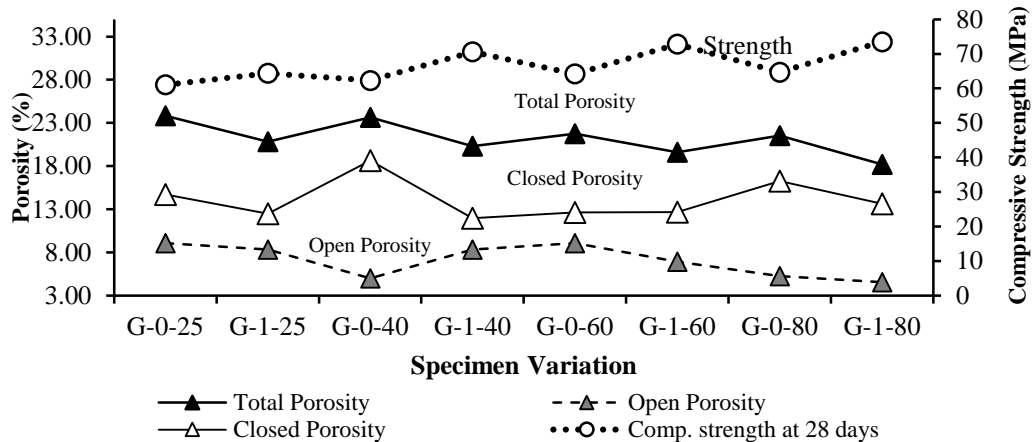


Fig 18. Porosity

## 4. Conclusions

- PVA fiber causes setting time becomes faster due to workability of fresh paste.
- Adding PVA fiber to 1% by paste volume shows less effect on density of paste.
- Curing temperature at 80°C generates the highest compressive strength of paste containing 1% of fiber.
- Tensile stress is contributed mostly by the presence of fibers, which expanded the ductility of paste. However, at higher curing temperature, even though the tensile stress increases, heat effect decreases the ductility.
- Stiffness of paste increases along with heat effect to the paste. However, the effect the fiber content contributes to decreasing of stiffness.
- Porosity has a strong relation with compressive strength. PVA fibers contribute to decrease the total pores which support the strength of paste.
- It is recommended to apply PVA fiber up to 0.6% by volume to increase the ductility of geopolymer paste.

## References

- [1] McCaffrey, Climate Change and the Cement Industry, Enviromental Special Issue 2002 (eds.), GCL Magazine, London.
- [2] K. Zerfu and J.J. Ekaputri, Review on Alkali-Activated Fly Ash-Based Geopolymer Concrete, MSF 841 (2016) 162-169
- [3] J. J. Ekaputri, Triwulan, S. Junaedi, Fansuri and R. Bayuaji, Light Weight Geopolymer Paste made with Sidoarjo Mud (Lusi), MSF 803 (2015) pp 63-74
- [4] M. M. A. B. Abdullah, M. Md Mohtar, L. Y. Ming, M. F. M Tahir, K. Hussin, and J. J Ekaputri, Flood Mud as Geopolymer Precursor Materials: Effect of Curing Regime on Compressive Strength, AMM 815 (2015) pp 177-181
- [5] A. N. Hashim, K. Hussin, N. Begum, M. M. A. B. Abdullah, K. A. Razak and J. J. Ekaputri, Effect of Sodium Hydroxide (NaOH) Concentration on Compressive Strength of Alkali-Activated Slag (AAS) Mortars, AMM 754-755 (2015) 300-304.
- [6] J. J. Ekaputri, M. B. Ulum, Triwulan, R. Bayuaji, T. E. Susanto and M. M. A. B. Abdullah, A Comprehensive Characterization and Determination of Fly Ashes in Indonesia using Different Methods, AMM. 754-755 (2015) pp 320-325
- [7] N. Ratni, J.J. Ekaputri, M. Bahrul Ulum, Triwulan and P. Suprobo, Characterization of Fly Ash on Geopolymer Paste, MSF 841 (2016) pp 118-125
- [8] S. Junaedi, A. Haris, N. Nurhayati, A. Irhamsah and J.J. Ekaputri, The Influence of Si:Al and Na:Al on the Physical and Microstructure Characters of Geopolymers Based on Metakaolin, MSF 841 (2016) 170-177

- [9] D.N.D. Triani, J.J. Ekaputri, Triwulan, S. Hardono and T. E. Susanto, Application of Pozzolan as Materials of Geopolymer Paste, MSF 841 (2016) pp 111-117
- [10] J. Davidovits, Properties of Geopolymer Cements, Proceedings First International Conference on Alkaline Cements and Concretes, Scientific Research Institute on Binders and Materials, KIEV State Technical University, Kiev, Ukraine, 1994, pp 131-149.
- [11] J. J. Ekaputri, K. Maekawa and T. Ishida, The Use of Geopolymerization Process for Boron Fixation in Fly Ash, 7th ISCC and the 11th ICACTSD, Jinan, China, 2010, pp 225-232.
- [12] Song, Durability of Fly Ash based Geopolymer Concrete Against Sulphuric Acid Attack, Proceeding of International Conference On Durability of Building Materials and Components, Lyon, France, 2005.
- [13] R. Bayuaji, M. S. Darmawan, B. Wibowo, N. A. Husin, S. Subekti and J. J. Ekaputri, The Influence of Chloride Environment on Compressive Strength of Geopolymer Concrete with Fly Ash using Taguchi Approach, AMM 754-755 (2015) pp 400-405
- [14] T. W. Cheng and J. P. Chiu, Fire Resistant Geopolymer Produced by Granulated Blast Furnace Slag, Mineral Eng.16, 2005, 205-210
- [15] J. J. Ekaputri, Triwulan and T. E. Susanto, Lightweight Geopolymer Paste made with Sidoarjo Mud, the 6th ACF 2014, 21-24 September, Gangnam, Seoul, South Korea, pp. 1053-1057
- [16] ASTM C 191, Standard Test Methods for Time of Setting of Hydraulic Cement by Vicat Needle, ASTM International, 2013
- [17] ASTM C1693, Standard Specification for Autoclaved Aerated Concrete (AAC), ASTM International, 2009
- [18] ASTM C 39, Standard Test Method for Compressive Strength of Cylindrical Concrete Specimens, ASTM International, 2013
- [19] ASTM C 496, Standard Test Method for Splitting Tensile Strength of Cylindrical Concrete Specimens, ASTM 2011
- [20] CRD-C 260-01, Standard Test Method for Tensile Strength of Hydraulic Cement Mortars, 2001
- [21] A. Noushini, B. Samali and K. Vessalas, Influence of Polyvinyl Alcohol Fibre Addition on Fresh and Hardened Properties of Concrete, Proceeding of EASEC 2013 pp: B-5.
- [22] J. J. Ekaputri, H. Limantono, Triwulan, T. E. Susanto, and M. M. A. B. Abdullah, Effect of PVA Fiber in Increasing Mechanical Strength Paste Containing Glass Powder, KEM 673 (2016) pp 83-93
- [23] J. J. Ekaputri, K. Maekawa, T. Ishida, Experimental Study on Internal RH of BFS Mortars at Early Age, MSF 857, pp 305-310
- [24] D. Hardjito and B. V. Rangan, Factors Influence the Compressive Strength of Fly Ash- Based Geopolymer Concrete, Civil Eng. Dimension 6, 2, pp 88-93.
- [25] M. Ohno and V. Li, A Feasibility Study of Strain Hardening Fiber Reinforced Fly Ash – Based Geopolymer Composites, Cons. and Build. Ma. 57, pp 163-168.
- [26] W. Hu, Experimental Research on the Mechanical Properties of PVA Fiber Reinforced Concrete, Research Journal of Applied Sciences, Eng. and Tech. 5, 18, pp 4563-4567.



Sustainable Civil Engineering Structures and Construction Materials, SCESCM 2016

## Geopolymer concrete: a sustainable cement based concrete for the future

Jay Sanjayan<sup>a,\*</sup>

<sup>a</sup>*Department of Civil and Construction Engineering, Swinburne University of Technology, P O Box 318, Hawthorn, Victoria 3122, Australia*

---

### Abstract

Portland cement manufacture creates carbon emissions at the rate of 1 ton per ton of cement produced and is second only to fossil fuels. Commercial implementations of concretes produced without Portland cements is starting to take place in recent years. The paper outlines the major technological advances in Geopolymer Concrete which is made without any Portland cement in the concrete mix.

Geopolymer is a broad term currently used to describe the alkali activated fly ash, slag or combination of both. This paper outlines the authors and his co-workers work in the area during the last two decades. These cements have great potential to be used as a building material alternative to Ordinary Portland Cement (OPC) concrete because their strength, stiffness and other mechanical properties are comparable to OPC concrete. This new generation of concrete is currently attracting increasingly widespread attention because their manufacture does not directly create carbon emissions like OPC concrete. The main base materials for these concretes are slag and/or fly ash, which are industrial by-products from blast furnace and coal power stations. The paper outlines the past research in this area and future research needs to fully utilize this new material effectively in construction.

© 2017 The Authors. Published by Elsevier Ltd.

Peer-review under responsibility of the organizing committee of SCESCM 2016.

*Keywords:* Geopolymer Concrete; Alkali Activated Concrete; Fly Ash; Slag; Sustainability; Construction Materials.

---

---

\* Corresponding author. Tel.: +0-000-000-0000 ; fax: +0-000-000-0000 .

*E-mail address:* [jsanjayan@swin.edu.au](mailto:jsanjayan@swin.edu.au)

Author contact details: Tel: +61 3 9214 8034; Email: [jsanjayan@swin.edu.au](mailto:jsanjayan@swin.edu.au)

1877-7058 © 2017 The Authors. Published by Elsevier Ltd.

Peer-review under responsibility of the organizing committee of SCESCM 2016.

## 1. Introduction

It is estimated 22 billion tons of concrete is used worldwide per annum, and this Fig. is increasing rapidly with the current worldwide infrastructure boom. Concrete is the highest consumed material far exceeding the coal, oil and steel all of which are used in quantities which are unsustainable in the long term. Almost all the materials to manufacture concrete are virgin materials mined from the earth. Recycled concrete is a term used for concrete containing aggregates which are crushed concrete, but the recycled concrete making still requires virgin cement and admixtures. In fact, crushed concrete is often weaker than conventional aggregate, hence requires higher cement content to compensate for strength development resulting in concretes with higher carbon emissions. Crushed concretes are better utilised as road base or other aggregate substitutes where it does not lead to increased carbon emissions.

Fig. 1 shows the most highly consumed materials by human beings (these Fig.s are compiled by the author from various sources). Consumption of these virgin materials at these levels is unsustainable and any discussion on the sustainable future should include sustainable alternatives to these materials.

Carbon emission due to concrete manufacture is fourth largest contributor to man-made global carbon emissions, which falls behind only to oil, coal and natural gas. Carbon emissions due to concrete manufacture range between 0.3 to 0.4 ton of CO<sub>2</sub> per cubic meter of concrete depending on the type of concrete as estimated by Flower et al (2005) shown in Fig. 2. The Fig. shows the carbon emissions of various grades of concrete and relative contributions of each of constituents of concrete for the carbon emissions. However, this will not directly translate into increased price due to carbon tax. Due to very generous allowances for untaxed emissions, only a fraction of the full cost of the carbon tax of \$23 will be passed on to the price of concrete, which would be negligible (about 20 cents per cubic meter of concrete).

Portland cement is the dominant source of carbon emissions in all of the concrete mixes. Major part of carbon emissions in Portland cement manufacture comes from the limestone releasing the CO<sub>2</sub> which would otherwise be buried in the ground; this is similar to CO<sub>2</sub> emissions from coal and oil. It can be seen in Fig. 2 (Flower et al, 2005) that the percentage of the total carbon emissions associated with Portland cement increases considerably in the higher strength concrete mixes. However, the other processes and materials in concrete still generate substantial amounts of carbon emissions and must be considered in the calculation of total emissions estimates. It is also clear that if the emissions of a concrete are to be reduced significantly, Portland cement is the main component that should be targeted.

Carbon emissions due to Portland cement in concrete can be reduced by partially replacing with supplementary cementitious materials (SCMs), which are industrial by-products with little carbon emissions. Most commonly used SCMs are fly ash, ground granulated blast furnace slag (GGBFS) and condensed silica fume. These SCMs have long track records in construction in many countries, typically well over three decades.

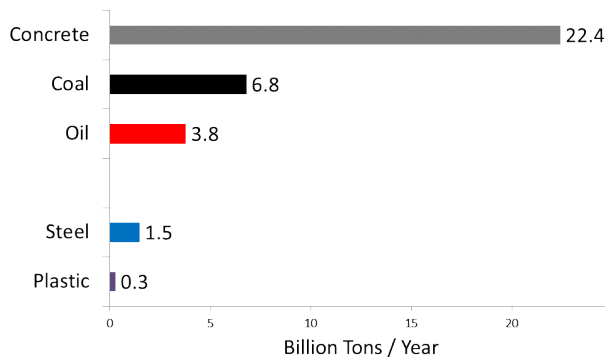


Fig. 1: Highest Consumed Materials

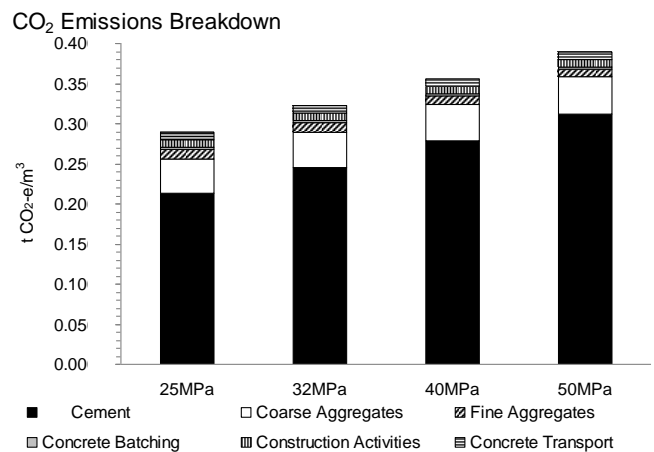


Fig. 2: CO<sub>2</sub> Emissions Generated by Concretes

To investigate two of the methods by which the amount of CO<sub>2</sub> generated by concrete can be reduced, four mixes are considered with binders including SCMs. The first two mixes (25 MPa and 32 MPa) have 25% of the Portland cement replaced by fly ash. The second two mixes (25 MPa and 32 MPa) have 40% of the Portland cement replaced by GGBFS. These percentages are chosen because they are commonly applied in construction projects in Australia. It is also noted that large cement replacements in lower grade concretes such as these are not desired by construction industry due to construction process being slowed down by slow early strength development of these concretes. The most commonly used standard strengths defined in Australian Standards (AS1379) are 25 MPa and 32 MPa concretes. Fig. 3 (Flower et al., 2005) show the results of this analysis.

Portland cement is the dominant source of emissions in all of the concretes, blended or otherwise. The fly ash blended concretes show reduced CO<sub>2</sub> emissions (13–15%), but it is the GGBFS blended concretes that show more substantial reductions (22%). This is because high percentage of GGBFS can be included in a blended mix without changing the engineering properties of the concrete, due to its natural cementitious properties. So while GGBFS has a higher material emission factor than fly ash, it can replace more cement, which leads to lower total emissions.

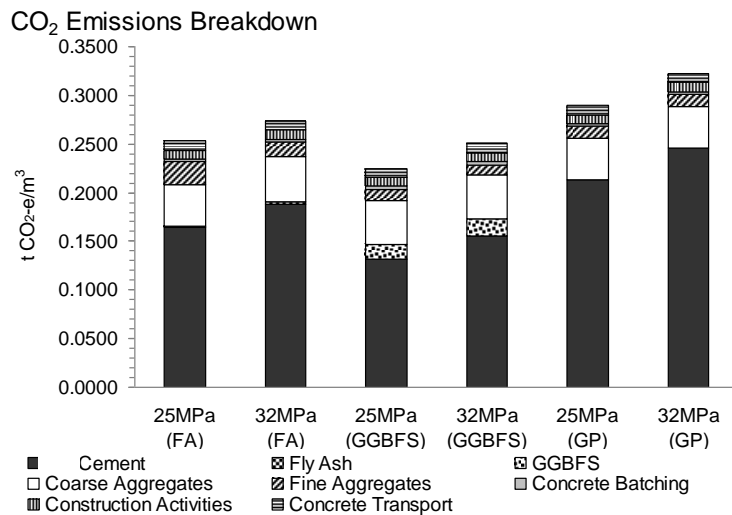


Fig. 3 CO<sub>2</sub> Emissions Generated by SCM Blended Cement Concretes

In recent years, high performance concrete has become popular in construction due to its superior mechanical properties, such as high elastic modulus and high compressive and tensile strengths, and superior durability in variety of environments. The high performance concrete utilises about twice the amount of cement to produce the same volume of concrete as conventional concrete. Widespread use of high performance concrete would significantly increase the greenhouse gas emission due to concrete construction. High strength concrete is usually used in construction to reduce the size of compression members (eg. columns), thereby reducing the amount of concrete used. However, often in precast or prestressed concrete constructions, high strength concrete is used for obtaining high early strengths, which may not be necessary for service conditions. The high strength concrete is commonly produced by reducing the water/cement ratio to around 0.35 to 0.3, but in some instances as low as 0.2. At these levels of water/cement ratios a large part of the cement used is left unhydrated, effectively using the cement as a filler material. Considering the environmental and other costs of cements, this is a waste of resources. Research needs to be focused in this area to make high performance concrete without the wastages of Portland cement. This paper summarises the work in the area of low carbon concretes carried out in the last two decades, primarily by the author and his co-workers.

## 2. Blended Cements

Many research studies have demonstrated that high strength, high performance concrete can be made with slag blended cements, with slag replacement of Portland cements of 30, 50 and 70% levels without any loss of the



advantages the high performance concrete offers (Sioulas and Sanjayan, 1997). Some of the advantages of using slag-blended cement in high performance are summarised as below:

- Using slag replacements, such as a 50% replacement of Portland cement, high performance concrete can be made with the same level of consumption of Portland cement as in the conventional concrete. A higher percentage replacement, such as 70%, will even reduce the Portland cement usage in high performance concrete.
- Due to the high levels of Portland cement usage in high performance concrete, high levels of heat are generated by hydration in high performance concretes increasing the risk of thermal cracking. With the use of slag replacements, the risk of thermal cracking can be reduced (Sioulas and Sanjayan 2000a).
- High performance concretes made with slag-blended cements offers superior durability, especially in marine applications.

However, it should be noted that the use of slag-blended cements also comes with some limitations. Since the hydration of slag relies on the release of  $\text{Ca(OH)}_2$  from the hydration of Portland cement, the rate of strength development of concretes made with blended cements are very low (Wainwright,1986). Also, as the hydration of slag occurs over an extended period of time, the extended curing period is essential to obtain the desirable properties. While the standard test cylinder specimens are kept in 100% moist conditions, the in-situ concretes do not receive the same treatment. As a result, there exists a significant difference between the in-situ strength properties of concrete made with slag blended cements and the control cylinders (Sioulas and Sanjayan, 1998). Sanjayan and Sioulas (2000b) found that lack of strength development in in-situ concrete is due to self-desiccation phenomenon which is caused by lack of access for curing water in the middle of large concrete members, resulting in significant part of GGBFS left un-hydrated.

The use of slag is sometimes viewed with suspicion due to its tendency to develop a distinct blue-green coloration a few days after casting of concrete. This discoloration can cause some degree of concern, usually associated with speculation of adverse consequences. Research studies have demonstrated that these concerns are unfounded and the colourations are no indications of inferior engineering properties (Sioulas and Sanjayan, 2001).

There are some in construction industry is of the view that concrete containing slag blended cement have higher drying shrinkage than concretes made with Type GP cement. This is a result of the peculiar test method used by the Australian standard (Sanjayan and Aly, 2005). The Australian test method for shrinkage (AS1012.13) requires the measurements to commence after 7 days of moist curing of the samples. However, during the first 7 days, slag concretes undergo expansions of the order of 100 microstrains, which would reduce the 56 days shrinkage results by that amount (Fig. 4) (Aly and Sanjayan, 2008). This expansion is not included in the Australian test method. However, other international test methods such as ASTM C157 method commences after 1-day, hence the slag blended concretes are not disadvantaged.

Further, for structural designers, the main issue is cracking due to shrinkage rather than the drying shrinkage itself. Concretes with slag blended cements develop elastic modulus at a slower rate than Type GP cement concretes. As a result, the less stress is generated in slag blended cement concretes, as compared to Type GP cement concretes for the same level of shrinkage. Models for elastic modulus, creep, shrinkage and tensile strength development of concretes containing slag blended cements are available for design calculations (Aly and Sanjayan, 2009). When using these models to calculate cracking of concrete and cracks widths, it is evident that concretes containing slag blended concretes are no different to Type GP cements.

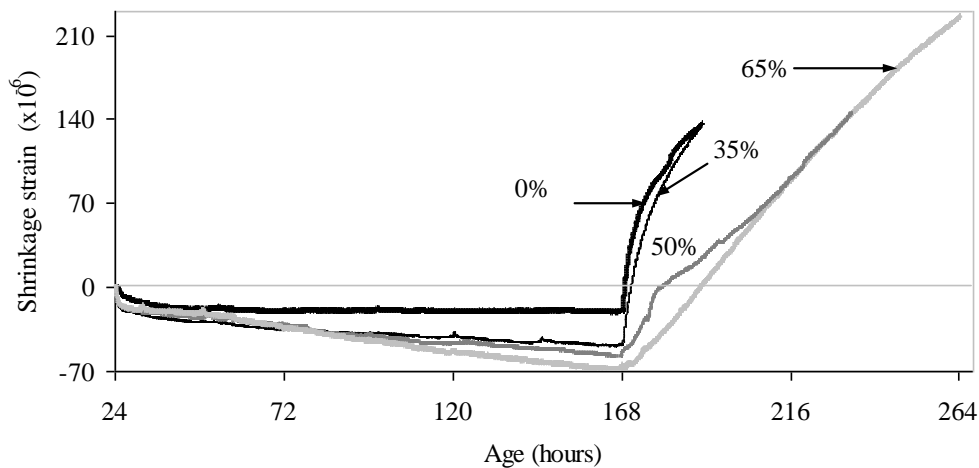


Fig. 4 Free expansion and shrinkage for all mixes (% indicates slag level) (Aly and Sanjayan, 2008)

### 3. Geopolymer / Alkali Activated Cements

These types of binders are Portland cement free, and produced without major capital investments in cement plants. They typically use fly ash, slag (ground granulated blast furnace slag) or metakaolin as the main resource, and combine small amounts of alkaline activators such as sodium silicate and/or sodium hydroxide. In some instances, slag and fly ash are used in combination, and sometimes small amounts of Portland cement may also be used. The chemical structure of the binder can vary significantly depending on the source materials and the activators. The alkali activated fly ash forms a Si-O-Al polymer, hence the name geopolymer. Geopolymer is a name first introduced by Davidovits (1991) for inorganic polymers made from metakaolin. The other names used are alkali activated metakaolin or fly ash or inorganic polymers. Alkali activated slag (AAS) binder predominantly forms C-S-H structure, which is more closely aligned with Portland cement. However, many of the mechanical and acid resistant properties resemble geopolymers. AAS concrete can yield high early strength, a characteristic currently not achieved by slag blended cements, while overcoming two shortcomings of ordinary Portland cements, namely, high heat of hydration and inferior durability in acid environments and accidental fire.

These cements have great potential to be used as a building material alternative to Ordinary Portland Cement (OPC) concrete because their strength, stiffness and other mechanical properties are comparable to OPC concrete. This new generation of concretes are currently attracting increasingly widespread attention because their manufacture does not directly create CO<sub>2</sub> emissions like OPC concrete. The main base materials for these concretes are slag and/or fly ash, which are industrial by-products from blast furnace and coal power stations. The processes involved in making these materials are carbon intensive, such as the burning of coal. However, it is not a secret that the coal is burnt to produce energy and not to make fly ash. Hence, the carbon emissions from these processes should be attributed to the energy production rather than to the fly ash. A similar consideration should also be given to the carbon footprint of activators. One of the activators, NaOH is produced from chlor-alkali process, where the primary purpose is to produce chlorine. It would be a difficult negotiation to decide what proportion of the carbon emissions from chlor-alkali process should be allocated to NaOH production. If we split in the middle at 50:50, then NaOH activator will have an emission about 0.5 ton/ton of NaOH. Typical amounts of sodium hydroxide activator used in geopolymers concrete is about 12 kg per cubic metre of concrete (Zhao and Sanjayan, 2011), resulting in about 6 kg CO<sub>2</sub> per cubic metre, as compared to Portland cement concrete emissions of 300 kg of CO<sub>2</sub> per cubic metre of concrete. While the activators emissions are not zero, due to the small amount of activators used in geopolymers concrete, large reductions in carbon emissions are possible.

Fig. 5 shows the number of research publications in refereed journals in this subject since 1990. In the 1990's world wide interest was negligible (<10 per year), but during the last couple of years the publications are well over 100 per year. It is inevitable that the level research interest worldwide will translate into commercial realities not so far into the future.

Extensive research studies conducted have shown that AAS concretes are suitable for construction purposes. Studies (Collins and Sanjayan, 1998, 2001a) based on the paste and mortar investigation showed that a multi-component activator based on powdered sodium silicate, hydrated lime and calcium sulphate was the most suitable activator based on one day strength and workability. AAS pastes showed better dispersion than OPC pastes. It was also found that partial replacement of slag with ultra-fine slag or ultra-fine fly ash improves workability, whereas condensed silica fume significantly reduces workability (Collins and Sanjayan, 1999a). AAS concrete made with liquid alkali activators, namely NaOH plus  $\text{Na}_2\text{CO}_3$  and also liquid sodium silicate showed rapid loss of workability with time (Collins and Sanjayan, 1999b). The one-day strength of AAS concrete was almost identical to OPC concrete for various water/binder ratios. Up to 25 MPa one-day strength was achievable with AAS concrete (Collins and Sanjayan, 1999c).

Long-term strength studies, up to 365 days, showed that certain AAS concrete mixes may exhibit limited strength retrogression under certain curing conditions. The behaviour of AAS concrete is associated with continuous microcracking and capillary pore network. A more detail account of this behaviour is explained in Collins and Sanjayan (2001b).

Testing up to 365 days showed that drying shrinkage of AAS concrete is greater than OPC concrete, which is a limitation in certain construction applications. The likely reason for higher drying shrinkage of AAS concretes has been explained by studying the pore size distributions of pastes of AAS and OPC (Collins and Sanjayan, 2000a). Studies focused on reducing the shrinkage of AAS concretes showed that up to 54% reduction in shrinkage could be achieved by the incorporation of a glycol-based shrinkage reducing chemical admixture into AAS concrete. Further the examination of the effect of gypsum content on shrinkage and compressive strength of AAS concrete showed 2%  $\text{SO}_3$  to be the optimum gypsum content. Further, it was found that replacement of normal weight coarse aggregate with saturated porous air-cooled blast furnace slag aggregate into AAS concrete achieved 38% less drying shrinkage at 365 days. This is most likely due to the "internal curing" effect whereby saturated blast furnace slag aggregate releases moisture into the cementitious paste during drying (Collins and Sanjayan, 1999c). The cracking tendency of AAS concrete was also studied by numerical modelling (Collins and Sanjayan, 2000b) and experimental investigation (Collins and Sanjayan, 2000c) and was compared with the OPC equivalent concretes.

Concretes developed in the laboratory are not necessarily suitable for construction use, as the problems in construction sites can be of different nature. To investigate these type of problems, a large column was constructed using AAS concrete batched and mixed at a commercial operating concrete plant using a mobile mixer. The investigation (Collins and Sanjayan, 1999d) showed that unlike concretes made with slag-blended cements, AAS concretes do not show significant difference in in-situ strength properties and control cylinder properties.

Detailed studies on microstructure of AAS concrete to investigate binder behaviour, including isothermal calorimetry, nuclear magnetic resonance, scanning electron microscopy and X-Ray micro-analysis confirm that the AAS concrete is suitable for most types of construction (Bakharev et al, 2001a, 1999a, 1998). Research has also shown that elevated temperature curing of AAS can produce superior strength and durability properties (Bakharev et al, 1999b), making AAS concrete highly suitable for precast concrete construction. Further studies of AAS concrete for compatibility for various admixtures (Bakharev et al, 2000), and long term durability against various attacks, such as alkali aggregate reaction (Bakharev et al, 2001b), sulphate attack (Bakharev et al, 2002) and carbonation (Bakharev et al, 2001c) ensure that AAS concrete is a viable alternative to the conventional Portland cement based concrete.

The primary difference between geopolymer concrete and OPC concrete is its binder. The geopolymer binder is synthesised by alkali activation of aluminosilicate raw materials, which are transformed into reaction product by polymerisation in a high pH environment and hydrothermal conditions at relatively low temperatures (up to 120°C). The reaction product is a polymer incorporating Al, Si and O, which is chemically very different from the hardened Portland cement which is calcium silicate hydrates (C-S-H) and calcium hydroxides. This difference in chemical structure gives geopolymer certain advantages over its OPC counterpart, such as a better strength performance when

geopolymer materials are exposed to fire as seen in Fig. 6 (Kong and Sanjayan, 2007, 2008, 2010; and Pan et al, 2009).

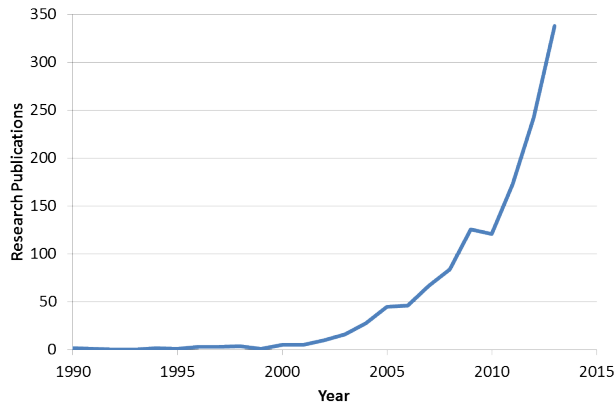
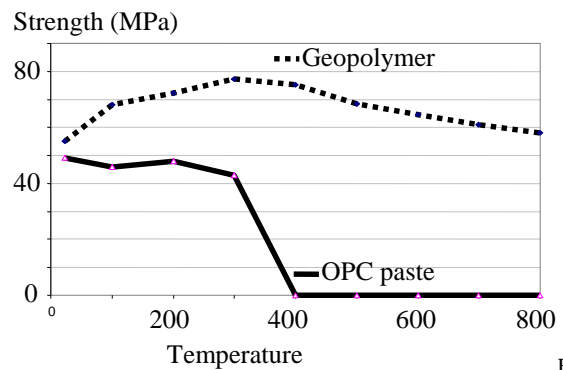


Fig. 5 Research Publications in Geopolymer (Scopus Database)



6 OPC and Geopolymers in Elevated Temperatures

Fig.

Geopolymer also possesses excellent resistance to acid environments, similar to alkali activated slag concrete (Bakharev et al 2003, Bakharev 2005). This provides technical advantages in applications such as sewer pipes, dairy floors and other acid industrial applications where the conventional Portland cement concretes long term durability problems because it does not possess sufficient acid resistance.

High performance concrete made from Portland cement concrete suffer from explosive spalling when exposed to accidental fire (Sanjayan and Stocks, 1993). Widely suggested reason for this phenomenon is the high steam pressure development in low permeable environment of high performance concrete. However, it has been found that the brittleness of the material (high performance concrete) and thermal incompatibilities between aggregate and paste also contribute to the spalling (Kong and Sanjayan, 2010). Geopolymer becomes highly flexible material at a temperature around 700°C, which allows the material to accommodate large strains without fracturing (Pan and Sanjayan, 2010). Further, hardened Portland cement pastes (C-S-H) dehydrate and disintegrate at high temperatures (>200°C), whereas geopolymer gains strength when exposed to fire (Kong and Sanjayan, 2010).

#### 4. Conclusions

Fly ash and ground granulated slag are abundantly available in many parts of the world, far in excess of quantities to replace Portland cements as construction material. Currently, they are used in limited quantities to partially replace Portland cement in concrete making. However, these industrial by-products can potentially replace the entire Portland cement in concrete making by utilising the rapidly advancing technologies of geopolymer concrete and alkali activated slag concretes. They have shown to provide superior fire resistance and acid resistance. There are also other materials currently in research and development phase, such as finely ground waste glass and rice husk ash, which can potentially become more viable with the development of advancing technologies. Further incentives, such as price on carbon will trigger rapid advancement and use of these technologies in practice.

#### Acknowledgements

I acknowledge my PhD students for their contributions to the research and development of the alternative and blended cement systems, namely, Zhu Pan, Ren Zhao, Daniel Kong, Tarek Aly, Frank Collins, Tatiana Bakharev and Bill Sioulas. Some of their work is presented in this paper.

#### References

- [1] Aly, T., and Sanjayan, J.G., (2008), "Factors Contributing to Early Age Shrinkage Cracking of Slag Concretes subjected to 7-days Moist Curing", *Materials and Structures*, Volume 41, Issue 4, pp. 633-642.

- [2] Aly, T., and Sanjayan, J.G., (2009), “Development of Model Parameters for Early-age properties and Crack-width Prediction of Slag-concretes”, Magazine of Concrete Research, Vol. 61, Issue 5, June, pp. 379-386.
- [3] Bakharev, T., Sanjayan, J. G., Cheng, Y. B., (1998), “Hydration of Slag Activated by Alkalis”, Journal of the Australasian Ceramic Society, Vol. 34, No. 2, 1998, pp. 195-200.
- [4] Bakharev, T., Sanjayan, J. G., Cheng, Y. B., (1999a) “Alkali Activation of Australian Slag Cements”, Cement and Concrete Research, January, 1999, Vol. 29, Issue 1, pp. 113-120.
- [5] Bakharev, T., Sanjayan, J.G., Cheng, Y.B., (1999b) “Effect of Elevated Temperature Curing on Properties of Alkali Activated Slag Concrete”, Cement and Concrete Research, Vol. 29 (10), 1999, pp. 1619-1625.
- [6] Bakharev, T., Sanjayan, J.G., Cheng, Y.B., (2000), “Effect of Admixtures on Properties of Activated Slag Concrete”, Cement and Concrete Research, Vol. 30, Issue. 9, 2000, pp. 1367 – 1374.
- [7] Bakharev, T., Sanjayan, J.G., Y.-B.Cheng, (2001a), “Microstructure and Properties of Alkali-Activated Slag Concrete”, Journal of the Australasian Ceramic Society, 37(1), pp. 115-120, 2001.
- [8] Bakharev, T., Sanjayan, J.G., Y.-B.Cheng, (2001b), “Resistance of Alkali Activated Slag Concrete to Alkali Aggregate Reaction”, Cement and Concrete Research, Vol. 31, Issue. 2, 2001, pp.331-334.
- [9] Bakharev, T., Sanjayan, J.G., Y.-B.Cheng, (2001c), “Resistance of Alkali Activated Slag Concrete to Carbonation”, Cement and Concrete Research, 31, 2001, pp. 1277-1283.
- [10] Bakharev, T., Sanjayan, J.G., Y.-B.Cheng, (2002), “Sulphate Attack on Alkali Activated Slag Concrete”, Cement and Concrete Research, Vol. 32 (2), pp. 211-216.
- [11] Bakharev, T., Sanjayan, J.G., Cheng, Y.-B., (2003) “Resistance of alkali activated slag concrete to acid attack”, Cement and Concrete Research, Vol. 33, No.10, October, 2003, pp. 1607-1611.
- [12] Bakharev, T., (2005), “Resistance of geopolymer materials to acid attack”, Cement and Concrete Research, Volume 35, Issue 4, April 2005, pp. 658-670.
- [13] Collins, F., Sanjayan, J. G., (1998) “Early age strength and workability of slag pastes activated by NaOH and Na<sub>2</sub>CO<sub>3</sub>”, Cement and Concrete Research, 28 (5), 1998, pp. 655-664.
- [14] Collins, F., Sanjayan, J. G., (1999a) “Effects of ultra fine materials on workability and strength of concrete containing alkali activated slag as the binder”, Cement and Concrete Research, 29, (3), 1999, pp.459-462.
- [15] Collins, F., Sanjayan, J. G., (1999d), “Strength and shrinkage properties of alkali activated slag concrete placed into a large column”, Cement and Concrete Research, 29(5), 1999, pp. 659-666.
- [16] Collins, F., Sanjayan, J.G., (1999b) “Workability and Mechanical Properties of Alkali Activated Slag Concrete”, Cement and Concrete Research, May, 1999, Vol. 29, Issue.3, pp. 455-458.
- [17] Collins, F., Sanjayan, J.G., (1999c) “Strength and shrinkage properties of alkali activated slag concrete containing porous coarse aggregate”, Cement and Concrete Research, 1999, 29(4), pp. 607 – 610.
- [18] Collins, F., Sanjayan, J.G., (2000a) “Effect of Pore Size Distribution on Drying Shrinkage Of Alkali Activated Slag Concrete”, Cement and Concrete Research, Vol. 30, Issue. 9, 2000, pp. 1401 – 1406.
- [19] Collins, F., And Sanjayan, J.G., (2000b) “Numerical Modeling of Alkali Activated Slag Concrete Beams subjected to Restrained Shrinkage”, ACI Materials Journal, American Concrete Institute, Vol. 97, No. 5, September-October, 2000, pp. 594-602.
- [20] Collins, F., Sanjayan, J.G., (2000c) “Cracking Tendency of Alkali-Activated Slag Concrete Subjected to Restrained Shrinkage”, Cement and Concrete Research, Vol. 30, No. 5, 2000, pp. 791-798.
- [21] Collins, F.G., Sanjayan, J.G., (2001a) “Early Age Strength and Workability of Slag Pastes Activated by Sodium Silicates”, Magazine of Concrete Research, Vol.53, No. 5, October 2001, pp. 321-326.
- [22] Collins, F.G., Sanjayan, J.G., (2001b) “Microcracking and Strength Development of Alkali Activated Slag Concrete”, Cement and Concrete Composites, Vol. 23/4-5, September 2001, pp. 345-352.
- [23] Davidovits, J., (1991) “Geopolymers: Inorganic Polymeric New Materials”, Journal of Thermal Analysis 37(8) (1991) 1633-1656.
- [24] Flower, D.J., Sanjayan, J.G., Baweja, D., (2005) “Environmental Impacts of Concrete Production and Construction”, Proceedings of the 22nd Biennial Conference of the Concrete Institute of Australia, Melbourne, October, published on CD, 10 pages.
- [25] Kong, D., Sanjayan, J.G., Sagoe-Crentsil, K., (2007) “Comparative performance of geopolymers made with metakaolin and fly ash after exposure to elevated temperatures”, Cement and Concrete Research, 37(12) (2007) 1583-1589.
- [26] Kong, D., Sanjayan, J.G., (2008) “Damage behavior of geopolymer composites exposed to elevated temperatures”, Cement & Concrete Composites, 30(10) (2008) 986-991.
- [27] Kong, D., Sanjayan, J.G. (2010) “Effect of elevated temperatures on geopolymer paste, mortar and concrete”, Cement and Concrete Research, 40(2) (2010) 334-339.
- [28] Pan, Z., Sanjayan, J.G., Rangan, B.V. (2009) “An investigation of the mechanisms for strength gain or loss of geopolymer mortar after exposure to elevated temperature”, J. Mater. Sci., 44(7) (2009) 1873-1880.
- [29] Pan, Z., Sanjayan, J.G., (2010) “Stress-strain behaviour and abrupt loss of stiffness of geopolymer at elevated temperatures”, Cement and Concrete Composites, Volume 32, Issue 9, October 2010, Pages 657-664.
- [30] Sanjayan, J.G., Aly, T., (2005), “A Review of the current Australian Standard Test for Shrinkage of Modern Concretes and its relevance in Concrete Specifications”, Concrete in Australia, Concrete Institute of Australia, June-August, pp. 25-28.
- [31] Sanjayan, G., and Stocks, L., (1993) “Spalling of High-Strength Silica Fume Concrete in Fire”, ACI Materials Journal, American Concrete Institute, Vol.90, No.2, March-April, 1993, pp.170-173.
- [32] Sioulas, B., Sanjayan J. G., (1997) “Use of Slag Blended Cements in Large High Strength Concrete Columns”, Proceedings of the International Conference on New Technologies in Structural Engineering, Lisbon, Portugal, July 1997, pp. 79 - 86.
- [33] Sioulas, B., Sanjayan, J.G., (1998), “Vertical Strength Variations in Large Columns using High Strength Concrete incorporating Slag”, Magazine of Concrete Research, Vol.50, No.4, Dec, 1998, pp. 329-337.
- [34] Sioulas, B., Sanjayan, J.G., (2000a) “Hydration Temperatures in Large High-Strength Concrete Columns incorporating Slag”, Cement and Concrete Research, Vol. 30, Issue, 11, 2000, pp.1791-1799.
- [35] Sanjayan, J.G., Sioulas, B., (2000b), “Strength of Slag-Cement Concrete cured in Place and in Other Conditions”, ACI Materials Journal,

Journal of the American Concrete Institute, Vol. 97, No. 5, September-October, 2000, pp. 603-611.

- [36] Sioulas, B., Sanjayan, J.G., (2001), “The Coloration Phenomenon associated with Slag Blended Cements”, *Cement and Concrete Research*, Vol. 31, Issue. 2, 2001, pp.313-320.
- [37] Wainwright, P. J., (1986), “Properties of fresh and hardened concrete incorporating slag cement”, In: Swamy, R. N. (ed.) *Concrete Technology and Design, Volume 3, Cement Replacement Materials*, Surrey University Press, Bishopbriggs, Glasgow, 1986, pp.100-133.
- [38] Zhao, R., and Sanjayan, J.G., (2011), “Geopolymer and Portland cement concretes in simulated fire”, *Magazine of Concrete Research*, V.63 (3), pp.163 – 173.



Sustainable Civil Engineering Structures and Construction Materials, SCESCM 2016

## An alternative method for determining tensile properties of engineered cementitious composites

Benny Suryanto<sup>a\*</sup>, Blair Cockburn<sup>a</sup>, Han Ay Lie<sup>b</sup>, W. John McCarter<sup>a</sup>

<sup>a</sup>Heriot-Watt University, Edinburgh EH14 4AS, Scotland, United Kingdom

<sup>b</sup>Diponegoro University, Semarang 5027, Indonesia

---

### Abstract

The framework of a practical test method that can be used to provide indirect assessment of the tensile properties of ECC is presented. Particular emphasis is placed on providing the underlying concept, modelling strategy and constitutive relations underpinning the proposed framework. An analysis case study, examining the effect of tensile stress-strain profiles on the flexural response of an ECC beam, is presented to demonstrate the capability of the modelling approach. The results of further parametric analysis are also provided to establish equations that can be used for determining equivalent tensile properties of ECC based on a given set of flexural test data. A web portal is provided as a simple tool for practitioners and researchers involved in mix development and quality control testing.

© 2017 The Authors. Published by Elsevier Ltd.

Peer-review under responsibility of the organizing committee of SCESCM 2016.

*Keywords:* ECC; practical test; tensile properties; quality control; virtual laboratory; website.

---

### 1. Introduction

An Engineered Cementitious Composite (ECC) is a fiber reinforced cement-based composite which possesses ultra-ductile tensile properties, typically a few hundred times larger than those possessed by concrete with no and regular fiber reinforcement [1–3]. The material's high tensile strain capacity is attributed to its ability to form closely-spaced fine cracks when subjected to tension, allowing it to deform plastically like a metal – a response which is known as a strain hardening [4]. This is in contrast to the post-cracking response of ordinary concrete which

---

\* Corresponding author. Tel.: +44-131-451-3817; fax: +44-131-451-4617

E-mail address: [b.suryanto@hw.ac.uk](mailto:b.suryanto@hw.ac.uk)



is characterized by a brittle, strain softening response. Apart from its high ductility, ECC is known for its crack control ability, with crack widths typically less than 100µm during the strain hardening [5]. It is these two ECC features that have attracted widespread interest from the engineering community.

In the United Kingdom, where this research is conducted, ECC has yet to be used in civil engineering applications, with the work still being at a research and development stage (see, for example, [6–9]). In order to promote the use of ECC in the construction industry, this work seeks to develop a simple test procedure that can be used for quality control testing in large volume applications. While the uniaxial tensile test has been the primary method used for ascertaining the tensile stress-strain properties of ECC and provides results which are easy to analyze, the test is often difficult to perform to an acceptable quality and thus can be impractical for use in normal construction practice. It is for this reason that a simpler test method is developed in this work. Although the proposed method can stand alone, it is not the intention of the authors to replace the standard tensile test, but rather to use it alongside the existing test method which should be used for validating the results periodically.

## 2. Heriot-Watt University (HWU) Method

A flowchart detailing the work undertaken to develop the HWU method is presented in Fig. 1, with the dashed lines highlighting the scope of this paper. The proposed method is similar in many respects to the University of Michigan (UM) method [10,11] on the basis that it only requires the peak load and the corresponding point-load deflection to be measured from a test. Similar to the UM method, the proposed method also does not require the use of special devices to take strain readings; rather, this can be determined using predefined equations, which can also be used to determine tensile strength. The proposed method is distinct from the UM method in that it offers an improved representation of the effect of micro-cracking on beam curvature and deflection profiles, making it more closely aligned with the principles of mechanics (Fig. 2). Another important aspect of the HWU method, when compared to the UM method, lies in the use of refined stress-strain relations which are used consistently throughout the calculation process. Fig. 3(a) presents the test setup used to derive equations used in the proposed method.

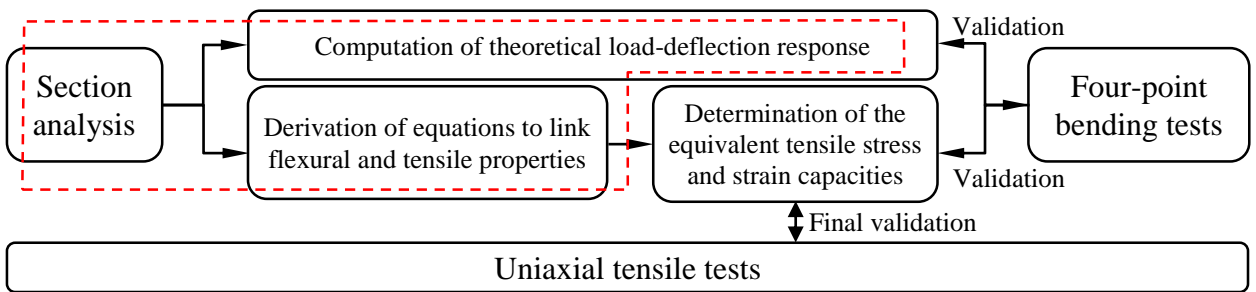


Fig. 1. Framework for the development of the HWU method.

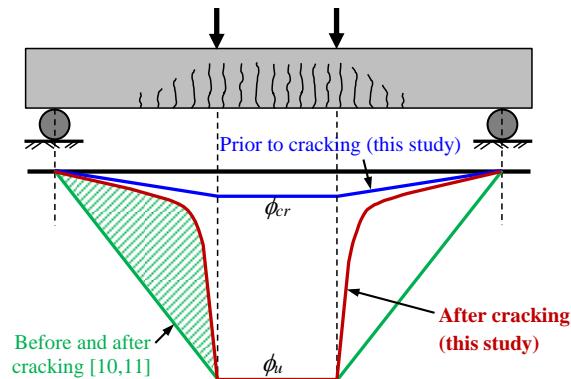
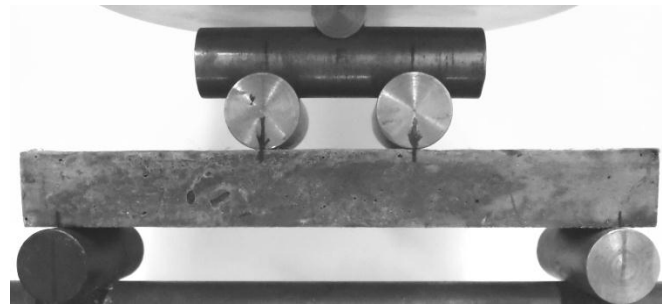
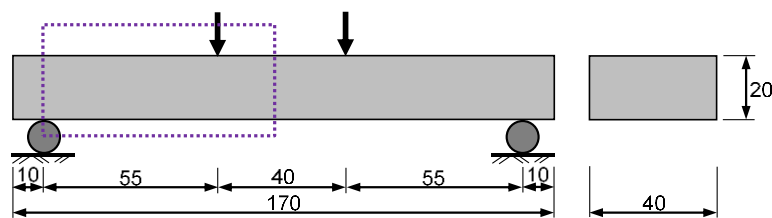


Fig. 2. Comparison of the assumed curvature profile in HWU and UM methods, with the hatched area highlighting the difference.

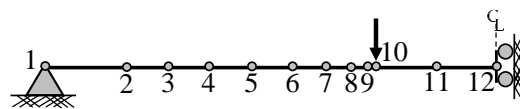




(a)



(b)



(c)

Fig. 3. (a) Proposed test setup; (b) schematic and dimensions of test sample (in mm); and (c) structural model representation of half of the test sample (marked with a dotted rectangle in (b)).

### 3. Analytical Model

#### 3.1. Modelling

Fig. 4 presents the analytical model used to predict the full-response of the beam, with only half of the beam being modeled due to the symmetry in load and support conditions. A total of 12 nodal points (or, accordingly, 11 elements) were used to represent half of the beam. On this individual point, it was assumed that the beam cross-section comprises a stack of ECC layers having the same width  $b$  and depth  $dh$ . It was also assumed that plane sections remain plane, provided that the shear span-of-depth ratio of the test specimen used in the HWU method is large enough ( $a/d = 2.75$ ; see Fig. 3a). It is on this basis that the calculation employs a linear strain profile.

Section analysis was performed at multiple locations along the beam (Points 2–12) and at each point, the depth of the beam was divided to 1000 layers, with the strain and stress values on each layer assumed to be uniform (see Fig. 4). Although significantly smaller number of layers could actually be used without significantly affecting the accuracy of the analysis, it was decided to use such a large number in order to obtain smooth strain and stress profiles and guarantee the highest levels of accuracy. The stress and strain on each layer were then individually analyzed using predefined stress and strain relations shown in Fig. 4, which are based on the work by [12–14]. On each section, iterative calculations were carried out to obtain the longitudinal strain and stress profiles whilst satisfying, respectively, the compatibility and equilibrium requirements. Two tensile stress profiles were used to form the tensile stress-strain response: a constant stress distribution ( $\alpha = 1.0$ ) and a bilinear stress distribution ( $\alpha < 1.0$ ). To suit the typical tensile properties of the ECC mix developed at Heriot-Watt [6],  $\alpha$  for the bilinear stress model was taken to be 0.7.

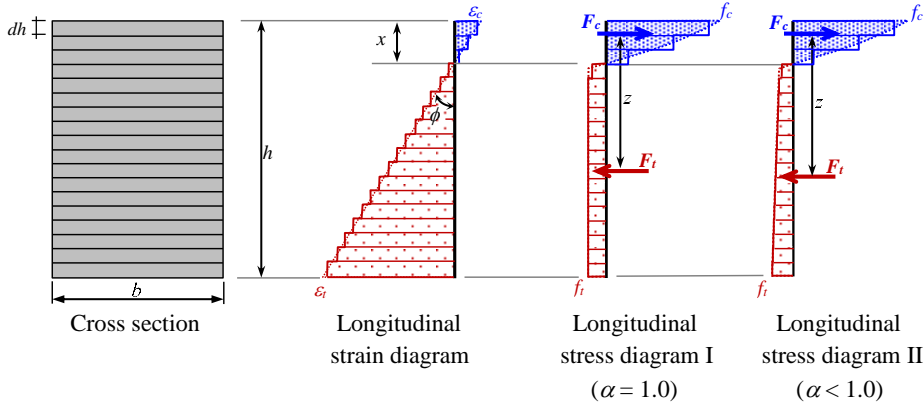


Fig. 4. ECC sample discretized into layers and the corresponding strain and stress profiles across the depth.

### 3.2. Constitutive models

The constitutive relations proposed by Suryanto *et al* [12,13] were used. The curve describing the monotonic response in compression is based on the elasto-plastic fracture model for concrete [15]:

$$f_c = \omega_c K_0 E_0 (\varepsilon - \varepsilon_p) \quad (1)$$

where fracture parameter  $K_0$ , initial stiffness  $E_0$  and plastic strain  $\varepsilon_p$  are defined as

$$K_0 = \exp \left( -0.73 \frac{\varepsilon}{\varepsilon_c} \left( 1 - \exp \left( -1.25 \frac{\varepsilon}{\varepsilon_c} \right) \right) \right) \quad (2)$$

$$E_0 = 2 \frac{f_c'}{\varepsilon_c} \quad (3)$$

$$\varepsilon_p = \beta \left( \frac{\varepsilon}{\varepsilon_c} - \frac{20}{7} \left( 1 - \exp \left( -0.35 \frac{\varepsilon}{\varepsilon_c} \right) \right) \right) \quad (4)$$

where  $f_c'$  is the ECC compressive strength,  $K_0$  is a fracture parameter,  $\varepsilon_c$  is the plastic strain,  $\varepsilon_c'$  is the strain at the peak compressive strength and  $\beta$  is the strain-rate factor. The strength reduction factor due to transverse cracking,  $\omega_c$ , is taken as 1.0. The base response in tension is assumed to be bilinear, with the first part describing the elastic response of the ECC and the second part describing the strain-hardening response, as given by

$$f_t = \omega_t E_e \varepsilon_t \quad 0 < \varepsilon_t < \varepsilon_{tcr} \quad (5)$$

$$f_t = \omega_t E_{sh} \varepsilon_t \quad \varepsilon_{t,cr} < \varepsilon_t < \varepsilon_{tu} \quad (6)$$

where  $E_e$  is the initial elastic modulus of the ECC (approximately 20GPa) [7],  $\varepsilon_t$  is the tensile strain,  $\varepsilon_{tcr}$  is the tensile strain at first cracking,  $\varepsilon_{tu}$  is the tensile strain capacity,  $\omega_t$  is a reduction factor to account for transverse cracking.

Given that the principal stress direction remained constant throughout the testing, it was anticipated that there was no transverse cracking forming and hence the strength reduction factor,  $\omega_t$ , was taken as 1.0. Failure was defined as the moment when the tensile strain at the utmost bottom layer reached the tensile strain capacity,  $\varepsilon_{tu}$ , and no post-peak response was considered. Section analyses at multiple locations along the beam were carried out using Microsoft Excel.

#### 4. Analysis Results and Discussion

To demonstrate the capability of the calculation framework described in Section 3, two series of analysis were undertaken to simulate the response of an ECC sample with sample dimensions and test set-up following the schematic presented in Fig. 3(a). In total, eighteen analysis cases were performed (nine for each tensile stress model). In each analysis case, different tensile strain values were used at the utmost bottom layer, including 0.03%, 0.075%, 0.15%, 0.30%, 0.45%, 0.75%, 1.50%, 2.25% and 3.0%. The mechanical properties of the ECC were taken as  $f_c' = 30$  MPa,  $f_{tu} = 4$  MPa and  $\varepsilon_{tu} = 3.0\%$ . In the bilinear stress analysis case,  $f_{cr}$  was taken as 2.8 MPa, whereas  $E_{sh}$  was taken as 40.2 MPa throughout.

Fig. 5 presents the computed load versus point-load deflection of the ECC beam using the assumed two tensile models. It is evident that the post-cracking tensile stress-strain profiles had a profound effect on the nonlinear part of the load versus deflection curves, which represents the post-cracking response of the beam. The elastic-plastic model ( $\alpha = 1.0$ ) produces a much sharper load-deflection response after first cracking, a flatter post-cracking response during the intermediate to final parts of the curve and a slight increase in load capacity. The sharp increase in response along with lower deflection values could be attributed to the value of the stress at first cracking,  $f_{cr}$  which is taken equal to that at ultimate state,  $f_{tu}$ . The same theory applies to the approximately flat-top response with increasing deflection, as well as to the marginal increase in load capacity. It is interesting to note that the assumed tensile stress-strain profiles also affect the deflection at the peak load. This can be attributed to the difference in the crack distribution at the underside of the two beams. The larger deflection at peak load shown by the bilinear stress distribution indicates that the cracks that form at the bottom of the beam are more uniform. The evidence for this can be seen from Fig. 6, which shows that the elastic-plastic stress distribution ( $\alpha = 1.0$ ) produces a much more drastic curvature profile as it reaches the center span than that of the bilinear distribution ( $\alpha = 0.7$ ). In addition, regardless the tensile models used, it is evident that the computed curvature profile is highly nonlinear which is in sharp contrast to the linear profile assumed by [10,11] (see Fig. 2). The assumption in linear curvature distribution may affect the accuracy of the deflection prediction, and hence the equivalent tensile strength and tensile strain capacity.

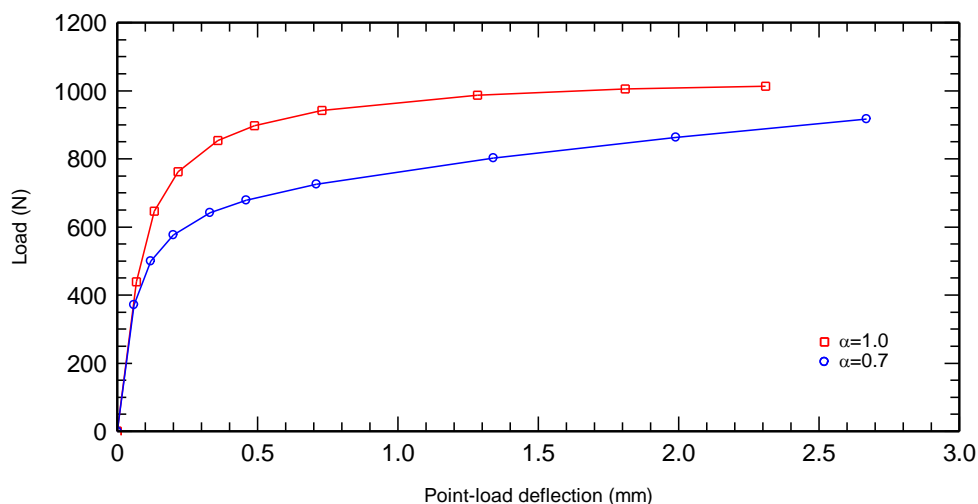


Fig. 5. Predicted load versus load-point deflection responses of an ECC sample presented in Fig. 3(a) and 3(b). The mechanical properties of the ECC are taken to be  $f_c' = 30$  MPa,  $f_{tu} = 4$  MPa and  $\varepsilon_{tu} = 3\%$ .

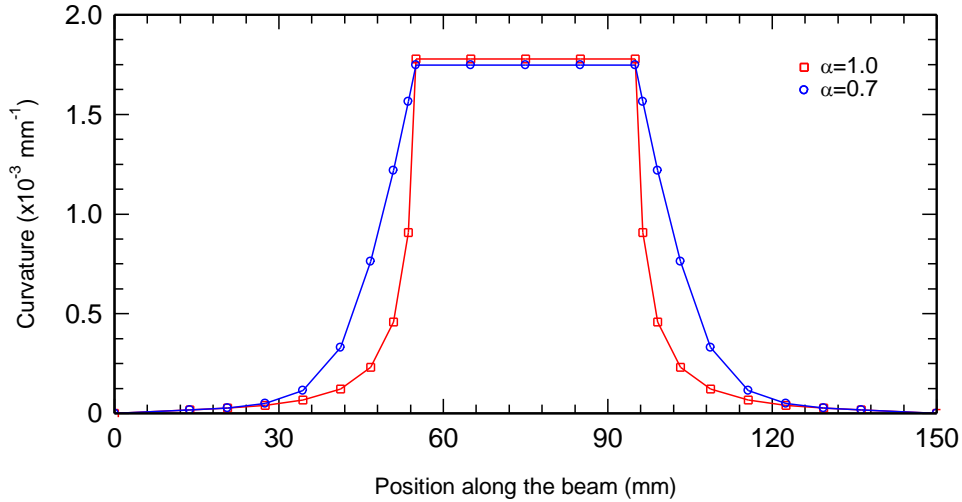


Fig. 6. Predicted curvature profiles for bilinear ( $\alpha = 0.7$ ) and elastic-plastic ( $\alpha = 1.0$ ) tensile models.

The analytical framework was then used to undertake a parametric study to investigate the influence of a wide range of possible ECC mechanical properties. In total, 56 analysis cases were run for the two tensile stress-strain models considering a variety of compressive and tensile strength and tensile strain values. The parameters considered in the parametric study include compressive strength (30, 40 and 50 MPa), tensile strength (3.5, 4 and 5 MPa) and tensile strain capacity (0.5, 1, 3 and 4%). It is interesting to note from the results of the parametric analysis that although the beam exhibits a highly nonlinear response, the tensile strain capacity,  $\varepsilon_{tu}$  exhibits an almost linear relationship with point-load deflection,  $\delta_u$  at peak load and is, to a lesser extent, affected by compressive strength,  $f'_c$ . Based on this finding, the following empirical equations are proposed to determine the equivalent tensile strain capacity,  $\varepsilon_{tu}$  from a given point-load deflection and compressive strength

$$\varepsilon_{tu} = \frac{f'_c}{10}(0.028\delta_u + 0.017) + 1.43\delta_u - 0.29 \quad \text{for elastic-plastic model } (\alpha = 1.0) \quad (7)$$

$$\varepsilon_{tu} = \frac{f'_c}{10}(0.015\delta_u + 0.021) + 1.21\delta_u - 0.21 \quad \text{for bilinear model } (\alpha = 0.7) \quad (8)$$

To determine the equivalent tensile strength, further derivations were performed using the analytical procedure described in Section 3. To summarise the findings from the derivations, the tensile strength can be found for either tensile model by

$$\left[ \left( -0.5 \frac{(h-x)}{E\varepsilon_{tu}} \right) f_{tu}^2 + (h-x)f_{tu} \right] b(0.52h) = 27.5P \quad \text{for elastic-plastic model } (\alpha = 1.0) \quad (9)$$

$$\left[ \left( \frac{\alpha + 1}{2} \right) (h-x) \right] 0.54bh f_{tu} + \left[ 0.5 \frac{\alpha^2(h-x)}{E\varepsilon_{tu}} - \left( \frac{\alpha + 1}{2} \right) \left[ \frac{\alpha}{E\varepsilon_{tu}} (h-x) \right] \right] 0.54bh f_{tu}^2 = 27.5P$$

$$\text{for bilinear model } (\alpha = 0.7) \quad (10)$$

where  $x$  is the neutral axis depth,  $E$  is the Young's Modulus and  $P$  is the applied load. For more details on the derivations of Equations 7–10, the reader should refer to [16].

To aid with the use of Equations 7–10, which are tedious to solve by hand, an Excel spreadsheet was developed along with a user-friendly website 'ECC Calc', built using HTML and CSS scripting languages. The JavaScript library was used to generate the equations and perform intermediate calculations according to the user's input. The

first generation of the website is now available at <http://dkwebsolutions.net/ECC-Calc/>. The webpage was designed in such a way that the browser can perform calculations quickly even through a dial-up connection, allowing access from around the world including countries with limited internet access. Fig. 7 shows the main interface of the website. A user can simply populate the form shown on the right and click the ‘Calculate’ button to perform the calculation. The results will be then shown automatically as presented in Fig. 8. The website can also be downloaded to a smartphone for use in a laboratory setting. New features will be incorporated in the near future to give users an option to visualize the calculated results.

Fig. 7. Screenshot of the *ECC Calc*'s main interface with boxes shown in the right for user input (available at <http://dkwebsolutions.net/ECC-Calc/>).

ECC Calc Results:	
Bilinear	Elastic-Plastic
$f_{tu}$ 4.39 N/mm <sup>2</sup>	$f_{tu}$ 3.90 N/mm <sup>2</sup>
$\epsilon_{tu}$ 3.01 %	$\epsilon_{tu}$ 3.51 %
$f_{cr}$ 3.07 N/mm <sup>2</sup>	$\epsilon_{cr}$ 0.019 %
$\epsilon_{cr}$ 0.015 %	

Fig. 8. Screenshot of the calculated output provided by *ECC Calc*.

#### 4. Concluding summary

The framework of a practical test method for characterizing the tensile properties of ECC is presented. The proposed framework comprises three primary parts: (i) a test method, which is based on the well-known four-point bending test; (ii) an analytical framework, which is based on the beam theory and incorporates nonlinear constitutive relations of ECC, and; (iii) a web portal, which can be accessed either on-site or in the laboratory via a computer or smartphone. This framework is called the Heriot-Watt University (HWU) test platform. In this paper, the proposed framework was used to simulate the response of an ECC sample under four-point bending and to develop relationships between flexural tests and tensile properties. It has been shown that the assumed tensile stress-strain response has a significant influence on the load capacity, deflection capacity, computed tensile strength and tensile strain capacity. Choosing an appropriate tensile stress-strain profile is shown to be essential to achieve the necessary level of accuracy with regard to the computed tensile strain and stress capacities. Future work will be directed towards extending the modelling platform for use with existing test methods. The first generation of a web portal is introduced to provide a practical tool for ascertaining the tensile properties of ECC.

#### Acknowledgements

The authors acknowledge the support of Kuraray Japan and Kuraray Europe GmbH for providing the PVA fibers and BASF UK for providing chemical admixtures. Financial support from the School of Energy, Geoscience, Infrastructure and Environment, Heriot Watt University, is gratefully acknowledged. Thanks also expressed to GV Ludford-Jones, EA Menzies, SJ Donnan, CO Sweeney, SD Taylor RM Traynor and D Kay for their assistance.

#### References

- [1] V.C. Li, Engineered cementitious composites (ECC) – material, structural and durability performance, in: E. Nawy (Ed.), *Concrete Construction Engineering Handbook*, CRC Press, New York, 2008, pp. 24-1–46.
- [2] V.C. Li, S. Wand, C. Wu, Tensile strain-gardening behavior of polyvinyl alcohol engineered cementitious composite (PVA-ECC), *ACI Mater. J.* 98 (2001) 483–492.
- [3] T. Kanda, V.C. Li, Practical design criteria for saturated pseudo strain hardening behavior in ECC, *J. Adv. Concr. Tech.* 4 (2006) 59–72.
- [4] A.E. Naaman, H.W. Reinhardt, Characterization of high performance fiber reinforced cement composites – HPFRCC, in: A.E. Naaman, H.W. Reinhardt (Eds.), *High Performance Fiber Reinforced Cement Composites 2*, E&FN Spon, London, 1996, pp. 1–24.
- [5] V.C. Li, On engineered cementitious composites (ECC) - a review of the material and its applications, *J. Adv. Concr. Tech.* 1 (2003) 215–230.
- [6] S. Pourfalah, B. Suryanto, Development of engineered cementitious composite mixtures using locally available materials in the UK, *Proc. Infra. Envi. Scot. 1<sup>st</sup> Post. Conf.*, Heriot-Watt University, Edinburgh, 2013, pp. 75–78.
- [7] B. Suryanto, S.A. Wilson, W.J. McCarter, Self-healing of micro-cracks in engineered cementitious composites, *Civ. Eng. Dimen.* 17 (2015) 187–194.
- [8] B. Suryanto, W.J. McCarter, G. Starrs, S.A. Wilson, R.M. Traynor, Smart cement composites for durable and intelligent infrastructure, *Proc. Eng.* 125 (2015) 796–803.
- [9] B. Suryanto, S.A. Wilson, W.J. McCarter, T.M. Chrisp, Self-healing performance of engineered cementitious composites under natural environmental exposure, *Adv. Concr. Res.* 28 (2016) 211–220.
- [10] S. Qian, V.C. Li, Simplified inverse method for determining the tensile strain capacity of strain hardening cementitious composites, *J. Adv. Concr. Tech.* 5 (2007) 235–246.
- [11] S. Qian, V.C. Li, Simplified inverse method for determining the tensile properties of strain hardening cementitious composites (SHCC), *J. Adv. Concr. Tech.* 6 (2008) 353–363.
- [12] B. Suryanto, K. Nagai, K. Maekawa, Modeling and analysis of shear-critical ECC members with anisotropic stress and strain fields, *J. Adv. Concr. Tech.* 8 (2010) 239–258.
- [13] B. Suryanto, K. Nagai, K. Maekawa, Smear-crack modeling of R/ECC membranes incorporating an explicit shear transfer model, *J. Adv. Concr. Tech.* 8 (2010) 315–326.
- [14] K. Nagai, B. Suryanto, K. Maekawa, Space-averaged constitutive model for HPFRCCs with multi-directional cracking, *ACI Mater. J.* 108 (2011) 139–149.
- [15] K. Maekawa, H. Okamura, A. Pimanmas, *Nonlinear Mechanics of Reinforced Concrete*, CRC Press, London, 2003.
- [16] B. Cockburn. *Developing a Practical Test to Determine the Tensile Properties of Engineered Cementitious Composites*, MEng Thesis, Heriot-Watt Univ., Edinburgh, 2016.



Sustainable Civil Engineering Structures and Construction Materials, SCESCM 2016

## Effect of temperature on precipitation rate of calcium carbonate produced through microbial metabolic process of bio materials

Prima Yane Putri<sup>a,b,\*</sup>, Keiyu Kawaai<sup>a</sup>, Isao Ujike<sup>a</sup>, Saya Yamamoto<sup>a</sup>

<sup>a</sup>Graduate School of Science and Engineering, Ehime University, Matsuyama 790-8577, Japan

<sup>b</sup>Department of Civil Engineering, Universitas Negeri Padang, Padang 25000, Indonesia

---

### Abstract

The cracking in concrete promotes deterioration such as the corrosion of reinforcing rebar, therefore, repair in filling the crack is often carried out. Recently, repair methods using bio-based materials associated with microbial metabolic processes leading to precipitation of calcium carbonate have been intensively studied. In this study, influencing factors on the precipitation rate depending on the constituents of bio-based material comprising yeast, glucose and calcium acetate mixed in tris buffer solution was examined for improving the rate of initial reactions. In addition, effect of temperature change on the amount of calcium carbonate precipitation was also investigated. The precipitates were identified by X-ray diffraction. It was shown that the increase of temperature lead to a change on calcium carbonate precipitation and caused the pH decrease under 7.0

© 2017 The Authors. Published by Elsevier Ltd.

Peer-review under responsibility of the organizing committee of SCESCM 2016.

*Keywords:* bio-based repair materials; yeast; calcium carbonate precipitation; temperature.

---

### 1. Introduction

Concrete is one of the most versatile, economical, and universally used construction material. Concrete has a great variety of applications because it not only meets structural demands but also lends itself readily to architectural treatment. In buildings, concrete is used for footings, foundations, columns, beams, girders, wall, slabs, and roof units-in short, all important building elements. Other important concrete applications are in road pavements, airport runways, bridges, dams, irrigation canals, water-diversion structures, sewage-treatment plants, and water-distribution pipelines. Although quality control of concrete used in these structures is strictly required, initial defects are likely to occur owing to structural constraints and poor workmanship. For example, construction-joint or gap tends to form especially at joints between structural members used in bridges structures. When it rains, it may cause leakage from the gap leading to a decrease in serviceability and should be aesthetically unacceptable. Difficulties associated with repair techniques for such defects are that conventional repair materials are less effective in sealing the gap formed spatially distributed in large areas, especially deeper zones in concrete structures.

For example, organic materials e.g. cement-based grout materials with higher viscosity are less practical in repairing deeper zones of cracks or gaps in large areas. In addition, they may cause adverse effect on the natural environment if they flow out through the gaps or cracks which are not completely repaired. Therefore, it is advantageous if the materials are not based on such materials, however, it should have similar materials properties of concrete.

---

\* Corresponding author. Tel.: +81-80-8638-0656

E-mail address: [prima.yane.putri.15@cee.ehime-u.ac.jp](mailto:prima.yane.putri.15@cee.ehime-u.ac.jp)



Recently, liquid-based repair techniques in the field of self-healing through the use of microbial induced precipitation (MIP) have been intensively investigated [4-6,8,10-12]. The mixtures are comprised of a microorganism, an organic carbon source and a calcium source which is readily available in concrete. When dry yeast is selected as the microorganism, carbon dioxide produced through the microbial metabolic processes consuming an organic carbon source such as glucose provides carbonate ions. The carbonate ions lead to react with calcium ions present in the mixture, leading to the precipitation of calcium carbonate depending on the pH levels in the alkali environment. The  $\text{CaCO}_3$  precipitates according to the following reactions:



It should be noted that the material produced through the reactions is no harmful to concrete materials because the precipitates are mainly comprised of calcium carbonate which is one of the reaction products formed by carbonation of hydration products. Besides the material properties, the mixture is a less viscous material compared to conventional materials. This may overcome shortcomings associated with the conventional repair materials as mentioned previously. Thus, it would be beneficial if the mixtures penetrate into deeper zones of gaps formed between concrete members and could effectively improve the water tightness of concrete with defects. However, the precipitation rate especially at early stages depending on the concentrations and initial pH levels.

Many studies have been carried out to investigate the effect of temperature on the  $\text{CaCO}_3$  precipitation and its incorporation into the calcite crystal lattice. H. Karoui et al [3] studied the effect of magnesium and sulphate ions on the kinetics precipitation and morphology of aragonite at fixed temperature of  $60^\circ\text{C}$ . It was shown that the magnesium ions were inserted in the aragonite crystal structure by substituting calcium ions. This substitution depends on the  $\text{Mg}^{2+}$ ,  $\text{Ca}^{2+}$  and  $\text{SO}_4^{2-}$  ions concentrations. Weiss et al [9] investigated the effect of synthesis temperature on the abundance of vaterite, aragonite, and calcite, thus delineating regions that are favorable for the formation of these different calcium carbonate polymorphs at temperatures ranging from  $25$  to  $80^\circ\text{C}$ . Therefore, in this research, the effects of temperature change were examined to enhance the precipitation rate of the calcium carbonate in bio based repair materials comprising yeast, glucose and calcium acetate. In order to evaluate the effect of temperature, X-ray powder diffraction (XRD) analysis was conducted. Finally, the relation between XRD analysis and polymorph of calcium carbonate precipitated was examined.

## 2. Methodology

### 2.1. Selection of basic constituents of mixtures

Along this study, calcium carbonate precipitation was promoted by microbial metabolic process of bio-materials mixtures as shown in Fig. 1. In addition to the reaction, it is essential to control the pH levels in mixtures to facilitate the precipitation of calcium carbonate. Tris (tris hydroxymethyl aminomethane) buffer solution with an alkali buffering function was used in this study. The initial pH in the Tris buffer solution was adjusted to 8.0 when mixed hydrochloric acid. The use of hydrochloric acid should be minimized in adjusting pH levels for ensuring no adverse effect on the integrity of hardened concrete.

The source of calcium ions used for mixtures was chosen taking into consideration higher solubility and no adverse effect on concrete materials. The material should be also commercially available and cost-effective. Based on the considerations above mentioned, calcium acetate was chosen in this study.

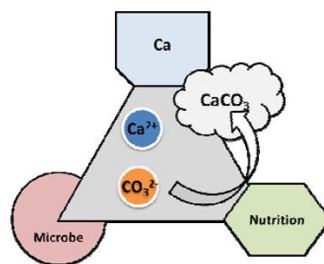


Fig. 1. Basic constituents of bio-based repair material

In addition, dry yeast commercially available was used as a microorganism, which is anaerobic and active in the oxygen-free environment. Organic carbon sources are necessary for the metabolism of the microorganism. Through the anaerobic fermentation, the yeast converts carbohydrates to carbon dioxide and alcohols in the presence of glucose ( $\text{C}_6\text{H}_{12}\text{O}_6$ ) which was selected as an organic carbon source.

It is known that highly alkaline environment in which pore solution in concrete exhibits is a severe condition for the yeast. It is crucial for the microorganism to exist in the mixtures with relatively lower pH, which is adjusted as low as possible initially.



According to previous research, it has been reported that the precipitation of calcium carbonate was likely to be smaller when pH decreased less than 7.5 [8]. In order to maintain the appropriate pH levels in mixtures tested, the pH was initially adjusted as 8.0 in room conditions controlled at 20°C. With the above materials, the mixtures as shown in Table. 1 were tested in different temperature conditions controlled at 10°C, 20°C and 30°C.

Table 1. Mix Proportion of dry yeast, glucose, calcium acetate and temperature changing.

Cases	Dry yeast	Glucose (mol/L)	Calcium acetate (mol/L)	Tris buffer solution		Temperature	Elapsed time (hours)
				pH	(Mol/L)		
A1							12
A2							24
A3	9.0	0.1	0.05	8.0	0.5	30°C	36
A4							48
A5							60
A6							72
B1							12
B2							24
B3	9.0	0.1	0.05	8.0	0.5	20°C	36
B4							48
B5							60
B6							72
C1							12
C2							24
C3	9.0	0.1	0.05	8.0	0.5	10°C	36
C4							48
C5							60
C6							72

## 2.2. Testing Procedures

In order to measure the concentration of calcium ion present and pH in mixtures after reaction was started, each mixture was prepared in a test tube. First, each material based on mix proportion specified as shown in Table. 1 was prepared and they were mixed with Tris buffer solution in a beaker. The mixture in the beaker was subsequently stirred until each material was dissolved into the solution. And the Tris buffer solution was further added to make solution 30 mL totally. The test tubes were placed in conditions controlled at 10°C, 20°C, and 30°C for the measurement. The concentration of calcium ions and pH were measured in filtered mixtures using commercially available meters (pH/mv meter model SK-620PH and calcium ion electrode model CA-2031). Each test was carried out using two test tubes to confirm the consistency of results obtained.

Based on the results of calcium ions measured, precipitated calcium carbonate was estimated using the following formula:

$$CaCO_3 = Q(\text{mol/L}) \times m(L) \times M(\text{g/mol}) \times \frac{C_0 - C_a}{C_0} \quad (2)$$

Where CaCO<sub>3</sub>: the amount of precipitates (g), Q: concentration of calcium acetate (mol/L), m: amount of solution (L), M: molar mass of calcium carbonate (100.09), C<sub>0</sub>: Initial concentration of calcium ion and C<sub>a</sub>: concentration of calcium ion measured. The precipitates were also tested for X-Ray Diffraction analysis to examine the crystals formed through the microbial metabolic process of bio-based materials in mixtures.

## 2.3. XRD analysis

XRD analysis was carried out using the residue left in the test tube after 24 hours, 48 hours and 72 hours. Each sample was crushed and pulverized to an average particle size of less than 10 microns, and then mounted onto an instrument-specific plastic slide plates. Then the mass absorption coefficient of the sample was determined by x-ray transmission. The XRD pattern was obtained by scanning from 5 to 50 degrees, 2 theta using a vertical x-ray diffractometer. The components of the sample were identified by comparing them with database powder diffraction PDF-4/Mineral 2015 established by the International Center for Diffraction Data [2].

### 3. Results and Discussion

#### 3.1. Influence of temperature on precipitates

Effect of temperature was examined with respect to precipitation rate up to 72 hours later after mixed. The mixtures cases were as shown in Table 1. Fig. 2 shows the precipitates left in tubes after filtering up to 24 hours elapsed time. Visually, calcium carbonate precipitation adhering to test tube increased with increasing temperature. Precipitation of  $\text{CaCO}_3$  in the case of A mixtures was observed to be greater than precipitation in B and C mixtures. Fig. 3 shows the precipitates left in tubes after filtering up to 72 hours elapsed time. Precipitation of  $\text{CaCO}_3$  up to 72 hours elapsed time was observed to be greater than those to 48 hours and 24 hours.

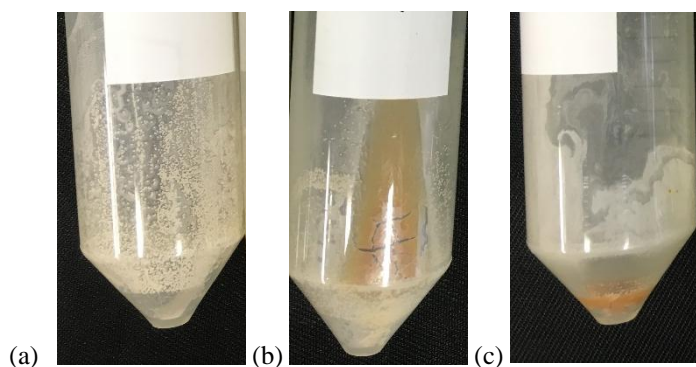


Fig. 2. Precipitates left after 24 hours; a) test tube in 30°C, b) test tube in 20°C and c) test tube in 10°C

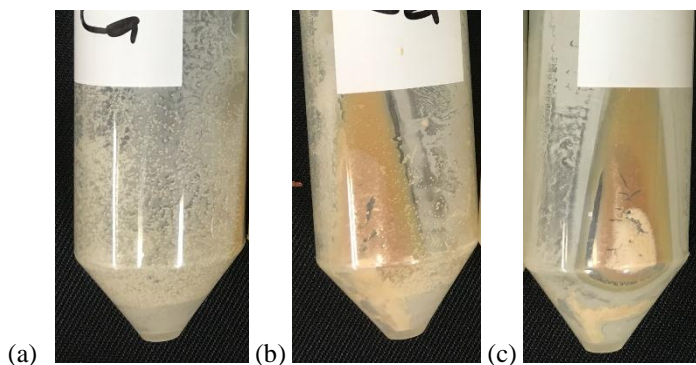


Fig. 3. Precipitates left after 72 hours; a) test tube in 30°C, b) test tube in 20°C and c) test tube in 10°C

Based on the weight of precipitates left in tubes after filtering, precipitation of  $\text{CaCO}_3$  in the case of A mixtures up to 24 hours elapsed time was 0.13 g. After 36 hours, it reached 0.14 g at most until 72 hours elapsed time. In the case of B mixtures, precipitates left in tubes after filtering up to 24 hours elapsed time was 0.06 g. The precipitation increased to 0.09 g after 36 hours, 0.10 g after 48 hours, and gradually increased to 0.13 gram during 60 to 72 hours elapsed time. On the other hand, in the case of C mixtures precipitates left in tubes after filtering were less than 0.05 g. Precipitation of  $\text{CaCO}_3$  up to 24 hours elapsed time was 0.02 g. After 48 hours elapsed time it reached 0.04 g and it subsequently reached 0.05 gram during 60 to 72 hours elapsed time. Furthermore, in the case of A mixtures, after 24 hours elapsed time the amount of precipitation was constant until 72 hours. In the case of B mixtures, after 24 hours elapsed time precipitation of  $\text{CaCO}_3$  increased gradually until 60 hours. After 60 hours, precipitation was constant until 72 hours. Otherwise, in the case of C mixtures, the amount of precipitation was below 0.05 g up to 72 hours elapsed time. Fig. 4 shows the weight of precipitates left in tubes after filtering for each mixtures up to 72 hours elapsed time.

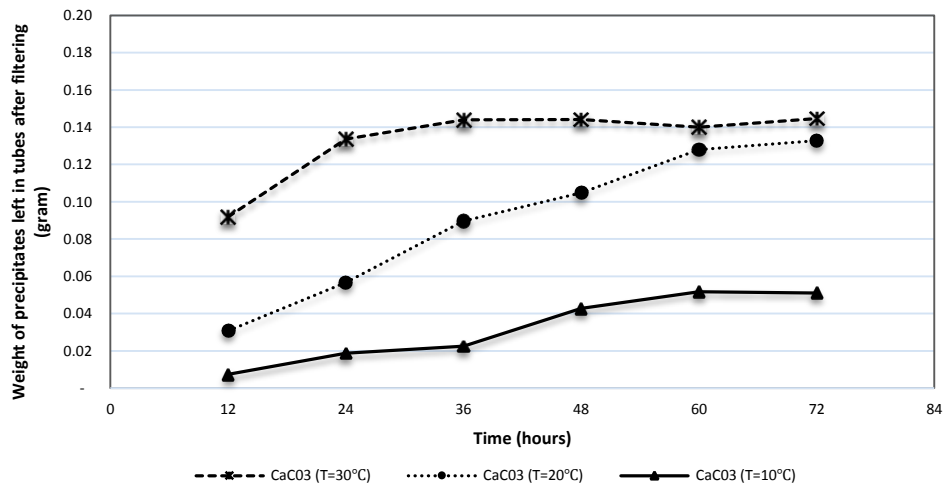


Fig. 4. Weight of precipitates left in tubes after filtering

The results were clearly confirmed by the calcium ion measurement in the mixtures tested. Fig. 5 shows the decreasing rate of calcium ion and changes of pH measured in the mixture tested. As can be seen, the concentration of calcium ion measured in the C mixtures was decreased by 5% after 12 hours. The decreasing rate reached about 15% after 36 hours and reached about 40% until 72 hours later. On the other hand, in this temperature, the pH decreased from 8.0 to 7.8. In the case of B mixtures, the decrease in the concentration of calcium ion was also notably observed in 12 hours of the monitoring after mixing. The decreasing rate reached about 20% up to 12 hours of elapsed time and reached almost 90% after 72 hours. In this condition, the pH slightly decreased from 7.8 to about 7.5. On the third condition, in the case of A mixtures after 24 hours elapsed time, the concentration of calcium ion was decreased by greater than 90%. On the other hand, the pH was gradually lowered below 7.0. According to past research, 80°F–90°F (27°C–32°C) temperature condition are optimum temperature range for yeast to grow and reproduce at fermentation stage [1]. So, it could increase the amount of calcium carbonate precipitation.

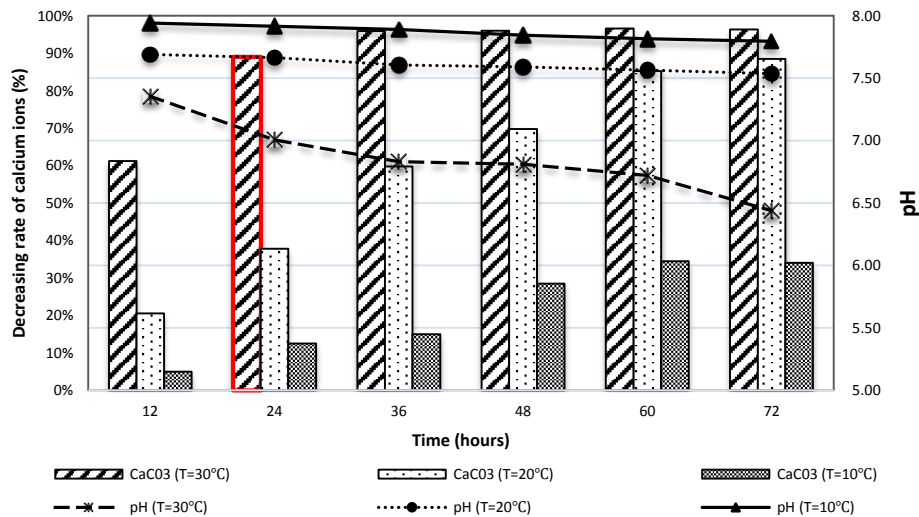


Fig. 5. Concentration of calcium ions and pH

Furthermore, the relation between decreasing rate of precipitation and precipitation rate by filtered paper is shown in Fig. 6. Decreasing precipitation rate was measured by using initial concentration of calcium ion ( $C_0$ ) and concentration of calcium ion measured ( $C_a$ ) based on Eq.2. The average difference between of decreasing rate of precipitation measured over precipitation rate calculated by filtered paper was less than 30%. The results were clearly confirmed that decreasing rate of precipitation similar to precipitation rate by measuring filter paper. The maximum precipitation of calcium carbonate was reached at 30°C temperature.

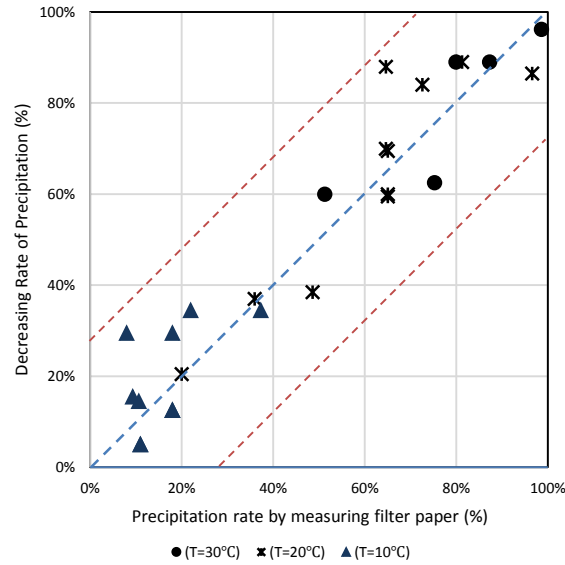


Fig. 6. Relation between decreasing rate of precipitation and precipitation rate by filtered paper

### 3.2. Effect of temperature on mineral microstructure

Calcium carbonate has three anhydrous polymorphs which are, in order of increasing solubility, calcite (rhombohedral), aragonite (orthorhombic) and vaterite (hexagonal). The calcium carbonate polymorph and precipitation rate depend on several parameters; i.e. water composition, temperature, and supersaturation. At ambient temperature, calcite is the most predominant phase [7].

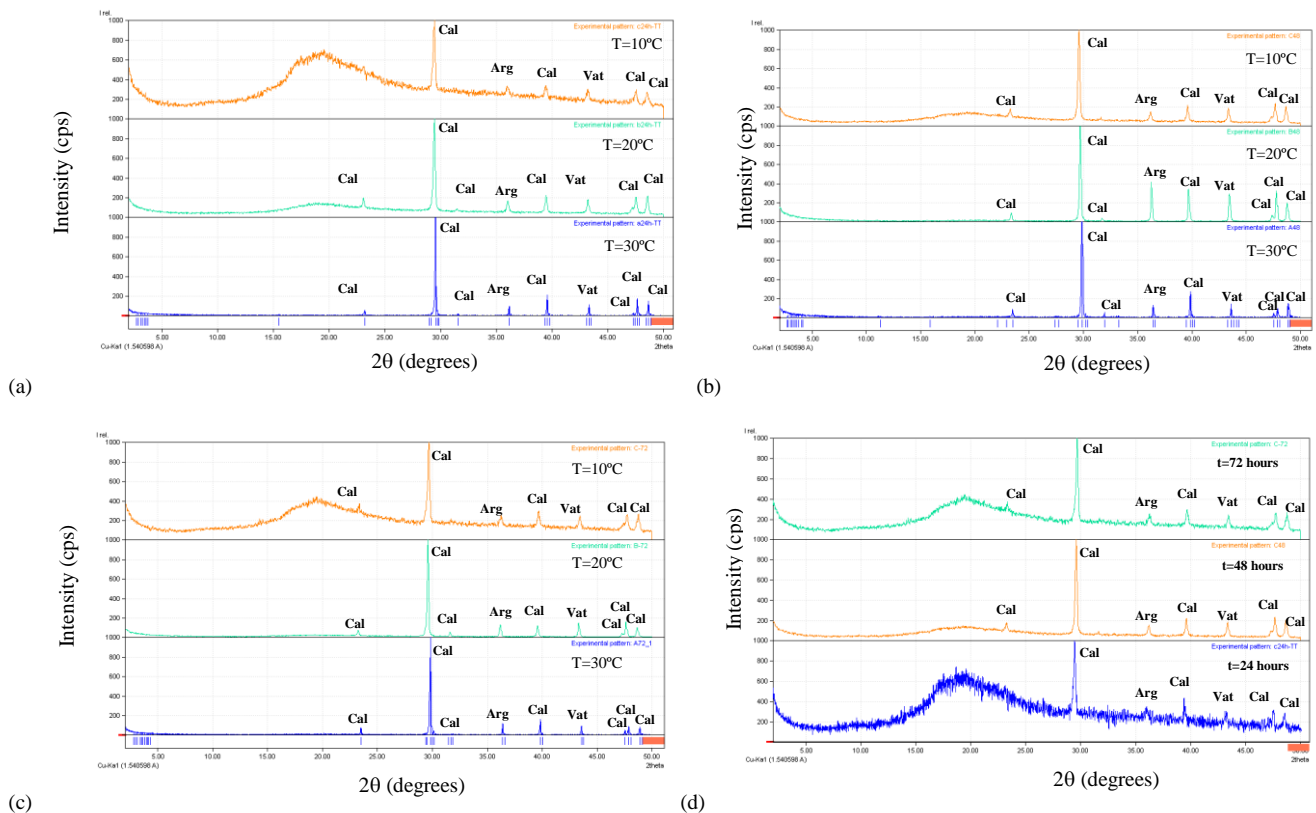


Fig. 7. Superposition of XRD Pattern obtained at different temperature; (a) after 24 hours elapsed time, (b) after 48 hours elapsed time, (c) after 72 hours elapsed time, (d) sampel in 10°C after 24, 48 and 72 hours elapsed time

The XRD patterns of the precipitates obtained at three temperature conditions in the presence of  $\text{CaCO}_3$  are presented in Fig. 7. At 10°C, the three polymorph of  $\text{CaCO}_3$  (aragonite, calcite, and vaterite) coexisted. However, after 24 hours elapsed time there was fluorite in this condition. It is because the growth rate of yeast was significantly reduced at temperatures under 20°C [1]. After

48 hours, intensities with respect to calcite increased. Correspondingly, after 72 hours calcite was the dominant polymorph of  $\text{CaCO}_3$  material as shown in 5 peaks of calcite in XRD pattern.

Similarly, in the 20°C, there were aragonite, calcite and vaterite polymorph in the calcium carbonate precipitation. After 24 hours elapsed time, there were 6 peaks of calcite, 1 peak of aragonite and 1 peak of vaterite. After 48 hours, the number of calcite polymorph pattern increased to 7 peaks. In the same way, after 72 hours elapsed time reached the same pattern. Otherwise, in the 30°C temperature, same pattern for 24 hours, 48 and 72 hours elapsed time. There were 7 peaks indicating the presence of calcite from 24 hours elapsed time. It is shown that calcite should be the dominant or only polymorph of  $\text{CaCO}_3$  formed by the loss of carbon dioxide if the temperature is the controlling factor. Moreover, when the temperature increased, the intensities of calcite reflections increased and became the major phase. Accordingly, the increase of the temperature promotes the calcite phase. It suggested that the crystals were mainly comprised of calcite.

#### 4. Conclusion

The result showed the effects of the temperature changes on the precipitation rate of calcium carbonate. Based on the weight of precipitates left in tubes after filtering, the maximum precipitation of  $\text{CaCO}_3$  was observed in the case of A mixtures (30°C temperature) and the lowest precipitation was in the case of (10°C temperature). The results were clearly confirmed by the calcium ion measurement in the mixtures. In the case of A mixtures, after 24 hours elapsed time the concentration of calcium ion was decreased by greater than 90%. On the other hand, the pH was gradually lowered below 7.0. Furthermore, the XRD method also showed effect of temperature changes. When the temperature increased, the intensities of calcite reflections increased and became the major phase. XRD analysis confirmed calcite should be the dominant polymorph of  $\text{CaCO}_3$ .

#### Acknowledgements

The authors acknowledge the scholarship from Government of Republic of Indonesia through Directorate General of Human Resource for Science, Technology and Higher Education. This research was supported by Grant-in-Aid for Scientific Research (B): 15H04025, the authors would like to express his sincere appreciation.

#### References

- [1] Gardiner, A. & Wilson, S. (1998). *Inquisitive Cook: Discover How a Pinch of Curiosity Can Improve Your Cooking*. New York: Henry Holt and Co.
- [2] International Center for Diffraction Data. (2015). *The Powder Diffraction File (PDF)-4/Minerals*. USA.
- [3] Karoui, H., Korchef, A., Tlili, M. M., Mosrati, H., Gil, O., Mosrati, R. & Ben Amor, M. (2008). Effects of  $\text{Mg}^{2+}$ ,  $\text{Ca}^{2+}$  and  $\text{SO}_4^{2-}$  Ions on Precipitation Kinetics and Microstructure of Aragonite. *Ann. Chim. Sci. Mater*, 33(2), 123–134.
- [4] Kawaai, K., Ujike, I. & Yamamoto, S. (2016). Some Considerations on Precipitation Rate of Calcium Carbonate in Bio-based Materials Used for Concrete Repair. *Proceeding of Concrete Solutions (imprinting)*
- [5] Kawasaki, S. et al., (2006). Fundamental Study on Novel Grout Cementing Due to Microbial Metabolism. *Journal of Japan Society of Engineering Geology*, Vol. 47:1, 2-12.
- [6] Kubo, K., Okazaki, S. & Ujike, I. (2013). Development of Microbial Metabolic Processes to Repair Concrete Joint Leakage. *Advanced Material Research*, Vol. 845, 158-162.
- [7] Mejri, W., Korchef, A., Tili, M. & M. Ben Amor. (2014). Effect of Temperature on Precipitation Kinetics and Microstructure of Calcium Carbonate in The Presence of Magnesium and Sulphate Ions. *Desalination and Water Treatment*, Vol. 52, 4863-4870.
- [8] Ujike, I., Kubo, F., Kawaai, K. & Okazaki, S. (2014). Influencing Factors Affecting Microbial Metabolic Processes of Bio Materials Used for Leakage Repairs. *Concrete Solutions*, 127-133.
- [9] Weiss, C.A., Torres-Cancel, K., Moser, R.D., Allison, P.G., Gore, E.R., Chandler, M.Q. & Malone, P.G. (2013). Influence of Temperature on Calcium Carbonate Polymorph formed from Ammonium Carbonate and Calcium Acetate. *Journal of Nanotechnology and Smart Materials*, Vol 1:105, 1-6.
- [10] Wiktor, V. & Jonkers, H.M. (2010). Quantification of Crack Healing in Novel Bacteria-Based Self-Healing Concrete. *Cement & Concrete Composites*. Vol. 33), 763-770.
- [11] Wiktor, V. & Jonkers, H.M. (2015). Field Performance of Bacteria-Based Repair System: Pilot Study in a Parking Garage. *Case Studies in Construction Materials*, Vol. 2, 11-17.
- [12] Wiktor, V. & Jonkers, H.M. (2015). Assessment of The Functionally of Bacteria-based Repair System for Concrete through ESEM Analysis. *15th Euro Seminar of Microscopy Applied to Building Materials*, 165-169.



Sustainable Civil Engineering Structures and Construction Materials, SCESCM 2016

## Mechanical properties of concrete with *Enterococcus faecalis* and calcium lactate

J.M.Irwan<sup>a,\*</sup>, L.H.Anneza<sup>a</sup>, N.Othman<sup>b</sup>, A.Faisal Alshalif<sup>a</sup>, M.M.Zamer<sup>a</sup>, T.Teddy<sup>a</sup>

<sup>a</sup>Jamilus Research Centre for Sustainable Construction (JRC), Faculty of Civil and Environmental Engineering, University Tun Hussein Onn, Malaysia.

<sup>b</sup>Micropollutant Research Centre (MPRC), Faculty of Civil and Environmental Engineering, University Tun Hussein Onn, Malaysia

---

### Abstract

Concrete is an important material used globally, diverse as it can be applied in all construction type or modify to be apply in specialize construction fields. Adding bacteria in concrete can improve the concrete properties and increase durability due deposited calcite by bacteria. However, calcite deposition by bacteria is limited by calcium available in cement. The objective of this research is to determine the effect of adding calcium lactate as an additional calcium source and bacteria on the concrete properties. The bacteria used is locally isolated and enriched to suite concrete environment. The type of the bacteria used is identified as *Enterococcus faecalis*. The calcium lactate is added into concrete mix with concentrations of 0.001 mol/l, 0.005 mol/l and 0.01 mol/l. Whereas, the bacteria is added as 3% Enterococcus Faecalis. Mechanical properties test such as compressive strength, flexural strength and tensile strength was conducted. Cubes of size 150mm × 150mm × 150mm were prepared for compressive strength test while of Dia 150mm by 300mm cylinder were prepared for tensile strength test. Flexural strength test was performed on prism of size 100mm × 100mm × 500mm. The result of compressive strength shows that adding *Enterococcus faecalis* with 0.005 mol/l of calcium lactate gave the highest strength of 42.8 MPa compared to control of 36 MPa. The tensile strength and flexural strength has a similar trend as compressive strength results. Where, both results were optimum with 0.005 mol/l concentration of calcium lactate. The result of tensile strength shows that *Enterococcus faecalis* with 0.005 mol/l obtained 3.18 MPa compared to control of 2.54 MPa. Flexural strength test result was 6.67 MPa for *Enterococcus faecalis* with 0.005 mol/l compared to control of 4.78 MPa. The overall results of bacteria with added calcium lactate showed promising result and further study on self healing capability is encouraging.

© 2017 The Authors. Published by Elsevier Ltd.

Peer-review under responsibility of the organizing committee of SCESCM 2016.

**Keywords:** Compressive strength; Flexural strength; Tensile strength; Enterococcus faecalis; Calcium lactate

---

\* Corresponding author. Tel.: +60 197758186

E-mail address: [irwan@uthm.edu.my](mailto:irwan@uthm.edu.my)



## 1. Introduction

Bacteria is a common microorganism found everywhere from soil, lakes, water dams and etc. Siddique and Chahal[1] states that there are approximately 40 million bacterial cells in 1g of soil and a million bacterial cells in a millimeter of fresh water. There are approximately five nonillion ( $5 \times 10^{30}$ ) of bacteria on earth. The bacteria species discovered by scientist from various places all around the world barely scratch the surface as there are constantly new discovery being made. Bacteria are able to promote the precipitation of calcium carbonate in the form of calcite. Calcium carbonate precipitation occurs as a by-product of a common microbial metabolic process which would help produce microbial calcite precipitation [2]. Bacterium added into concrete is able to improve concrete properties by production of calcium carbonate. This has been proven by several researchers done all over the world [1, 2, 3]. However, the bacterium used in this research varies from those used by others. The bacterium identified as *Enterococcus faecalis* is used in this research, isolated and enriched to suit concrete environment. This process was initiated during the early stage of research by Irwan [4]. The optimum percentage of 3% is used in this research based on previously research trial by Irwan [5]. Based on this trial, it was determine that 3% would provide the optimum results on strength and durability. Determining the optimum concentration of calcium lactate and the effect on compressive strength, flexural strength and tensile strength is the main reason of this research.

## 2. Experimental program

### 2.1 *Enterococcus faecalis* and calcium lactate

*Enterococcus faecalis* is added into concrete as a partial replacement of water. This bacterium is added into concrete in the form of bacteria liquid culture. One colony of bacteria was added into nutrient broth and shaken for ten days, based on bacteria growth curve. After ten days, the bacteria liquid culture was measured and used in fabrication. The calcium lactate added is measured based on the total amount of water used for fabrication. The calculation can be seen in Table 1. The amount of calcium lactate used in this study is adopted from Xu and Yao [6].

Table 1. Calcium lactate used in fabrication

Chemical formula of calcium lactate	$C_6H_{10}CaO_6$
Molar mass of calcium lactate	218 g/mol
$0.001 \text{ mol/L} \times 218 \text{ g/mol}$	0.22 g/L
$0.005 \text{ mol/L} \times 218 \text{ g/mol}$	1.09 g/L
$0.01 \text{ mol/L} \times 218 \text{ g/mol}$	2.18 g/L

### 2.2 Materials

The bacteria used is isolated from fresh urine and enriched to suit concrete environment. Concrete environment is high in alkaline and near to zero oxygen. All materials used in this study for concrete mixing and the 3% of *Enterococcus faecalis* is based on previously conducted study by Irwan [5]. Whereas, calcium lactate added into fabrication was done in several concentrations, which are 0.001 mol/l, 0.005 mol/l and 0.01 mol/l. The amount of material used for every batch casted in fabrication can be seen in Table 2. The calculated amount is based on G30 using DOE method. The fabrication of concrete was done according to BS 1881-125:2013 [7]. The samples were removed after 24 hour and are air dry until tests are conducted.

Table 2. Amount of materials prepared for fabrication

Materials	Cement (kg)	Sand (kg)	Aggregate (kg)	Water (kg)	<i>Enterococcus faecalis</i> (g)	Calcium lactate (g)
Control	16	28.15	45.70	8.63	-	-
3% <i>Ent.f</i>	16	28.15	45.70	8.37	259	-
3% <i>Ent.f</i> + 0.001 mol/l CL	16	28.15	45.70	8.37	259	1.90
3% <i>Ent.f</i> + 0.005 mol/l CL	16	28.15	45.70	8.37	259	9.40
3% <i>Ent.f</i> + 0.01 mol/l CL	16	28.15	45.70	8.37	259	18.80

\* Note: *Ent.f* (*Enterococcus faecalis*); CL (Calcium Lactate)

### 2.3 Test procedure

Mechanical tests that were performed are compressive strength, tensile strength and flexural strength test. All three tests were conducted using Universal Testing Machine (UTM). All tests were conducted on three samples after 28 days of curing. The average results are reported. Compressive strength test was performed using cubes of size 150mm × 150mm × 150mm. The test was done in accordance to BS EN 12390-3:2009[8]. Flexural strength test was conducted using prism of size 100mm × 100mm × 500mm based on BS EN 12390-5:2009 [9]. Tensile strength test was conducted using cylinder of Dia 150 by 300mm. The test was accordance to BS EN 12390-6:2009 [10].

## 3. Results and discussion

### 3.1 Compressive strength

The average results obtained for compressive strength test are presented in Table 3 and Fig. 1. The compressive strength of concrete containing calcium lactate and *Enterococcus faecalis* have significant increment towards the compressive strength. The highest compressive strength is obtained by 0.005 mol/L CL (42.8MPa) followed by 0.01mol/L CL (39MPa) then 0.001 mol/L CL (38.5MPa). After 28 days, there was a 18.9% improvement in the compressive strength of concrete specimens with 0.005 mol/L CL compared to control. Addition of 0.001 mol/L CL in concrete specimens obtained an increment of 6.9%. Whereas, 0.01 mol/L CL in concrete specimens increased compressive strength by 8.3%. The increment of compressive strength with 0.001 mol/L, 0.005 mol/L and 0.01 mol/L of CL compared to concrete specimens of *Ent.f* are 0.8%, 12% and 2% respectively. The improvement of compressive strength with the addition of CL in concrete specimens containing *Ent.f* is due to microbial precipitation of calcium carbonate. The precipitation of calcium carbonate increased with the addition of calcium source which increases the compressive strength [1-3].

Table 3. Average results of compressive strength, Tensile strength and Flexural strength

Materials	Compressive strength (Mpa)	Tensile strength (Mpa)	Flexural strength (Mpa)
Control	36.00	2.50	4.78
3% <i>Ent.f</i>	38.20	2.70	6.60
3% <i>Ent.f</i> + 0.001 mol/l CL	38.50	2.72	6.65
3% <i>Ent.f</i> + 0.005 mol/l CL	42.80	3.20	6.74
3% <i>Ent.f</i> + 0.01 mol/l CL	39.00	2.74	6.67



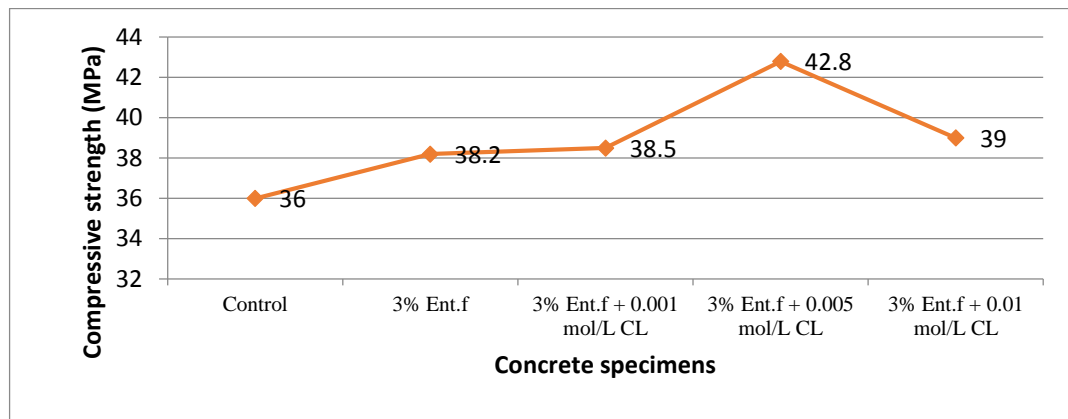


Fig. 1. Influence of different concentrations of calcium lactate on bioconcrete containing *Ent.f*

### 3.2 Tensile strength

Tensile strength test was conducted to determine the influence of bacteria and calcium lactate on tensile strength. The average result of tensile strength is shown in Table 3 and Fig. 2. The tensile strength results increases significantly with the addition of CL in concrete specimens containing *Ent.f*. The highest increment of tensile strength is with 0.005 mol/L CL. The tensile strength increased by 25.2% with concrete specimens containing 0.005 mol/L CL and *Ent.f* compared to control. The addition of 0.001 mol/L CL in concrete specimens containing *Ent.f* increased tensile strength by 4%. Whereas, 0.01 mol/L CL increased tensile strength by 8%. The increment tensile strength obtained with 0.001 mol/L, 0.005 mol/L and 0.01 mol/L CL compared to concrete specimens containing *Ent.f* are 0.7%, 18.5% and 1.5% respectively. The increment of tensile strength of bioconcrete containing calcium lactate is due to deposition of calcium carbonate. The addition of calcium lactate in the bioconcrete facilitated by acting as a food source for the bacteria. Previous researchers such as Faiz and Steve [11] and Gavimath [12] has reported similar results in which the addition of bacterial precipitation increases the strength of concrete.

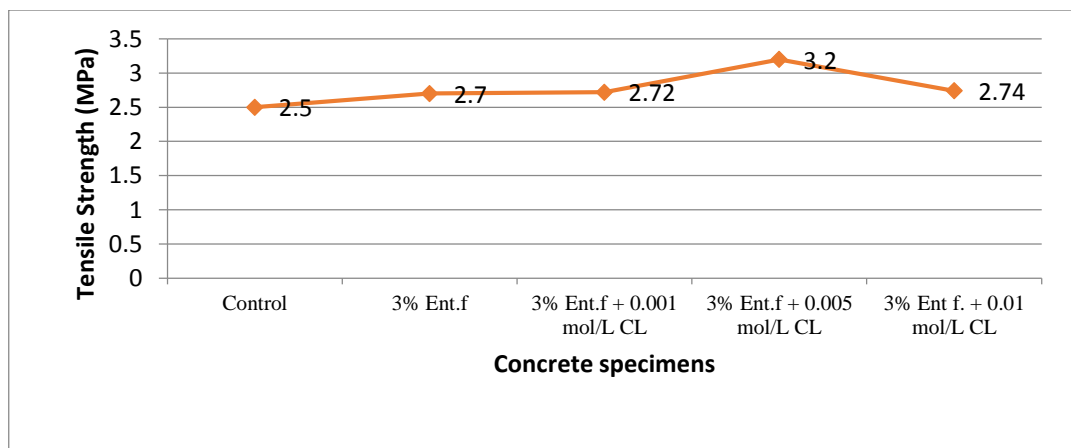


Fig. 2. Tensile strength of different concentrations of calcium lactate in bioconcrete containing *Ent.f*

### 3.3 Flexural strength

Resistance to flexure is tested by conducting flexural strength test. The average results of the test are presented in Table 3 and Fig. 3. The precipitation of calcium carbonate with calcium lactate by bacteria has increased the flexural

strength of concrete. The addition of 0.005 mol/L of calcium lactate in concrete containing *Ent.f* has increased the flexural strength by 39.5% compared to control. This is followed by 35.4% increment by 0.01 mol/L CL then 33.3% increment by 0.001 mol/L of specimens containing *Ent.f* compared to control. The addition of 0.001 mol/L, 0.005 mol/L and 0.01 mol/L has increased the flexural strength by 0.7%, 2.1% and 1% respectively compared to concrete with *Ent.f*. The highest increment of flexural strength is with 0.005 mol/L CL. The addition of microbial activity within the concrete by addition of calcium lactate has aided in the increment of flexural strength. The flexural strength of concrete correlates well with previous study which states that the addition of bacteria has profound impact on the flexural strength of prism by deposition of calcium lactate by bacteria [14].

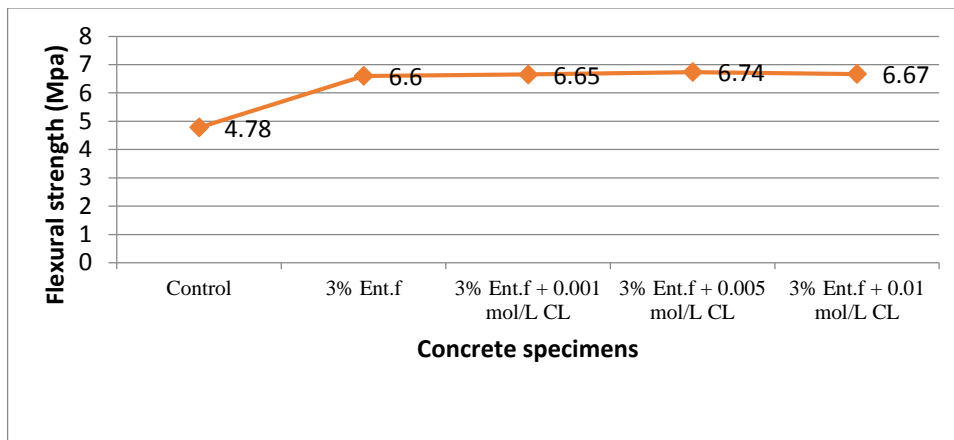


Fig. 3. Comparison between different concentrations of calcium lactate with bioconcrete containing *Ent.f*

#### 4. Conclusion

The calcium lactate added into 3% *Enterococcus faecalis* have positive results attributed to the increment of strengths obtained from the tests. The calcium lactate added act as an additional food source for the bacteria to precipitate calcium carbonate. The precipitated calcium carbonate fills the pores within the concrete matrix which creates a more compact concrete. This compact concrete is able to withstand higher load thus increasing the strength. The optimum concentration of calcium lactate added into 3% *Enterococcus faecalis* is 0.005 mol/L CL. This concentration has contributed to the increment of 16.4% of compressive strength, 25.2% increment of tensile strength and 39.5% increment of flexural strength.

#### Acknowledgements

This research was supported by Universiti Tun Hussein Onn Malaysia (UTHM) and The Ministry of Higher Education Malaysia through Fundamental Research Grant Scheme (FRGS), Vot 1211.

#### References

- [1] Siddique, R. and Chahal, N.K. Effect Of Ureolytic Bacteria On Concrete Properties. *Construction and Building Materials*. 2011, 25, 3791-3801.
- [2] Chahal, N., Siddique, R. Permeation properties of concrete made with fly ash and silica fume: Influence of Ureolytic bacteria. *Construction and Building Materials*, 2013, 49, 161-174.
- [3] Ramachandran, S.K., Ramakrishnan, V. and Bang, S.S. Remediation Of Concrete Using Micro-Organisms. *American Concrete Institute: Materials Journal*. 2001.
- [4] J.M.Irwan, A.FaisalAlshalif, N.Othman and R.M Asyraf, Isolation of Ureolytic and Sulphate reduction bacteria: Acclimatize to concrete environment. *International conference on civil, Biological and Environmental Engineering (CBEE)*, Istanbul, Turkey, 2014.

- [5] J.M.Irwan, A.FaisalAlshalif, N.Othmanand L.H.Anneza, Effect of Ureolytic Bacteria on Compressive strength and Water Permeability on Bio-concrete. International Conference on Civil, Architectural, Structural and Construction Engineering. August 21-23, Dong-A University, Seoul, Korea, 2015.
- [6] Xu.Jing and Yao, Wu. Multiscale mechanical quantification of self healing concrete incorporating non-ureolyticbacteria-based healing agent. Cement and concrete research. 64, 2014, 1-10.
- [7] British Standard Institution. Testing Concrete: Part 125: Methods for mixing and sampling fresh concrete in the laboratory. London, BS 1881-125:2013.
- [8] British Standard Institution. Part 3: Compressive strength of test specimens, London, BS EN 12390-3:2009.
- [9] British Standard Institution. Testing hardened concrete part 5: Flexural strength of test specimens.BS EN 12390-5:2009.
- [10] British Standard Institution Testing hardened concrete part 6: Tensile splitting strength of test specimens. BS EN 12390-6:2009.
- [11] Faiz.U.A,Shaikh and Steve. W.M.Supit. Mechanical and durability properties of high volume fly ash (HVFA)concrete containing calcium carbonate (CaCO<sub>3</sub>) nanoparticles.Construction and building materials.70(2014),309-321.
- [12] GavimathC.C.,Mali B.M.,Hooli V.R.,Mallpur J.D.,Patil A.B, Potential application of bacteria to improve the strength of cement concrete, International Journal of Advanced Biotechnology and Research, ISSN 0976-2612,Vol 3, Issue 1,2012, pg 541-544.
- [14] Majumdar.Sudipta,Sarkar.Manas,Chowdhury.Trinath,Chattopadhyay.Brajadulal and Mandal.Soraj. Use of bacterial protein powder in commercial fly ash pozzolana cements for high performance construction materials. Open journal of civil engineering, 2012, 2, 218-228.



Sustainable Civil Engineering Structures and Construction Materials, SCESCM 2016

## Recommendations based on experimental observations to design a printable cement-based material for construction

Imane Krimi<sup>a,b</sup>, Zoubeir Lafhaj<sup>a,\*</sup>, Laure Ducoulombier<sup>b</sup>

<sup>a</sup>*Civil Engineering departement, Ecole Centrale de Lille, Villeneuve d'Ascq, France.*

<sup>b</sup>*R&D division, Bouygues Batiment Nord Est, Villeneuve d'Ascq, France.*

---

### Abstract

The objective of this study was to define specifications of a printable cement based material. This paper proposes a definition and recommendations to design a « printable cement based material ». These recommendations are based on experimental work and observations carried out in the laboratory. A dedicated tool was designed for this experimental phase to simulate the implementation of cement-based material using a 3D printer. In the first part of this paper, an analysis of the literature overview on 3D printing for construction is detailed and analyzed. In the second part the experimental device designed especially for this study is presented and discussed. Finally in the third part a synopsis record of key parameters and properties to design a « printable cement-based materials » is proposed and discussed.

© 2017 The Authors. Published by Elsevier Ltd.

Peer-review under responsibility of the organizing committee of SCESCM 2016.

*Keywords:* Type your keywords here, separated by semicolons ;

---

### 1. Introduction

Additive Manufacturing (AM) consists in building an object layer by layer using a 3D CAD model, an appropriate material and a special machine [1]. Various technologies are associated with AM, going from paste extrusion to the deposition of a binder on a powder layer.

Additive manufacturing with cement based materials emerged in the world of construction in 1997 within the first paper on printing cement-based materials published by Pegna [2]. The technique used was based on applying a binder

---

\* Corresponding author. Tel.: +33 320 335 365; fax: +33 320 335 300.

E-mail address: [zoubeir.lafhaj@ec-lille.fr](mailto:zoubeir.lafhaj@ec-lille.fr)

on a cement powder. The idea of building layer on layer was proposed by the architect Nader Khalili [3]. Number of initiatives emerged thereafter. In 2010, Prof. Behrokh Khoshnevis of the University of Southern California presented 3D printed walls made with cement-based materials extrusion. Khoshnevis proposed the idea of building individual homes using a large-scale 3D printers [4], and named this technology ‘Contour Crafting’. A gantry system on which a printing head can move in the XYZ system was used for this technology. In the same year, Enrico Dini [5] unveiled a machine able to create large-scale elements from a powdered stone material bound together with a binder. A 2m high element was manufactured using Enrico Dini’s technology. The objective of using this technology was to build houses on earth and also on the moon [5]. In 2012, researchers from Loughborough University unveiled a large-scale 3D printer capable of extruding cement-based materials [6, 7]. In 2014 Loughborough University started collaboration with a construction company on the development of AM applied to construction. In the same year, additive manufacturing was used to produce 10 houses in 24 hours. This was achieved by “Winsun Corp” in China [8]. At the Institute of Advanced Architecture of Catalonia in Spain [9], an architectural element was printed using cement. Three mini-robots called ‘Minibuilders’ were used in this case. In 2015, The University of Berkeley [10] built a structure of 2.7 meters. This element, called ‘Bloom’, was made from 804 parts. These parts were manufactured using small-scale 3D printers. During the same year, a company [11] based in Netherlands published pictures of 3D printed concrete elements. A robotic arm was used to produce these elements. Recently an Italian company [12] unveiled a 3D printer that was 12m height. It was announced that this printer was able to print in cement and clay. Moreover, Andrey Rudenko developed a 3D printing machine for cement based materials. He announced that development was inspired from a desktop 3D printer. The printing system is moved using a gantry. The development started in the United States where elements of nearly 1m50 height were printed. In 2015 a collaboration in Philippines was started to build massive 3D printed expansion of a hotel [13].

Additive manufacturing applied to construction is still in a research and development phase. In fact large-scale industrial machines are not available on the market, neither suitable materials nor clear business models. The construction sector faces numerous challenges within the current economic context. Numbers of initiatives have pledged to reduce construction duration and find innovative solutions to respond to the growing need of housing. The completion of a construction project can range from few months to several years, which is relatively long compared to industry. New trends have emerged to reduce construction schedules: Modular construction- Prefabrication - automation. etc.

### *1.1 Previous work*

The current trend in AM applied to construction is the development of a cement based material usable for large-scale 3D printing. The formulation of a cement based material needs specifications of key properties. Only few studies were carried out to determine these key properties [6, 14]. Two printability indicators: extrudability and buildability were identified [6]. These indicators were controlled by the workability. Extrudability was defined as the capacity of fresh mortar to flow through pipes and nozzle to form a continuous filament. The extrudability test consisted in printing a range of 1 to 5 filaments of 300 mm. The test was passed if the extrusion occurred without blocking or cracking. The Buildability was defined as the ability to build a monolithic part layer by layer with minimal deformation. It is mainly influenced by the handling time. 34 layers were built without notable defaults. A complementary rheological characterization has identified a range of shear stress value between 0.3 kPa and 0.9 kPa to extrude cement based materials. The link between structural built up of cement based materials and 3D printing was studied [14]. A model to study the impact of layers superposition was presented. Cylinders of fresh cement-based materials were submitted to a 1.5 N load according to different frequencies. The loading frequency was correlated to printing velocity. Loading stopped once cracks appeared on sample’s surface.

### *1.2 Cement-based materials: the liquid stone*

Rheology is the science that study matter flow, in its liquid, semi-solid or solid state. The objective is to understand the behavior of a material under a shear stress. When a shear stress  $\tau$  is applied to a soft material a deformation will result. The shear rate is represented with  $\dot{\gamma}$  (1/s). When the relationship between shear stress  $\tau$  and shear rate  $\dot{\gamma}$  is

constant the material is described as a Newtonian fluid (Eq 1) where  $\eta$  is the apparent viscosity. In other cases the material is viscoplastic. In this case the apparent viscosity depends on the deformation rate (Eq 2).

$$\tau = \eta \cdot \dot{\gamma}' \quad (\text{Eq 1})$$

$$\tau = \eta(\dot{\gamma}') \cdot \dot{\gamma}' \quad (\text{Eq 2})$$

$$\tau = \tau_0 + \mu \cdot \dot{\gamma}' \quad (\text{Eq 3})$$

Concrete and cement based-materials can be considered, with good accuracy as yield stress materials [15, 16]. It is necessary to overcome a certain yield stress  $\tau_0$  to initiate flow. The relationship between the yield stress and the deformation rate in the case of cement based materials is generally expressed by the Bingham model (Eq 3) where  $\mu$  is the plastic viscosity [15].

The objective of this paper is to:

- Give a definition to printable cement based materials through literature review and highlight main properties to monitor.
- Propose a methodology to measure key properties.
- Propose a framework/guideline to design a printable cement based material.

## 2. Methodology

The objective of this paper was to suggest a definition and define recommendations to design a printable cement based material. These recommendations are based on experimental work and observations carried out in the laboratory. A dedicated system was designed for this experimental phase to simulate the implementation of cement based material using a 3D printer. Two reference printable materials were taken from literature: ‘LG’ from [6] and ‘CC’ from [17]. An extrudable cement paste ‘CP’ and a mortar ‘MO’ were added for comparison. We tried to get as close as possible to formulations gathered from literature review to carry out laboratory testing and check some data and results.

A printable cement based material should be soft enough to flow through pipes and in same time have the behavior of a solid once deposited. The literature review and the experimental work showed that mortars can have a semi solid behavior when no stress was applied. Two printability indicators were defined in literature: Extrudability and Buildability [6, 14]

### 2.1 Material

So as to able to reproduce formulations from literature, the type of cement and sand granular distribution were considered. In a 3D printing process material is supposed to extrude through an orifice. Considering material used for concrete projection or pumping [18] sand is chosen according to the diameter of the hose. The largest aggregate size must be four times smaller than orifice diameter ( $D_{\max} < D_{\text{orifice}}$ ). In University of Loughborough an extrusion orifice of 9 mm was combined with a sand maximum size of 2 mm. The used binder was a mix of CEM I 52.5, fly ash and silica fume. Details about components used in Contour Carafing’s material (CC) were unfortunately not specified.

In this study a normalized sand AFNOR EN 196-1 was used, this sand was sieved and corrected to obtain a sand (S) with same granular distribution as Loughborough’s sand (LG-S). Graphic in Fig. 1 shows the granular distribution of the sand used in this study compared to ‘LG-S’ sand. A plasticizer was used for the Contour crafting mix. A CEM I 52.5 N was used in the binder.

The composition of the studied materials is shown in Table 1. “CC” designates the material developed through Contour crafting project, the material contains 29 % of cement (binder) and 57 % of sand. “LG” is the material developed in the University of Loughborough, it contains 34 % of binder (70 % cement+20 % Fly ash+ 10 % Silica fume). “CP” is a cement paste and “MO” is a mortar, these materials were designed in the laboratory for comparison.

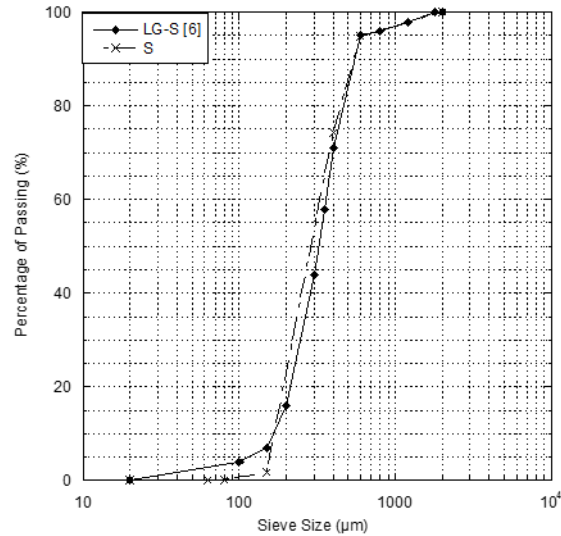


Fig. 1 Granular distribution of sand: 'S' sand used in this study and 'LG-S' sand used in [6]

Mixes were prepared by mixing water and the binder for 2 min at 140 rpm in a 5L mixer. Then sand was added and the mixing continued for 2 min at a speed of 280 rpm. For each batch series of tests were conducted: Slump test-Density measure-Extrudability-Buildability.

Table 1 Proportions of Mix designs

	B (%)	S (%)	W (%)	PI (%)	W/B
<b>CP</b>	77	0	23	0	0.30
<b>MO</b>	47	36	17	0	0.35
<b>LG</b>	34	51	15	0	0.45
<b>CC</b>	29	57	12	2	0.40

## 2.2 Extrudability

The ability of tested mixes to extrude was tested through a piston system. This system was designed in the laboratory for this purpose. It was composed of a tube of  $D=50$  mm diameter and 200 mm of length, the tube has an orifice of  $d=10$  mm in its bottom to allow material extrusion.

Once a mix was ready, the fresh material was introduced inside the tube and the piston applied a controlled displacement of 5mm/s. The length of the extruded material was recorded. A similar system was used by [19] to measure rheology of semi-solid mortars.

## 2.3 Buildability

In 3D printing material is deposited layer on layer. Which implies that the fresh mortar should be able to bare the deposited layers. A device was developed in laboratory to simulate this layer deposition. The test was performed by applying incremental loads to a sample and measuring its deformation.

An incremental loading was used in our case. After mixing, fresh mortar samples of 60 mm diameter and 30 mm were manufactured and tested. A roughened plate was added to the bottom and the up of the consolidation system to avoid sample's slipping. Stress was applied in the vertical direction, lateral deformations were allowed. The loading was incremented each 30 s to simulate a 3D printer that deposits layer each 30 s. Fractures in the surface of the sample were monitored and the applied stress was recorded until the cracking of the sample as shown in Fig. 3.

### 3. Results & Analysis

Fresh mortars characterization included slump test and density measurement. After these values were recorded extrusion and buildability tests were carried out.

Table 2 Results of fresh material characterization

	Slump (mm)	$\rho_{\text{fresh}}$ (kg/m <sup>3</sup> )	Extrusion speed (cm/s)	Critical vertical stress (kPa)
<b>CC</b>	4	2206	25	6
<b>LG</b>	20	2694	15	11
<b>MO</b>	30	2585	21	16
<b>CP</b>	20	2796	63	21

Test results are shown in Table 2. The slump value ranges from 4 mm to 30 mm. According to the EN 206-1:2000 standard these values corresponds to ‘S1 class’ which represents stiff mortars. ‘CC’ is stiffer than ‘LG’ and CP which are stiffer than MO. Fresh density ranges from 2206 to 2796 kg/m<sup>3</sup>. The cement paste ‘CP’ has the highest density while ‘CC’ has the lowest value. This may be explained by sand adding. Sand changes the microstructural structure of the homogenous cement paste. Voids are created between aggregates. These voids are filled with air which reduces the density of the fresh mortar.

The recorded extrusion output velocity for ‘CP’ was 63 cm/s, 25 cm/s for ‘CC’, 21 cm/s for ‘MO’ and 15 cm/s for ‘LG’. The ability of ‘CP’ to extrude was 4 times the ability of ‘LG’ to extrude. The critical vertical stress was recorded when first fractures appeared on samples. This value goes from 6 kPa to 21 kPa. The highest value was recorded for ‘CP’ and the lowest for ‘CC’. It was noticed that the extrusion speed and the critical vertical stress were linked to sand and cement content. In the following these values are analysed considering cement and sand content.

#### 3.1 Extrusion

Fig. 2 shows the representation of Extrusion Speed according to cement and sand content. The extrusion speed of ‘CP’ was higher than ‘MO’ and ‘CC’ which were also higher than the extrusion speed of ‘LG’. The sand content of CP was 0 %, 36 % for MO, 51 % for LG and 57 % for CC. The cement content of ‘CP’ was 77 %, 47 % for MO, 34 % for LG.

Considering slump values ‘LG’ and ‘CC’ are stiffer than ‘MO’ and ‘CP’. The extrusion speed of ‘LG’ and ‘CC’ is lower. These materials require higher piston pressure to extrude than ‘MO’ or ‘CP’.

It was noticed that the extrusion speed decreased with sand content and increased with cement content. A pressure on the piston was required to extrude the material. In our case the pressure was constant, which explains speed changes. In theory this phenomenon is due to the tribology of cement based materials [20]. These materials tend to stiffen when no constraints are applied and to flow when sufficient shear is applied. The adding of sand increased friction constraints. To equilibrate these additional constraints, the piston pressure should be increased to overcome the critical friction stress  $Kw_0$  [21].

The ‘CC’ sample didn’t follow this general tendency. This may be explained by the migration of the cement paste (matrix) through the particle skeleton due to plasticizer content [22]. Mortars are two-phase materials, they are composed of a cement paste matrix and of aggregates suspensions. Flow velocity in the case of two-phase fluids is the combinations of the matrix velocity and of the particle skeleton velocity. This difference in velocity involves segregation. Further tests should be carried out on this mix. The piston system may also contribute to the disconnection between sand aggregates and cement paste.



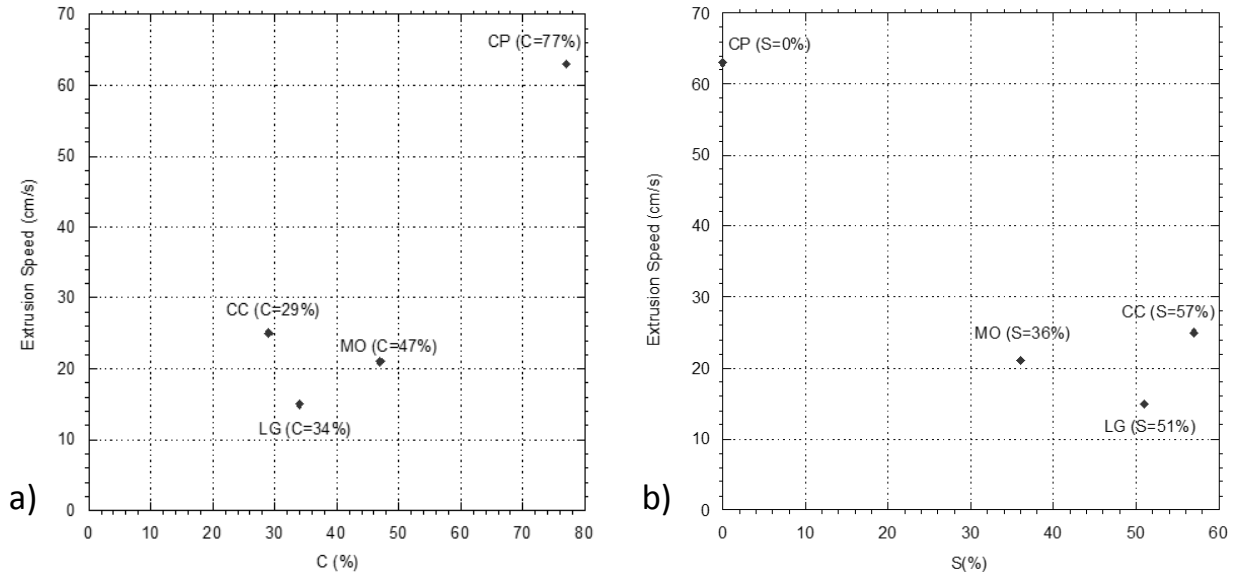


Fig. 2 Representation of the Extrusion Speed according to cement content (a) and to sand content (b)

### 3.2 Buildability

The critical constraint was recorded when a fracture appeared on the sample. Fig. 3 shows a sound sample (a) and a fractured sample (b). The vertical constraint was increased with increments of 5 kPa each 30 s. Fig. 4 shows the representation of the critical vertical stress according to cement and sand content. The vertical strength of ‘CP’ was higher than ‘MO’, ‘LG’ and ‘CC’. The sand content of CP was 0 %, 36 % for MO, 51 % for LG and 57 % for CC. The cement content of ‘CP’ was 77 %, 47 % for MO, 34 % for LG. The critical stress decreases with sand content and increased with cement.

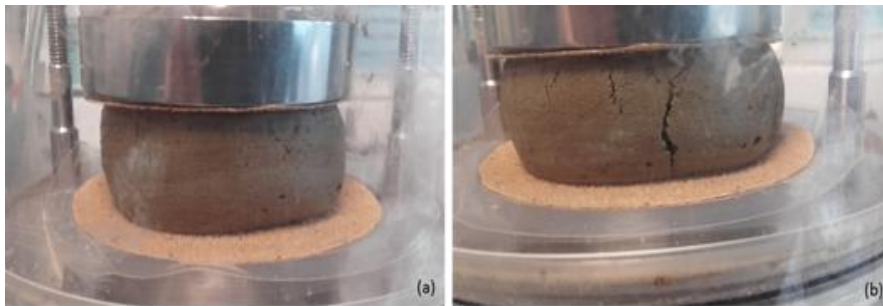


Fig. 3 Sound sample at the beginning of the incremental loading (a) and Cracked sample at the end of the incremental loading (b).

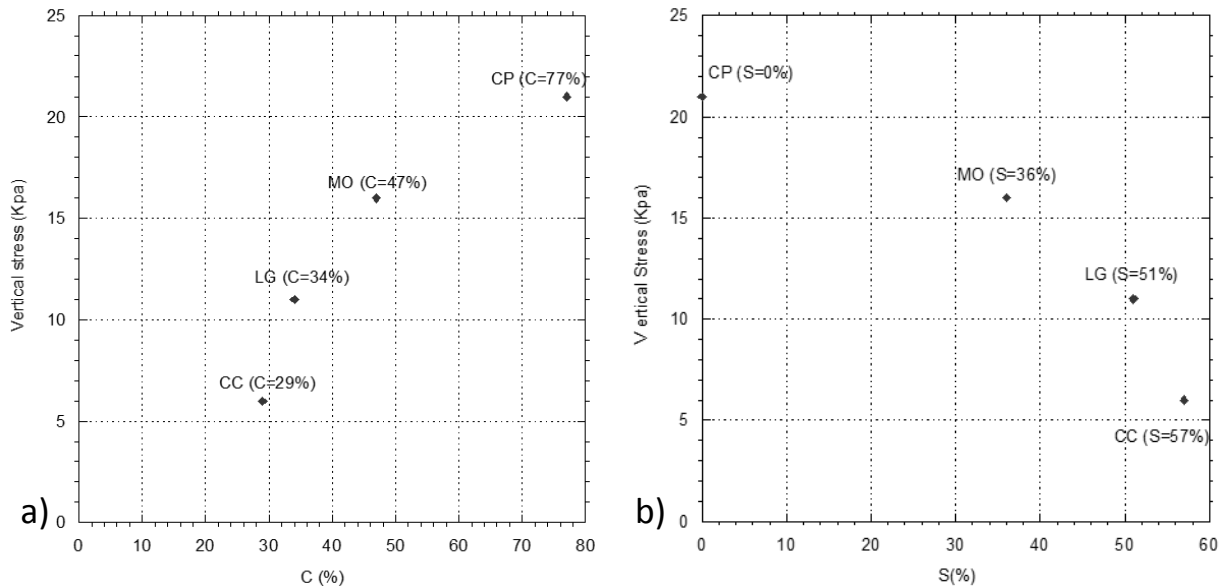


Fig. 4 Representation of the critical stress according to cement content (a) and sand content (b)

Cement based materials have a shear-thinning behaviour, these materials need a mechanical solicitation to flow. This behaviour is modelled by the Bingham model. The yield stress  $\tau_0$  reflects the consistency of fresh concrete, high shear rate concrete tends to have a semi-solid behaviour. On the other hand, the plastic viscosity  $\mu$  reflects the ability of the material to flow.

During piston extrusion, a pressure was applied to the material. When the applied stress exceeded the shear yield stress of the material ( $\tau_0 < \tau_{\text{piston}}$ ) and the critical friction stress, the system flowed according to the plastic viscosity. A similar study was carried out by [19]. Series of orifice extrusion tests were conducted on highly concentrated semi-solid cement mortars under various extrusion velocities. The orifice extrusion was used as a tool to quantify the rheological behaviour of tested materials. In our case, extrudability can be linked to the plastic viscosity of the material and is controlled by the applied pressure. The extrudability decreases with sand content.

In buildability tests, the material was subjected to a vertical constraint which simulated the loading of next layers above. The material must withstand these layers without cracking. A similar study was led by [14]. A theoretical framework was presented where the vertical stress acting on the first deposited layer was compared to the critical stress of material. This framework was validated by simulating layer deposition using a loading device. The compression principle was inspired from the squeezing test which is a tool used in rheology measurement [23, 24]. The material remains solid as  $\tau_{\text{applied}} < \tau_0$ . The normal stress  $\sigma$  and the shear stress  $\tau$  are linked through a relationship that depends on sample's geometry [14, 24]. The cement content contribute to increase materials buildability. However cement is expensive and have a negative impact on the environment. Other materials, like sand, are generally added to cement reduce its cost and environmental impact.

#### 4. Conclusion and perspectives

In this paper a literature review highlighted main fresh properties of a printable cement based materials. An experimental device was specially designed to simulate 3D printing based on key properties. Some materials were taken from literature for laboratory testing. The printability of fresh mortars depends on the rheological behaviour of materials. Main parameters are the yield stress and the plastic viscosity. To formulate a printable cement based material, the operator should take into account these parameters and extrusion system characteristics. Materials with low sand content seems to extrude easily than materials with high percentage: the extrusion speed was 63cm/s when 0% of sand was used and 15 cm/s with 51 % of sand. This is due to the friction stress. On the other hand, material with

high cement content developed a 21 kPa vertical green strength. This can be attributed to cement based materials thixotropy. This study is a part of an ongoing research project, the objective is to achieve a  $1 \times 1 \times 1 \text{ m}^3$  3D printed element.

## References

- [1] ASTM International, ASTM F2792-12a, Standard Terminology for Additive Manufacturing Technologies, (Withdrawn 2015), (2012). [www.astm.org](http://www.astm.org).
- [2] J. Pegna, Exploratory investigation of Solid freeform construction, *Autom. Constr.* 5 (1997) 427–437.
- [3] Nader Khalili, Emergency Sandbag Shelter and Eco-village: Manual-How to Build Your Own with Superadobe/Earthbag, 2012.
- [4] B. Khoshnevis, Automated construction by contour crafting-related robotics and information technologies, *Autom. Constr.* 13 (2004) 5–19.
- [5] G. Cesaretti, E. Dini, X. De Kestelier, V. Colla, L. Pambaguian, Building components for an outpost on the Lunar soil by means of a novel 3D printing technology, *Acta Astronaut.* 93 (2014) 430–450.
- [6] T. Le, S. Austin, S. Buswell, A. G. Gibb, A. Thorpe, Mix design and fresh properties for high-performance printing concrete, *Mater. Struct.* 45 (2012) 1221–1232.
- [7] T.T. Le, S. a. Austin, S. Lim, R. a. Buswell, R. Law, a. G.F. Gibb, et al., Hardened properties of high-performance printing concrete, *Cem. Concr. Res.* 42 (2012) 558–566. doi:10.1016/j.cemconres.2011.12.003.
- [8] Winsun & Co, YINGCHUANG Integrated 3D Printing Technology for Buildings, (2014). <http://www.yhbm.com/index.php?a=lists&c=index&catid=67&m=content> (accessed January 26, 2016).
- [9] IAAC, Minibuilders, Small Robot. Print. *Big Struct.* (2014). <http://robots.iaac.net/> (accessed January 26, 2016).
- [10] M. Cocoma, UC Berkeley unveils first-of-its-kind 3-D-printed cement structure, (2015). <http://news.berkeley.edu/2015/03/06/bloom-3-d-printed-cement-structure/> (accessed January 26, 2016).
- [11] CyBe, Redefining Construction By Enabling 3D Concrete Printing, (2014). <http://www.cybe.eu/> (accessed January 26, 2016).
- [12] WASP Project, BigDelta- La storia , (2014). <http://www.wasproject.it/w/bigdelta-la-ricerca/> (accessed January 26, 2016).
- [13] 3Ders, Lewis Grand Hotel teams with Andrey Rudenko to develop world’s first 3D printed hotel, planning construction of homes | 3D Printer News & 3D Printing News, (n.d.). <http://www.3ders.org/articles/20150909-lewis-grand-hotel-andrey-rudenko-to-develop-worlds-first-3d-printed-hotel.html> (accessed April 13, 2016).
- [14] a. Perrot, D. Rangeard, a. Pierre, Structural built-up of cement-based materials used for 3D-printing extrusion techniques, *Mater. Struct.* (2015). doi:10.1617/s11527-015-0571-0.
- [15] O.H. Wallevik, J.E. Wallevik, Rheology as a tool in concrete science: The use of rheographs and workability boxes, *Cem. Concr. Res.* 41 (2011) 1279–1288. doi:10.1016/j.cemconres.2011.01.009.
- [16] N. Roussel, A thixotropy model for fresh fluid concretes: Theory, validation and applications, *Cem. Concr. Res.* 36 (2006) 1797–1806. doi:10.1016/j.cemconres.2006.05.025.
- [17] D. Hwang, B. Khoshnevis, CONCRETE WALL FABRICATION BY CONTOUR CRAFTING Dooil Hwang and Behrokh Khoshnevis, (2004).
- [18] F.E.F. du Béton, Le pompage des bétons, 2008. [www.efbeton.com/\\_template/\\_.../POMPAGE\\_EFB\\_V3\\_12\\_08\\_part1.ppt](http://www.efbeton.com/_template/_.../POMPAGE_EFB_V3_12_08_part1.ppt).
- [19] X. Zhou, Z. Li, M. Fan, H. Chen, Rheology of semi-solid fresh cement pastes and mortars in orifice extrusion, *Cem. Concr. Compos.* 37 (2013) 304–311. doi:10.1016/j.cemconcomp.2013.01.004.
- [20] A. Perrot, Y. Mélinge, D. Rangeard, F. Micaelli, P. Estellé, C. Lanos, Utilisation d ’ une extrudeuse a piston pour étudier le comportement rhéologique et tribologique d ’ un matériau à fort seuil de cisaillement à faible taux de cisaillement, in: XXXe Rencontres AUGC-IBPSA Chambéry, Savoie, 6 Au 8 Juin 2012, 2012.
- [21] N. Roussel, C. Lanos, Plastic Fluid Flow Parameters Identification Using a Simple Squeezing Test, in: *Appl. Rheol.*, 2003: pp. 132–141. doi:10.3933/ApplRheol-13-132.
- [22] M. Chaouche, F. Chaari, G. Racineux, a. Poitou, Comportement de fluides pâteux en écoulement d’écrasement, *Rhéologie(Châtenay-Malabry)*. 3 (2003) 46–52.
- [23] Z. Toutou, N. Roussel, C. Lanos, The squeezing test: A tool to identify firm cement-based material’s rheological behaviour and evaluate their extrusion ability, *Cem. Concr. Res.* 35 (2005) 1891–1899. doi:10.1016/j.cemconres.2004.09.007.
- [24] J. Engmann, C. Servais, A.S. Burbidge, Squeeze flow theory and applications to rheometry: A review, *J. Nonnewton. Fluid Mech.* 132 (2005) 1–27. doi:10.1016/j.jnnfm.2005.08.007.



Sustainable Civil Engineering Structures and Construction Materials 2016, SCESCM 2016

## *Bacillus subtilis* HU58 immobilized in micropores of diatomite for using in self-healing concrete

Nguyen Ngoc Tri Huynh<sup>a</sup>, Nghi Mai Phuong<sup>a</sup>, Nguyen Phung Anh Toan<sup>a</sup>, Nguyen Khanh Son<sup>a,\*</sup>

<sup>a</sup>Faculty of Materials Technology, Ho Chi Minh city University of Technology (HCMUT),, District 10, Ho Chi Minh city, Vietnam

---

### Abstract

Recent studies reveal that using bacteria to mix into concrete material promote generating specific precipitated product. Such product allows improving physio-mechanical properties of concrete materials at both early and later age. This experimental study deals with the use of *Bacillus subtilis* HU58 and natural diatomite Lam Dong as controlled release agent to formulate bacterial concrete. We investigated self-healing effect during long period of curing time up to 24 months. Given in the result of material analysis, there is an increasing crystallinity of precipitated calcite by bacteria. At a smaller scale in bacteria modified mortar (prismatic samples 40x40x160 mm), both compressive and flexural strengths increase in comparison with those of normal sample, 57 → 61 MPa (in compression) and 9 → 11 MPa (in flexion). At greater scale in bacterial concrete (cube samples 150x150x150 mm), compressive strengths are higher (about 18 %) than obtained results of normal concrete sample at age of 2 months. For the reason of better control of process of precipitation, *Bacillus subtilis* HU58 and nutrient were first immobilized in diatomite Lam Dong, before introducing in cement matrix. We examined self-healing capacity of crack opening that were artificially prepared (1-1.8 mm by width) after early setting of cement mortar. Results of the water permeability test, developed in laboratory presented the evidence of remediating crack and fissure due to bacteria.

© 2017 The Authors. Published by Elsevier Ltd.

Peer-review under responsibility of the organizing committee of SCESCM 2016.

**Keywords:** Bacteria modified mortar, self-healing concrete, *Bacillus subtilis*, precipitated calcite.

---

---

\* Corresponding author. Tel.: +84-0933-623-629.

E-mail address: [ksnguyen@hcmut.edu.vn](mailto:ksnguyen@hcmut.edu.vn)

## 1. Introduction

Smart materials with self-healing capacity are now regarded as a good candidate material solution for sustainable development. Bio-concrete or bacteria modified concrete, recently developed in laboratory, is a promising solution in the sector of construction materials. In general, biological approach in self-healing materials takes inspiration from the natural phenomenon of bone regeneration in human body. Micro cracks or cracks opening, generated in the material matrix were able to heal themselves progressively with such natural glue. In comparison with other techniques based on chemical and natural processes, more advantage in term of effectiveness and environment-friendly results are attributed to bacteria-based technique [1]. In concrete material, process of cement hydration permits to establish the microstructure and to specify the mechanical resistance of structural elements. Bio-mineralization process of calcite in its turn permits to remediate cracks, fissures, capillary pores in microstructure for durable concrete at later age. Current research issues on this topic tend to explore different species of bacteria in laboratory study and technology development of this laboratory proven concept in construction sites.

Bacteria genera of *Bacillus* are well-known by its anaerobe and activity in high alkali solution. Recent studies reveal the use of *Bacillus pasteurii* and *Bacillus pseudofirmus* cohnii DSM 8715 in self-healing concrete [2]. Nutrient solution of calcium lactate or urea/  $\text{CaCl}_2$  almost were feed with a high concentration of microbial in order to mineralize calcite as precipitated product [2]. According to the review of Al-Thawadi et al. and Ghosh et al., most of researchers agree that the phenomenon of calcite precipitation occurs initially on the bacteria spores and progressively develop toward outer bound [3]. We focus on two objectives in the following paragraphs. First, we attempt to clarify the mechanism of combination of *Bacillus subtilis* HU58 bacteria and diatomite, name controlled release agent. To do so, bacteria and nutrient solution were mixed with natural diatomaceous earth to produce pellet capsule of diatomite. Then, we use such particle as aggregate components in mix proportion of bacterial mortar and concrete. Second, we conduct studies on the self-healing behavior at later age of concrete sample and the variation of mechanical resistance of cement mortar. In closing, we discuss on the performance of *Bacillus subtilis* HU58 immobilized in microporous structure of diatomite with regard to the result of water permeability test on different self-healing samples.

## 2. Materials and experimental method

Bacterial solution were prepared from urea,  $\text{CaCl}_2$ , and *Bacillus subtilis* HU58 ( $10^9$  cfu/g) with proportional mixture given in table 1. We used the resource of natural diatomaceous earth Lam Dong. Such diatomite had a moderate grade with silica content about 70 wt% in the form of silica gels and 20 wt% alumino-silicate compound. Homogeneous mixture of bacterial solution and dry diatomite powder could be obtained after 10 minutes in laboratory planetary mixer. Taking into account the presence of clay content, we applied the plastic forming technique to granulate the mixture in pellet capsule 10 mm diameter, 10 mm height (figure 1). The ratio of bacterial solution/solid powder was fixed at 1.26 wt%. These pellet capsules were then coated with cement paste ( $w/c=0.5$ ) and placed for drying in dry air before using as normal aggregate component of concrete.

Table 1. Mixing proportion of bacterial solution (1.26 wt% of cement in bacteria modified mortar sample)

	<i>Bacillus subtilis</i> HU58	Urea	$\text{CaCl}_2 \cdot \text{H}_2\text{O}$	Nutrient Broth	Total
wt%	0.49	0.44	0.22	0.11	1.26



Fig. 1. (a) diatomite pellet capsule (b) coated capsule with cement paste ( $w/c=0.5$ )

Other concreting materials were Portland cement PC40 – Ha Tien, standard sand, well-graded coarse aggregate ( $D_{max}=20$  mm) and tap water. Those materials went through series of quality control tests conforming to the specific requirement of Vietnamese standard TCVN. A small amount 1.26 wt% (cement) of the bacterial solution was seeded in fresh mortar as a chemical admixture to formulate bacteria modified cement mortar. Prismatic samples  $40\times40\times160$  mm of (bacterial modified mortar and controlled mortar without bacteria) were casted in mold and cured in laboratory condition (TCVN 6016:1995) until appropriate time for mechanical resistance test. Controlled sample of concrete grade M300 without bacteria was manufactured as reference. Two others batches of bacterial concrete were manufactured with diatomite pellet 0.5 wt% (mixing as coarse aggregate) and with bacterial solution 0.5 wt% (mixing directly with tap water). All concrete samples were casted in cubic molds  $150\times150\times150$  mm. Demolded samples were then cured in laboratory condition until time interval 60 days for compression test. Relating to the self-healing test, we produced cylindrical samples (90 mm diameter) of bacteria modified mortar. 20 mm thick slices of mortar were cut from 14 age day samples and then broken into two pieces during a splitting test. Broken slices of mortar were kept in the right position to submerge for curing in water tank. We examined the state of cracked samples after another 28 days of curing time and also had recourse analytical analysis of healing glue material.

### 3. Results

#### 3.1. Precipitated calcite in diatomite pores

As mentioned, we relied on the assumption that diatomite capsule could contribute to the process of controlled release bacterial solution in cement matrix. Figure 2 describes the test of two pellet capsules immersing in water: the first one (a) is original pellet with cement paste coating and the second one (b) is cut in half. As given in the figure 1c and 1d, we found on the broken surface of diatomite pellets (after 3 days) many white and small particles. In particular, for the second sample, these scattering products were generated clearly in the matrix binder and we can observe with the naked eyes. That is not evident in case of the first sample.

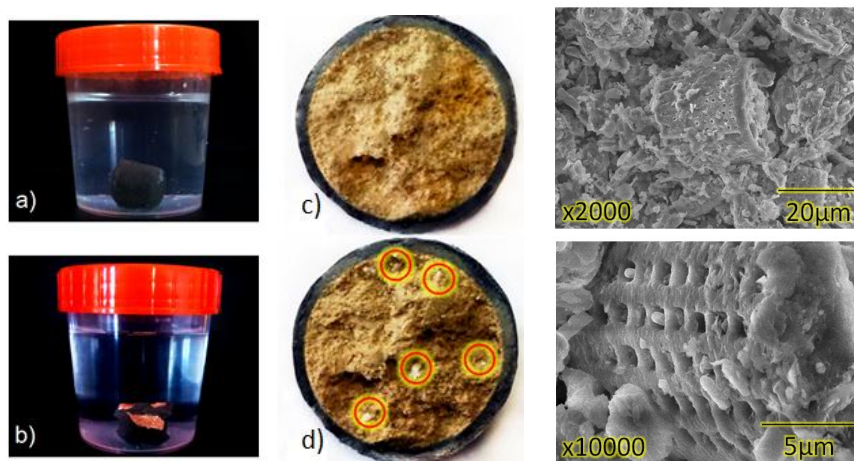


Fig. 2. left: (a) diatomite pellet in water; (b) broken diatomite pellet in water; (c) inside the broken pellet; (d) calcite precipitation inside diatomite pellet. Right: SEM images of diatomite immobilized bacteria

We collected these generating products as sieve residue  $90\mu\text{m}$  for analytical analysis. Results of XRD analysis (figure 2) shows that there is a continuous increase of peak intensity of calcite mineral. Thermal analysis by DSC confirms the existing product of precipitation with an endothermic peak of calcite decomposition at  $840^\circ\text{C}$ . It means, over curing time in high moisture content, bio-mineralization process by *Bacillus subtilis* HU58 occurred inside micropores of diatomite matrix. To examine the porous microstructure of diatomite in high solution SEM clichés (figure 2-right), we noted that some microbial spore occupied pore position. That resulted probably from normal



dissolution during mixing period. We attempted to confront the obtained result with the previous study of Zweers et al., [4] and TEM images of *Bacillus subtilis* spores by Yoon et al. [5]. There is a great similarity in spore-like structure of bacteria. Furthermore, in term of microbial concentration, after 5 months, there was a small deduction of  $2.7 \times 10^8$  cfu/g from the initial concentration of *Bacillus subtilis* HU58  $10^9$  cfu/g. Indeed, up to 80 % bacteria spore still be active in the producing diatomite pellets.

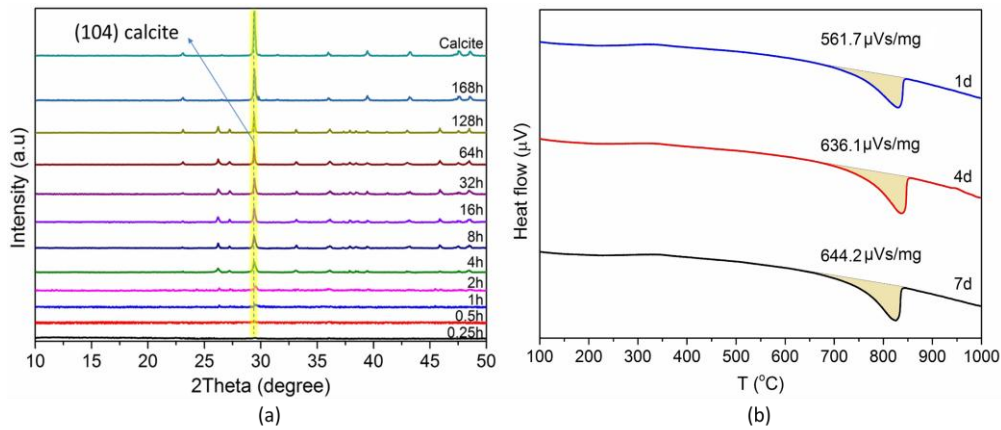


Fig. 3. (a) XRD patterns of precipitated product inside the broken diatomite pellets; (b) result of thermal analysis DSC of precipitated product.

### 3.2. Mechanical properties of bacterial sample

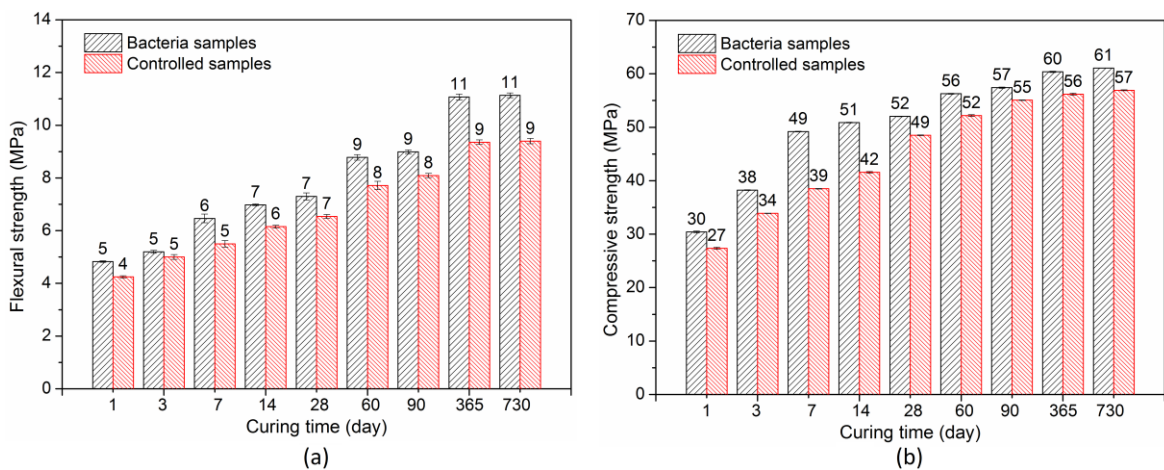


Fig. 4. Compressive strength of bacterial mortar and controlled samples.

Both compressive and flexural strength of mortar sample were registered in the figure 4. Till the age of 2 years cured in normal condition, results figure out the evidence of higher resistance of bacteria-modified mortar: 61 MPa in compression and 11 MPa in flexion comparing to result values respectively 57 MPa and 9 MPa for controlled samples. It is noted that due to small sample size, bacterial solution was dispersed directly into mixer without using capsule pellets. It seems that generating product of calcite in cement matrix is responsible for such strength gain. With regard to the different bacteria species, we also highlight better results with *Bacillus subtilis* HU58 (+ 36 % strength gain relative to controlled sample) of compressive strength than those mentioned in the study of Ghosh et al., [6] with an aerobic microbial *Shewanella* (+ 25 % strength gain relative to controlled sample).

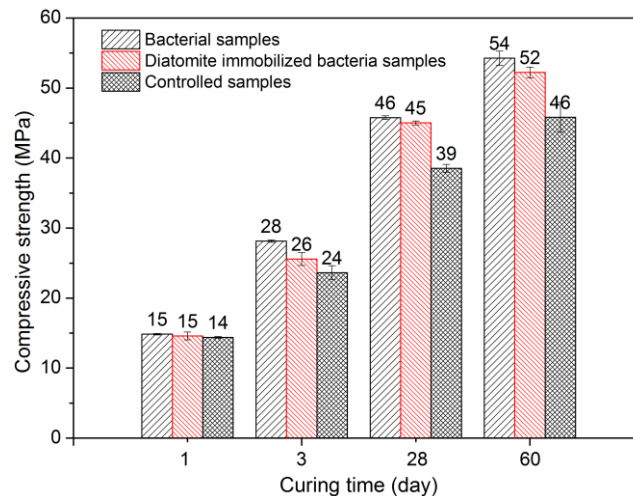


Fig. 5. Compressive strength of two bacterial concrete and controlled samples.

As given in figure 5, all concrete samples showed an expected increase in compressive strength over time of curing. Among three series of concrete sample, higher resistance was highlighted for two types of bacterial concrete in comparison with controlled concrete. Actually, concrete mixing with bacterial solution pointed out the highest strength development and concrete mixing with capsule pellets revealed slightly lower compressive strength. It is probably that we can explain such variation due to fact that coating layer around diatomite pellet prevents the direct contact with water. We note that high moisture condition is necessary to activate the bio-mineralization progress. But, in fact, obtained result (17 % higher than controlled samples) in case of concrete mixing with diatomite pellet still greater than those of Wang [7] while the author used *Bacillus subtilis* incorporated into the concrete specimens as part of the mixing water (15 % higher than controlled samples). At this point, we need back to the interest of using diatomite as controlled release agent. Thank to the immobilization of *Bacillus subtilis* HU58 in diatomite pores, which could help us keeping protect microbial from rigorous concrete mixing process and increasing the bacteria concentration for healing effect on meso/microstructure defaults.

### 3.3. Self-healing behavior

Test of self-healing material were conducted on mortar sample (90 mm diameter, 20 mm thickness) including artificial crack 1.8 mm in width. First, figure 6a illustrates that such crack which crossed diatomite pellet position and made it broken in two pieces. Second, in the course of curing period 3-28 days, two pieces of broken slices healed well together. To analysis the healing material in the crack opening by using SEM and EDX technique, we obtained relevant results in the figure 7. Calcite products was crystallized clearly in rod-like shape in the figure 7. Such qualitative and quantitative analyses proved useful to conclude the presence of precipitated calcite in material testing. It is obvious that the existing calcite precipitated product acted as glue on the cutting area of mortar sample for self-healing issue. Indeed, there was an release of bacterial solution from diatomite pellet into wide crack 1.8mm in order to activate the bio-mineralization process. Comparing to previous study in literature of Wang [8], thank to using *Bacillus sphaericus* LMG 22557 the author reported healing phenomenon on crack 0.97 mm in width. That mean, higher performance is attributed to the use of *Bacillus subtilis* HU58 immobilized in microporous structure of diatomite. They could heal an artificial crack wide 1.8 mm in this study.



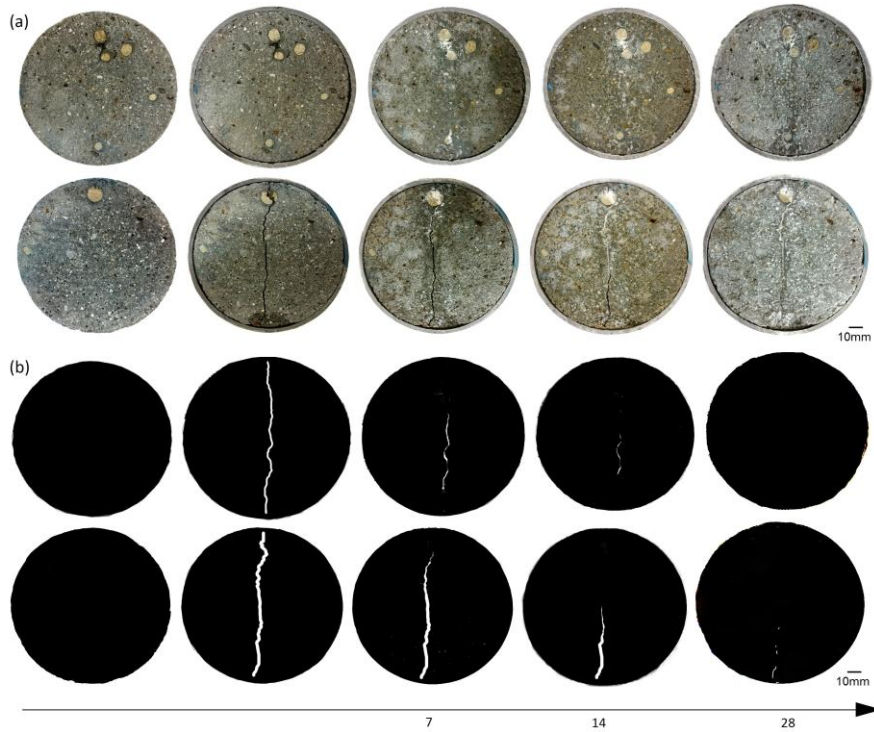


Fig. 6. (a) photos of healing crack 1.8mm in width over curing time; (b) negative cliches of healing progress

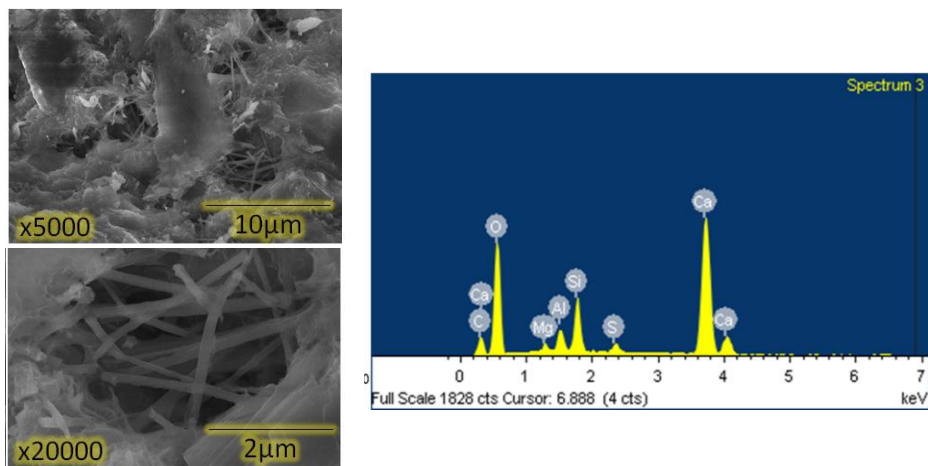


Fig. 7. SEM photo of the healing glue in the artificial cracks. EDX patterns of the rod-like shape crystalline mineral.

Figures 7 describes the experimental disposition in order to investigate water penetration progress throughout 20 mm mortar slices. Measured result of water permeability test was recorded in figure 7. As might be expected, the healing effect of mortar sample affected to degree of permeability of sample. We defined the value of anti-seepage rate =  $(V_0 - V_t)100\%/V_t$ , where  $V_0$  is the water permeation velocity of initial sample,  $V_t$  is the water permeation velocity of healed sample at time t). There was a significant difference in the slope of the area repair rate diagram at 14 and 28 days test in case of mortar mixing with bacterial solution (bacteria without controlled release agent of

diatomite). We might explain that due to the gradual decrease of microbial concentration, the healing capacity of unprotecting bacteria decreased over time. On the contrary, no difference was remarked on the anti-seepage rate diagram at 14 and 28 days test in case of mortar mixing with diatomite pellets (bacteria immobilized in diatomite micropores). It means there are no decline in the healing capacity of bacterial sample between two time interval. Taken together, these results provide the evidence of positive effect of diatomite pore in order to immobilize bacteria.

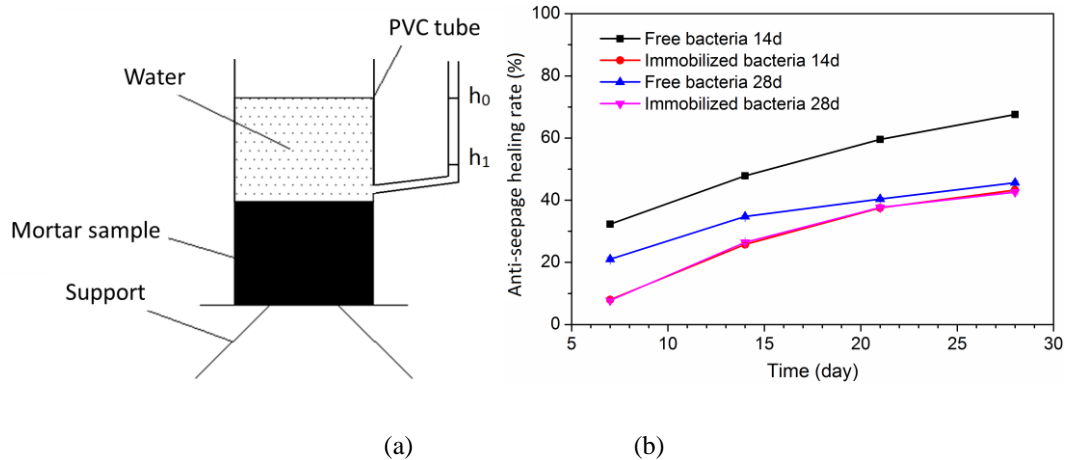


Fig. 8. (a) the water permeability test setup. (b) the healing rate diagram of free bacteria and immobilized bacteria mortar samples after different healing time.

#### 4. Conclusion

In the course of this study, we used natural diatomaceous earth Lam Dong as controlled release agent for bacterial solution. Precipitated product could be generated in diatomite's porous matrix due to the bio-activity of *Bacillus subtilis* HU58 in contact with nutrient including chlorite calcium, urea and nutrient broth. While mixing these pellet capsules into cement mortar and concrete, such precipitated calcite was able to contribute to the improvement of mechanical properties of cement matrix. Comparing to controlled sample without bacteria, 2 years old sample of bacteria-modified mortar attribute to respectively 7 % and 22 % higher compressive and flexural strength. By using diatomite pellets as coarse aggregate in bacterial concrete, we also obtained positive effect in compressive strength of concrete samples (14 % at 60 days). Others result of material analysis permit to conclude the role of calcite product in healing glue of mortar sample. The result of water permeability test provide the evidence of self-healing capacity in case of bacteria immobilized in diatomite. High capacity of bacteria immobilized in diatomite pellets explain for great stability in the result of permeability after 28 days. Our on-going studies serve to quantify bio-mineralization progress (kinetic reaction) by *Bacillus subtilis* HU58 in concrete over different interval of curing time and to investigate the durability of bacterial concrete in marine environment.

#### Acknowledgements

This research is funded by Vietnam National University HoChiMinh City (VNU-HCM) under grant number C2016-20-29.

#### References

- [1] A. Talaiekhazan, A. Keyvanfar, A. Shafaghat, R. Andalib, M.A. Majid, M.A. Fulazzaky, et al., A Review of Self-healing Concrete Research Development, *J. Environ. Treat. Tech.* 2 (2014) 1–11.
- [2] S.K. Ramachandran, V. Ramakrishnan, S.S. Bang, Remediation of concrete using microorganisms, *ACI Mater. J.* 98 (2001).

- <http://www.concrete.org/Publications/InternationalConcreteAbstractsPortal.aspx?m=details&i=10154> (accessed February 26, 2015).
- [3] S.M. Al-Thawadi, Ureolytic bacteria and calcium carbonate formation as a mechanism of strength enhancement of sand, *J Adv Sci Eng Res.* 1 (2011) 98–114.
- [4] J.C. Zweers, I. Barák, D. Becher, A.J. Driessen, M. Hecker, V.P. Kontinen, et al., Towards the development of *Bacillus subtilis* as a cell factory for membrane proteins and protein complexes, *Microb. Cell Factories.* 7 (2008) 10.
- [5] K.-Y. Yoon, J.H. Byeon, J.-H. Park, J. Hwang, Susceptibility constants of *Escherichia coli* and *Bacillus subtilis* to silver and copper nanoparticles, *Sci. Total Environ.* 373 (2007) 572–575.
- [6] V. Wiktor, H.M. Jonkers, Quantification of crack-healing in novel bacteria-based self-healing concrete, *Cem. Concr. Compos.* 33 (2011) 763–770.
- [7] R. Pei, J. Liu, S. Wang, M. Yang, Use of bacterial cell walls to improve the mechanical performance of concrete, *Cem. Concr. Compos.* 39 (2013) 122–130.
- [8] J.Y. Wang, H. Soens, W. Verstraete, N. De Belie, Self-healing concrete by use of microencapsulated bacterial spores, *Cem. Concr. Res.* 56 (2014) 139–152.



Sustainable Civil Engineering Structures and Construction Materials, SCESCM 2016

## The use of alkaliphilic bacteria-based repair solution for porous network concrete healing mechanism

Senot Sangadji<sup>a,\*</sup>, Virginie Wiktor<sup>b</sup>, Henk Jonkers<sup>b</sup>, Erik Schlangen<sup>b</sup>

<sup>a</sup>*Civil Engineering Department, Faculty of Engineering, Universitas Sebelas Maret, Surakarta, Indonesia*

<sup>b</sup>*Section of Materials & Environment, Delft University of Technology, Delft, the Netherland*

---

### Abstract

Bacteria induced calcium carbonate precipitation based on metabolic conversion of nutrients has been acknowledged for having potentials in self-healing cement-based materials. Recent studies have shown the development of bacteria-based repair solution (liquid) for concrete surface repair. This article demonstrates the feasible application of the solution as healing agent to be injected into porous network concrete (PNC). This type of concrete has a porous core which can be used as a media to transport healing agents into the fracture zone. The repair capacity of the solution have been assessed by monitoring the bio-mineral precipitation in the porous cylinder cores. The X-ray tomography and permeability tests at certain time interval were carried out before and after injection of the solution. Polished sections were prepared and examined under ESEM after healing period to investigate healing capacity. The healing potential was then tested by injecting the solution into PNC. The injection of tap water and bacteria based solution was performed through porous network until it reached and flew out through the crack which was formed by three-point bending loading. The healing efficiency was measured by water permeability test before and after injection at several time intervals. The specimens injected with bacteria based solution and cured in wet condition showed higher healing efficiency compared to dry cured specimens.

© 2017 The Authors. Published by Elsevier Ltd.

Peer-review under responsibility of the organizing committee of SCESCM 2016.

*Keywords:* Self-healing concrete, Bio-based healing agent.

---

---

\* Corresponding author. Tel.: +62-82137659700

E-mail address: [s.sangadji@ft.uns.ac.id](mailto:s.sangadji@ft.uns.ac.id)

## 1. Introduction

For many people not well trained in biology, the word ‘bacteria’ means something not so friendly to human. They associate bacteria with *pathogen* – agent that cause disease and infection. Though there are several deadly bacteria, the great number of bacterial communities have no connection with human. Recent studies show that bacterial ecosystem inhabits in healthy human skin, mouth, genital areas and intestine. This human microbiome – *a complex mutualism symbiotic of host-microbe* – is essential in maintaining human basic physiological processes.

Apart from aforementioned unique intricate human-bacteria relation, countless bacterial communities have direct positive effects in human life. these bacteria help human in digestion, food fermentation, and soil fertility maintenance, to name a few.

Specific to concrete technology, the potential benefit of bacteria has been investigated. Bacteria have been utilized in improving mortar strength, cleaning weathered concrete surface, restoring deteriorated limestone, and healing / sealing concrete cracks. Bacteria based concrete healing/sealing have been carried out through carbonate precipitation.

In nature, bio-mineralization (microbiologically induced calcium carbonate precipitation, MICP) precipitates calcium carbonate in three different polymorphs, calcite, aragonite, and vaterite, where calcite is the most thermodynamically stable mineral. This  $\text{CaCO}_3$  precipitation is mediated by bacteria via different pathways – e.g. urea hydrolysis, metabolic conversion of salt and carbon, denitrification. Currently in the lab scale, several research of bacterially mediated self-healing concrete have successfully develop techniques that make use alkaliphilic calcite precipitating bacteria [9-11].

As research project spin-off, the bacteria-based repair system has been developed recently by Wiktor and Jonkers at Microlab TU Delft [1]. This bio-based system was designed in particular for repairing cracks in existing (aged) concrete. This is a liquid system comprises of three components: [a] alkaliphilic calcite precipitating bacteria, [b] nutrients and [c] transport solution. The solution is sprayed on to a concrete surface and seals the cracks leading to porosity reduction of concrete matrix.

For designing new durable building component, this contribution investigates the feasibility of the solution to block crack opening by injecting the solutions via porous core in Porous Network Concrete (PNC). PNC which was designed by imitating concrete mammalian bone morphology has pervious (porous/enhanced porosity) concrete embedded in the interior of concrete main body [2]. This air void network system constitutes an alternate means for channeling the healing agent to cracks in the main structure. Once crack mouth opens wider than a prescribed threshold value and detected by sensors, the solution may be injected automatically by the actuator.

## 2. Materials

### 2.1. Bacteria based repair solution

Jonkers and Schlangen [7], Jonkers et al. [1, 8], and Wiktor and Jonkers [3] designed self-healing concrete by means of bacteria mediated calcite precipitation through metabolic conversion of nutrients. It is required that the bacteria resistant to alkaline environment as in fresh concrete matrix and have sufficient tolerances to oxygen. The bacteria should be able to form spores in order to be viable in very long time. As the encapsulated bacteria convert the nutrients when crack intersects the capsule, the microenvironment next to the bacteria cell is conducive for calcite to precipitate. With this mechanism bacteria help sealing crack for newly designed concrete.

On the other hand, existing aged concrete shows distress and crack due to mechanical or environmental load. This damaged concrete was not designed in first place to have self-healing capability. They demand repair using ecologically friendly repair material. This situation motivated Wiktor and Jonkers to design a bacteria-based repair system with easy and quick application [1]. The solution is applied by spraying the solution onto the surface of a cracked concrete structure, where it yields to crack closure.

For this investigation the solutions were prepared based on Wiktor and Jonkers [1]. The bacteria-based repair system consists of two types of solutions namely A which is composed of bacteria, nutrients and pH buffer compound and B containing a calcium source to promote massive calcium carbonate precipitation.

## 2.2. Porous core and Porous Network Concrete

One important aspect to make concrete self-healing is the transport of healing agent into the damage i.e. fracture or crack zone. In organisms, nutrients transport appear at micro level by means of cellular transport and via vascular system in the macro level. In concrete, transport of substance is influenced by several factors; such as gradients of temperature, pressure, humidity, or solution concentration. Without external driving force, these intrinsic factors, however, might not enough to transfer healing agent to the fracture zone.

Imitating bone shape, Porous Network Concrete was designed by Sangadji and Schlangen [2], by embedding this porous concrete core as interior of conventional concrete. PNC consist of two type of concrete; normal (dense) concrete and pervious concrete as porous core. Both concretes are made of cement, water, and aggregate where some admixtures may be added to achieve specified criteria. In pervious concrete, fine aggregate is not used and narrow distribution of coarse aggregate is employed. The porous core which has interconnected void, thus liquid to certain level of viscosity can flow easily, is used as a channel for healing agent.

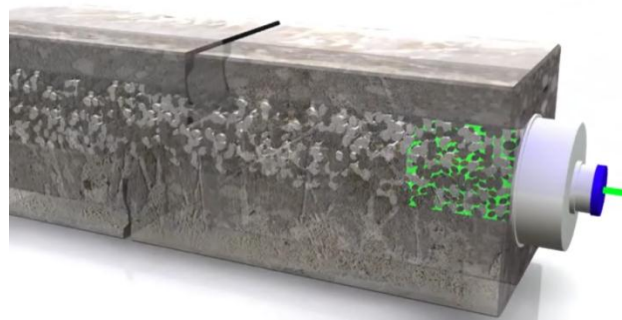


Fig. 1. Conceptual working principle of healing agent transport in the Porous Network Concrete.

Fig. 1 shows a semi-transparent picture depicting PNC with porous concrete core inside of dense concrete beam. The system shows healing agent start flowing through the porous core which eventually will reach the crack and sealing it inside out.

In this research program, PNC was prepared as described by Sangadji and Schlangen [2] as concrete prisms with dimension of  $55 \times 55 \times 285$  mm PNC specimen. Each specimen center interior is  $23 \times 23 \times 285$  mm porous concrete and  $\varnothing 2$  mm threaded steel rebar was installed under the core. Bacteria based solution was injected from point of injection.

## 3. Research Methods

### 3.1. Calcite precipitation in the porous core

It is predicted that the bacteria-based repair solution can seal the crack in the concrete after it is injected via porous network core. To determine whether the hypotheses work well, it is necessary to investigate biomineralization process takes place in the concrete core when the solution is injected. Porous concrete cores with diameter of 2.5 cm and height of 3 cm of were cut form longer core which was prepared according to Sangadji and Schlangen [1].

Five series (A,B, C, D and Control) of test were designed to assess repair capacity of the solution in porous concrete core. Two replicates were used per time and series where test have been conducted 3, 7, 14, 21 and 28 days after injection except for series D (only 28 days is tested). Porous core in series A were treated with 1 time injection and sequence: sol A and then sol B. Series B were treated with 1 time injection with static mixing nozzle by which solution A and B were mixed. Series B were treated with 3 times injection and injection sequence as series 'A'. Series D were treated as series 'A' but only food solution is injected without bacteria. And lastly, Control series were injected with tap water only.



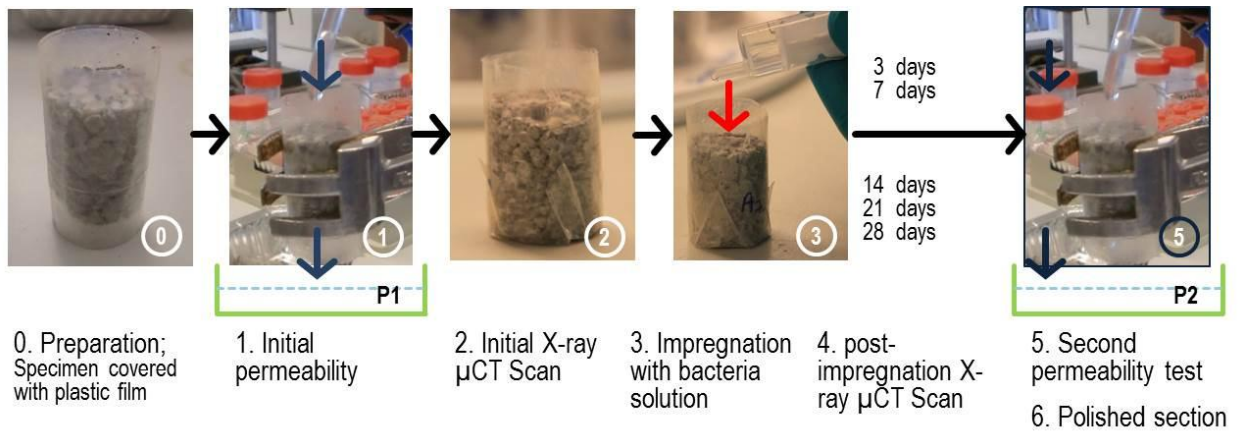


Fig. 2. Sequence of the test.

To assess the repair capacity of the system the bacteria-based solution is injected into porous cores, and the production of bio-minerals in time is monitored by X-ray micro-tomography. In parallel, water permeability test is conducted before and after the injection of the bacteria-based solution at regular time interval to determine the sealing efficiency of the system. Finally, at the end of the healing period, polished sections of injected specimens are observed with ESEM/EDS to analyze and locate bio-minerals. The sequence of the test form material preparation, injection and permeability test is shown in Fig. 2.

### 3.2. Crack sealing in the main body

A research program has been devised to implement injection of bacteria based solution into Porous Network Concrete (PNC) prism. Two type of treatments were implemented with 2 replicates. The ‘control’ series received injection of tap water and ‘bacteria’ series received injection of bacteria-based solution. Two different curing were conducted in which ‘wet’ series were cured in  $\pm 95\%$  RH and  $\pm 20^\circ\text{C}$  curing chamber while ‘dry’ series were cured under lab condition with RH  $\pm 30\%$  and temperature  $\pm 20^\circ\text{C}$ .

Initial permeability test was performed by flowing water from point of injection (a) to the opposite point outflow (b) prior to crack formation, as depicted in Fig. 3.a. Then, crack formation in the prism mid-span was carried out by means of strain controlled three point bending, as depicted in Fig. 3.b. Initial crack width in the beam bottom side was achieved around  $\pm 250 \mu\text{m}$  [2]. The pre-healing permeability test, the, was performed by blocking point (b), therefore water leaked out from crack opening. After the core achieved saturated surface dry, then PNC prism was injected with 30 ml of water for ‘control’ series and ‘bacteria’ series specimens were injected with solution A and B into. Afterwards, specimen were cured under lab condition and in the humid fog room prior to after-healing permeability test and second mechanical three point loading.

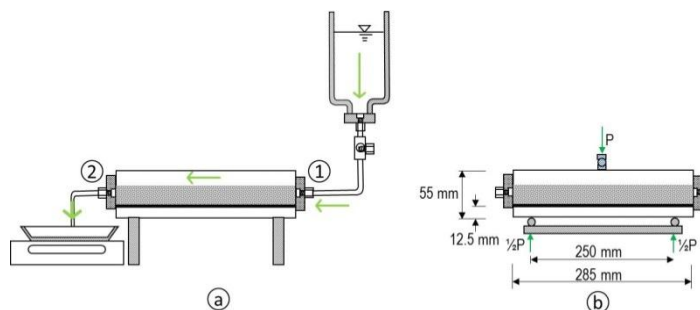


Fig. 3. a. Falling head permeability test, b. strain controlled three-point bending

Crack closure has been monitored before and 7, 14, 21, and 28 days after injection under stereomicroscope. Quantification of crack-healing has been carried out using the method as described by Wiktor and Jonkers [3]. 28 days post-healing permeability test was executed to measure permeability reduction.

## 4. Result

### 4.1. Repair capacity of bacteria-based solution in the porous core

There is a diverse data observed from water permeability test in porous concrete before and after bacteria-based solution injection with setup as depicted in panel 1 Fig. 2. The reason is that the specimens are very porous with average void diameter of 1 – 1,5 mm and the volume  $\text{CaCO}_3$  precipitation is not enough to block the total void. In line with the observation above, data processed from micro CT-scan reveal similar outcome. Three day after injection, approximately 6% new material is found in the porous core which decreased to 2% after 7 days and remain constant up to 28 days. The bacteria injected may not produce high amount of  $\text{CaCO}_3$  precipitation and after 3 days only solution is detected with the CT-scan. Further the solution dries out over time and the volume detected decrease leading to difficulty to distinguish between organic precipitates (from nutrients) and bio-minerals. It can be deduced that both techniques, permeability and CT-scan, provide no meaningful indicator of bacteria-based solution's repair capacity within porous core.

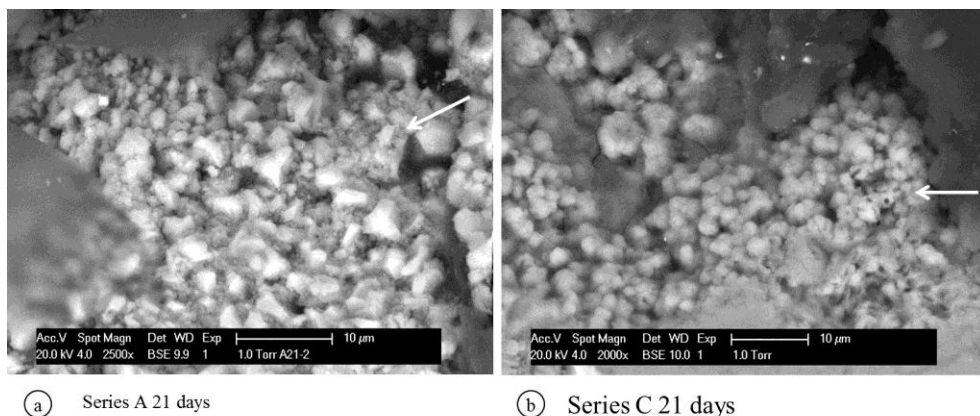


Fig. 4. a. Ca-based crystal formation within the specimen Series A at 21 days after injection, b.  $\text{CaCO}_3$  formation in the porous core where bacteria imprints indicate that it entombed after crystal formation grows in the vicinity of the bacteria.

Observing porous core polished section under ESEM, however, it was found several cavity between epoxy and the porous core matrix in series containing nutrients, but not in ‘control’ series injected with tap water only. The reason was the nutrients entrapped dissolved when the polished specimens were ground on top of sand paper for 45 minutes with water. Yet, this ‘bad bonding’ is a good sign to locate the existence of nutrients and bio-minerals converted from it by bacteria.

Calcium based crystal are observed to be exist in the series A at 21 days after injection even though in small volume. The crystal is shown in the Fig. 4.a. More Ca-based crystals are detected in specimens of 28 days after injection which may be induced by bacteria. Similar indication is observed in series B though it seems that the amount of crystal formation is smaller than series A.

Larger number of cavity in between epoxy and concrete matrix is observed in series C. This is coherent with the case that more nutrients and bacteria are injected into the porous core series C by factor of 3 compared to series A. Furthermore, it is found a strong indication of bacterial activity in the concrete matrix in the form of bacteria imprint, as depicted in Fig. 4.b, for specimens of 21 and 28 days after injection. Found in several location this imprints indicated bacteria are active and consume the nutrients to cultivate and reproduce. While bacteria growing, the chemistry in the area next to its cell wall changed and with the present of Ca ions the supersaturation condition is



achieved leading to the formation of  $\text{CaCO}_3$ . As nutrients dissolved in the series D, many cavities are observed in the specimens but no bacteria mediated calcite precipitation is observed.

It is deduced from the experiment that there is potential of healing capacity by means of  $\text{CaCO}_3$  formation where alkaliphilic bacteria are an indispensable element of the system. Nevertheless more external Ca-salt is needed in the system to produce more  $\text{CaCO}_3$  formation amount necessary to seal crack formation.

#### 4.2. Self-healing capacity in PNC prism

For PNC prisms the results of initial permeability showed that porous core is pervious and after crack formation in the mid-span there was water leakage from the crack opening. Fig. 5.a. and 5.c. show the crack path in the bottom of the PNC specimen after three-point bending test. From this crack formation liquid can flow out or in to the concrete matrix.

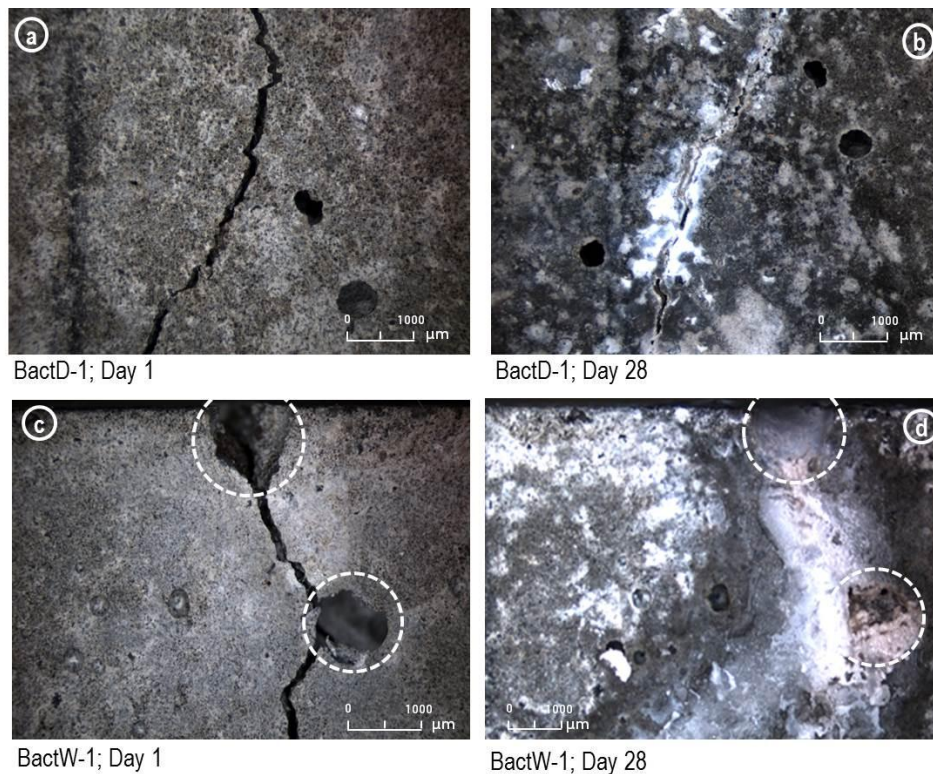


Fig. 5. a. Crack of in the PNC prism after three point bending test (1 day), b.  $\text{CaCO}_3$  formation in the crack of dry cured PNC, c. Crack of in the PNC prism after three point bending test (1 day), d. precipitation of bio-minerals in the crack zone for wet cured PNC.

The experiment showed that wet cured bacteria series exhibited complete permeability reduction as it can be seen from the Fig. 5.d., where precipitation of bio-minerals blocks the crack path therefore no water cannot flow out from permeability test. Meanwhile dry cured specimen shows limited reduction as seen in Fig. 5.b. It can be deduced from the experiment and visual observation under microscope that the liquid tightness of the healed specimen is obtain fully using bacteria based solution injected provided enough humidity for the bio-mineralization process.

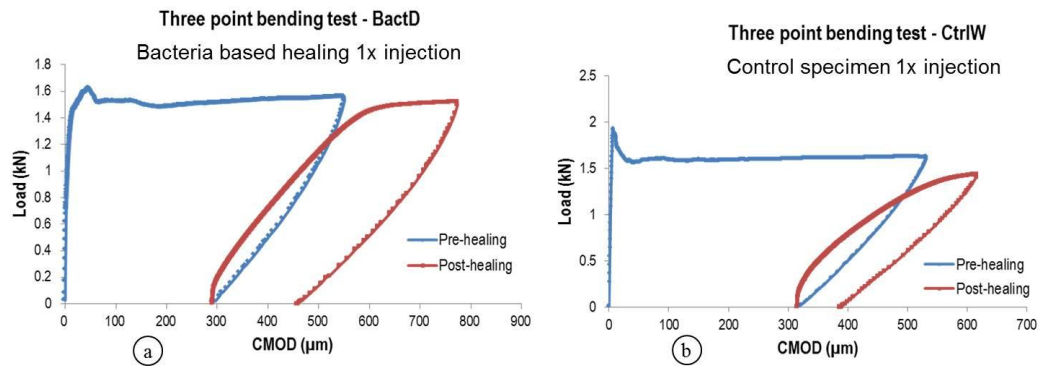


Fig. 6. a. Load-crack mouth opening displacement (CMOD) graphs of bacteria based healing specimen, b. Loading cycle graphs of control specimen.

Load versus Crack Mouth Opening Displacement (CMOD) is obtained from three-point bending test. This mechanical test is used to indicate the strength of PNC in pre- and post-healing state. Fig. 6 show the result of PNC with bacteria based healing system (a) and control specimen which only receive tap water injection after crack formation. Second cycle three-point loading was carried out to assess whether the bio minerals precipitated in the crack zone contribute to regain the strength as it is compared to pre-healing loading cycle. The curves of loading cycle obviously show limited strength and stiffness regain in both bacteria based or control specimen. The peak load of post-healing specimen is lower than the peak load of the virgin specimen. The post-healing stiffness of both systems are also far less than the pre-healing. It was observed that the crack formation was just reopened due to the second loading cycle and the post-healing strength and stiffness more less was provided only by the rebar embed in the PNC.

## 5. Conclusions

The bacteria based repair solution, firstly designed for concrete surface crack repair, showed promising potential as healing agent which can be injected via porous network. The precipitation of bio-minerals, mainly  $\text{CaCO}_3$ , can seal the crack formed in the PNC main body, where multiple injection appear to be the most efficient way to obtain sufficient volume of the bio-minerals. The bio-mineralization indeed is induced by alkaliphilic bacteria as bacterial activity in the form of bacteria imprint is found in the system. Even though mechanical regain in term of strength and stiffness of bacteria-based post-healing PNC prism is quite limited, crack sealing works effectively and liquid tightness may be assured.

## Acknowledgements

The project was executed at Microlab, Section of Materials and Environment, TU Delft. The authors would like to thank the Government of the Republic of Indonesia for its financial support in the form of scholarship for S. Sangadji and the Technology Foundation STW for the financial support for the project 11342. The authors acknowledge Mr. Ger Nagtegaal and Mr. Arjan Thijssen for their support.

The continuation of the project is funded by Universitas Sebelas Maret, Surakarta, Indonesia through Hibah Doktor Baru, 2016, granted to the first author.

## References

- [1] V. Wiktor, H.M. Jonkers, Application of bacteria-based repair system to damaged concrete structures, Proceedings of the 2nd International Workshop on Structural Life Management of Underground Structures, Daejeon, 2012, pp. 31-34.
- [2] S. Sangadji, E. Schlagen, Self-healing of Concrete Structures - Novel approach using porous network concrete, Journal of Advanced Concrete Technology, 10 (2012) 185-194.

- [3] V. Wiktor, H.M. Jonkers, Quantification of crack-healing in novel bacteria based self-healing concrete, *Cement and Concrete Composite*, 33 (2011) 763-770.
- [4] V. Wiktor, S. Sangadji, H.M. Jonkers and E. Schlangen, Potential of Bacteria-based Repair Solution as Healing Agent for Porous Network Concrete, *Proceedings of 4<sup>th</sup> International Conference on Self-Healing Materials*, Ghent, 2013, pp 592-596.
- [5] S. Sangadji, V. Wiktor, H.M. Jonkers and E. Schlangen, Injecting a liquid bacteria-based repair system to make porous network concrete healed, *Proceedings of 4<sup>th</sup> International Conference on Self-Healing Materials*, Ghent, 2013, pp 118-122.
- [6] S. Sangadji, *Porous Network Concrete: a bio-inspired building component to make concrete structures self-healing*, PhD Thesis, TU Delft, 2015
- [7] Jonkers, H.M. and E. Schlangen, *Crack Repair by Concrete-Immobilized Bacteria*, in the First International Conference on Self Healing Materials. 2007: Noordwijk aan Zee, The Netherlands.
- [8] Jonkers, H.M., *Self Healing Concrete: A Biological Approach*, in *Self Healing Materials*, S. Zwaag, Editor. 2008, Springer Netherlands. p. 195-204.
- [9] Van Tittelboom, K., *Self-Healing Concrete through Incorporation of Encapsulated Bacteria or Polymer-Based Healing Agents*, in *Faculty of Engineering and Architecture*. 2012, University of Gent: Gent, Belgium.
- [10] Van Tittelboom, K. and N. De Belie, *Self-Healing in Cementitious Materials—A Review*. *Materials*, 2013, 6(6): p. 2182-2217.
- [11] Mario de Rooij, K.V.T., Nele De Belie, Erik Schlangen, *Self-Healing Phenomena in Cement- Based Materials*, in *State-of-the-Art Report of RILEM Technical Committee 221-SHC: Self-Healing Phenomena in Cement-Based Materials*. 2013, Springer Netherlands.



Sustainable Civil Engineering Structures and Construction Materials, SCESCM 2016

## Determining moisture levels in straw bale construction

Julian Robinson<sup>a</sup>, Hynda Klalib Aoun<sup>a\*</sup>, Mark Davison<sup>a</sup>

<sup>a</sup>*School of Architecture, Design and the Built Environment; Nottingham Trent University; Burton Street, Nottingham NG1 4BU, UK*

---

### Abstract

With the growing interest in sustainable building materials that are able to provide reductions in energy consumption, the viability of straw bale construction has recently been investigated, in particular, its resistance to moisture. The level of moisture that a construction is exposed to may have an adverse effect on its durability. Concerns are raised about the susceptibility of straw to decay when used as a walling system. It is an organic material, therefore is at risk of biodegradation under certain conditions. The research uses a range of measurement techniques to assess the effects of atmospheric conditions and wet render application on straw bale's moisture content, and it requires an understanding of the complexities of the transition of water vapour through the material and the interaction of moisture with the bale. Deviations in the moisture content within the straw bale caused by the second application of wet render were shown to be insignificant. Straw bale can withstand 25% moisture content for prolonged periods of time without degradation at temperatures not exceeding 10°C.

© 2017 The Authors. Published by Elsevier Ltd.

Peer-review under responsibility of the organizing committee of SCESCM 2016.

*Keywords:* Straw bale construction; Sustainable material; Moisture content; Relative humidity; Temperature; Monitoring devices

---

### 1. Introduction

The EPBD (Energy Performance of Buildings Directive) advises that all new buildings be “nearly zero-energy” by December 2020 [1]. Straw bale construction can be designed and built to achieve energy efficiencies [2] that surpass those required for the environmental assessment of buildings such as the BREEAM [3] and CSH [4] rating systems. In the UK, the NHPAU (National Housing and Planning Advice Unit) estimates that construction of between 223,000 and 255,000 new homes per year is required until 2026 to provide enough housing for the growing population.

---

\* Corresponding author. Tel.: +44 (0)115 848 4873.

*E-mail address:* [hynda.klalib@ntu.ac.uk](mailto:hynda.klalib@ntu.ac.uk)

It has been estimated that in the UK alone [5], the surplus of yearly produced straw is around 4 million tonnes, enough for the walls of 450,000 new houses. Globally, a billion people live in slums [6] and are in need of the economical, insulated constructions that could be provided by straw bale [7].

Straw bale can be used for non-load-bearing and limited load-bearing wall [8] or in panel applications. These types of walls have good structural capacity and thermal efficiency, are durable [9, 10] and have been awarded a two hour fire safety rating [11, 12].

The overall research aim is to quantify and evaluate straw bale constructions' resistance to moisture using different monitoring techniques. This paper contributes by determining the effect of wet render application, assessing limitations of resistance meters and comparing atmospheric conditions to moisture content results taken in a test rig.

An extensive literature review [13] was conducted to critically examine, quantify and evaluate the risk posed to straw bale constructions by moisture. There has been a lack of conclusive agreement concerning the resilience of straw exposed to raised levels of moisture [14]. However, Straube [14, 15], Lawrence et al. [16] and Carfrae et al. [17], have rationalised the apparent ability of straw to tolerate moisture content but have recommend that it should not exceed 25% when in service [17].

Wihan [19] and Straube [15] highlighted the complexity of moisture interaction within a straw bale and associated deterioration or decay of the material. Furthermore, there has been a lack of critical analysis concerning moisture storage regimes [15] and factual descriptions of how moisture interacts with the straw [13]. In assessing moisture content, Lawrence et al. [16] developed, through Sorption Isotherms, a simple conversion scale that defines the interaction of moisture with straw by identifying desorption and adsorption trends.

## 2. Experimental program

### 2.1. Test rig description

A test rig (Figs.1 and 2) was constructed to provide facilities to assess different measurement systems whilst being subjected to a dynamic environment (seasonal variations in Lincolnshire, UK).



Fig. 1. Erection of test rig blocks



Fig. 2. Completed rig construction

The rig consists of twelve modular straw blocks (Figs. 3 and 4), comprised of three  $\frac{1}{2}$  wheat straw bales (1100x330x225mm) laid vertically and compressed into place. The modular-blocks are labelled 1 to 7 (Fig. 4); 'B' represents the lower blocks and 'T' the upper blocks. Prior to construction, the bales had been kept together in dry storage for nearly a year. A lime mortar mix was applied to the bales to a thickness of around 20mm externally and 10mm internally.



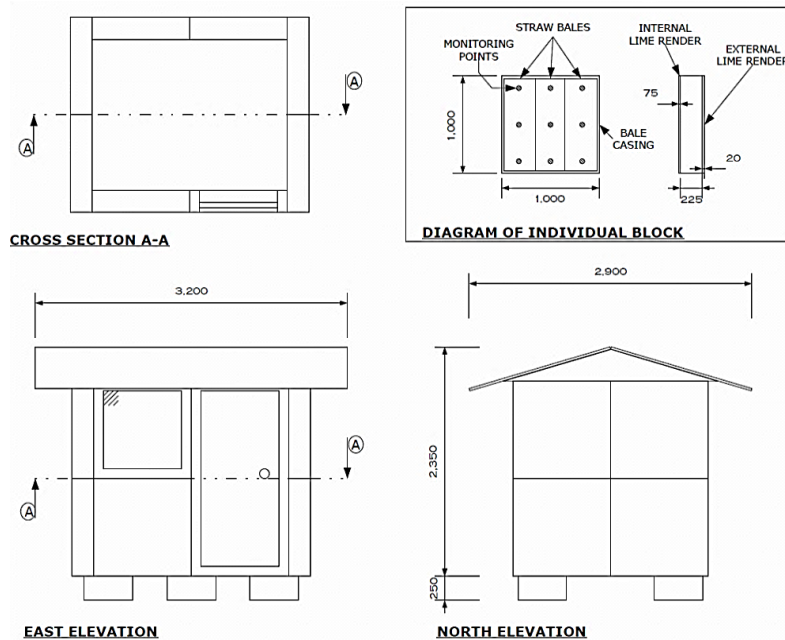


Fig. 3. Test rig plan

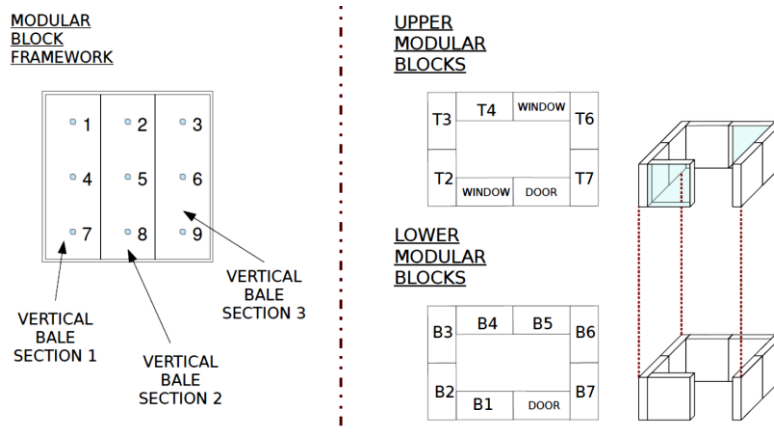


Fig. 4. Test rig block diagram

The test rig is exposed to the north (Fig. 5), shadowed by a large farm building four meters in height to the east and a three meter high hedge two meters to the south. The east façade butts up to a concrete path and the other walls are surrounded by vegetation. The north is unsheltered and a weather station was set up there to provide a comparison of internal and external conditions. Each block (Fig. 4) has nine monitoring points for the insertion of the Balemaster probe (Fig. 6), to a depth of 112 mm (approximately half the wall thickness). Moisture content measurements were taken weekly, based on the assumption that, barring dramatic failure, moisture would not be transferred through the bale at a significant enough rate to justify additional monitoring [18].

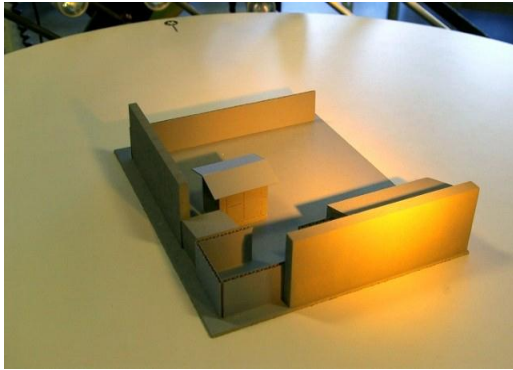


Fig. 5. Model of test rig location



Fig. 6. Balemaster probe with Timbermaster and Balemaster resistance meters, and thermocouples

## 2.2. Materials characterisation

The physical properties of the wheat straw used in the test rig are shown in Table 1. Table 2 presents the microstructural constituents of the straw.

Table 1. Straw bale physical properties.

Straw properties	Measured values
Bale dry bulk density	100–130 kg/m <sup>3</sup>
Porosity	46–84%
Initial moisture content	11–16%
Water absorption	65–75%

Table 2. Straw bale microstructure constituents.

Straw microstructure	Proportion
Cellulose	41%
Hemicellulose	29%
Lignin	11%

## 2.3. Test rig method

The straw bale test rig walls were rendered in lime, a first layer of render was applied to the external walls on the first day of the 45 day experiment. Subsequently, on day 12, a second layer of render was applied to the external walls, and on day 21, a layer of render was applied to the internal walls. As the render cures, it absorbs CO<sub>2</sub> and expels water, which will theoretically raise the moisture content of the wall material.

The purpose of the test rig investigation was therefore to establish the impact of wet render applied to the straw bales and to identify the limitations of using the Protimeter Balemaster as a reliable monitoring method. When using the GE Protimeter Balemaster, it is required to compensate the moisture result for temperature [20] using the following equation (1):

$$C = 0.1r(20 - t) \tag{1}$$

C: Moisture content (%)

t: Temperature (°C)

r: Balemaster reading

The US version of the Balemaster, used in this study, returns the results in a wet basis while the Timbermaster returns results in a dry basis. Fig. 7 shows how the moisture content is obtained using the Balemaster resistance meter, Balemaster probe and a digital thermometer.

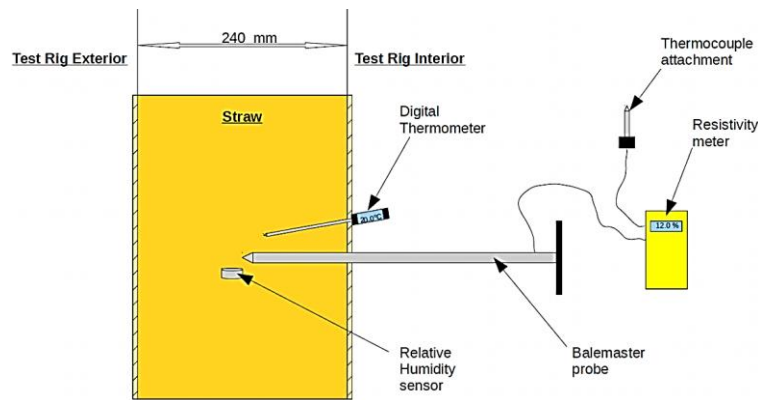


Fig. 7. Test rig measurement method

The study also compares the moisture content levels measured by the Balemaster meter to the weather conditions and to the value estimated from equation (2), developed by Lawrence et al [16] and based on relative humidity.

$$C = \frac{C_s}{1+n\left(\frac{K_m}{\phi}-1\right)^{\frac{i}{3}}} \quad (2)$$

C: Moisture content (%)

$\phi$ : Relative humidity (%)

$K_m = 0.9773$  ;  $C_s = 400$  ;  $i = 1.6$  or  $1$  ;  $n = 44$

In addition, a cyclic study was adopted in order to assess the effect of temperature on the moisture content of straw over a 24 hour period. A cyclic study records an output over a set time, and gauges whether the analysed system returns to the initial starting position.

### 3. Results and discussion

Firstly, an analysis of the effect of render application on the moisture content of straw bales is performed, then, a study of individual bale moisture content. The results are shown below, followed by a 20 hour study looking into the cyclical data obtained by both a Timbermaster and Balemaster resistance meter from several monitoring positions within the test rig. Finally, the results assess the impact of atmospheric conditions on the straw moisture levels.

#### 3.1. Application of render

Fig. 8 illustrates the standard deviation of moisture content for each monitoring point, recorded over the 45 day period. The standard deviation has been used as it can highlight the differences in deviations between mean moisture contents under different atmospheric conditions. The results reveal two stages of moisture increase; the first between days 0 and 12 corresponding to the first application of the external render, the second between days 21 and 37 corresponding to the application of the internal render. The application of the second layer of render to the external



walling on day 12 shows no effect. Moreover, Fig. 8 shows the distribution of the moisture content on day 0, spreads over a moisture content range of 5%. This range is unexpected as the bales had been equilibrated in the same atmospheric conditions for over a year prior to construction. Another surprising finding is that the moisture content of the straw varied for not only each individual bale, but for each monitoring point within the same bale. This variation demonstrates that other factors could be affecting the results, such as temperature, density, relative humidity or the resistance meter itself.

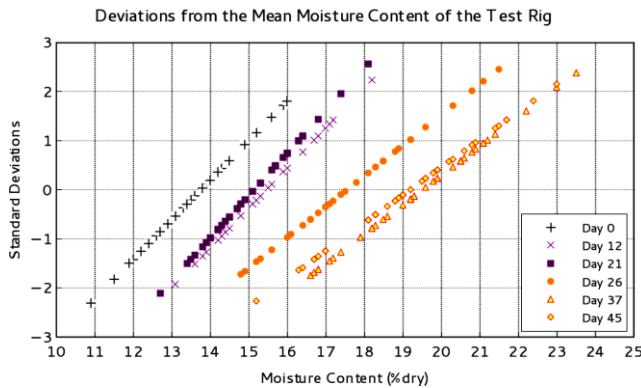


Fig. 8. Statistical analysis of the test rig

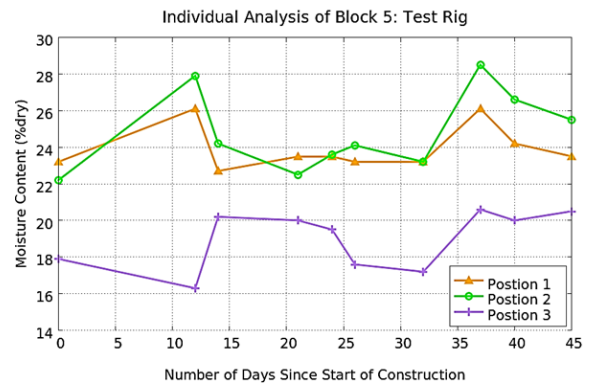


Fig. 9. Individual bale analysis

### 3.2. Individual bale study

Fig. 9 shows the difference in moisture readings between three points within the same bale. Although positions 1 and 2 return similar moisture contents, position 3 returns results 3-7% lower. The starting moisture content of the bales, and the relative humidity and temperature of each measurement position within the bale may be assumed the same due to the pre-construction storage conditions. The density of the straw at the point of measurement should be the influencing parameter, as it is likely to vary, in part due to the way a baling machine operates. This is supported by Carfrae et al's [17] conclusions. Therefore, further investigation into the effect of straw density on moisture readings is essential. Other influencing parameters that are potentially responsible for the increase in moisture and the irregularity of the initial readings include rainfall, relative humidity and internal and external temperature. However, it is important to mention that the only rainfall within the 45 day period was from the north and west combined with light winds of a speed less than  $5\text{ms}^{-1}$ . The rain during this period is believed unlikely to have had a significant effect on the overall increase of moisture content of the bales.

Fig. 9 also illustrates that the moisture content of position 2 exceeded 25% on days 12 and 37. On day 45 a sample of straw was extracted and examined. However, on inspection there was no sign of degradation. This observation confirms Carfrae et al's study [21] that moisture contents that do not exceed 37% (at the highest reading) may be tolerated by the straw. The data however must be interpreted with caution as the temperature at the time of the measurement did not rise above  $15^{\circ}\text{C}$ , averaging at around  $10^{\circ}\text{C}$ , since at that temperature, biological decay is slowed [16].

### 3.3. Cyclic study

Figs 10 to 13 show a comparative study of data collected using the Balemaster and Timbermaster resistance meters over a 20 hours period, together with the temperature data from points of measurement within the bale. The study looked at part of a cycle relating temperature within the bale to moisture content in order to assess both moisture transition and the effectiveness of using resistance meters. It can be noted that the moisture contents in each figure increase during the measurement phase. One hypothesis drawn from this result would suggest that warmer air containing more moisture is driven into the bale from the external straw-render interface; this maybe a product of wetting of the render from rain or overnight dew followed by heating of the render surface at dawn as external air

temperatures rise or as the wall is subjected to solar gain. The warm moist air condenses on the cooler straw within the bale and also at the point of measurement, thus raising the moisture content. The effect of vapour transition could then reversed as the external atmosphere cools. The accuracy of the GE Protimeter’s equation (1) has to be validated by further investigation so as to remove alternate hypotheses for the effects of moisture transfer rates through a bale. The data reveals differences between the Balemaster and the Timbermaster meters.

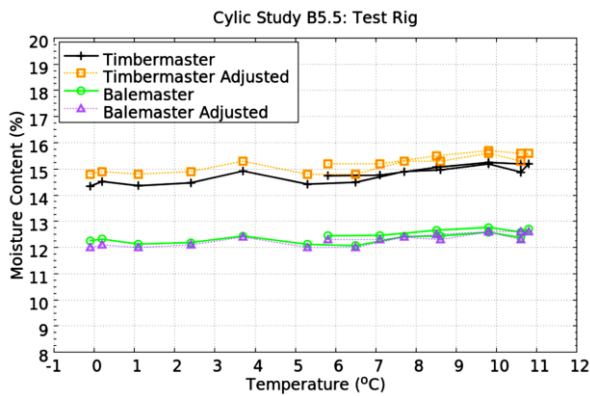


Fig. 10. Moisture content at B5.5 position

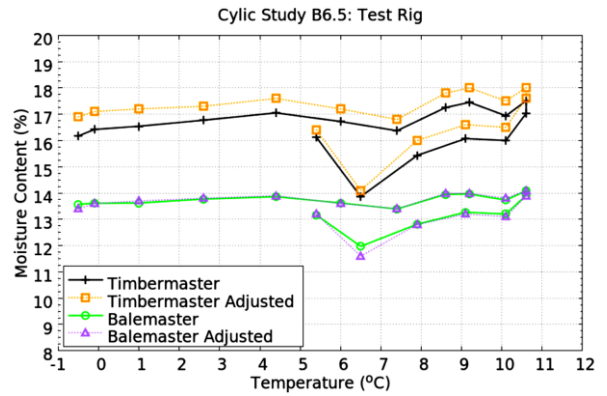


Fig. 11. Moisture content at B6.5 position

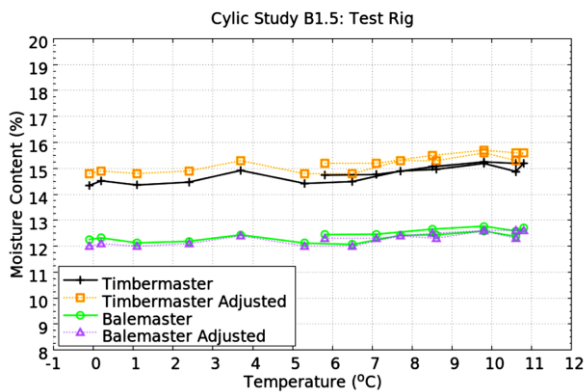


Fig. 12. Moisture content at B1.5 position

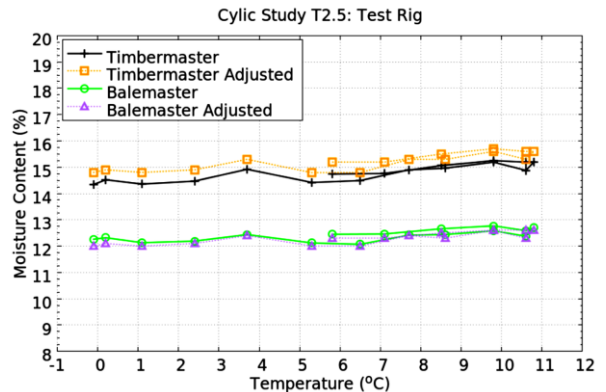


Fig. 13. Moisture content at T2.5 position

### 3.4. Atmospheric conditions

Regarding the moisture transfer, the effect of atmospheric conditions on the straw was studied. Analysing the data obtained over the initial 45 day study, the study compares the effect of external relative humidity and temperature on the measured straw moisture content. Fig. 14 illustrates the measured and estimated moisture content using the GE Protimeter equation (1). The experimental values are adjusted by approximately 1% when using the Timbermaster, with temperature compensation. The Bezier formula has been used to shape the moisture content curve. The rise from 16% moisture content to 20% took around 16 days and the average relative humidity recorded during the test rig experiment is between 80 and 85%.

On the other hand, utilising Lawrence et al’s [16] equation (2), the equivalent moisture content as affected by the atmospheric conditions would average between 20 and 24.5%. This would suggest that the surrounding environment has affected the straw moisture content to bring it towards an equilibrium. However, this raises the issue of moisture transfer rate and the rate at which humidity can affect the moisture content of straw. It is possible to hypothesise from

the results obtained in the first section of this paper that the application of the wet render has increased the moisture content of the straw up to the point at which it is in equilibrium with the exterior. This hypothesis assumes that the exterior could not have influenced the straw moisture content at the rate directly associated with the resultant moisture content. Therefore, the rate at which the moisture content increases is a product of the curing of the first layer application of lime render; as the render cures it releases water into the bale's interior, thus influencing the rate at which the straw would react to the external environment. It is therefore necessary based on the hypotheses presented that further work is undertaken to understand moisture transfer through straw bales.

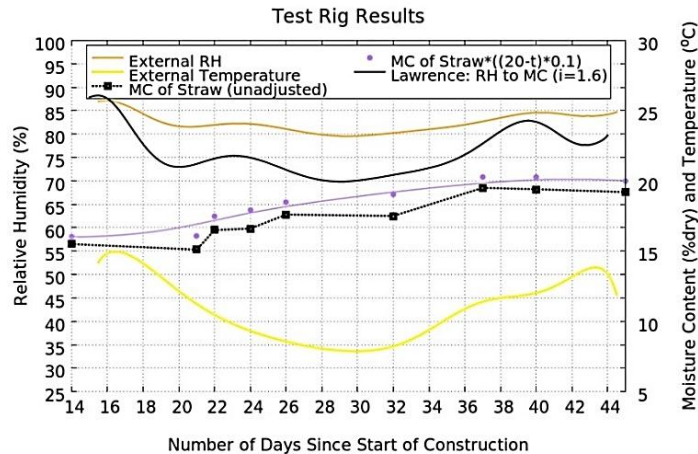


Fig. 14. Relative humidity and temperature influences

#### 4. Conclusion

The results present a level of moisture to be expected in straw bale walls. They are part of a larger study conducted to evaluate and quantify the risk posed to straw bale constructions by moisture. Highlighted are various gaps in knowledge including the effect of straw density, vapour transition and moisture transfer rates through a bale, and the accuracy of the Protimeter resistance meter and equation.

The results however do provide evidence to suggest that the application of wet render directly onto straw affects the moisture content throughout the bale, although additional applications of render on top of existing layers appear to have no further effect. The differences in starting moisture contents of the monitoring points within the bales indicate that the density of the straw is an important variable, as is the temperature at the point of measurement. The effect of density is reasoned as the differences in starting moisture content from an assumption that other influencing variables would have been equal within each bale.

Other observations included the apparent ability of straw to withstand moisture contents in excess of 25%, however other influencing factors must be taken into account regarding time and temperature. The obtained moisture content values conform to those estimated by the Lawrence equation. However, the rate at which equilibration occurs raises an important question concerning the moisture transfer rate through a bale when affected solely by relative humidity. It is proposed that the application of wet render accelerated the rate at which atmospheric moisture could have influenced the straw within the bale. The results also raise concerns about using the GE Protimeter equation, as the obtained values do not fulfil accuracy requirements.

#### References

- [1] Directive 2010/31/EU of European parliament and of the council on the energy performance of buildings, Official Journal of the European Union (2010).

- [2] S. Goodhew, R. Griffiths, Sustainable earth walls to meet the building regulation, *Energy and Buildings*, Elsevier, vol. 37, n°5 (2005) 451–459.
- [3] BREEAM UK New Construction, Code for a sustainable built environment, Technical manual, version: SD5076, n°1 (2014). [http://www.breem.com/filelibrary/BREEAM%20UK%20NC%202014%20Resources/SD5076\\_DRAFT\\_BREEAM\\_UK\\_New\\_Construction\\_2014\\_Technical\\_Manual\\_ISSU\\_0.1.pdf](http://www.breem.com/filelibrary/BREEAM%20UK%20NC%202014%20Resources/SD5076_DRAFT_BREEAM_UK_New_Construction_2014_Technical_Manual_ISSU_0.1.pdf).
- [4] Code for Sustainable Homes, Technical guide, Communities and Local Government, November (2010). [http://www.planningportal.gov.uk/uploads/code\\_for\\_sustainable\\_homes\\_techguide.pdf](http://www.planningportal.gov.uk/uploads/code_for_sustainable_homes_techguide.pdf)
- [5] G. Grams, Policies and strategies for ecological building design, Part 3: Building elements and services, Red Eye Publications (2005) 73–74.
- [6] UN-Habitat, The challenge of slums, Global report on human settlements 2003, Management of Environmental Quality, Emerald, vol. 15, n°3, (2004) 337–338.
- [7] B. King et al., Design of straw bale buildings: The state of the Art, Green Building Press (2007).
- [8] T. Ashour, A. Bahnasawey, W. Wu, Compressive strength of fibre reinforced earth plasters for straw bale buildings, *Australian Journal of Agricultural Engineering*, Southern Cross Publishers, vol. 1, n°3 (2010) 86–92.
- [9] T. Ashour, H. Georg, W. Wu, Performance of straw bale wall: A case of study, *Energy and Buildings*, Elsevier, vol. 43, n°8 (2011) 1960–1967.
- [10] P. Walker, Compression load testing straw bale walls, Research report (2004). <http://people.bath.ac.uk/abspw/straw%20bale%20test%20report.pdf>.
- [11] V.B. Apte, B. Paroz, A. Bhargava, A fire safety testing and modelling of rendered straw bales for construction in bushfire prone areas. Proceedings of the Fourth International Seminar, Fire and explosion hazards, Belfast, University of Ulster Edition, September (2004) 537–546.
- [12] ASTM E119-05, Standard test methods for fire tests of building construction and materials, ASTM International, West Conshohocken, PA (2005). [www.astm.org](http://www.astm.org).
- [13] J. A. Robinson, Quantifying and evaluating the risk posed to straw bale constructions from moisture, PhD thesis, Nottingham Trent University, School of Architecture, Design and the Built Environment (2014).
- [14] J. Straube, BSD-112: Building science for straw-bale buildings, *Building Science Digest* (2009). <http://www.buildingscience.com/documents/digests/bsd-112-building-science-for-strawbale-buildings>.
- [15] J. Straube, C. Schumacher, Monitoring the hygrothermal performance of straw bale walls, *BalancedSolutions.com* (2003). [http://www.ecobuildnetwork.org/images/Straw\\_Bale\\_Test\\_Downloads/monitoring\\_the\\_hygrothermal\\_performance\\_of\\_strawbale\\_walls\\_straube\\_Schumacher\\_2003.pdf](http://www.ecobuildnetwork.org/images/Straw_Bale_Test_Downloads/monitoring_the_hygrothermal_performance_of_strawbale_walls_straube_Schumacher_2003.pdf).
- [16] M. Lawrence, A. Heath, P. Walker, Determining moisture levels in straw bale construction, *Construction and Building Materials*, Elsevier, vol. 23, n°8 (2009) 2763–2768.
- [17] J. Carfrae, The moisture performance of straw bale construction in a temperate maritime climate, PhD thesis, University of Plymouth, School of Architecture, Design and Environment (2011).
- [18] S. Goodhew, R. Griffiths, T. Woolley, An investigation of the moisture content in the walls of a straw-bale building, *Building and Environment*, Elsevier, vol. 39, n°12 (2004) 1443–1451.
- [19] J. Wihan, Humidity in straw bale walls and its effect on the decomposition of straw, MSc thesis, East London University (2007).
- [20] G. E. Protimeter, Sensing. [http://www.damp-meter-direct.co.uk/PDF/manual/Protimeter\\_Timbermaster\\_Manual.pdf](http://www.damp-meter-direct.co.uk/PDF/manual/Protimeter_Timbermaster_Manual.pdf)
- [21] J. Carfrae, P. De Wild, J. Littlewood, S. Goodhew, P. Walker, Development of a cost effective probe for the long term monitoring of straw bale buildings, *Building and Environment*, Elsevier, vol. 46, n°8 (2011) 156–164.



Sustainable Civil Engineering Structures and Construction Materials, SCESCM 2016

## The Influence of PET Plastic Waste Gradations as Coarse Aggregate towards Compressive Strength of Light Concrete

Nursyamsi<sup>a,\*</sup>, Winner Syukur Berkat Zebua<sup>a</sup>

<sup>a</sup>*Department Of Civil Engineering, University Of Sumatera Utara, Jalan Perpustakaan No.5, Medan, 20155, Indonesia*

---

### Abstract

In recent years, the use of substitute materials of concrete aggregate such as industrial wastes and other aggregates, which are light, is being a concern. It is due to these materials can be a solution in order to manage wastes from industry and also to reduce the weight of building structures. This study utilizes *Poly Ethylene Terephthalate* (PET) plastic waste which is light as coarse aggregates. The coarse aggregate from PET plastic waste is the result of the PET-heated to produce agglomeration, and then it is cooled and crushed into aggregates that have variety of sizes with certain gradations. The purpose of this study is to determine the compressive strength of light concrete of PET plastic waste as coarse aggregate and the influence of aggregate gradations towards the compressive strength of concrete that is produced. The material testing with various fineness modulus (FM) produces various results. The maximum compressive strength is achieved on sample using the maximum fineness modulus of PET plastic waste aggregate. According to SNI 03-3994-2002, the weight and compressive strength of the material should fit the standard. As the result, the gradation of coarse aggregate of PET plastic waste can affect the compressive strength of light concrete.

© 2017 The Authors. Published by Elsevier Ltd.

Peer-review under responsibility of the organizing committee of SCESCM 2016.

*Keywords: light concrete, coarse aggregate, PET plastic waste, compressive strength.*

---

---

\* Corresponding author. Tel.: +0-000-000-0000 ; fax: +0-000-000-0000 .

E-mail address: [njnursyamsi@gmail.com](mailto:njnursyamsi@gmail.com)

## 1. Introduction

### 1.1. Background

The use of *Poly Ethylene Terephthalate* (PET) for food or beverage packaging is already familiar in public. After the contents are consumed, the PET plastic containers usually are directly discharged. In essence, this type of plastics is not reused one, but it is recycled plastic producing several other products. However, in the real life, PET plastics are commonly reused by society not only for foods packaging but also for beverages and other uses. The hazardous contents contained in this plastic can be mixed with food and drinks that are packed in it. Time by time, the increasing of the plastics usages cause the inclining of the amount of plastic wastes. The non-biodegradable characteristic of plastic is the reason why plastics take hundreds of years to decompose completely. Most people maintain the plastic wastes by burning them freely, whereas the burning process of this waste will release a variety of harmful substances to the environment. Certainly, the efficient waste plastic management is strongly needed nowadays. One of ways is by utilizing the waste to be useful materials, such as the utilization of plastic wastes to be artificial aggregate in light concrete mixture. Most of the existing plastic wastes are polyethylene plastic type. Polyethylene is produced from the polymerization process of ethylene gas molecules that are together to form long molecules to be a form of plastic (polymer).

The author, in this study, will use *Poly Ethylene Terephthalate* (PET) plastic waste as coarse aggregate, in which this material is also light weight. This light PET plastic waste will be designed to produce mixtures for producing structural light concrete based on SNI-03-2461-2002 with maximum weight of content is 1,850 kg/m<sup>3</sup>. The coarse aggregate of PET plastic waste is the result of the heating process of the PET plastic producing agglomeration, and then it is cooled and crushed into aggregates that have various sizes with certain gradations. The gradation of the aggregate expressed numerically by fineness modulus. Fineness Modulus (FM) is an empirical factor that determines the fineness of the aggregate. The aggregate with greater value of FM is coarser and aggregate with the smaller FM value is finer. SK SNI S-04-1989-F determines that a coarse aggregate has 6.0 to 7.1 of fineness modulus. From this standard, the author will also make variations of the coarse aggregate FM of PET plastic waste in order to determine the effect of compressive strength of concrete that has been produced. This research is expected to have contributions for society, industry, and science development. The structural light concrete from aggregates of PET plastic waste could be an alternative way to utilize PET plastic waste and light concrete which is suitable for earthquake-prone areas.

### 1.2. Nature of Problems

This study focuses on the manufacturing the PET plastic waste into coarse aggregate, to help recycling and reusing the plastic waste for the construction industries. The coarse aggregate is used on building structure as an effort to implement the lightweight concrete to minimize the building failure, especially in the earthquake-prone areas. The coarse aggregate in this study has various gradations which then compared to obtain the maximum and optimum strength for the lightweight concrete structure.

### 1.3. Study Objectives

The benefits of this study are to provide alternative utilizations of PET plastic waste and to produce light concrete for building structures, especially in many areas prone to earthquakes. Furthermore, this study provides information on the effects of variation gradations of coarse aggregate of PET plastic waste in light concrete and also to inspire other researchers to create other light concretes for building structures.



## 1.4. Problem Limitation

This study is conducted to obtain the compressive strength of 28-day-concrete for each variation with mix design calculations based on ACI 211.2-98 method. The plan compressive strength is 17.5 MPa. The gradations of coarse aggregate of PET plastic waste are reviewed by three variations of manual mixing, in which fineness modulus within specified limits for coarse aggregate.

## 2. Methodology

The PET waste such as bottles and other kinds of PET products are cut into small pieces (flakes) to make them melt easier in the heating process. The PET flakes are heated until they are melted. The melted PET is then poured into the molding plate and then left to be cooled. The molded PET waste is then crushed using hammer to form the coarse aggregate with various gradation.

After the coarse aggregate of PET plastic waste is produced, the variations of gradations are manufactured. This following pictures are the manufacturing process of the coarse aggregate to the variation of PET plastic waste gradations:

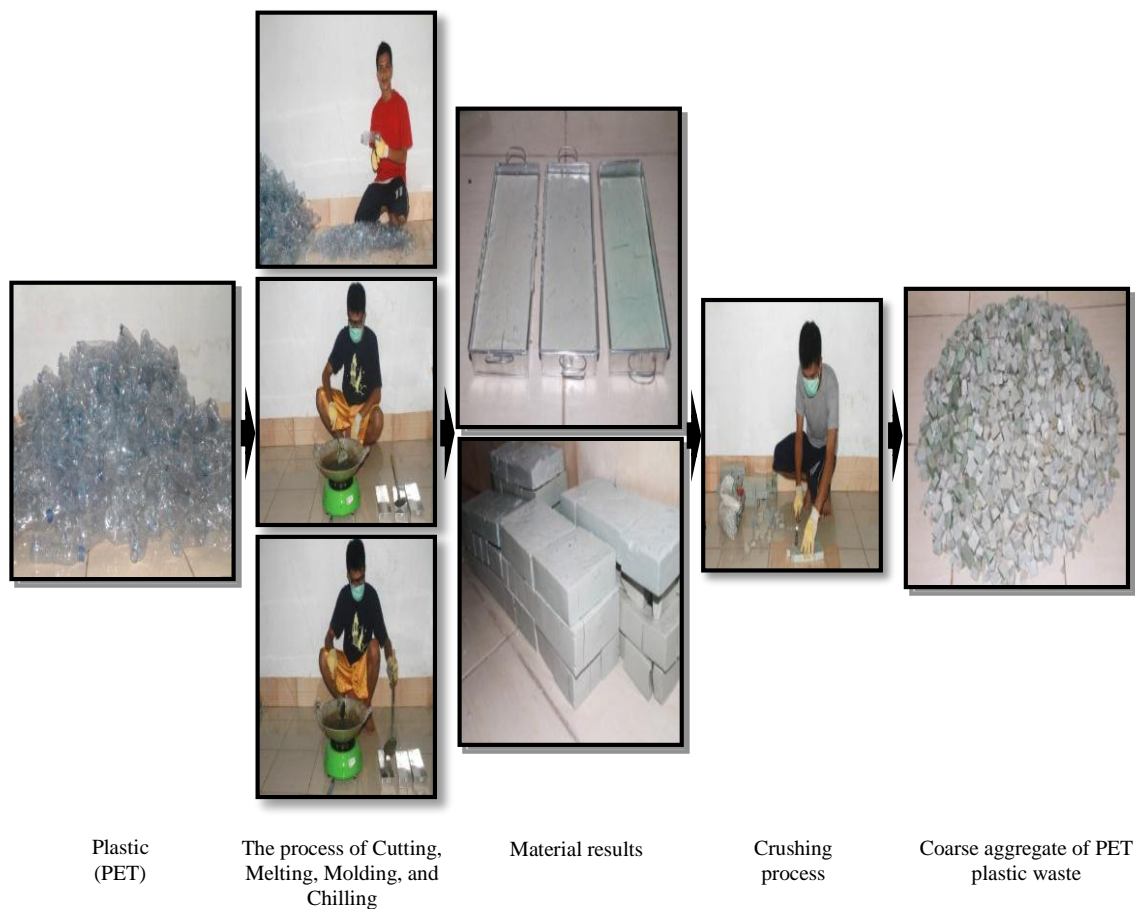


Figure 1. The manufacturing process of coarse aggregate of PET plastic waste



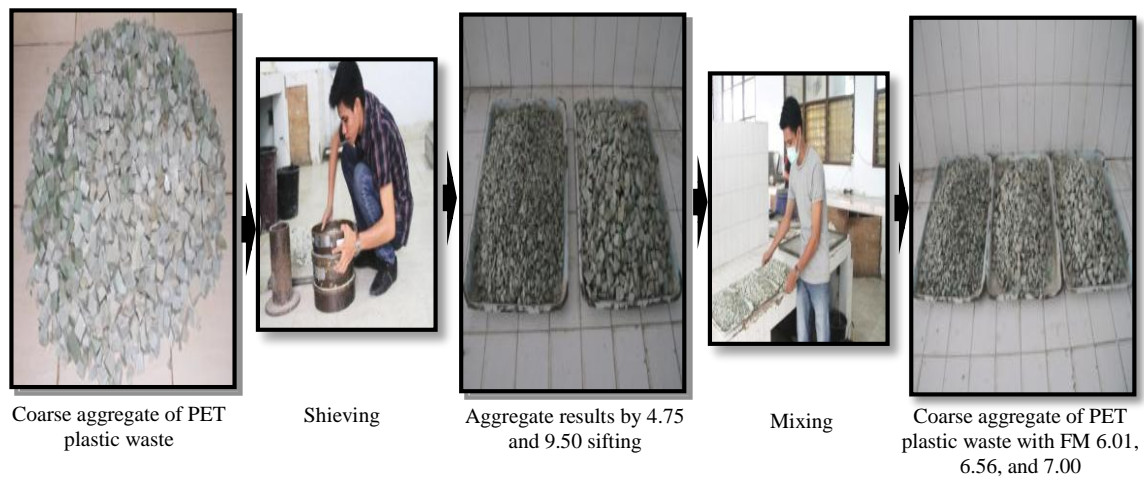


Figure 2. The manufacturing process of coarse aggregate gradation of plastic waste

After the manufacturing of coarse aggregate, the properties tests of fine aggregate and cement are done to obtain the data for the concrete mix design. Based on ACI 211.2-98, the stages of mixing design determine the designated compressive strength, the designated slump, the maximum diameter of the aggregate, the air-water requirements, the ratio of water-cement, and the coarse aggregate requirements in the mixing design. The mixing can be done when every stage or aspect has completed.

The mixing process requires the designated weight of the materials including aggregates, cement and water. The aggregates and cement are initially poured into the mixer and then the water. Afterwards, the homogeneous concrete is poured or casted into the molds. The molds used for the fresh concrete are a cube of 15 x 15 x 15 cm.

After the casting process, the concrete is left for 24 hours for the initial setting. After 24 hours, the molds are released and the samples are sunk in the water for 28 days. After the 28 days sunk and 24 hours of drying, the compressive strength test is done.

### 3. Results

The form of the coarse aggregate of PET plastic waste is similar to or even equal to the form of the coarse aggregate of crushed stone. Texture of aggregates surfaces is shiny (glassy). The result of material testing:

Table 1. The result of coarse aggregate of PET plastic waste

Types of testing	Coarse aggregate of PET plastic waste
Fineness Modulus (FM)	6.01 – 6.5 – 7.00
Water content (%)	0.002
Density of SSD condition	1.31
Density (kg/m <sup>3</sup> )	812
Absorption Percentage (%)	0.4

Table 2. The result of light aggregates

Types of testing	Sand
Fineness Modulus (FM)	2.39
Water content (%)	4.93
Density of SSD condition	2.45
Absorption Percentage (%)	1.94

The content of clay lump (%)	2.56
The content of organic substances (colour)	Same
Density (kg/m <sup>3</sup> )	1,678

Table 3. The proportion of light concrete by mix design on ACI 211.1-98 method

Material	kg/m <sup>3</sup>
Cement	367.27
Sand	518.85
Coarse aggregate of PET plastic waste	600.88
Water	202.00

The results of the concrete weighing and compressive strength testing of this study can be seen in the following tables:

Table 4. The result of concrete weight

The gradation of coarse aggregate of PET plastic waste (FM)	Concrete weight per m <sup>3</sup> (kg/m <sup>3</sup> )
FM 6.01	1,741.23
FM 6.5	1,784.69
FM 7.00	1,801.48

Table 5. The result of concrete compressive strength

The gradation of coarse aggregate of PET plastic waste (FM)	Compressive strength (MPa)
FM 6.01	13.89
FM 6.5	16.27
FM 7.00	16.57

## 4. Conclusions and Recommendations

### 4.1. Conclusions

1. The maximum size of aggregate coarse grain of PET plastic waste can be produced about 3-4 cm.
2. The use of coarse aggregate of PET plastic waste with variation of 6.01; 6.56; and 7.00 FM can produce 1,741.23 kg / m<sup>3</sup>, 1,784.69 kg / m<sup>3</sup>, and 1,801.48 kg / m<sup>3</sup> light concrete respectively.
3. The smaller FM of coarse aggregate of PET plastic waste that is used in concrete, the lighter the concrete that is produced.
4. The maximum compressive strength is 16.57 MPa, which is the coarse aggregate of PET plastic waste with FM 7. The respective value of compressive strength with the FM 6.01 and 6.56 are 13.89 and 16.27 MPa that do not achieve the target of structural concrete compressive strength.
5. The gradation of coarse aggregate of PET plastic waste can affect the compressive strength of structural light concrete. This is influenced by the coarse aggregate surface areas and densities of PET plastic waste in concrete. The smaller the FM of aggregate, the broader surface area of aggregate and more solidified in concrete. Its broad surface area of aggregate makes concrete attachment becoming weak that is caused by shiny texture (glassy). Therefore, the more solidified aggregate, the more concrete is filled by coarse aggregate of PET plastic waste with weak destruction.

#### 4.2. Recommendations

1. The use of coarse aggregate of PET plastic waste in concrete as an alternative to reduce self-weight on the building needs to be studied more such as compressive strength and other characteristics. The light concrete results in this study can be used for light structural only.
2. It is recommended for researchers to conduct further research about the minimum and maximum variation of aggregates gradations of PET plastic waste that can be used as concrete structural or light concrete structural.
3. It is needed to do further research about the effect of coarse aggregate gradation variation of PET plastic waste on other concrete properties.
4. It is recommended to continue this research with other types of plastics.

#### References

- [1] Anonim 1, Metode Pengujian Kuat Tekan Beton (SNI 03-1974-1990), Badan Standarisasi Nasional, 1990.
- [2] Anonim 2, Tata Cara Rencana Pembuatan Campuran Beton Normal (SNI T-15-1990-03), Departemen Pekerjaan Umum: Yayasan Lembaga Penyelidikan Masalah Bangunan, 1991.
- [3] Anonim 3, Standard Practice for Selecting Proportions Structural Lightweight Concrete (ACI 211.2-98), ACI Committee 211, 1998.
- [4] Anonim 4, Tata Cara Pembuatan Rencana Campuran Beton Normal (SNI 03-2834-2000), Badan Standarisasi Nasional, Bandung, 2000.
- [5] Anonim 5, Spesifikasi Agregat Ringan untuk Beton Ringan (SNI 03-2461-2002), Standarisasi Bidang Konstruksi dan Bangunan, Jakarta, 2002.
- [6] Anonim 6, Tata Cara Rencana Pembuatan Campuran Beton Ringan dengan Agregat Ringan, SK SNI T-03-3449-2002, SNI 03-3449-2002, Departemen Pekerjaan Umum, Yayasan LPMB, Bandung, 2002.
- [7] Alqahtami Fahad K, Lightweight Concrete Containing Recycled Plastic Aggregates, International Conference on Electromechanical Control Technology and Transportation (ICECTT 2015)
- [8] Anju Remesan et al, Performance of Light-Weight Concrete with Plastic Aggregate, Int. Journal of Engineering Research and Applications, ISSN: 2248-9622, Vol.5, Issue 8, (Part-5), August 2015.
- [9] Mulyono, Tri, Teknologi Beton, CV Andi Offset, Yogyakarta, 2003.
- [10] Murdock, L.J, Brook, K.M, Hendarko, Stephanus, Bahan dan Praktek Beton, Erlangga, Jakarta, 1991.
- [11] Nawy, Dr. Edward G., P. E. Beton Bertulang, Refika Aditama, Bandung, 2008.
- [12] N, Venkata Ramana et al, Regression Models to Elevate Compressive Strenght of Polyethylene Terephthalate (PET) Fibre Reinforced Recycle Aggregate Concrete, International Journal of Engineering Research and Development e-issn : 2278-067x, p-issn : 2278-800x, www.ijerd.com volume 8, issue 5, August 2013.
- [13] Nugraha, Paul. dan Antoni, Teknologi Beton dan Material, Pembuatan Beton Kinerja Tinggi, Andi Offset Yogyakarta, 2007.
- [14] Pratikto, Beton Ringan ber-agregat Limbah botol plastik jenis PET (Poly Ethylene Terephthalate), Seminar Nasional Teknik Sipil Politeknik Negeri Jakarta, 2010.
- [15] Segel, R., Kole, P., dan Kusuma, Gideon, Pedoman Pengerjaan Beton, Erlangga, Jakarta, 1993.
- [16] Tjokrodinuljo, K, Teknologi Beton, Gramedia, Yogyakarta, 1992.
- [17] Wicaksono, Adi Purwoko, Kajian Kuat Tekan, Kuat Tarik, Kuat Lentur, dan Redaman Bunyi pada Panel Dinding Beton Ringan dengan Agregat Limbah Plastik PET dan Limbah Sekam Padi, e-Jurnal Matriks Teknik Sipil, 2014.
- [18] Widyawati, Ratna, Perbandingan Kuat Tekan Beton Ringan dengan Metoda Rancang-Campur ACI dan Dreux-Corrise, Jurnal Rekayasa Vol. 15 No. 2, 2011.
- [19] Yessi Rismayasari, Utaridan Usman Santosa., Pembuatan Beton dengan Campuran Limbah Plastik dan Karakteristiknya, Indonesian Journal of Applied Physics (2012) Vol. 2 No.1 halaman 21, 2012.
- [20] Riyadi, Mohtarom dkk, Pemanfaatan Limbah Plastik Simpul Sebagai Pengganti Agregat Kasar Pada Beton. Jurnal Politeknologi Vol. 14 No. 1. Jakarta: Politeknik Negeri Jakarta, 2015.
- [21] Rommel, Erwin, Pembuatan Beton Ringan dari Agregat Buatan Berbahan Plastik, Jurnal Gamma vol. 9 no.1 September 2013.
- [22] Vikran Kathe et al, Green Concrete using Plastic Waste, International Journal of Engineering and Technology (IJETT) Volume 19 Number 4 Jan 2015.



Sustainable Civil Engineering Structures and Construction Materials, SCESCM 2016

## Experimental study of fly ash density effect to the mortar compressive strength with recycled fine aggregate

Altho Sagara<sup>a,\*</sup>, Johannes Adhijoso Tjondro<sup>a</sup>, Dinda Karina Putri<sup>a</sup>

<sup>a</sup>Department of Civil Engineering, Parahyangan Catholic University, Ciumbuleuit 94, Bandung 40140, Indonesia

---

### Abstract

Massive production of fly ash and recycled concrete aggregate from various sources such as industries, demolished buildings and so on has been seen as a threatening environmental waste from the conservative material engineering perspective. However, in recent years, the utilization of waste materials in mixed concrete have been turned upside down to become an alternative in producing eco-friendly construction materials. Therefore, this study is aimed to observe the mortar compressive strength that consists of cement, water, recycled fine aggregate and specifically fly ash whose amount is determined based on the packing density method. Several mixing variations are used to derive the correlation between fly ash density and mortar compressive strength. Three different fly ash percentages, which are 25% (loose), 35% (completely) and 45% (over) are used in the laboratory test with the variations of mixing ratios of 0.2, 0.35, and 0.5. The mortar under completely packaged condition delivers the highest compressive strength in any mixing ratio, which are found at 27.02 MPa, 30.26 MPa, and 32.15 MPa for respectively 0.2, 0.35 and 0.5 mixing ratio. Conclusively, this particular pattern indicates the suitability of packing density method usage as the basic to determine the optimum fly ash amount in mortar mixing.

© 2017 The Authors. Published by Elsevier Ltd.

Peer-review under responsibility of the organizing committee of SCESCM 2016.

*Keywords:* Fly Ash; Recycled Concrete Aggregate; Packing Density; Compressive Strength; Mortar Mixing.

---

### 1. Introduction

Innovations in civil engineering field have developed quite significantly in recent years. These innovations are mostly contributed by material research developments which are the most interested area in green building concept.

---

\* Corresponding author. Tel.: +62-819-2935-3768.

E-mail address: [altho.sagara@unpar.ac.id](mailto:altho.sagara@unpar.ac.id)

One of these developments leads to the use of fly ash in mortar as a substitute to a part of cementitious materials. The use of this material is expected to reduce the contributing wastes which are byproducts of coal power plants. Moreover, this material can be a better filler than common fine aggregates. This is due to the fact that it has a smaller particle sizes that averaged at 0.075 mm.

Although several concrete code like ACI (American Concrete Institute) and SNI (Indonesian National Standard) have provided the value of fly ash that can be added in concrete mix as pozzolan material which at 15%-25% [1], it doesn't govern the behavior of fly ash beyond these percentages. Considering the behavior of fly ash from the previous research [2], the fly ash would be considered as fine aggregate in mortar mix for this study.

Aside from the use of fly ash, reducing the waste material in constructions can also be achieved by using recycled fine aggregate in mortar mix. Although the use of these materials would likely to produce a significantly smaller compressive strength, it can be overcome with decent researches in this field. Recycled fine aggregate used in this study have particle size with the range 0.6 mm – 4.75 mm.

The objective of this study is to find an optimum percentage for fly ash in recycled aggregate concrete mortar mix and to observe the relation between packing density of mortar mix and its compressive strength. This percentage would be obtained by observing the relation between the packing density of mortar mix with the percentage of fly ash in that mortar mix. This relation is predicted to have a similar Fig. as seen in Fig 1 [3]. With the increasing percentage of fly ash (filler aggregate), the packing density would increase until it reached an optimum point (point 3). The value of packing density would decrease beyond this point.

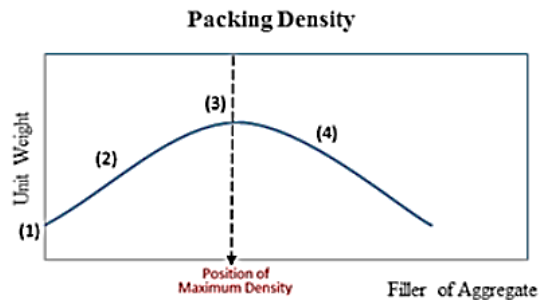


Fig. 1. Packing density prediction

## 2. Experimental

### 2.1. Packing density method

Mortar's mix packing density with a variety of fly ash percentage are tested to obtain the effect of fly ash percentage in the mix to its packing density. For each percentage of fly ash, the mortar's mix packing density is tested with the increments of 5 percent until it reached a few point beyond the optimum. It is compacted directly in a mold using a bar and rubber hammer. These result of present study can be seen in Fig 2

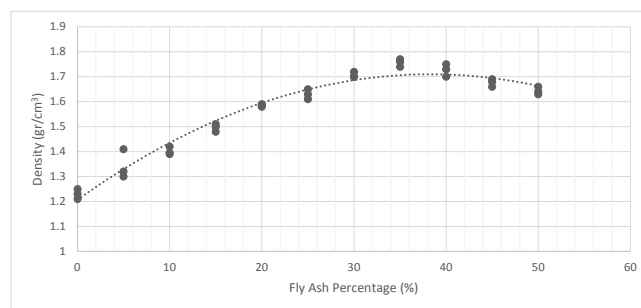


Fig. 2. Packing density testing

Based on the result as seen on the Fig. 2, it can be seen the packing density reached its optimum point at 35 percent of fly ash. This condition is named completely package. Whereas, the condition with 25 percent and 45 percent of fly ash is named loosely and over package respectively. These three points are points of interest in this study that would be discussed later.

## 2.2. Mix proportions and specimens

Mix proportions that used in this research are 0.2, 0.35, and 0.5. With bigger mix proportion, the more amount of cement in the mix. The mass requirement of mortar mix materials for each mix proportions and fly ash percentage can be seen in Table 1. These value are only for a single cylinder mold. The mortar specimens have a dimension of 5 cm diameter and 10 cm height (Fig. 3)

Table 1. Mix proportion

Mix Proportion	Fly Ash Percentage (%)	Cement Mass (gram)	Fly Ash Mass (gram)	Aggregate Recycled mass (gram)
0.2	25	103.3	43.95	179.90
0.35	25	160.27	39.07	159.91
0.5	25	206.06	35.16	143.92
0.2	35	103.03	61.53	179.90
0.35	35	160.27	54.70	159.91
0.5	35	206.06	49.23	143.92
0.2	45	103.03	79.11	179.90
0.35	45	160.2	70.32	159.91
0.5	45	206.06	63.29	143.92



Fig. 3. Steel mold and mortar specimens

These mix proportions would be tested with a variety of fly ash percentage and mortar's age. This would result a total of 9 type of specimens that would be tested on 3, 7, 14, 21, and 28 days of age. There is 3 specimens for each type and age. Each type of specimens with its label can be seen in Table 2.

Table 2. Variety of specimens

Label	Fly ash percentage (%)	Packing condition	Mix proportion (cement / aggregates)	Age (days)
C2-25	25	Loosely Package	0.20	3, 7, 14, 21, 28
C3-25	25		0.35	3, 7, 14, 21, 28
C5-25	25		0.50	3, 7, 14, 21, 28
C2-35	35	Completely Package	0.20	3, 7, 14, 21, 28
C3-35	35		0.35	3, 7, 14, 21, 28
C5-35	35		0.50	3, 7, 14, 21, 28
C2-45	45	Over Package	0.20	3, 7, 14, 21, 28
C3-45	45		0.35	3, 7, 14, 21, 28
C5-45	45		0.50	3, 7, 14, 21, 28

### 2.3. Mortar's compressive strength measurement

Mortar's compressive strength measurement would be conducted with the standard method of ASTM C-109/C109M-12 using a Universal Testing Machine (UTM) [4]. Experimental setup can be seen on Fig.4. From the result of UTM, the peak load of mortar compressive strength is obtained along with the load – displacement curve.



Fig. 4. Experimental setup

## 3. Results and discussion

Based on the experimental results, the relation between fly ash percentage, mortar's compressive strength, and the mortar mix age with varying mix proportion is obtained. These curved is fitted using polynomial functions as seen in the following Fig.s.

As seen in the Fig.s below, the results have a varying trend which depends on mortar's fly ash percentage and its mix proportion.

The results of each 0.2 mix proportion specimen have a matching trend where at completely package condition, it has the highest compressive strength. This compressive strength is 27.02 MPa which 7% higher than loosely package condition, and 12% higher than over package condition.

As for 0.35 mix proportion specimen, the results have a slightly different trend for each specimen. Smaller fly ash percentage specimen has highest compressive strength on the early age (before 14 days). On the other hand, this trend isn't true for later age which the highest compressive strength is found in completely package specimen. It is about 30.26 MPa which has a difference of 5% and 1.5% with loosely and over package condition respectively.

Unlike the previous 2 type of proportions, the 0.5 mix proportion doesn't have a significant compressive strength differences in each varying fly ash percentage and its age. The highest compressive strength in this mix proportion is 32.15 MPa, and found in completely package specimen which has 3.5% difference with other condition.



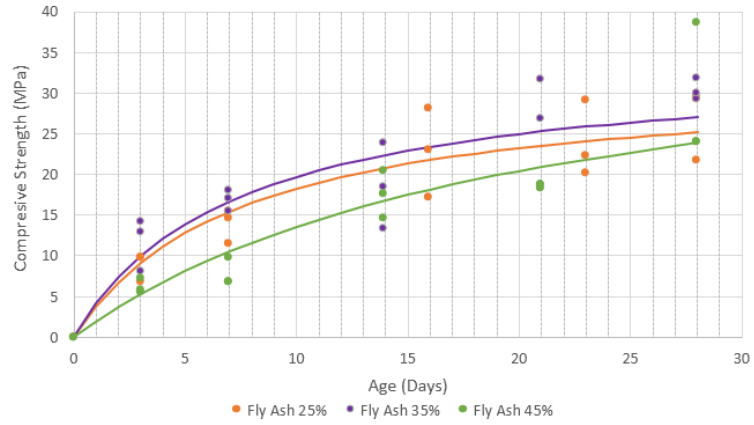


Fig. 5. Mortar's compressive strengths with 0.2 mix proportion

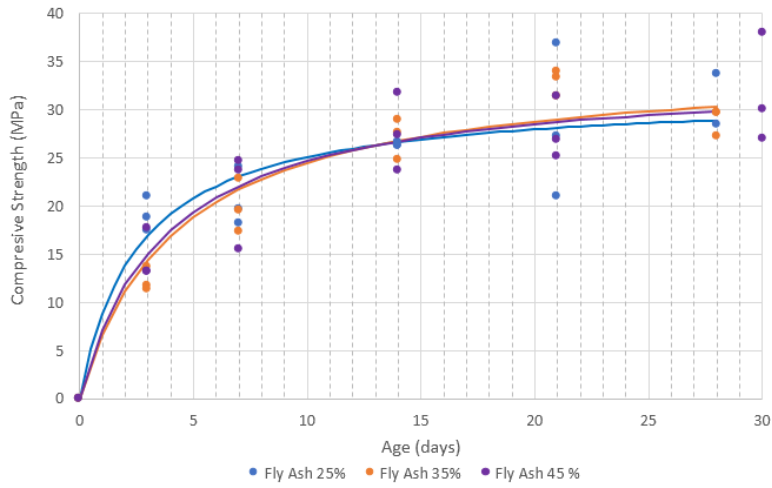


Fig. 6. Mortar's compressive strengths with 0.35 mix proportion

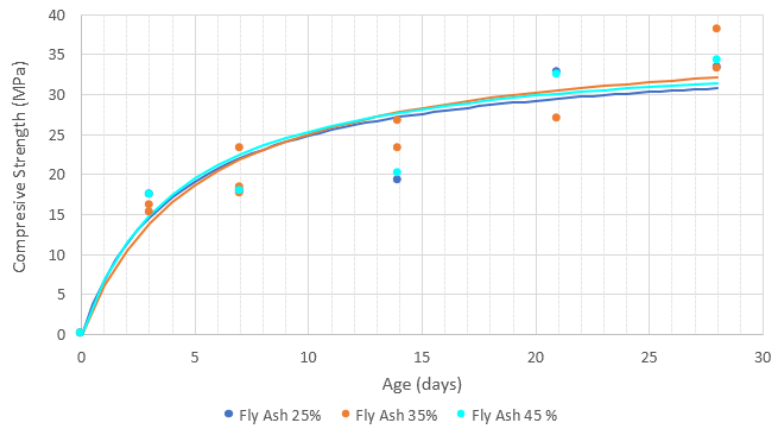


Fig. 7. Mortar's compressive strengths with 0.5 mix proportion

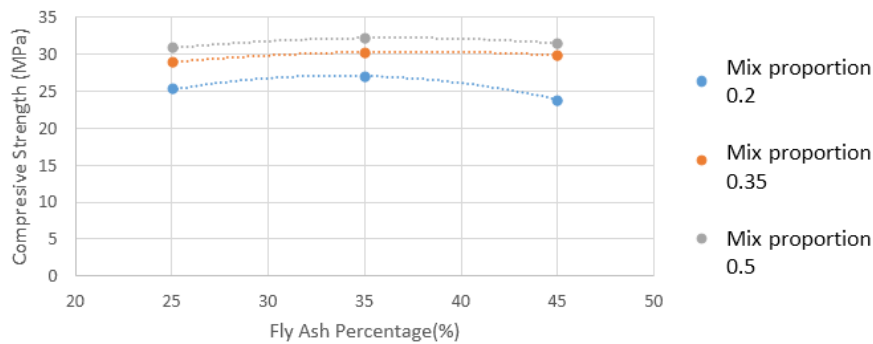


Fig. 8. The Relation between fly ash percentage and compressive strength

Fig. 8 shows the relation between fly ash percentage and its compressive strength for every mix proportions. Every mix proportions have the same trend which the highest compressive strength is always achieved by completely package condition. This can be concluded that the fly ash percentage of completely package condition is the optimum amount of fly ash that can be added. Furthermore, the amount of cement in the mix is also affecting the mortar's compressive strength. With higher cement content, it would produce a higher mortar's compressive strength.

#### 4. Conclusion

The packing density approach can be used to determine the optimum fly ash percentage that can be added in the mix. Based on the result of this research, the optimum fly ash percentage is found to be 35 percent (completely package). It is proven by compressive testing which the highest compressive strength is always achieved by this condition. The resulting compressive strengths are 27.02 MPa, 30.26 MPa, and 32.15 MPa for 0.2, 0.35, and 0.5 mix proportions respectively. It is also noted that a mix's density is directly proportional with its compressive strength.

Although the higher cement content would likely to produce higher compressive strength, it is not true fly ash content. Due to this fact, fly ash can't replace cement as a full supplementary cementitious materials. But it can act as a partially supplementary of the cement and also a well-performed filler.

#### Acknowledgements

The writer would like to acknowledge Bambang Suryatmono, Dina Rubiana Widarda, Buen Sian, Julius Belen, and Sisi Nova from Civil Engineering Department, Parahyangan Catholic University for technical input to improve the research and their continued advisement.

#### References

- [1] ACI Committee 318M-08, "Building Code Requirements for Structural Concrete" American Concrete Institute, Detroit, MI (2008).
- [2] Musekh, L. Meddah, M.S. Ouchagour, Y. (2012). Use of Recycled Concrete in Fly Ash Concrete. Kingston University, London.
- [3] Hwang, Fuller (2012). Pozzolan Concrete Mixture Design by Hwang-Fuller Densified Mixed Design Algorithm. Construction Material Research Laboratory (CMRL)
- [4] American Society for Testing and Materials (2012). Standard Test Method for Compressive Strength of Hydraulic Cement Mortar, ASTM C-109/C109M-12, Annual Books of ASTM Standards, USA.
- [5] American Society for Testing and Materials (2004). Standard Specification for Mortar Cement, ASTM C1329-04, Annual Books of ASTM Standards, USA.
- [6] American Society for Testing and Materials (1989). Standard Test Method for Compressive Strength of Cylindrical Concrete Specimens, ASTM C-39. Pennsylvania, United States.
- [7] Hansen, T.C (1992). Recycling of Demolished Concrete and Masonry. 1st ed. Taylor & Francis Group.
- [8] Mehta, P.K. and Monteiro, P.J.M (2002). Concrete: Microstructure, properties, and materials. Ottawa, Canada.



Sustainable Civil Engineering Structures and Construction Materials, SCESCM 2016

## Mechanical properties of concretes with recycled aggregates and waste brick powder as cement replacement

Viviana Letelier<sup>a,\*</sup>, Ester Tarela<sup>a</sup>, Giacomo Moriconi<sup>b</sup>

<sup>a</sup>Department of Civil Engineering, Universidad de la Frontera, Av. Fco. Salazar 01145, Temuco-Chile

<sup>b</sup>Department of "Scienze e Ingegneria della Materia, dell'Ambiente e Urbanistica" (SIMAU) Università Politécnica delle Marche, Via Breccie Bianche - 60131 Ancona - Italy

---

### Abstract

The cement industry is responsible for around a 5 % of the CO<sub>2</sub> emissions worldwide and considering that concrete is one of the most used materials in construction its total effect is significant. An alternative to reduce the environmental impact of concrete production is to incorporate certain amount of residuals in the dosing, limiting the replacement percentages to avoid significant losses in the mechanical properties of the final material. This study analyses the variation in the mechanical properties of structural concretes with recycled aggregates and waste brick powder as cement replacement to test the effect of the simultaneous use of different residuals in the same material. All concretes are dosed for a compressive strength of 30 MPa. The recycled aggregates are obtained from prefabricated pipe debris with a compressive strength of 20 MPa. The waste bricks are obtained from construction demolitions. Four levels of replaced cement by waste brick powder are considered: 0 %, 5 %, 10 % and 15 %. Also, two kinds of samples are studied regarding the amount of recycled aggregates: 0 % and 30 %. All these levels are combined to analyze the effect of both residuals in the mechanical properties of the concrete through compressive strength tests, flexural strength tests and elasticity modulus tests, all of them after 28 curing days. Results show that when no recycled aggregates are used, the cement can be replaced up to a 15 % by waste brick powder. But when both residuals are combined the amount of waste brick powder recommended without significant losses in the final material properties is limited to a 5 %. Replacing a 30 % of the aggregates together with a 5 % of the cement can considerably reduce the environmental impact of the final material.

© 2017 The Authors. Published by Elsevier Ltd.

Peer-review under responsibility of the organizing committee of SCESCM 2016.

*Keywords:* Recycled aggregates; waste brick powder; replacement of cement; mechanical behaviour of recycled concrete.

---

---

\* Corresponding author. Tel.: +56-45-2596533.

E-mail address: [viviana.letelier@ufrontera.cl](mailto:viviana.letelier@ufrontera.cl)

## 1. Introduction

Concrete is one of the most used materials in construction and, at the same time, one of the materials with higher contribution to the amount of construction and demolition waste (CDW) generation. In concrete production the main responsible for CO<sub>2</sub> production is the use of ordinary Portland cement with a contribution rate roughly equivalent to 80–90 % [1]. Hence, an effective way to reduce the environmental impact of concrete production is to minimize the CO<sub>2</sub> emission related to cement.

Viera et al. [2] studied the effect of adding fine aggregates from waste bricks and ceramic sanitary ware in concretes, concluding that these fine aggregates contribute to the pozzolanic activity. They found that the use of these residuals increased the strength of the concretes compared to a traditional control one. Puertas et al [3] found that ceramic materials, used as cement replacement, have pozzolanic activity after at least 8 curing days. Kulovaná et al [4] study the replacement of up to a 60 % of brick residuals as cement, with a 0.4 water/cement ratio, concluding that the use of up to a 20 % does not compromise the mechanical properties of the concrete and it enhances up to a 50 % its heat conductivity. On the other hand, Katzer [5] analyzes mortars with 10 % and 50 % brick waste replacements, finding that these residuals can be used in materials with low mechanical requirements (over 0.6 water/cement ratios). This disparity in the results can be attributed to the particle size distribution of the residual, while Katzer [5] uses material with particles under 8 mm, Kulovaná et al [4] mainly replace material under 100 microns.

Moreover, the use of ceramic brick residuals enhances the durability due to a refinement in the pore structure. Bignozzi and Bonduà [6] found that the use of a 25 % of ceramic residuals as cement supplement increases the cement durability compared to ordinary Portland cements. Similar results are obtained by Pacheco and Jalali [7,8] using 20 % of brick and sanitary ware ceramic waste. On their behalf, Toledo et al [9] and Vejmelková et al. [10] conclude that the use of up to a 20 % of ceramic brick has no influence in the compressive strength and elasticity modulus of the mortar, and Lavat et al. [11] establish that 20 % to 30 % of the cement can be replaced by adequately grinded ceramic roof tile.

Besides, the replacement of up to a 25 % of cement by brick waste has been tested along with the use of waste glass as sand replacement. Results have proven that the brick powder is able to counteract the negative effects of the use of glass in the alkali-silica expansive reaction responsible of the production of fissures in the concrete [12].

An alternative to reduce even more the CO<sub>2</sub> emissions and the amount of CDW from concrete production is to replace, not only some amount of cement but also other of the raw materials, such as coarse aggregates. Several studies [13-23] have proven the feasibility of the use of recycled aggregates (RA) if the percentage of replacement is limited [16-23]. Differences between the mechanical properties of traditional concrete and concretes with RA have been mainly attributed to the old mortar adhered to the surfaces of the RA. Two interfaces have to be considered when using RA rather than one, the old interface, between the old mortar and the RA, and the new one, between the RA and the new cement mixture [14]. The quality of these interfaces, given by the quantity and quality of the old adhered mortar, is a key factor influencing the mechanical behavior of recycled concrete [15,24].

Despite the use of RA and waste brick powder (WBP) has been studied in construction materials, there is still a lack of information about the mechanical behavior of concretes produced with both residuals simultaneously. Therefore, the goal of this research is to analyze the effects of the simultaneous replacement of WBP as cement and RA as natural coarse aggregates, in particular, in the mechanical properties (compressive strength and flexural strength) of concrete mixtures, to efficiently maximize the reuse of concrete waste. The aim of this study is to optimize the mixture combining the considered parameters, maximizing the amount of WBP and RA reused.

## 2. Methods and Materials

### 2.1. Cement and Bricks

Pozzolanic cement, equivalent to ASTM type P cement, was used. The targeted 28-days-compressive concrete strength was set at 30 MPa.

WBP, used as cement replacement, was obtained from industrial brick residuals from demolition debris.

## 2.2. Natural and recycled aggregates

RA were obtained from precast concrete debris and their nominal sizes are 19.3 mm, 12.5 mm and 9.5 mm. The amount of mortar adhered to the surface of RA has been mechanically reduced by applying a 300 rev abrasion using a Los Angeles machine. This way the effect of the double interface problem is minimized.

The physical properties of the coarse aggregates were obtained following the ASTM C127–15 and ASTM C128–15. The results are shown in Table 1. Natural sand was used in all of the concretes. Natural aggregates (NA) present higher values of density than recycled ones. This decrease, of around 6 %, in the density is caused by the presence of remaining adhered mortar in RA. This has been proven measuring the density and the water absorption both before and after the abrasion treatment. On the other hand, the water absorption is around 2.5 times bigger in RA than in NA.

Table 1: Physical properties of the coarse aggregates

Aggregates	Size	$\rho_{R_{ss}}$	$\rho_{rs}$	$\rho_n$	Absorption
NA (Natural Aggregates)	6.3-9.5	2678	2629	2765	1.9 %
	9.5-12.5	2687	2642	2767	1.7 %
	12.5-19	2699	2661	2765	1.4 %
RA (Recycled Aggregates)	6.3-9.5	2510	2390	2720	5.0 %
	9.5-12.5	2530	2430	2720	4.4 %
	12.5-19	2530	2440	2700	4.0 %

## 2.3. Sample preparation

In order to assess the effects of WBP as partial replacement of cement on the behavior of concrete, a constant water/binder (cement + fine addition) ratio of 0.42 was used for all samples.

The experimental phase consisted in analyzing the differences in the mechanical properties between concrete made with different amounts of WBP (0 %, 5 %, 10 % and 15 %) and NA, and concretes with the same amounts of WBP and 30 % of RA. This way not only the effect of the WBP can be assessed but also the combined effect of both residuals.

The manufactured samples and series are shown in Table 2.

Table 2: Concrete dosages

	Natural Aggregate (2.36-19 mm) kg	RA (6.3-19 mm) kg	Cement kg	WBP kg	Sand kg	Water Lt
B0-R0	1266.00	-	382.00	-	542.00	192.63
B5-R0	1266.00	-	362.90	19.10	542.00	192.63
B10-R0	1266.00	-	343.80	38.20	542.00	192.63
B15-R0	1266.00	-	324.70	57.30	542.00	192.63
B5-R30	886.2	379.8	362.90	19.10	542.00	192.63
B10-R30	886.2	379.8	343.80	38.20	542.00	192.63
B15-R30	886.2	379.8	324.70	57.30	542.00	192.63

Compressive strengths, flexural strengths and static modulus of elasticity were tested after 28 curing days. The compressive strength was tested using a hydraulic press with a maximum capacity of 3000 KN and was determined using the standard ASTM C39/C39 on three 150 $\phi$ ×300 mm cylindrical specimens. The flexural strength was

measured following the ASTM C78 specifications on three 150×150×530 mm prism specimens. The static modulus of elasticity was determined on three 150φ×300 mm cylindrical specimens according to ASTM C469 for each type of concrete produced.

### 3. Results and discussion

The results obtained for the compressive strength, flexural strength and static elasticity modulus after 28 curing days are shown in Fig. 1. The samples are named following the code: B(% of WBP)-R(% of RA).

Most of the series without RA present no significant negative effects, even when a 15 % of WBP is used, agreeing with several authors that conclude that up to a 20 % of the cement can be replaced by ceramic materials with almost no effect in the mechanical properties of the concretes [4,7,8]. Only when the WBP replacement exceeds a 5 % and is combined with the use of RA a slight decrease in the mechanical properties is observed.

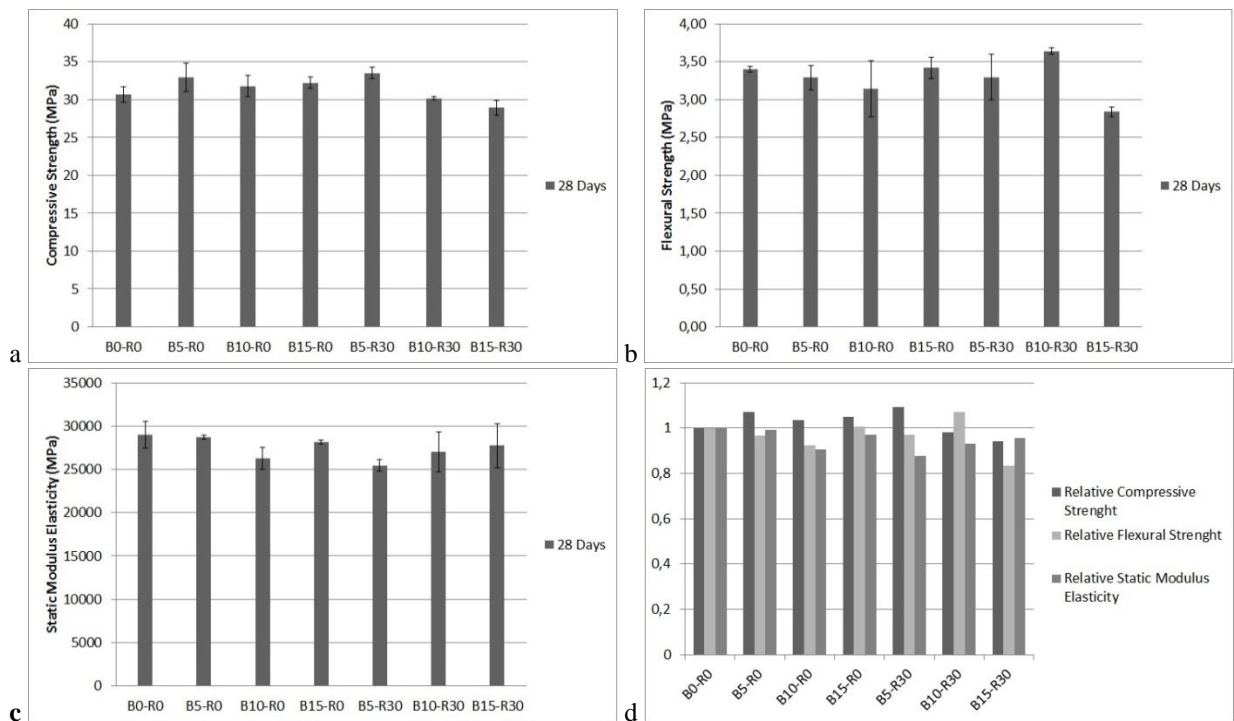


Fig. 1: (a) Compressive strength. (b) Flexural strength. (c) Static elasticity modulus. (d) Compressive strength, flexural strength and elasticity modulus related to CC (B0-R0) values.

Compressive strength (Fig.1a) varies between an increase of 9 % and a reduction of 6 % compared to the B0-R0 sample or the control concrete (CC). Series B5-R0 and B5-R30 present the highest values. Both series contain a 5 % WBP replacement. Agreeing with the conclusions presented by Ergün [5], the fineness and the amount of residue improved the initial porosity of the mix due to the obstruction of pores as a filler effect. This effect would improve the simultaneous behavior of RA and WBP. Nassar and Soroushian [29] studied the use of glass powder as cement replacement together with RA, concluding that a pozzolanic reaction occurs between the silicates in the glass powder and the calcium hydroxide ( $\text{Ca}(\text{OH})_2$ ) in the cement of the mortar of RA, forming hydrated calcium silicate (CSH), enhancing the quality of the interface.

Flexural strength (Fig. 1b) ranges between an increase of 1 % and a decrease of 16 %. Here the amount of RA seems to have low influence on the results. The most significant reduction is obtained for series B15-R30, with a 16 % loss in relation to CC. Fig. 1d shows the relative compressive and flexural strength related to CC. The use WBP and RA has more effects in the flexural strength than in the compressive strength.

Static modulus of elasticity (Fig. 1c) decreases between a 1 % and a 12 %. The amount of RA seems to have low influence on these results. The most significant reduction is obtained for series B5-R30, with a 12 % loss respect to CC. Fig. 1d shows the relative static modulus of elasticity related to CC. As it happened with flexural strength, the static elasticity modulus suffers the effect of the use of WBP and RA more significantly than the compressive strength.

ACI 318-11 proposes Eq. 1 to calculate the ultimate tensile strength or flexural strength and Eq. 2 to calculate the static modulus of elasticity:

$$f_r = 0.62\sqrt{f'_c} \quad (1)$$

Where  $f_r$  is the ultimate flexural strength (MPa) and  $f'_c$  the cylindrical compressive strength (MPa).

$$E_c = 4700\sqrt{f'_c} \quad (2)$$

Where  $E_c$  is the static elasticity modulus (MPa) and  $f'_c$  is the cylindrical compressive strength (MPa).

The experimental results and those obtained using Eq. 1 and Eq. 2 for the studied specimens are shown in Fig. 2. Almost all of the specimens show higher values than the ones specified by ACI 318, except for the flexural strength in series B15-R30. As the values established by ACI 318 are quite conservative it is possible to state that concretes with recycled aggregates exceed expected resistances.

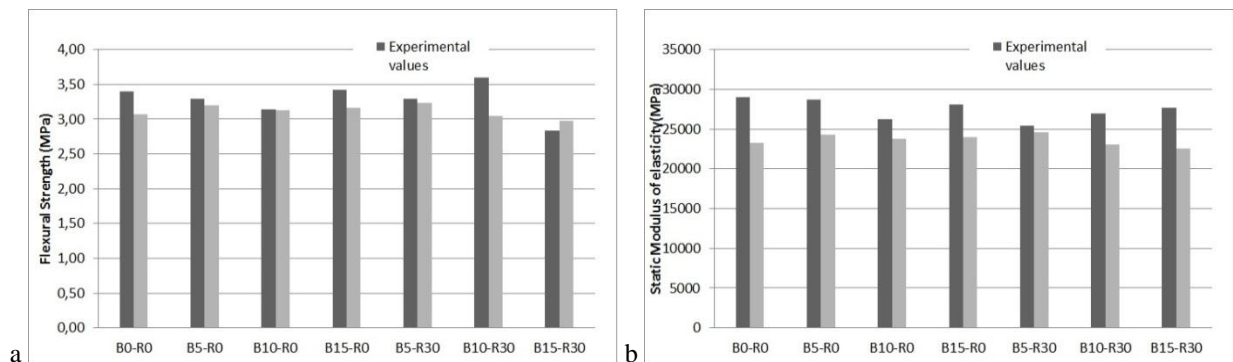


Fig. 2. (a) Flexural strength: experimental and ACI values. (b) Static elasticity modulus: experimental and ACI values.

#### 4. Conclusions

- The best compressive strength results are obtained using 30 % of RA, and 5 % of WBP.
- Low percentages of replaced cement by WBP were found to be beneficial, compensating the strength losses due to the use of RA because of the filler effect.
- Flexural strength and static elasticity modulus are slightly more affected than compressive strength by the use of recycled materials. However, most of the series obey theoretical strength values provided by ACI-318.
- Further studies are needed to establish and quantify the combined effects of WBP and RA on the durability of recycled concretes.

#### Acknowledgements

This analysis is part of the Project CORFO 15IPPID-45706 ‘Áridos reciclados de alta calidad a partir de escombros de hormigones’-‘Evaluación de metodología para la eliminación de mortero por abrasión en áridos reciclados’ (High quality recycled aggregates from concrete debris-Evaluation of the methodology to reduce mortar through abrasion in recycled aggregates), funded by CORFO-CHILE.



## References

- [1] K.H. Yang, Y.B. Jung, M.S. Cho, S.H. Tae, Effect of supplementary cementitious materials on reduction of CO<sub>2</sub> emissions from concrete, *Journal of Cleaner Production*. 103 (2015), 774-783.
- [2] T. Vieira, A. Alves, J. de Brito, J.R. Correia, R.V. Silva, Durability-related performance of concrete containing fine recycled aggregates from crushed bricks and sanitary ware, *Materials & Design*. 90 (2016) 767–776.
- [3] F. Puertas, A. Barba, M.F. Gazulla, M.P. Gómez, M. Palacios, S. Martínez-Ramírez, Ceramic wastes as raw materials in Portland cement clinker fabrication: Characterization and alkaline activation, *Materiales de Construcción*. 56 (2006) 73-84.
- [4] T. Kulovaná, E. Vejmelková, M. Keppert, P. Rovnaníková, Z. Kersner, R. Cerný, Mechanical, durability and hygrothermal properties of concrete produced using Portland cement-ceramic powder blends, *Structural Concrete*. 17 (2015) 105–115.
- [5] J. Katzer, Strength performance comparison of mortars made with waste fine aggregate and ceramic fume, *Construction and Building Materials*. 47 (2013) 1–6.
- [6] M.C. Bignozzi, S. Bonduà, Alternative blended cement with ceramic residues: Corrosion resistance investigation on reinforced mortar, *Cement and Concrete Research*. 41 (2011) 947-954.
- [7] F. Pacheco-Torgal, S. Jalali, Reusing ceramic wastes in concrete, *Construction and Building Materials*. 24 (2010) 832–838.
- [8] F. Pacheco-Torgal, S. Jalali, Compressive strength and durability properties of ceramic wastes based concrete, *Materials and Structures*. 44 (2011) 155–167.
- [9] R.D. Toledo Filho, J.P. Gonçalves, B.B. Americano, E.M.R. Fairbairn, Potential for use of crushed waste calcined-clay brick as a supplementary cementitious material in Brazil, *Cement and Concrete Research*. 37(2007) 1357-1365.
- [10] E. Vejmelková, M. Keppert, P. Rovnaníková, M. Ondráček, Z. Keršner, R. Černý, Properties of high performance concrete containing fine-ground ceramics as supplementary cementitious material, *Cement and Concrete Composites*. 34 (2012) 55-61.
- [11] A.E. Lavat, M.A. Trezza, M. Poggi, Characterization of ceramic roof tile wastes as pozzolanic admixture, *Waste Management*. 29 (2009) 1666–1674.
- [12] M.C. Bignozzi, A. Saccani, Ceramic waste as aggregate and supplementary cementing material: A combined action to contrast alkali silica reaction (ASR), *Cement & Concrete Composites*. 34 (2012) 1141-1148.
- [13] G. Lee, H. Choi, Study on interfacial transition zone properties of recycled aggregate by micro-hardness test, *Construction and Building Materials*. 40 (2013) 455-460.
- [14] V.W.Y. Tam, X.F. Gao, C.M. Tam, Microstructural analysis of recycled aggregate concrete produced from two-stage mixing approach, *Cement and Concrete Research*. 35(6) (2005) 1195-1203.
- [15] D.S. Seo, H.B. Choi, Effects of the old cement mortar attached to the recycled aggregate surface on the bond characteristics between aggregate and cement mortar, *Construction and Building Materials*. 59 (2014) 72-77.
- [16] A. Gonzalez, M. Etxeberria, Experimental analysis of properties of high performance recycled aggregate concrete, *Construction and Building Materials*. 52 (2014) 227-235.
- [17] D. Pedro, J. de Brito, L. Evangelista, Influence of the use of recycled concrete aggregates from different sources on structural concrete, *Construction and Building Materials*. 71 (2014) 141-151.
- [18] V.W.Y. Tam, K. Wang, C.M. Tam, Assessing relationships among properties of demolished concrete, recycled aggregate and recycled aggregate concrete using regression analysis, *Journal of Hazardous Materials*. 152(2) (2008) 703-714.
- [19] A.K. Padmini, K. Ramamurthy, M.S. Mathews, Influence of parent concrete on the properties of recycled aggregate concrete, *Construction and Building Materials*. 23(2) (2009) 829-836.
- [20] X. Li, Recycling and reuse of waste concrete in china; Part ii. Structural behaviour of recycled aggregate concrete and engineering applications, *Resources, Conservation and Recycling*. 53(3) (2009) 107-112.
- [21] W.H. Kwan, M. Ramli, K.J. Kam, M.Z. Sulieman, Influence of the amount of recycled coarse aggregate in concrete design and durability properties, *Construction and Building Materials*. 26(1) (2012) 565-573.
- [22] S. Ismail, M. Ramli, Mechanical strength and drying shrinkage properties of concrete containing treated coarse recycled concrete aggregates, *Construction and Building Materials*. 68 (2014) 726-739.
- [23] M. Etxeberria, A. Mari, E. Vásquez, E.; Recycled aggregate concrete as structural material. *Materials and Structures*, 40 (2007), 529-541.
- [24] F. Agrela, M. Sánchez de Juan, J. Ayuso, V. Galdes, J.R. Jimenez, Limiting properties in the characterization of mixed recycled aggregates for use in the manufacture of concrete, *Construction and Building Materials*. 25 (2011) 3950-3955.
- [25] A. Ergün, Effects of the usage of diatomite and waste marble powder as partial replacement of cement on the mechanical properties of concrete, *Construction and Building Materials*. 25(2) (2011) 806-812.
- [26] R. Nassar, P. Soroushian, Strength and durability of recycled aggregate concrete containing milled glass as partial replacement for cement, *Construction and Building and Environment*. 29 (2008) 368-377.



Sustainable Civil Engineering Structures and Construction Materials, SCESCM 2016

## Potential of substituting waste glass in aerated light weight concrete

Lim Sheau Hooi<sup>a,\*</sup>, Phang Jia Min<sup>a</sup>

<sup>a</sup>*Environmental & Water Technology Centre of Innovation, Ngee Ann Polytechnic, Singapore*

---

### Abstract

This paper investigates the potential of substituting the waste glass in making aerated light weight concrete. The physical, chemical and activity index properties of the ground waste glass are first investigated. Subsequently, the waste glass is incorporated in the aerated light weight concrete formulation as cement substitution at different ratios. The density and initial compressive strength of aerated light weight concrete result are then compared. Based on the initial experiment results, the ground waste glass can be potentially substituted up to 20% as pozzolanic material in making aerated light weight concrete.

© 2017 The Authors. Published by Elsevier Ltd.

Peer-review under responsibility of the organizing committee of SCESCM 2016.

*Keywords:* Waste glass; Aerated light weight concrete; Pozzolanic material; Cement replacement; Sand replacement

---

### 1. Introduction

According to 2014 Singapore National Environment Agency (NEA) annual statistic report, 79,500 tons of waste glass was generated in Singapore and only 20% of the amount was recycled [1]. The remaining quantity of waste glass was either disposed at landfills or recycled back to low cost glass product at the neighbouring countries [2]. The deposition of waste glass to landfills is definitely not a sustainable environmental solution to Singapore. Although, the waste glass can be recycled back to new glass products; however, the process of sorting, crushing and re-melting which require high energy is not favourable in long run. Furthermore, these recycling process may also instigate air pollution if there is any mishandling.

Aerated light weight concrete or also known as cellular concrete is a light weight building material that has been aerated to reduce its density before to the setting of Portland cement in the formulation. The LWC offers not only low density, they also possess superior insulation and acoustic performance, fire resistant properties as well as relatively

---

\* Corresponding author. Tel.: +0-000-000-0000 ; fax: +0-000-000-0000 .

E-mail address: [lsh52@np.edu.sg](mailto:lsh52@np.edu.sg)

high strength coupled with dimensional stability. The LWC can be used to make partitions, prefabricated unit, floating platform and many other applications in building and construction that require low load application. The quick and easy installation of LWC also can significantly reduce the intensive labour and overall load of buildings.

Therefore, the main objective of this study is to investigate the potential of substituting the increasing waste glass number as in the production of aerated light weight concrete (LWC). Furthermore, converting the waste glass into raw materials in building material open up an attractive option in the building and construction industry. The benefits not only reduce the reliance on natural resources, lower the disposal cost and landfill volume but also help to reduce the carbon dioxide emission to our environment [3]. Utilizing industrial by-products such as bottom ash, pulverize fly ash and steel slag as fine aggregate for cement substitute has been common in the building and construction industry [4]. However, there are still very limited studies focusing on the use of waste glass as the replacement raw material in making LWC.

This paper therefore present the preliminary investigation of using finely ground waste glass in making LWC in terms of physical (dry bulk density) and mechanical (compressive strength) as a partial replacement of cement or sand. The LWC sample are water cure by conventional method and the properties are investigated and compared. This research hopes to improve the building and construction industry by increasing the usage of waste glass while sustaining good LWC performance and enhance the waste glass recycling rate. By substituting waste glass in LWC as partial replacement of cement can pose an advancement towards the development of a sustainable environment, energy efficient concrete-based building and construction industry.

## 2. Materials and experiment

### 2.1. Materials

The main materials used to produce the LWC samples were Ordinary Portland Cement (OPC) CEM I 42,5N, water, sand, lime, gypsum, ground granulated blast furnace slag (GGBS) and aluminum powder. The waste glass used in this research was a typical clear soda-lime glass that obtained from post-consumer glass product.

### 2.2. Waste glass

Two types of post-consumer waste glass (colored and non-colored clear type) were used on this study. The post-consumer waste glass was crushed into cullet size and followed by grinding process to fine particles using a Fritsch Planetary Mill PULVERISETTE 5. The glass particles were then sieved into desired particle size range. The ranges of glass particle size used in the experiment were:

- Waste glass having particle size in the range of  $>90\mu\text{m}$
- Waste glass having particle size in the range of  $45\text{--}75\mu\text{m}$

The chemical properties of both color and non-colored clear glass were first compared using X-ray fluorescence (XRF).

### 2.3. Mixtures

The basic materials used to produce the LWC sample is summarized in Table 1. Milled waste glass, foaming agent (aluminum powder), water, lime, cement, GGBS and gypsum were added at different proportions with varying the ratio. The bulk density of the waste glass and cement are  $1051\text{ kg/m}^3$  and  $1522\text{ kg/m}^3$  respectively. To investigate the potential of replacing the waste glass in making LWC, a specific proportion of waste glass is incorporated in LWC formulation as cement.

Table 1 summarizes the LWC formulations prepared in this paper. The finely grounded waste glass was mixed and casted into  $100\times 100\times 100\text{mm}$  steel mould based on the formulation in Table 1. Six LWC mould samples were prepared for each formulations. The LWC samples were demoulded after 24 hours, the excess expanded portion of the sample

were trimmed and oven dried for 24 hours at  $80^{\circ}\text{C} \pm 5^{\circ}\text{C}$ , until the constant weight was obtained before the water-curing for 7 and 28 days at room temperature.

To study the influence of the finely grounded waste glass to the properties of LWC, the waste glass was incorporated as cement substitute in sample C at 10% and 20% by weight percentage. The control samples contained the same set of raw material except without any glass replacement.

Table 1: LWC formulations with different loadings of waste glass as partial replacement of cement or sand

Formulations	OPC (g)	Glass (g)	GGBS (g)	Gypsum (g)	CaO (g)	Water (g)	Al powder (wt% of binder)
Control C	100	0	500	5	30	450	0.08
C10	90	10	500	5	30	450	0.08
C20	80	20	500	5	30	450	0.08

## 2.4. Experiment

### 2.4.1. Waste glass characterization

The chemical composition of both finely grounded colored and non-colored glass were analyzed using an X-ray Fluorescence (XRF) ARL 8400 based on BS EN 196-2:2013 [5].

### 2.4.2. Activity indexes of waste glass and cement mortars

During the initial stage, the activity index of waste glass was investigated accordance to BS EN 196-1:2005 [6]. The mixed waste glass was crushed into cullet, milled and sieved into particle size range (a)  $>90\ \mu\text{m}$  and (b)  $45\text{--}75\ \mu\text{m}$ . These waste glasses were then incorporated 10% and 30%, as cement replacement in making standard mortar bars. The mortar bars were water-cured for 7 and 28 days at room temperature. The evaluation of the activity indexes of test mortar bars would give an estimated of optimum waste glass percentage and particle size can be used in the LWC formulations.

### 2.4.3. Dry bulk density and compressive strength

The LWC formulations with various proportion of waste glass incorporated as substitution for cement are summarized in Table 1. Six cubes ( $100 \times 100 \times 100\ \text{mm}$ ) were casted. Prior to compression test, the dry bulk densities of the LWC samples were measured in accordance to ASTM C567 [7]. The LWC samples were tested in accordance to BS EN 12390-3:2000 [8] for the compressive strength at 7 and 28 days curing age.

## 3. Results and discussion

### 3.1. Waste glass characterization

The chemical composition of both the colored and non-colored clear waste glass is shown in Table 2. From Table 2, the major composition of both the colored and non-colored clear glass are mainly  $\text{SiO}_2$ . Although some traces of elements such as  $\text{TiO}_2$  and  $\text{Cr}_2\text{O}_3$  are present in the colored waste glass, while  $\text{BaO}$ ,  $\text{Pb}$ ,  $\text{ZnO}$  are found present in non-colored clear waste glass. But the percentage is fairly minor as compared to  $\text{SiO}_2$ ,  $\text{Na}_2\text{O}$ ,  $\text{CaO}$  and  $\text{Al}_2\text{O}_3$ .

Table 2: Chemical compositions of clear and mixed waste glass used in this research

Element	Colored	Clear
SiO <sub>2</sub>	66-67%	66-68%
Na <sub>2</sub> O	14-16%	14-16%
CaO	14-16%	14-16%
Al <sub>2</sub> O <sub>3</sub>	1-2%	1-2%
K <sub>2</sub> O	<1%	<0.5
Fe <sub>2</sub> O <sub>3</sub>	<0.5	<0.1
TiO <sub>2</sub>	<0.5%	0.0
Cr <sub>2</sub> O <sub>3</sub>	<0.1%	0.0
SO <sub>3</sub>	<0.1%	<0.5
SrO	<0.1%	<0.5
MnO	<0.1%	0.0
BaO	0.0	<1
Pb	0.0	<0.1
ZnO	0.0	<0.5

### 3.2. Activity indexes of waste glass and cement mortars

To investigate the potential use of the waste glass in replacing the cement in making aerated light weight concrete (LWC), the activity index of powdered waste glass is investigated. In this studies, both the colored and non-colored waste glass was mixed as one sample since no significant difference in chemical composition is found based on the previous studies. The activity index results of the sample are indicated in Fig. 1.

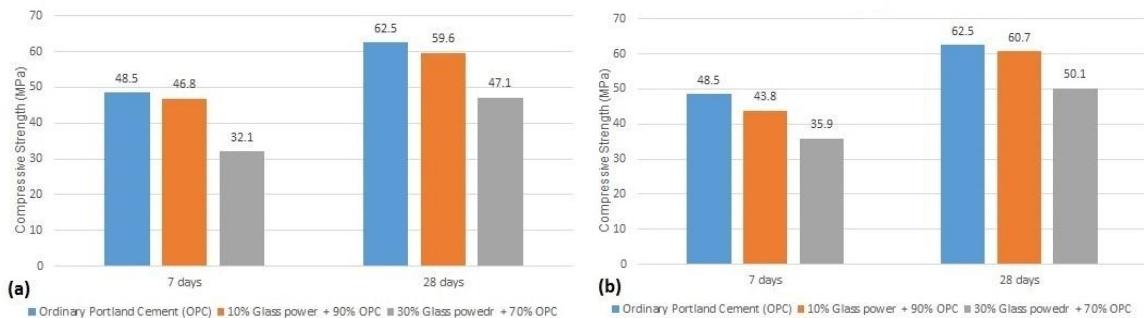


Fig. 1: Activity indexes of mortar bar with (a) >90 μm, (b) <75 μm

First, it is evident that the incorporation of waste glass as cement replacement is possible at the percentage of not more than 10%. It is obvious that the early activity index (7 days) of mortar bar with 10% waste glass substitution shown insignificant difference with the control mortar bar which uses only the OPC cement. The compressive strength for mortar bars with waste glass of particle size >90 μm and <75 μm is 46.8 MPa and 43.8 MPa respectively as compared to the standard cement mortars of 48.5 MPa. Subsequently, the attained 28 days activity index rise almost close to standard cement 59.6 MPa and 60.7 MPa as compared to the standard cement mortars of 62.5 MPa.

On the other hand, both the 7 and 28 days activity index of the sample decrease obviously when the waste glass content is increased to 30% replacement as compared with the 10% replacement in cement content. The early activity index (7 days) of the mortar bars with 30% loading of waste glass particle size of >90 μm and <75 μm is 32.1 MPa and 35.9 MPa respectively as compared to that of the standard cement mortar (48.5 MPa). While the early activity

index (28 days) of the mortar bars with 30% loading of waste glass particle size of  $>90\ \mu\text{m}$  and  $<75\ \mu\text{m}$  is 47.1 MPa and 50.1 MPa respectively as compared to that of the standard cement mortar (48.5 MPa). The reduction of the activity index is almost by 25 - 32%.

In addition, it is observed that the mortar bar with waste glass particle  $<75\ \mu\text{m}$  performs better than mortar bar with waste glass particle  $>90\ \mu\text{m}$  in both 10% and 30% substitution samples. Such observations could possibly relate to the amorphous content in waste glass increases with decreased glass particle size. Based on such result, the waste glass with particle size range of  $<75\ \mu\text{m}$  seem to provide better pozzolanic properties [9].

### 3.3. Dry bulk density and compressive strength

The density of the LWC samples at different loading proportion are measured and summarized in Table 3. In this studies, the glass particle is milled and sieve to  $<75\ \mu\text{m}$  to cast the sample. The density is calculated based on the LWC samples dry bulk weight after oven dried. As can be observed, the density of the LWC samples decrease when the waste glass is used to substitute the cement portion in the formulation. The bulk density of the waste glass and cement used in this studied are measured and compared. The density of waste glass and cement are found to be  $1051\ \text{kg/m}^3$  and  $1522\ \text{kg/m}^3$  respectively. Hence, it is expected that the replacement of the waste glass in the cement can reduce the overall density of the LWC.

Table 3: Effect of glass content on the dry bulk density of LWC samples

Formulation	Dry bulk density ( $\text{kg/m}^3$ )
Control C	738
C1	719
C2	620

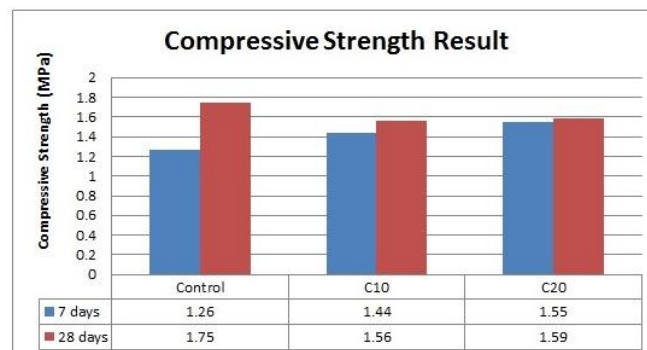


Fig. 2: Compressive strength result

Generally, compressive strength of aerated light weight concrete has a lower mechanical properties in comparison with ordinary concrete. For the sake of early investigation, this study focus on the potential use of waste glass to replace the cement content in LWC. Hence the LWC is cured in room temperature condition instead of autoclaving. The compressive strength of the LWC samples is represented at Fig. 2.

The result clearly indicated that the early compressive strength of the LWC increased with waste glass loading. The compressive strength of the C10 and C20 LWC sample are 1.44 MPa and 1.55 MPa as compared to that of the control sample 1.26 MPa. This observation could be contributed by the high amorphous structure of the finely grounded waste glass offers excellent pozzolanic properties and hence provides early strength development within the LWC.

Conversely, it is notice that the compressive strength of C10 & C20 LWC samples is slow down at the age of 28 days. The compressive strength of C10 and C20 LWC samples are 1.56 MPa and 1.59 MPa respectively as compared to control sample 1.75 MPa. One of the possibility reasons is that the addition of waste glass in LWC formulation decreases the Dicalcium Silicate ( $\text{C}_2\text{S}$ ) formation within the LWC which usually formed at a slower rate. Therefore,

the reduced of cement content in C10 and C20 retard the overall strength at 28 days. This further indicates that the replacement of waste glass as cement need to be controlled and optimized so that to prevent the weakening of the LWC.

#### 4. Conclusion

This study aim to investigate the potential of recycle the waste glass in light weight concrete. The activity index, density and the preliminary compressive strength of the LWC were studied and compared. In this investigation, the LWC was prepared and cured at room temperature. The activity index, density and preliminary compressive strength were then analyzed and compared. Based on the work, the following conclusions can be drawn:

- The ground waste glass can be used to replace cement in LWC.
- The fineness of the waste glass used has a strong influence on the activity index of cement.
- The bulk density of LWC were decreased as the ground waste glass was incorporated into the LWC samples. Such observation is mainly due to the overall bulk density of ground waste glass is less dense that cement material.
- The use of ground waste glass as cement substitute is possible at maximum of 10% and the compressive strength gain is mainly control by the pozzolanic characteristics in the waste glass

#### References

- [1] Singapore National Environment Agency, Neagovsg. [Online] Waste management: Waste statistic and overall recycling. <<http://www.nea.gov.sg/energy-waste/waste-management/waste-statistics-and-overall-recycling>>.
- [2] Singapore National Environment Agency, Neagovsg. [Online] Waste management: Recycling processes <<http://www.nea.gov.sg/energy-waste/3rs/recycling-processes>>.
- [3] M. C. Bignozzi, A. Saccani, F. Sandrolini, Matt waste glass from glass separated collection: An ecosustainable addition to new building materials. *Waste Management* 29, (2009) 329-334.
- [4] P. Walczak, J. Małolepszy, M. Reben, P. Szymański and K. Rzepa, Utilization of Waste Glass in Autoclaved Aerated Concrete. *Innovative solutions in Construction Engineering and Management Flexible Approach*. 122 (2015) 302–309.
- [5] EN 196-2. Methods of testing cement. Chemical analysis of cement, 2013.
- [6] EN 196-1. Methods of testing cement Part 1: Determination of strength, 2005.
- [7] ASTM C567. Standard test method for determining density of structural lightweight concrete, 1991.
- [8] EN 12390-3. Testing hardened concrete. Method of determination of compressive strength of concrete cubes, 2000.
- [9] S. O. Nwaubani and K. I. Poutos. The influence of waste glass powder fineness on the properties of cement mortars. *International Journal of Application or Innovation in Engineering & Management (IJAIEM)*, 2(2), (2013).





Sustainable Civil Engineering Structures and Construction Materials, SCESCM 2016

## Improving of recycled aggregate quality by thermal-mechanical-chemical process

Ni Nyoman Kencanawati<sup>a</sup>, Akmaluddin<sup>a</sup>, I Nyoman Merdana<sup>a</sup>, Nonik Nuraida<sup>a</sup>, Imam Robbani Hadi<sup>a</sup>, Mitsuhiro Shigeishi<sup>b,\*</sup>

<sup>a</sup>*Civil Engineering Dept., Mataram University, Jl. Majapahit 62, Mataram, 83125, Indonesia*

<sup>b</sup>*Graduate School Science and Technology, Kumamoto University, 2-39-1 Kurokami, Kumamoto, Japan*

---

### Abstract

To save natural resources and promote the sustainable development of construction industry, the use recycled coarse aggregate (RCA) from waste concrete has been encouraged recently. However, it is widely accepted that RCA concrete has lower performance about 15% to 20% than that of natural aggregate concrete. The adhered mortar on RCA surfaces causes lower quality of RCA produced through conventional recycling process. Therefore, it is necessary to provide higher quality of RCA from waste concrete by detaching old mortar as much as possible; so that the quality of RCA concrete can be improved as well. This research proposes a thermal-mechanical-chemical process to produce better properties of RCA from waste concrete. Then, new concrete was produced by utilizing the RCA. Results indicate that the physical properties of RCA are close to natural aggregate and meet the requirement of Indonesian Standard for concrete aggregate. Furthermore, the mechanical performance of RCA concrete produced by the proposed method has better mechanical properties to that of conventional RCA. It is about 3-8% lower than the mechanical properties of natural coarse aggregate concrete.

© 2017 The Authors. Published by Elsevier Ltd.

Peer-review under responsibility of the organizing committee of SCESCM 2016.

*Keywords:* Recycled aggregate; mechanical properties; thermal-mechanical-chemical process.

---

---

\* Corresponding author. Tel.: +62-370-638436; fax: +62-370-636126.

*E-mail address:* [nkencanawati@ts.ftunram.ac.id](mailto:nkencanawati@ts.ftunram.ac.id)

## 1. Introduction

Construction wastes are increasing as the growth of the construction industry; therefore, the issue of waste concrete recycling has become more important in the world nowadays. After the service period is over, the concrete construction might be demolished and disposed. It causes the problem of accumulation of waste concrete in the near future and leads to environmental problem. In addition, significant exploitation of natural resources for concrete production is highly prohibited in some parts in the world. Thus, in favor of the reducing of waste concrete and pointing at sustaining environment, the utilizing of recycled aggregate from waste concrete has been encouraged, recently.

However, the conventional method of recycling does not meet the demand of recycled aggregate to re-utilized for making a new concrete. This recycling process only produces smaller part from concrete lumps [1]. It only can be applied as road bed materials due to low quality of recycled aggregate. The surface of recycled aggregate is still attached by the old cement paste leading to low density and high water absorption of this aggregate [2,3].

To solve this problem, a new recycling technique has been developing in our laboratory using combination of thermal-mechanical-chemical techniques. Heating exposure up to 100°C – 200 °C weakens bonding between cement past and aggregate [2]. It should be noted that heating up to 500 °C does not affect the structure of the aggregate in concrete. After heating, the hot concrete lumps are then grinded to obtain the size of recycled aggregate. In addition, the recycled aggregate is soaked in acid solution to clean the residue of attached cement paste. Before the recycled aggregate manufactures will be used in, it needs to have the correct physical and mechanical properties. A series of research to examine the recycled aggregate will be discussed in this paper.

## 2. Related Works

It is widely recognized that compressive strength in recycled aggregate concrete is lower than that of normal concrete with the same water-to-cement ratio. Therefore, the utilization of recycled aggregate in producing new concrete is often associated with physical and mechanical deterioration of concrete as well as its durability. Concrete manufactured from recycled aggregate has compressive strength as much as 26% lower than that of concrete made by natural aggregate [3]. This can be understood because generally the recycled aggregate produced by conventional method, the aggregate is still attached by cement paste; therefore, the adhesion of interface between recycled aggregate and cement paste on new concrete reduce. As a result, the mechanics strength of concrete also decreases.

In attempt of producing higher quality recycled aggregate from waste concrete, a pulsed power (PP) technique was implemented [4]. The high quality recycled coarse aggregate (RCA) produced by PP has been conducted. Density and absorption test results of the aggregate meet the requirement for H (high) class set by Japanese Industrial Standard for recycled aggregate. Other research has concentrated on mechanical properties of concrete made using the pulsed power recycled coarse aggregate (PP-RCA). It is clarified that the concrete made by high grade PP-RCA has sufficient compressive strength and Young's modulus to be utilized as construction material [5] and furthermore, analysing of kind of recycled aggregate concrete under acoustic emission testing show the similar behaviour to that of normal concrete aggregate [6].

## 3. Experiment

### 3.1. Material

There were several steps in producing recycled coarse aggregate. First, concrete lumps were heated up to 1000C for 24 hours. Second is mechanical grinding by 500 cycles using Los Angeles machine. These processes were objected to produce heating-grinding (H-G) recycled coarse aggregate. The addition treatment; which was soaked in acid solution (H<sub>2</sub>SO<sub>4</sub>) in 24 hours, was objected to produce heating-grinding-acid (H-G-A) recycled coarse aggregate.

Then new concrete was made using two types of recycled coarse aggregate. For analysis consideration, normal fresh coarse aggregate concrete was also produced taken from the same quarry as material for recycling. Water cement ratio was 48%. Specimens were cylinder concrete. Mixture proportion is shown in Table 3.

Table 1. Mixture proportion of concrete in 1 m<sup>3</sup>

Concrete type	Concrete ingredients (kg)			
	Cement	Water	Sand	Gravel
Normal coarse aggregate concrete	427	205	675	1013
H-G recycled coarse aggregate concrete	427	205	667	1001
H-G-A recycled coarse aggregate concrete	427	205	671	1007

### 3.2. Method

After demoulding, they were placed in a water until the time of testing. Curing was performed in accordance with the ASTM C511 standard. The compressive strength tests were carried out in accordance with ASTM C39 -86 at 28 days. The splitting tensile strength tests were performed according to ASTM C496-87 at 28 days. Meanwhile, flexural strength was determined according to ASTM C597. Each testing of concrete consisted of five samples. Specimens were cylinder concrete in size of 150 mm in diameter and 300 mm in height for compressive and tensile testing. While the specimen for flexural testing were concrete prisms in size of 150 mm x 1500 mm x 500 mm. All experiments were conducted in Material and Structural Engineering Laboratory, Civil Engineering Department, Mataram University.

## 4. Result and Discussion

### 4.1. Physical Properties of Recycled Aggregate.

According to visual examination as shown in Fig. 1, in margin part of recycled coarse aggregate surfaces is still attached by cement paste. However, H-G-A recycled coarse aggregate surfaces are much cleaner than H-G recycled coarse aggregate surfaces. For further investigation, the quality examination of recycled aggregate includes density, water absorption, fineness modulus, and sieve analysis are examined. Almost similar properties are obtained compare to normal coarse aggregate, indicating the improvement quality of the recycled aggregate. Table 2 and Fig. 2 show the physical properties of recycled coarse aggregate along with normal coarse aggregate as comparison.



Fig. 1. Recycled Aggregate (a) H-G; (b) H-G-A.

Table 2. Properties of recycled coarse aggregate

Physical properties	Normal	H-G	H-G-A
Density	2.61	2.56	2.59
Water absorption (%)	1.23	2.62	2.43
Fineness modulus	7.10	7.05	7.03

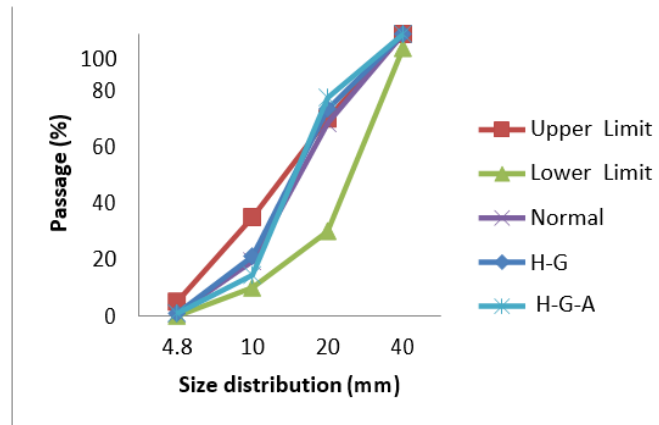


Fig. 2. Sieve analysis

#### 4.2. Mechanical Properties

Mechanical properties of recycled aggregate concrete along with those of normal concrete are written in Table 3. Generally, the mechanical properties of normal concrete aggregate (NCA) are slightly higher than those of both types of recycled concrete aggregate (RCA). Different impact on mechanical properties of two types of RCA is caused by their different quality. H-G-A RCA possesses better mechanical properties than those of H-G RCA. The continued treatment process by soaking in acid solution enables to improve the mechanical properties of H-G-A concrete. However, that mechanical properties improvement is not in significant different so H-G RCA can be potential as well as H-G-A RCA in utilization.

Table 3. Mechanical properties of concrete

Average of mechanical properties (MPa)	Normal aggregate concrete	H-G-A concrete	H-G concrete
Compressive strength	41.77	39.79	39.32
Modulus of elasticity	30280	29643	29472
Splitting tensile strength	4.57	4.49	4.31
Flexure strength	6.29	5.73	5.58

#### 5. Conclusion

Both H-G and H-G-A coarse aggregate almost have similar quality to natural coarse aggregate in terms of density, water absorption, and sieve analysis. However, the Compressive Strength, Modulus of Elasticity, Splitting- Tensile Strength, and Flexure Strength of H-G recycled coarse aggregate concrete is less than those of H-G-A recycled coarse aggregate concrete. The acid solvent treatment of H-G-A enables to remove the cement paste from aggregate surface more effectively than that of H-G, therefore the H-G-A recycled aggregate gives better performances than those of H-G. Continued delamination process increases bonding mechanism between new cement paste and recycled coarse aggregate surface. However, that mechanical properties of both RCA concrete are not in significant different so that they can be potential as construction material in near future.

#### References

- [1] Anwar SNR, Pemanfaatan Limbah Struktur sebagai Alternatif Pengganti Agregat Kasar Beton, e-Journal FT Unram, Vol 3 (2007) 84-93 (in Indonesian).
- [2] Ni Nyoman Kencanawati, Jauhar Fajrin, Buan Anshari, Akmaluddin, and Mitsuhiro Shigeishi, Evaluation of High Grade Recycled Coarse Aggregate Concrete Quality Using Non-Destructive Testing Technique, Applied Mechanics and Materials Vol 776 (2015) pp 53-58

- [3] Xiao J., Li J., and Zhang C., Mechanical Properties of Recycled Aggregate Concrete under Uniaxial Loading, *Cement and Concrete Research*, vol. 35, issue 6 (2005), 1187-1194.
- [4] Narahara S., Namihira T., Nakashi K., Inone S., Iizasa S., Maeda S., Shigeishi M., Ohtsu M., and Akiyama H., Evaluation Of Concrete Made From Recycled Coarse Aggregates by Pulsed Power Discharge, *Digest of Technical Paper- IEEE International Pulsed Power Conference (2007)* 748-751.
- [5] Maeda, S. and Shigeishi, M.: Controlling of fracture using pulsed power: 3R technology for concrete aggregate, *Proc. the 5th Kumamoto International Workshop on Fracture, Acoustic Emission and NDE in Concrete, 2009*.
- [6] Kencanawati NN, Iizasa S, Shigeishi M, Fracture Process and Reliability of Concrete Made from High Grade Recycled Aggregate using Acoustic Emission Technique Under Compression, *Materials and Structures, Volume 46, Issue 9 (2013), 1441-1448*.



Sustainable Civil Engineering Structures and Construction Materials, SCESCM 2016

## Proportioning, microstructure and fresh properties of self-compacting concrete with recycled sand

Carro-López, Diego<sup>a\*</sup>; González-Fonteboa, Belén<sup>a</sup>; Martínez-Abella, Fernando<sup>a</sup>;  
González-Taboada, Iris<sup>a</sup>; de Brito, Jorge<sup>b</sup>; Varela-Puga, Fernando<sup>a</sup>

<sup>a</sup>Department of Construction Technology; Civil Engineering School; Universidade da Coruña; Campus de Elviña s/n, 15071, A Coruña, Spain

<sup>b</sup>CERIS, Department of Civil Engineering, Architecture and Georresources, Instituto Superior Tecnico, Universidade de Lisboa, Av. Rovisco Pais, 1 - 1049-001 Lisboa, Portugal

---

### Abstract

The use of fine recycled aggregates from recycled concrete is limited due to the high absorption of the material and the subsequent reduction in mechanical performance. At the same time, Self-Compacting Concrete (SCC) uses large amounts of fines to ensure its flowability. Therefore, this type of concrete could allow the use of fine recycled aggregates. Hence, the aim of this work is to study the proportioning and the effects in the microstructure and the fresh basic properties of the use of recycled sand to produce SCC.

The concrete mixes analyzed incorporate recycled sand (in percentages of 0%, 20%, 50% and 100 %) and natural coarse aggregates. The mix design used an equivalent mortar, which allowed obtaining a suitable concrete that could be at the same time comparable between different replacement ratios and usable in real-life applications.

During the design of the mixes with the mortars, the workability was measured from 10 min to 90 min using mini-cone and mini-funnel tests and the suitable ones were chosen to perform self-compacting concrete. Once this was done, these mixes were produced at concrete scale, and with these, basic properties were measured.

The fine recycled aggregate changes the workability and the rheology of the mortar and concrete. These differences also affect the microstructure in terms of bonding and porosity distribution. There is a severe reduction of compressive and splitting strength as a result of the use of recycled sand, and this could be linked directly to these changes of the microstructure. The recommended substitution ratio with small decrease of mechanical performance is up to 20%.

© 2017 The Authors. Published by Elsevier Ltd.

Peer-review under responsibility of the organizing committee of SCESCM 2016.

---

\* Corresponding author. Tel.: +34-881-015-249

E-mail address: [diego.carro@udc.es](mailto:diego.carro@udc.es)

*Keywords:* recycled aggregate; self-compacting concrete; recycled sand; microstructure; proportioning.

---

## 1. Introduction

As the population grows and improves its lifestyle, a proportional increase of the consumption of natural resources and energy occurs. One of the industries with greater responsibility in the consumption of natural resources and generation of waste is the construction industry. Construction and demolition waste (CDW) is undoubtedly one of the main centers of attention in the search for waste reduction.

This research is focused on the determination of the influence of the use of recycled sand on self-compacting concrete in terms of proportioning and microstructure. With this, the variables of interest in this research are the percentage of replacement of natural sand and the workability measured over time.

There are different ways of obtaining the composition of a SCC and in this work the objective is an appropriate workability, i.e., the resulting concrete should present fresh-state SCC behavior. This research involves the replacement of 0%, 20%, 50% and 100% of natural sand by recycled sand and this type of sand presents a high absorption. Thus, it is expected that the mortars and concrete with high substitution ratios of these aggregates will present lower workability. This could be dealt with by increasing the content of superplasticizer but in the extreme case of 100% of replacement this was not enough to provide acceptable workability. However, if the amount of superplasticizer varies, the different mixes would not be comparable. Therefore, the superplasticizer quantity was adjusted for the control concrete and kept constant for all substitution ratios.

### 1.1. Use of fine recycled aggregate concrete

The possibility of the use of Fine Recycled Aggregates (FRA) in self-compacting concrete (SCC) was demonstrated by Kou & Poon [1], who obtained SCC with acceptable workability and compressive strength using even 100% of both fine and coarse recycled aggregates. The authors found out that the values of slump flow grew with the replacement ratio, and this indicated that the recycled aggregates did not absorb 100% of the water at 24 hours (W24h). They repeated this test after 1 hour and they found a positive correlation between the substitution ratio and the loss of workability.

Other interesting reference of the use of FRA in SCC is the work of Corinaldesi & Moriconi [2] who achieved SCC concrete with coarse and fine recycled aggregates separately in percentages of 0 and 100%. In this work the w/c ratio was established as 0.45 and the content of cement as 440 plus 100 kg of filler. These fines were alternatively limestone, fly ash and also powder from recycled aggregates. The main effect of this last type of powder was to reduce over time the workability of the paste; this was evidenced in terms of yield stress values and plastic viscosity values. Finally, this work also refers a significant reduction in compressive strength, much larger in the case of FRA than in recycled coarse aggregates.

There are also works about recycled coarse aggregates (RCA) in SCC, recent examples of these could be the work of Silva [3], or the ones of Safiudin et al. [4] and Grdic et al. [5]. All results agree in two points:

- The effect of the absorption of the recycled aggregates must be compensated. This adjust is done by means extra water or adding superplasticizer;
- There is a reduction in compressive strength and modulus of elasticity with the substitution's percentage.

Research on the use of FRA in ordinary concrete is not extensive. The main effect that is reported in the literature is the loss of compressive strength with the substitution ratio. Khatib [6] refers that concrete with 25% and 100% suffer reductions of 15% and 30% relative to the reference mix. Evangelista & de Brito [7] refer that with percentages of substitution up to 30% there were no significant reductions. The other important effect described is the loss of workability due to the high absorption of the FRA. Some authors add more water to compensate this effect; others add more superplasticizer and a few of them deal with the effects of the loss of workability.

Another significant question is the variability of the quality of the FRA. For example, Pereira et al. [8] refer a FRA with 13.1% of absorption; on the other hand, Khatib [6] refers one with 6.3% of absorption and Zega et al. [9] uses a



FRA with an absorption of 8.5%. These differences obviously should produce significant effects on the properties of the resulting concrete. However, in all cases this absorption is higher in the recycled aggregate than in the natural one. The main idea is that there is a negative relationship between the absorption of the recycled sand and the quality of the resulting concrete. This follows the same trend that is well established with coarse recycled aggregates [10].

### 1.2. Fresh properties & rheology of SCC

SCC is designed and produced with fresh-state properties in mind. SCC exhibits enhanced capabilities substantially different than the ones of the ordinary concrete. The enhanced properties that are looked for in SCC are: flowability, viscosity (measure of the speed of flow), passing ability (flow without blocking) and segregation resistance [11,12]. The priority of these properties depends on the use of the concrete: in a section strongly reinforced the crucial property is the passing ability; on the other hand, when casting a slab, the emphasis is on the flowability and the segregation resistance. Thus, different SCC are designed with a specific behavior corresponding to its use [11].

The SCC fresh-state properties are used as reception criteria and one or two tests are performed when the concrete arrives at the construction site allowing acceptance or not of the concrete batch [13]. However, the evolution of the fresh properties over time is a key factor in the properties of concrete, i.e. the open time can be adjusted to the type of superplasticizer or retarders [11,13,14]. It has been observed that the rheological parameters worsen with time [15] and the open time varies in different mixes. This evolution can be observed in the equivalent mortar, where it is enhanced by the absence of coarse aggregate.

The fresh-state properties are measured by means of several specific empirical tests. For the flowability, the slump-flow is widely used; for the viscosity of the mix,  $T_{50}$  is used but also the V-funnel; for the passing ability, the L-box and J-ring are the most common and, finally, for the segregation resistance, the sieve segregation is one of the most widely used [11,14].

The empirical approach is useful but it is possible to study the phenomena in further detail. Fresh SCC can be modelled as a viscoelastic fluid with a model that relates the shear stress ( $\tau$ ) and shear rate ( $\dot{\gamma}$ ). There are various models for the equation that relates both properties, but the Bingham model is one of the simplest and most widely accepted [16]. This model describes concrete flow in terms of yield stress ( $\tau_0$ ) and plastic viscosity ( $\mu$ ) with this equation:  $\tau = \tau_0 + \mu \cdot \dot{\gamma}$ . Yield stress represents the stress necessary to initiate or maintain flow, whereas plastic viscosity expresses the increase in shear stress with increasing shear rate once the yield stress has been exceeded [17].

There is a significant difference between the SCC when it is at rest for a long period of time or when it has been recently mixed, due to its thixotropy. The resistance to deformation varies substantially, so that two parameters could be defined: static yield stress, that relates to undisturbed concrete, and dynamic yield stress that relates to disturbed concrete [18,19].

## 2. Materials

A Portland cement, CEM I 42.5 R according to European Standard EN197-1, was used. In addition to this, the powder fraction was completed with limestone filler.

The superplasticizer used to achieve suitable SCC mixes was a modified polycarboxylate type usual in SCC production. No retarder was used to control the hydration or the open time.

Three types of aggregates were used. The coarse fraction was a natural limestone gravel. Two fine aggregate were used: a natural limestone sand that was partially replaced by a recycled sand. The source of the natural aggregates was a crushed aggregate from a northern-western Spain stone quarry. The fine recycled aggregate came from crushed concrete from a local recycling plant (RECINOR).

The natural and recycled sands need to be well graded and have a size distribution as similar as possible. To achieve both objectives, it was necessary to adjust the grain size curve of one of the aggregates. In this case it was decided to divide the natural sand in three fractions: below 0.25 mm, between 0.25 mm and 2 mm and above 2 mm. After this, these three fractions of natural sand were remixed to obtain a “corrected natural sand” with a size distribution similar to that of the recycled sand.

In addition to the regular absorption test, a continuous measurement of water absorption of the aggregates was conducted. At the usual reference time of 10 min the absorption of the recycled sand was 72% of the absorption at 24 h, and in the case of natural gravel and sand it was 50% and 70% respectively.

### 3. Mix proportioning of self-compacting concrete with fine recycled aggregates

#### 3.1. Proportioning methods

There are many references about the design of SCC with different methodologies. Mainly, there are two groups of procedures to adjust the composition: on the one hand, one can set the strength level to be achieved and then the components' content necessary to meet this objective. On the other hand, one can start from a given standard formulation that will be corrected to achieve the workability appropriate to the target application. In this work, the second option was used.

Schwartzentruber and Catherine [20] proposed the use of the concrete equivalent mortar (CEM) to study the rheology of fresh concrete with the assumption that the rheological properties of CEM should be correlated with those of the corresponding concrete. For the CEM design it is considered that all friction phenomena take place at the cement paste/aggregate interface. Therefore, the total specific area of the aggregates is a fundamental variable to understand the level of workability of concrete.

When the composition of the CEM is determined the main following relationships concerning the original concrete composition should be kept constant: cement and filler content, water-cement ratio, and fine aggregate content necessary to achieve the same total surface area of coarse aggregate replaced. An example of this procedure can be seen in the Rubio-Hernández et al. work [21].

Since the start of the CEM method there have been various approaches to obtain the equivalent mortar of a specific concrete. In this context, the Nepomuceno et al. method [22] used in this work is a generalization of the one proposed by Ouchi et al. [23] and it centers its efforts on the characterization of the mortar and correlates the behavior of mortar and the one of concrete. This method uses two parameters,  $G_m$  and  $R_m$  measured in mortars that are correlated with the slump-flow and the  $T_{50}$  time of concrete.

Because of easier preparation, mixing, and sampling, CEM mixes consume less materials, energy, and time for testing, which can greatly simplify and speed up testing of concrete [24]. This represents a solution to adjust the mortar that would produce a SCC. In addition, as in this research the interest is centered on the recycled sand, the study of mortar is more useful in the aspects where the effect of the properties of the recycled aggregate is magnified.

#### 3.2. Concrete composition and mixing

The design of the reference SCC is based on the Nepomuceno's method [25] using some recommendations from the CEM and rational methods. This methods can give guidelines of how to adjust a mix to a set of properties like compressive strength and fresh-state parameters. However, it is not known how to ensure that a reference concrete with SCC behavior, once some fraction of it is replaced, would remain in the domain of acceptable quality SCC. For instance, if the replacement of FRA is set to 100% and no water is compensated, the result is a conventional concrete with no SCC behavior (Fig. 10).

Regarding the high water absorption of the recycled aggregates, it was necessary to adjust the mixing water, which was done by adding extra water. However, not all the 24 h water absorption was compensated, rather the absorption at 10 min. This criterion was also used before by other authors [8] [26]. To ensure comparability, all materials were oven dried before their use.

In order to study the effect of FRA in the SCC proportioning and microstructure, the designed concrete included an increasing proportion of recycled sand. With this same idea, the incorporation of coarse aggregate was fixed to 30% in volume of natural gravel. This criterion corresponds to the recommendations of the rational method [23] [14]. Besides, this allows to study the mortar fraction of the SCC separately.

To start correctly the adjustment of the mix, the paste (with a previously fixed w/c ratio) was tested alongside with variable percentages of superplasticizer additive (Fig. 1). The test showed that the optimum quantity was 2% of sp. However, this high content produced segregation and finally it was set to a value of around 1.7% of superplasticizer.

The use of the mortar fraction to adjust the mix has proved to be a powerful tool to find and compare mix proportions. The batches are only of 1.6 liters and this reduces the quantities of materials to prepare: oven dry the aggregates, mixing the fractions of the sand, weight all components, etc.; so tests are substantially faster and/or it is possible to perform a much larger number of tests. Once a mix proportion that fulfilled the Nepomuceno's recommendations was found, it was tested in full-scale concrete performing the empiric fresh-state tests: slump-flow, V-funnel, L-box and J-ring.

This mix design in two stages, first mortar and later full concrete, was helpful to achieve in a rapid way suitable compositions of SCC with FRA. Additionally, it should be emphasized that the only variable that affected the flowability and viscosity of the mix was the presence of FRA. Based on this, the other mixes were designed by replacing a given volume of natural sand with recycled sand. The replacement ratios were 0%, 20%, 50% and 100 %.

The mortar approach allowed designing a suitable SCC concrete mix. This mix was tested at concrete scale, obtaining a SCC with acceptable slump-flow results but with high values in the V-funnel test. With these data, and focusing on obtaining a robust but flowable mix, small increases in w/c ratio and superplasticizer content were introduced. Therefore, the final mix was obtained (Table 1) with only minor changes from the composition adjusted in the mortar phase.

As the research's interest is to understand the influence of the replacement of natural with recycled sand, it was important not to include other adjustment or variation in the mixture proportioning. With this, the effects could be attributed to the recycled material.

Table 1. Concrete composition of the mixes

Material	Volume (l)	Mass (kg) of the mixes % of recycled sand replacement (in volume)				SSD Density (kg/l)	Absorption 24 h (%)
		0 %	20 %	50 %	100 %		
Cement	128.7	400.0	400.0	400.0	400.0	3.11	
Limestone filler	66.4	180.0	180.0	180.0	180.0	2.71	
Water	184.0	184.0	184.0	184.0	184.0	1.00	
Additional water <sup>(1)</sup>		10.36	13.39	31.74	53.12	1.00	
Recycled sand <sup>(2)</sup>		-	63.6	365.9	731.9	2.30	9.3
Natural sand <sup>(2)</sup>	318.2	865.6	692.4	432.8	-	2.72	1.0
Natural gravel <sup>(2)</sup>	300.0	768.0	768.0	768.0	768.0	2.56	1.1
<i>Water/cement</i>		<i>0.46</i>	<i>0.46</i>	<i>0.46</i>	<i>0.46</i>		
<i>Superplasticizer (% in mass of cement + filler)</i>		<i>1.70</i>	<i>1.70</i>	<i>1.70</i>	<i>1.70</i>		

<sup>(1)</sup> Water absorbed by the aggregates after 10 min and correspondent with the mixing time

<sup>(2)</sup> All materials were oven dry before its use

To obtain all the mixes with the different substitution ratios, given volumes of natural sand were replaced with the same volumes of recycled sand. No other adjustment was introduced because the focus was on studying the effect of the use of different percentages of recycled sand. Also, a detailed protocol for the mixing of concrete and mortar was set (Fig. 2).

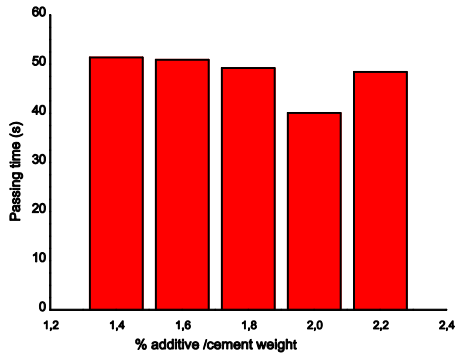


Fig. 1. Marsh cone test results

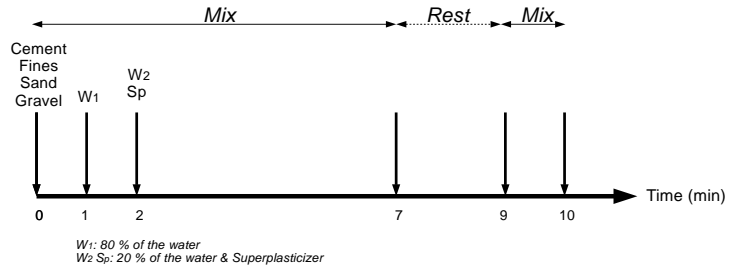


Fig 2. Mixing procedure for concrete and mortar

## 4. Results and discussion

### 4.1. Comparability of mixes with different substitution ratios of FRA

As mentioned previously, the general procedure to obtain the mortar content was based on the Nepomuceno method [25] [27]. It would have been possible to strictly follow the CEM method [20] [21] and include an extra content of recycled sand equivalent to the specific surface of the gravel. This would lead to an equal specific surface, but the absorption of this extra amount of sand would be much higher than the one of the gravel (their water absorption at 24 h are 9.3% and 1.1% respectively). In this way, the equivalent mortar would only be equivalent in terms of specific surface but the influence of the absorption would be quite more relevant. So, finally, it was decided not to include this extra sand and assume that the mortar phase correlated accurately with the concrete. It should be noted that all mixes included 30% in volume of natural gravel, so the only variable of influence was the presence of FRA.

During the adjustment phase the only tests performed were the ones related with the fresh state, i.e. mini-cone and mini-funnel. The Nepomuceno’s limits were complied with [25,27] so the target spread values in mini-cone and flow time in mini-funnel were 251-263 mm and 7.7-8.7 s respectively. These limits were unreachable for all the mixes at the same time. If it were adjusted for 0% replacement, the mixes with 50% and above of FRA would not exhibit SCC behavior. They were conventional mortars with fluid consistency and low values in spread in mini-cone; and also with high passing times in mini-funnel, when they did pass at all. On the other hand, if the mix were adjusted for 100% of FRA incorporation the result would be a severe increase in fluidity and reduction of viscosity. This would lead to severe segregation in the substitution percentages of 0% and 20%. This can be seen in the sections of Fig. 3 of a rejected mix with excessive fluidity and low viscosity that produced segregation for low substitution ratios.

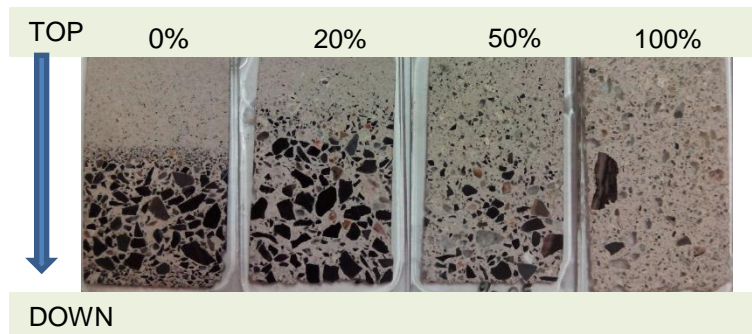


Fig 3. Segregation in some mortar tests, increased with low substitution ratios

It was detected that if the 100% FRA mix was adjusted and exhibited acceptable parameter in both mini-cone and mini-funnel tests (according to Nepomuceno's criterion), the mix with 0% replacement showed complete segregation of paste and aggregates (Fig. 3). When the 0% mix was the reference, the 100% mix lost the SCC behavior. Therefore, it was clear that the complete fulfillment of the criterion was impossible, so new limits were set. In this way, it was possible to find out mixes where all batches showed SCC behavior even though with some variability in viscosity and flowability. However, at least there were groups of SCC products under comparison, not conventional concrete compared to SCC.

This new criteria is represented in Fig. 4, where it can be seen that the narrow range that Nepomuceno's method indicates is widely expanded (mini-cone: 251-263 mm & mini-funnel: 7.7-8.7 s). However, when the values of mini-cone spread grew substantially, segregation problems started to appear. Therefore these mixes are also not valid.

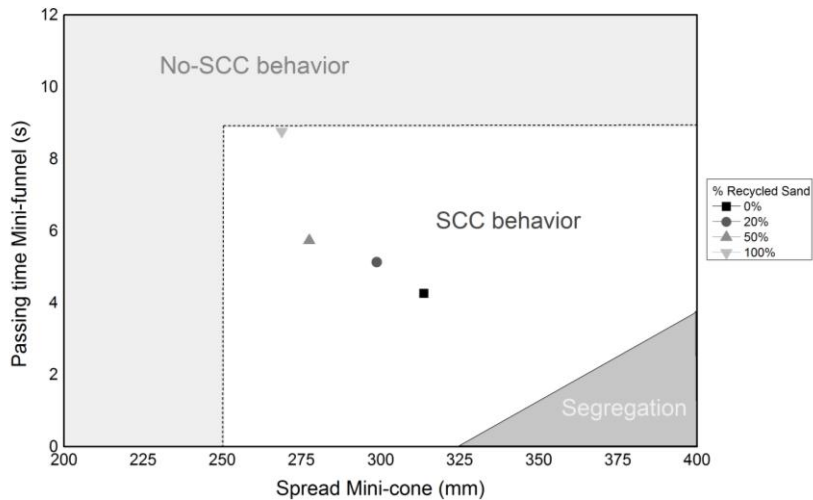


Fig 4. Criterion of acceptance of equivalent mortars to produce SCC concrete

Another question that should be addressed properly is the time at which the mix is adjusted. In this work, the fresh-state parameters were measured just after finishing the mixing process (at 10 minutes). However, as seen in Fig. 6; these parameters change with time and, in the case of the 100% substitution, a mix that presented complete SCC behavior lost all fluidity and passing ability after 90 minutes. Maybe, 30 minutes or 45 minutes could represent better the SCC fresh-state characteristics of a specific mix. Testing at one of these times could be more representative of the real behavior in the construction site, but this is impractical from a production control point of view.

#### 4.2. Microstructure of SCC equivalent mortars

The selected mixes were studied under optic microscopy at the age of 14 days in a preparation of petrographic thin sections. The pictures (Fig. 5) show a significant increase in porosity with the percentage of FRA. These pores are clean with no precipitate in them and with size varying from 50 to 250  $\mu\text{m}$ .

It was not possible to visualize the different interfacial transition zone (ITZ) of the aggregates, because this is easier in coarse aggregates and rather difficult with recycled sand. This ITZ has been referred to be the weak part of the microstructure [28].

However, in the 100% replacement mix there was a fraction of natural aggregate - from the original concrete - that seemed to be separated from the original paste. This could be attributed to the processing of the aggregates.

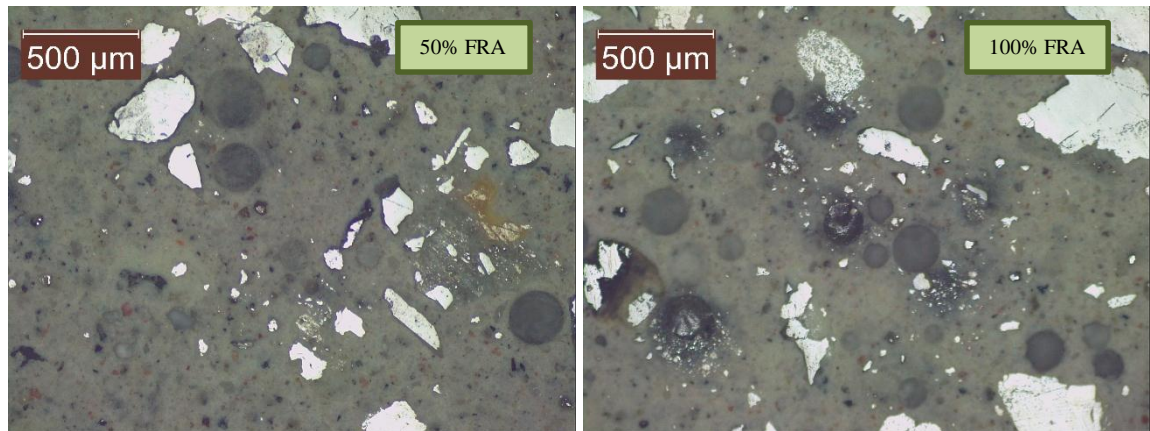


Fig 5. Microstructure of the mortar phase with FRA in percentages of 50% (left) and 100 % (right).

### 4.3. Mortar results

The mortars were tested over time by means of the mini-cone and mini-funnel tests (0). In the mix that includes 100% of recycled sand, at 90 minutes the mini-funnel test was unfeasible due to the rigidity of the mix.

The spread is higher with low sand substitution percentages. However, for the reference mortar, and also for the one with 20% of sand substitution there is a slight increase in the spread values from 15 to 60 minutes. Regarding the passing time (V- funnel), it could be said that there is a clear trend towards reduced values with time and with replacement percentage. This contrasts with the results reported by Jin [15], who found out a continuous decrease of spread and increase of the passing time over time.

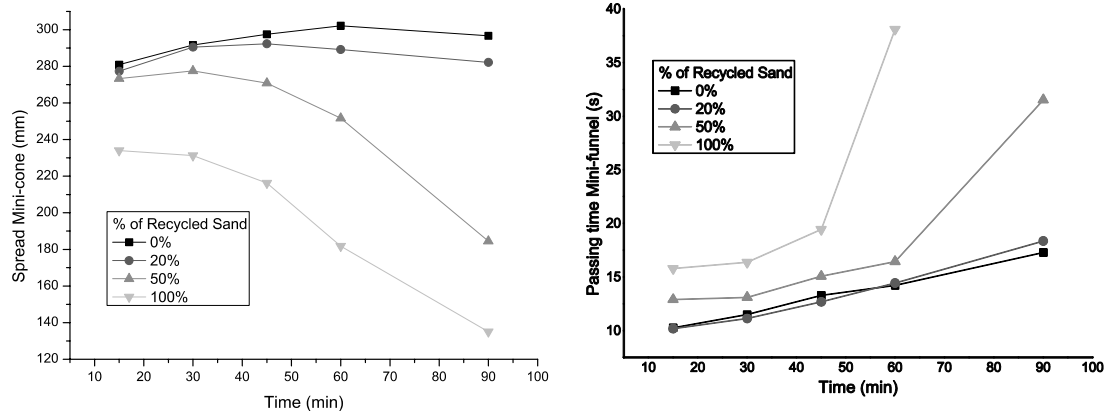


Fig. 6. Left: Spread results of the mortar on mini-cone test. Right: Passing time results of the mortar on mini-funnel test

The density and compressive strength of the mortars are substantially influenced by the presence of the recycled sand (Fig. 7). In the case of the 100% substitution, the decrease of compressive strength at 28 days is 48%. Concerning the density, it is reduced with the same trend.



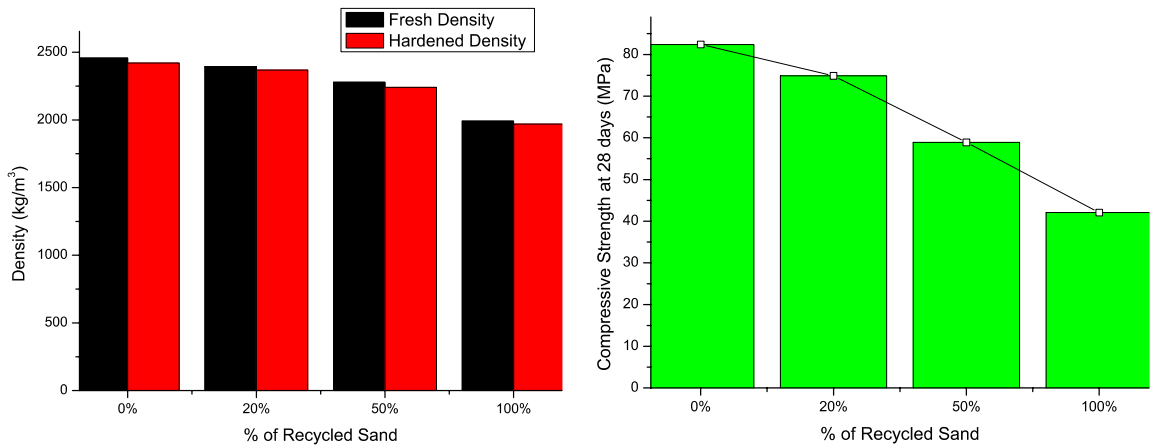


Fig. 7. Left: Hardened density at 28 days and fresh density of mortars. Right: Compressive strength at 28 days of mortars

#### 4.4. Concrete results

Once the mix proportion was tested in the mortar phase, the next step was to produce equivalent concrete mixes. At this stage the empirical tests used were the usual slump-flow test and V-funnel. In addition, tests with rheometer were performed: stress growth test and flow curve test. In the two first all substitution ratios were performed but in the case of the concrete with a 100% of replacement the results at 90 min showed a complete loss of the SCC behavior. After these results, it was decided to go on only with 0 and 50% replacement. This allows studying the effect of the incorporation of the recycled sand.

In Fig. 8 the results of slump-flow test are presented. A reduction over time of the spread and an increase in the T500, higher with the substitution ratios, can be seen. A similar trend was detected in the case of the V-funnel results (Fig. 9), but there were substantial differences between the 0% and 20% and the 50% and 100% group. In this last group, the effect of time is stronger; it seems that the concrete loses flowing ability with the incorporation of recycled sand.

The flowability of the 50% and 100% mixes suffered a severe reduction, losing their SCC behavior. In the case of the 100% mix, it was even impossible to achieve a flowable concrete (Fig. 10).

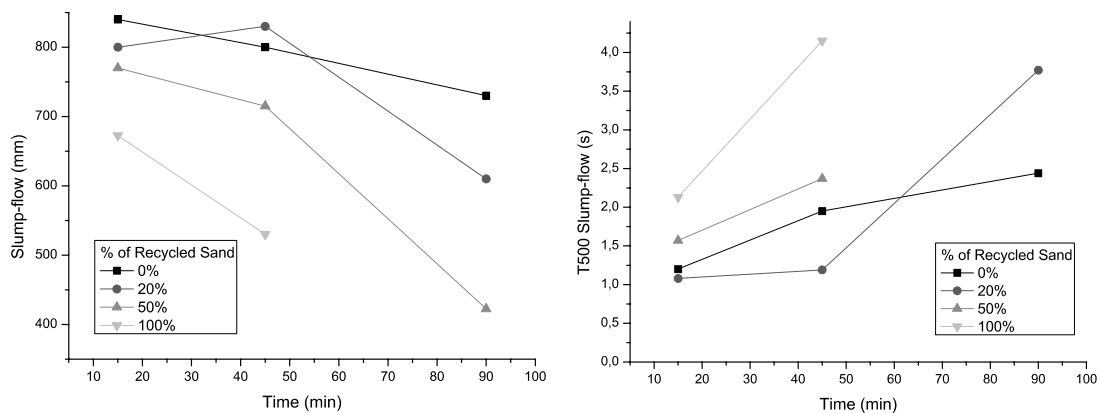


Fig. 8. Results of the slump-flow test (spread & T<sub>500</sub>)



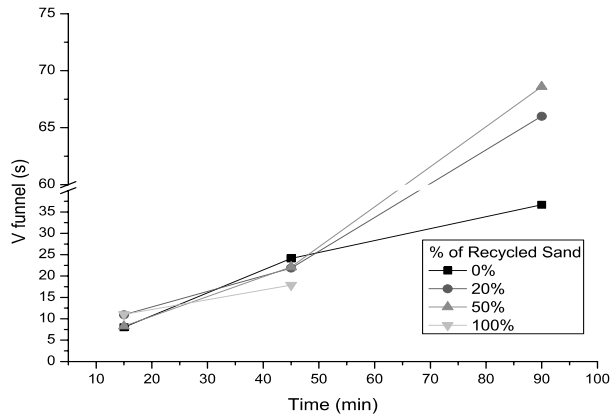


Fig. 9. Results of the V-funnel test



Fig. 10. Slump test of the mix with 100% of recycled sand at 90 minutes. The slump-flow test was unfeasible even though at 15 min it was a SCC with a spread of 680 mm

### 4.5. Mechanical properties of SCC

Fig. 11 presents the compressive strength of the mixes. There are substantial reductions of the mechanical properties with the incorporation of recycled sand. At the same time, the evolution with the concrete age is slightly lower in the case of concretes with fine recycled aggregate. The trends are similar to those of mortars.

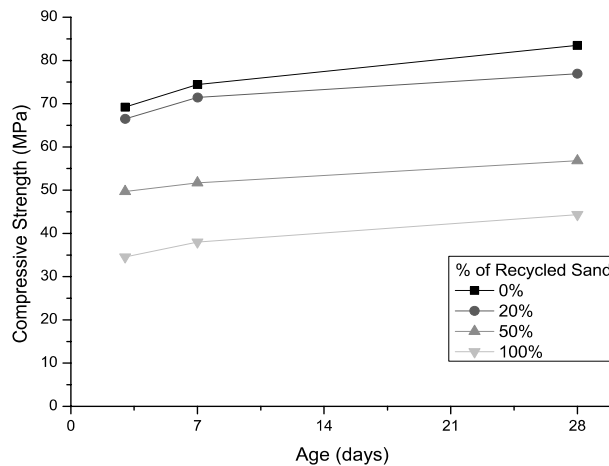


Fig. 11. Evolution of compressive strength in concrete samples

## 5. Conclusions

The following conclusions can be drawn:

- The use of some fixed parameters as 30% of gravel content and 1.7% of superplasticizer for all the replacement ratios (0%, 20%, 50% & 100%) leads to comparable SCC's and allows studying the mortar phase separately;
- Criteria of comparability for the mixes that included recycled sand were established: they should present SCC behavior to be comparable, if not, the reference proportion should be readapted. It is not possible to comply with all recommendations when the nature of the aggregates is changed;
- The microstructure of the pastes was homogeneous and no different ITZ was observable, some aggregates were detached from the paste. The incorporation of recycled sand resulted in an increase in porosity;
- With this mix design it was possible to produce self-compacting concrete with a substitution of up to 100% of recycled concrete sand. However, 50% and 100% mixes started to lose this behavior after 60 min;
- There was a reduction of filling capability and flow ability over time and the loss of properties was substantially higher as the percentage of recycled sand increased;
- The mechanical properties are affected by the incorporation of recycled sand: the influence is low in the case of 20% but, for larger substitution ratios, the losses are severe.

## References

- [1] Kou SC, Poon CS. Properties of self-compacting concrete prepared with coarse and fine recycled concrete aggregates. *Cem Concr Compos* 2009;31:622–7. doi:10.1016/j.cemconcomp.2009.06.005.
- [2] Corinaldesi V, Moriconi G. The role of industrial by-products in self-compacting concrete. *Constr Build Mater* 2011;25:3181–6. doi:10.1016/j.conbuildmat.2011.03.001.
- [3] Carro-López, D.; González-Fonteboa, B.; Brito, J. de; Martínez-Abella, F.; González-Taboada, I.; Silva, P.: "Study of the Rheology of Self-Compacting Concrete with Fine Recycled Concrete Aggregates", *Construction and Building Materials*, V. 96, Elsevier, UK, October 2015, pp. 491-501.
- [4] Safiuddin M, Salam M a., Jumaat MZ. Effects of recycled concrete aggregate on the fresh properties of self-consolidating concrete. *Arch Civ Mech Eng* 2011;11:1023–41. doi:10.1016/S1644-9665(12)60093-4.
- [5] Grdic ZJ, Toplicic-Curcic G a., Despotovic IM, Ristic NS. Properties of self-compacting concrete prepared with coarse recycled concrete aggregate. *Constr Build Mater* 2010;24:1129–33. doi:10.1016/j.conbuildmat.2009.12.029.
- [6] Khatib JM. Properties of concrete incorporating fine recycled aggregate. *Cem Concr Res* 2005;35:763–9. doi:10.1016/j.cemconres.2004.06.017.
- [7] Evangelista L, de Brito J. Mechanical behaviour of concrete made with fine recycled concrete aggregates. *Cem Concr Compos* 2007;29:397–401. doi:10.1016/j.cemconcomp.2006.12.004.
- [8] Pereira P, Evangelista L, de Brito J. The effect of superplasticisers on the workability and compressive strength of concrete made with fine recycled concrete aggregates. *Constr Build Mater* 2012;28:722–9. doi:10.1016/j.conbuildmat.2011.10.050.
- [9] Zega CJ, Di Maio AA. Use of recycled fine aggregate in concretes with durable requirements. *Waste Manag* 2011;31:2336–40. doi:10.1016/j.wasman.2011.06.011.
- [10] ACHE. Use of recycled aggregates for production of structural concrete. (In Spanis. Madrid: Asociación Científica del Hormigón Estructural; 2005.
- [11] EFNARC, BIBM, ERMCO, CEMBUREAU, EFCA. The european guidelines for self-compacting concrete. Specification, production and use. 2005.
- [12] Khayat KH. Workability, testing, and performance of self-consolidating concrete. *ACI Mater J* 1999;96:346–53.
- [13] EFNARC. Specification and guidelines for self-compacting concrete. vol. 44. 2002.
- [14] ACHE. Self-compacting concrete: design and appliances (in Spanish). (In Spanis. Madrid: Asociación Científica del Hormigón Estructural; 2008.
- [15] Jin J. Properties of mortar for self-compacting concrete. University of London, 2002.
- [16] Banfill PFG. The rheology of fresh cement and concrete - A review. 11th Int. Cem. Chem. Congr., Durban: 2003.
- [17] Billberg PH. The structural behaviour of SCC at rest. In: Singapore Concrete Institute, editor. *Our world Concr. Struct.*, Singapore: 2011.
- [18] Khayat H, Omran A, Magdi A. Evaluation of thixotropy of self-consolidating concrete and influence on concrete performance. I SIMLAMCAA - IBRACON, 2012, p. 14.
- [19] Kovler K, Roussel N. Properties of fresh and hardened concrete. *Cem Concr Res* 2011;41:775–92. doi:10.1016/j.cemconres.2011.03.009.
- [20] Schwartzentruber A, Catherine C. La méthode du mortier de béton quivalent ( MBE ) - Un nouvel outil d'aide à la formulation des bétons adjuvés. *Mater Struct* 2000;33:475–82.
- [21] Rubio-Hernández FJ, Velázquez-Navarro JF, Ordóñez-Belloc LM. Rheology of concrete: a study case based upon the use of the concrete equivalent mortar. *Mater Struct* 2012;46:587–605. doi:10.1617/s11527-012-9915-1.

- [22] Nepomuceno M, Oliveira L, Lopes SMR. Methodology for mix design of the mortar phase of self-compacting concrete using different mineral additions in binary blends of powders. *Am Concr Institute, ACI Spec Publ* 2012;26:317–26. doi:10.1016/j.conbuildmat.2011.06.027.
- [23] Ouchi M, Hibino M, Ozawa K OH. A rational mix-design method for mortar in self-compacting concrete. *Proc. sixth east-asia- pacific Conf. Struct. Eng. Constr.*, 1998, p. 1307–12.
- [24] Assaad JJ, Harb J, Chakar E. Relationships between key ASTM test methods determined on concrete and concrete-equivalent-mortar. *J ASTM Int* 2012;6:1–13.
- [25] Nepomuceno M, Oliveira L, Lopes SMR. Methodology for mix design of the mortar phase of self-compacting concrete using different mineral additions in binary blends of powders. *Constr Build Mater* 2012;26:317–26. doi:10.1016/j.conbuildmat.2011.06.027.
- [26] Pereira P, Evangelista L, de Brito J. The effect of superplasticizers on the mechanical performance of concrete made with fine recycled concrete aggregates. *Cem Concr Compos* 2012;34:1044–52. doi:10.1016/j.cemconcomp.2012.06.009.
- [27] Nepomuceno M, Oliveira L. Parameters for self-compacting concrete mortar phase. *Am. Concr. Institute, ACI Spec. Publ. (253 SP)*, 2008, p. 311–27.
- [28] Sidorova A, Vazquez-Ramonich E, Barra-Bizinotto M, Roa-Rovira JJ, Jimenez-Pique E. Study of the recycled aggregates nature's influence on the aggregate–cement paste interface and ITZ. *Constr Build Mater* 2014;68:677–84. doi:10.1016/j.conbuildmat.2014.06.076.



Sustainable Civil Engineering Structures and Construction Materials 2016, SCESCM 2016

## Properties of concrete containing ground waste cockle and clam seashells

Monita Olivia<sup>a,\*</sup> Revina Oktaviani<sup>a</sup>, Ismeddiyanto<sup>a</sup>

<sup>a</sup>Universitas Riau, Kampus Bina Widya Simpang Baru, Pekanbaru Riau 28293, Indonesia

---

### Abstract

Seashells from marine by-product are potentially used in concrete as partial replacement of cement or fine aggregates substitute. The shells generally have high calcium content (CaO) which can improve the concrete physical and mechanical properties. In this research, two types of shells, namely cockle/blood clam (*Anadara granosa*) and marsh clam (*Polymesoda expansa*) were burnt and ground as powders to be used as the cement replacement. The shells were ground and replaced the cement at 4% by weight. Specimens were prepared from three different mixtures, i.e. Ordinary Portland Cement (OPC) as a control mix, concrete contains ground marsh clam (OPC Clam) and blood clam concrete (OPC Cockle). Setting time, density, compressive strength, tensile strength of the concrete mixtures were determined for each mixture. Test results indicate that the replacement of cement using different type of shells could yield to different concrete performance. Setting time, density, compressive and tensile strength of the OPC Cockle concrete are considerable lower than the OPC concrete up to 91 days. However, the OPC Clam concrete performed faster setting, higher density, higher compressive and tensile strength than the OPC concrete. Therefore, the CaO content of different type of seashells has the possibility of influencing the physical properties and strength development of concrete.

© 2017 The Authors. Published by Elsevier Ltd.

Peer-review under responsibility of the organizing committee of SCESCM 2016.

*Keywords:* clam; concrete; ground; setting time, properties

---

### 1. Introduction

Molluscs in fishery industry provide nutritious food source, jewellery, pharmaceutical, medicine and ornaments for domestic and international markets. In term of mollusc production, the method of production is divided into

---

\* Corresponding author.

E-mail address: [monita.olivia@lecturer.unri.ac.id](mailto:monita.olivia@lecturer.unri.ac.id)

capture and aquaculture. It was estimated approximately 236,564 tones of mollusc was captured in Indonesia between 1950-2011. Approximately 38.8% and 8.26% of the total amount were blood cockles and hard clams, respectively. In aquaculture industry, about 206.605 tones of mollusc was produced in 1950-2011, with 79.63% and 20.15% of the total amount were pearl oyster and penguin wing oyster, respectively [1]. The post consumer shells are part of molluscs with low economic value and usually disposed in land fill as solid waste. However, the seashells can be recycled and processed, then use them in concrete as fine aggregate, coarse aggregate, cement filler, and cement replacement for structures in coastal area.

Various type of shells, including oyster, mussel, periwinkle, clam, crepidula, scallops, and conk shells in form of complete, crushed, ground or powder in concrete, paver block, brick, and road pavement were investigated previously [2-6]. Some researcher used the ground shells approximately 5-20% by weight of cement as a cement replacement. It was reported that the shell powder in concrete generally could increase setting time, reduce compressive strength, reduce drying shrinkage, and decrease flexural strength [5, 7].

As a cement replacement, the chemical content of the shells will determine the properties of concrete. Ground shells is produced by washing, grinding, miling and calcining to obtain cementitious benefit of CaO that takes part in cement hydration. Typical raw seashells contain mainly 95-97% of calcium carbonate ( $\text{CaCO}_3$ ), small quantity of mineral and organic materials. The amount  $\text{CaCO}_3$  is considered very high, but it is more important as CaO to increase strength development and density of concrete. According to Lertwattanaruk et al. [5], the  $\text{CaCO}_3$  is transformed into calcium oxide (CaO) and carbon by burning the shells at high temperature exceeding  $550^\circ\text{C}$ . The CaO percentage of burnt shells is reported between 52 to 57% depends on the type and  $\text{CaCO}_3$  content of shells. One study by Islam et al. [8] concluded that the cockle shells could contain more calcium, carbon and other trace elements than the commercial calcium carbonate. Although majority of previous studies focused on using shells as aggregate substitution to avoid energy cost and difficulty in processing the shells, the ground shells powder is still an alternative to replace cement to obtain high cementitious benefit in concrete. In this research, two types of shells from local waters, namely blood cockle and marsh clam were studied to determine setting time, density, compressive strength, and tensile strength values.

## 2. Material and method

General purpose Ordinary Portland Cement was used as a main binder for the OPC concrete, OPC Cockle and OPC Clam specimens. Fine aggregate was river sand with specific gravity of 2.69, fineness modulus of 1.90, and water absorption of 2.24%. The coarse aggregates used had specific gravity of 2.72 and water absorption of 2.64%. The cockle/blood clam (*Anadara granosa*) and marsh clam (*Polymesoda expansa*) shells were collected from local seafood vendors (Figure 1).



Figure 1. The seashells a) Cockle/Blood Clam, b) Marsh Clam.

The shell powder was produced by cleaning, drying, burning the shells at a brick furnace for 3 days at approximately  $600^\circ\text{C}$ , crushing, grounding and sieving the shells using #200 sieve. The chemical composition of the OPC, cockle and clam shells are given in Table 1. It can be seen that the calcium oxide (CaO) content of the clam and cockle was 67.70% and 51.91%, respectively.

Table 1. Chemical composition of OPC, Cockle and Marsh Clam

Oxides (%)	Type of material		
	Ordinary Portland Cement/ OPC*	Cockle**	Marsh Clam**
CaO	65.21	51.91	67.70
SiO <sub>2</sub>	20.92	0.38	0.39
Al <sub>2</sub> O <sub>3</sub>	5.49	0.65	0.28
Fe <sub>2</sub> O <sub>3</sub>	3.78	0.05	0.02
MgO	-	-	-

\*Salain (2009)

The OPC control mix was designed to produce concrete with target strength  $\pm 35$  MPa at 28 days. The concrete mix consisted of cement (531.58 kg), water (190.39 kg), fine aggregates (862.15 kg) and coarse aggregates (750.89 kg). The cement was replaced by 4% of ground seashells based on the trial mix results and a recommendation of the previous study [9]. The specimens were prepared by casting the concrete mix in 100x200mm cylinders for compressive strength test, and 150x300mm cylinders for tensile strength test. The specimens were cured for 28 days in a water pond and left to air dry until the testing date. The specimens were tested for setting time (SNI 15-2049-2004), density (SNI), compressive strength test (SNI 03-1973-1990), and splitting tensile strength (SNI 03-2491-2002).

### 3. Material and method

#### 3.1. Setting time

Setting time test for all types of cement paste (OPC, OPC Cockle and OPC Clam) was conducted to determine the initial and final setting times. Those values are useful to observed the impact of adding seashells in the mixture and to determine strength development of concrete at early age. Figure 1 shows that the final setting time of OPC Cockle and OPC Clam concretes are shorter than the OPC concrete. Incorporating ground seashells into concrete mixture will increase the cement hydration reaction rate due to high calcium oxide (CaO) content. This is particularly important for concrete in application that needs to be hardened quickly with high early strength gain.

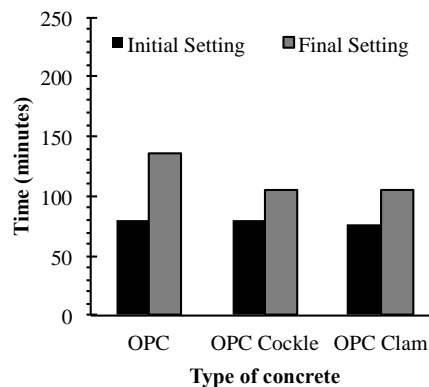


Figure 2. Setting time of OPC and seashell concretes.

#### 3.2. Density

The effects of replace cement with ground seashells on the density of concrete at 7, 28, and 91 days are presented in Figure 2. It can be seen that the density increases with the concrete age. As shown in the figure, the OPC Cockle has the lowest density and the OPC Clam showed the highest density among the concrete types. This is probably due to the fact that the densification of hydration product in OPC Clam is related to high CaO content that

could reduce porosity and increase density of the specimens. The lowest density of the OPC Cockle could indicate smaller content of hydration product that could pack the particles closely.

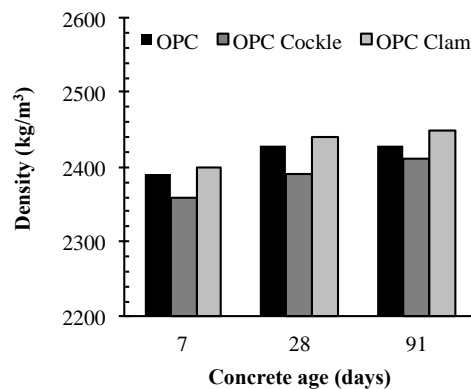


Figure 3. Density of OPC and seashell concretes.

### 3.3. Compressive strength

The compressive strength of concrete mixtures is shown in Figure 3. As the strength increased with age, the compressive strength increased accordingly. The compressive strength developed with type of cement and shells. The OPC Clam concrete showed higher compressive strength values than the OPC and OPC Cockle concretes, indicating that the replacement of the cement with the ground clamshell improves the later strength of the concrete.

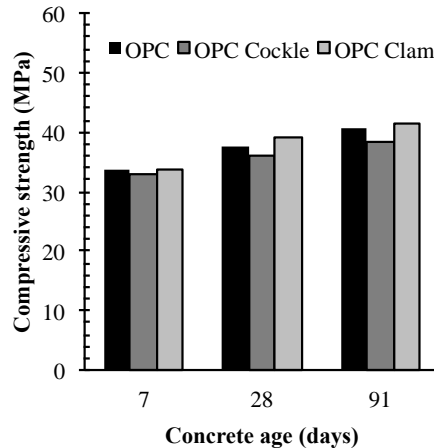


Figure 4. Compressive strength of OPC and seashell concretes at 7, 28, and 91 days.

On the other hand, at 28 and 91 days the OPC Cockle concrete had the smallest strength values than other concretes. This finding confirms that replacement of cement in the OPC could yield to different strength properties due to type of seashells and the CaO content in concrete. The result is consistent with those of other studies and suggest that a decrease in strength is related closely to the replacement of cement content that possibly disturb the rate of cement hydration at early ages [5]. This phenomenon was not applied to the OPC Clam concrete, since the amount of CaO in ground clamshells was significantly higher than the cockle shells.



### 3.4. Tensile strength

Results showed that the tensile strength of the OPC concrete was higher than the OPC seashell concretes. In this research, the tensile strength had a similar trend with the compressive strength values. The tensile strength of the OPC Cockle and OPC Clam concretes was considerably lower than the OPC concrete. Other researchers reported similar findings about the tensile strength values of OPC seashells since the bonding strength of the aggregate-cement paste interface was disrupted by the cement replacement. On the contrary, a previous study showed that the OPC seashells specimen performed higher tensile strength than the compressive strength due to a good adhesion between aggregates and cement paste for the OPC cockle concrete [10].

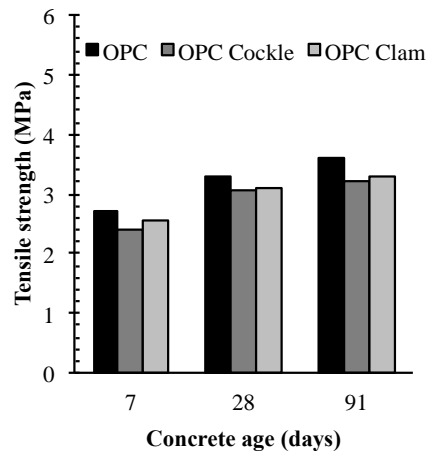


Figure 5. Tensile strength of of OPC and seashell concretes at 7, 28, and 91 days.

For overall performance, the OPC Clam specimens containing 4% of shell powder produced high initial setting, high density, good compressive strength and more flexible material than the OPC concrete that useful for early strength material in aggressive environment such as coastal areas. The replacement of cement using the seashells actually provide a practical solution for structures in remote coastal areas that need high strength and durable concrete to by reusing of marine by products disposed in landfill. According to [11], utilization of seashells is still not favorable as cement replacement material in concrete due to high energy cost for calcining the shells. However, when compared with the environmental benefit of using the seashell waste in concrete, the cost of shells processing for cement replacement is considered cheaper than use the Ordinary Portland Cement in remote coastal areas.

## 4. Conclusions

In this study, two types of local seashell were processed to produce ground shells for cement replacement in concrete. Setting time, density, compressive and tensile strength were studied. Replacement of the Portland cement with the ground cockle shells and clamshells by 4% of weight led to different physical and mechanical properties of the concrete. The OPC Cockle concrete showed lower setting time, density and tensile strength than the OPC concrete. The OPC Clam concrete performed faster setting, higher density, higher compressive and tensile strength than the OPC and OPC Cockle. The type and CaO content of seashells has the possibility of determining the physical and mechanical strength development in concrete.

## Acknowledgments

The authors acknowledge the support from Structural and Concrete Laboratory staff and assistants for their support during the laboratory work. We wish to thank the final year project students batch 2. This research is also use partial funding from Penelitian Unggulan Perguruan Tinggi (PUPT) 2016, No 492/UN.19.5.1.3/LT/2016,

Lembaga Penelitian, Universitas Riau, Pekanbaru, Indonesia.

## References

- [1] S. Kartika, Y. Mu. A study on Indonesian mollusc fishery and its prospect for economy. *International Journal of Marine Science*. 4(2014) 61-66.
- [2] B. Safi, M. Saidi, A. Daoui, A. Bellal, A. Mechekak, K. Toumi. The use of seashells as a fine aggregate (by sand substitution) in self-compacting mortar (SCM). *Construction and Building Materials*. 78(2015) 430-438.
- [3] A.A. Umoh, K.O. Olusola. Performance of periwinkle shell ash blended cement concrete exposed to magnesium sulphate. *Civil Engineering Dimensions*. 15(2013) 96-101.
- [4] D.H. Nguyen, M. Boutouil, N. Sebaibi, L. Leleyter, F. Baraud. Valorisation of seashell by-products in pervious concrete pavers. *Construction and Building Materials*. 49(2013) 151-160.
- [5] P. Lertwattanaruk, N. Makul, C. Siripattaraprat. Utilization of ground waste seashells in cement mortars for masonry and plastering. *Journal of Environmental Management*. 111(2012) 131-141.
- [6] W-T. Kuo, H-Y. Wang, C-Y. Shu, D-S. Su. Engineering properties of controlled low-strength materials containing waste oyster shells. *Construction and Building Materials*. 46(2013) 128-133.
- [7] G-L. Yoon, B-T. Kim, B-O. Kim, S-H. Han. Chemical-mechanical characteristics of crushed oyster-shell. *Waste Management*. 23(2003) 825-834.
- [8] K.N. Islam, M.Z.B.A. Bakar, M.M. Noordin, M.Z.B. Hussein, N.S.B.A. Rahman, M.E. Ali. Characterisation of calcium carbonate and its polymorphs from cockle shells (*Anadara granosa*). *Powder Technology*. 213(2011) 188-191.
- [9] M. Olivia, A.A. Mifshella, L. Darmayanti. Mechanical properties of seashell concrete. *The 5th International Conference of Euro Asia Civil Engineering Forum (EACEF-5) 2015*.
- [10] N.H. Othman, B.H.A. Bakar, M.M. Don, M.A.M. Johari. Cockle shells ash replacement for cement and filler in concrete. *Malaysian Journal of Civil Engineering*. 25(2013) 201-211.
- [11] J.M. Paris, J.G. Roessler, C.C. Ferraro, H.D. Deford, T.G. Townsend. A review of waste products utilized as supplements to Portland cement in concrete. *Journal of Cleaner Production*. 121(2016) 1-18.



Sustainable Civil Engineering Structures and Construction Materials, SCESCM 2016

## Utilization of polystyrene waste for wall panel to produce green construction materials

Suprpto Siswosukarto<sup>a,\*</sup>, Ashar Saputra<sup>a</sup>, I Gede Yohan Kafrain<sup>b</sup>

<sup>a</sup>*Department of Civil and Environmental Engineering, Faculty of Engineering, Universitas Gadjah Mada, Indonesia*

<sup>b</sup>*Engineering Faculty, Universitas Sariputra Indonesia Tomohon, Indonesia*

---

### Abstract

The wall structure separating floor areas significantly contribute the weight of the building that put it into a greater risk to earthquake event. The use of lighter wall materials is more desirable to reduce the potential risk of damage due to earthquake treat. This development of polystyrene wall panel is an effort to achieve two objectives, namely development light wall material and promoting green construction materials by utilizing polystyrene waste. The paper present the study on the development of polystyrene waste wall panel by pre-compacted method. In this research, the shredded polystyrene was blended with cement Portland and water at various certain proportion. When the mixed already properly blended, it was poured into the steel mold of 30x80cm. The mixed within the mold was subjected to compaction stress for up to 2 MPa that reduce the thickness of the mixed into about 1 cm. The polystyrene panel was kept in the humid zone for curing for about 28 days. They were 12 wall panel specimens made for this purpose. Result of test show that at the same compaction stress, higher cement content produces stronger polystyrene concrete. The average compressive strength of specimens with 250 kg/m<sup>3</sup> and 300 kg/m<sup>3</sup> cement content are 4.9 MPa and 5.3 MPa, respectively, and for flexural strength are 2,4 MPa and 3.3 MPa, respectively. The result show that the compressive strength of concrete matrix and and flexural strength panel are significantly high. However, under repeated loading of about 10% of maximum load, the panels experience decrease in stiffness in each load cycles suggesting the low tensile capacity of the concrete matrix. These results indicate the potential use of polystyrene wall panel for construction materials purposes with further attention on improvement the tensile characteristic of the concrete matrix.

© 2017 The Authors. Published by Elsevier Ltd.

Peer-review under responsibility of the organizing committee of SCESCM 2016.

*Keywords:* Polystyrene; panels; pre-compaction, waste, flexural, stiffness.

---

---

\* Corresponding author. Tel.: +0-000-000-0000 ; fax: +0-000-000-0000 .

*E-mail address:* [suprpto.siswosukarto@ugm.ac.id](mailto:suprpto.siswosukarto@ugm.ac.id)

## 1. Introduction

Wall is one component of building structure that is generally made of bricks, concrete blocks, concrete panels, wood boards, plywood and gypsum. The use of brick, concrete brick and concrete walls will produce large self-weight of wall resulting in large building's dead weight. The use of lighter wall materials is more desirable to reduce the potential risk of damage due to earthquake treat. To reduce the dead load of building, lighter weight wall has been widely used, such partition walls from plywood or gypsum. This study is attempted to take advantage the nearly weightless polystyrene waste into light weight wall panels. Polystyrene waste is well known as waste material that is hardly decomposed by nature. In a view of nature conservation, this situation is alarming since the volume of this waste is increasing by time. It is expected that this research will be able to bring a hope of the potential utilization of waste polystyrene as environmentally friendly building materials to support nature conservation efforts. This study has been started for quite a while but has not been able to produce some potential finding worth to be developed. The potential use of polystyrene waste began to appear with the application of pre-compaction processes in the manufacturing process of wall panel specimens. The polystyrene used in this study is limited to polystyrene from the pack of electronic goods.

## 2. Research objectives

The long term objectives of the research is the utilization of polystyrene waste as construction material thereby developing a green concept in construction program. This paper presents the extent of research result. The more detail of the objective of study presented in this paper are as follows:

- Developing procedures for processing polystyrene waste into a lightweight concrete based construction materials.
- Studying the mechanical characteristics of polystyrene wall panel, such as compressive strength, flexural strength, density, water absorption,
- Studying the behavior of polystyrene wall panel under repeated load to simulate the action of forces on wall.

## 3. Literature review

Lightweight concrete is defined in the literature as concrete with bulk density of less than  $1800 \text{ kg/m}^3$  [1]. Research on the development of lightweight concrete has been widely carried out, and one of an attempt to achieve a lightweight concrete is to replace aggregate with nearly weightless polystyrene [2-7]. There are several studies of lightweight concrete using polystyrene waste. Musana (2006) carried out research where the polystyrene was cut into small cube shape of less than 1 cm to replace the coarse aggregate [2]. Various PCC cement proportion of  $250 \text{ kg/m}^3$ ,  $300 \text{ kg/m}^3$  and  $350 \text{ kg/m}^3$  was used. The test results showed that compressive strength of polystyrene concrete is very low ( $<1 \text{ MPa}$ ). Ndale (2010) conducted study on the use of polystyrene into wall panel of concrete with various thickness of 6 cm and 8 cm [3]. The concrete polystyrene panel was reinforced with wire mesh of 4 mm diameter. The result of study showed that the flexural strength of panel is too low (flexural strength  $<1 \text{ MPa}$ ). Atmoko (2012), Aidil (2012) and Siregar (2012) conducted similar study and they introduced pre-compacting process in casting panel specimens [8,9]. Unfortunately, the wooden mold used for casting was capable only to withstand limited pre-compaction forces and hence the result of specimens were also unsatisfactory.

### 3.1. Wall panel

The idea of utilization of polystyrene waste for wall panel come from the availability of light wall panel products that basically consists of super foam sandwiched between steel wire mesh and concrete. One of factory product of polystyrene wall panels is M-System, originally developed in Italy ([www.M-Systemindonesia.com](http://www.M-Systemindonesia.com)) [10]. M-System wall panels consists of thick super foam core reinforced with wire mesh and concrete at both surfaces than for residential house, high rise buildings and special applications such as swimming pools, tribunes and others. The M-system panel is bearing wall that can be used for up to four floors of building structure. The panel wall size of  $15 \text{ cm} \times 270 \text{ cm} \times 112 \text{ cm}$  is capable to sustain load up to 1,700 KN. Another product of lightweight wall concrete panels is

Qui Panel which has a density of  $700 \text{ kg/m}^3$  [11]. Qui panels have a core made of a mixture of cement and EPS (Expanded Polystyrene) and coated with fiber cement. Qui Panel can be used for external walls, roofs, floors, partition walls. It can be used as a load bearing wall for one and two-story buildings.

### 3.2. Three Dimensional Steel Wire Mesh Panel

In Indonesia, the use of lightweight wall of super foamed based is stipulated in SNI 7392:2008 [12]. The lightweight wall system is called Three Dimensional Steel Wire Mesh Panel (PJKB-3D) which consists of expanded polystyrene core reinforced with steel wire mesh. The wall panel system is similar to M-System. PJKB-3D acts as a load bearing wall or floor plate and can be used for building. Steel wire existing on both sides are plastered using mortar with minimum cement content of  $250 \text{ kg/m}^3$  (proportion of cement: sand = 1: 4) to result in a minimum compressive strength of 17.5 MPa. The EPS (Expanded Polystyrene) has minimum density of  $16 \text{ kg/m}^3$  and thickness of 40 mm to 150 mm. The wall can serve as a barrier to noise and temperature. The thickness of one side plaster is 40 mm up to 50 mm that result in thickness of the entire wall panel of 120 mm to 250 mm.

The initial stage of research was tried to imitate the fabricated wall panel system by introducing polystyrene concrete of wall core. Despite numerous trial have been carried out, but the result is still unsatisfactory owing the poor quality of polystyrene concrete. It is only after the application of pre-compaction process that the quality of polystyrene concrete seems to be promising for further development. Owing to limited strength of polystyrene concrete, the latter research is not focusing to use polystyrene wall panel for bearing purposes but rather for partition to substitute wooden or gypsum panels.

## 4. Materials, specimens and testings

The research process was carried out into three main stages, namely the examination of materials, manufacturing of specimens and the testing of specimen. The examination process included evaluation of cement condition and investigation the unit weight of polystyrene. The second stage of research include a trial mix to determine adequate proportion of PPC cement and polystyrene, formulating procedures mixing and preparing specimen to investigate mechanical properties of polystyrene concrete used for research. The last stage was testing to investigate both mechanical properties and also strength characteristic of lightweight polystyrene wall panels.

This research used Portland Composite Cement (PPC) with proportion of  $250 \text{ kg/m}^3$  and  $300 \text{ kg/m}^3$  and water cement ration 0.3. The water cement ratio is determined considering the result of previous research. In the application of pre-compaction process, the use of higher water cement ration will result in more bleeding during the pre-compaction. The polystyrene used in the research is a type of polystyrene waste from packaging electronic goods so that it is relatively hard and stiff. Using shredding machine, the polystyrene was made into tiny shredded shaped with average length of less than 1 cm. The shredded polystyrene is nearly weightless so that it is easy being blown by air and is kept under dry condition until prior mixing process. The mold for casting specimen is steel mold from steel plate of 6mm thickness and has dimension of 80 cm length, 30 cm wide and 30 cm height (Fig. 1). After pre-compaction at 2 MPa, the resulted specimen of polystyrene concrete panel is 80 cm x 30 cm x 1 cm. The specimen was then placed in the humid area for curing for at least 28 days when it is ready for testing.



Fig. 1. Steel mold for casting specimen made of steel plate of 6 mm thick.

The experiment was initiated to find appropriate polystyrene concrete mix to be used for panel. During concreting process, the mixing of shredded polystyrene was very tricky since the polystyrene dry and is easy to fly. Therefore, the polystyrene need to be poured into the mixing bowl slowly with extra care. Cement and water of certain amount according to the intended proportion were then poured into the bowl and was mixed slowly for about 5 minutes. A proper mix was achieved when all shredded polystyrene was fully covered with cement paste. The mix was then poured into steel mold into 3 stage, each stage about 10 cm height and compacted using steel stick with round end. When the mold is full, the surface was trimmed to make it flat and uniformly thick. The mold cover was put in place, and then the mold was placed in the steel frame for application of pre-compaction. Attention should paid so that the point of loading at the mold cover coincide with its center area to ensure uniform distribution of forces in the mix within the steel mold. The forced was gradually applied through hydraulic jack connected to data logger were the load can be monitored. The loading process was stopped when the stress reached 2 MPa. The application of pre-compacting process on concrete panel is shown in Fig. 2a. The resulted polystyrene concrete panel after pre-compaction is shown in Fig. 2b.

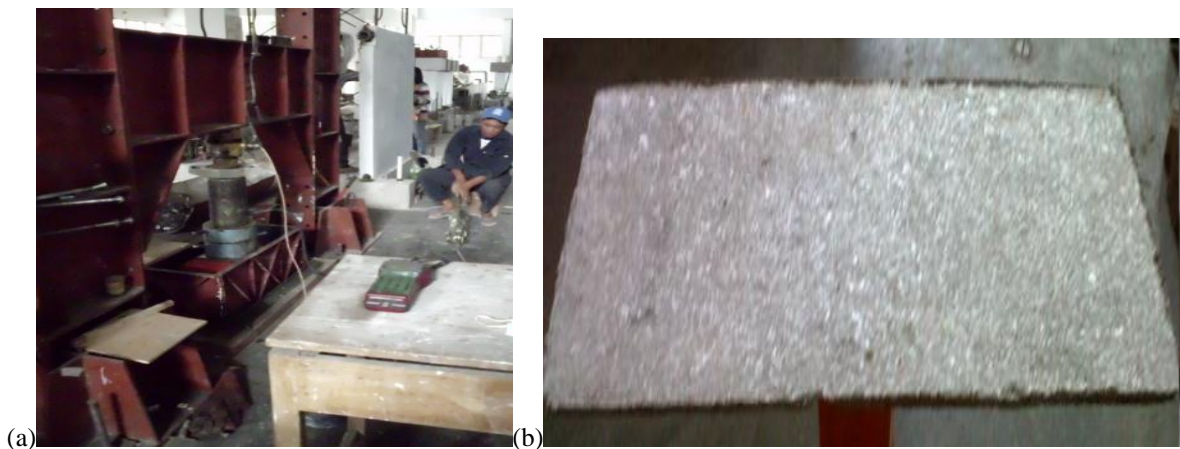


Fig. 2. (a) The application of pre-compaction process in manufacturing polystyrene concrete panels; (b) The resulted polystyrene concrete panel from pre-compaction process.

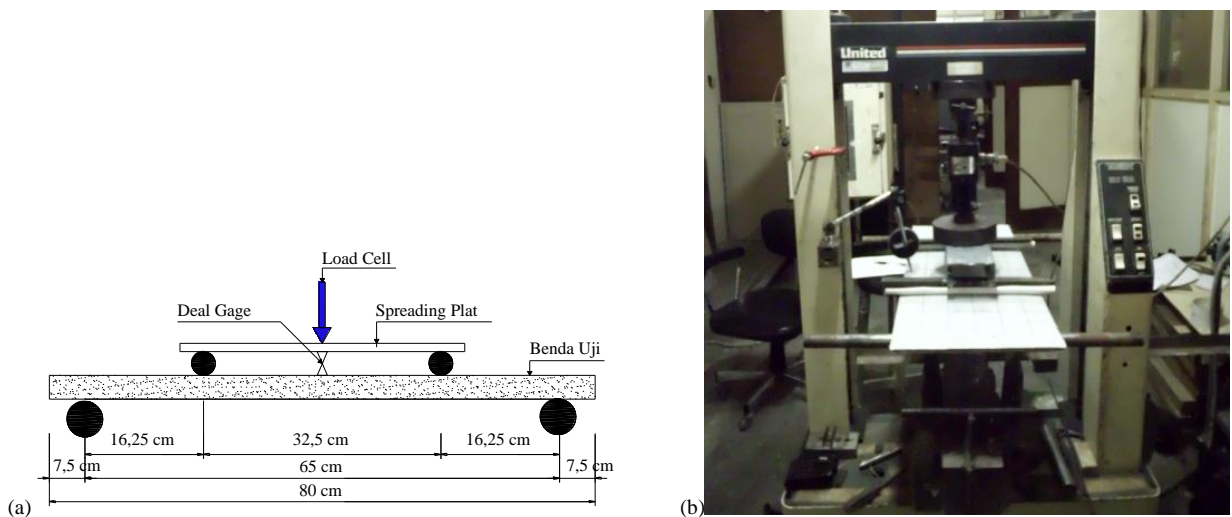


Fig. 3. (a) Schematic flexural test for polystyrene concrete panels; (b) Configuration of polystyrene concrete panel under flexural test



After all the specimens were made and appropriately cured in humid area for at least 28 days, the next stage was the testing process that include investigation of mechanical properties concrete matrix and strength characteristics of polystyrene concrete panels. The physical and mechanical properties of polystyrene concrete tests carried out on cube specimens of 5cmx5cmx5cm and cube specimens of 10cmx10cmx10cm, respectively that include the determination of water content, water absorption and compressive strength. While testing on wall panels were intended to investigate the compressive and flexural strength of panel, and the panel behavior under repeated loading. Fig. 3 shows the configuration of flexural test of panel, while Fig. 4 shows the set-up of test for panel under compressive load.

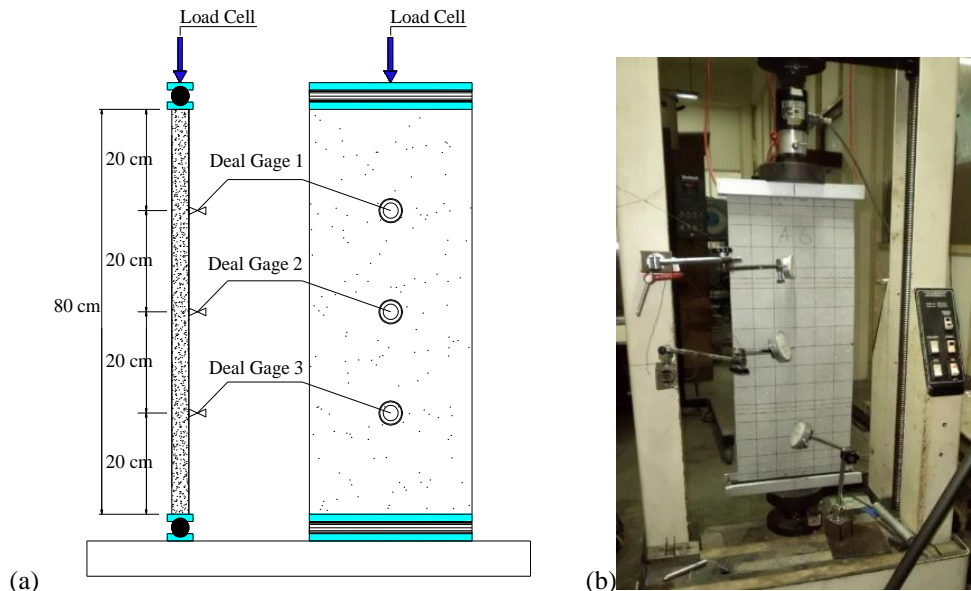


Fig. 4. (a) Schematic test set-up of polystyrene concrete under compression; (b) The testing configuration of polystyrene concrete panel under compression.

## 5. Results and Discussions

### 5.1. Results of physical and mechanical properties

The results of tests show that the unit weight of polystyrene in dry conditions being used in the research is 15.9 kg/m<sup>3</sup>. The study also indicates that there are many variety of polystyrene with different unit weight. The use of polystyrene of different type might result in difficulties in assessing its unit weight and hence may jeopardize the uniformity of one concrete mix to another. As a result, the physical and mechanical properties of each specimens might be different one to another. Therefore, in order to minimize the diversity of the mixes, the polystyrene waste was collected from one source and from one type of package, namely packaging of electronic goods.

The physical test results show that the water content of polystyrene concrete with 250 kg/m<sup>3</sup> and 300 kg/m<sup>3</sup> are 7.20% and 6.68%, respectively. Meanwhile, the value of water absorption of mix with cement content of 250 kg/m<sup>3</sup> and 300 kg/m<sup>3</sup> are 9.27 % and 8.23 %, respectively. Polystyrene concrete mixes with higher cement content tend to have lower water content as well water absorption. This is might be attributed to the volume of polystyrene, where a mix with higher cement content use less polystyrene, hence less wet surface area during mixing and also less porosity. It is suggested that the water content and water absorption will indicate the characteristics of mix against humidity change that may lead to strength deterioration when the water content and water absorption are high. Referring to the technical requirement of plywood [13], where the water content should be less than 14%, the polystyrene concrete panels have values that meet the requirement.



Another results show that the bulk density of polystyrene concrete mixes with cement content 250 kg/m<sup>3</sup> and 300 kg/m<sup>3</sup> are 1,467 kg/m<sup>3</sup> and 1,533 kg/m<sup>3</sup>, respectively. The result of bulk density of polystyrene concrete mix under pre-compaction stress of 2 MPa are significantly greater that the results of previous studies without pre-compaction [2-9]. The result also suggests that the density of mix tends to be close to the density of cement, and referring to previous study, it is suggested that the higher pre-compaction stress will result in mix's density that is closer to cement.

## 5.2. Compressive strength

The test results show that the compressive strength of polystyrene concrete mixes with cement content of 250 kg/m<sup>3</sup> and 300 kg/m<sup>3</sup> are 4.9 MPa and 5.3 MPa. This resulted compressive strength of specimens under pre-compaction stress of 2 MPa is significantly higher that the previous research without pre-compaction process since the concrete matrix becomes denser. According to lightweight concrete classification given by Neville and Brooks (1987) [1], the polystyrene concrete used in this might be included as type of lightweight concrete for retaining heat (insulating concretes).

## 5.3 Polystyrene concrete Panel Testing Results

Results of experimentation show that polystyrene concrete panels with cement content of 250 kg/m<sup>3</sup> and 300 kg/m<sup>3</sup> have an average weight of 14.4 kg/m<sup>2</sup> and 14.9 kg/m<sup>2</sup>, respectively. These values are about 3 times than that for gypsum panel (5.5 kg/m<sup>2</sup>). However, in comparison with the weight of red brick wall (250 kg/m<sup>2</sup>) and also hollow concrete blocks (200 kg/m<sup>2</sup>), the weight per square area of polystyrene concrete panel is still significantly lighter.

### 5.3.1. Compressive and Flexural Strength of Polystyrene Panels

The compressive test was carried out according to SNI 7392:2008 [10] for testing wall panel for structural purpose. Meanwhile, in the current research the specimen is of 80cmx30cmx1cm, hence the specimen is very slender (Fig. 4b). The results of test show that the polystyrene concrete panel with cement content of 250 kg/m<sup>3</sup> and 300 kg/m<sup>3</sup> have average compressive strength of 0.63 MPa and 0.83 MPa. The resulted compressive strengths are so low that make the polystyrene concrete panel is not available for bearing wall purposes.

Results of flexural test of polystyrene concrete panel yield average stiffness values of 17 N/mm and 31 N/mm for cement content of 250 kg/m<sup>3</sup> and 300 kg/m<sup>3</sup>, respectively. While the average flexural strength of panels are 2,4 MPa and 3,3 MPa for panels with cement content of 250 kg/m<sup>3</sup> and 300 kg/m<sup>3</sup>, respectively. The resulted flexural strength is significantly larger than previous research on flexural strength of gypsum [14]. The results of this study suggests that by increasing cement content can improve strength as well as stiffness of polystyrene concrete panels.

### 5.3.2. Panel Behavior under Repeated Loading

Repeated loading is intended to simulate the imposed load on the wall. This testing was carried out under flexural test at load level of 10% from the maximum bending load. Repetition was carried out up at the total of 20 cycles. In each load cycle, a curve describing the relationship between load (P) and deflections ( $\delta$ ) was obtained. The results of repeated load tests on the panel with cement content of 250 kg/m<sup>3</sup> and 300 kg/m<sup>3</sup> is shown in Fig. 5a. In Fig. 5a, each line of (P- $\delta$ ) relationship shows one loading cycle. Each line is shifted to another due to a shift of the LVDT readings during to pause between one cycles to the next loading cycle. The flexural stiffness of panel is determined as value of slope at each line. To clarify the extent change in slope of every loading cycle, the magnitude of slope of each line is then drawn in accordance with the order of its loading cycles, and the result is shown in Fig. 5b. Fig. 5b clearly shows that the value of slope is decreasing from cycle to cycle indicating the decrease in stiffness of panel in every loading cycles. The decrease in stiffness of polystyrene panel might be attributed to the occurrence of micro raking within the concrete matrix. The crack propagates, as shown by further decrease in slope in the next cycle, as the load was repeated. This finding is very important in understanding the behavior of polystyrene panel as it

experience micro crack propagation under relatively low level of repeated loading ( $10\% P_{\max}$ ). It can be concluded that the tensile strength capacity of polystyrene concrete matrix is low that result in panel of low stiffness.

The results of repeated testing for polystyrene concrete panel with cement content of  $300 \text{ kg/m}^3$  also exhibits similar characteristics of decreasing stiffness in every load cycle. The rate of decrease in stiffness for mix with cement content of  $300 \text{ kg/m}^3$  is nearly similar to that of lower cement content. The results of this study suggests that the polystyrene concrete panels has insufficient strength and stiffness to sustain repeated load as low as  $10\%$  of its maximum flexural capacity that might occur in wall structure. However, the flexural test results show the significantly high flexural strength of panels that indicates its potential to be further developed as wall panels. In further research efforts are required to improve the tensile capacity of concrete matrix, for example by adding fiber in the concrete mix or introduction of reinforcement either paper based or wire mesh on panel surfaces to improve its flexural strength and stiffness.

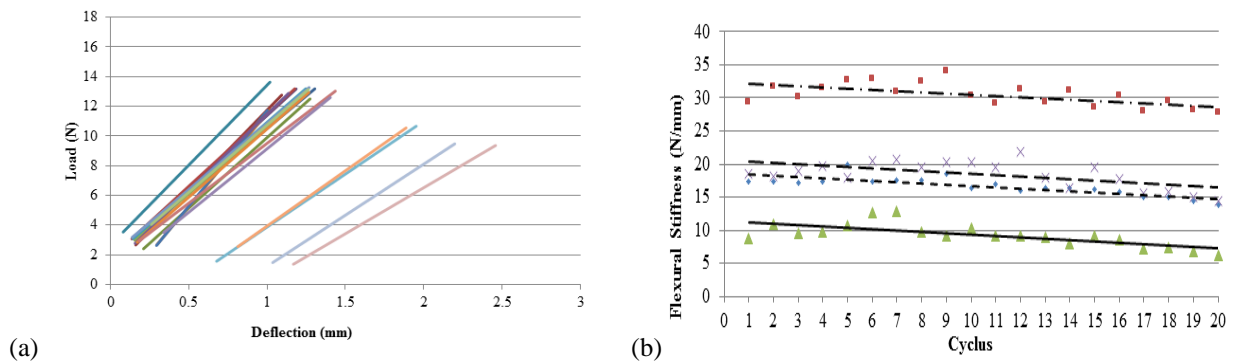


Fig. 5. (a) The relationship between  $P - \delta$  for each cycle of loading on the panel with cement content of  $250 \text{ kg/m}^3$ ; (b) The change in slope in every loading cycle as drawn according the order of occurrence.

## 6. Conclusion and Suggestion

Based on the results of this study, some conclusions can be drawn as follows:

- The application of pre-compaction method in concreting process can effectively improve the mechanical characteristic of polystyrene concrete.
- At the same level of pre-compaction stress, the higher cement content on mix of polystyrene concrete may increase strength, reduce water content as well as and water absorption.
- Polystyrene concrete panel under pre-compaction stress of  $2 \text{ MPa}$  has significant flexural strength and stiffness indicating its potential to be developed as lightweight wall panel of non-bearing type.
- Polystyrene concrete panel exhibits decrease in stiffness under repeated loading suggesting the low tensile capacity of the concrete matrix that need further improvement.

The research finding suggest that one of the main disadvantage of polystyrene concrete is the low tensile capacity of the concrete matrix. Therefore, considering the potential utilization of polystyrene waste for construction materials, further efforts should be addressed to improve the tensile characteristics of concrete matrix, such as:

- The use polystyrene of smaller particles to increase bonding surfaces and bonding concrete matrix.
- The addition of fibers within concrete mix to improve tensile characteristics of polystyrene concrete matrix.
- The application of reinforcement on surfaces panels, such as wire mesh or membrane from plastic or paper based.

## Acknowledgements

The research was supported by Hibah Penelitian from the Department of Civil and Environmental Engineering, Faculty of Engineering, Gadjah Mada University, 2015.

## References

- [1] Neville dan Brooks, K.M., 1987. *Properties of Concrete*, McGraw-Hill.
- [2] Musana, 2006, Pemanfaatan Limbah Polystyrene Sebagai Bahan Campuran Beton Ringan dengan Semen PCC 250, 300, 350 Kg/m<sup>3</sup>, Tesis, Magister Teknologi Bahan Bangunan Jurusan Teknik Sipil Universitas Gadjah Mada Yogyakarta
- [3] Ndale, 2010, Penggunaan Beton Ringan Polystyrene dengan Perkuatan Wiremesh untuk Panel Dinding Tebal 6 cm, Tesis, Magister Teknologi Bahan Bangunan Jurusan Teknik Sipil Universitas Gadjah Mada Yogyakarta.
- [4] Pudiasri, 2012 Aplikasi Beton Ringan Polystyrene Untuk Panel Dinding Tebal 8 cm Dengan Metode Pengempaan Terukur, Magister Teknologi Bahan Bangunan Jurusan Teknik Sipil Universitas Gadjah Mada Yogyakarta.
- [5] Sambodo, 2003, Beton Ringan Polystyrene, Magister Teknologi Bahan Bangunan Jurusan Teknik Sipil Universitas Gadjah Mada Yogyakarta.
- [6] Sireggar, 2012, Beton Ringan Polystyrene untuk Panel Dinding Tebal 7 cm dengan Metode Pengempaan Terukur, Magister Teknologi Bahan Bangunan Jurusan Teknik Sipil Universitas Gadjah Mada Yogyakarta.
- [7] Sulistyorini, 2010, Perilaku Dinding Beton Ringan dari Limbah Polystyrene Dengan Perkuatan Wiremesh, Tesis, Jurusan Teknik Sipil dan Lingkungan, Program Pascasarjana Universitas Gadjah Mada Yogyakarta.
- [8] Aidil, 2012, Penggunaan Polystyrene Sebagai Beton Ringan dengan Pra Pemasangan untuk Panel Dinding 10 cm, Magister Teknologi Bahan Bangunan Jurusan Teknik Sipil Universitas Gadjah Mada Yogyakarta.
- [9] Atmoko, 2012, Beton Ringan Polystyrene untuk Panel Dinding Tebal 9 cm dengan Metode Pengempaan Terukur dan Perkuatan Kawat Loket, Magister Teknologi Bahan Bangunan Jurusan Teknik Sipil Universitas Gadjah Mada Yogyakarta.
- [10] [www.m-systemindonesia.com](http://www.m-systemindonesia.com) (Diakses pada Juli 2015)
- [11] [quipanel.co.id](http://quipanel.co.id) (July 2015)
- [12] SNI 7392:2008, Tata cara perencanaan dan pelaksanaan bangunan gedung menggunakan panel jaring kawat baja tiga dimensi (PJKB-3D) las pabrikan, Badan Standardisasi Nasional, Jakarta.
- [13] SNI 03-2105-1996, Papan Partikel. Badan Standardisasi Nasional, Jakarta.
- [14] Trisna H. and Mahyudin A., 2012, Analisis sifat fisis dan mekanik papan komposit gypsum serat ijuk dengan penambahan boraks (dinatrium tetraborat decahydrate), *Jurnal Fisika Unand* Vol. 1, No. 1, Oktober 2012, ISSN 2302-8491.
- [ ] Raju. K.N, 1983, *Design of Concrete Mixes*. CBS Publish and Distributor.



Sustainable Civil Engineering Structures and Construction Materials 2016, SCESCM 2016

## Valorization of the crushed dune sand in the formulation of self-compacting-concrete

Farid Benmerioul<sup>a,\*</sup>, Abdelkadir Makani<sup>b</sup>, Ahmed Tafraoui<sup>b</sup>, Said Zaouai<sup>a</sup>

<sup>a</sup>Laboratoire de Fiabilité des Matériaux et des structures (FIMAS), Université Tahri Mohammed – Béchar BP 417 - Béchar (08000), Algeria.

<sup>b</sup>Laboratoire de Fiabilité du Génie Mécanique (LFGM), Université Tahri Mohammed – Béchar BP 417 - Béchar (08000), Algeria

---

### Abstract

In this paper, the crushed dune sand and limestone filler were using as mineral addition in the formulation of self-compacting concrete (SCC), for that a comparison was carried out on their effect on the properties and behaviour of SCC in a fresh and hardened state. The results of the mechanical tests showed that there is a light difference between the concrete containing limestone filler or crushed dune sand. Moreover, the SCC containing crushed dune sand presents a better behavior at the shrinkage than the SCC with limestone filler.

© 2017 The Authors. Published by Elsevier Ltd.

Peer-review under responsibility of the organizing committee of SCESCM 2016.

*Keywords:* SCC; crushed dune sand; limestone filler; compressive strength; shrinkage.

---

### 1. Introduction

The self-compacting-concrete (SCC) makes a new family of concrete and a new technological step in civil engineering. It is very fluid concrete whose putting in place without vibration, it has several advantages so much at the environmental level, technological that economic which interests the industrialists more and more [1-3]. It is essential that the self-compacting-concrete preserves its stability and ensures a perfect homogeneity; these two contradictory properties are ensured by the employment of superplastifiant and the incorporation of the mineral additions as binary or ternary blended cement in their compositions [3-7]. The aim of this study is to valorize the crushed dune sand ( $D_{\max} \leq 80 \mu\text{m}$ ) in order to use it like a mineral addition in the formulation of self-compacting-

---

\* Corresponding author. Tel.: +0-000-000-0000 ; fax: +0-000-000-0000 .

E-mail address: [faridbba37@yahoo.com](mailto:faridbba37@yahoo.com)

concrete. In this work, incorporation was made for the limestone filler and crushed dune sand producing by crushing the western dune sand in the formulation of the SCC in order to evaluate their effects on the properties fraiche and hardened of these concretes. This document carried out a comparison on the effect of limestone filler and crushed dune sand in term of behavior on the fresh states, compressive strength, loss mass, and free shrinkage of these concretes.

## 2. Materials and experimental method

### 2.1. Basic materials

#### 2.1.1. Cement

The cement used is Portland cement composed CPJ CEM II / B resistance real Matine 425 bars under the trade name.

#### 2.1.2. Additions

- Limestone fillers are type calcaire according to norm (NF P 18-508 1995a).
- The crushed dune sand coming from crushing dune sand which is on the level of Taghit, wilaya of Bechar (Algeria), the maximum coarse aggregate of crushed dune sand does not exceed 80 $\mu$ m. it has high content of quartz silica [8].

The results of DRX analysis carried out on the sand of Taghit and limestone fillers are presented graphically on Fig. 1. It was noticed a peak of approximately 100 % of silica with crashed sand and calcite for limestone fillers which translated the predominance of SiO<sub>2</sub> and CaCO<sub>3</sub>, the others revealed elements present at small percentages.

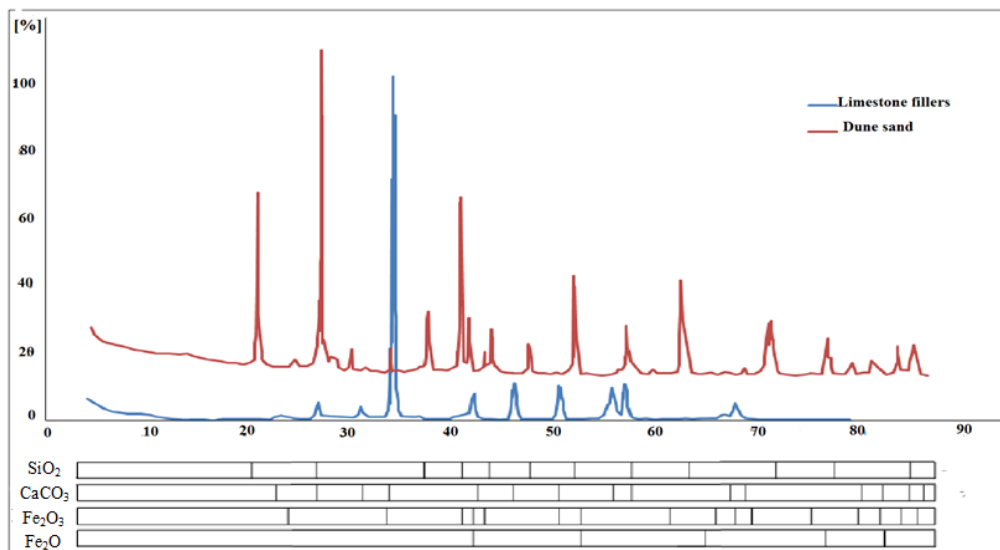


Fig. 1. DRX analyze of limestone filler and dune sand.

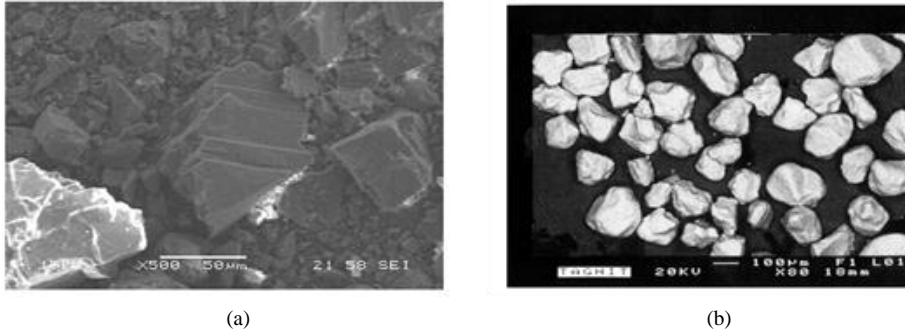


Fig. 2. MEB photographs of (a) Limestone filler; (b) Dune sand.

From Fig. 2, it was observed that the shape of filler calcaire particle is angular, dapped, broken or round forms observed for crushed dune sand.

Table 1. Physical properties of Limestone filler and crushed dune sand.

Items	Limestone filler (0/0.63)	Crushed dune sand ( $\leq 80 \mu\text{m}$ )
Specific density	2.71	2.8
specific surface $\text{cm}^2/\text{g}$	4060	3000
Unit weight ( $\text{kg}/\text{m}^3$ )	1120	1300
Activity index $i_{28j}$	0.79	-

### 2.1.3. Aggregates

The aggregates play an important role in the behavior of concrete. Their influence is very strong in terms of mechanical performance, shrinkage and durability [9-10]. Rolled sand class (0/3) from the quarry Mahmoudi (Bechar), gravels are class 3/8, 8/15 from Hassi EL 20 (Bechar).

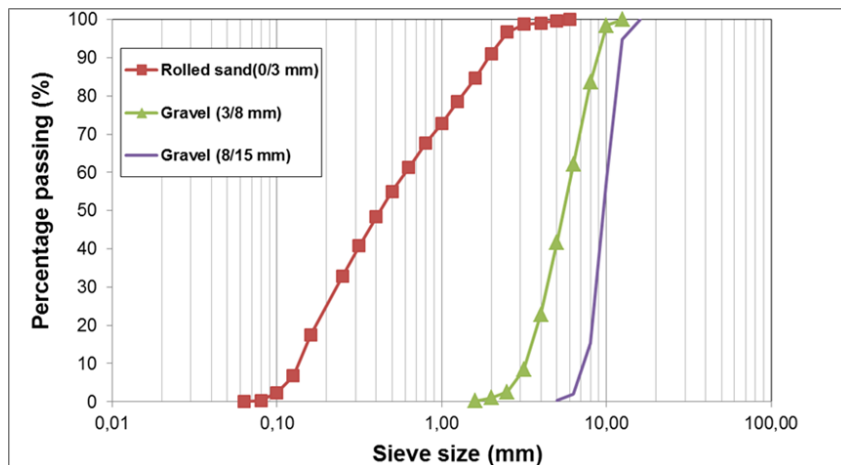


Fig. 3. Particle size distribution curves of the aggregates used.

Table 2. Physical characteristics of materials.

	Rolled sand (0/3)	Gravel (3/8)	Gravel (8/15)
Sand Equivalent (%)	74	—	—
Fineness modulus	2.1	—	—
Absolute volumetric mass (kg/m <sup>3</sup> )	2604	1606	1444
Apparent volumetric mass (kg/m <sup>3</sup> )	1761	2630	2666

#### 2.1.4. Superplasticizer

Superplasticizer SIKAPLAST 5045 / High Reducer Water / retarder for concrete ready and compacting concretes according to norm NF EN 934 -2. [11].

#### 2.1.5. Mixing water

The water abstraction is done on the conduct of drinking water supply for the town of Bechar. This water is treated for drinking.

### 2.2. Formulation of concrete

For this purpose, we first made a self-compacting-concrete (SCC) based solely on the criteria recommended by AFGC [12] (report (Gravel / Sand) to be close to 1, the volume of the paste must be between 330 and 400 l / m<sup>3</sup>, cement dosage is between 300 and 350 kg / m<sup>3</sup>, dosage of Superplasticizer must ensure the fluidity of the mixture.) The final formulation of the self-compacting-concrete is given in table 1. Two concretes were thus obtained, one with the limestone filler is named SCC LF, and another with crushed dune sand is named SCC CS.

Table 3. Composition of self-compacting-concrete.

Constituents	Binder (C+A)	Addition	Rolled Sand (0/3 mm)	Gravel (3/8mm)	Gravel (8/15mm)	Superplasticizer	E/B
Dosage (kg/m <sup>3</sup> )	520	104	903	151	578	6.8	0.4

### 2.3. Experimental method

#### 2.3.1. Tests in fresh state

The SCC must satisfy many tests, we chose three that are recommended by AFGC [12] that allow to characterize the principal properties of SCC in the fresh state (fluidity, static and dynamic stability, free and confined environment) spreading Abrams cone flow box L and stability through a sieve. The test slump flow is carried with the Abrams cone consists of measuring the diameter of concrete spread on two perpendicular lines and takes the mean. The test L-box is used to check the mobility of confined concrete and verify the implementation of concrete will not be thwarted by blocking phenomena. The test of stability [1,13] by sieve can qualify compacting concrete vis-a-vis the risk of segregation and indicates the degree of segregation of SCC.

#### 2.3.2. Tests in hard state

The tensile strength in bending according to norm [NF P18-407] was determined using bending machine 3 points. For the mechanical compressive strength according to norm [NF P18-406], The compression test is to break the test specimen between the two plates of a compression press. The press used is a compression machine (ELE AUTOTEST).

The measurements of shrinkage were recorded from 24h after the casting. All testing was completed on three samples and the average value reported.



### 3. Results and discussion

#### 3.1. Fresh state of concrete

From those results (Fig. 4), it was observed that all the self-compacting concretes (SCC) respect the criteria of autoplacibilité recommended for testing [AFGC.2008] [12]. For all SCC, the aureole laitance at the periphery of concrete patties was absent or very low (1 to 2 mm). In addition, the coarse aggregates have been properly trained by the cement matrix and are not remains piled in the midst of galette of concrete.

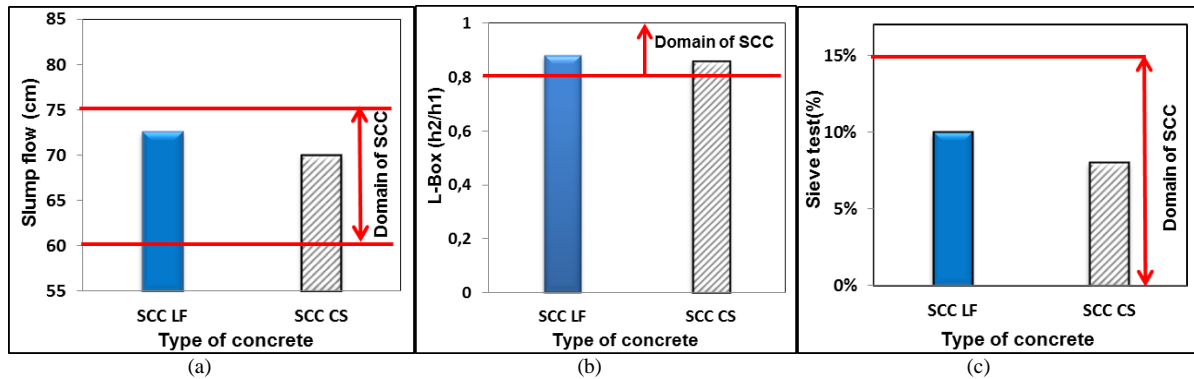


Fig. 4. Effect of the mineral additions on fresh properties of SCC. (a) Slump flow; (b) L-Box; (c) stability in sieve.

The influence of the mineral additions on the flow of concretes is according to their dosage and of their state (inert or active)[14-16], while, the time of flow more noticeable by the concrete containing siliceous fines is dependent on the fineness of additions and its high demand of water [10]. The fine particle of the addition fills the voids available between the particles of the mortar, thus increasing the compactness of the mixture by improving total arrangement of the particles in the matrix. Consequently, the quantity of water which occupied these voids is liberated in the interstitial solution, which results a better fluidity. [13, 17]. The Fig 4 presents the slump flow of the different formula. It is seen that the two concretes having a better fluidity what is acceptable for a SCC according to recommendations of the AFGC. However, one rather notes a light reduction in slump flow, particularly for the SCC CS compared with SCC CS.

The results obtained by the L – Box test are presented on fig 4, it can show that these concretes have a good mobility in confined milieu, the SCC shows a better rate of filling.

According to the criteria of the AFGC, [12]. The role of volume of paste is more important to limit the risks of segregation and sweating. These mixtures have a satisfactory stability (fig.4), it is marked laitance  $p \leq 10\%$  who signifies any risk for the static segregation. The SCC CS has a resistance for the static segregation a little improved that SCC LC, the concrete is too viscous to run out through the sieve.

#### 3.2. Hardened state of concrete

##### 3.2.1. Compressive strength

The mechanical strength is an essential characteristic for the material concrete and one of the fundamental parameters of our study. The introduction of mineral additions involves a modification of the porosity of the cementing matrix and improving the mechanical strength of the concretes at the young age by physical effect mainly and pozzolanic effect when they are chemically active, in the longer term [18].

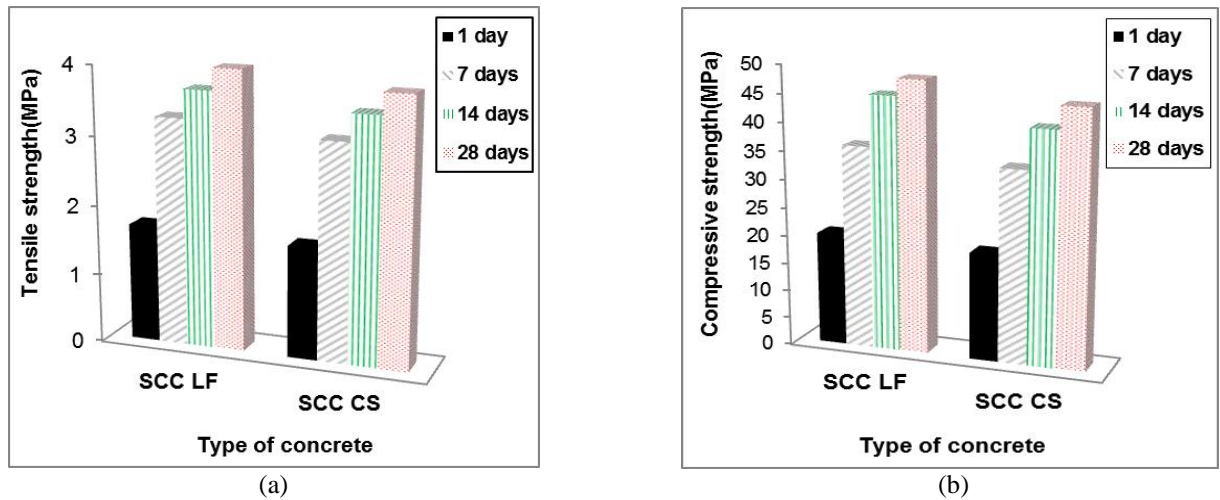


Fig. 5. (a) Compressive strength of concretes; (b) tensile strength.

Consequently, the evolution of compressive and tensile strength in time was followed for the various compositions of concrete and the results so obtained are represented graphically in Fig. 5. It is noted, according to Fig. 5, that the mechanical compressive strength of the two compositions of SCC is almost equivalent. Nevertheless, SCC LF has better compressive strength at the expiry of 7 and 28 days while for SCC CS.

### 3.2.2. Shrinkage

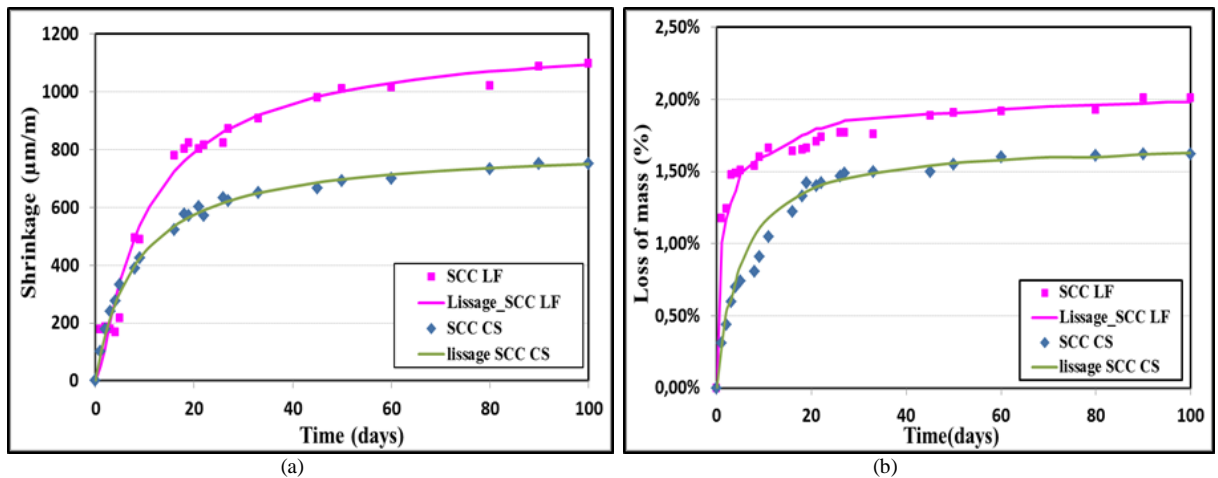


Fig. 6. Effect of the mineral additions on: (a) free shrinkage; (b) loss of concrete mass.

The analysis of the curves of Fig. 6 shows that the shrinking of concrete SCC LF is more significant than that of concrete SCC CS that can be justified by the extreme fineness of crushed dune sand and the absence of sweating. The results of the loss of mass could confirm this differed behavior. Fig. 6 illustrates the percentage of the loss in mass of the two compositions of concrete. From Fig. 6, it is notable that the loss of mass of concrete SCC LF is much more significant compared to those of concrete SCC CS. The weak loss of mass of concrete SCC CS is due mainly to the reduction in porosity by the pozzolanic reaction of the silica which contributes to the containment of the pores in the cementing matrix [4].

#### 4. Conclusion

This study contributed to the research tasks undertaken on the valorization of crushed dune sand of the western erg. Our first experimental results showed that the mechanical resistance in compression of the limestone filler concrete is slightly higher than that of the crushed dune sand of concrete, the fineness is the principal reason to improve this characteristic. With regard to the free shrinkage in desiccation, the use of crushed dune sand is very satisfactory. Indeed, the concrete containing crushed dune sand presented shrinkage remarkably lower than that of the concrete containing limestone filler. To finalize, it was deduced that the incorporation of crushed dune sand of the western erg in the composition of the SCC as a mineral addition was generally beneficial and can bring solutions to future in certain work of our country.

#### References

- [1] H. Okamura, M. Ouchi, Self-compacting concrete, *Journal of advanced concrete technology*, 1 (2003) 5-15.
- [2] A. Neville, The confused world of sulfate attack on concrete, *Cement and Concrete Research*, 34 (2004) 1275-1296.
- [3] A.Castel, T. Vidal, R. François, Bond and cracking properties of self-consolidating concrete, *Constr. Build. Mater.* 24 (2010) 1222–1231.
- [4] M. Uysal, K. Yılmaz, Effect of mineral admixtures on properties of self-compacting concrete, *Cem Con Com*,33 (2011) 771–6.
- [5] M.Sahmaran, H.A. Christianto, I.Ö.Yaman ,The effect of chemical admixtures and mineral additives on the properties of self-compacting mortars, *Cem Con Comp*, 28 (2006) 432–440.
- [6] W. Wongkeo, P.Thongsanitgam, A.Ngamjarrojana, A. Chaipanich, Compressive strength and chloride resistance of self-compacting concrete containing high level fly ash and silica fume. *Materials & Design*, 64 (2014) 261-269.
- [7] S. Zaoiai, A. Makani, A. Taфраoui, F. Benmerioul (2016), Optimization and mechanical characterization of self-compacting concrete incorporating rubber aggregates, *Asian journal of civil engineering (bhrc)* 17 (2016) 817-829.
- [8] A.Taфраoui,Valorisation du sable de l'erg occidental (Algérie): Application aux nouveaux bétons, Editions universitaires europeennes, 2012.
- [9] A. Makani, Correlation between Young's modulus and uniaxial compressive strength of aggregates, *International Review of Civil Engineering*, 5 (2014) 187-192.
- [10] M. Valcuende, F. Benito, C. Parra ,Shrinkage of self-compacting concrete made with blast furnace slag as fine aggregate, *Construction and Building Materials*, 76 (2015) 1-9.
- [11] EN, T. S. 934-2 ,Admixtures For Concrete, Mortar and Grout-Part 2: Concrete Admixtures; Definitions, Requirements, Conformity, Marking and Labelling". TSE (Turkish Standards Institute), 2002.
- [12] AFGC, association française de génie civil ,2008.
- [13] B.Poulson., Specification and Guidelines for Self-Compacting Concrete., EFNARC, Annex D, 2002.
- [14] A.Yahia, M.Tanimura,Y. Shimoyama, Rheological properties of highly flowable mortar containing limestone filler-effect of powder content and W/C ratio, *Cement and concrete Research*, 35 (2005) 532-539.
- [15] A. Taфраoui, G. Escadeillas ,S. Lebaïli,T.Vidal, Metakaolin in the formulation of UHPC ,*Construction and Building Materials* 23 (2009) 669-674.
- [16] A.Taфраoui, G.Escadeillas,T.Vidal,Durability of the Ultra High Performances Concrete containing metakaolin." *Construction and Building Materials*,112 (2016) 980-987.
- [17] B. Elbahi, S. M. A. Boukli Hacene, Influence of limestone fillers and natural pozzolan on engineering properties of concrete, *Journal of Adhesion Science and Technology*, (2016),DOI: 10.1080/01694243.2016.1161970.
- [18] P. Billberg, Influence of filler characteristics on SCC rheology and early hydration, In : *Proceedings of the Second International RILEM Symposium on Self-compacting Concrete*, Tokyo. 2001. p. 285-294.



Sustainable Civil Engineering Structures and Construction Materials, SCESCM 2016

## Improvement of Roller-Compacted Concrete's Workability for Pavement by using Poly Naphtalene Sulfonate superplasticizer

<sup>a</sup>Chamroen Chhorn, <sup>b</sup>Seung Hwan Han, <sup>c</sup>Beom Jun Chon, <sup>a</sup>Seung Woo Lee\*

<sup>a</sup>Department of Civil Engineering, Gangneung-Wonju National University, Jukheon-gil 7, Gangneung city, 210-702, Korea

<sup>b</sup>Korea Expressway and Transportation Research Institute, 50-5 Sancheok, Dongton city, 445-615, Korea

<sup>c</sup>Samwoo IMC Co.Ltd, 33-8 Ogeum-dong, Songpa-gu, Seoul city, 138-855, Korea

---

### Abstract

Roller-compacted concrete or RCC is a zero slump concrete that requires compaction in order to reach its final form. It has the same composition as conventional concrete with different proportioning. Its cement content is typically lower than that of conventional concrete which can be beneficial in term of economic and environmental friendliness. To use this concrete in actual construction, proper consistency is necessary for supporting compacting machine and minimizing compaction energy. Vebe time is used as consistency measurement due to RCC's dryness. The Vebe time ranged from thirty to seventy five seconds is considered to be appropriate consistency for RCC in pavement application. The purpose of this study is to improve consistency and working time of RCC. The workable time of reference mixture (normal RCC mixture) was found to be less than fifty minutes. Poly Naphtalene Sulfonate superplasticizer was discovered to be very effective in lowering down Vebe time and maintaining it. 0.3% of this admixture was learned to extend the working time up to four hours without influence RCC's compressive strength.

© 2017 The Authors. Published by Elsevier Ltd.

Peer-review under responsibility of the organizing committee of SCESCM 2016.

*Keywords:* Roller-compacted concrete; Consistency; Poly Naphtalene Sulfonate superplasticizer;

---

### 1. Introduction

RCC or roller-compacted concrete is a dry concrete that consists of the same components as conventional concrete with different proportioning. Its construction characteristic, however, is a little different from the later. Due

---

\* Corresponding author. Tel.: +82-33-640-2419; fax: +82-33-641-1391.

E-mail address: [swl@gwnu.ac.kr](mailto:swl@gwnu.ac.kr)

to its dryness, heavy vibratory steel drum and rubber-tired rollers are required in order to compact this concrete into its final form. Its cement content is typically lower than that of conventional concrete which can be beneficial in term of economic and environmental friendliness. With less demand of cement, its production can be reduced which lead to less CO<sub>2</sub> productivity. Moreover, due to light surface colour of RCC pavement, lighting requirements can be reduced and thus a lot of energy can be saved. In the past few decades, the use of RCC in public and private applications has been increasing steadily in low-volume roads and parking lots [1]. For instance, RCC pavement was used in Intermodal yard paving projects at the Port of Tacoma, Washington due to a substantial cost savings over conventional Portland cement concrete and asphaltic concrete pavement when used in heavy wheel load applications [2]. The railroad intermodal hub faculty for Burlington Northern at Houston, Texas, is the first heavy-duty RCC pavement constructed by the private sector in the U.S [3]. The structure was inspected several months after operation showed the structure to be functioning satisfactorily under the heavy loading and service conditions.

Appropriate consistency is very important for roller-compacted concrete workability. If the mixture is too dry, high compaction energy would be required. In contrast, if the mixture is too wet, the concrete would be disintegrated and thus the vibrating roller cannot be applied. Many researches and experiences have indicated that appropriate Vebe time for pavement application (a consistency parameter obtained from vibrating table test, [4]) is between 30 to 75 seconds. Recommended ranges of consistency in term of Vebe time measured by vibrating table test [4] from other researches are given in table 1.

Table 1. Modified Vebe time range of RCC for pavement application.

Modified Vebe time range (seconds)	References
30 to 40	[5]
30 to 40	[6]
50 to 75	[7]

Getting a good consistency to work with is important but maintaining it within the working period is even more crucial. For typical RCC, it can be only worked with within 45 minutes to 1 hour after mixing [8]. In actual construction, more time may be required to get RCC compacted due to transportation duration and limitation of compacting machine. The design mixture may not have the desired consistency by the time it is compacted even though its initial consistency (right after mixing) is satisfied. Thus, maintaining a good consistency of RCC until the compaction is finished is necessary. Extending workability of an RCC mixture can be especially beneficial during hot weather, RCC startup activities, long haul distances and placement of thick lifts. Various admixtures such as water reducer, retarder and superplasticizer have been used on RCC mixtures for reducing required water and working time extension. It was suggested by PCA [9] that dry cast surfactant can extend working time and improve the finishability of RCC. The effect of this admixture on RCC's consistency, however, was not well defined. Thus, a study on the effect of this product on RCC's consistency shall be conducted here.

## 2. Experimental program

In this research, variation of RCC's consistency due to time and usage amount of Poly Naphtalene Sulfonate superplasticizer (a dry cast surfactant product) was study. Vebe test [4] was used to measure RCC's consistency.

### 2.1. Materials

Ordinary Portland cement was used in this study. Fine aggregate was taken from Jumunjin and maximum 19 mm coarse aggregate was selected from Tanyang of South Korea. The aggregate gradation is shown in figure 1. The admixture used in this study is Poly Naphtalene Sulfonate (PNS) superplasticizer and its properties are given in table 2.

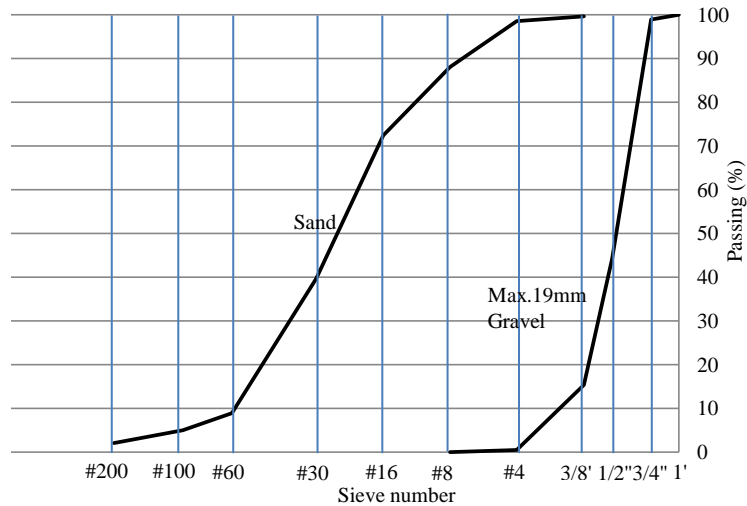


Fig. 1. Sand and gravel gradation

Table 2. Standard and inspected properties of Poly Naphtalene Sulfonate.

Modified Vebe time range (seconds)	References	
	Standard	Inspection
Appearance	Light brown powder	Light brown powder
Bulk density (kg/m <sup>3</sup> )	700±50	700
Dry loss (%)	-	-
PH	8 to 10	8.04
Solid content (%)	≥92	92.1
CI (%)	≤0.10	-
Solubility	-	-
Stability	-	-
Cement paste flow (mm)	-	-
SO <sub>4</sub> content (%)	≤3.5	2.36
HCOH (%)	≤0.10	0.014

## 2.2. Study cases

To evaluate the effect of PNS on RCC's consistency, various usage amounts of this material were applied to reference mixture in term of binder's mass percentage. RCC mixture cases in this study are given in table 3. The consistency of each case was tested at 0 to 4h after mixing.

Table 3. RCC mixture proportions for a cubic meter.

Mixture	PNS (%)	Water (kg)	Cement (kg)	Sand (kg)	Gravel (kg)
Ref	0.0	147.3	280.0	1285.0	864.0
PNS1.0	1.0	147.3	280.0	1285.0	864.0
PNS0.3	0.3	147.3	280.0	1285.0	864.0
PNS0.2	0.2	147.3	280.0	1285.0	864.0
PNS0.1	0.1	147.3	280.0	1285.0	864.0

### 3. Test results

Variation of Vebe time according to time for each studied case is given in table 4. The data from this table was used to plot Vebe time and time relationship curves in figure 2 and 3. It should be pointed out again that workable range of RCC is from 30 to 75 seconds of Vebe time. From the test result, it was found that normal RCC or reference mixture’s consistency tended to change rapidly exceeding the desirable range within less than 50 minutes (figure 2). The addition of PNS to the reference RCC mixture was tested in order to extend the working time of RCC. By maintaining the same mixture, the admixtures were simply added to the mixture according to the amount of binder (percentage of binder’s mass). From figure 3, it was found that RCC’s Vebe time tends to low down when the amount of PNS is increased. The results showed that it is possible to maintain RCC workable consistency within desirable duration by using appropriate amount of the additive (figure 3). Moreover, the replication of Vebe test on their mixtures gave more consistent result than that of the normal RCC mixture did. This signifies that this additive can control RCC’s consistency very well. 0.3% of Poly Naphtalene Sulfonate superplasticizer was learned to be an optimal usage amount which can extend working time up to 4 hours.

Table 4. Variation of Vebe time according to time for studied mixtures.

Mixture	Vebe time (seconds) at					
	0 min	30 min	60 min	120 min	180 min	240 min
Ref	62	63	75	77	105	120
PNS1.0	14	16	18	26	-	25
PNS0.3	20	41	44	51.5	70	75.5
PNS0.2	26	48	48	75	-	-
PNS0.1	35	45	44	56	120	-

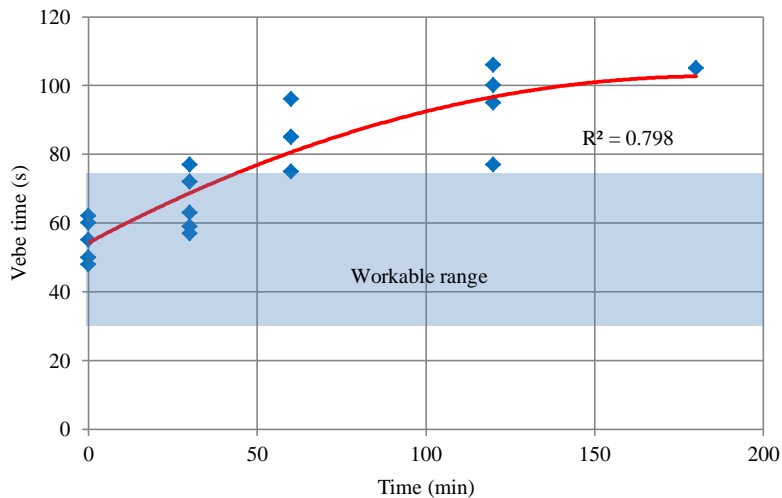


Fig. 2. Variation of Vebe time according to time for reference RCC mixture



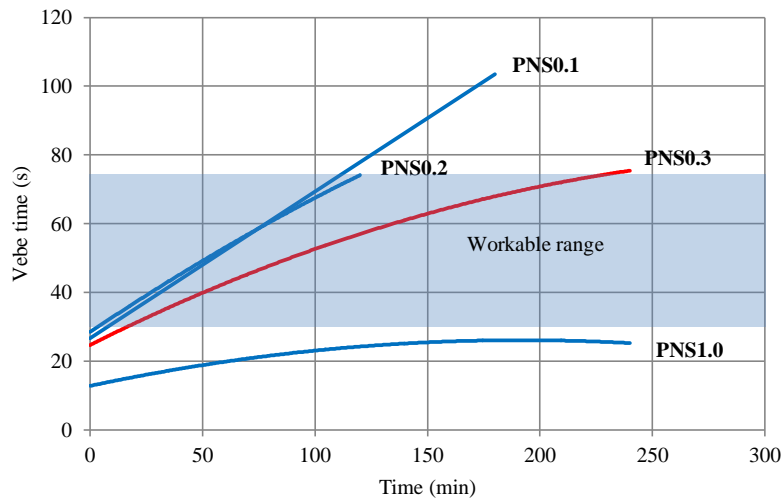


Fig. 3. Variation of Vebe time according to time for RCC mixture with 0.1-1.0% of PNS

Compressive strength of Ref and PNS0.3 were tested at 3, 7 and 28 days, and the result is shown in figure 4. The compressive strengths in both cases were found to be similar which indicated that the use of 0.3% of PNS in RCC does not significantly affect its compressive strength. Further test shall be conducted if more PNS is required.

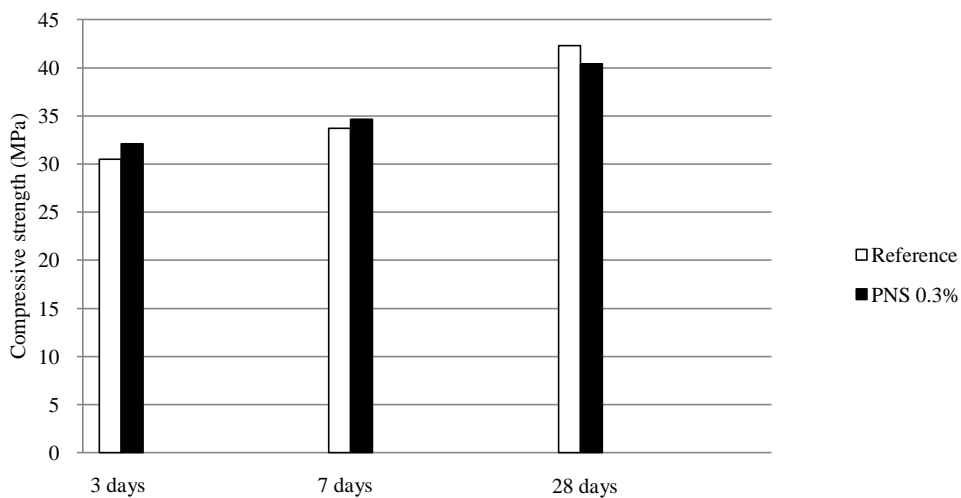


Fig. 4. Compressive strength of RCC's reference mixture and PNS0.3 mixture at 3, 7 and 28 days

## 4. Conclusion

Having an appropriate consistency during construction is very important for RCC. It was confirmed that a normal RCC mixture permits less than one hour of working time which may not be sufficient for some constructions.

However, it was found that it is possible to maintain RCC workable consistency within desirable duration by using appropriate amount of Poly Naphtalene Sulfonate superplasticizer. Moreover, the replication of Vebe test on RCC consisted of this admixture gave more consistent result than that of the normal RCC mixture did which shows that this additive can control RCC's consistency very well. 0.3% of PNS was found to be an optimum amount; it can provide up to four hours of working time without influencing compressive strength. The effect of this admixture on RCC's durability, however, shall be discussed in the next study.

## Acknowledgements

This study was conducted under research project (Development of Eco-Friendly Pavements to Minimize Greenhouse Gas Emissions) funded by the Ministry of Land, Infrastructure and Transport (MOLIT) and the Korea Agency for Infrastructure Technology Advancement (KAIA). The authors would like to thank the members of research team, MOLIT and KAIA for their guidance and supports throughout the project. (No. 15LRPB07926102)

This research was also financially supported by the Ministry of Education (MOE) and National Research Foundation of Korea (NRF) through the Human Resource Training Project for Regional Innovation (No. 2014H1C1A106708)

## References

- [1] Pittman, D.W. and G.L. Anderton. The use of roller-compacted concrete pavements in the United States. Presented at the Sixth International Conference on Maintenance and Rehabilitation of Pavements and Technological Control (MAIRE PAV 6), Torino, 2009.
- [2] Larson, J. L. Roller-Compacted Concrete Pavement Design Practices for Intermodal Freight Terminals at the Port of Tacoma. Presented at Facing the Challenge. The intermodal Terminal of the Future, New Orleans, Louisiana, 2-5 March (pp. 22-29). Washington, D.C., 1986.
- [3] Logie, C. V. and J. E. Oliverson. Burlington Northern Railroad Intermodal Hub Faculty. Concrete International, Vol. 9, No. 2, 1987, pp. 37-41.
- [4] ASTM C1170 / C1170M. Standard Test Method for Determining Consistency and Density of Roller-Compacted Concrete Using a Vibrating Table.
- [5] Abdo, M.J. et al. (1993). The use of Roller Compacted Concrete for Roads. Spain: Permanent International Association of Road Congresses.
- [6] ACI 325.10R-95. Report on Roller-Compacted Concrete Pavements.
- [7] Marchand, J., Gagne R., Ouellet E. and Lepage S. (1997). "Mixture proportioning of roller-compacted concrete: a review". ACI Special Publication, Vol. 171.
- [8] Harrington, Dale et al. (2010). Guide for Roller-Compacted Concrete Pavements. National Concrete Pavement Technology Center, Institute for Transportation, Iowa State University, Ames.
- [9] Chetan, V.Hazaree et al. (2013). Use of Chemical Admixtures in Roller-Compacted Concrete for Pavements. National Concrete Pavement Technology Center, Institute for Transportation, Iowa State University, Ames.



Sustainable Civil Engineering Structures and Construction Materials, SCESCM 2016

## Calcium Silicate Board As Wall-Facade

Luciana Kristanto<sup>a\*</sup>, Handoko Sugiharto<sup>b</sup>, Dwi Agus S.W.<sup>b</sup>, Aditya Pratama S.<sup>b</sup>

<sup>a</sup>Architecture Department Petra Christian University, Siwalankerto 121-131, Surabaya 60236, Indonesia

<sup>b</sup>Civil Engineering Department Petra Christian University, Siwalankerto 121-131, Surabaya 60236, Indonesia

---

### Abstract

Wall as spatial partition and facade of a building gives impact not only for building aesthetic, but especially for the occupant's convenience. In the preference of wall material, especially for high rise apartments, hotels or offices, its mass/m<sup>2</sup> and its noise reduction become an important criteria that must be considered by the building owner and architect in order to give a more lightweight construction and a quieter interior for occupant's convenience and privacy. In this paper, lightweight material that has been investigated is calcium silicate board, as an alternative to brick as a common wall material. The findings of this research, by flexural strength test in normal condition, are generally categorized in class 2 and 3. By soak-dry test as durability test for outside uses, there are no cracks found in all samples and the flexural strength decreases but less than 30% so that it meets the SNI 7705:2011 standard. By warm water test, this material cannot withstand against temperature at 60 degree centigrade or higher. By heat and rain test, this material can withstand the heat and rain conditions. By noise reduction as sound isolating enclosure, this material is unable to perform as a noise barrier.

© 2017 The Authors. Published by Elsevier Ltd.

Peer-review under responsibility of the organizing committee of SCESCM 2016.

*Keywords:* calcium silicate board; durability; flexural strength; noise reduction

---

\* Corresponding author. Tel.: +62312983375; fax: +62318417658.

*E-mail address:* lucky@petra.ac.id

## 1. Overview

Construction development nowadays is supported by the newest invention in building materials. A more lightweight, more sustainable and easier installation material is being considered in material preferences. In the preference of wall material, especially for high rise apartments, hotels or offices, its weight (mass/m<sup>2</sup>) and its noise reduction become an important criteria that must be considered by the building owner and architect in order to give a more lightweight construction and a quieter interior for occupant's convenience and privacy. Such preference of lightweight wall material, being researched here is calcium silicate board.

## 2. Calcium silicate board in building construction

Calcium silicate board mainly consists of inorganic material such as silica sand, Portland cement, cellulose and water. It is widely used as an alternative to gypsum and asbestos cement board that have some disadvantages. Asbestos cement board gives a bad influence to building occupants health, while the gypsum board will dissolve in the water so that it can not be used on the building exterior.

Formerly calcium silicate board was used for indoor partition and ceiling, but later it is widely used for wall facade as it is waterproof, lightweight, has a wide dimension and is easy to install; even it is the solution for a sloping and bending opaque wall surfaces. That is why it has the advantage compared to the brickwall and lightweight concrete. Compared to lightweight concrete, it has the same drywall construction, but at a lower cost.

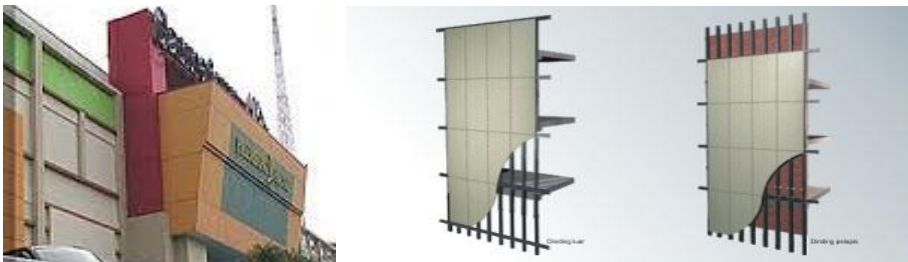


Fig. 1. Calcium silicate board uses as façade and room partition

Besides its advantages, some of the disadvantages are the high installation cost compared to gypsum and asbestos; and it has limitation in its rain, heat and fire resistance. That is why some modification are needed.

A research in cold-formed steel wall frame with calcium silicate board sheathing conducted by Lin, Pan and Hsu [1] noted that the crack happened mostly at the bottom of the track of wall specimen. That is why modification of the wall with calcium silicate board sheathing is needed. Wang, Chuang and Lin [2] studied the performance of calcium silicate partition fireproof drywall assembly with a junction box and found that the quality of the calcium silicate board plays a big role in the fireproof effectiveness. Different composition may impact the heat and fire resistance of this material. The poorer formula it has, such as substitution of cement with the coal ash to reduce the production cost; the poorer its fire-proofing will be. Since this material needs modification in its application in many kinds of performances, this paper aims to find its capability as facade material by flexural strength test, warm water test, soak-dry test, heat-rain test in tropical climate as well as the sound reduction test.

The warm water test was needed to know its flexural strength due to increase in temperature, compared to normal condition. The soak-dry test was done to get known the flexural strength after soaking in the water and dried while the heat-rain test was conducted to find its durability against the rain and the heat of the sun. The sound reduction test was conducted to find its noise reduction as sound isolating enclosure. The samples were taken from 2 different kinds of thickness and 4 brand products in Indonesia for each thickness ; the 6mm was used for outside ceiling, while the 8 mm thickness was used for outside wall or facade.

### 3. Flexural strength of calcium silicate board

According to SNI (Indonesian National Standard) 7705:2011[3] the flexural strength standard of calcium silicate board is as follows:

Table 1. Calcium Silicate Board Standard Flexural Strength (SNI 7705:2011)

Class	Category	
	A	B
Class 1	4	4
Class 2	7	7
Class 3	13	10
Class 4	18	16
Class 5	24	22

Note: A category for saturated condition of outside uses; B for inside uses  
Flexural strength in M Pa; 1 M Pa = 10.03735 kg/cm<sup>2</sup>

Table 2 shows the quality standard of Calcium silicate board according to SNI 7005:2011 [3]

Table 2. Quality standard of Calcium Silicate Board (SNI 7705:2011)

No	Item	Unit	Quality standard
1	Flexural strength	M Pa	See Table 1
2	Density	g/cm <sup>3</sup>	≥0.8
3	Water resistance	-	No leakage
4	Warm-water resistance	-	Li of average ratio $r \geq 0.7$ ; no cracks
5	Soak-dry resistance	-	Li of average ratio $r \geq 0.7$ ; no cracks
6	Heat-rain resistance	-	SNI 03-1027-2006 [4]
7	Noise reduction	decibel	See Table 3

#### 3.1. Flexural strength test

Flexural strength test was conducted by proving ring machine that gave loading in 1000 grams per second until the sample put along its transverse fiber was broken.



Fig. 2. Flexural strength test with proving ring machine

#### 3.2. Warm water test

To get the flexural strength of warm water, the sample was soaked in water with the temperature of 60 degrees centigrade for 24 hours. After that, the flexural strength test was conducted with proving ring machine.



Fig. 3. Warm water test

### 3.3. Soak-dry test

Soak-dry test was conducted to the sample until 10 cycles to sample where one cycle consisted of soaking the sample in 5 degree centigrade room temperature for 2 hours and drying it by heating it to 60 degree centigrade for 2 hours. After settling for 24 hours then the flexural strength was conducted.



Fig.4. Soak-dry test

### 3.4. Heat-rain test

Heat-rain test was conducted to the sample until 10 cycles where one cycle consisted of spraying it with 2.5 liter/minute water for 2 hours, and after settling for 10 minutes, the sample was heated to 33 degree centigrade for two hours. After 10 minutes being settled, then the sample was checked whether there was any seepage water.



Fig. 5. Heat-rain test

## 4. NoiseReduction of Calcium Silicate Board

### 4.1. Sound and Noise

Sound emerges from a sound source, and transmits in air as the medium to the ear as the receiver. Noise is defined as a sound, especially one that is loud or unpleasant or that causes disturbance. ([www.oxforddictionaries.com/definition/./noise](http://www.oxforddictionaries.com/definition/./noise)) For any person, noise is subjective; but there is some sound that makes noise for any person such as a sudden high sound level, a loud and continuous sound like the rock music, the engine planting, and the sound of vehicles as well [5]. In terminology, noise can be distinguished into background noise, noise, and ambient noise. Background noise is the sound around us that appears regularly and stable at a certain level, usually lower than 40 deciBel. Noise is a sudden sound with the degree of hardness exceeds the background noise in the area. Meanwhile, ambient noise is the combination of background noise and noise. Noise disturbance is determined by the sound level (in deciBel) and the sound frequency (in Hz). Both factors are considered in the Noise Criteria that determine the level of sound comfort in a particular room[5].

### 4.2. Noise reduction (NR) test

The NR between rooms is simply the arithmetical difference in room intensity levels. It means the noise in the source room at an intensity level of IL1 is less than the transmitted noise in the receiving room at a reduced intensity level of IL2[6]. Table 3 shows standard for noise reduction in SNI 7705:2011.

Table 3. Standard of Sound Reduction Index of Calcium silicate board (SNI 7705:2011)

No	Sample thickness(mm)	SRI (dB) density $0.8 \leq D < 1.25 \text{ gram/cm}^3$	SRI (dB) density $1.25 \leq D < 1.35 \text{ gram/cm}^3$	SRI (dB) density $D \geq 1.35 \text{ gram/cm}^3$
1	$\leq 5$	19	23	25
2	5 s.d. 10	21	25	27
3	> 10 s.d. 15	24	28	31
4	>15 s.d. 20	27	32	35
5	>20	31	37	41

This research, because of the limitations of the reverberation room, adopted here the ASTM E 596-96 “Laboratory Measurement of the Noise Reduction of Sound-Isolating Enclosures” [7]. By using this method, the noise reduction of the sound isolating of the wall materials tested can be obtained.

According to ASTM, the effective reverberation room volume should not be less than  $200 \text{ m}^3$ . The reverberation chamber in this research was only  $53.4 \text{ m}^3$  volume. However, if the point requirement 9.1.2 and 9.5 of the standard are satisfied, room volume is not critical. The 9.1.2 requires that the enclosure is at least one-half wavelength away from the reverberation walls and ceiling and any diffusing surfaces at the center frequency of the lowest one-third octave band in which the noise reduction is to be measured. The wavelength of the 125 Hz as the lowest frequency here is 2.72 m, so the one-half wavelength must be 1.36 m.

The 9.5 requires that microphone positions shall be at least one-half wavelength away from any solid surface of the test frequency; thus it is in the same distance, 1.36 m. From the layout and section in the Figure 6, it will be found that both requirement are fulfilled. To maintain its validity, we refer to Section 11 of the standard that the room has to fulfill sound diffusion condition and the measurement result reaches 95% confidence to within 1 dB at all test frequencies, except the lowest, should be in 95% confidence to within 2 dB. To make sure that the reverberation chamber is diffuse, the preliminary measurement has been done. After doing some adjustment so that the diffusion in all points reach the 95%, the reverberation chamber is ready to be used.

The noise reduction was measured with 2 microphones that has been calibrated. The first was put at the sound source area and the second one was put inside the enclosure. Then, the result was read on each sound level meter. To get the NR, the calculation was taken by using this formula:

$$NR = L_1 - L_2 \tag{1}$$



Fig.6. Noise reduction test

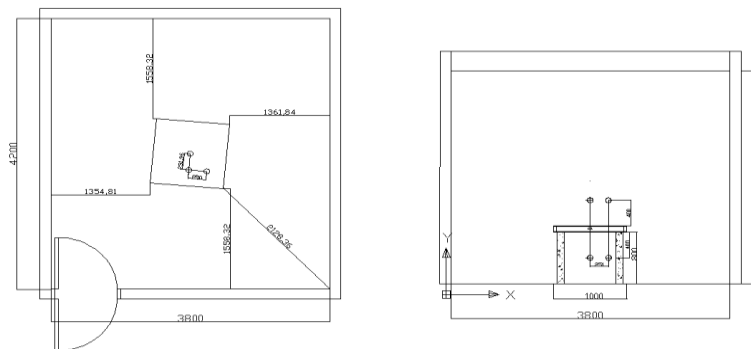


Fig.7. Reverberation room layout and section (length 4.26m x width 3.80m; height 3.30m)



## 5. Results and Discussions

### 5.1. Flexural strength test

Table 4. Flexural strength result and class summary

No	Code	Load (kg)	Moment (kg.cm)	Flexural strength (M Pa)	Class Category	Average Flexural strength (M Pa)	Class summary
1	S 6 I	27.58	148.23	11.00	Class 2	13.95	Class 3
2	S 6 II	41.37	222.35	16.89	Class 3		
3	K 6 I	34.47	185.29	9.61	Class 2	10.47	Class 2
4	K 6 II	38.61	207.53	11.33	Class 2		
5	N 6 I	48.26	259.41	14.99	Class 3	15.07	Class 3
6	N 6 II	42.75	229.76	15.15	Class 3		
7	G 6 I	44.13	237.17	17.04	Class 3	18.01	Class 4
8	G 6 II	49.64	266.82	18.98	Class 4		
9	K 8 I	41.37	222.35	8.68	Class 2	8.76	Class 2
10	K 8 II	44.13	237.17	8.85	Class 2		
11	N 8 I	121.35	652.23	21.57	Class 4	20.76	Class 4
12	N 8 II	113.07	607.76	19.95	Class 4		
13	S8 I	68.95	370.58	11.18	Class 2	12.76	Class 2
14	S8 II	89.63	481.76	14.34	Class 3		
15	G8 I	82.74	444.70	15.98	Class 3	15.34	Class 3
16	G8 II	75.84	407.64	14.70	Class 3		

The results show that the average flexural strength of the sample was 14.39 M Pa. In average, the flexural strength of the sample were categorized in class 2 and class 3; except the G6 and N8 were categorized in class 4.

Table 5. Warm-water test result

No	Code	Load (kg)	Moment (kg.cm)	Flexural strength (M Pa)	Class category	Ratio	Warm water test	SNI requirement
1	G6	48.26	259.41	16.76	Class 3	0.93	No crack	Passed
2	G8	55.16	296.47	10.22	Class 2	0.67	No crack	Failed
3	K6	26.20	140.82	7.79	Class 2	0.74	No crack	Passed
4	K8	34.47	185.29	6.63	Class 1	0.76	No crack	Passed
5	N6	39.99	214.94	12.73	Class 2	0.84	No crack	Passed
6	N8	57.91	311.29	10.62	Class 2	0.51	No crack	Failed
7	S6	28.96	155.65	12.21	Class 2	0.88	No crack	Passed
8	S8	71.70	385.41	11.88	Class 2	0.93	No crack	Passed

From table 5, it was found that the flexural strength of all samples decreased compared to its normal condition. After 24 hours warm water treatment, no crack was found in all samples; but after the flexural strength test was conducted, it was found that there were sample that could not pass the requirement of SNI ratio has to be  $\geq 0.7$ . The samples with a ratio of flexural strength lower than 0.7 were the G8 and N8. This meant that calcium silicate board could not stand well against hot temperature at 60 degree centigrade or higher.

Table 6. Soak-dry test result

No	Code	Load (kg)	Moment (kg.cm)	Flexural strength (MPa)	Class Category	Ratio	Soak-dry test	SNI requirement
1	G6	34.473	185.29	12.74	Class 2	0.71	No crack	Passed
2	G8	71.704	385.41	14.18	Class 3	0.92	No crack	Passed
3	K6	41.368	222.35	12.62	Class 2	1.21	No crack	Passed
4	K8	55.157	296.47	10.91	Class 2	1.25	No crack	Passed
5	N6	44.125	237.17	14.37	Class 3	0.95	No crack	Passed
6	N8	96.524	518.82	18.20	Class 4	0.88	No crack	Passed
7	S6	39.989	214.94	17.09	Class 3	1.23	No crack	Passed
8	S8	62.051	333.53	9.68	Class 2	0.76	No crack	Passed

From the soak-dry test, it was found that all samples passed the SNI 7705:2011 requirement that the ratio of the flexural strength compared to the normal condition should be  $\geq 0.7$ . There were no cracks found in all samples as well. This meant that calcium silicate board withstood against the soak-dry condition.

Table 7. Heat-rain test result

No	Code	Heat-rain test	Crack length (mm)
1	G6	No crack	---
2	G8	No crack	---
3	K6	No crack	---
4	K8	No crack	---
5	N6	No crack	---
6	N8	No crack	---
7	S6	No crack	---
8	S8	No crack	---

SNI 7705:2011 requirement for heat and rain conditions that any cracks should be less than 50 mm were fulfilled by all samples. From the heat-rain test, no cracks were found in all samples. This meant that calcium silicate board withstood against the heat-rain condition.

Noise reduction of calcium silicate board as sound isolating enclosure measured in deciBel (dB) was taken in low to high frequency: 125 Hz, 250 Hz, 500 Hz, 1kHz, 2kHz and 4 kHz. Table 8 shows the result.

From the noise reduction test result, it was found that all samples could not fulfill the SNI 7705:2011 standard. However, from the result we can find that calcium silicate board as sound isolating enclosure can reduce better the low frequency especially at 125 Hz and 250 Hz than sound with high frequency.

Because the result was not satisfying, a modification has been done to get a better noise reduction by inserting some types of local sand into the frame of the enclosure in order to increase its mass/kg. By this insertion, the mass increased from 25.4 kg/m<sup>2</sup> to 62–65.9 kg/m<sup>2</sup>. The result shows in Figure 8 that as long as the mass increases, the noise reduction increases as well. But the best frequency of noise reduction was the 125 Hz and 250 Hz, that increased 120-410% its noise reduction; while the 4 kHz increased only 10-27%. From the result, it was found that all samples could not reduce noise required by SNI standard.

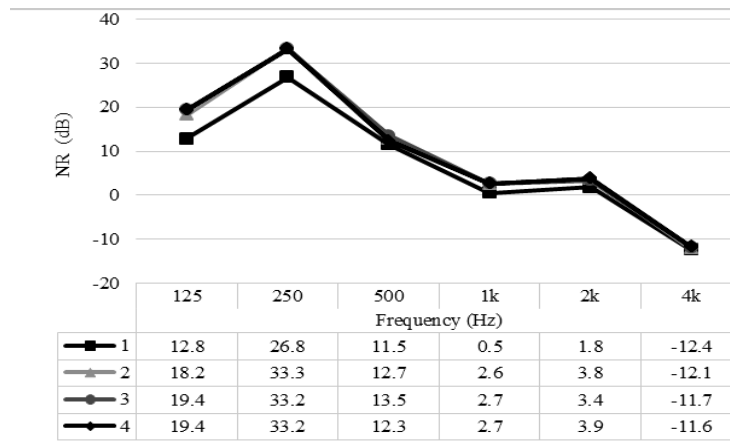


Fig.8. Increases of noise reduction with sand insertion

Table 8. Noise Reduction test result

No	Code	Frequency (Hz)	NR			Average NR	Density (g/m <sup>3</sup> )	Mass (kg/m <sup>2</sup> )
			1	2	3			
1	G6	125	14.3	12.9	11.1	12,8	1,645	9,56
		250	34.6	33.2	32.7	33,5		
		500	11.5	10.5	10	10,7		
		1K	1.2	0.2	0.2	0,5		
		2K	3.3	2.8	2.8	3,0		
		4K	-9.8	-8.4	-9.1	-9,1		
2	K6	125	13.3	12.8	12.5	12,9	1,267	8,54
		250	31.4	34.2	34.6	33,4		
		500	11.8	13.7	13.4	13,0		
		1K	3.5	3.5	4.1	3,7		
		2K	5.4	6.5	6.5	6,1		
		4K	-8.8	-7.1	-7.9	-7,9		
3	N6	125	16,3	14,4	5,4	12,0	1,242	7,78
		250	34,0	31,2	31,7	32,3		
		500	13,4	14,4	14,9	14,2		
		1K	3,1	3,6	3,2	3,3		
		2K	5,8	5,6	5,2	5,5		
		4K	-8,2	-7,9	-8,5	-8,2		
4	S6	125	13,5	12,6	12,4	12,8	1,276	7,28
		250	33,8	33,5	31,8	33,0		
		500	8,8	8,6	9,2	8,9		
		1K	-0,4	-0,7	-1,6	-0,9		
		2K	2,4	1,3	2,0	1,9		
		4K	-10,1	-9,8	-10,0	-10,0		
5	G8	125	16,7	16,7	15,5	16,3	1,554	12,78
		250	33,9	34,5	33,0	33,8		
		500	15,4	15,2	14,3	15,0		
		1K	3,2	2,6	2,0	2,6		
		2K	4,7	4,2	4,5	4,5		
		4K	-8,2	-8,7	-8,9	-8,6		
6	K8	125	15,5	15,3	13,7	14,8	1,334	10,64
		250	33,8	32,2	32,0	32,7		
		500	16,0	16,7	13,6	15,4		
		1K	3,9	4,0	2,4	3,4		
		2K	7,1	6,8	7,1	7,0		
		4K	-7,8	-8,1	-7,6	-7,8		
7	N8	125	18,0	13,7	16,3	16,0	1,390	11,89
		250	35,2	33,8	33,8	34,3		
		500	14,4	13,7	14,5	14,2		
		1K	4,0	4,5	4,4	4,3		
		2K	5,5	5,4	5,2	5,4		
		4K	-8,2	-8,8	-8,5	-8,5		
8	S8	125	16,4	16,8	14,5	15,9	1,418	12,77
		250	35,1	32,2	33,0	33,4		
		500	13,2	11,6	12,8	12,5		
		1K	3,3	1,9	1,9	2,4		
		2K	4,3	4,6	3,8	4,2		
		4K	-9,4	-8,4	-8,6	-8,8		

## 6. Conclusion

By the test of its strength, durability and noise reduction according to Indonesian National Standard (SNI) 7705:2011, it can be concluded that:

- By flexural strength test in normal condition, the 6 mm and 8 mm thickness were generally categorized in class 2 and 3; only one sample in each thickness was categorized class 4 (G6 and N8 samples).
- By soak-dry test as durability test for outside uses, there were no cracks found in all samples. The flexural strength decreased but less than 30%. Thus, it met the standard.
- By warm water test, no cracks were found in all samples. For 6 mm thickness, all samples met the standard; however, for 8 mm thickness there were two samples that decreased strength  $> 30\%$ , so they could not pass the standard (G8 and N8). It means this material can not withstand against temperature at 60 degree centigrade or higher.
- By heat and rain test, no crack was found in all samples. Thus, this means that this material can withstand the heat and rain conditions.
- By noise reduction as sound isolating enclosure, all samples could not fulfil the SNI standard. By sand insertion to increase its masses, this standard could not be fulfilled as well. It means this material is unable to perform as a noise barrier.

From the result above, the calcium silicate board can be recommended as building facade or outside ceiling as long as the building surface is not exposed to heat and hot water exceeding 60 degree centigrade and the sound performance is not crucial since this material can not perform well as a noise barrier.

## References

- [1] S.H. Lin, C.L. Pan, W.T.Hsu, Monotonic and cyclic loading tests for cold-formed steel wall frames sheathed with calcium silicate board, Elsevier Thin-Walled Structures 74 (2014) 49-58.
- [2] Y.Wang, Y.J. Chuang, C.Y. Lin, The performance of calcium silicate board partition fireproof drywall assembly with junction box under fire, Advances in Materials Science and Engineering ID 642061 (2015) 1-12.
- [3] Badan Standarisasi Nasional, SNI 7705:2011 Lembaran Rata Kalsium Silikat, Departemen Pekerjaan Umum, Jakarta, 2011.
- [4] Badan Standarisasi Nasional, SNI 03-1027-2006 Lembaran Serat Krisotil Semen Rata, Departemen Pekerjaan Umum, Jakarta, 2006.
- [5] C.E. Mediastika, Akustika Bangunan: Prinsip-prinsip dan Penerapannya di Indonesia, Erlangga, Jakarta, 2005.
- [6] M.D. Egan, Concepts in Architectural Acoustics, McGraw-Hill, Inc., 1972.
- [7] American Society for Testing and Materials, ASTM E 596-96 Laboratory Measurement of The Noise Reduction of Sound-isolating Enclosures, 2009.



Sustainable Civil Engineering Structures and Construction Materials, SCESCM 2016

## Compressive strength of mortar containing ferronickel slag as replacement of natural sand

Ashish Kumer Saha<sup>a\*</sup>, Prabir Kumar Sarker<sup>a</sup>

<sup>a</sup>*Department of Civil Engineering, Curtin University, GPO Box U1987, Perth, WA 6845, Australia*

---

### Abstract

Uses of various industrial by-products have been extensively studied in the past few decades in order to enhance the sustainability of construction industry. By-products can be used as alternatives to binders as well as aggregates in concrete. A large quantity of granulated ferronickel slag (FNS) is produced as a by-product in the smelting of nickel ore. This paper presents the effects of using ferronickel slag as a replacement of natural sand in cement mortar. The slag was produced by sea water-cooling of the by-product from the smelting of garnierite nickel ore. The grain size distribution of the slag was found suitable for using as fine aggregate in concrete. It was found that flow of fresh mortar increased with the increase of FNS up to 50% replacement of sand and then declined with further increase of FNS. The compressive strength of the hardened mortar specimens increased with the increase of FNS up to 50% and then declined with further increase of FNS. Use of fly ash as 30% cement replacement together with FNS as replacement of sand increased the flow of fresh mortar and decreased the strength of hardened specimens.

© 2017 The Authors. Published by Elsevier Ltd.

Peer-review under [responsibility](#) of the organizing committee of SCESCM 2016.

*Keywords:* Ferronickel slag; fly ash; compressive strength; flow value; mortar.

---

### 1. Introduction

Construction works require a significant amount of earth's natural resources. Sand has been used as a fine aggregate in concrete for decades. The demand for concrete is increasing with the growth in both developed and developing countries. However, our natural resources are limited, and sand is not extensively available in every country. Therefore, use of industrial by-products as aggregate can help solve this scarcity of natural sand and reduce

---

\* Corresponding author. Tel.: +0-000-000-0000 ; fax: +0-000-000-0000 .

*E-mail address:* [author@institute.xxx](mailto:author@institute.xxx)

the disposal cost of these by-products. Moreover, the production cost of concrete may also reduce, which will have a positive impact on the economic growth of the society.

In search of suitable alternatives to natural sand, research is being conducted on different types of industrial by-products, for instance, steel slag, blast furnace slag, copper slag and FNS. Aggregates constitute almost 70% to 80% of the volume of concrete. As a result, aggregates affect the fresh and hardened properties of concrete to a great extent. For example, steel slag aggregate was shown suitable for producing high strength concrete [1, 2, 3]. Furthermore, steel slag aggregate also performed better than the natural aggregate to produce hot mix asphalt concrete [4]. However, blast furnace slag as a replacement of fine aggregate showed poor strength performance in concrete [5] though, ground granulated blast furnace slag and fly ash are usually found effective in improvement of the durability properties [6, 7]. The strength properties of mortar and concrete are influenced by the density, gradation and particle shape of aggregates used in the mix [5, 8]. Granulated FNS showed higher density and lower water absorption compared to natural sand [10, 11]. The fresh concrete properties were also influenced by ferronickel slag. Concrete bleeding was shown to increase with an increment of ferronickel slag in concrete [12]. Compressive strength was found to increase by the replacement of sand by FNS [12]. However, there is a difference in opinion among the researchers. Sakoi et al. [11] pointed out that compressive strength remained same regardless the presence of FNS. Using industrial waste in construction works may impose a threat of leaching out of heavy metals and pollute the environment. However, FNS was found to be safe to use in land reclamation works as well as in construction works [13].

The properties of the ferronickel slag largely depend on the source of ore as well as the smelting process. No literature is available on the use of this particular slag as a fine aggregate. The slag used in this study was produced by sea water-cooling of the by-product from the smelting of garnierite nickel ore. The aim of the present study is to determine the workability and strength of cement mortar containing FNS in different percentages of the fine aggregate. Furthermore, the effects of fly ash on the workability and strength of mortar are evaluated. A concurrent study is being conducted on using the ground FNS as a supplementary binder in concrete [14].

## 2. Materials and Methods

Ordinary portland cement (OPC), class F fly ash, FNS and natural sand were used in this study. Density and fineness modulus were determined for both natural sand and FNS. The FNS ( $2.78 \text{ kg/m}^3$ ) had a higher density compared to sand ( $2.16 \text{ kg/m}^3$ ). Furthermore, the fineness modulus of FNS (4.07) was higher than that of sand (1.95). The FNS particles are angular in shape and coarser than sand in size. The gradations of natural sand, FNS and their combinations in different percentages are plotted in Figure 1. It can be seen that the grain size distribution becomes well-graded when the two aggregates are combined together. The best-graded combination is obtained for 50% replacement of sand by FNS.

Ten different mixtures were prepared in this study. In Series A, only OPC was used as the binder and sand was replaced in five different proportions (0%, 25%, 50%, 75% and 100%) with FNS. In series B, fly ash was used as 30% replacement of cement. Same combinations of the fine aggregates as in Series A were used in the mixtures of Series B. The water to cement ratio was kept constant at 0.47 for all the mixes. The reason for selecting 30% replacement of OPC with a class F fly ash was that it can reduce the  $\text{CO}_2$  emission to a considerable extent [15]. The mixture proportions are given in Table 1.

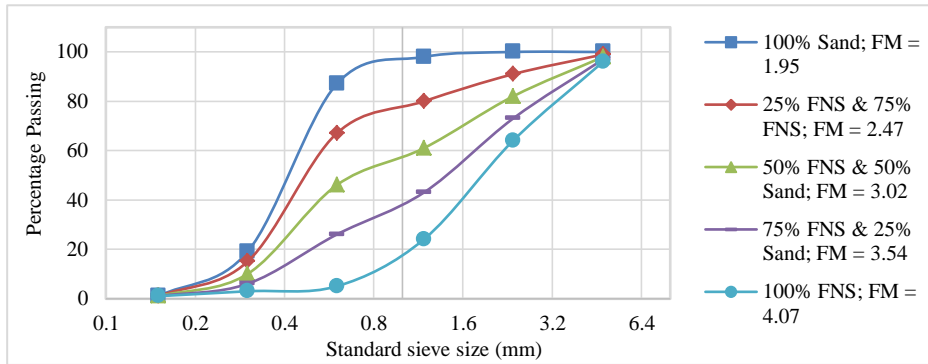


Fig. 1. Gradation of fine aggregates

Table 1. Mix proportions of concrete

Series	Sample ID	Binder (Kg/m <sup>3</sup> )		Fine aggregate (Kg/m <sup>3</sup> )		W/C
		OPC	FA	Sand	FNS	
A	A1	602	0	1355	0	0.47
	A2	602	0	1015	338	
	A3	602	0	678	678	
	A4	602	0	338	1015	
	A5	602	0	0	1355	
B	B1	421	181	1355	0	0.47
	B2	421	181	1015	338	
	B3	421	181	678	678	
	B4	421	181	338	1015	
	B5	421	181	0	1355	

Flow test was conducted to determine the workability of the freshly mixed mortar. The flow table with the mortar was dropped 25 times in 15 seconds after removing the mould. The percentage of the final diameter of the spread after the drops to the original diameter is used as the flow value of the mortar. Figure 2 shows the flow value measurements of the mixes. Mortar cubes (50 mm) were cast for compressive strength tests. The samples were left in the mould for one day and then stripped from the moulds. The samples were then cured in a water tank in fully submerged condition. The compressive strength of mortar was determined at 3, 7, 28 and 56 days after casting.



Fig. 2. Flow test (a) 100% sand; (b) 50% FNS and 50% sand (c) 100% FNS



### 3. Results and discussion

#### 3.1 Workability of mortar

The flow value was used to determine the workability of the mortar mixes. Figure 3 shows the plot of flow value with the FNS content. From the plot, it can be seen that the flow of mortar increased with the increase of FNS. However, the flow declined for replacement of sand by FNS beyond 50%. The particle shape of sand is a round; on the other hand, particle shape of FNS used in this experiment is angular. Since FNS particles are coarser than sand particles, less water is required to wet the FNS particles [16]. Moreover, Workability of mortar largely depends on the gradation of fine aggregates in the mix [17]. Since the 50% sand replacement resulted in the well-graded aggregate combination, this also showed the highest flow value of the mortar. The flow declined by FNS content of more than 50% because of the increase of angular particles in the mixture. Furthermore, fly ash has a positive effect on the workability of the mix. Fly ash blended mixes exhibited higher flow value than the OPC-only mixes. This is because of the well-known ball bearing effect of the fly ash particles.

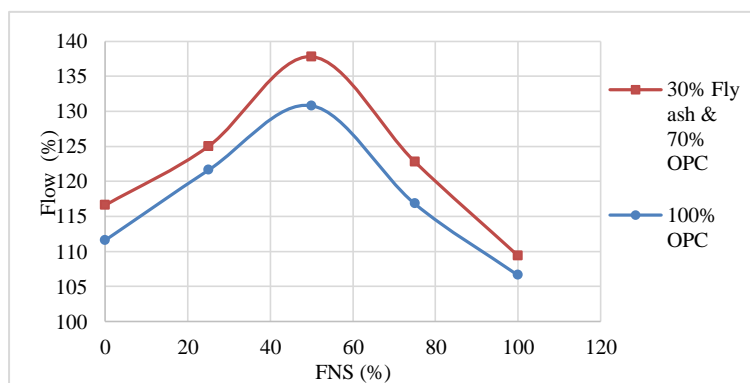


Fig. 3. Flow value of mortar mixes

#### 3.2 Compressive Strength

The samples were dried in air before testing for the compressive strength. The compressive strength results for series A are given in Figure 4. It can be observed from the figure that compressive strength increased with the increase of FNS content up to 50% replacement level and then it declined with further increase of FNS. The similar phenomenon was observed at the ages of 3, 7, 28 and 56 days. The maximum 28-day compressive strength of 57 MPa was achieved for 50% FNS (Mix A3). The 28-day compressive strength of the samples with no FNS was 38 MPa. Therefore, 50% FNS resulted in about 50% increase of the 28-day compressive strength. Moreover, the compressive strength of samples containing 100% FNS (Mix A5) aggregate is 44 MPa, which is higher than that of the control sample.

The compressive strength results of the mixtures containing 30% fly ash as cement replacement are presented in Figure 5. It can be seen that compressive strength increased with the increase of FNS content up to 50% and then declined with further increase of FNS. The similar trend is observed at 3, 7, 28 and 56 days of age. Maximum 28-day compressive strength was 35 MPa for 50% FNS content. As expected, the compressive strength of the specimens of this series was less than the corresponding mixtures of series A because of the use of 30% fly ash as cement replacement.

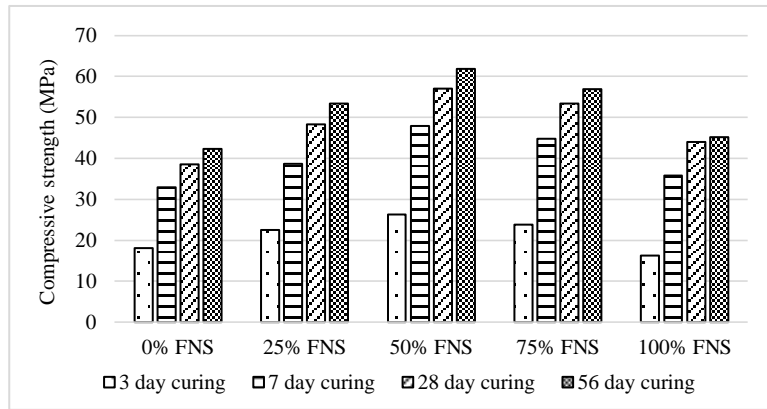


Fig. 4. Compressive strength of the mixtures with 100% OPC (Series A)

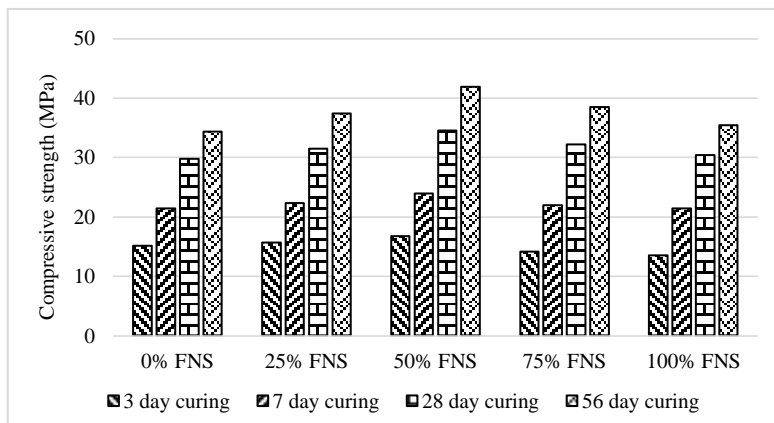


Fig. 5 Compressive strength of the mixtures with 30% fly ash and 70% OPC (series B)

Figure 6 exhibits the effect of 30% fly ash on the strength development of the mixtures containing 50% FNS. It can be seen that the strength development is slowed down by the fly ash from the early ages. However, the difference between the strengths at early ages is reduced by the pozzolanic reaction of fly ash with the increase of age.

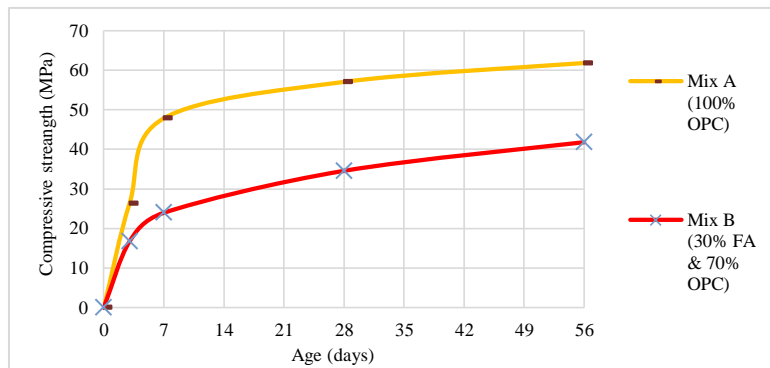


Fig. 6 Effect of fly ash on compressive strength development (50% FNS as aggregate)

From the above discussion, it is observed that FNS can improve the compressive strength considerably upto 50% replacement of sand. This is attributed to the particle packing effect of the well-graded aggregates for 50% replacement of sand by the FNS.

#### 4. Conclusion

The workability and compressive strength of cement mortars containing different percentages of FNS as replacement of natural sand were evaluated. The results show that the optimum level of sand replacement by FNS is 50% for maximizing the compressive strength of mortar. This is because of the best particle packing achieved by the well-graded aggregates at this combination. Furthermore, 50% FNS also resulted in improved the workability of the mortar mix as determined by the flow test. The increase of flow by FNS is attributed to its relatively larger size compared to natural sand. Use of a class F fly ash as 30% replacement of cement improved the workability of the mixture because of the ball bearing effect. Fly ash decreased compressive strength of the mortars with and without FNS at both early and late ages up to 56 days.

#### Acknowledgements

This research was funded and supported by SLN, New Caledonia. The authors gratefully acknowledge the contribution and continuous support from SLN through its research department and its consultant, Mr. D.J. Sassoon Gubbay.

#### References

- [1] J. A. Polanco, J. M. Manso, J. Setién, and J.J. Gonzalez. "Strength and durability of concrete made with electric steelmaking slag." *ACI Materials Journal* 108, no. 2 (2011): 196-203.
- [2] L. Dongxue, F. Xinhua, W. Xuequan, and T. Mingshu. "Durability Study of steel slag cement." *Cement and Concrete Research* 27, no. 7 (1997): 983-987.
- [3] M. Maslehuddin, A.M. Sharif, M. Shameem, M. Ibrahim, and M. S. Barry. "Comparison of properties of steel slag and crushed limestone aggregate concretes." *Construction and building materials* 17, no. 2 (2003): 105-112.
- [4] P. Ahmedzade, and B. Sengoz. "Evaluation of steel slag coarse aggregate in hot mix asphalt concrete." *Journal of Hazardous Materials* 165, no. 1 (2009): 300-305.
- [5] I. Yüksel, Ö. Özkan, and T. Bilir. "Use of granulated blast-furnace slag in concrete as fine aggregate." *ACI Materials Journal* 103, no. 3 (2006): 203-208.
- [6] G. Li, and X. Zhao. "Properties of concrete incorporating fly ash and ground granulated blast-furnace slag." *Cement and Concrete Composites* 25, no. 3 (2003): 293-299.
- [7] I. Yüksel, T. Bilir, and Ö. Özkan. "Durability of concrete incorporating non-ground blast furnace slag and bottom ash as fine aggregate." *Building and Environment* 42, no. 7 (2007): 2651-2659.
- [8] A.I. Al-Negheimish, F.H. Al-Sugair, and R.Z. Al-Zaid. "Utilization of local steel making slag in concrete." *J King Saud Univ Eng Sci* 9, no. 1 (1997): 39-55.
- [9] E. Güneyisi, & M. Gesoğlu, (2008). A study on durability properties of high-performance concretes incorporating high replacement levels of slag. *Materials and Structures*, 41(3), 479-493.
- [10] T. Sato, K. Watanabe, A. Ota, M. Aba, and Y. Sakoi. "Influence of Excessive Bleeding on Frost Susceptibility of Concrete Incorporating Ferronickel Slag as Aggregates." In 36th Conference on Our World in Concrete & Structures. 2011.
- [11] Y. Sakoi, M. Aba, Y. Tsukinaga, and S. Nagataki. "Properties of Concrete used in Ferronickel Slag Aggregate." In Proceedings of the 3rd International Conference on Sustainable Construction Materials and Technologies, Tokyo, Japan, pp. 1-6. 2013.
- [12] K. Kokubu and M. Shoya, Guidelines for construction using Ferronickel slag fine aggregate concrete, Concrete library of JSCE No. 24, December 1994.
- [13] S.S. Kang, K. Park, and D. Kim. "Potential Soil Contamination in Areas Where Ferronickel Slag Is Used for Reclamation Work." *Materials* 7, no. 10 (2014): 7157-7172.
- [14] M.A. Rahman, and P. Sarker, and F. Shaikh, 2015. Fresh and Early-Age Properties of Cement Pastes and Mortars Blended with Nickel Slag, in J. Sanjayan and K. Sago-Crentsil (ed), 27th Biennial National Conference of the Concrete Institute of Australia in conjunction with the 69th RILEM Week, Aug 30 2015. Melbourne, Australia: Concrete Institute of Australia.
- [15] P. Nath, and P.K. Sarker, "Effect of mixture proportions on the drying shrinkage and permeation properties of high strength concrete containing class F fly ash." *KSCE Journal of Civil Engineering* 17, no. 6 (2013): 1437-1445.
- [16] J.C. Santamarina, "Flow test evaluation." (2008) retrieved from "[https://smartech.gatech.edu/bitstream/handle/1853/23048/e-20-k79\\_9124.pdf](https://smartech.gatech.edu/bitstream/handle/1853/23048/e-20-k79_9124.pdf)"
- [17] J. Hu, and K. Wang. "Effects of aggregate on flow properties of mortar." In Proceeding of the Mid-Continent Transportation Research Symposium, p. 8. 2005.



Sustainable Civil Engineering Structures and Construction Materials, SCESCM 2016

# The effect of seawater curing to the correlation between split tensile strength and modulus of rupture in high strength concrete incorporating rice husk ash

Galuh Chrismaningwang<sup>a,\*</sup>, Achmad Basuki<sup>a</sup>, Kusno Adi Sambowo<sup>a</sup>

<sup>a</sup>*Department of civil engineering, Sebelas Maret University, Surakarta, Indonesia*

---

## Abstract

This paper presents an experimental and analytical methods conducted to study the effect of seawater curing on the correlation between split tensile strength and modulus of rupture (MOR) in high strength concrete incorporating rice husk ash. Rice husk ash was added into the mix partially replacing cement content, replacements were done at 0,5,10,15, and 20%. To resemble marine environment, concrete samples were cured in seawater. The results showed that addition of rice husk ash increased the modulus of rupture and split tensile strength value, and also increased the resistance to seawater exposure. The correlation between split tensile strength and MOR had the empirical  $f_{st} = 125,3\% \times \text{MOR}$  for fresh water curing, and  $f_{st} = 115,8\% \times \text{MOR}$  for seawater curing.

© 2017 The Authors. Published by Elsevier Ltd.

Peer-review under responsibility of the organizing committee of SCESCM 2016.

*Keywords:* split tensile, MOR, rice husk ash, high strength concrete

---

## 1. Introduction

Waterfront city is one of building concepts to be developed in Indonesia. Observing the other countries such as Singapore, Japan, the United Kingdom, and the USA that have successfully applied this concept, the Indonesian government is very supportive of waterfront city projects to improve economy and infrastructure development throughout the nation.

---

\* Corresponding author. Tel.: +62-821-3641-8888

E-mail address: [galuh.chrismaningwang@gmail.com](mailto:galuh.chrismaningwang@gmail.com)

The aggressive characteristic of seawater requires building materials that are resistant to seawater effects. Concrete becomes the appropriate selection of building materials to be used in coastal areas, considering that it is noncorrosive, formable, and workable materials, which are great benefits for coastal area construction, particularly on a big scale level. The consideration in coastal and marine areas have a high concentration of chloride and sulfate, which can decrease the performance or even destroy the concrete (Al-Rabiah, 1997; Rostam, 1997; Swamy, 2003; Bader, 2003). Not to mention that the effects of seawater abrasion also have to be considered.

The challenge in construction is to make concrete as an environmentally friendly building material but still completely supports sustainable development. Sustainable development requires a sustainable construction industry, in particular, concrete sustainability in structural design and performance, also building’s life-cycle (Susilorini,2008).

Additive materials usage in concrete can improve concrete quality. Rice Husk Ash (RHA) is one of the additive material innovations which can improve concrete strength in certain dosages. The aim of the study is to develop RHA as additive material in high strength concrete that’ exposed to seawater abrasion

## 2. Experimental Details

Figure 1 shows the experimental details of this study that includes preliminary test, mix proportion, curing, and hardened concrete test.

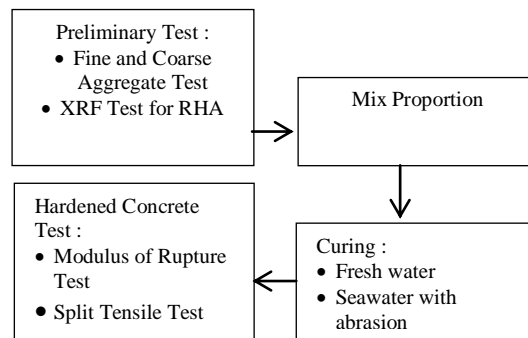
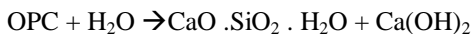


Figure 1 Experimental Details

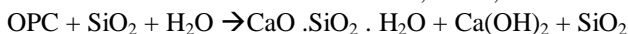
Rice Husk Ash (RHA) as an additive material on the concrete was obtained from Sragen, Central Java, Indonesia. XRF Test is a spectroscopic method commonly used in solids, in which secondary X-ray emission is generated by excitation of a sample with X-ray.

Table 1 shows that the largest component of RHA is SiO<sub>2</sub>, this resembles same conditions of cement matrix. The reaction between cement, water, and rice husk ash are shown below :

1. Chemical reaction between OPC and water



2. Chemical reaction between OPC, water, and rice husk ash (RHA)



The reaction between RHA and CH resulted in the decreased amount of CH, which decreased alkalinity and added cement paste endurance to an outer chemical reaction. The reaction also resulted in increased amount of CSH which retained liquid infiltration to cement paste, and in result decreased the permeability level making the concrete more solid.

Table 1 Chemical Properties of RHA According to XRF Test

Formula	Concentration
	%
SiO <sub>2</sub>	82.59
CaO	4.81
K <sub>2</sub> O	3.05
Al <sub>2</sub> O <sub>3</sub>	2.05
P <sub>2</sub> O <sub>5</sub>	2.00
Fe <sub>2</sub> O <sub>3</sub>	1.65
MgO	1.48
SO <sub>3</sub>	1.18
Cl	0.57
MnO	0.29
TiO <sub>2</sub>	0.16
Nd <sub>2</sub> O <sub>3</sub>	0.03
SrO	0.02
ZnO	0.02
V <sub>2</sub> O <sub>5</sub>	0.02
Rb <sub>2</sub> O	0.01

In order to understand the effect of Rice Husk Ash (RHA) and seawater effect on hardened concrete, various tests were executed in the laboratory. Standards that were used in the making and curing of the samples were SNI 03-2493-1991. Concrete samples were in cylinder and beam shape, and the details such as sample size, number of samples, the age of tests, and standards are shown in Table 2.

The variations of sample treatment that were used in this study were :

- Normal samples soaked in fresh water
- Normal samples soaked in seawater
- Modulus of Rupture Test Samples with RHA Addition (0%,5%,10%,15%, and 20%) soaked in fresh water and seawater
- Split Tensile Test Samples with RHA Addition (0%,5%,10%,15%, and 20%) soaked in freshwater and seawater

Table 2 Macro structures experimental details

Test	Sample Description			Standard	Unit	Measurement	Equipment
	Size (mm)	No	Age (days)				
Modulus of Rupture	100x100x500	30	28	ASTM C-78	MPa	Modulus of Rupture	Loading frame dan Dial Gauge
Split Tensile Strength	80 x 150	30	28	SNI 03-2491-2002	N/mm <sup>2</sup>	Split/tensile	Compression Testing Machine

This study used trial-error mix design method to gain the number of  $f_c' > 40 \text{ N/mm}^2$ . Recapitulation for the mix design used in Modulus of Rupture Tests and Split Tensile Tests are shown in Table 3.

*Table 3 Concrete mix design for samples*

RHA		Super plasticiser	Cement	FA	CA	Water
%	kg/m <sup>3</sup>	kg/m <sup>3</sup>	kg/m <sup>3</sup>	kg/m <sup>3</sup>	kg/m <sup>3</sup>	kg/m <sup>3</sup>
0	0.00	7.59	505.73	641.5	1025.8	166.73
5	25.24	9.69	504.85	641.5	1025.8	164.90
10	50.40	11.79	503.98	641.5	1025.8	163.08
15	75.47	13.88	503.11	641.5	1025.8	161.27
20	100.4	15.96	502.24	641.5	1025.8	159.46

### 3. Results and Discussions

#### 3.1. Split Tensile Strength

The method used in this study were tensile splitting cylinder tests. Tensile strength was monitored at ages 28 days using Compression Testing Machine. The formula used to find the tensile strength is shown in Eq. 1 below.

$$f_{st} = \frac{2 \times P}{\pi \times D \times L \times f_d} \tag{1}$$

where  $P$  = maximal load applied;  $D$  = diameter of sample;  $L$  = length of sample;  $f_d = 1,06$  (correction factor for diameter variation of cylinder samples). The correction factor is according to SNI 1974-2011.

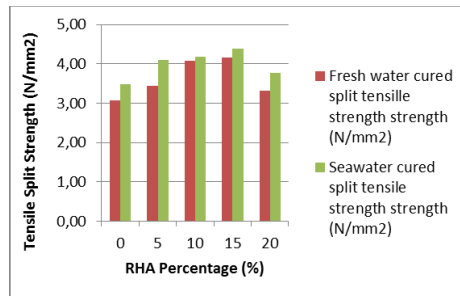


*Figure 2 Split tensile strength at 28 days*

#### 3.2. Modulus of Rupture

The modulus of rupture was monitored at ages 28 days using Loading frame and dial gauge. The formula used to find the tensile strength is shown in Eq. 2 below.

$$MOR = \frac{P \times L}{b \times d^2} \tag{2}$$

where  $P$  = maximal load applied;  $b$  = breadth of sample;  $d$  = height of sample;  $L$  = length of sample

In modulus of rupture testing, all samples were perfectly broken in the center of effective length. This condition indicated that samples were broken by a flexural load. Modulus of rupture test results was shown in Figure 3.



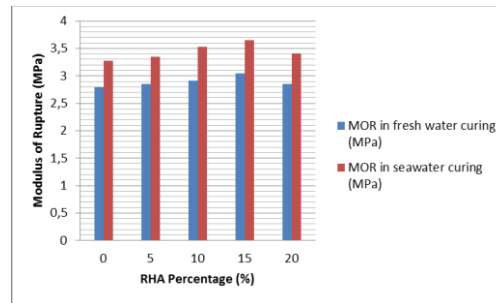


Figure 3 Modulus of rupture in 28 days

### 3.3. The correlation between split tensile strength and modulus of rupture

Figure 2 and Figure 3 show the addition of RHA could increase split tensile strength and modulus of rupture value both in fresh water and seawater curing. Tensile split strength and MOR value in seawater cured concrete were higher than fresh water cured. This is caused by chemical reaction between the concrete and seawater formed  $\text{CaCl}_2$  that was used as an accelerator.  $\text{CaCl}_2$  increased tensile split strength value faster compared to split tensile strength value for fresh water cured concrete at the same age.

Seawater could cause corrosion in reinforced concrete for a long term period. The chemical reaction between calcium in concrete and sulfate salt from seawater formed ettringite ( $6\text{CaO} \cdot \text{Al}_2\text{O}_3 \cdot 32\text{H}_2\text{O}$  or  $\text{C}_6\text{AS}_3\text{H}_{32}$ ). Ettringite caused concrete volume swelling, so that the concrete cracked and became porous. The addition of RHA as a filler reduced porosity. The high level of  $\text{SiO}_2$  reduced calcium hydroxide content and made concrete more resistant to sulfate salt.  $\text{SiO}_2$  reacted to calcium hydroxide and changed it into calcium silicate hydrate which became the source of concrete strength. The more RHA used inside the concrete, the more  $\text{Ca}(\text{OH})_2$  area, thus more calcium silicate hydrate was formed so that concrete became stronger and more impermeable.

The empirical formulae of correlation between split tensile strength and modulus of rupture shown in Eq. 3 (Raphael, 1984)

$$f_{st} = \frac{3}{4} MOR. \tag{3}$$

Where  $f_{st}$  = split tensile strength and  $MOR$  = Modulus of Rupture

Table 4 The comparison between split tensile strength and MOR

Curing environment	RHA percentage (%)	Average MOR (MPa)	Average split tensile strength (MPa)
Fresh water	0	2.79	3.08
	5	2.85	3.43
	10	2.91	4.08
	15	3.04	4.15
	20	2.85	3.31
Seawater	0	3.28	3.49
	5	3.35	4.10
	10	3.53	4.19
	15	3.65	4.39
	20	3.41	3.77

The comparison between split tensile strength and MOR in this research are shown in Table 4. Correlation between split tensile strength and MOR were obtained by using modified SK SNI T-15-1990-03, shown in Figure 4 and Figure 5.

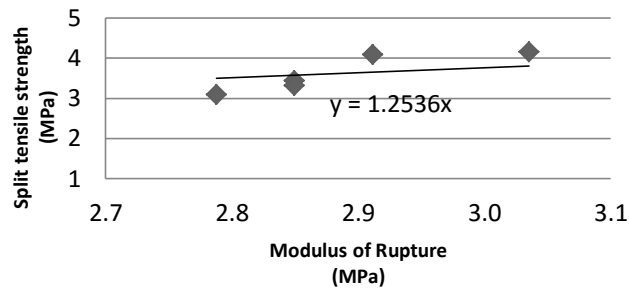


Figure 4 Chart of split tensile strength and MOR comparison in fresh water curing

Based on Figure 4, the empirical formulae of split tensile strength and MOR correlation for high strength concrete incorporating RHA in fresh water curing is :

$$f_{st} = 125,3\% \times MOR \tag{4}$$

Where  $f_{st}$  = split tensile strength and MOR = Modulus of Rupture

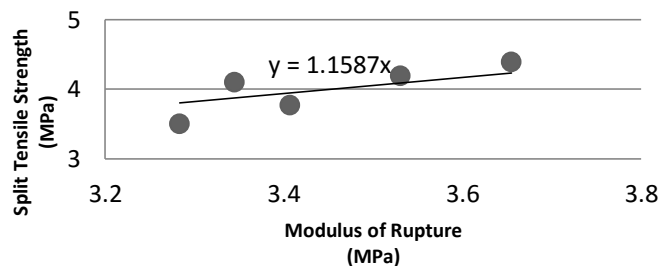


Figure 5 Chart of split tensile and MOR comparison in seawater curing

Based on Figure 5, the empirical formulae of split tensile strength and MOR correlation for high strength concrete incorporating RHA in sea water curing is :

$$f_{st} = 115,8\% \times MOR \tag{5}$$

Where  $f_{st}$  = split tensile strength and MOR = Modulus of Rupture

#### 4. Conclusions

In conclusion, the addition of Rice Husk Ash increased the value of modulus of rupture and split tensile strength both in fresh water and seawater cured concrete. It also increased concrete’s resistance to seawater exposure.

The correlation between split tensile strength and MOR had the empirical formulae  $f_{st} = 125,3\% \times MOR$  for fresh water curing, and  $f_{st} = 115,8\% \times MOR$  for seawater curing.

## Acknowledgements

The authors wish to express their sincere appreciation to Sebelas Maret University and Ministry of Research, Technology, and Higher Education of Indonesia, for providing the facilities and financial grant in conducting this research.

## References

- [1] Amri, Syaifei, ST, Dipl. E. Eng. 2005. *Teknologi Beton A-Z*. Yayasan John Hi-Tech Idetama. Jakarta.
- [2] Armesto, L., Bahillo, A., Veijonen, K. Cabanillas, A., and Otero, J. 2002. Combustion Behaviour of Rice Husk in a Bubbling Fluidised Bed. *Biomass and Bioenergy*. 23: 171 – 179.
- [3] Bakri, Jurnal Perennial, 5(1): 9-14 Lab. Keteknikan dan Diversifikasi Produk Hasil Hutan Fakultas Kehutanan Universitas Hasanuddin Jl. Perintis Kemerdekaan Km. 10 Tamalanrea, Makassar.
- [4] Bui, D. D., Hu, J. and Stroeven, P. 2005. Particle Size Effect on the Strength of Rice Husk Ash Blended Gap-Graded Portland Cement Concrete. *Cement & Concrete Composites*. 27: 357–366
- [5] Ismail, M. S. and Waliuddin, A. M. 1996. Effect of Rice Husk Ash on High Strength Concrete. *Construction and Building Materials*. 10 (1): 521 – 526
- [6] Kencanawati, Ni Nyoman dan Merdana, I Nyoman, 2012. *Perbandingan Penggunaan Pozolan Alami (Abu Sekam Padi) dan Pozolan Buatan (Sika Fume) Pada Kuat Tekan Beton Mutu Tinggi*. Jurnal Teknik REKAYASA, Volume 13, Prodi Teknik Sipil, Fakultas Teknik Mataram, Mataram
- [7] Kodoatie & Sjarief. 2010. *Jurnal Abrasi*. UPI : Yogyakarta
- [8] Meyer, C. 2002. “Concrete and Sustainable Development”, *Special Publication ACI 206, Concrete Materials to Application – A Tribute to Surendra P. Shah*, American Concrete Institute, Farmington Hills, MI
- [9] Mulyono, T. 2004. *Teknologi Beton*. CV Andi Offset, Jogjakarta
- [10] Nawy, E.G. 1990. *Beton Bertulang Suatu Pendekatan Dasar*. Eresco. Bandung
- [11] Neville, AM. 1995. *Properties of Concrete*. The English Language Book Society and Pitman Publishing : London
- [12] Sahureka, T.B.J.M., 1997. *Pengaruh Penambahan Abu Sekam Padi pada Kuat Tekan dan Ketahanan Asam Beton*. Tesis, Prodi Teknik Sipil, Fakultas Teknik Sipil, UGM, Yogyakarta
- [13] Sambowo, Kusno Adi. 2001. *Engineering Properties and Durability Performance of Metakaolin and Metakaolin PFA Concrete*. Thesis. Faculty of Engineering at University of Sheffield. Sheffield
- [14] Suhendro, B. 2007. “Beton Hijau (*Green Concrete*)- Dambaan, Realisasi, dan Permasalahannya”, Prosiding Seminar Nasional “Sustainability dalam Bidang Material, Rekayasa, dan Konstruksi Beton”, KK Rekayasa Struktur FTSL ITB, Bandung, pp.20- 38
- [15] Tjokrodimuljo, K. 1996. *Teknologi Beton*. Arif: Yogyakarta
- Mehta, P Kumar, dan Monteiro, PJM. (1993). *Concrete ~ Structure, Properties, and Materials*. Prentice-Hall, New Jersey



Sustainable Civil Engineering Structures and Construction Materials, SCESCM 2016

## Physical and mechanical properties of WPC board from sengon sawdust and recycled HDPE plastic

Yudhi Arnandha<sup>a, \*</sup>, Iman Satyarno<sup>a</sup>, Ali Awaludin<sup>a</sup>, Inggar Septia Irawati<sup>a</sup>, Yoga Prasetya<sup>a</sup>, Deki Agung Prayitno<sup>a</sup>, Dui Cakra Winata<sup>a</sup>, Mochammad Hardito Satrio<sup>a</sup>, Astri Amalia<sup>a</sup>

<sup>a</sup>*Civil Engineering Department, Engineering Faculty, Gadjah Mada University, Yogyakarta, Indonesia*

---

### Abstract

Wood Plastic Composite (WPC) is a composite material made from sawdust and plastic as polymer bonding, that used in a variety of structural and non-structural applications. Nowadays, In Indonesia WPC is made from Sengon sawdust and recycled HDPE plastic. This research was conducted in order to investigate the physical and mechanical properties of WPC from Sengon sawdust in accordance with ASTM D7031. From the physical test, due to its water restrains, WPC has low moisture content, water absorption and swelling. For the mechanical properties, the bending strength and shear strength are around 40.49 MPa and 27.35 MPa, respectively. However, the WPC tensile strength is lower than common tropical wood, which is only 5.54 to 12.75 MPa, due to the absence of grain in WPC. Furthermore, the modulus of elasticity is only 2113 to 3398 MPa or around one tenth of that wood or concrete modulus of elasticity. From the withdrawal test shows that sheet metal screw type has the highest withdrawal strength compared to cut thread wood, and fine thread drywall screw. Hence, for structural application it is suggested that the WPC board is used for structural element with high moment inertia such as shear wall as its lower modulus of elasticity but has high shear strength.

© 2017 The Authors. Published by Elsevier Ltd.

Peer-review under responsibility of the organizing committee of SCESCM 2016.

*Keywords:* wood plastic composite; sengon sawdust; HDPE; physical properties; mechanical properties.

---

---

\* Corresponding author. Tel.: +6285770200000.

*E-mail address:* [yudhiarnandha@untidar.ac.id](mailto:yudhiarnandha@untidar.ac.id)

## 1. Introduction

### 1.1. Background

Wood has become one of the major material that been used for structural and also non-structural civil engineering purpose. Wood offers many structural advantages, such as low density, high toughness, non-toxic, low in thermal conductivity. However, wood has primary disadvantage which is low water resistance due to its natural hygroscopic characteristic. Wood can be used as timber product, sawn timber, plywood and other processed wood products. Since the enforcement of forest conservation regulations that prevent illegal logging, high quality timber product become expensive due to difficult to find. Sengon (*Paraserianthes falcataria*) is one tropical wood that has good strength and also short harvesting time, not more than 5 years. Sengon was usually being used for wood product such as plywood, laminated veneer lumber (LVL) and wood plastic composite (WPC).

Nowadays wood wastes and plastic garbage have been a main environmental concern. [1] Wood–plastic composites (WPCs) are obtaining a great attention in industrial sectors and academics due to their favorable properties, which include low density, low cost, renewability and recyclability as well as desirable mechanical properties. Nowadays WPC only used for non structural purpose such us flooring, decking, fence and any other use. [2] As the use of wood-plastic composite (WPC) materials extends to include more structural applications, there is an increasing need to determine design values appropriate for designing structural WPC elements. [3] The decision to use a WPC product in place of another, generally speaking, should be predicated on achieving greater performance, reduced price, or reduced environmental impact. [4] There are a number of published studies in WPC research, most of them were held in overseas using its local kind of wood and using compression mold method. This research was conducted to observed physical and mechanical properties of WPC in order for being used for structural material purpose.

Yadaf studied about mechanical and physical properties of wood-plastic composites made of polypropylene, wood flour and nanoclay, [5] Adhikary studied about dimensional stability and mechanical behavior of wood–plastic composites based on recycled and virgin high-density polyethylene (HDPE) [6], Rafighi studied about mechanical properties of composite made of sawdust and high density Polyethylene [7] Nugraha studied about compression molded composites based on a combination recycled PET and Sengon chips [8], Susanti studied about compression molded composites based on a combination of recycled PP and HDPE and Sengon chips [9]. The research about physical and mechanical WPC using Sengon sawdust and recycled HDPE plastic using extrusion method never been conducted before.

## 2. Experimental

### 2.1. Materials

Materials that been used for this research was WPC board produced by local factory in Magelang, Central Java. WPC board with 12 mm thickness, 60 cm width and 3 m length from Sengon sawdust dust and recycled HDPE plastic was selected to be observed its physical and mechanical properties. WPC board was made and shape using hot extrusion method, thus can improve and reassure the homogeneity from WPC board better than using molding method. Sengon sawdust in the form of sawdust were collected from local plywood production industry. Recycled HDPE granules were collected from local plastic recycling plant.

### 2.2. Physical Properties Measurements

Moisture content, water absorption and thickness swelling tests were conducted according with ASTM D7031 (Standard Guide for Evaluating Mechanical and Physical Properties of Wood Plastic Composite Products). [10] This guide covers test methods appropriate for evaluating a wide range of performance properties for wood-plastic composite products. According to this guide, in order to measure water absorption and thickness swelling, the specimens were soaked in water for 2 hours, 2 + 22 hours and directly 24 hours. The physical properties

measurements were conducted to different direction of WPC extrusion in order to figure out the isotropic properties of WPC board.

### 2.3. Mechanical Properties Measurements

Several mechanical properties measurements of WPC Sengon were carried out such as bending test, tensile test, compression test, shear test and screw withdrawal test in accordance with ASTM D7031 (Standard Guide for Evaluating Mechanical and Physical Properties of Wood Plastic Composite Products). Due to WPC thickness, several modifications were made in specimens without influenced the scheme of testing procedure. The mechanical properties measurements were also conducted to different direction of extrusion in order to figure out the isotropic properties of WPC board.

Different treatment used as variation in this research, that is normal dry condition and wet condition (soaked into water for 7 days). This kind of treatment had been carried out in order to indicate the possibility of mechanical strengths loss during 7 days' condition in the water.

## 3. Results and Discussions

### 3.1. Physical Properties Results

Physical properties measurement of WPC Sengon were carried out according to ASTM D7031 (Standard Guide for Evaluating Mechanical and Physical Properties of Wood Plastic Composite Products). For the moisture content measurement, the specimens dimension was 2 by 2 inch in size, the weight of each specimen was measured before and after soaked in distilled water at room temperature for 24 hours. The moisture content is the percentage difference of the specimen's weight before and after drying. As shown in Fig. 1, WPC has very small moisture content approximately in the value of 0.917%. The result showed that moisture content from WPC board is less than given standard for particle board moisture content such as mention in JIS (5–13%) [11], FAO (<12%) [12] and SNI (<14%) [13].

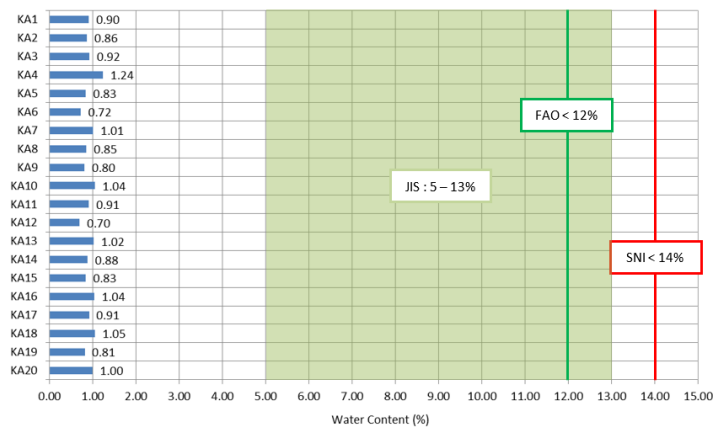


Fig. 1. Moisture content of WPC Sengon

The density of WPC Sengon is around  $1.511 \text{ ton/m}^3$ , higher than molding Sengon board in the value around  $0.86 \text{ ton/m}^3$ . [9] The increase in density (decrease in porosity) affects practically all important properties of WPC. The higher the density, the higher the flexural strength and the flexural modulus. [14]

For the water absorption test, the test specimen dimension was 6 by 6 in. (152 by 152 mm) in size with all four edges smoothly and squarely trimmed. The weight of 20 specimens being measured first, then the specimens soaked in water for 2 hours, 2 + 22 hours and directly 24 hours. The specimens were removed from the water, then patted dry and measured again. According to the result, WPC has small water absorption approximately in the value of

0.091% (2 hours), 0.258% (2+22 hours) and 0.242% (24 hours), see Fig. 2.a and Fig. 2.b. This result is less than given standard for particle board water absorption from FAO (20-75%). From thickness swelling test showed WPC has small swelling approximately in the value 0.702% (2 hours), 1.738% (2+22 hours) and 0.982% (24 hours), see Fig. 3.a and Fig. 3.b. From length swelling test showed WPC has also small swelling approximately in the value 0.017% (2 hours), 0.053% (2+22 hours) and 0.041% (24 hours), see Fig. 4.a and Fig. 4.b. Physical properties results for WPC from Sengon and recycled HDPE given in Table 1.

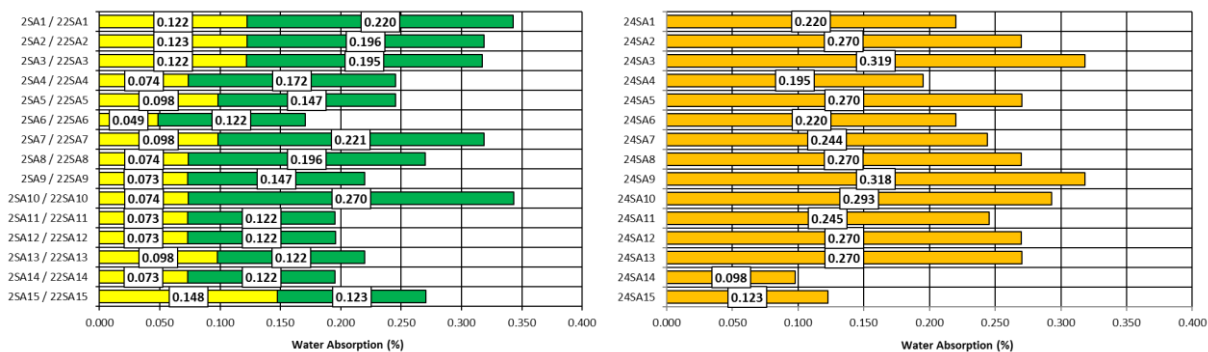


Fig. 2. (a) Water absorption for 2 hours and then 22 hours; (b) Water absorption for 24 hours

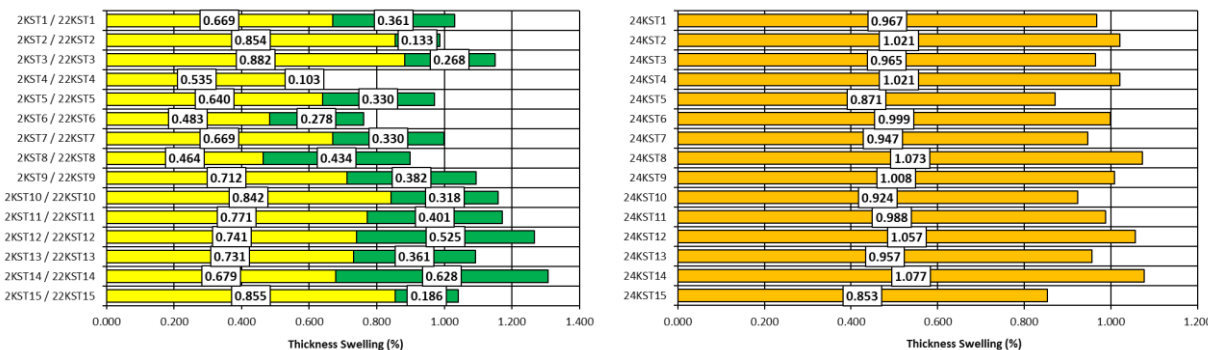


Fig. 3. (a) Thickness swelling for 2 hours and then 22 hours; (b) Thickness swelling for 24 hours

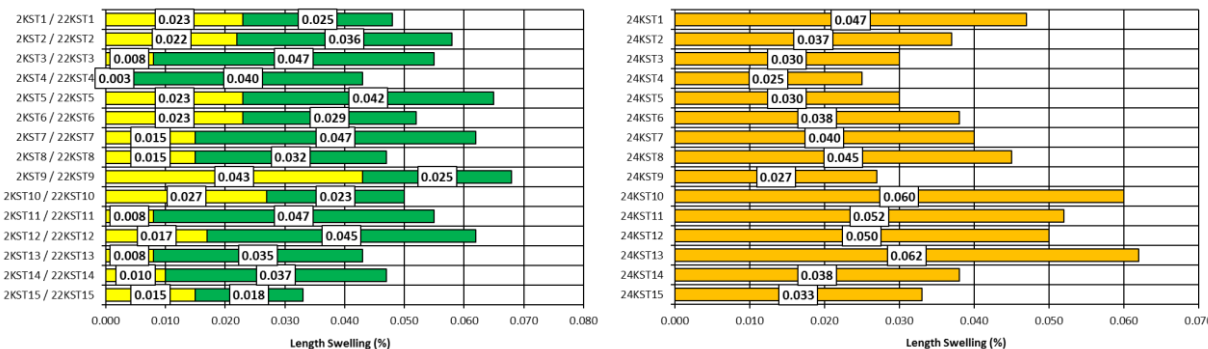


Fig. 4. (a) Length swelling for 2 hours and then 22 hours; (b) Length swelling for 24 hours

Table 1. Physical Properties Results.

Physical Properties	2 hours	2 + 22 Hours	24 Hours	Moulding Sengon Board by Susanti [9]
---------------------	---------	--------------	----------	--------------------------------------



Density (ton/m <sup>3</sup> )	-	-	1.511	0.86
Moisture content (%)	-	-	0.917	1.99 – 4.67
Physical Properties	2 hours	2 + 22 Hours	24 Hours	Moulding Sengon Board by Susanti [9]
Water Absorption (%)	0.091	0.258	0.242	19.2 – 26.36
Swelling Thickness (%)	0.702	1.038	0.982	2.82 – 4.75
Swelling Length (%)	0.017	0.053	0.041	-

### 3.2. Mechanical Properties Results

#### 3.2.1. Compression Test

According to mechanical properties measurement using ASTM D7031 (Standard Guide for Evaluating Mechanical and Physical Properties of Wood Plastic Composite Products), short column compression strength shall be determined in accordance with the principles of ASTM D4761 (Standard Test Methods for Mechanical Properties of Lumber and Wood-Base Structural Material) [15] where the specimen is loaded at a prescribed rate until failure occurs or a preselected load is reached, see Fig. 5.a. The dimension of the specimen was 2 x 10 x 1,2 cm with 10 specimens used for the parallel to extrusion and also 10 specimens used for the perpendicular to extrusion. Compression test conducted for different direction of extrusion in order to Fig. out the isotropic properties of WPC board. Furthermore, using ANOVA as statically method, different direction of extrusion from both test did not indicate statically significant different results. Different treatment in dry and wet condition also did not indicate statically significant different results. WPC has high compression strength approximately in the value 44.97 MPa (parallel to extrusion) and 43.91 MPa (perpendicular to extrusion), thus showed WPC has isometric compression strength, see Fig. 5.b.

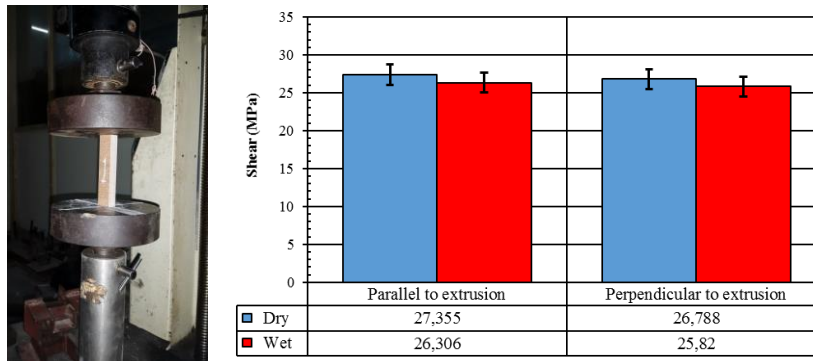


Fig. 5. (a) Schematic of compression Test of WPC Sengon; (b) Compression Test Result of WPC Sengon

#### 3.2.2. Bending Test

According to mechanical properties measurement using ASTM D7031 (Standard Guide for Evaluating Mechanical and Physical Properties of Wood Plastic Composite Products), bending tests were conducted in accordance ASTM D1037 (Standard Test Methods for Evaluating Properties of Wood-Base Fiber and Particle Panel Materials) [16] which provides procedures for the determination of bending strength (MOR) and modulus of elasticity (MOE) flat-wise bending on short spans under third-point load. The specimens were loaded at the center of span with the load applied to the finished face at a uniform rate through a loading block rounded as is shown in Fig. 6.a for horizontal position and Fig. 6.b. for vertical position. Static bending tests were made both on specimens when dry and when soaked. Each test specimens were 3 inch in width and 24 times the nominal depth in length.

From the bending test, MOE of WPC approximately in the value 3562.55 MPa (parallel to extrusion) and 3398.39 MPa (perpendicular to extrusion), respectively. According to rupture failure, MOR of WPC approximately in the value 40.49 MPa (parallel to extrusion) and 26.83 MPa (perpendicular to extrusion). This result higher than WPC from Pine that had MOE around 840 – 1970 MPa and MOR around 14.4 – 24.9 MPa. [6]

From this test, different direction of extrusion indicates different significant results in MOR and MOE. MOR from bending tests result given in Fig. 7.a. and MOE result given in Fig. 7.b.

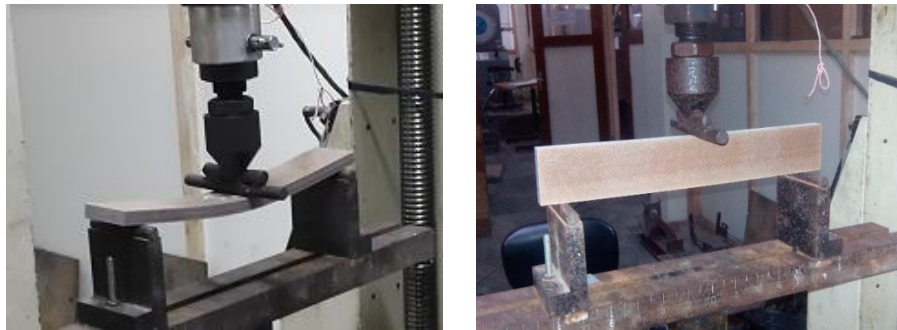


Fig. 6. (a) Schematic of Static Bending Test (Horizontal); (a) Schematic of Static Bending Test (Vertical)

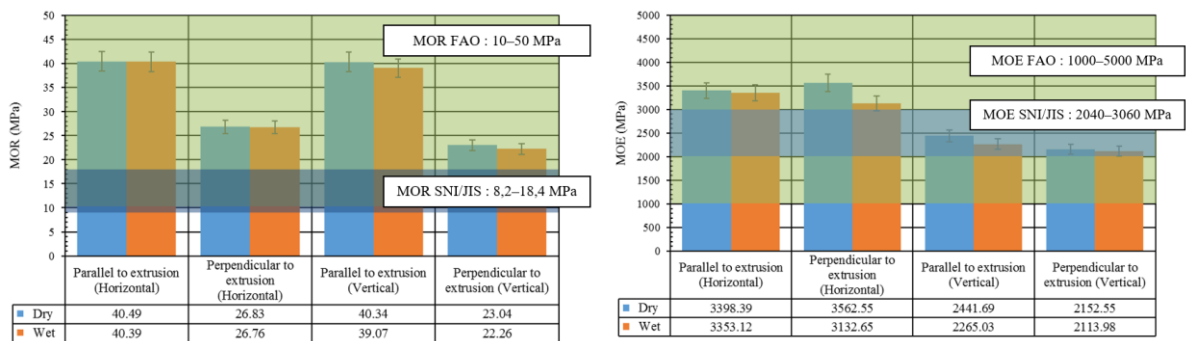


Fig. 7. (a) MOR of WPC Sengon; (b) MOE of WPC Sengon

### 3.2.3. Shear Test

According to mechanical properties measurement using ASTM D7031 (Standard Guide for Evaluating Mechanical and Physical Properties of Wood Plastic Composite Products), shear strength shall be determined in accordance with the principles of Test Method D143 (Standard Test Methods for Small Clear Specimens of Timber). [17] The shear test specimens dimension was 2 by 2 in, see Fig. 8.a. The test used a shear apparatus similar to that illustrated in Fig. 8.b. Specimen failure due to shear test can be seen in Fig. 9.a. Shear test also conducted for different direction of extrusion. WPC has high shear strength approximately in the value 27.355 MPa (parallel to extrusion) and 26.788 MPa (perpendicular to extrusion), this showed WPC has isometric shearing strength. From ANOVA statically method, different direction of extrusion did not indicate significant results. (Fig. 9.b)



Fig. 8. (a) Specimens of Shear Test; (b) Shear Apparatus for Shear Test

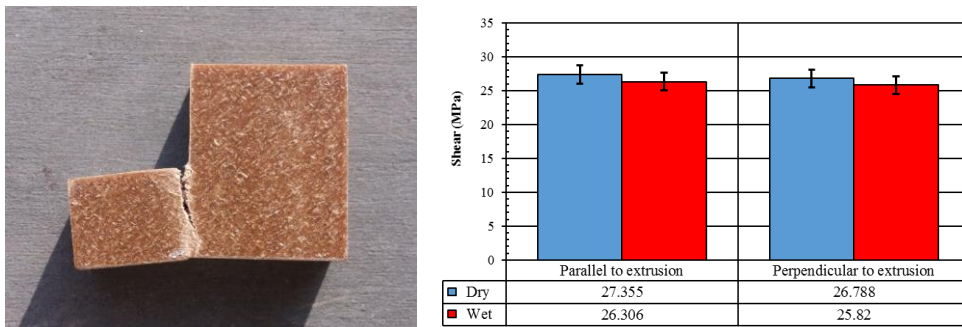


Fig. 9. (a) Specimen failure due to Shear Test; (b) Shear strength of WPC Sengon

### 3.2.4. Tensile Test

According to mechanical properties measurement using ASTM D7031 (Standard Guide for Evaluating Mechanical and Physical Properties of Wood Plastic Composite Products), tensile strength for wood product in accordance with ASTM D1037 (Standard Test Methods for Evaluating Properties of Wood-Base Fiber and Particle Panel Materials). The specimens for tensile test were made both in the dry and in the soaked condition. The specimen made both in long dimension parallel (parallel to extrusion) and perpendicular to the long dimension of the board (perpendicular to extrusion).

Each test specimens were shaped as shown in Fig. 10.a and prepared for test as shown in Fig. 10.b. From the test showed that WPC tensile strength approximately in the value 10.331 MPa (parallel to extrusion) and 5.986 MPa (perpendicular to extrusion). In the generally, this result higher than WPC from Fir (5.1 – 6.4 MPa) and WPC from Beech (7 – 8 MPa). [7] Different from its original Sengon wood, WPC as wood composite has brittle characteristic because the absence of grain. From tensile test, different direction of extrusion indicates different significant results. (Fig. 11).

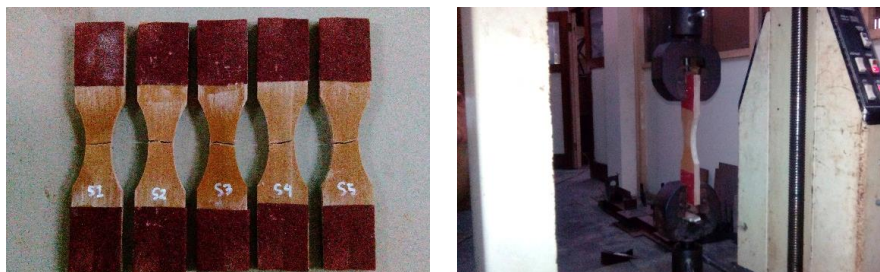


Fig. 10. (a) Specimen failure due to Tensile Test; (b) Schematic of Tensile Test

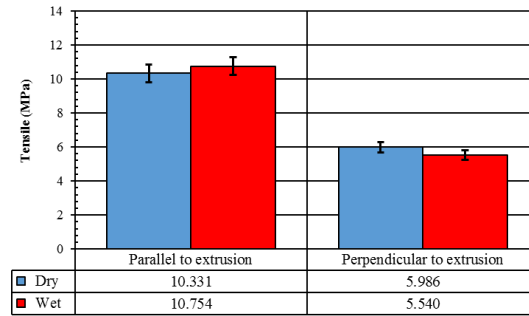


Fig. 11. Tensile strength of WPC Sengon

### 3.2.5. Screw Withdrawal Test

According to mechanical properties measurement using ASTM D7031 (Standard Guide for Evaluating Mechanical and Physical Properties of Wood Plastic Composite Products), screw withdrawal test for wood product accordance to ASTM D1037 (Standard Test Methods for Evaluating Properties of Wood-Base Fiber and Particle Panel Materials). The test specimens were made in dimension of 3 in. (76 mm) in width and 6 in. (152 mm) in length, see Fig. 12.a. Different type of screw with several diameters used as variation such as sheet metal, cut thread wood, and fine thread drywall wood, and fine thread drywall, see Fig. 12.b. Each withdrawal tests were prepared as shown in Fig. 13.

The withdrawal test results showed that sheet metal screw type has the highest withdrawal strength in the value 20.43 MPa for root diameter 3.21 mm, slightly higher than root diameter 2.72 mm in the withdrawal value 20.27 mm. Thus, both diameter can be use for common WPC connection. Screw withdrawal result of WPC Sengon can be seen in Fig. 14. Using ANOVA statistical method, the difference condition of dry and wet specimen did not indicate significantly different results.



Fig. 12. (a) Specimens for Withdrawal Test; (b) Sheet metal, cut thread wood, and fine thread drywall screw



Fig. 13. Schematic of Screw Withdrawal Test

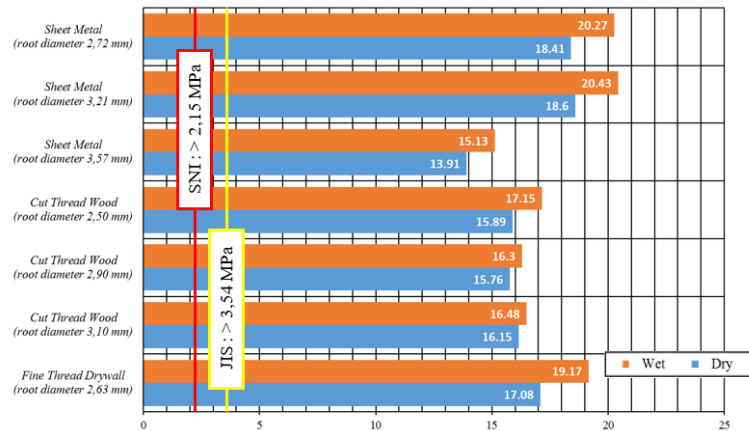


Fig. 14. Screw withdrawal test of WPC Sengon

#### 4. Conclusion and Recommendation

In this research, study about physical and mechanical properties of Wood Plastic Composite (WPC) from Sengon and recycled HDPE had been conducted. From physical properties showed that WPC has low moisture content, swelling and absorption respectively. Thus showed that WPC suitable for both outdoor or indoor application. From mechanical test result, WPC has higher compression and shear strength than common Sengon wood itself. This study has shown that the WPC Sengon will be most useful as building materials because its stability and mechanical properties. Since WPC has high moment inertia and low modulus of elasticity, it is suggested that the WPC board is preferred for shear wall as its lower modulus of elasticity but has high shear strength.

#### References

- [1] El-Haggag, M. Salah, Kamel and A. Mokhtar, "Wood Plastic Composites," in *Advances in Composite Materials - Analysis of Natural and Man-Made Materials*, P. Tesinova, Ed., Rijeka, Croatia, InTech, 2011.
- [2] Z. X. Zhang, C. Gao, Z. X. Xin and J. K. Kim, "Effects of extruder parameters and silica on physico-mechanical and foaming properties of PP/wood-fiber composites," *Composites Part B: Engineering*, vol. 43(4), p. 2047–2057, 2012.
- [3] H. P. San, L. A. Nee and H. C. Meng, "Physical and Bending Properties of Injection Moulded Wood Plastic Composites Boards," *ARP Journal of Engineering and Applied Sciences*, vol. 3, no. 5, pp. 13-19, October 2008.
- [4] M. J. Schwarzkopf and M. D. Burnard, *Wood-Plastic Composites—Performance*, Springer Science+Business Media, 2016.
- [5] S. M. Yadav and K. B. Yusoh, "Mechanical and Physical Properties of Wood-plastic Composites Made of Polypropylene, Wood flour and Nanoclay," in *Kuala Lumpur International Agriculture, Forestry and Plantation*, Kuala Lumpur, 2015.
- [6] K. B. Adhikary, S. Pang and M. P. Staiger, "Dimensional stability and mechanical behaviour of wood–plastic composites based on recycled and virgin high-density polyethylene (HDPE)," *ScienceDirect*, pp. 807-815, 2008.
- [7] A. Rafighi, A. Dorostkar and M. Madhoushi, "Investigation on mechanical properties of composite made of sawdust and high density Polyethylene," *International Journal of Lignocellulosic Products*, vol. 1, no. 2, pp. 134-141, 2014.
- [8] D. P. Nugraha, "Pemanfaatan Rajangan Kayu Sengon dan Plastik sebagai Bahan Baku Pembuatan Papan Partikel," Thesis, Magister Sistem Teknik, Fakultas Teknik, Universitas Gadjah Mada, Yogyakarta, 2011.
- [9] A. Susanti, "Pemanfaatan Limbah Plastik dan Serbuk Kayu Sengon sebagai Bahan Komposit Plastik," Thesis, Magister Sistem Teknik, Fakultas Teknik, Universitas Gadjah Mada, Yogyakarta, 2014.
- [10] "ASTM D7031-11, Standar Guide for Evaluating Mechanical and Physical Properties of Wood-Plastic Composite Products," ASTM International, West Conshohocken, 2011.
- [11] "JIS (A) 5908 - Particleboards," Japan, 2003.
- [12] "International Consultation on Plywood and Other Wood Based Panel Products," FAO, 1966.
- [13] "SNI 03-2105-2006 - Papan Partikel," Badan Standar Nasional, Jakarta, 2006.
- [14] A. A. Klyosov, *Wood-Plastic Composite*, Hoboken, New Jersey: John Wiley & Sons, Inc., 2007.

- [15] “ASTM D4761-13, Standard Test Methods for Mechanical Properties of Lumber and Wood-Base Structural Material,” ASTM International, West Conshohocken, PA, 2013.
- [16] “ASTM D1037-12 Standard Test Methods for Evaluating Properties of Wood-Base Fiber and Particle Panel Materials,” ASTM International, West Conshohocken, PA, 2012.
- [17] “ASTM D143-14, Standard Test Methods for Small Clear Specimens of Timber,” ASTM International, West Conshohocken, PA, 2014.





Sustainable Civil Engineering Structures and Construction Materials, SCESCM 2016

## Characterization of fly-ash using electrochemical impedance spectroscopy

Benny Suryanto<sup>a</sup>, W. John McCarter<sup>a,\*</sup>, Gerry Starrs<sup>a</sup>, T. Malcolm Chrisp<sup>a</sup>

<sup>a</sup>*School of Energy, Geoscience, Infrastructure and Society, Heriot-Watt University, Edinburgh EH14 4AS, Scotland, UK*

---

### Abstract

Electrochemical impedance spectroscopy is used to obtain the electrical properties of fly-ash over the frequency range 100Hz-10MHz. A range of presentation formalisms are exploited to characterize and assess this material in terms of its unburnt carbon content and pozzolanic reactivity. Fly-ash from a number of power stations within the UK, which differ in carbon content and fineness are used within the experimental programme. It is shown that the methodology could be exploited to index both the pozzolanicity and the presence of carbon in the ash. A number of additional features make this testing methodology of interest: the method is non-destructive and non-invasive; samples need not be restricted to cement pastes as mortars and concretes can also be studied.

© 2017 The Authors. Published by Elsevier Ltd.

Peer-review under responsibility of the organizing committee of SCESCM 2016.

*Keywords:* Fly-ash; Carbon; Pozzolanicity; Monitoring; Electrical properties

---

### 1. Introduction

The use of alternative cementitious binders, whereby Portland cement is partially (or even totally) replaced by the by-products of traditional industries, have an important role to play both in the design of durable cementitious systems and also in the reduction of CO<sub>2</sub> emissions. Because of the quantities of concrete produced world-wide, even a small reduction in CO<sub>2</sub> emission can result in significant environmental benefits. It is incumbent upon all nations to reduce total CO<sub>2</sub> emissions and contribute to achieving the targets initially set at the Kyoto Conference in 1997 and reaffirmed at the more recent UN Climate Change Conference in 2015 in Paris. For the foreseeable future,

---

\* Corresponding author. Tel.: +44-131-451-3318; fax: +44-131-451-4617.

E-mail address: [w.j.mccarter@hw.ac.uk](mailto:w.j.mccarter@hw.ac.uk)



extensive use will be made of materials such as ground granulated blast-furnace slag, micro-silica and fly-ash. Characterization of these materials is thus of considerable importance because the amount and quality of the replacement added to the binder are, ultimately, decisive parameters in concrete performance.

The two most important factors which determine the suitability of fly-ash are its fineness (45µm residue), to ensure reactivity, and its free carbon content which is quantified by the loss-on-ignition (LOI). In the case of low-lime fly ashes produced from anthracitic and bituminous coals, the cellular nature of the carbon particles results in a high specific surface area which can adsorb significant quantities of chemical admixtures. This can have a direct influence on the effectiveness of air-entraining agents, water-reducing admixtures and retarders; furthermore, the higher the carbon-content of the ash, the higher the water demand to maintain workability. There is also scope for direct activation of fly-ash to produce construction materials requiring lower strengths, for example, masonry mortars, grouts, backfill, non-clay bricks or slurry trench cut-off walls for containment purposes. This would further increase their utilization, particularly those fly-ashes which would not satisfy BS EN450 [1] code requirements as contributing towards all (or part) of the cementitious component.

In this paper, electrochemical impedance spectroscopy (EIS) is used to study fly-ash binders; more specifically, it is shown that EIS techniques could be developed as a *signature* for fly-ash and in the study of the pozzolanicity of fly-ash by direct chemical/thermal activation thereby extending previous work [2, 3].

### 1.1. Electrochemical Impedance Spectroscopy

The electrical response of a saturated porous material can be quantified in terms of its resistance (or its reciprocal, conductance) and capacitance. Monitoring these intrinsic electrical parameters as a function of frequency of applied electrical field represents the area of EIS. The underlying mechanisms responsible for impedance behaviour are directly related to the physical and chemical properties of the material – the capacitance is a quantitative measure of the polarization of charges within the material, and the conductance accounts for any direct transfer of charge through the material (i.e. ionic conduction) together with the dissipation of energy incurred due to relaxation of polarization processes.

The complex impedance,  $Z^*(\omega)$ , of a porous, ionic conductor at any angular frequency,  $\omega$ , of applied electrical field, can be represented by the equation [4],

$$Z^*(\omega) = Z'(\omega) - iZ''(\omega) \tag{1}$$

where  $Z'(\omega)$  and  $Z''(\omega)$  represent, respectively, the resistive (or in-phase component) and reactive (or quadrature component) of the complex impedance and  $i = \sqrt{-1}$ . Both these components can be monitored as a function of frequency of applied field and values presented on a Nyquist plot, i.e. values  $Z'(\omega)$  vs.  $-iZ''(\omega)$ . These are the basic concepts involved in impedance spectroscopy, with the frequency range over which measurements are made

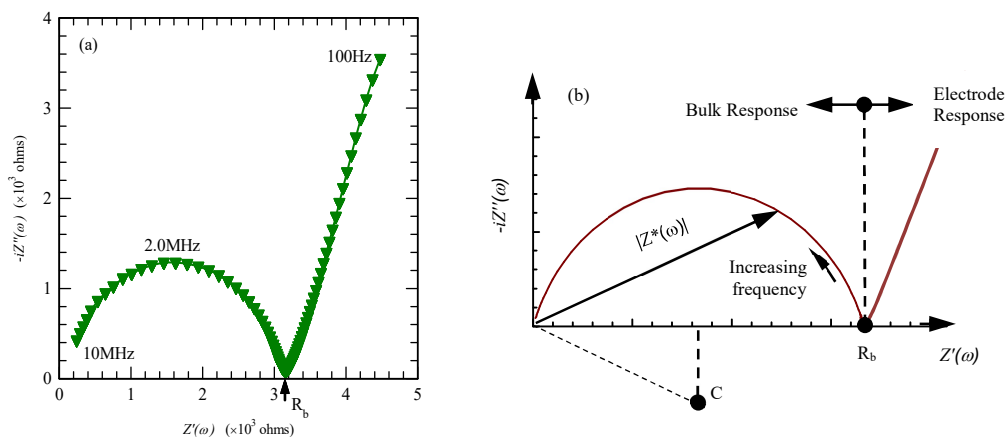


Fig. 1. (a) A typical Nyquist plot for hardened concrete, and (b) schematic showing electrode and bulk response and location of bulk resistance,  $R_b$ .

extending over several decades. A typical response for a hardened concrete is presented in Fig. 1(a) over the frequency range 100Hz-10MHz with frequency increasing from right to left across the curve [5]. The Nyquist plot comprises two distinct regions, a high frequency, bulk arc whose centre,  $C$ , is depressed below the real axis and a low-frequency spur representing the response from the electrode/sample interface. The true bulk resistance of the sample, denoted  $R_b$ , is obtained at the cusp-point between the bulk arc and low-frequency spur shown schematically in Fig. 1(b). In this paper, use is made of both the Nyquist and bulk resistance presentation formalisms.

## 2. Experimental Programme

### 2.1. Impedance Measurements

The EIS characterization studies were developed on two fronts:

(i) Frequency-effect. In this phase of the work, EIS measurements were obtained on both the fresh (i.e. plastic) and hardened samples using a Solartron 1260 frequency response analyser (FRA) with measurements presented in the form of equation (1) above.

(ii) Pozzolanicity/Activation. Within this phase of the work, fly-ash was mixed with an activator and the electrical response monitored using an Agilent 4263B LCR meter. Measurements were undertaken at a fixed frequency of applied electrical field.

Both the FRA and LCR meter operated in voltage-drive mode with a signal amplitude of 100mV used throughout. FRA measurements were obtained over the frequency range 100Hz-10MHz using a logarithmic frequency sweep with 20 spot frequencies per decade. The LCR meter was programmed to operate at a fixed frequency of 10kHz which was optimised through EIS measurements to ensure that electrode polarization effects had a negligible influence on evaluation of  $R_b$  (see Fig. 1(b)). Connections to the FRA and LCR meter were by means of individually screened coaxial leads with measurements taken every 10 minutes over periods extending up to 150 hours. Lead inductive effects were *nulled* from the data at each measurement frequency utilising an open-circuit, short-circuit and load calibration algorithm.

### 2.2. Test Cells, Materials and Sample Preparation

Paste and mortar samples were compacted into rigid, sealed Plexiglas cells. The cells had internal dimensions 5×5×5cms with electrical contact established by means of 5×5×0.3 cm (thick) stainless steel electrodes attached to two opposite cell walls. For concretes, the test cell had internal dimensions 15×15×15cms with electrical contact established by means of 15×15×0.3 cm (thick) stainless steel electrodes.

Table 1: Chemical and physical properties of fly-ashes used within the experimental programme

Oxide%	FA1	FA2	FA3	FA4	FA5	FA6
SiO <sub>2</sub>	46.5	51.0	50.5	49.6	48	44.3
Al <sub>2</sub> O <sub>3</sub>	28.2	27.4	24.7	25.3	27	24.7
Fe <sub>2</sub> O <sub>3</sub>	4.9	4.6	7.4	10.3	9	9.2
CaO	3.3	3.4	2.6	2.0	3.3	5.9
MgO	1.2	1.4	1.5	1.9	2.0	1.9
SO <sub>3</sub>	1.09	0.7	0.8	0.77	0.6	0.69
TiO <sub>2</sub>	1.3	1.6	1.0	1.1	0.9	1.4
K <sub>2</sub> O	1.1	1.0	3.0	3.7	3.3	1.7
Na <sub>2</sub> O	0.7	0.2	0.8	1.2	1.2	0.6
LOI	10.9	5.5	5.3	3.7	4.0	1.9
Fineness (% retained on 45 μm sieve)	20.6	8	9.5	26.2	29.8	11.6

The fly-ashes (FA) used within the current study were obtained from power stations using anthracitic/bituminous coals. Their oxide analysis is presented in Table 1. For the pozzolanicity studies, the following standard, base-mix formulation was used: samples were prepared by dry-mixing fly-ash and reagent grade calcium hydroxide in the ratio 4:1 and then mixing with distilled water at a water:solids ratio of 0.5. In addition to the base-mix, sodium sulphate ( $\text{Na}_2\text{SO}_4$ ), at a dosage of 10g/100g water (0.7Moles/l) was used. The paste samples were contained in the 5×5×5cms cell; the tops of the samples were covered before placing in a temperature controlled cabinet at ambient temperatures of 20°C, 37°C and 54°C ( $\pm 1^\circ\text{C}$ ).

For the frequency-effect studies a CEM I 42.5N cement [6] was used throughout and specimens comprised cement-pastes, mortars and concretes. Cement pastes were prepared using a fly-ash replacement levels of 0%, 10%, 25% and 40% with a water/binder ratio = 0.3. A BS EN 196-1 mortar [7] was used which had a 3:1 sand:binder ratio and a water:binder ratio = 0.5; a CEN reference sand [7] was used and the binder comprised CEM I cement and CEM I cement partially replaced with 33% (by mass) of fly-ash. The concrete mixes used are presented in Table 2 and also had fly-ash replacement levels of 0%, 10%, 25% and 40%. A 10dm<sup>3</sup> planetary motion mixer was used in the preparation of paste and mortar samples and a 0.1m<sup>3</sup> pan mixer was used in the preparation of concrete samples.

Table 2: Summary of cement-paste and concrete mixes studied.

Mix	CEM I kg/m <sup>3</sup>	FA kg/m <sup>3</sup>	Fine (<4mm) kg/m <sup>3</sup>	Coarse kg/m <sup>3</sup>		Water l/m <sup>3</sup>
				10mm	20mm	
C1	405	-	608	406	811	183
C2	363	40	605	403	806	181
C3	300	100	600	400	800	180
C4	237	158	593	395	791	178

### 3. Results and Discussion

This experimental program focusses on the use of electrical property measurements, obtained using EIS, in the study of fly-ash based systems. Results are presented to highlight the direct application of electrical property measurements in the evaluation of the pozzolanic reactivity of fly-ash through chemical and thermal activation and show the influence of the unburnt carbon within the ash on electrical response.

#### 3.1. Pozzolanicity Studies

The bulk resistance,  $R_b$ , of the specimens (obtained at 10kHz) was converted to conductivity,  $\sigma$ , through the relationship,

$$\sigma = \left( \frac{L}{R_b A} \right) \text{ Siemens/cm (S/cm)} \quad (2)$$

where  $A$  is the area of the electrodes ( $=5 \times 5 \text{ cm}^2$ ) and  $L$  is their spacing ( $=4.4 \text{ cm}$ ). The conductivity of the mixture will be dependent upon the fractional volume of aqueous phase; the continuity and tortuosity of the interstitial aqueous path between the electrodes, and the ionic concentration within the aqueous phase; hence, as the mixture reacts and increases in rigidity, all these factors will be affected which will, in turn, change the conductivity of the mixture.

For illustrative purposes, Fig. 2(a) displays the conductivity versus time response for the base-mix using, in this instance, FA2 and for clarity, measurement points have been omitted. The conductivity decreases by approximately 15% over the initial 2-days and remains virtually constant over the remainder of the test period. This would indicate a very sluggish reaction between the fly-ash particles and lime with little strength development; regarding the latter,

this was the case as samples could easily be crushed by hand and would agree with published work [8]. Fig. 2(b) presents the conductivity response for all ashes using  $\text{Na}_2\text{SO}_4$  in the gauging water. It should be noted that the conductivity of these mixtures is almost an order of magnitude higher than their base-mix counterpart values due to the increased ionic content within the gauging water. All curves now display a central region where there is a reduction in conductivity which would signify an increase in rigidity of the mixture, although the time at which this decrease occurs, the time-scale over which the central region occurs, and the rate of the decrease of conductivity are different for each material. These features could be used to quantify the pozzolanic reactivity of each ash; moreover, the derivative of the conductivity/time curves (i.e.  $d\sigma/dt$ ) could be considered as indicative of reaction

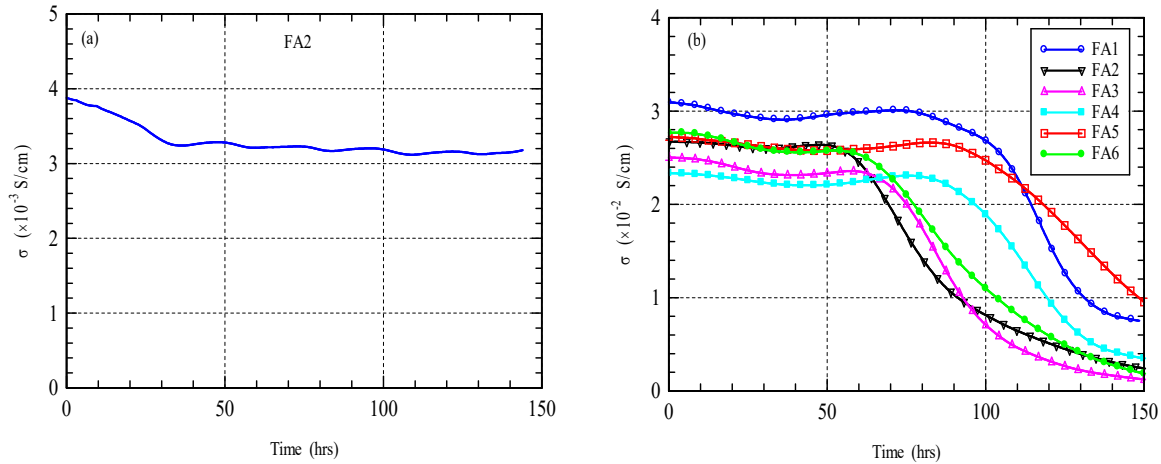


Fig. 2. Change in conductivity for (a) base-mix with FA2, and (b) base-mix with  $\text{Na}_2\text{SO}_4$  dissolved in gauging water.

kinetics, hence microstructural development [3].

Fig. 3 presents the conductivity/time response for FA4 and the resulting  $d\sigma/dt$  curve. Four regions can be identified: Region I, from initial gauging up to approximately 75 hours, over which time  $d\sigma/dt$  displays minor fluctuations, perhaps indicating some initial chemical activity; Region II, from 75-113 hours, representing an acceleratory period with more rapid chemical activity and is taken to signify stiffening of the mixture; Region III, from 113-145, representing a deceleration period and indicating a reduction in intensity of chemical activity; this leads into Region IV, where there is a more gradual decrease in conductivity over the remainder of the test period. Parallels can be drawn with calorimetry methods used to follow the hydration of Portland cement comprising a dormant period, an acceleratory period, a deceleration period followed by a diffusion controlled period.

A number of metrics can be identified from the electrical responses presented in Figs. 2(b) and 3 which could quantify the pozzolanic reactivity of a particular fly-ash. For example, Table 3 presents,

- (a) the extent and duration of Region II; the shorter the duration of Region II, the more reactive the fly-ash;
- (b) the ratio  $\sigma_0/\sigma_{150}$  where  $\sigma_0$  and  $\sigma_{150}$  are, respectively, the values of conductivity at the beginning and end of the test period (i.e. at 150 hours); this ratio would give a semi-quantitative measure of the increase in rigidity of the

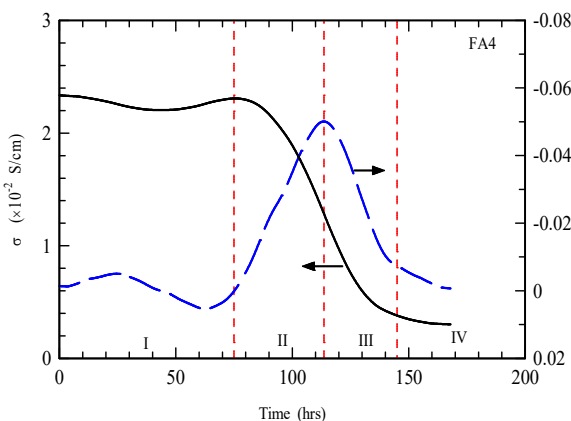


Fig. 3. Change in conductivity for FA4 in Fig. 2(b) and its derivative,  $d\sigma/dt$ .

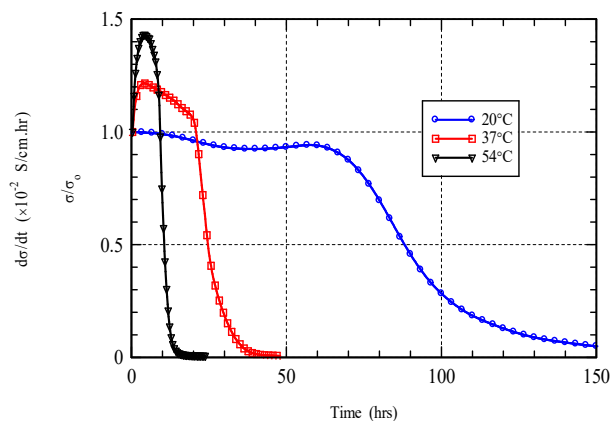


Fig. 4. Relative change in conductivity for FA3 at different ambient temperatures.

Table 3. Summary of derivative data for fly-ashes (at 20°C)

Ash	Extent (duration) of Region II (hrs)	$\sigma_o/\sigma_{150}$	$ d\sigma/dt _{max}$ ( $\times 10^{-4}$ S/cm.hr)	Time, T, to $ d\sigma/dt _{max}$ (hrs)
FA1	75-117 (42)	4.11	5.3	117
FA2	48-73 (33)	11.07	6.2	73
FA3	57-85 (28)	20.28	6.2	85
FA4	75-113 (38)	6.70	5.4	113
FA5	81-130 (49)	2.89	3.5	130
FA6	50-82 (32)	14.86	4.7	82

- specimen, with increasing rigidity reflected by increasing values of  $\sigma_o/\sigma_{150}$ .
- (c) the maximum value of the derivative,  $|d\sigma/dt|_{max}$ , which would increase with increasing reactivity of fly-ash; and,
  - (d) the time, T, to the maximum value of  $|d\sigma/dt|$ ; as with (a) above, the shorter the time, T, the more reactive the fly-ash.

It is evident that there is a good correlation between the values presented in Table 3 and the fineness/coarseness of the ash.

A limited study was undertaken on the influence of ambient temperature on reaction kinetics. Fig. 4 presents the response for FA3 using the base-mix with  $Na_2SO_4$  dissolved in the gauging water; in this Figure, the change in conductivity,  $\sigma$ , relative to the value at the start of the,  $\sigma_o$ , is presented. This Figure clearly indicates that the reaction process is also thermally activated with increasing temperature reducing the time zones over which Regions I-IV start/end.

### 3.2. Frequency Effect Studies

Fig. 5(a) and (b) displays, respectively, the Nyquist plot for mortar samples obtained ~20 minutes after gauging

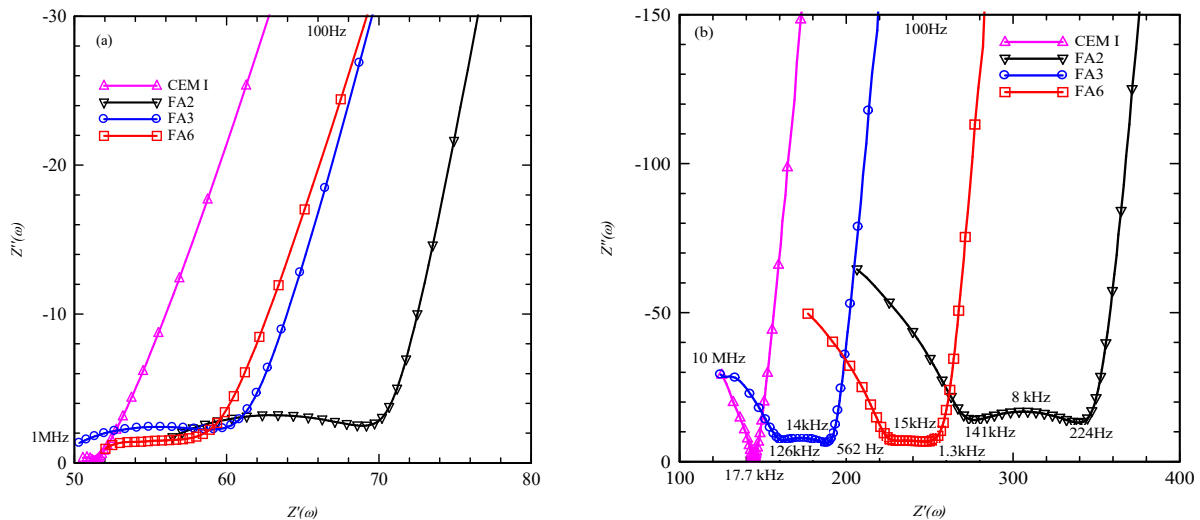


Fig.5. Nyquist plots for mortars (a) 20 minutes after mixing, and (b) 3-days after mixing.

and ~3 days after gauging, with data presented within the frequency range 100Hz-10MHz. For clarity only selected measurement points are highlighted, although plots are drawn through all measurement points. A plain CEM I cement mortar and CEM I mortars with FA2, FA3 and FA6 ashes are presented; some salient frequencies are

indicated on these plots.

The plot for the plain cement mortar displays a typical two-region response which is well documented [4], with the electrode polarization arc forming the right-hand-side of a 'V' shaped plot, and a small arc forming the left-hand-side representing the bulk (sample) response. This feature is more evident in Fig. 5(b). The addition of fly-ash results in several significant changes in the Nyquist plot:

- i) the two regions associated with the plain mortar response become separated by a distinctive *plateau* region creating a response which is now characterised by three distinct zones: the electrode response, a *flat* region associated with the inclusion of fly-ash, and a bulk arc;
- ii) the addition of fly-ash results in an overall displacement of the Nyquist plot to the right; and,
- iii) the different fly-ashes produce detectable differences; for example, FA2 displays a distinct plateau region, which takes the form of a circular arc whose centre is depressed below the real axis; FA3 also displays a circular arc, but the extent of the *plateau* region is reduced in comparison to FA2; FA6, although having similar resistances to FA3, displays a plateau region which is not as prominent or *arc-shaped* as FA2 or FA3.

Fig. 5(b) also illustrates the persistence of the effect of the fly-ash even after the cement component has set and entered the hardening process. Regarding (iii) above, this feature is more clearly seen in Fig. 6(a) whereby the Nyquist plots in Fig. 5(a) are *normalized* by dividing both  $Z'(\omega)$  and  $Z''(\omega)$  by the respective value of bulk resistance ( $R_b$ ) obtained at the junction between the electrode arc and sample response [9]. This allows a better comparison between the three different ashes as there will be minor variations in the pore fluid chemistry (hence bulk resistance) resulting from differing oxide compositions. Regarding their composition, the most significant difference between these three ashes lies in their carbon content, which is quantified by their LOI. FA2 and FA3 have similar LOI's (5.5% and 5.3% respectively) hence a similar response as shown in Fig. 6(a); however, FA6 is approximately 60% less (1.9%). The electrically conductive nature of the unburnt carbon [9] would explain the reason as to why the plateau region is not as prominent in FA6. It is also interesting to note that this plateau region between the electrode spur and the bulk arc has been identified in fibre reinforced cement composites containing (electrically conductive) carbon/steel fibres [10, 11]. Fig. 6(b) shows the cellular morphology to unburnt carbon in fly-ash.

Fig. 7(a) and (b) present the Nyquist plots taken ~20 minutes after mixing for, respectively, neat cement pastes and concretes with different fly-ash replacement levels (FA2 used in this set of tests). This further highlights the influence of the fly-ash on the electrical response with the plateau region increasing almost in direct proportion to the fly-ash content. The Nyquist plots also become more progressively displace to the right as the samples become more resistive and would imply that the fly-ash is acting as an inert filler at this early stage in the hydration process.

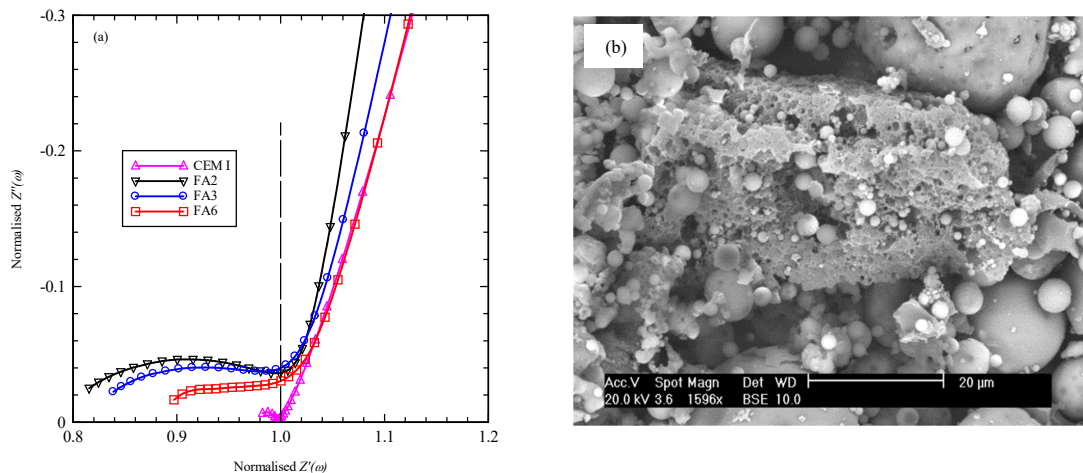


Fig.. 6. (a) Normalised Nyquist plots in Fig. 5(a) allowing comparison of the extent of the plateau region, and (b) micrograph showing cellular nature of unburnt carbon.

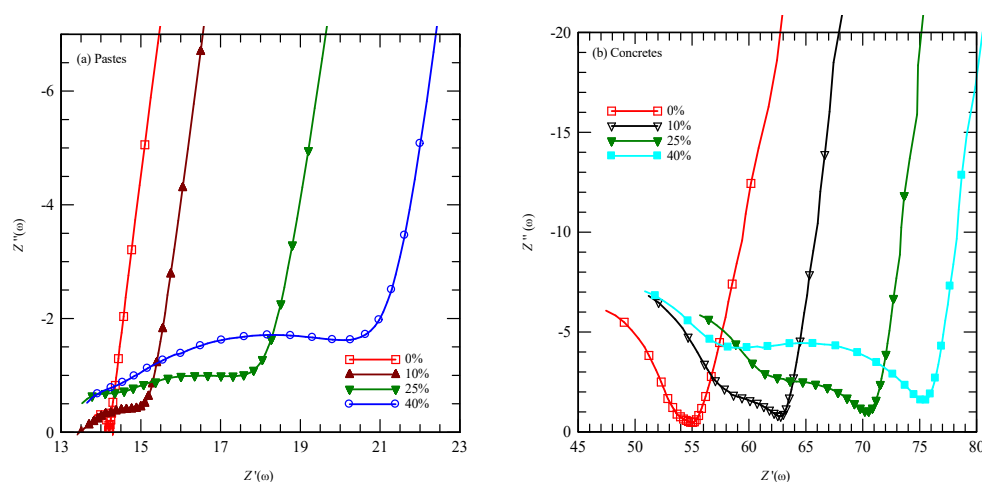


Fig. 7. Nyquist plots for (a) paste and (b) concrete specimens with replacement levels of 0%, 10%, 25% and 40%

#### 4. Concluding Comments

This paper has extended the range of application of EIS to characterise fly-ash in terms of its unburnt carbon content and reactivity with chemical activators. It was shown that single frequency (10kHz) electrical property measurements could be exploited in following the reaction kinetics – at ambient and elevated temperatures - when FA is activated with a suitable activator or combination of activators; it was found that the fineness of the ash played an important role in this respect. A number of salient features were identified from the conductivity vs. time response and the  $d\sigma/dt$  curve which could be exploited in evaluating the efficacy of different activators. In connection with the unburnt carbon-content of the ash, this results in the emergence of the distinctive plateau when plotted using the Nyquist formalism. As strict requirements are set on the LOI of the ash, EIS techniques could be exploited as a rapid means of quality control in this respect.

#### Acknowledgements

The authors wish to thank the Engineering and Physical Science Research Council (UK) for financial support.

#### References

- [1] British Standards Institution, BS EN450-1:2012. 'Fly ash for concrete-Part 1: Definition, specifications and conformity criteria', BSI, London.
- [2] C. Tashiro, K. Ikeda, Y. Inoue, Evaluation of pozzolanic activity by the electric resistance measurement method, *Cem. Concr. Res.*, 24(6), 1994, pp1133-1139.
- [3] W.J. McCarter, D. Tran, Monitoring pozzolanic activity by direct activation with calcium hydroxide, *Constr. Build. Matls.*, 10(3), 1996, pp179-184.
- [4] W.J. McCarter, R. Brousseau, The A.C. response of hardened cement paste, *Cem. Conc. Res.*, 20(6), 1990, pp891-900.
- [5] W.J. McCarter, H. Ezirim, A.C. Impedance profiling within cover-zone concrete: influence of water and ionic ingress, *Advs. Cem. Res.*, 10(2), 1998, pp57-66.
- [6] British Standards Institution, BS EN197-1:2011, Cement: Composition, specifications and conformity criteria for common cements, BSI, London.
- [7] British Standards Institution, BS EN 196-1:2005, Methods of testing cement – Part 1: Determination of strength, BSI, London.
- [8] C. Kulasuriya, V. Vimonsatit, W.P.S. Dias, P. De Silva, Design and development of Alkali Pozzolan Cement (APC), *Constr. Bldg. Matls.*, 68(15 Oct.), 2014, pp426-433.
- [9] W.J. McCarter, T.M. Chrisp, G. Starrs, The complex impedance response of fly-ash cements revisited, *Cem. Conc. Res.*, 34(10), 2004, pp1837-1843.
- [10] T.O. Mason, M.A. Campo, A.D. Hixson, L.Y. Woo, Impedance spectroscopy of fiber-reinforced cement composites, *Cem. Conc. Comp.*, 24(5), 2002, pp457-465.
- [11] S. Wansom, N.J. Kidner, L.Y. Woo, T.O. Mason, AC-impedance response of multi-walled carbon nanotube/cement composites, *Ibid*, 28(6), 2006, pp509-519.





Sustainable Civil Engineering Structures and Construction Materials, SCESCM 2016

# Creep Behaviour of Self-Compacting Concrete Incorporating High Volume Fly Ash and Its Effect on the Long-Term Deflection of Reinforced Concrete Beam

Stefanus A Kristiawan<sup>a,\*</sup>, Agung P Nugroho<sup>b</sup>

<sup>a</sup>SMARTCrete Research Group, Civil Engineering Department, Sebelas Maret University, Indonesia

<sup>b</sup>PT Wijaya Karya Tbk, Indonesia

---

## Abstract

Sustainable infrastructures may be achieved by utilizing green construction materials. In term of reinforced concrete structure, this could be attained by the use of concrete with less cement content. In this research, self-compacting concrete has been developed with an inclusion of high volume fly ash as cement replacement. The benefit of incorporating high volume fly ash on the creep behaviour self-compacting concrete was investigated through experimental laboratory. The short-term data were then used to estimate long-term creeps with the ACI 209 model. A computation of creep effect on the long-term deflection of reinforced self-compacting concrete beam was accomplished to study the influence of major parameters on the magnitude of deflection.

© 2017 The Authors. Published by Elsevier Ltd.

Peer-review under responsibility of the organizing committee of SCESCM 2016.

*Keywords:* creep; deflection; deformation; fly ash; self-compacting concrete

---

## 1. Introduction

Infrastructure has a significant impact on sustainability, and promoting sustainable infrastructure is an urgent need. Sustainable infrastructure may be achieved by utilizing green construction materials. It is recognized that concrete, one of the major construction materials utilized for the development of various infrastructures, is not sustainable for a variety of reasons. First, the production of concrete consumes a huge quantities of virgin materials.

---

\* Corresponding author. Tel.: +0-000-000-0000 ; fax: +0-000-000-0000 .

E-mail address: [s.a.kristiawan@ft.uns.ac.id](mailto:s.a.kristiawan@ft.uns.ac.id)

Second, the principle binder of concrete is Portland cement, the production of which is a major contributor to greenhouse gas emissions that are implicated in global warming and climate change. Third, many concrete structures suffer from lack of durability which has an adverse effect on the resource productivity of industry [1].

A special type of concrete, namely self-compacting concrete (SCC), has been developed and widely used in the concrete industry to efficiently reduce the need for vibration in order to obtain a good quality of hardened concrete. The ability of SCC to flow, pass through obstacle, and fill any spaces in the congested area offers advantages in terms of concreting practices over conventional concrete. However, the composition of SCC tends to have a higher cement content compared to that of normal concrete. Hence, a reduction of cement content in the SCC composition becomes necessary to promote more sustainable concrete. The reduction can be accomplished by a partial replacement of cement with a high volume fly ash i.e. at least 50% by weight of cement is replaced with fly ash.

SCC incorporating high volume fly ash has been the subject of various investigations. Based on the previous works [2-5], the strength of SCC could be expected to reach in the range of 15-25 MPa at 28 day; but the compressive strength is still increased to 25-32 MPa at 90 day. A high strength SCC with high volume fly ash is also possible. An inclusion of high volume fly ash in SCC could improve the durability of the concrete. The chloride penetration resistance of this concrete is optimum at about 55% fly ash replacement level. A better resistance of this concrete against sulfuric acid attack is found when a higher volume fly ash is incorporated. The presence of high volume fly ash could also reduce the shrinkage of SCC. In addition to all of these properties, the design and utilization of structural SCC containing high volume fly ash should also consider time-dependent effect of creep which control serviceability of structural member.

Concrete with higher cement content as that of SCC tends to show a higher creep than that of normal concrete. A higher creep leads to a higher long-term deflection. In the normal reinforced concrete element, creep contributes to the long-term deflection of reinforced concrete beam by a factor of 2. If SCC is used instead of normal concrete, the portion of deflection due to creep will be much higher [6]. Hence, to reduce the deflection of reinforced self-compacting concrete element, a modification in the ingredients of SCC is proposed. It is known that the influencing parameters that affect creep are similar with that of shrinkage [7]. One of the major influencing parameters is cement content. Since cement is the source of both shrinkage and creep in the concrete, replacing a portion of cement with fly ash at high volume level could be justified to lower creep [5].

Modern design codes of structures require that a structure must be designed to simultaneously satisfy a number of different limit states including strength and serviceability. One of the specified criteria to satisfy the serviceability limit states is that the magnitude of deflection must be limited [8]. To be able to assess the deflection of reinforced concrete element that utilizing SCC with high volume fly ash, it is necessary to, first, quantify the creep behaviour of this type of concrete. Two methods may be employed to quantify creep i.e. quantification of creep based on the mix composition of concrete and quantification of creep based on the short-term data. The ACI 209.2R-08 [9] model for estimating long-term creep does not recognize the influence of fly ash as cement replacement at high volume level. Most of other codes have also been developed using data of normal concrete. Hence, for the current research the best way to quantify the long-term creep behaviour of SCC containing high volume fly ash is by measurement of this concrete for short-term period. The obtained short-term data of creep are then used to estimate the magnitude of long-term creep using ACI 209 model. The procedure of estimating long-term creep adopted in this research is similar to that for shrinkage [5,10-11]. After creep has been quantified, the next step is to calculate creep effect on the structural concrete and check if the serviceability limit is satisfied.

Method to calculate long-term deflection with respect to the effect of creep proposed in the ACI 209R-92 [12] is to calculate the time-dependent deflection based on empirical formula that gives the time-dependent deflection as the instant deflection multiplied by the factor  $\lambda$  where  $\lambda$  representing the effect of creep and reinforcement ratio. The effect of creep may also be calculated using analytical model instead of empirical formula [8,13]. The gradual development of creep strain in the compression zone of a reinforced concrete cross-section causes an increase of curvature and a consequent increase in the deflection of the member. Creep in the compression zone causes a lowering of the neutral axis and a consequent reduction in the compressive stress level. Creep is slowed down as the compressive stress reduces, and the increase in curvature is proportional to a small of the creep coefficient. For a cracked beam, the tensile zone of concrete below the neutral axis is assumed to carry no load and thus, does not creep. For this reason, the relative increase in deflection caused by creep is greater in an uncracked beam than in a cracked beam, although the total deflection in the cracked beam is significantly greater [8]. For the current research,

ACI 209 method of estimating creep effect on concrete structures is adopted to assess the influence of high volume fly ash on the deflection of reinforced concrete beam.

## 2. Laboratory Investigation of Creep

### 2.1 Mixture Proportion

The composition of SCC was determined following the recommendation by Okamura and Ozawa [14]. First, coarse aggregate (CA) having a maximum size of 10 mm was proportioned at 50% of the total volume of solid ingredients. Fine aggregate (FA) was selected to be 40% of the volume of mortar. Volume ratio of water/cement (W/C) was chosen in the range of 0.9-1; and finally the superplasticizer (Sp) dosage was determined to meet the self-compacting concrete criteria. After several trials, the following proportion of SCC was obtained as per m<sup>3</sup>: 670 and 671 kg of CA and FA, respectively; 677 kg of cement (C) and 151 kg of water (W). The mixture required 7.72 kg of Sp. The amounts of fly ash were then determined to replace cement at 35%, 55% and 65% by weight of binder. Hence, three mixture composition were proposed and identified as SCC-35, SCC-55 and SCC-65. To reduce excessive water in the mixture as a consequence of cement replacement with fly ash, the amount of water was adjusted to maintain the mixture possessing similar flowability. Table 1 summarizes the proportion of SCC used in this research.

Table 1. Proportion of SCC

Mix Identification	Cement (kg)	Fly ash (kg)	Sand (kg)	Coarse Aggregate (kg)	Water (kg)	Superplasticizer (kg)
SCC-35%	440	237	671	670	151	7.72
SCC-55%	305	373	671	670	149	7.72
SCC-65%	237	440	671	670	124	7.72

### 2.2 Fresh Properties of SCC

The following test methods were carried out to assess the fresh characteristics of SCC i.e. flow table, J-Ring, L-Box, Box-Type and V-funnel test. These test methods followed reference [15]. All three mixes meet the requirements of SCC as shown in Table 2.

Table 2. Fresh Properties of SCC

Type of test	Parameter	Results		
		SCC-35%	SCC-55%	SCC-65%
Flow Table	diameter (mm)	745	740	765
	t <sub>500</sub> (sec)	3.70	3.57	3.27
	velocity (mm/sec)	32.533	37.463	54.255
J-Ring	diameter (mm)	605	680	665
	t <sub>500</sub> (sec)	9.58	8.36	7.15
	velocity (mm/sec)	17.958	35.380	35.395
L-Box Type	t <sub>200</sub> (sec)	3.34	4.20	5.40
	t <sub>400</sub> (sec)	6.50	6.70	7.20
	h <sub>2</sub> /h <sub>1</sub>	0.73	0.90	0.85
Box Type	h <sub>2</sub> (mm)	350	350	350

	h2/h1	1	1	1
V funnel	t (sec)	24.73	22.98	16.00

### 2.3 Measurement of Creep

Five cylinder specimens of 7.5 mm x 275 mm were cast for each mix proportion of SCC. The shape and size of the specimens followed RILEM TC 107-CSP [16]. On each surface of cylinder specimen, 4 pairs of demec points with gauge lengths of 200 mm at equidistant of 90° were glued using epoxy adhesive. All the gluing process of demec points were conducted at 1 day after casting. Three of these specimens were prepared for measuring time-dependent deformation without loading (shrinkage). While the rest of the specimens would be arranged in series and axially under a sustained compressive load in the creep loading frame (see Fig. 1). The compressive load was applied by tightening loading nuts to give an axial stress equals to 30% of the compressive strength. For the current study, the following compressive strengths were obtained at 28 day: 54.5, 46.9 and 40.1 MPa for SCC-35, SCC-55 and SCC-65, respectively. The target loading stress could be determined by measuring the deformation of steel dynamometer that had been calibrated. The instantaneous (elastic) deformation due to the applied axial compressive stress and the subsequent time-dependent deformation due to the sustained compressive stress were observed by measuring the change in length of the distance between a pair of demec points. Both deformation (change in length) on the unloaded and loaded specimens were measured using a demountable mechanical (Demec) strain gauge with a resolution of 1 micron. For every single specimen, the deformation was calculated as an average of four measurements of changes in length. The obtained values of change in length were then divided by the original length (gauge length) to determine the deformation in a strain unit. The time-dependent deformation on the loaded specimen represents the total deformation due to both shrinkage and creep. Hence, to determine the deformation due to creep, this total deformation must be subtracted by the time-dependent deformation on the unloaded specimen (shrinkage). Both deformations on the loaded specimens and their concurrent deformations on the unloaded specimens were measured for a period of 90 days under laboratory environment.

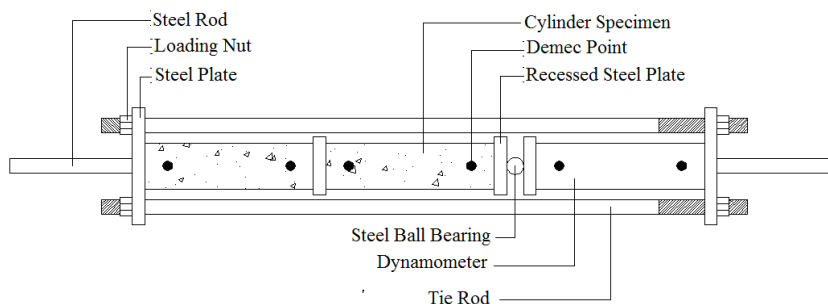


Fig. 1. Arrangement of specimens in creep loading frame

## 3. Creep Behaviour of SCC Incorporating High Volume Fly Ash

### 3.1 Short-term creep

The time-dependent total deformations measured on the loaded specimens are presented in Fig. 2. (a). These magnitude of total deformations must be deducted by the deformations due to shrinkage measured on the unloaded specimens (Fig. 2. (b)) to obtain the time-dependent deformations due to creep (Fig. 2. (c)). The magnitude of creep is influenced by the level of sustained load; so it is convenient to convert the value into creep coefficient for structural creep analysis. Creep coefficient is defined as a ratio between deformation due to creep and that of due to elastic property of the concrete. The value of creep coefficients for the type of concretes investigated in this study are summarized in Fig. 2. (d). The figure clearly shows that incorporating high volume fly ash into SCC has a benefit of reducing creep. A lower creep is observed in SCC with a higher inclusion of fly ash. The effect is consistent with

that observed on shrinkage. These results indicate that both creep and shrinkage are influenced by the similar parameters. For this current study, it is the proportion of the binder which gives a significant effect. SCC with 55-65% fly ash could reduce the value of creep coefficient by 50-60% compared to that of SCC with 35% fly ash. It is recognized that cement is the most important factor in creep because the hydrated cement paste is the seat of the phenomenon. The effect of cement is twofold: that arising from the physical and chemical properties of cement, and that due to variation in the amount of the hydrated cement paste. The first effect will be significant when a different type of cement or binder is used. For similar cement or binder, the later effect could be prominent. Creep decreases with a decrease in the cement paste content [17]. For this current study, there are no differences on the type of cement and fly ash which are used for the production of all SCC mixtures. The difference is only on the amount of the proportion of the binder. Thus, this difference in the proportion of the binder could be responsible to the creep behaviour of SCC observed in this study. SCC with a higher level of fly ash (or lower cement content) tends to have a lower creep.

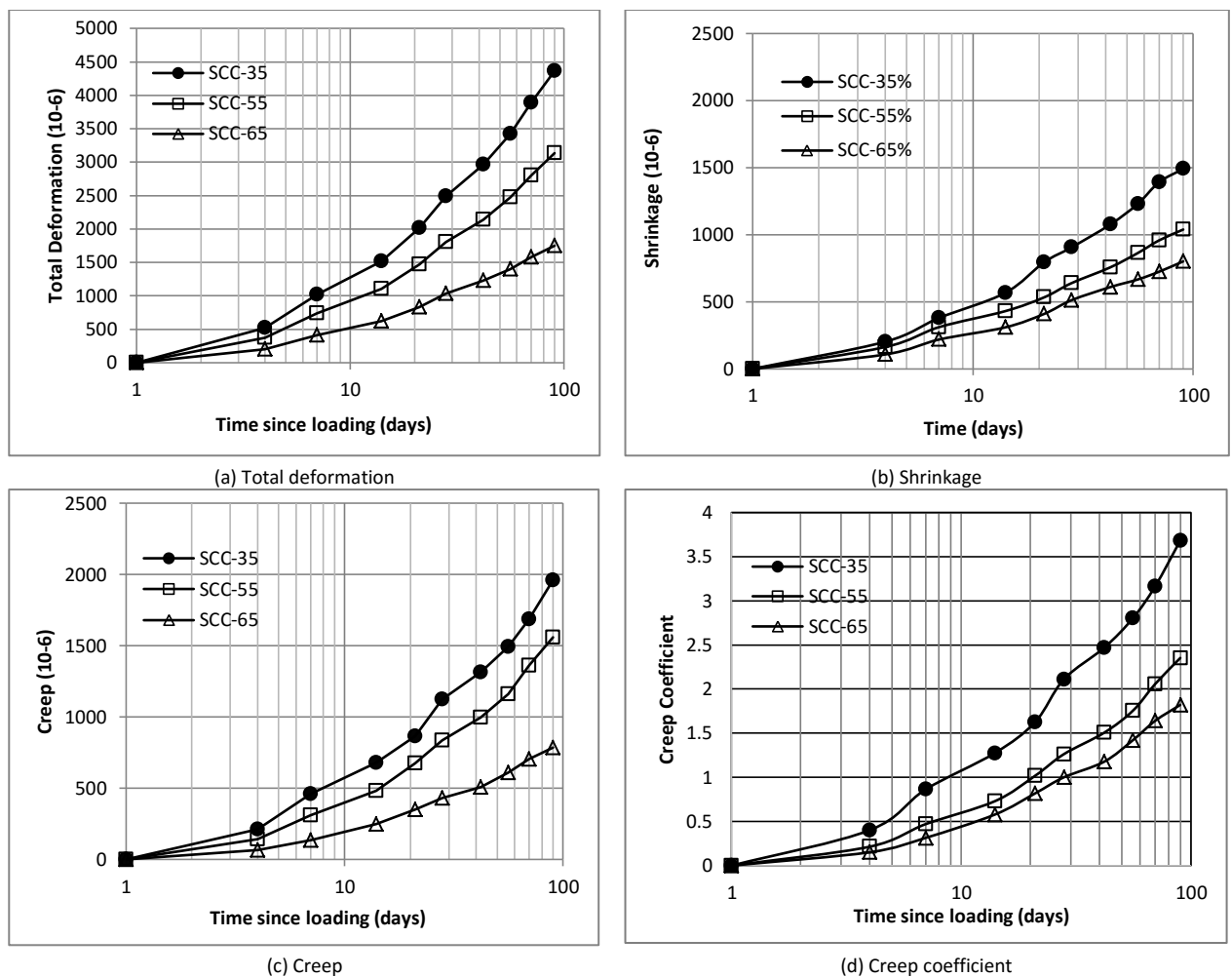


Fig. 2. Short-term time-dependent deformation properties of SCC

### 3.2 Prediction of long-term creep

ACI 209.2R-08 [9] provides a guide for modeling and calculating shrinkage and creep in hardened concrete. The model is applicable for typical composition of concretes having a compressive strength within a range of at least 20

to 70 MPa. Concrete with fly ash content larger than 30% is excluded. ACI 209 model has two components that determine the asymptotic value and the time development of creep is presented in Eq. (1) where the predicted parameter is in the form of creep coefficient.

$$\phi_{(t,t_0)} = \frac{(t-t_0)^{0.6}}{10+(t-t_0)^{0.6}} \phi_u \tag{1}$$

- $\phi_{(t,t_0)}$  = creep coefficient
- $\phi_u$  = ultimate creep coefficient
- $t$  = duration of loading (days)
- $t_0$  = time at first loading (days)

For the standard conditions, the average value proposed for the ultimate creep is 2.35. This value needs to be modified by correction factors to account for conditions other than the standard conditions. For concrete with composition of fly ash larger than 30% and conditions difference to those specified as standard conditions, the model may be applied by providing the short-term data of creep. Thus, the model is used to extrapolate the tendency of creep as obtained from the short-term measurement. The extrapolation procedure is, first, to determine the ultimate creep value. This can be evaluated from the time ratio of Eq. 1 and the short-term creep coefficient data. Based on this evaluation technique, the obtained ultimate creep coefficients are summarized in Table 3. The ultimate creep coefficients of these SCCs are likely to be higher than the ultimate creep coefficient proposed in ACI 209 model. The fewer amount of coarse aggregate in the SCC mixtures may be the cause of this phenomenon. While the cement paste is the source of deformations both due to shrinkage and creep, the present of aggregate will restrain the deformations. Thus, the restraint of deformations on concrete with fewer coarse aggregate will be certainly lesser.

The next step in the prediction of creep coefficient is to use the ultimate creep coefficients to extrapolate the creep coefficients in time using Eq. 1. The results are presented in Fig. 3. It can be shown that the creep coefficients at 3 months and 1 year after loading could reach about 60% and 80% of the ultimate value, respectively, for all the SCC mixtures. After 1 year of loading, the development of creep coefficient is very slow and it requires at least 5 years for creep coefficient to attain 90% of the ultimate value.

Table 3. Ultimate creep coefficient

Concrete	$\phi_u$
SCC-35	5.26
SCC-50	3.28
SCC-65	2.59

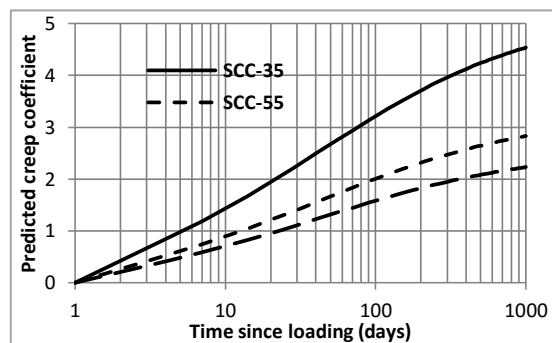


Fig.3. Predicted creep coefficient of SCC

## 4. Prediction of Creep Effect on the Deflection of Reinforced Concrete Beam

Prediction of structural response of reinforced concrete due to creep effect is complicated by a continuous redistribution of stress: the neutral axis is lowered with a consequent decrease in the stress in concrete and an increase the stress in steel. However, an exact analysis of creep effect is not always necessary in most cases. A simplified method of creep analysis may be used as an alternative which still delivers an acceptable result. ACI 209R-92 [12] provides simplified methods of creep analysis for two cases. One of the cases is when the gradual time change of stress due to creep and shrinkage is small and their effect is negligible. For this particular case, the deflection of reinforced concrete beam due to creep,  $\Delta_{(t,t_0)}$ , is calculated using Eq. (2) as follows:

$$\Delta_{(t,t_0)} = \xi_r \phi_{(t,t_0)} \Delta_i \tag{2}$$

where  $\Delta_i$  is instantaneous (elastic) deflection at time  $t_0$  when the load is first applied and  $\xi_r$  is a factor to account for the movement of neutral axis and the presence of compression steel in reinforced member  $A_s'$ , and the inclusion of tension reinforcing steel  $A_s$ . The value of  $\xi_r$  is estimated using Eq. (3):

$$\xi_r = 0.85 - 0.45 \left( \frac{A_s'}{A_s} \right), \text{ but not less than } 0.40 \tag{3}$$

The instantaneous deflection  $\Delta_i$  could be calculated from a static analysis as given in Eq. (4)

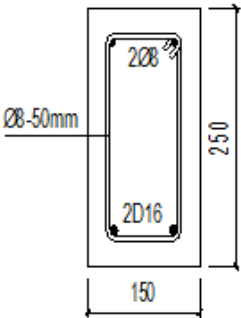
$$\Delta_i = \frac{\xi M l^2}{E_{ci} I} \tag{4}$$

where  $\xi$  is a constant depending on the type of loading and of support,  $M$  is a maximum bending moment,  $l$  is the span length,  $E_{ci}$  is an initial elastic modulus and  $I$  is the moment of inertia of the cross section of the reinforced concrete beam.

Table 4. Material and cross section properties of the reinforced concrete beam

Reinforced Concrete Beam Section	Properties	SCC-35	SCC-55	SCC-65	Unit	
	Compressive strength	$f_c$	54.5	46.9	40.1	MPa
	Flexural strength	$f_r$	6.21	5.52	4.51	MPa
	Elastic modulus	$E_{ci}$	31702	32823	32911	MPa
	Ultimate creep coefficient	$\phi_u$	5.26	3.28	2.59	NA
	Compression steel	$A_s'$	100.53	100.53	100.53	mm <sup>2</sup>
	Tension steel	$A_s$	402.12	402.12	402.12	mm <sup>2</sup>
	Yield strength of steel	$f_y$	437.89	437.89	437.89	MPa
	Elastic modulus of steel	$E_s$	200000000	200000000	200000000	MPa
	Gross Moment of Inertia	$I_g$	209527370	208962949	208920229	mm <sup>4</sup>
	Cracked Moment of Inertia	$I_{cr}$	60272160	58737240	58621174	mm <sup>4</sup>
	Cracking Moment	$M_{cr}$	10670544	9621418	7722728	N.mm
	Yield Moment	$M_y$	31568109	31852019	31874306	N.mm
	Effective Moment of Inertia	$I_e$	105371841	108603056	108844832	mm <sup>4</sup>



Effective depth (d) = 200 mm  
Span length (l) = 3 m

Reinforced Concrete Beam Section	Properties	SCC-35	SCC-55	SCC-65	Unit	
	Compressive strength	$f_c$	54.5	46.9	40.1	MPa
	Flexural strength	$f_r$	6.21	5.52	4.51	MPa
	Elastic modulus	$E_{ci}$	31702	32823	32911	MPa
	Ultimate creep coefficient	$\phi_u$	5.26	3.28	2.59	NA
	Compression steel	$A_s'$	100.53	100.53	100.53	mm <sup>2</sup>
	Tension steel	$A_s$	402.12	402.12	402.12	mm <sup>2</sup>
	Yield strength of steel	$f_y$	437.89	437.89	437.89	MPa
	Elastic modulus of steel	$E_s$	200000000	200000000	200000000	MPa
	Gross Moment of Inertia	$I_g$	209527370	208962949	208920229	mm <sup>4</sup>
	Cracked Moment of Inertia	$I_{cr}$	60272160	58737240	58621174	mm <sup>4</sup>
	Cracking Moment	$M_{cr}$	10670544	9621418	7722728	N.mm
	Yield Moment	$M_y$	31568109	31852019	31874306	N.mm
	Effective Moment of Inertia	$I_e$	105371841	108603056	108844832	mm <sup>4</sup>



For the purpose of illustrating the effect of SCC creep incorporating high volume fly ash on the deflection of reinforced concrete beam, a parametric study is executed. The material and cross section properties of the reinforced concrete beam for this parametric study are summarized in Table 4. A simple beam having a span length of 3 m and an effective depth of 200 mm are considered in this study. For this deflection analysis, an area of any part of the composite section is replaced by a transformed area. Deflection of the beam will be examined on two conditions of loading. First, a distributed sustained load which gives a maximum bending moment ( $M_D$ ) below cracking moment ( $M_{cr}$ ) is analyzed to represent the uncracked reinforced concrete beam. Second, a higher distributed sustained load causing a maximum bending moment ( $M_D$ ) greater than cracking moment ( $M_{cr}$ ) but less than first yield moment ( $M_y$ ) is evaluated as an example of cracked reinforced beam. The results of predicted instantaneous and time-dependent deflection due to creep of SCC incorporating high volume fly ash are given in Table 5 and Fig. 4, respectively.

Table 5. Instantaneous and ultimate deflection due to creep

Level of loading $M_D$ (N.mm)	Instantaneous deflection $\Delta_i$ (mm)			Ultimate deflection due to creep $\Delta_{(\mu,t)}$ (mm)		
	SCC-35	SCC-55	SCC-65	SCC-35	SCC-55	SCC-65
$600000=M_D < M_{cr}$	0.85	0.82	0.82	3.28	1.98	1.54
$12000000=M_D > M_{cr}$	2.15	3.16	3.14	8.35	7.63	5.93

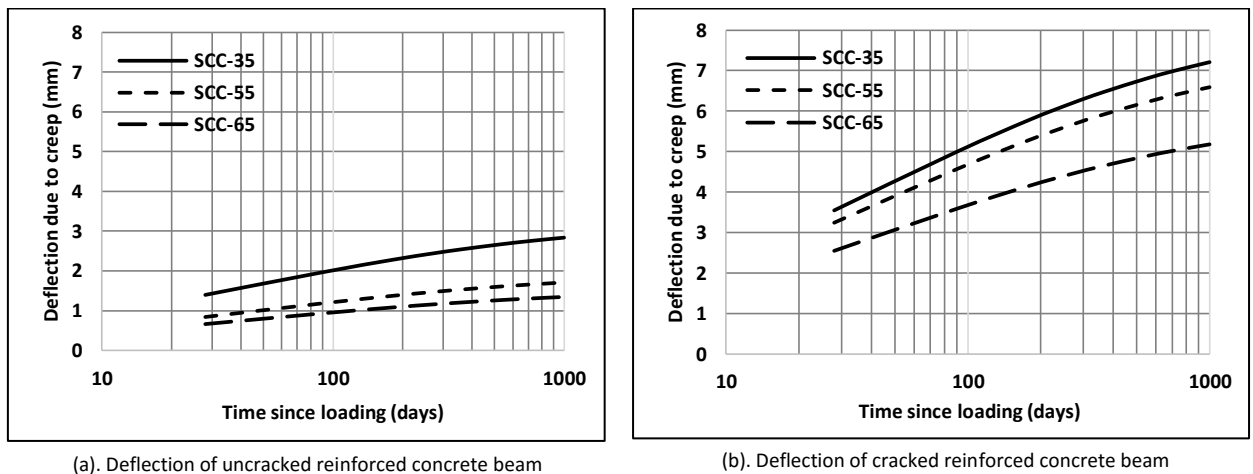


Fig. 4. Time-dependent deflection due to creep

The instantaneous deflection of uncracked reinforced concrete beam is similar for all SCC mixtures as the gross elastic modulus of all the concretes is almost the same. On the other hand, for cracked beam the instantaneous deflection of SCC-35 is the lowest. The reason is that the flexural capacity of this concrete is the highest and so for similar level of loading, the SCC-35 beam would crack with the least intensity. Given the least intensity of cracks, SCC-35 would maintain the highest rigidity. Consequently, under similar level of loading SCC-35 exhibits the lowest instantaneous deflection.

For the time-dependent deflection due to creep (Fig. 4), the trends are consistent with the contribution of SCC creep. SCC with a higher creep coefficient would produce a higher deflection both on the uncracked and cracked reinforced concrete beam. It is noticed that the gap of the time-dependent deflection on cracked beams between SCC-35 and SCC-55 is closer than that of uncracked beam. The explanation is as follows: the rigidity of the uncracked beams is almost similar and so the magnitude of time-dependent deflection is merely dependent on the creep coefficient. In the meantime, for cracked beam a higher rigidity of the SCC-35 beam plays a significant contribution to reduce the deflection. Hence, the difference in the magnitude of time-dependent deflection becomes closer.

The ultimate contribution of SCC creep on the deflection of reinforced concrete beam is in the range of 1.89-3.89 multiplied by instantaneous deflection (Table 5). For SCC-65, the contribution (1.89) is similar to the contribution of

normal concrete creep. At 3 months and 1 year of loading, the deflection due to creep counts to about 60% and 85% of its ultimate value.

## 5. Conclusions

A high magnitude of SCC creep could be reduced by incorporating a high volume fly ash as partial cement replacement. A reduction of creep by 50-60% could be expected when the fly ash replacement level is increased from 35% to 55-65%. The predicted ultimate creep coefficients of SCCs using ACI 209.2R-08 model confirms that the values are higher than that of standard concrete proposed in the model. However, an inclusion of fly ash at 65% by weight of cement will diminish the predicted ultimate creep coefficient of SCC to a similar level with that of normal concrete suggested by ACI 209.2R-08 model. The long-term deflection of reinforced concrete beam due to creep as calculated using ACI 209R-92 model is influenced by both the initial instantaneous deflection and the creep coefficient of the concrete. At an uncracked level of loading, the instantaneous deflection of all SCCs is similar but at a cracked level of loading, SCC-35 gives the lowest instantaneous deflection which is associated with its highest rigidity (least cracks intensity) as a consequence of its higher flexural capacity. However, the ultimate deflection of SCC-35 is the highest since the portion of long-term deflection due to its creep is the largest compared the other SCCs. Generally, SCC creep contributes to the long-term deflection by a factor of 1.89-3.89.

## Acknowledgements

The authors acknowledge the financial support by the University of Sebelas Maret, Indonesia through Hibah Maintenance Research Group 2016.

## References

- [1] P. K. Mehta, High Performance, high-volume fly ash for sustainable development, in *Proceedings of the International Workshop on Sustainable Development and Concrete Technology*, Edited by K Wang, Beijing, China, 2004, pp. 3-14.
- [2] Sunarmasto., S.A. Kristiawan, Effect of fly ash on compressive strength and porosity of self-compacting concrete, *Applied Mechanics and Materials* 754-755 (2015) 447-451.
- [3] S.A. Kristiawan., Wibowo., S. As'ad., B.S. Gan., D.P. Sitompul, Effect of high volume fly ash n the chloride penetration resistance of self-compacting concrete, in *Advances in Civil, Architectural, Structural and Constructional Engineering*, CRC Press, 2016. pp. 31-35.
- [4] S.A. Kristiawan., Sunarmasto., G.P. Tyas, Degradation of self-compacting concrete (SCC) due to sulfuric acid attack: Experiment investigation on the effect of high volume fly ash content, *IOP Conference Series: Materials Science and Engineering* 107 No 1 (2016).
- [5] S.A. Kristiawan., M.T.M. Aditya, Effect of high volume fly ash on shrinkage of self-compacting concrete, *Procedia Engineering* 125 (2015) 705-712.
- [6] W.C. Choi., H.Y. Yun., Long-term deflection and flexural behaviour of reinforced concrete beams with recycled aggregate, *Materials and Design* 51 (2013) 742-750.
- [7] R.A. Mari., J.M. Bairan., N. Duarte, Long-term deflection in cracked reinforced concrete flexural members, *Engineering Structures* 33 (2010) 829-842.
- [8] I. Gilbert, The serviceability limit states in reinforced concrete design, *Procedia Engineering* 14 (2011) 385-395.
- [9] ACI 209.2R-08, Guide for modeling and calculating shrinkage and creep in hardened concrete, American Concrete Institute, Farmington Hills, Michigan, 2008.
- [10] S.A. Kristiawan., S. Sangadji, Prediction model for shrinkage of lightweight aggregate concrete, *Asian Journal of Civil Engineering (Building and Housing)* 10 No. 5 (2009) pp. 549-558.
- [11] S.A. Kristiawan, Evaluation of current models for estimating long-term shrinkage of lightweight aggregate concrete, in *Proceeding of the 3rd International conference of EACEF (Euro Asia Civil Engineering Forum)*, Yogyakarta, Indonesia, 2011, pp. B-57-64.
- [12] ACI 209R-92, Prediction of creep, shrinkage and temperature effects in concrete structures, American Concrete Institute, Farmington Hills, Michigan, 1992.
- [13] A. Ghali., R. Favre., M. Elbdabry, *Concrete Structures: Stress and Deformation*, E&F SPON, 11 New Fetter Lane, London, 2002.
- [14] H. Okamura and K. Ozawa, Mix design for self-compacting concrete, *Concrete Library of JSCE* 25 (1995), pp. 107-120.
- [15] K. Takada and S. Tangtermsirikul, Part IV: Testing of fresh concrete, in A. Skarendahl, O. Petersson (Eds), *Self-compacting concrete*, State of the Art Report of RILEM Technical Committee; 2000, pp. 25-39.
- [16] RILEM TC107-CSP, Measurements of time dependent strains in concrete, *Materials and Structures* 31 (1998), pp. 507-512.
- [17] A.M. Neville, W.H. Dilger, J.J. Brooks, *Creep of plain and structural concrete*, Construction Press, 1983.



Sustainable Civil Engineering Structures and Construction Materials, SCESCM 2016

## Investigation of agro-concrete using by-products of rice husk in Mekong delta of Vietnam

Nguyen Khanh Son\*, Nguyen Phung Anh Toan, Tran Thi Thuy Dung, Nguyen Ngoc Tri Huynh

*Faculty of Materials Engineering, Ho Chi Minh city University of Technology (HCMUT), VNU-HCM  
Building C4, 268 Ly Thuong Kiet street, District 10, Ho Chi Minh city, Vietnam*

---

### Abstract

Agro-concrete concept seems to create interesting links between agriculture sector and building industry. Over the last years, researcher around the world have reported their investigation on such material made out of different type of agricultural by-products mixed with lime-based binder. Based on the locally use natural aggregate and good thermo-physical properties, they are considered as as eco-material for more comfortable low carbon building. Indeed, energy efficiency or thermal conform are improved from optimization of building envelopes. In this paper, we focus on producing concrete block under mechanical compaction method from two types of rice husk (natural and reusing) mixing with binder (hydrate lime and metakaolin). Physio-mechanical properties of concrete block were characterized at appropriate period of curing condition in dry air. Empirical results show that both compressive strength and splitting strength of concrete block evolve over time due to pozzolanic reactivity and natural carbonation reaction. Low thermal conductivity 0.27 W/mK with normal density 880 kg/m<sup>3</sup> in mixed formulation deal with the purpose of using in thermal and acoustic insulating solution. In the current context of rural development in the delta region, the objective of using rice husk concrete for non-load bearing wall building as filling material or non-fired brick would be discussed.

© 2017 The Authors. Published by Elsevier Ltd.

Peer-review under responsibility of the organizing committee of SCESCM 2016.

*Keywords:* Rice husk;agro-concrete;hempcrete;non-fired brick, metakaolin; carbonation, sustainable.

---

---

\* Corresponding author. Tel.: +84 933 623 629; fax: +84 8 38 66 18 43  
E-mail address:ksnguyen@hcmut.edu.vn

## 1. Introduction

In building sector, the passive house is now a sustainable construction concept that provides for affordable, high-quality buildings as well as comfortable, healthy living conditions [1]. In general, specific requirement of passive house standard are rigorous for helping us to improve energy efficiency and to reduce environmental impact of house building. Researchers and professional engineers around the world contribute to practical implementation of passive house certificate from this point of view after considering local climate condition for regionally optimised. For example in tropical climate, they require protecting measure from solar load such as using fixed shading devices for windows, using reflective, cool colours, low-e solar windows with high selectivity and moderate level of insulating materials for thermal comfort. Technically, good practice to build a passive house combine firstly an appropriate architecture design, secondly a new technology in energy saving system and thirdly a relevant material solution. The third one should be negative carbon building material or eco-friendly material. Currently, that is the case of hemp concrete that met such requirement and becoming increasingly demand in some European country and US. We mainly use in housing as filling material or casting material around load-bearing wooden structure for wall application (figure 1). Neutral carbon footprint of vegetable aggregate deduce from the fact that plants store carbon during their growth and the carbon remains locked within the plant material until it decays. Moreover, the absorption of CO<sub>2</sub> by lime partially offsets its release during the production of the binder. Furthermore, using lime helps regulate temperature and humidity within building because it is moisture permeable [2]. In the same way of hemp concrete, eco-friendly materials using locally available agriculture waste are in full development, for example bagasse fibres [3], flax shives [4], hemp hurds [5–8], sawdust [9] and rice husk [10].



Fig. 1. Hemp concrete and practical application in wall building, redrawn with photo from ref. [11].

In Mekong delta (South of Vietnam), rice cultivation is one of the most important economic sector in agriculture. It contributes to overall performance of rice export 6.7 million ton per year of Vietnam. Rice husk is protective shell of the grain, represent about 20 wt% of the whole grain. Hence, in Mekong delta of Vietnam, rice farming produces nearly 1.9 million ton per year of rice husk and almost Vietnamese farmer regard this by-product as waste materials often buried in the ground. In larger scale, recently rice husk was consumed for electricity generation because of their high calorific value. Amorphous silica resulted from rice husk burning process could be used in cement industry as pozzolanic admixture. However, burning process in general makes impact on the environment and not easy to obtain high content of silica in rice husk ash because of their peculiar silica–cellulose structural arrangement [12]. Therefore, rice husks cause critical problems in Mekong delta of Vietnam because significant volumes are generated and not used in a beneficial way. The fact that using of raw and whole rice husk in concrete has rarely been investigated is due to common concern about durable properties of natural aggregate and about mechanical performances essentially studied in practical application of concrete material. This study combines the use of lime-based binder and rice husk to design lightweight concrete block or commonly name non-fired brick. In this regard, rice husks would be considered as natural aggregates like hemp hurds in above hemp concrete. In the following paragraph, we investigate using two types of rice husks as raw product for concreting. Different mix proportions of

rice husks and lime-based binder were formulated concrete block in order to analyse variation of their physio-mechanical properties over curing time.

## 2. Experimental study

In practice, to produce lightweight concrete, there is a compromise between thermal conductivity and compressive strength. The more we use natural aggregate, the more we obtain lightweight concrete with low thermal conductivity. Less mixing water are added in concrete producing, more we obtain high resistance in compression. Hence, concrete mixture correspond to different binder on aggregates mass ratios and water content.

### 2.1. Sampling procedure

As we know, one of the difficulties encountered during the mixing period of hemp concrete is competition for water absorption between the binder and natural aggregate. For this reason, it is essential to take into account the water absorption capacity of the raw natural particles. But in general, rice husks absorb less water due to their low-porous microstructure. Short particle with boat-like shape and spherical extremities of rice husk also permit to disperse easily in binder matrix. Water demand of lime-based binder 0.73 was tested according to standard ASTM C110. Water mixing in concrete was taken at 0.70 for laboratory concreting condition.

First type of rice husk is natural product that collected from a nearby rice milling station in Long An province. Respectively, 15 wt% and 20 wt% of natural rice husk were added in two series of concrete sample, named RH15 and RH20. Second type of rice husk is collected from water filter material of wastewater-treatment plant Binh Hung - Binh Chanh. We rely on the point of view that using solidification/ stabilization technology stabilize the heavy metal contaminant and reduce their mobility. 15 wt% of these reusing rice husk (RHW) was added in formulating lightweight concrete.

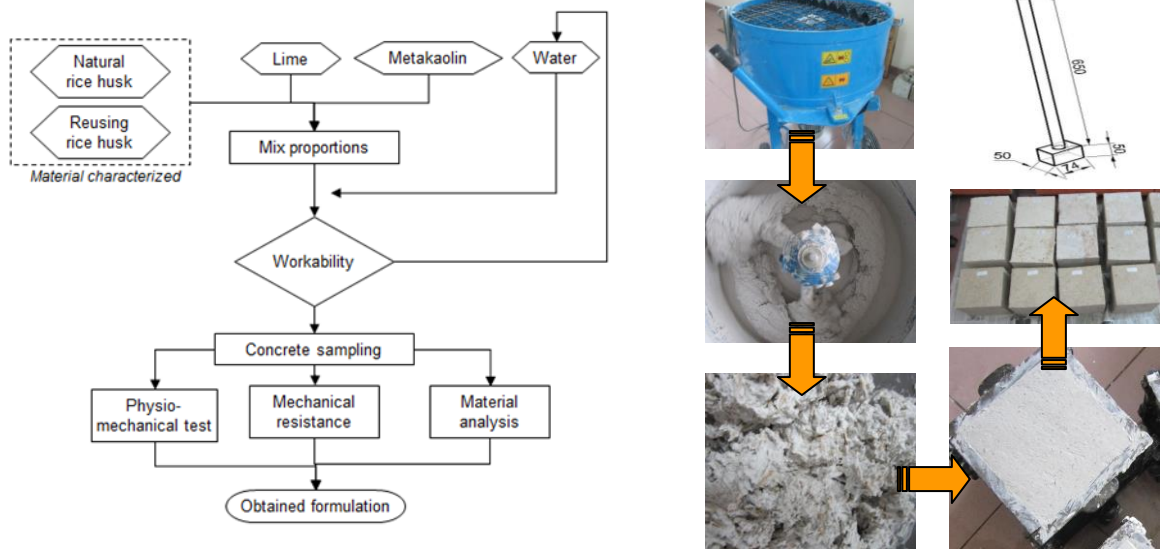


Fig. 2. (a) Schema of experimental campaign; (b) Different step in producing rice husk concrete.

Different step in experimental campaign are summarized in figure 3a. Before casting in molds, mixture of raw material and binder was realized in laboratory pan mixer. Total mixing time in mixer was around 20 minutes including first mixing of lime binder and final incorporating of natural aggregate little by little. The mixture was then placed in cubic mold 15x15x15cm and cylindrical mold  $\phi 15 \times 30$ cm. A mechanical tamping device (figure 3b) was used for sample compaction. For cubic specimens, the height of a single layer is equal to one-third of the total height of the concrete specimen (5cm) and the compacting action 18 times (eq. 3 rounds) is the same for all layers.



By increasing water content, we could obtain lower viscous concrete mixture for sampling in spraying machine. That could be an important factor to increase production yield in practical application. Concrete samples were demolded after 24 hours kept in room condition ( $T=28-30^{\circ}\text{C}$ ,  $\text{RH}=80\pm 10\%$ ). The process of sample curing was applied until hydric stabilization. These specimens kept outdoors for curing period. It is noted that cylindrical samples must be kept carefully from deformation during first time of drying period due to their important height.

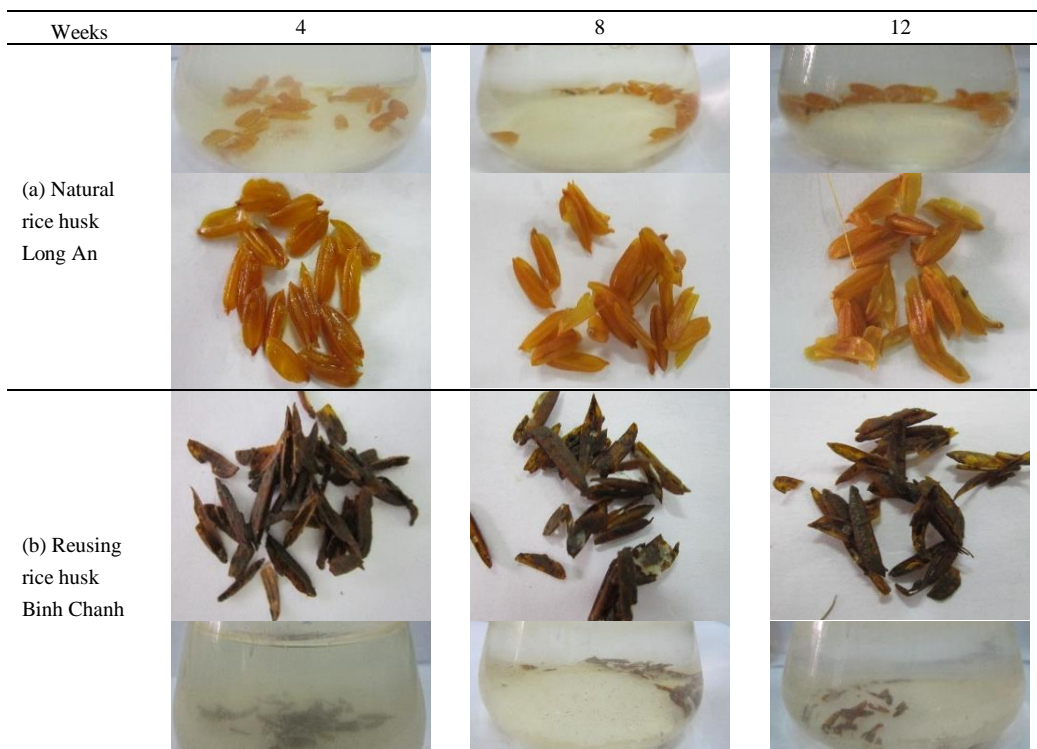
## 2.2. Lime binder and rice husk aggregate

Lime is now regarded as better candidate material than cement for sustainable development. In term of mechanical resistance, rapid setting time, cement is more suitable material solution. But that is not the case of non load-bearing element in housing. Aerial lime Minh Duc (90% of  $\text{Ca}(\text{OH})_2$ ) has been chosen for its great capacity to generate carbonation reaction to convert calcium hydroxide into calcium carbonate. This process starts mostly when the lime has dried enough and it can last for month even years. That is also reason for using metakaolin as mineral admixture. This is high quality supplementary cementing material. We obtained such material from heat treatment of natural kaolinite Lam Dong. Chemical composition of local resource metakaolin is given in table 1. More we use metakaolin, more we attribute short-term resistance to concrete material. However, we limited the use of metakaolin 5 wt% in mixture for reasonable cost of binder.

Table 1. Chemical composition of lime binder and metakaolin Lam Dong.

Oxides	CaO	SiO <sub>2</sub>	Al <sub>2</sub> O <sub>3</sub>	Fe <sub>2</sub> O <sub>3</sub>	MgO	Others	LOI
Hydrate lime Minh Duc	62.1	0.14	0.05	0.05	0.08	9.68	27.9
Metakaolin Lam Dong	0.53	55.1	40.46	1.09	0.56	1.44	0.82

Table 2. (a) natural rice husk from Long An; (b) reusing rice husk from Binh Chanh.



Natural rice husk was selected as a local resource. Literature reveals that depending on the resource, there are in rice husk 75% organic compound and 25% silica inorganic compound. 75% organic compound consists of 45-60%

cellulose/hemi-cellulose and 25-30% lignin [13]. To compare with other lignocellulose material, total amount of cellulose/hemi-cellulose compound is quite high as those of coconut fibre, but smaller than those of hemp hurd (65-70%). In reusing rice husk, the heavy metal contaminant include Pb 32.76ppm, Cd 0.596ppm, Cu 142.9ppm, Zn 382.4ppm and they showed dark colour, smaller particle size than natural resource.

Table 2 shows the result of dissolution two type of rice husk in high alkali solution. These test consisted in immersing the particles in pure limewater solution during period of 12 weeks and following photo taken at appropriate interval of time respectively 4-8-12 weeks. After 10 weeks, natural rice husk exposed small dissolution but remaining the integrity of grain particle. Reusing rice husk exposed dissolution of black coating layer and made appear spherical particle inside. The results suggest that reusing rice husk remain good character and could be recycled if we apply an appropriate technique.

### 3. Results

All concrete samples were kept 1 – 2 – 6 months indoors for hardening period. We discuss on the variation of material character over that curing time.

#### 3.1. Thermo-physical properties

Volumetric mass were registered on three type of concrete sample RH15, RH20, RHW at 2 months (table 3). Average result shows only small difference:  $880\pm 10$  kg/m<sup>3</sup> for RH15,  $690\pm 5$  kg/m<sup>3</sup> for RH15 and  $920\pm 15$  kg/m<sup>3</sup> for RHW. Those values are equivalent to plaster, foam concrete's case but still higher than those of autoclave aerated concrete block. By using more aggregate (5 wt% in case of RH20) permit us to decrease average density by 21.5%. Smaller particle size of reusing rice husk contributes to produce denser concrete block.

Table 3. Physical characteristics of rice husk concrete.

Sample series	RH15	RH20	RHW
Volumetric mass, kg/m <sup>3</sup>	$880\pm 10$	$690\pm 5$	$920\pm 15$
Thermal conductivity, W/mK	$0.27\pm 0.015$	$0.25\pm 0.012$	$0.31\pm 0.012$
Water absorption, %wt	$61.9\pm 1.5$	$62.5\pm 2.0$	$56.4\pm 1.8$

During the test of water absorption, all concrete samples were attributed same behavior: first, floating on the water and then gradual wetting of sample skin and sinking in the water tank. In reality, high water absorption of agro-concrete decrease gradually conforming to the progress of carbonation reaction. Among 3 series of concrete samples, the densest specimens RHW attribute less water absorption result and that is not the case RH20.

Thermal conductivity of concrete block were measured on the apparatus QTM 500 at room temperature  $T=28^{\circ}\text{C}$ , RH<85%. Obtained results on table 3 show that thermal conductivity of RH20 0.25 W/mK is lowest, following by RH15 0.27 W/mK and the one of RHW 0.31 W/mK. From the binder on aggregates mass ratio point of view, it seems that we improve thermal isolation by using higher content of rice husk in mixture. High density of RHW concrete sample was also penalized by the most important thermal conductivity result. Also we noted that, experimental result is very sensitive with relative humidity of sample storage.

#### 3.2. Mechanical properties

Compressive strength test were conducted on concrete block 15x15x15cm at different interval of curing period 1-2-6 months. For 2 months sample, average results of drying shrinkage were about 1-3%. Compression load (kN) vs time (s) curves on the figure 3a describe the global mechanical behavior of material under a constant load rate 1,7kN/s. 4 stages include OA (beginning) → AB (linear quasi-elastic behavior) → BC (recovery) → CP (towards an elasto-plastic behavior). In general, such elasto-plastic behavior is revealed in almost case of polymeric composite material. After the recovery stage (BC), the mineral binder and the interface between the natural aggregates and the binder are progressively damaged. This fact makes compress aggregate part and cause significant deformations of



concrete specimens. However, the stress continues to involve due to the compaction ability of rice husk aggregates without complete crack as usual brittle concrete [10]. Meanwhile, we pay attention to two peaks of compression load, corresponding to early resistance (B) and to total failure (D) at 25s after B. Average result of compressive strength are  $0.38\pm 0.03$  MPa and  $0.36\pm 0.02$  MPa, respectively mixture RH15, RH20 after 6 months. That means a lower compressive strength of RHW samples than those of RH15. Regarding the effect of curing time, it seems that the carbonation progress attribute more elasticity to 3 months samples. But in general the variation of resistance at different interval of curing time was not so net.

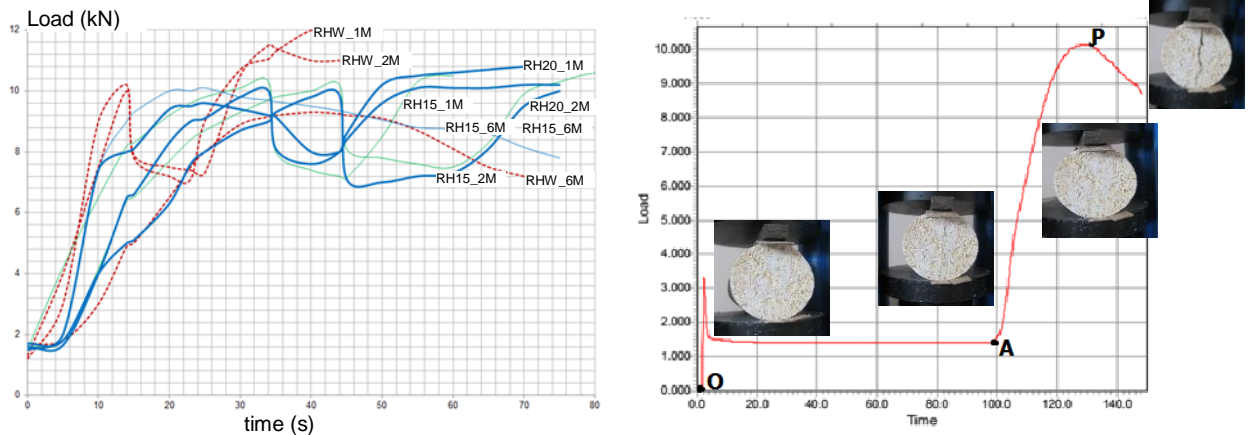


Fig. 3. Curve of compression load vs time during (a) compression test; (b) a splitting test of concrete samples.

Splitting test was also conducted on concrete block  $\phi 150 \times 300$  mm after 6 months of curing time. We applied stress constant rate  $0.00002$  N/mm<sup>2</sup>/s conforming to the requirement of ASTM standard. Figure 3b shows the behavior of material until total failure, including 3 stages: OA (beginning)  $\rightarrow$  AP (critical resistance at P)  $\rightarrow$  after P (sample splitting, decreasing resistance). Average splitting strength was  $0.07\pm 0.003$  MPa,  $0.09\pm 0.002$  MPa and  $0.07\pm 0.003$  MPa respectively for RH15, RH20 and RHW sample series. That means there is a no difference in resistance between two sample series mixing with natural rice husk and reusing rice husk. To use 20 wt% of rice husk in concrete made increase splitting strength by 30%. Such result permit to conclude that tensile strength of agro-material is a relevant property for practical application in wall building.

### 3.3. Matrix analysis by mean of TG/DTA

Given in the figure 4a is the result of thermal analysis TG/DTA of powdered material that we extracted from concrete sample. Between  $30-200^{\circ}\text{C}$ , there is a continuous mass loss about 2.089 wt% corresponding to free water evaporation and/or combustion of organic compound. Between  $300-500^{\circ}\text{C}$ , a mass loss 12.851 wt% associated with endothermic peak on DTA curve corresponds to the dihydroxylation reaction of portlandite. Mass loss between  $575-800^{\circ}\text{C}$  is the most important 19.142 wt% that attributes to the decarbonation reaction of calcite. Last result confirms the presence of calcite after 6 months of hardening due to natural carbonation. In reality, after 1 month, hardening specimens are covered by a rigid skin, mostly composed of carbonate lime.

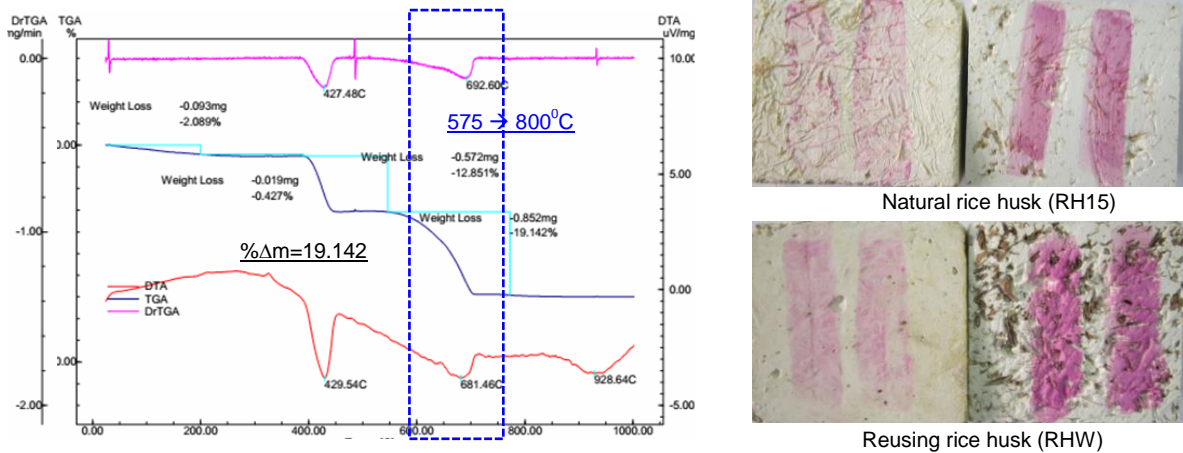


Fig. 4. (a) Diagram of thermal analysis TG/DTA of powdered material; (b) Test on carbonization depth by using phenolphthalein as indicator

Slow carbonation progress could take month or even year for extend the carbonation depth from surface to core of concrete specimens. We tested with phenolphthalein as indicator of carbonation depth. Respectively, they showed faint pink color on the surface skin and pink color on the cutting core of producing rice husk concrete (figure 4b). We explain such result by the fact that pH of portlandite decreased and replaced by neutral calcite product. They exist reaction product and reactant in the same time that may affect on overall resistance of material.

#### 4. Conclusion

By using local rice husk as a vegetable aggregate and a lime-based binder, we successful developed agro-concrete product in block. In comparison with common approach of rice husk recycling, we try valorise this residue in its natural state. We highlight that the formulated composite material could benefit from their low thermal conductivity for the purpose of using as insulating filling material in a wall timber frame or as non-fired brick in wall building. Rice husk concrete blocks have been fabricated in laboratory with the remaining dry density about 880 kg/m<sup>3</sup>. 15 wt% of rice husk and N/V=0.7 are appropriate for the formulation stage with mechanical tamping method. In term of mechanical resistance, both compressive and tensile strength of the concrete specimens was studied. Relevant results suggest that producing concrete block should be used for non-load bearing element, especially in building envelopes. As the carbonation process plays a key role in solidification/ stabilisation of contaminant, we also could reuse rice husk of wastewater treatment in such agro-concrete product to get over the current environmental impact.

#### Acknowledgements

First author would like to thank Ho Chi Minh city University of Technology for the financial support and Binh Hung wastewater treatment plant for supporting raw material.

#### References

- [1] Passipedia.org, the passive house resource: What is a Passive House?
- [2] Benfratello, S., C. Capitano, G. Peri, G. Rizzo, G. Scaccianoce, and G. Sorrentino. Thermal and structural properties of a hemp–lime biocomposite. *Construction and Building Materials* 48 (2013): 745-754.
- [3] Bilba, Ketty, and M-A. Arsene. Silane treatment of bagasse fiber for reinforcement of cementitious composites. *Composites Part A: Applied Science and Manufacturing* 39, no. 9 (2008): 1488-1495.
- [4] Khazma, Mahmoud, Adeline Goullieux, Rose Marie Dheilley, Boubker Laidoudi, and Michèle Queneudec. Impact of aggregate coating with a PEC elastomer on properties of lightweight flax shive concrete. *Industrial Crops and Products* 33, no. 1 (2011): 49-56.

- [5] Nguyen, Tai Thu, Vincent Picandet, Patrick Carre, Thibaut Lecompte, Sofiane Amziane, and Christophe Baley. Effect of compaction on mechanical and thermal properties of hemp concrete. *European Journal of Environmental and Civil Engineering* 14, no. 5 (2010): 545-560.
- [6] Nguyen, Tai-Thu, Vincent Picandet, Sofiane Amziane, and Christophe Baley. "Influence of compactness and hemp hurd characteristics on the mechanical properties of lime and hemp concrete." *European Journal of Environmental and Civil Engineering* 13, no. 9 (2009): 1039-1050.
- [7] Arnaud, Laurent, and Etienne Gourlay. "Experimental study of parameters influencing mechanical properties of hemp concretes." *Construction and building materials* 28, no. 1 (2012): 50-56.
- [8] Nozahic, V., S. Amziane, G. Torrent, K. Saïdi, and H. De Baynast. "Design of green concrete made of plant-derived aggregates and a pumice–lime binder." *Cement and Concrete Composites* 34, no. 2 (2012): 231-241.
- [9] Aigbomian, Eboziegbe Patrick, and Mizi Fan. Development of wood-crete from treated sawdust. *Construction and Building Materials* 52 (2014): 353-360.
- [10] Chabannes, M., Bénézet, J. C., Clerc, L., & Garcia-Diaz, E. Use of raw rice husk as natural aggregate in a lightweight insulating concrete: An innovative application. *Construction and Building Materials*, 70 (2014), 428-438.
- [11] A. Gacoin (2010), Hemconcrete - Insulation Plant, ERASMUS INTENSIVE PROGRAM, Multi-Disciplinary International Project in Passive Design & Construction
- [12] Beagle, Eldon C. Rice-husk conversion to energy. Food and Agriculture Organization of the United Nations, 1978.
- [13] Ali, M. (2012). Natural fibres as construction materials. *Journal of Civil Engineering and Construction Technology*, 3(3), 80-89.



Sustainable Civil Engineering Structures and Construction Materials, SCESCM 2016

## Delamination tendency of repair mortar incorporating crumb rubber

Stefanus A Kristiawan<sup>a,\*</sup>, Amanah N D Hapsari<sup>b</sup>

<sup>a</sup>*SMARTCrete Research Group, Civil Engineering Department, Sebelas Maret University, Indonesia*

<sup>b</sup>*PT Pembangunan Perumahan, Indonesia*

---

### Abstract

The success of repair material to extend the service life of infrastructures will be determined by its performance and durability. The delamination tendency of this material may be a crucial factor that governs its performance and durability. This paper investigates the delamination tendency of repair mortar incorporating crumb rubber at various contents. The beneficial effect of incorporating crumb rubber to reduce the risk of delamination is discussed. A simulation of shear stress due to differential shrinkage in the interface between repair mortar and substrate concrete is accomplished to highlight the important of material properties (elastic modulus, creep and shrinkage) with regards to delamination tendency.

© 2017 The Authors. Published by Elsevier Ltd.

Peer-review under responsibility of the organizing committee of SCESCM 2016.

*Keywords:* creep; crumb rubber; delamination; elastic modulus; repair mortar; shrinkage; shear stress.

---

### 1. Introduction

Reinforced concrete is one of the main materials used in the construction and development of various infrastructures. There are many reasons why this material turns out to be a preferable choice in the construction of countless infrastructures around the world. The widespread availability of concrete ingredients and the versatility of this material to be manufactured into any shapes and sizes could be those of the considerations. In spite of its advantages, it should be aware that a reinforced concrete will eventually deteriorate due to a number of factors. A reinforced concrete structure may experience some extreme circumstances during its service life. In the seismic zone for example, earthquake could trigger excessive loading on the structure causing structural damage. In aggressive environment, the service life of the structural concrete may be shortened due to the accelerated degradations. All of

---

\* Corresponding author. Tel.: +0-000-000-0000 ; fax: +0-000-000-0000 .

*E-mail address:* [s.a.kristiawan@ft.uns.ac.id](mailto:s.a.kristiawan@ft.uns.ac.id)

these situations should remind civil engineers that in addition to the creation of new infrastructures, there is a great challenge to maintain and rehabilitate the existing infrastructures.

Maintenance and rehabilitation are important schemes to extend the service life of existing reinforced concrete structures. A longer service life means preserving and limiting an exploitation of natural resources that would be utilized to replace the out of use structures. Thus, maintenance and rehabilitation are part of the holistic strategies to promote sustainable infrastructures. The type and technique of maintenance or rehabilitation are vary and these depend on the forms of degradations that would be tackled. Degradations of structural reinforced concrete element in the forms of spalling and delamination of the concrete cover may be repaired by patching method. The success of this method relies on the performance and durability of the repair material being used.

Experience shows that the design of durable concrete repair material can be more complex than the design of new structures, because each damaged structure imposes its own necessities. Mistakes in design, selection of materials, and execution of repair work lead to crack formation, with a drastic consequence on the durability of the repaired structure [1]. Matthews [2] investigated performance of repair materials via case histories and found a variety of modes of repair failure. The principle modes of repair failure were cracking (32 %), debonding (25 %), continues corrosion of embedded reinforcement (22 %), alkali aggregate reaction (4 %) and others (17 %). Most of the failures i.e. cracking and debonding (delamination) could be initiated by a dimensional incompatibility between the repair material and the substrate concrete. This dimensional incompatibility could be explained as follows: when a cement-based repair material is applied to seal the patching zone of concrete element, hydration of the repair material will promote adhesion in the interface between repair material and substrate concrete. After the repair material attains a hardened state, the two components become a composite system. Differential shrinkage and thermal expansion will exist due to the new repair material tends to exhibit higher shrinkage and thermal expansion than those of the old substrate concrete. For the case of differential shrinkage, the deformation of the repair material will be restrained by the substrate concrete which induces tensile stress in the repair material and compressive stress in the substrate concrete. The induced tensile stress could result in the formation of cracking in the repair material [3, 4]. In addition to these stresses, shear stress in the interface and tensile stress in the direction normal to the interface plane are also induced which may cause delamination and peeling [5-7].

Understanding the mechanisms in which cracking and delamination of a repair material may occur is a key to identify the influencing parameters. As explained in the previous paragraph, cracking and delamination of repair material are initiated by the development of shrinkage stresses. These stresses are controlled by the magnitude of differential shrinkage between the repair material and the substrate concrete. Thus, limiting the shrinkage of the repair material could be one of the approaches to obtain durable repair material. However, it is recognized that creep of the repair material also plays important role in releasing the shrinkage stresses. A repair material with a higher creep coefficient will be a better choice than that of a lower creep coefficient. Another parameter that must be taken into account is an elastic property of the two components of the composite system. A lower elastic modulus of the repair material will decrease the induced shrinkage stresses. A lower elastic modulus of the substrate concrete will reduce the degree of shrinkage restraint, which in turn minimizing the shrinkage stresses [4, 8-11]. Based on the above identified parameters and other relevant properties, Beushausen and Alexander [12] proposed design considerations for obtaining durable concrete patch repair. Meanwhile, Li and Li [13] proposed a repair material with special mechanical characteristics i.e. high strength and high ductility. These two characteristics are other important parameters to promote a higher resistance of repair material against cracking and delamination. Cracking can only occur when the induced shrinkage stress has attained the tensile strength of the repair material. The ductility of the repair material which is provided by a large inelastic strain capacity under tensile stress is beneficial to offset the shrinkage demand and so lowering a risk of delamination.

The effect of all the influencing parameters on the induced shrinkage stresses in the patch repair system could be formulated in the analytical model. A number of models to compute shrinkage stresses for this case have been developed by many authors [1, 5-7, 9-12, 14]. In the development of the models, the initiation and then the progress of shrinkage stresses can be divided into several stages. Firstly, it is assumed that the repair material can freely shrink. At this stage, there are two distinctive approaches in the consideration of the shrinkage of the repair material. Most of the models assume that shrinkage is constant across the depth of the repair material. It may be argued that as a result of drying, the surface of the repair material tends to experience higher shrinkage than the layers below. Hence, there exists a shrinkage gradient throughout its thickness. Wittmann and Martinola [1] proposed a model that

represents this shrinkage gradient. However, other researchers suggested that depending on the pore structure and moisture condition, drying of the repair layer might also take place at the interface. A relatively dry and porous substrate concrete may generate considerable capillary suction, which results in a higher shrinkage at the interface than at the layer above it. For simplicity, most of the models considers constant shrinkage profile throughout the depth of repair material. The second stage in the development of the models assumes that the shrinkage of the repair material is fully restrained by substrate concrete and thus induces tensile stress in the repair material. The magnitude of this tensile stress equals to the stress required to pull the shrinking repair material to its original length. The third step in the development of the model is that external compressive load is applied to the end of the composite system. This compressive load will balance all forces at the composite system into equilibrium state. At this stage, Bernoulli's principle is used to determine the stresses-strains distribution across the composite system. A Birkeland's model applies the compressive load to the center of gravity of the repair material. Since this compressive load is applied out of the center of gravity of the composite system, it also triggers a moment at the end of composite system. Meanwhile, Junghanns's model applies the compressive load to the center of gravity of the composite system and so, moment does not exist [14]. Different approach has been suggested by Beushausen and Alexander [12] with an argument that shrinkage is restrained along the whole length of the interface. Thus, transmission of stress due to differential shrinkage is initiated along the interface and not by external compressive load. An analytical model developed by Zhou et al [6,7] also used external compressive stress at the end of composite system but they determined the stresses-strains distribution across the composite system using plate theory and the assumption of the linear relation between shear stress and slip at the interface. In the final stage, the calculated stress in the previous step is used to superimpose the restrained tensile stress in the repair material.

This paper adopts the model of Zhou et al [6,7] to simulate shrinkage stresses in the repair material for the purpose of evaluating the delamination tendency. According to this model, the highest shear stress  $\tau_{xy}$  at the interface are situated at the two ends. This stress could initiate the delamination. The maximum value of the shear stress  $\tau_{xy}$  can be calculated by the following equation [7]:

$$\sigma_{xy,\max} = \frac{\varepsilon_{sh} E_r \lambda h_r}{1 + \frac{E_r h_r}{E_s h_s}} \frac{e^{\lambda L} - 1}{e^{\lambda L} + 1} \quad (1)$$

$$\text{where, } \lambda = \sqrt{\frac{K}{E_r h_r} + \frac{K}{E_s h_s}} \quad (2)$$

$\varepsilon_{sh}$  is the shrinkage of repair material,  $E_r$  and  $E_s$  is the elastic modulus of repair material and substrate concrete, respectively,  $h_r$  and  $h_s$  is the thickness of repair material and substrate concrete, respectively,  $K$  is the shear stiffness of the interface and  $L$  is the length of the repair system. To account for relaxation of stress due to creep ( $\phi$ ) and aging property of creep ( $\rho$ ), the age-adjusted effective modulus of elasticity  $E^*$  is employed as shown in Eq. (3):

$$E^* = \frac{E}{1 + \rho\phi} \quad (3)$$

where the value of  $\rho$  is in the range of 0.5-1 and a value of 0.8 can be chosen [7].

It has been shown in the preceding paragraphs about the major parameters affecting the shrinkage stresses and how a variety of models were developed to account for these parameters. Once the major parameters are identified and formulated into the models, strategies to design or choose durable repair material could be introduced. In the development of durable repair material, it may not be possible to accomplish all favorable properties to be included in the design of repair material. For example, designing a high strength repair material may also result in obtaining repair material with high elastic modulus. High elastic modulus will generate high shrinkage stresses and so, unless this material exhibits strain hardening behaviour, there is a little value of producing repair material with high strength. On the other hand, strength may be of little interest. Instead the target property that would like to be achieved is a deformability of the repair material. With this property, the gradual increase of shrinkage stresses in the



repair material will be slow and at some point later on it may decrease. The situation could be explained by the fact that the rate of shrinkage is slower at later age while the release of stresses by creep is greater at later time [3]. Thus, in any approaches to obtain durable repair material, it is always necessary to evaluate its restrained shrinkage performance by considering other factors. The assessment could be done either by laboratory investigation, numerical/analytical simulation or combination of both [1, 7, 13, 15, 16]. For the current research, a durable repair material is developed by introducing crumb rubber into a mortar mix. The main purpose of introducing crumb rubber is to modify the flexibility (deformability) of the mortar. It has been shown that an inclusion of crumb rubber could reduce the elastic modulus of the mortar and concrete [17, 18]. The increase in drying shrinkage of crumb rubberized-concrete was noticed when this material was used as partial aggregates replacement [19]. However, crumb rubber may have a little influence on shrinkage if the aggregate content of the concrete is maintained. The presence of crumb rubber is also expected to increase the creep coefficient of the mortar. The modification of the mortar properties in particular its deformability is supposed to raise the resistance of the repair mortar against delamination. Laboratory investigation and simulation of shear stress on the interface are carried out to confirm the proposition.

## 2. Materials and method

### 2.1. Materials

This research utilizes mortar containing various contents of crumb rubber as patch repair materials. The basic strength property of mortar was designed to be in the range of 20-30 MPa. Other consideration includes the workability of the mortar. Trial investigation showed that this could be achieved when mortar was proportioned at 1:2.5 by weight of cement/sand ratio and with a water/cement ratio of 0.50. The proportion of superplasticizer was determined at 2% by weight of cement. At this composition, 12 % of crumb rubber by volume of mortar was found to be the maximum level of crumb rubber that could be added into the mix while maintaining the workability of fresh repair mortar still suitable to be mixed, handled and applied manually. Fig. 1 and Table 1 show the physical properties of crumb rubber used in this research. It is noted that crumb rubber used in this research is that of passing grading size of No. 4.75. Meanwhile, the use of accelerator was necessary to increase the hardening rate of repair material since in practice the repair material should adhere to the substrate concrete and work as a composite system as fast as possible. Table 2 summarizes the proportions of the repair materials including the amount of accelerator needed. A commercial repair material (SK) was also investigated for a comparison purpose. A part from the repair materials, concrete with a target strength of 30 MPa was also proportioned to represent substrate concrete which eventually would be repaired. The obtained proportion of substrate concrete was 376 kg of cement, 622 kg of sand, 1207 kg of gravel and 180 kg of water as per m<sup>3</sup> of concrete.

Table 1. Properties of crumb rubber

Grading size	Length (mm)	Diameter (mm)	Cumulative passing
4.75	-	-	66.60%
2.36	21.50	1.8	56.50%
1.18	9.20	1.2	29.14%
0.85	2.35	0.8	7.80%

Table 2. Proportion of repair material

Identification	Crumb Rubber*	Composition of mortar
M-0%	0	All repair materials have proportion: cement: sand = 1: 2.5, w/c ratio =0.5, superplasticizer = 2%**, accelerator = 0.4%**
M-4%	4%	
M-8%	8%	
M-12%	12%	
SK		Commercial repair material

\* by volume of mortar; \*\* by weight of cement





Fig. 1. Crumb rubber used in the research

## 2.2. Specimens

Ten beams of concrete specimen with dimension of 100x100x1500 mm were cast as substrate concretes. The beams were stored and allowed to dry in the laboratory environment for 90 days. After 90 days of drying, a layer of repair material with a thickness of 30 mm was laid on top of the substrate concrete to obtain a composite beam (Fig. 2). Each repair material was used to produce two specimens of composite system. The preceding period of drying should limit the rate of shrinkage of the substrate concrete and so, a maximal differential shrinkage between the repair material and substrate concrete could be simulated.

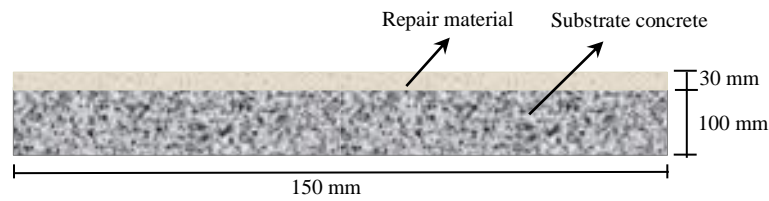


Fig. 2. Composite beam specimen to simulate delamination of repair material

In addition to the above beam specimens, 10 cylinder specimens of 75x275 mm were also prepared for measuring free shrinkage of repair materials. Each repair materials were represented by two cylinder specimens. The shape and size of the specimens followed RILEM TC 107-CSP [20]. The method and procedure of measuring shrinkage was similar to reference [21].

## 2.3. Measurement of delamination tendency

The differential shrinkage between repair layer and substrate concrete would induce shear and peeling stresses at the interface. These stresses could initiate delamination of the repair layer from the substrate concrete starting at the two ends of the composite beam. When delamination has occurred, the curling of repair layer could be observed. Hence, measurement of delamination tendency may be carried out by observing the curling behaviour of the repair layer. For this purpose dial gauges with a resolution of 1 micron were installed on top of the two end of beam (Fig. 3). The progress of curling could be detected continuously until the reading of the dial gauges showing a barely increment value. For the current research, the progress of curling would be presented by an increase of the surface elevation of repair material.

### 3. Results and discussion

#### 3.1. Delamination tendency observed in the laboratory

The surface elevations of the repair materials over time are presented in Fig. 4. A zero elevation was defined as the height of the surface repair material after 1 day being placed on top of the substrate concrete. Thus, observations of the surface elevation increments were started at this time for a period of 14 days. A higher surface elevation means a



Fig. 3. Measurement of delamination tendency

higher tendency of the repair material to separate from the substrate concrete. Generally, the inclusion of the crumb rubber into mortar tends to decrease the delamination tendency (Fig. 4 (a)). The decrease in the tendency of the repair material to detach from the substrate concrete is influenced by the amount of the crumb rubber. A higher amount of crumb rubber causes a lesser tendency of delamination. Compared to the SK repair material (Fig. 6 (b)), all of the repair materials with crumb rubber demonstrate a better performance.

Fig. 4(a) also indicates the progress of repair materials curling as shown by the increase of the surface elevation with time. At the beginning, a fairly fast rate of increment surface elevation could be expected up to 12 days. After this, the rate tends to slow down suggesting a steady state of curling is nearly reached. A different behaviour of curling is observed on SK repair material (see Fig. 4(b)). A very fast curling of this material is noted during the first four days after which the height of the surface layer is almost constant with a tendency of being lower. Investigation reveals that separation of SK repair material from the substrate concrete has occurred at 1 day (with a distance of up to 1000 mm). The progress of curling after this time is generated mainly by the shrinkage of this material since there is no more interface stresses after separation. Fig. 5 shows an example of the different in the extent of separation between repair mortar with crumb rubber and SK repair material.

The delamination behaviour of repair material is correlated with the shrinkage behaviour of the material even though other factors should also be considered. It is shrinkage which initiates the development of stresses in the repair materials that might cause delamination. Previous research by other investigators confirmed that an inclusion of crumb rubber as partial aggregate replacement would increase the shrinkage of concrete [19, 22]. The increase in the shrinkage of crumb rubberized-concrete could be related to the amount of aggregates. It is recognized that cement paste is the seat of the shrinkage phenomenon while aggregates act to restrain this shrinkage. Partial replacement of aggregates with crumb rubber will decrease the capacity of the bulk aggregates to restrain the shrinkage of cement paste as crumb rubber is obviously less stiffness than the original aggregates. For the current research, crumb rubber is introduced into mortar without aiming to partially replace fine aggregates. Hence, the capacity of aggregate to restrain shrinkage of the cement paste should be less influenced by the added crumb rubber. The shrinkage of the repair materials investigated in this research are likely confirmed this behaviour as presented in Fig. 6. An inclusion of no more than 8% crumb rubber into mortar is slightly reduced the shrinkage of repair material. While incorporating crumb rubber at 12% by volume of mortar will lessen a considerable shrinkage

especially at later time. It could be shown that the shrinkage of repair mortar decreases by 20-30% after 10 days of drying when 12% crumb rubber is used. Two factors might be responsible to this shrinkage reduction. Firstly, the addition of crumb rubber without modifying the original proportion of mortar will slightly alter the amount of cement paste. Less cement paste leads to less shrinkage. Secondly, the physical properties of the crumb rubber (see Table 1) indicates that some of this rubber could act as fiber. Dowel actions by the fibers might also contribute to the restraint of cement paste shrinkage.

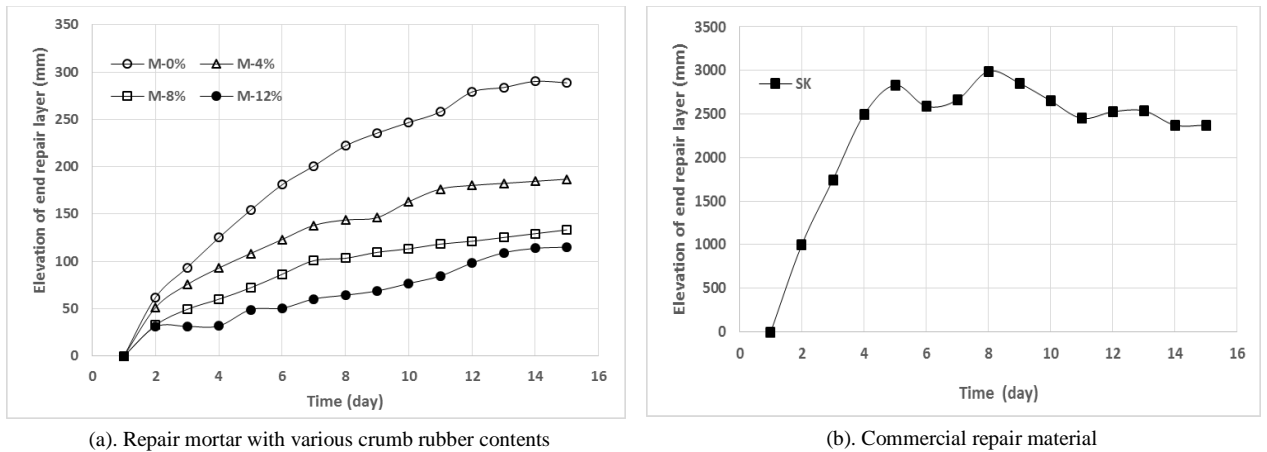


Fig. 4. An increase in the surface elevation of repair layers

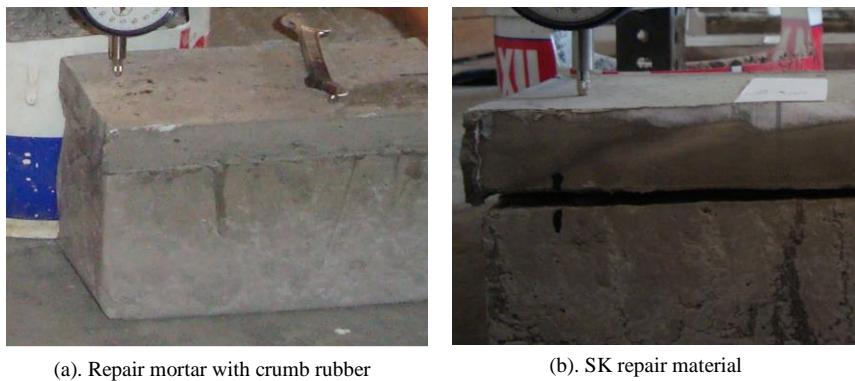


Fig. 5. The extent of separation between repair layer and substrate concrete

The shrinkage of SK repair material behaves in a different way in term of its rate and magnitude (see Fig. 6(b)). The rate is very fast at the first 3 days after which the rate diminishes. The magnitude of the shrinkage is higher compared to the repair mortar with crumb rubber. It is shown that the SK shrinkage at 3 days is similar in magnitude with the shrinkage of repair mortar with crumb rubber at 14 days. The high rate and magnitude of SK shrinkage could be a determining factor of the observed delamination of this repair material.

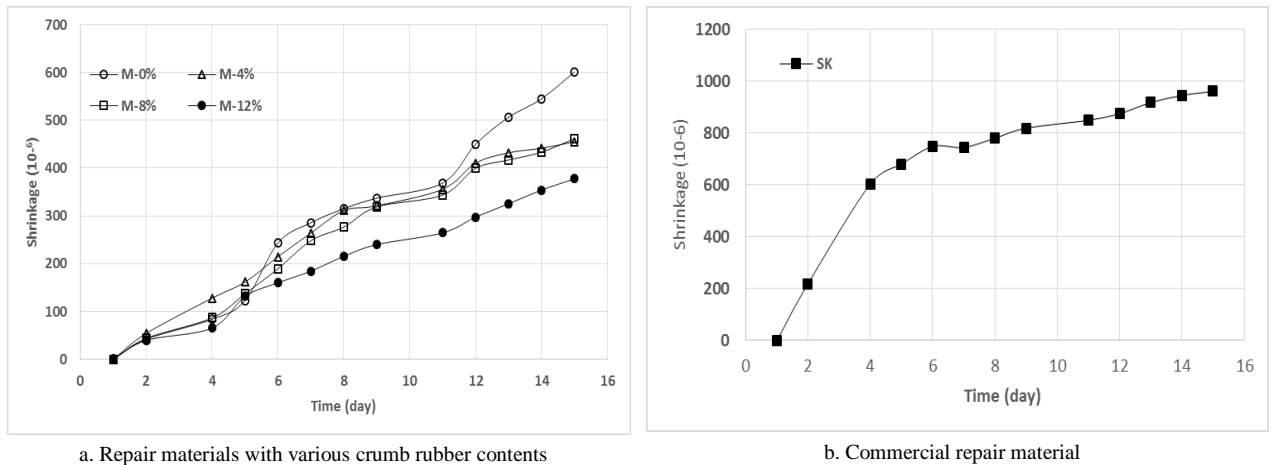


Fig. 6. Free shrinkage of the repair materials

### 3.2. Delamination tendency based on the shear stress simulation

Calculation of shear stress in the interface between repair material and substrate concrete could be useful to identify the effect of repair material properties on the tendency of delamination. Eq. (1) will be used for this purpose. It should be aware that Eq. (1) applies to compute shear stress at the interface situated at the ends of composite beam. If the repair layer at these zones already separate from the substrate concrete, the shear stresses at these area will be vanished. Based on the laboratory investigation presented in the previous section, delamination of repair materials did occur. Hence, exact shear stresses could not be simulated. However, exact shear stress may not be possible considering there exists time-dependent properties of both mechanical and deformation of the repair material. It is recognized that after repair material is laid on top of the substrate concrete, the progress of hydration will change the mechanical and deformation properties of the repair material continuously. For realistic calculation of shear stress, these time-dependent properties should be taken into account. For practical analysis, this may not be necessary. The purpose of the simulation in this research is to identify the effect of material properties on the delamination tendency of repair materials. This could be achieved by comparing the relative values of the shear stresses of various repair materials. Thus, the important thing that would like to be extracted from the simulation is how the relative shear stresses of various repair materials may provide an indication of the tendency of delamination. In the current research, the calculation assumes the following conditions: time-dependent mechanical properties are ignored and repair layer at the two ends of the beam are not separated yet. The mechanical and creep properties of the repair material are given in Table 3. These properties were determined at 1 day. The shrinkage of repair materials as presented in Fig. 6 are used. The compressive strength of the substrate concrete is 30 MPa with an elastic modulus predicted as  $4700\sqrt{30} = 25742$  MPa.

Table 3. Properties of repair materials

Repair Material	Compressive Strength (MPa)	Elastic Modulus (MPa)	Creep Coefficient
M-0%	13.71	17403	4.42
M-4%	10.51	15237	3.09
M-8%	7.12	12541	3.00
M-12%	5.33	10851	2.25
SK	8.85	13982	4.91

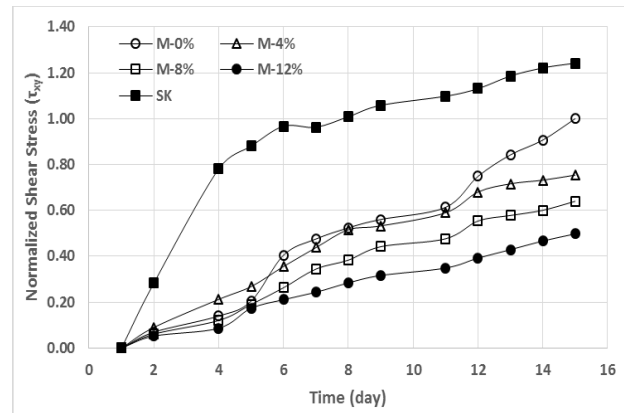


Fig. 7. The development of maximum shear stress (normalized) on the interface

The result of calculation of shear stress is presented in Fig. 7. The values of shear stresses are normalized by the magnitude of shear stress of M-0% at 14 days. In this way the relative shear stresses of all repair materials may be compared. It is obvious from Fig. 7 that the highest shear stress occurs on the SK repair material. This finding is in agreement with the observed delamination tendency of this repair material as given in Fig. 4 and 5. The effect of adding crumb rubber into mortar could also be estimated from the shear stress development. The tendency of delamination is reduced with an increase of crumb rubber content. The reduction of shrinkage by crumb rubber addition is the possible cause of reduction of delamination tendency in the overlay system. Moreover, the inclusion of crumb rubber also decrease the elastic modulus of repair material, which has positive effect on lowering the tendency of delamination. Thus, lower values of both shrinkage and elastic modulus of repair materials could be chosen as strategy toward designing durable repair material.

Creep of repair mortar with crumb rubber is expected to contribute further on decreasing the tendency of delamination. However, it seems that the trend of creep does not reflect the expectation. A higher amount of crumb rubber in the mortar results in lowering creep coefficient (see Table 3). Lower value of creep coefficient means lower contribution of creep to release the stress. Generally, concrete with lower stiffness will exhibit higher creep. This is not the case with the repair materials containing crumb rubber. The explanation might be as follows: when a stress is applied to the repair material, the stress instantly presses the body of the repair material causing elastic strain. The magnitude of elastic strain depends on the stiffness of the repair material which is also influenced by the stiffness of its ingredients. Crumb rubber obviously is the ingredient with the lowest stiffness. Consequently, a higher amount of crumb rubber will produce a higher elastic strain. Once the body of the repair material was compressed under influence of stress, the contribution of crumb rubber on the subsequence deformation (creep) will not be as much as in the preceding deformation (elastic). The crumb rubber is already in a squeezed state and so creep is more or less determined by other factors. The major factor is the cement content because it is the origin of the phenomenon. Repair mortar with a higher addition of crumb rubber will slightly contain lower cement. Even though this may not substantially reduce the value of creep, but in term of creep coefficient (i.e. ratio of creep to elastic strain) it could be significant as the elastic strain of the crumb rubberized mortar is higher. Thus, lower creep but high elastic strain will yield lower creep coefficient.

#### 4. Conclusions

Repair material is susceptible to delamination as a result of differential shrinkage between the repair material and the substrate concrete. Reducing the shrinkage of repair material could be one of the strategies to obtain durable repair material. Of course, other factors both positively or negatively influence the tendency of delamination should also be taken into account even though all favorable factors may not be possible to be accomplished. An inclusion of crumb rubber into mortar is beneficial to reduce the risk of delamination. Both experimental and simulation of shear stress at the interface confirm that a higher amount of crumb rubber tends to cause a lower tendency of

delamination. Reductions in both shrinkage and elastic modulus of the repair material as a consequence of adding crumb rubber could be the source of lowering the risk of delamination in the crumb rubberized repair material.

## References

- [1] F.H. Wittman, G. Martinola, Decisive properties of durable cement-based coatings for reinforced concrete structures, *International Journal for Restoration of Buildings and Monuments*. 9 No. 3 (2003) 235-264.
- [2] S. Matthews, CONREPNET: Performance based approach to the remediation of reinforced concrete structures: Achieving durable concrete structures, *Journal of Building Appraisal*. 3 No. 2 (2007) 6–20.
- [3] S.A. Kristiawan, Shrinkage cracking tendency of patch repair mortar modified with polymer, The 5<sup>th</sup> International Conference of Asian Concrete Federation, Pattaya, Thailand, October 2012.
- [4] S.A. Kristiawan, Evaluation of models for estimating shrinkage stress in patch repair system, *International Journal of Concrete Structures and Materials*. 6 No. 4 (2012) 221-230.
- [5] M. H. Baluch, M. K.Rahman, A. H. Al-gadhib, Risks of cracking and delamination in patch repair, *Journal of Materials in Civil Engineering*. 14 No. 4 (2002) 294–302.
- [6] J. Zhou, G. Ye, E. Schlangen, K. van Breugel, Modelling of stresses and strains in bonded concrete overlays subjected to differential volume changes, *Theoretical and Applied Fracture Mechanics*. 49 (2008) 199–205.
- [7] J. Zhou, G. Ye, E. Schlangen, K. van Breugel, Numerical study on predicting the performance of repair materials under differential volume changes, *International RILEM Symposium on Concrete Modelling- CONMOD'08*. Delft, The Netherlands, 26-28 May 2008.
- [8] S.A. Kristiawan, Shrinkage cracking resistance of repair materials made from unsaturated polyester resin (UPR)-mortar, The 6<sup>th</sup> International Conference of Asian Concrete Federation, Seoul, Korea, 21-24 September 2014.
- [9] J. Silfwerbrand, Differential shrinkage in normal and high strength concrete overlays, *Nordic Concrete Research*. 19 (1996) 55–68.
- [10] E. Denarie, J. Silfwerbrand, Structural behaviour of bonded concrete overlays, *Workshop on Bonded Concrete Overlays*, Stockholm, 7-8 June 2004.
- [11] J. Zhang, V.C. Li, Influence of supporting base characteristics on shrinkage-induced stresses in concrete pavements, *Journal of Transportation Engineering*, 127 No. 6 (2011) 455-462.
- [12] H. Beushausen, M. G. Alexander, Performance of concrete patch repair systems, *Advances in Construction Materials*. Edited by C. U. Grosse (2007) 255–262.
- [13] M. Li, C.C. Li, Influence of material ductility on performance of concrete repair, *ACI Materials Journal*. 106 No. 5 (2009) 419-428.
- [14] H. Beushausen, Long-term performance of bonded concrete overlays subjected to differential shrinkage, PhD Thesis, Department of Civil Engineering, University of Cape Town, South Africa (2006).
- [15] P. Range, H.C. Kuhne, Investigation on the performance of concrete repair mortars in composite specimen test, In *Concrete Repair, Rehabilitation and Retrofitting*. (2012) 377-378.
- [16] J. Zhou, G. Ye, T. Sui, Performance of engineered cementitious composite for concrete repairs subjected to differential shrinkage, In *Concrete Repair, Rehabilitation and Retrofitting*. (2012) 387-388.
- [17] S.A. Kristiawan, Dimensional compatibility between patch repair materials containing tyre fibers and concrete under short-term compressive stress, *Proceedings of the First Makassar International Conference on Civil Engineering*, Makassar, Indonesia, 9-10 March 2010.
- [18] C. Naito, J. States, C. Jackson, B. Bewick, Assessment of Crumb Rubber Concrete for Flexural Structural Members, *Journal of Materials in Civil Engineering*. 26 No. 10 (2014) 751-758.
- [19] I. Mohammadi, Investigation of the use crumb rubber concrete (CRC) for rigid pavements, MSc Thesis, Centre for Built Infrastructure Research, School of Civil and Environmental Engineering, University of Technology Sydney. (2014).
- [20] RILEM TC107-CSP, Measurements of time dependent strains in concrete, *Materials and Structures*. 31 (1998), pp. 507-512.
- [21] S.A. Kristiawan., M.T.M. Aditya, Effect of high volume fly ash on shrinkage of self-compacting concrete, *Procedia Engineering*. 125 (2015) 705-712.
- [22] I. Mohammadi, H. Kabbaz, Shrinkage performance of Crumb Rubber Concrete (CRC) prepared by water-soaking treatment method for rigid pavements, *Cement and Concrete Composites*. 62 (2015) 106-116.





Sustainable Civil Engineering Structures and Construction Materials, SCESCM 2016

## Effect of Phosphogypsum on the Properties of Portland Cement

G M Sadiqul Islam<sup>a</sup>, Fazlul Habib Chowdhury<sup>a,\*</sup>, Muhammad Tanveer Raihan<sup>a</sup>, Shishir Kumar Sikder Amit<sup>a</sup>, Mohammad Rafiqul Islam<sup>a</sup>

<sup>a</sup>*Department of Civil Engineering, Chittagong University of Engineering & Technology, Chittagong-4349, Bangladesh.*

---

### Abstract

Use of industrial by-products as construction material can help to achieve sustainability in this industry. Phosphogypsum, a by-product in phosphoric acid manufacturing process, produced in bulk quantity especially from the fertilizer industry, typically used as a supplementary fertilizer for soil treatment. Alternatively, disposal of these materials in the form of landfill also need huge land area although environmental hazard concern from these activities has been raised by researches. The material has therefore, tried to incorporate in cement manufacturing considering its sustainable use. Phosphogypsum could be used as a substitute of natural gypsum in the production of Portland cement to control the hydration reaction rate of cement. In this study, raw phosphogypsum was collected from a local fertilizer industry. Properties of phosphogypsum were evaluated and then the effect of various level phosphogypsum addition (2, 5, 10 and 15 percent by weight of cement) with Portland cement clinker was investigated. The raw material was treated to remove additional water and impurity by washing, air drying and oven drying. Both treated and untreated materials were used in experimental work. Setting time, flow and compressive strength behavior of the prepared paste, mortar and concrete samples were evaluated to find an effective percentage of phosphogypsum to be used in Portland cement manufacturing. By evaluating properties of cement paste, mortar and concrete it was concluded that 5-10% phosphogypsum addition in cement clinker gave good results. In general, the processing of phosphogypsum by washing and drying gave better performance in all the media.

© 2017 The Authors. Published by Elsevier Ltd.

Peer-review under responsibility of the organizing committee of SCESCM 2016.

*Keywords:* Phosphogypsum, Sustainability, By product, Portland cement clinker

---

---

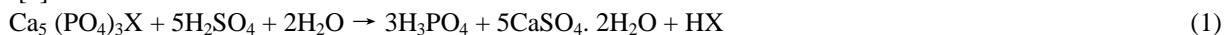
\* Corresponding author. Tel.: +8801710432022; fax: +88031714948.

*E-mail address:* [fnchy@yahoo.com](mailto:fnchy@yahoo.com)



## 1. Introduction

Phosphogypsum is a by-product from the wet manufacturing process of phosphoric acid (ammonium phosphate fertilizer) by the action of sulphuric acid on the rock phosphate. Approximately 4.5-5.5 tons of phosphogypsum is generated per ton of phosphoric acid production using wet process. Phosphoric acid is produced by reacting phosphate ore (apatite) with sulphuric acid according to the following reaction, where X may include OH, F, Cl, or Br. [1]



Dumping of phosphogypsum into open land could have environmental and health concerns. The stockpiled material dominated by calcium sulphate dehydrate (around 94-98% by wt.), also contains approximately 5-6% of impurities including heavy metals, fluoride and radionuclides [2]. These toxic substances can be transported by wind over long distances. In consequence, it could contaminate soil and or groundwater. Detailed studies are necessary in order to fully understand the transfer process of toxic sub-stances into the adjacent environment and to assess their impact [3, 4, 5] but not within the scope of this work.

Treated phosphogypsum can be used as an ingredient of plaster [6, 7, 8]. The most important and motivating use of phosphogypsum could be in the construction industry. In the manufacturing process of cement, phosphogypsum could be used as a replacement of natural gypsum which plays the role of a set retarder [9, 10], or to reduce the clinkerization temperature [11]. Study also conducted with weathered (stored in open air) phosphogypsum as a set retarder in Portland cement [10]. Partly refined boric acid and phosphogypsum mixture can be used in place of natural gypsum for Portland and Trass cements [12]. It can be processed by wet sieving and washing process in the plant. The impurities of phosphate, fluoride, organic matter and alkalis are reduced by considerable extent. The beneficiated phosphogypsum can be used as an additive in place of mineral gypsum in the manufacturing of Portland cement and Portland slag cement. Phosphogypsum-slag based aggregate was prepared and tested for compressive, flexural and splitting tensile strength by using in concrete. It was recommended that the slag aggregate performed well as a coarse aggregate in cement concrete and should perform satisfactorily in highway pavement system [13]. In the manufacturing of building materials phosphogypsum was used as raw and calcined materials, however, the mechanical properties was found unsatisfactory [14]. Heated phosphogypsum used as a binder, improved the compressive and flexure strength of the material. Phosphogypsum based aggregate used in Roller Compacted Concrete (RCC) slabs gave good result for set retardation and drying shrinkage compensation [15]. Study on partial replacement of cement by various percentage of phosphogypsum gave good result with concrete specimens [16]. Researches [17,18] on the basic engineering properties of phosphogypsum-based concrete mixtures concluded that the unique properties of dihydrate phosphogypsum under compaction-consolidation can significantly contribute to the compressive strength of concrete mixes. However, with higher percentage of phosphogypsum, the strength of concrete mixtures is affected by the moisture at the time of testing. Better compressive strength attained with calcined phosphogypsum [19]. Study with up to 40% cement replacement by phosphogypsum gave 10% level optimum [20]. Another study with both OPC and PPC replacement in mortars found decreased compressive strength but increased flexural strength comparing with conventional mix [21]. Phosphogypsum's presence in the cement has increased its initial strength rapidly. This strength development was due to the formation of anhydrate at higher temperatures. Self-compacting concrete mixes using 0-30% percent replacement of cement also gave maximum flexural strength with 10% phosphogypsum. Study on the properties of both cement pastes and mortars using Ordinary Portland cement, Limestone Blended cement and Slag cement gave compressive strengths at 7 and 28 days satisfactory up to 8% phosphogypsum replacement for all the three types of cements at standard mix proportion. These three types of cement also met the limit of initial setting time and soundness requirements set by standards [22]. Study suggested modification in concrete mix process to incorporate raw phosphogypsum as partial replacement in cement mortar and concrete [23].

In view of the characteristics of phosphogypsum and its attractive economic potential at the present time there is a prodigious curiosity in using phosphogypsum as an alternative raw material for many applications. Replacement of cement clinker with certain percentage of phosphogypsum could give positive outcomes in mortar and concrete although there is still debate in related literatures. This research mainly investigated the effect of phosphogypsum addition with cement clinker on the properties of paste, mortar and concrete. In this regard, both field condition and

calcined phosphogypsum were used in mortar and concrete at the replacement level of 0%, 2%, 5%, 10% and 15% where water cement ratio kept 0.45.

## 2. Materials & Specimen Preparation

### 2.1. Physical properties of phosphogypsum

Calcium sulfate can be either in dihydrate ( $\text{CaSO}_4 \cdot 2\text{H}_2\text{O}$ ) or hemihydrate ( $\text{CaSO}_4 \cdot 0.5\text{H}_2\text{O}$ ) form depending on the reaction temperature used to produce phosphoric acid. Usually free moisture content between 25-30% exists in the gypsum cake after filtration. The generated hemihydrate form of phosphogypsum, in the presence of free water can rapidly convert to dehydrate form [24]. Moreover, if the process is left undisturbed it will set up into a relatively hard cemented mass. Di-hydrate consists principally silt-size ( $<0.075\text{mm}$ ) and appear as soft aggregates of crystals [25]. It depends on the source of the phosphate rock and the reactor conditions.

### 2.2. Chemical properties of phosphogypsum

Phosphogypsum consists mainly calcium sulphate dehydrate with small amount of silica. The mineralogical composition of phosphate ore was described by various researchers [26, 27] and is dominated by fluorapatite, goethite and quartz, with minor amounts of Al-phosphates, anatase, magnetite, monazite and barite. X-ray Diffraction pattern of obtained phosphogypsum is given in Fig. 1 indicating the material mainly composed of Gypsum.

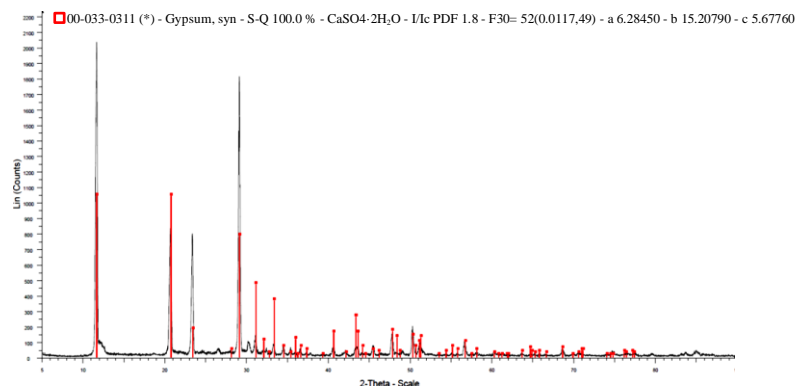


Fig. 1. X-ray Diffraction pattern of the Phosphogypsum sample

### 2.3. Other material property and specimen preparation

Ordinary Portland cement clinker, phosphogypsum, graded river sand and crushed stone was used to conduct the tests in this research. The fineness modulus of sand was 2.7 which was washed and dried before use to avoid presence of dust and clay particle. It was free from organic materials. Normal drinking water was used for paste, mortar and concrete works.

Phosphogypsum sample was collected from triple superphosphate (TSP) complex, Chittagong, Bangladesh. The industry has considerable production of phosphoric acid and eventually phosphogypsum. Two category of sample was prepared using phosphogypsum. One using raw phosphogypsum (found in field condition after production) and the other was washed sample. After washing the sample was oven dried in order to get dry phosphogypsum.

Setting time of paste and flow of mortar samples were conducted according to ASTM C191 and ASTM 1437, respectively. Compressive strength test of mortar and concrete was conducted as per ASTM C109 and ASTM C39, respectively.

### 3. Result & Discussion

#### 3.1. Setting time

Setting time test result is presented in Figs. 2 and 3. Consistency of cement paste was estimated before testing the setting time. Setting time was always found higher in processed condition than field condition. Using more than two percent of phosphogypsum, the setting time decreases gradually for processed condition, however, this was opposite with wet samples. In field condition adding 2% phosphogypsum in the mixture gives setting time up to 3 hours and 10 minutes. In dry condition more than 5% phosphogypsum decreases the setting time value than the control sample. This may be due to the formation of anhydrate at early stage [21]. The processed sample gave 10% addition as optimum for both initial and final setting time (comparable with control sample).

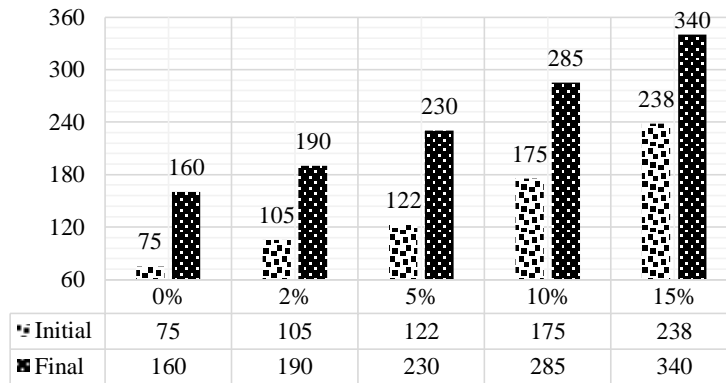


Fig. 2. Setting time of cement clinker and phosphogypsum (field condition)

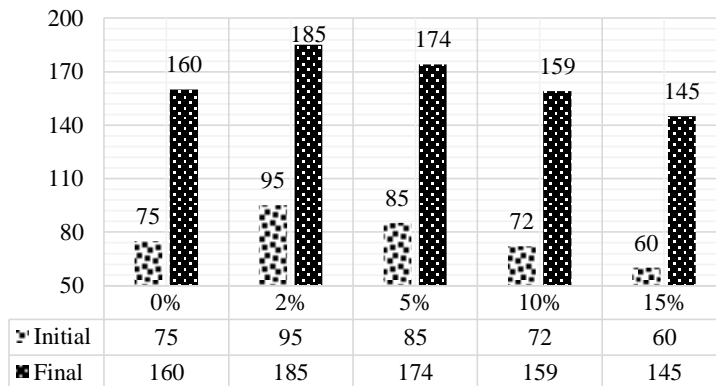


Fig. 3. Setting time of cement clinker and phosphogypsum (processed sample)

#### 3.2. Flow of mortar

Flow of mortar samples with different percentage of phosphogypsum is presented in Fig. 4. Higher flow of mortar was obtained with all replacement level compare to control mortar. The field samples gave better results than processed samples. This may be due to presence of higher amount of water in field condition. In addition, the processed sample may agglomerate during drying and might not separate fully during mixing and testing. For field and processed conditions 10% and 5% addition was found to be best for flow consideration, respectively.

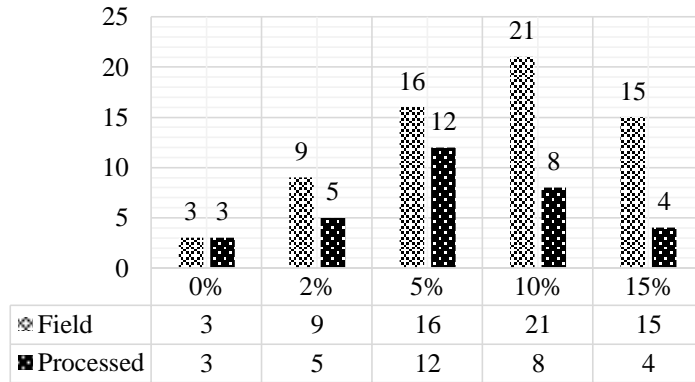


Fig. 4. Flow of mortar using various level field and processed phosphogypsum addition

### 3.3. Compressive strength of mortar

Compressive strength of the mortar sample at the age of 7 & 28 days curing is presented in Figs. 5(a) and 5(b). At 7 days the strength was decreased with the phosphogypsum content giving better results for processed samples. At 28 days the wet samples gave optimum at 5% replacement level while strength was increased up to 10% addition of processed samples.

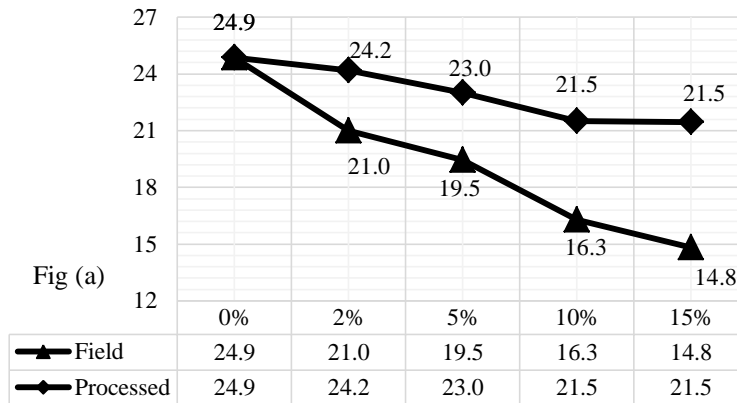


Fig (a)

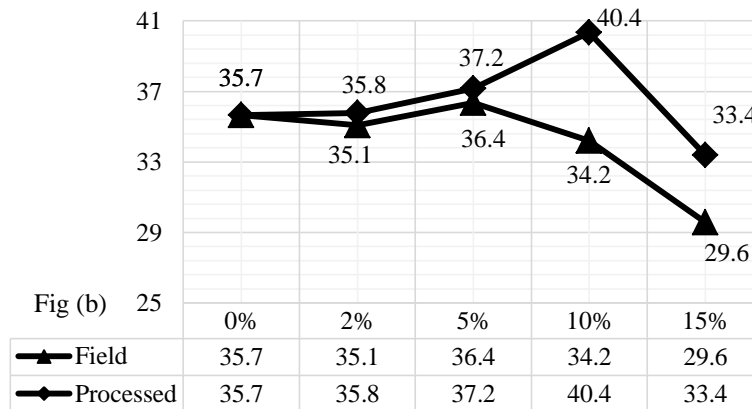


Fig (b)

Fig. 5. Compressive strength of mortar at (a) 7 days and (b) 28 days

This indicates superiority of processed samples over raw filed samples. The field condition contains a lot of water which might affected the w/c ratio of the mix. It may also be noted that on processing the samples impurities present in raw samples were removed which gave better results. To obtain the actual cause of strength increment with processed samples further research considering the chemical process involved is necessary.

### 3.4. Compressive strength of concrete

The concrete strength was designed for 28 MPa and calculated cement was replaced by phosphogypsum at 0%, 2%, 5%, 10% and 15% in terms of weight. Compressive strength test results of 7 days and 28 days are given in Figs. 6(a) and 6(b). As with mortar, it was generally observed that the processed material gave higher strength then the field sample. The results portrays that addition of 5% and 10% phosphogypsum addition in processed condition shows similar results to concrete without phosphogypsum at 7 days. At this age a decreasing trend in strength with phosphogypsum addition was noted for filed condition. At 28 days the processed materials gave higher concrete strength than the control sample at 10% addition and for field condition this level gave lower strength but found optimum considering all replacement level. Adding more than 10% phosphogypsum reduces the strength of concrete significantly for both field and processed condition.

This research studied different properties of paste, mortar and concrete by adding various proportion of phosphogypsum with cement. Addition of phosphogypsum up to 5-10% gave better results. In general, the processing of phosphogypsum by washing and drying gave better performance in all medium. Further detail investigation on the properties of phosphogypsum and reaction mechanism could provide better understanding.

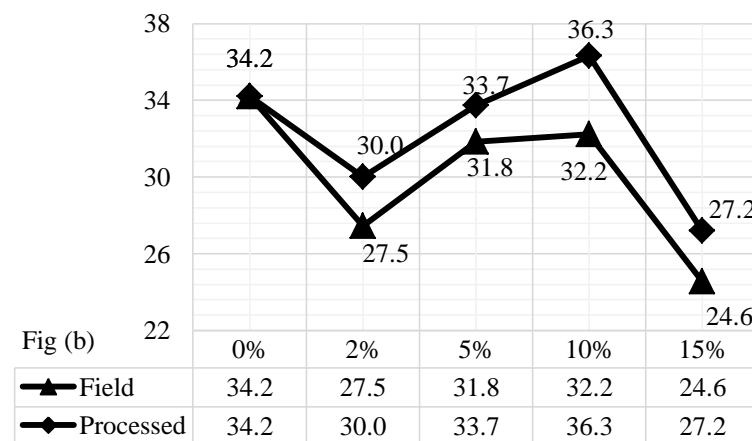
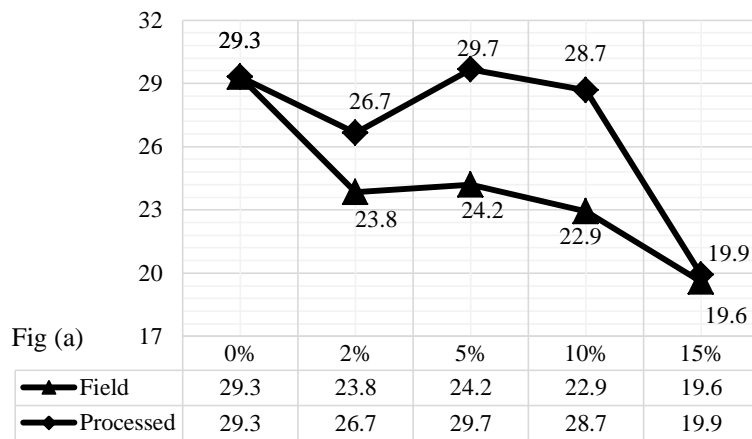


Fig. 6. Compressive strength of concrete with Phosphogypsum addition at (a) 7 days and (b) 28 days

#### 4. Conclusion

TSP complex at Chittagong is the main source of phosphogypsum production in Bangladesh. The industry occasionally sales the product at low price but mainly use for landfilling. 5-10% addition of phosphogypsum with Portland cement clinker gave promising results while tested various fresh and hardened properties of cement paste, mortar and concrete. The raw field sample was processed by washing and subsequent drying. In general, the processing of phosphogypsum gave better performance in all media. Processed sample gave better or at least similar performance than the control samples (100% clinker) in paste, mortar and concrete at 10% addition level. This indicated that the industrial by-product could sustainably be used as replacement of natural gypsum (generally used 5% of total cement) in cement manufacturing. Cement industry might then reduce the dependency on natural gypsum for their production. Environmental concern is an important issue in this regard. A more detailed research and development work might help to ensure better use of this material in construction industry.

#### 5. Acknowledgement

The laboratory support provided by Chittagong University of Engineering & Technology (CUET) and Dr. Abdul Gafur of Material Science and Engineering Division, Bangladesh Council of Scientific and Industrial Research (BCSIR) are gratefully acknowledged. Thanks also extended to TSP complex authority for material support.

#### 6. References

- [1] Banu, S. S., & Haq, M. N. A Study on the Mechanical Properties Such as Compressive Strength, Split Tensile Strength and Flexural Strength for Various Percentages of Phosphogypsum. *International Journal of Emerging Trends in Engineering and Development*, 2015, Issue 5, Vol. 4, pp. 264-387.
- [2] Szykowska, Małgorzata Iwona, Aleksandra Pawlaczyk, and Jacek Rogowski. *Characterization of Particles Transmitted by Wind from Waste Dump of Phosphatic Fertilizers Plant Deposited on Biological Sample Surfaces*. INTECH Open Access Publisher, 2011.
- [3] Al-Masri, M. S., et al. "Distribution of some trace metals in Syrian phosphogypsum." *Applied Geochemistry* 19.5 (2004): 747-753.
- [4] Arocena, J. M., P. M. Rutherford, and M. J. Dudas. "Heterogeneous distribution of trace elements and fluorine in phosphogypsum by-product." *Science of the total environment* 162.2 (1995): 149-160.
- [5] Rutherford, P. M., M. J. Dudas, and J. M. Arocena. "Radioactivity and elemental composition of phosphogypsum produced from three phosphate rock sources." *Waste Management & Research* 13.5 (1995): 407-423.
- [6] Singh, Manjit. "Treating waste phosphogypsum for cement and plaster manufacture." *Cement and Concrete Research* 32.7 (2002): 1033-1038.
- [7] Singh, Manjit. "Effect of phosphatic and fluoride impurities of phosphogypsum on the properties of selenite plaster." *Cement and Concrete Research* 33.9 (2003): 1363-1369.
- [8] Singh, Manjit. "Role of phosphogypsum impurities on strength and microstructure of selenite plaster." *Construction and building materials* 19.6 (2005): 480-486.
- [9] Potgieter, J. H., et al. "An investigation into the effect of various chemical and physical treatments of a South African phosphogypsum to render it suitable as a set retarder for cement." *Cement and concrete research* 33.8 (2003): 1223-1227.
- [10] Altun, İ. Akin, and Yesim Sert. "Utilization of weathered phosphogypsum as set retarder in Portland cement." *Cement and Concrete Research* 34.4 (2004): 677-680.
- [11] Kacimi, Larbi, et al. "Reduction of clinkerization temperature by using phosphogypsum." *Journal of hazardous materials* 137.1 (2006): 129-137.
- [12] Erdogan, Yunus, Ayhan Demirbas, and Hasan Genc. "Partly-refined chemical by-product gypsums as cement additives." *Cement and concrete research* 24.4 (1994): 601-604.
- [13] Foxworthy, Paul T., Elfriede Ott, and Roger K. Seals. *Utilization of phosphogypsum-based slag aggregate in portland cement concrete mixtures*. No. 1437. 1994.
- [14] Değirmenci, Nurhayat. "Utilization of phosphogypsum as raw and calcined material in manufacturing of building products." *Construction and Building Materials* 22.8 (2008): 1857-1862.
- [15] Nanni, Antonio, and Wen F. Chang. "Phosphogypsum-based roller compacted concrete." *Concrete International* 11.11 (1989): 48-53.
- [16] Bagade, Mahesh A., and S. R. Satone. "An experimental investigation of partial replacement of cement by various percentage of Phosphogypsum in cement concrete."

- [17] Ghafoori, Nader, and Wen F. Chang. "Investigation of phosphate mining waste for construction materials." *Journal of materials in civil engineering* 5.2 (1993): 249-264.
- [18] Lin, K. T., and W. F. Chang. "Strength properties of compacted phosphogypsum-based mixtures, Volume II." *Proceedings of the second International symposium on phosphogypsum*, University of Miami, Florida Institute of Phosphate Research, Bartow, Florida, (January 1988).
- [19] Taher, M. A. "Influence of thermally treated phosphogypsum on the properties of Portland slag cement." *Resources, Conservation and Recycling* 52.1 (2007): 28-38.
- [20] Reddy, T. Siva Sankar, D. Rupesh Kumarb, and H. Sudarsana Raoc. "A study on the strength characteristics of Phosphogypsum concrete" *Asian Journal of Civil Engineering (Building and Housing)* 11.4 (2010): 411-420.
- [21] Smadi, M. M., Haddad, R. H., & Akour, A. M. (1999). Potential use of phosphogypsum in concrete. *Cement and Concrete Research*, 29 (9), 1419-1425.
- [22] El Nouhy, Hanan, Enas Khattab, and Sayieda Zeedan. "Behavior of Cement Pastes and Mortar Containing Phosphogypsum." *Key Engineering Materials*. Vol. 668. Trans Tech Publications, 2015.
- [23] Bhadauria, S. S., and Rajesh B. Thakare. "Utilisation of phosphogypsum in cement mortar and concrete." *31st Conference on Our World in Concrete & Structures*. 2006.
- [24] Bhawan, Parivesh, and East Arjun Nagar. "Guidelines for Management and Handling of Phosphogypsum Generated from Phosphoric Acid Plants (Final Draft)." (2012).
- [25] Wissa, A. E. Z., M.A., Phosphogypsum Disposal and the Environment. Available online at: [www.ardaman.com/phosphogypsum\\_disposal.htm](http://www.ardaman.com/phosphogypsum_disposal.htm) (last accessed on October, 2015)
- [26] Carbonell-Barrachina, A., R. D. DeLaune, and A. Jugsujinda. "Phosphogypsum chemistry under highly anoxic conditions" *Waste Management* 22.6 (2002): 657-665.
- [27] de Oliveira, Sonia Maria Barros, and Rosely Aparecida Liguori Imbernon. "Weathering alteration and related REE concentration in the Catalão I carbonatite complex, central Brazil" *Journal of South American Earth Sciences* 11.4 (1998): 379-388.





Sustainable Civil Engineering Structures and Construction Materials, SCESCM 2016

## Optimizing polycarboxylate based superplasticizer dosage with different cement type

Antoni<sup>a,\*</sup>, James Gabriel Halim<sup>a</sup>, Owen Chandra Kusuma<sup>a</sup> and Djwantoro Hardjito<sup>a</sup>

<sup>a</sup>*Civil Engineering Department, Petra Christian University, Surabaya 60236, Indonesia*

---

### Abstract

The use of polycarboxylate ether (PCE) as superplasticizer (SP) in the manufacture of high strength concrete is increasingly common. Each brand of SP available on the market has different compositions, causing differences in dosage requirement and the resulting characteristics. Beside SP type, cement type and composition also affect the fresh and hardened concrete properties. In this study, the optimum dosages of several brands of PCE superplasticizer in making mortar were investigated. Two different cement types were used. The effect of SP on flowability, setting time, and resulting compressive strength were evaluated. The results show that with the increase of SP dosage in mortar mixture, the flowability increased. However, there is an optimum value for each brand and for each water cement ratio. The increase of flowability is accompanied by an increase in compressive strength until it reaches the optimum level. Nevertheless, excessive use of SP could lead to bleeding and segregation, and reduce the compressive strength. It was found that ordinary Portland cement (OPC) requires higher SP dosage than Portland Pozzolan cement (PPC) for the same flowability. Longer setting time was observed for all mixtures employing SP, at different degrees of extension. It correlates with the slump retention time. Simple method to determine the optimum dosage is suggested in this paper. © 2017 The Authors. Published by Elsevier Ltd.

Peer-review under responsibility of the organizing committee of SCESCM 2016.

*Keywords:* polycarboxylate; superplasticizer; setting time; dosage; cement type; OPC; PPC.

---

### 1. Introduction

High strength concrete essentially need to use superplasticizer to reduce cement interparticle force and to disperse the particle evenly in the concrete mix. High compressive strength could only be achieved when low water to

---

\* Corresponding author. Tel.: +62-81-931073728; fax: +62-31-8415274

*E-mail address:* [antoni@petra.ac.id](mailto:antoni@petra.ac.id)

cement ratio (w/c) is ensured in the concrete mix design, while maintaining adequate workability of the fresh mixture. Superplasticizer addition reduces the cohesiveness of the cement particles by electrostatic repulsion, in the case of naphthalene or melamine-based superplasticizer; and by a combination of electrostatic and steric repulsion mechanism in the case of polycarboxylate based superplasticizer [1,2].

Different brand of polycarboxylate ether (PCE) superplasticizer has different molecular structures, affected by the manufacturing process. Its chemical structures consist of main chain and side chains with different length and density, and will have different effectivity in increasing the workability of concrete mixture [3]. Several researches have been done on the dispersion mechanism based on the molecular structures of the materials, showing that it could cause changes in the dispersion behavior (slump flow), performance on slump retention (slump loss), delay on the reaction rate (setting time) and the particle packing improvement (compressive strength) with different chemical structures [4-8].

The effect of superplasticizer in concrete fresh mixture depends on its dosage and distribution in the mixture. Very low dosage will not affect the rheological behavior of the fresh mixture, and on the other hand very high dosage may cause detrimental effect such as bleeding and segregation. Yamada et al. [9] remark that there are critical dosage and saturation dosage of SP in the concrete mixture. Critical dosage is defined as minimal dosage needed to cause overall effect of SP in the mixture. Below critical dosage, the mixture will behave as if no SP is added. Saturation dosage implies that further addition of SP will not lead to improvement of rheology behavior of the concrete mixture. However, the SP dosage must also have an upper limit value, as higher dosage reduces cohesion of the mixture due to excessive bleed water, lowers the viscosity of the cement paste, and hence induces segregation. Interaction of SP in the concrete mixture is a complex process, as it has to compete with the dissolution of cement compound. Dissolution of sulfate ions from gypsum to control the setting time of cement occurs at the beginning of the process. The presence of gypsum, as well as other compounds, affects the effectivity of SP [9]. Direct addition of SP into mixing water may cause different SP dosage requirement compared to delayed addition. Lower SP dosage requirement was observed for delayed addition, however, delayed SP addition is not always possible when considering the mixing equipments and production cycle.

Different cement types may alter the critical dan saturation SP dosages, because of the differences of the chemical compositions of cement. Variation of chemical composition and physical properties of one brand of cement between shipments may occur, and thus the optimum SP dosage needs to be adjusted for a good and consistent result. The addition of supplementary cementitious material can also reduce or increase the SP dosage requirement. Adding fly ash tends to reduce the SP dosage required to achieve the same workability, because of its chemical and physical properties [10].

The PCE-based SPs currently available in the market in Indonesia, are supplied by several manufacturers, both local and international, competing one to each other. Each brand of PCE-based SP comes with different behavior and characteristics, aside from the availability and price range. The customization of the SP by adding other ingredient, such as retarder, accelerator, foam buster, causes further confusion on the dosage requirement of the SP to produce a good, homogeneous and predictable fresh concrete. The objectives of this research are to study the different characteristics of polycarboxylate-based (PCE) superplasticizer commonly available in the market and to evaluate the proposed simple testing method to determine its properties. Simple testing method is proposed to simplify the optimization process. Two cement types were used to show the influence of cementitious mixture on the optimum dosage needed.

## 2. Experimental methods

### 2.1. Materials and mixtures

Five brands of PCE-based SP that currently available in the local market in Indonesia, produced by four different manufactures, were used in this study. The codings for the SPs used are (a) CC, (b) SV, and (c) AS, produced by three different producers; (d) BA and (e) BS produced by the same producer. Two cement types, i.e. Ordinary Portland cement (OPC) and Portland Pozzolan cement (PPC) from two different cement producers were used in this research.

Distilled water was used throughout the experiment to avoid any contamination. Sand was obtained from local quarry in Lumajang, East Java, Indonesia. The sand gradation was controlled by sieving to conform to graded sand according to ASTM C778 [11] to avoid any unnecessary variation in sand gradation that may affect the workability of the fresh mortar mixture. This controlled gradation is necessary to avoid variation of flowability.

The effective SP dosage was investigated in mortar mixes with sand to cement weight ratio of 2. Three series of w/c ratio of 0.25, 0.30 and 0.35 was used to investigate the effect of water content in the mixture. Superplasticizer dosage intended was from 0 to 2% by cement weight at 0.1% increment, the test series was terminated when the mixture was showing sign of bleeding and/or segregation.

## 2.2. Test Methods

Workability of the fresh mixture was measured using flow table test apparatus in accordance to ASTM C230 [12]. SP was added directly into the water. Dry material was mixed thoroughly before adding water in the mixture, then the mortar mixture was mixed using small hand drill for two minutes. Afterwards, the mixture was placed in a converted cone on the flow table test apparatus. The initial diameter or static flow (D1) was measured after the cone was removed from the table, and final diameter or dynamic flow (D2) was measured after applying 25 drops. Fig. 1(a) shows an example of a flowability test result. The mortar mixture was then cast in 50×50×50 mm cube molds. Demolding was carried out on the following day and specimens were kept submerged in clear fresh water until taken out one day prior to test.

Compressive strength test were conducted on the mortar cube specimens at 7 and 28 days, on three specimens for each variable. Determination of setting time was performed from temperature measurement of the mortar, on 200 ml mortar that was placed in a sealed polystyrene container. Monitoring the temperature evolution was done for 48 hours. Initial setting time was determined as the time at the median of the temperature rise, while final setting time as the time when the maximum temperature was reached, as shown in Fig. 1(b). This measurement was to simplify testing method based on ASTM C1679 [13].

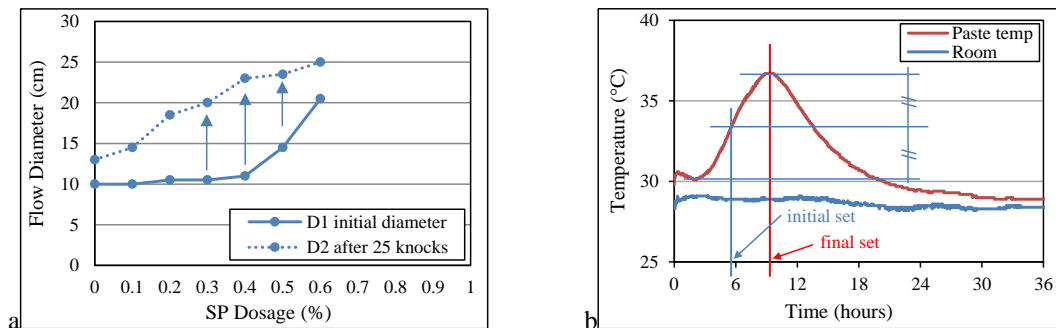


Fig. 1. (a) Result of flow table test, showing D1 and D2 with increase of SP dosage; (b) Measurement of initial and final setting time of the mortar mixture from temperature evolution of the mixture.

## 3. Results and discussions

### 3.1. Effect of superplasticizer type and water-to-cement ratio

Mortar mixture was tested for its flowability using flow table test. Initial diameter (D1) and final diameter (D2) were measured to determine the workability of the mixture. Fig. 2 to 6 show the correlation between the dosage of five SPs with the flowability of fresh mortar and the 28-day compressive strength. The water-to-cement ratios of mortar were varied, i.e. 0.25, 0.30 and 0.35, while maintaining the cement content, to investigate the influence of water content in the mixture. Adding water into the mixture increases the distance amongst the cement particles and reduces the viscosity. On the other hand, adding SP reduces the inter-particle attractive force, with slight change in

its viscosity. This difference causing intricate interaction between the mixture composition and the SP dosage required to achieve the targeted workability.

Water-to-cement ratio influences the static flowability of the mixture. Very low water-to-cement ratio ( $w/c=0.25$ ) does not cause any static flowability of mortar mixture, even when SP is continually added. The increase of workability was observed at the dynamic condition, when the table was dropped for 25 times. When the SP dosage was increased, it was observed that there was an inflection point. The mixture showed low flowability at low SP dosage. Increase in SP dosage linearly increased the flowability until the optimum SP dosage was reached, where only slight increase of flowability was acquired with the increase of SP dosage.

From the inflection point, the critical and saturation dosages can be identified for the specific mixture composition. Different optimum SP dosages observed are depending on the SP brand. This can be attributed to the concentration of the active component in the SP. Therefore, the active component of SP should be also known for better estimation of the dosage needed.

The 28-day compressive strength was also shown in the Figures, correlating with the SP product used, SP dosage and  $w/c$  ratio of the mortar mixtures. It is shown that the presence of SP definitely has positive impact in increasing the compressive strength of concrete with the increase of workability and dispersion of cement particles. The increase is more pronounce for mixtures with lower  $w/c$ . Fig. 3(b) shows an example of the increase of compressive strength for mortar with SV superplasticizer. There is an optimum dosage of 0.3-0.4% to achieve higher strength. Further dosage increment reduces the strength, indicating the occurrence of bleeding and segregation.

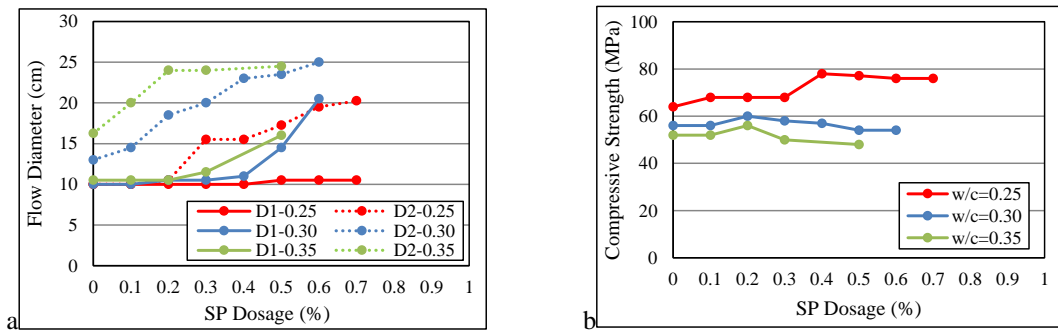


Fig. 2. (a) Flow diameter and SP dosage with different  $w/c$ ; (b) 28-day compressive strength of mortar with CC superplasticizer.

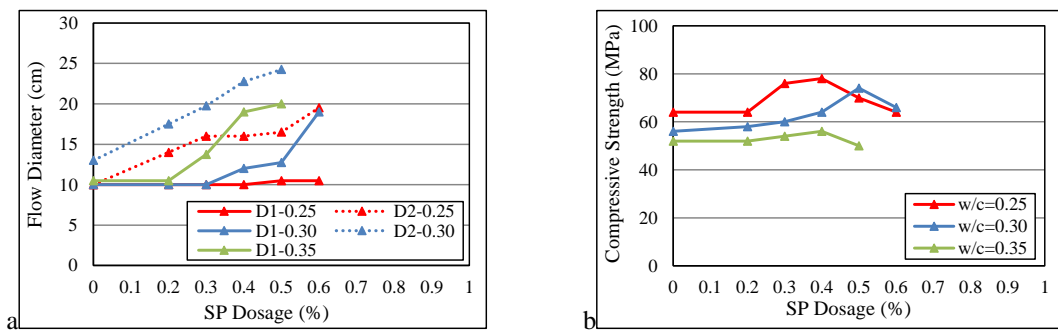


Fig. 3. (a) Flow diameter and SP dosage with different  $w/c$ ; (b) 28-day compressive strength of mortar with SV superplasticizer

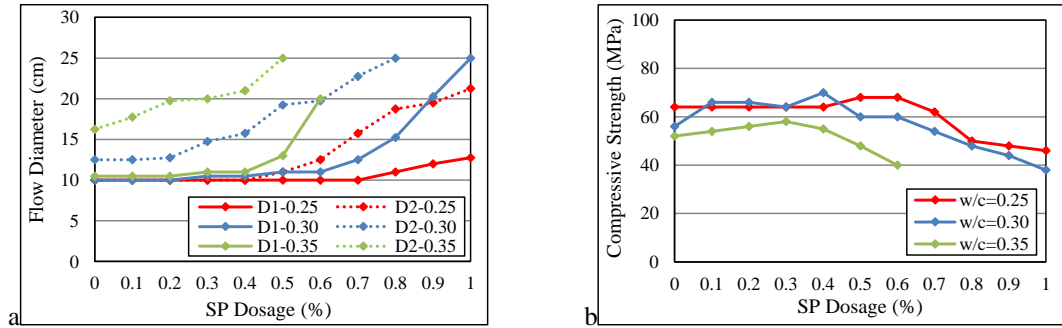


Fig. 4. (a) Flow diameter and SP dosage with different w/c; (b) 28-day compressive strength of mortar with AS superplasticizer

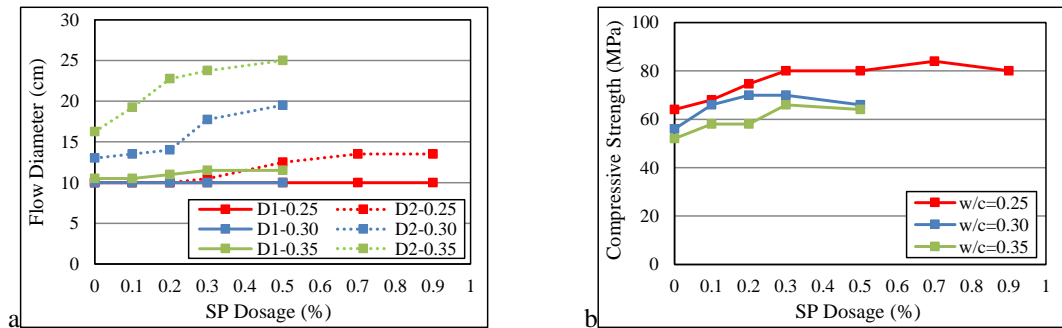


Fig. 5. (a) Flow diameter and SP dosage with different w/c; (b) 28-day compressive strength of mortar with BA superplasticizer

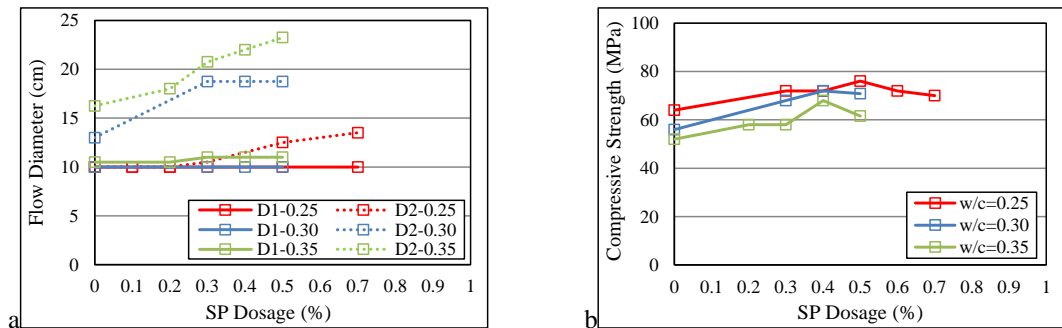


Fig. 6. (a) Flow diameter and SP dosage with different w/c; (b) 28-day compressive strength of mortar with BS superplasticizer

### 3.2. Effect of cement type

The SP dosage increment on mixture using Ordinary Portland cement (OPC) and Portland Pozzolan cement (PPC) are shown on Fig. 7-11. Distinct results are shown for mixtures with OPC and PPC, where PPC mortar mixture show better workability. Water-to-cement ratio was set constant at 0.3 in this experiment series. SP demand is lower for PPC mortar because in its composition there is additional pozzolanic material that contributes to lowering the inter-particle attraction force, and reduces the water demand of the mixture. OPC mortar is more benefitted from SP addition, because cement particles are distributed more evenly in the mixture. Its compressive strength is increased compared to the one without SP addition. Higher increase of strength with the increase of testing age is also observed on mortar mixture using OPC.

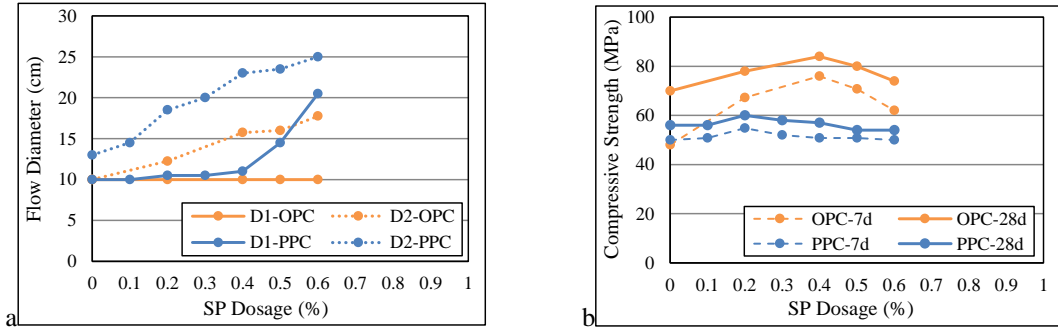


Fig. 7. (a) Flow diameter and SP dosage with OPC and PPC cement; (b) 7-day and 28-day mortar compressive strength with CC superplasticizer

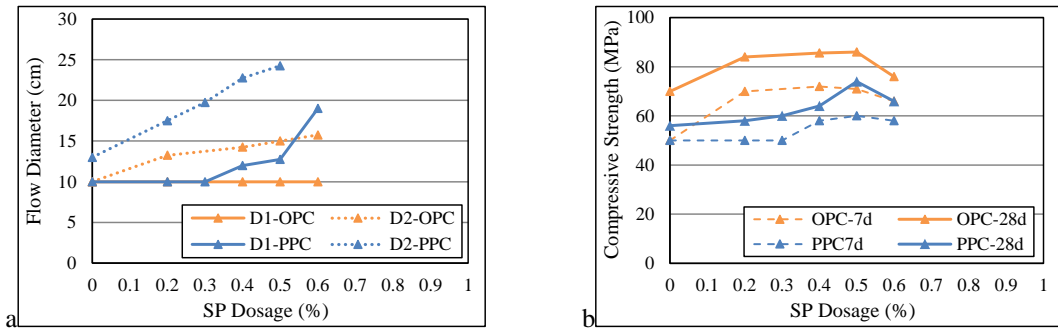


Fig. 8. (a) Flow diameter and SP dosage with OPC and PPC cement; (b) 7-day and 28-day mortar compressive strength with SV superplasticizer

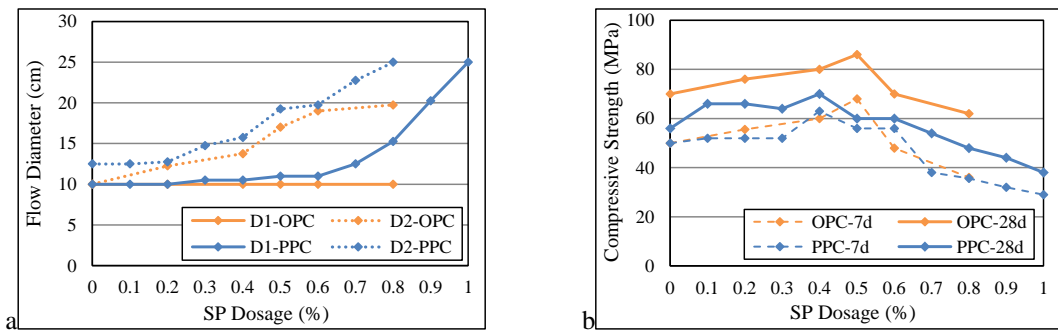


Fig. 9. (a) Flow diameter and SP dosage with OPC and PPC cement; (b) 7-day and 28-day mortar compressive strength with AS superplasticizer

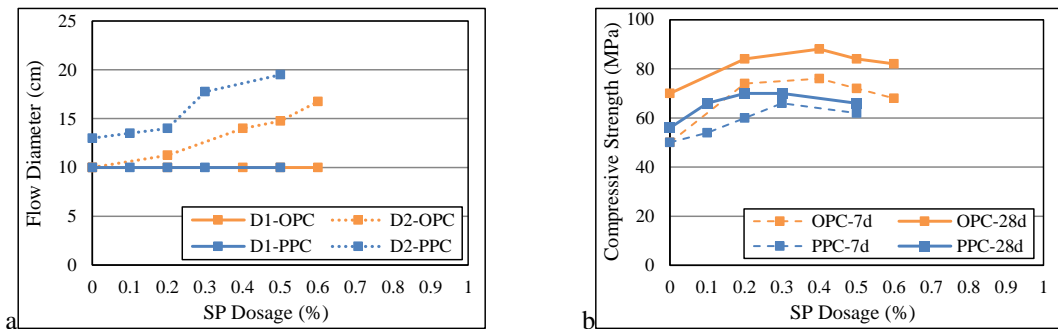


Fig. 10. (a) Flow diameter and SP dosage with OPC and PPC cement; (b) 7-day and 28-day mortar compressive strength with BA superplasticizer

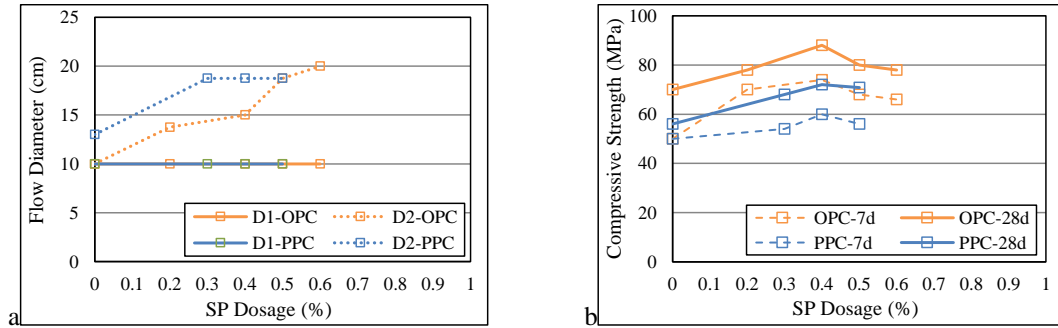


Fig. 11. (a) Flow diameter and SP dosage with OPC and PPC cement; (b) 7-day and 28-day mortar compressive strength with BS superplasticizer

### 3.3. Slump retention and setting time

The slump retention of mortar mixture with different SP was measured by dynamic flow (D2) at 30 minutes interval. Water-to-cement ratio was set constant at 0.3, with SP dosage was determined from previous step. Fig. 12 shows that there is reduction on slump flow for three SPs (CC, SV and AS) starting from 60 minutes after water addition. The other two SPs (BA and BS) show good slump retention even after 120 minutes.

The initial and final setting time measured from temperature evolution of the mixture is shown in Table 1. There is good correlation between setting time and slump retention time. The setting time is faster for OPC mortar compared to the one with PPC, as shown in the control mixture. However, the SP addition is also shown to retard the chemical reaction rate of the mixture with the longest retention time occurs for BS superplasticizer.

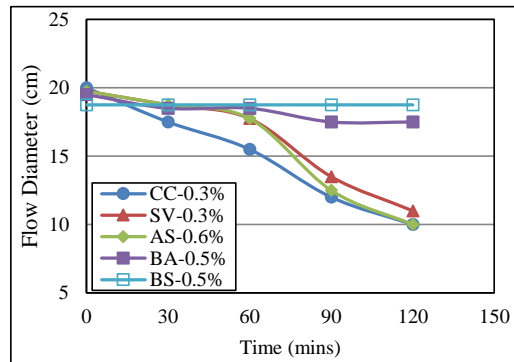


Fig. 12. Slump retention of PPC mortar mixture with SP dosage

Table 1. Initial and final setting time of PPC and OPC mortar with various SP addition for w/c=0.3

Superplasticizer	Type	PPC			OPC		
		Dosage (%)	Initial set (h)	Final set (h)	Dosage (%)	Initial set (h)	Final set (h)
Control	-	0	3.60	9.00	0	3.33	7.20
CC	PCE	0.3	5.75	11.50	0.4	5.75	8.78
SV	PCE	0.3	6.67	12.00	0.6	8.78	12.00
AS	PCE	0.6	6.00	11.20	0.6	6.00	10.00
BA	PCE	0.5	8.50	13.00	0.5	6.70	10.30
BS	PCE	0.5	12.70	18.00	0.4	12.00	16.67



#### 4. Conclusions

From this study, the following conclusions can be summarized:

1. The addition of superplasticizer improves the flowability of mortar mixture. However, there is an optimum dosage for each water content. Excessive use of SP causes bleeding and segregation.
2. The increase of flowability increases the compressive strength up to a point. Optimum dosage is depending on the superplasticizer and cement type. Compressive strength will be reduced with excessive usage of SP.
3. The difference in flowability and strength gain are also affected by the type of cement used. PPC mortar has higher flowability compared to the one with OPC, but it has lower compressive strength for the same water-to-cement ratio.
4. Optimizing the superplasticizer dosage using flow table test and temperature evolution measurement give satisfactory information on the different performance amongst various SP brands.
5. Each SP brand has different behavior with regards to the optimum dosage, setting time, strength development and slump retention time. Hence, the use of different cement type needs to be carefully considered.
6. The variation of SP and cement type should be considered when doing the material selection for better prediction on the behavior of the fresh and hardened concrete mixture.

#### Acknowledgements

The authors gratefully acknowledge The Ministry of Research, Technology and Higher Education, Indonesia, who provided the research grant under the Fundamental Research scheme.

#### References

- [1] R. Rixom & N. Mailvaganam, Chemical Admixtures for Concrete. E & FN Spon Publication, III Edition (2003).
- [2] H. Okamura & M. Ouchi, Self-Compacting Concrete. *J. of Adv. Con. Tech.*, 1 (1) (2003) 5–15.
- [3] E. Sakai, K. Yamada, A. Ohta, Molecular structure and dispersion-adsorption mechanisms of comb-type superplasticizers used in japan, *J. of Adv. Con. Tech.*, 1 (1) (2003) pp 16-25, <http://doi.org/10.3151/jact.1.16>.
- [4] F. Kong, L. Pan, C. Wang, D. Zhang, N. Xu, Effects of polycarboxylate superplasticizers with different molecular structure on the hydration behavior of cement paste, *Con. & Build. Mat.*, 105 (2016) 545-553. doi:10.1016/j.conbuildmat.2015.12.178.
- [5] A. K. H. Kwan & W. W. S. Fung, Effects of SP on Flowability and Cohesiveness of Cement-Sand Mortar. *Con. & Build. Mat.*, 48 (2013) 1050–57. doi:10.1016/j.conbuildmat.2013.07.065.
- [6] J. Gołaszewski, & J. Szwabowski, Influence of superplasticizers on rheological behaviour of fresh cement mortars. *Cem. & Con. Res.*, 34 (2004) 235–248. doi:10.1016/j.cemconres.2003.07.002.
- [7] V. Morin, F. Cohen Tenoudji, A. Feylessoufi, & P. Richard, Superplasticizer effects on setting and structuration mechanisms of ultrahigh-performance concrete. *Cem. & Con. Res.*, 31 (2001) 63–71. doi:10.1016/S0008-8846(00)00428-2.
- [8] S. Srinivasan, S. A. Barbhuiya, D. Charan & S. P. Pandey, Characterising cement-superplasticiser interaction using zeta potential measurements. *Const. & Build. Mat.*, 24 (12) (2010) 2517–2521. doi:10.1016/j.conbuildmat.2010.06.005.
- [9] K. Yamada, S. Ogawa, S. Hanehara, Controlling of the adsorption and dispersing force of polycarboxylate-type superplasticizer by sulfate ion concentration in aqueous phase, *Cem. & Con. Res.*, 31 (3), 2001, Pp 375-383, [http://dx.doi.org/10.1016/S0008-8846\(00\)00503-2](http://dx.doi.org/10.1016/S0008-8846(00)00503-2).
- [10] E. Tkaczewska, Effect of the superplasticizer type on the properties of the fly ash blended cement. *Const. & Build. Mat.*, 70 (2014) 388–393. doi:10.1016/j.conbuildmat.2014.07.096.
- [11] ASTM C778. Standard Specification for Standard Sand. ASTM International, 2002.
- [12] ASTM C230 / C230M-14, Standard Specification for Flow Table for Use in Tests of Hydraulic Cement, ASTM International.
- [13] ASTM C1679 – 14, Standard Practice for Measuring Hydration Kinetics of Hydraulic Cementitious Mixtures Using Isothermal Calorimetry, ASTM International.



Sustainable Civil Engineering Structures and Construction Materials, SCESCM 2016

## Influence of the Stiffness Modulus and Volume Fraction of Inclusions on Compressive Strength of Concrete

Han Ay Lie<sup>a,\*</sup>, Buntara Shently Gan<sup>b</sup>, Benny Suryanto<sup>c</sup>, Yulita Arni Priastiwi<sup>d</sup>

<sup>a</sup>Associate Professor, Civil Engineering Department, Diponegoro University, Semarang, Indonesia

<sup>b</sup>Professor, Department of Architecture, College of Engineering, Nihon University, Koriyama, Japan

<sup>c</sup>Assistant Professor, School of Energy, Geoscience, Infrastructure and Society, Heriot Watt University, Edinburgh, UK

<sup>d</sup>Research Associate, Structural and Material Laboratory, Diponegoro University, Semarang, Indonesia

---

### Abstract

The stiffness differences between aggregate and mortar matrix in concrete create stress concentration at their interface transition zones. Studies on 100 mm cubes with different volume and shape of inclusions, resembling aggregate particles within the concrete, suggested that it is always in this transition zone that cracks initiate. Further detailed finite element analysis brought to light that especially the mortar nodes in principal tension - compressive stresses were most vulnerable to premature failure. The study also suggested that as the relative stiffness between the inclusion and the surrounding mortar increases, the stress concentration problem increases, resulting in premature cracking and lower compressive strength, when compared to the specimens with more homogeneous stiffness profile. This study aims to investigate in more details the influence of inclusion volume fraction, compressive strength and stiffness modulus on the compressive strength of 100×100×50 mm<sup>3</sup> prisms. The inclusions were in cylindrical shape and made of mortar with a compressive strength ranging from approximately 20 MPa to 50 MPa; the matrix was also made of mortar but with a constant compressive strength of approximately 29 MPa. It is found that the compressive strength and initial stiffness of the concrete prisms are directly related to the volume fraction and compressive strength of the inclusions. Finite element analysis is conducted to investigate the influence of the relative strength of inclusion to the surrounding mortar.

© 2017 The Authors. Published by Elsevier Ltd.

Peer-review under responsibility of the organizing committee of SCESCM 2016.

*Keywords:* inclusion volume fraction; inclusion strength ratio; compressive strength.

---

---

\* Corresponding author. Tel.: +62-811288313; fax: +62-24-76480727.

E-mail address: [hanaylie@hccnet.nl](mailto:hanaylie@hccnet.nl)

## 1. Introduction

Extensive research work has been conducted to study the influence of aggregate inclusions on the mechanical behavior of mortar and concrete [1-6]. In these studies, the aggregate inclusions were much stronger and stiffer than the surrounding mortar matrix. As a result, when the mortar/concrete specimens were tested to failure, the inclusions remained elastic although the surrounding mortar exhibited highly nonlinear behavior. It was concluded as the inclusion volume fraction is increased, the initial stiffness increases and the compressive strength decreases. The reduction in compressive strength is likely attributed to the weak interfacial transition zone (ITZ) between the aggregate inclusions and the surrounding matrix. Apart from the volumetric ratio, the compressive strength and stress-strain response of the mortar/concrete specimens were found to be influenced by the geometry and configuration of the inclusions, the presence of sharp angles in the direction of loading, the number of inclusions and their distance. Other influencing factors include the absorption rate, surface roughness and material homogeneity of the inclusions. Apart from the study high strength inclusions, work has also been conducted on low strength inclusions such as in a soil mixture [7, 8] and in concrete using synthetic inclusions [9].

This study aims to study the effect of compressive strength and volume fraction of inclusions on the overall compressive strength and elastic modulus of concrete. The inclusions were cylindrical and core drilled from mortar slabs. The 28 days compressive strengths of the inclusions are presented in Table 1, together with the corresponding strengths at 56 days and their relative strengths to that of the surrounding mortar which has a cylinder compressive strength of 29.16 MPa at 56 days.

Table 1. Inclusion cylinder compressive strength

Testing age	Cylinder Compressive Strength (MPa)				
	A1	A2	A3	A4	A5
28 days	22.94	28.89	35.71	39.97	46.06
56 days	23.95	30.11	36.24	41.63	46.80
Strength ratio to mortar	0.82	1.03	1.24	1.43	1.60

This study also investigates the response of concrete as a composite material containing a mixture of aggregate inclusion and mortar. In theory, the behavior of a composite material can be approximated by the parallel (Voigt, constant-strain), series (Reuss, constant-stress), Hirsch and Counto model [10] using the following relationships:

$$\text{Parallel model: } E_s = V_a E_a + V_m E_m \quad (1)$$

$$\text{Series model: } \frac{1}{E_s} = \frac{V_a}{E_a} + \frac{V_m}{E_m} \quad (2)$$

$$\text{Hirsch model: } \frac{1}{E_s} = x \frac{1}{(V_a E_a + V_m E_m)} + (1 - x) \left( \frac{V_a}{E_a} + \frac{V_m}{E_m} \right) \quad (3)$$

$$\text{Counto model: } \frac{1}{E_s} = \frac{1 - \sqrt{V_a}}{E_m} + \frac{\sqrt{V_a}}{(1 - \sqrt{V_a}) E_m + E_a \sqrt{V_a}} \quad (4)$$

Where  $E$  and  $V$  represent the elastic modulus and volume fraction; the subscripts  $s$ ,  $a$  and  $m$  stand for the specimen, inclusion and mortar, respectively;  $x$  and  $(1-x)$  are the relative proportions corresponding to the upper and lower bound solutions for elastic materials, customary taken as 0.5 for concrete. It should be noted that the first two models are only a simple approximate as concrete does not exhibit either constant stress or strain even under uniform loading. The Hirsch model, which is a combination of the parallel and the series models, does not provide accurate predictions for soft inclusions. For example, when the aggregate stiffness approaches zero ( $E_a = 0$ ), this would result in zero composite stiffness (e.g.  $E_s = 0$ ) which is incorrect. The Counto model (Eq. 4) therefore appears to be the most accurate model and is useful for this study. The computed composite elastic modulus will be compared to experimental data to gauge the accuracy.

## 2. Experimental work

The work involved the testing of  $100 \times 100 \times 50$  (depth) mm concrete prisms with one single cylindrical inclusion aligned vertically at the center of the square surface. Two test parameters were investigated: inclusion volume fraction and inclusion compressive strength. Four inclusion diameters, 11.7, 20.6, 29.7 and 45.7 mm were prepared, resulting in a volume fraction  $V_a$  of 0.01, 0.03, 0.07 and 0.16. Control (mortar only) specimens were also produced representing a zero inclusion volume fraction. For every case, eight specimens were prepared to result in six valid data. The compressive strengths provided in Table 1 were used as the basis for the second parameter.

The specimens were prepared in two stages. The first stage involved the preparation of the inclusions and for this purpose, aggregate inclusions were core drilled from 70 mm thick mortar plates using a diamond core drill. The cylindrical core was then made in a saturated surface dry condition and positioned at the center of  $100 \times 100 \times 50$  mm five gang plywood molds (see Fig. 1). The mold had a 5 mm acrylic lid in order to secure the cores in place during casting. This vertical configuration was done to minimize the bleeding effect that could weaken the interface between the cylindrical inclusion and the surrounding mortar.

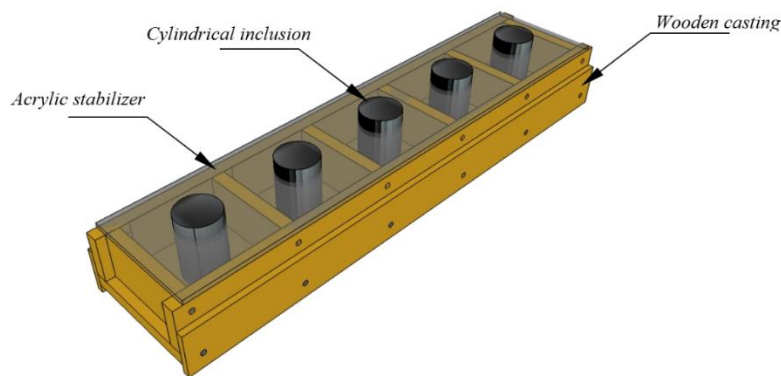


Fig. 1. Cylindrical inclusions placed at the center of a five gang plywood mold.

The second stage involved the mixing and pouring of mortar. Compaction was performed using a vibration table for a period of 30 seconds. The specimens were then submerged in water for 28 days and dried. The top surface of the specimen was made flush by cutting part of the inclusion that protruded 20 mm. The specimens were given label as  $A_{ij}$ , with  $i$  representing the inclusion strength ratio and  $j$  for the inclusion diameter such as 11, 20, 29 and 45.

The testing surfaces were further leveled, two  $100 \mu\text{m}$  Teflon layers separated by bearing grease were placed on the top and on the bottom face of the specimen to prevent the loading platen's confinement on the specimen. A uniform compression load was applied to each specimen at a rate of 800 N/sec. Four linear variable displacement transducers (LVDTs) with a sensitivity of  $2000 \times 10^{-6}$  strain/mm and a load cell with a capacity of 1000 kN were used to record the load, which was applied incrementally, and the corresponding displacements. Each test specimen was monitored visually using a high definition digital camera to observe the initiation and propagation of cracks under monotonic loading.

## 3. Test Results

### 3.1. Compressive strength

Figure 2 shows the relationship of the inclusion volume fraction for a range of inclusion strengths ratios. It can be seen that an increase in inclusion volume fraction resulted in a decrease in the specimen's load carrying capacity. The behavior followed a linear pattern and all specimens exhibited lower compressive strengths when compared to the control (mortar only) specimen. With regards to the effects of inclusion compressive strength, it appears that the

lower the strength ratio, the more pronounced the reduction in the specimen’s capacity relative to that of the control specimen. A1 specimens exhibited an almost identical pattern to A2 specimens, which can be seen from comparable gradients of the plots presented in Fig. 2. This indicates that when the compressive strength ratio is close to unity, it has only minor influence on the reduction rate in compressive strength with increasing inclusion content.

To better analyze the influence of inclusion strength ratio, the load carrying capacity of specimens were plotted against this variable, for every inclusion volume fraction variation. The results are presented in Fig. 3.

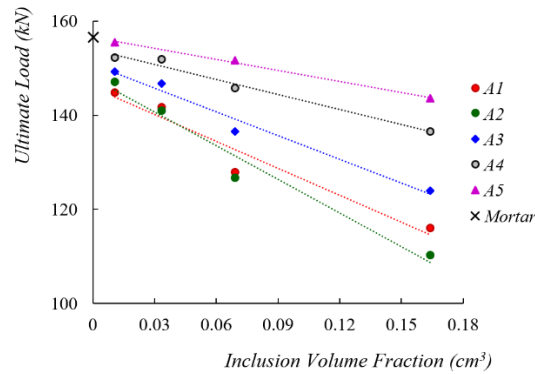


Fig. 2. Influence of inclusion volume fraction on compressive strength

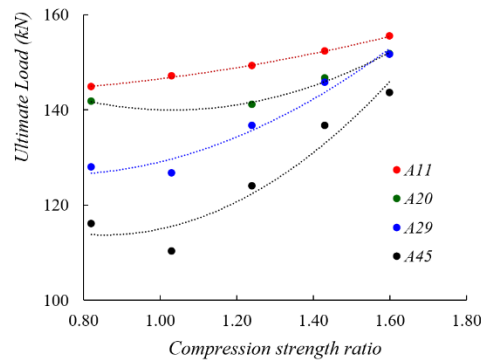


Fig. 3. Influence of strength ratio on compressive strength

The behavior was best described by a quadratic convex path. For all inclusion volume fractions, an increase in compressive strength ratio has a positive influence on the compressive strength of the bulk composite. Larger inclusion volume fractions were more sensitive to strength degradation, which can be seen from the patterns of curves A<sub>11</sub>, A<sub>20</sub>, A<sub>29</sub> and A<sub>45</sub>. The 0.8 volume fraction resulted from the 11.7 mm inclusion had the most moderate curve’s tangent.

### 3.2. Initial Failure and Crack Propagation

The control (mortar only) specimen failed due to tensile strains in the direction perpendicular to the line of loading, resulting in a columnar pattern (Fig. 4a). For specimens with inclusions, two modes of failure were observed: a columnar pattern with crack passing through the inclusion (Fig. 4b) and a columnar pattern with crack passing around the inclusion due to interface debonding (Fig. 4c).

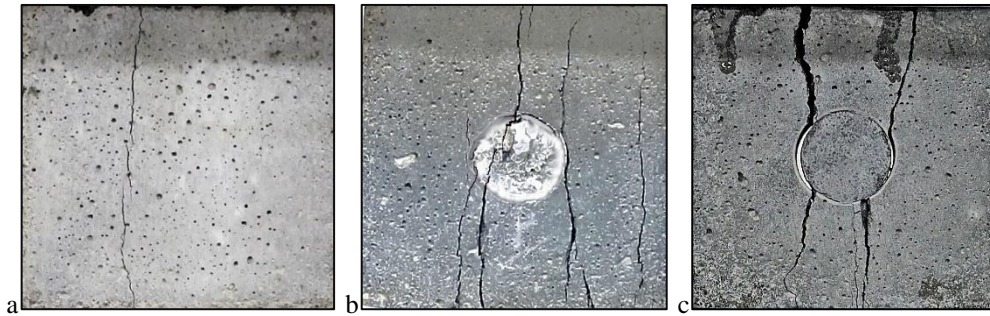


Fig. 4. (a) mortar specimen cracking; (b) cracking in the inclusion; (c) columnar and interface debonding

Cracking in the inclusions was only detected for compressive strength ratios lower than 1.0 (A1 series). In this series, it was found that cracks formed vertically and some of them passed through the cylindrical inclusion (see Fig. 4b). In specimens with larger compressive strengths ratio (A3 to A5 series), the same vertical crack formation was observed. However, it was found that cracks propagated around the cylindrical inclusion along the inclusion/matrix interface, creating an en-echelon formation (Fig. 5a) as explained by van Mier in 1997 [11].

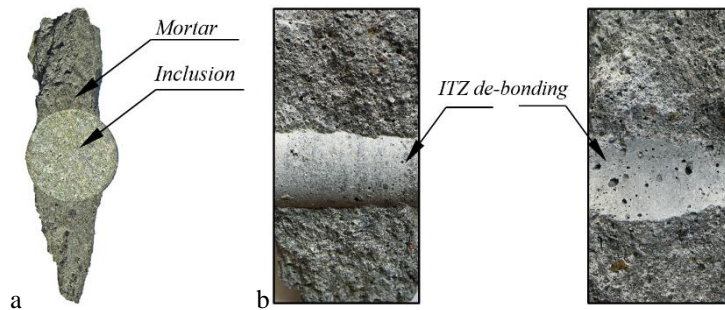


Fig. 5. (a). En-echelon formations; (b). ITZ tension debonding failure surfaces

Close observation of the cracked surface revealed that no mortar fragments were detected in the failure surface (Fig. 5b), indicating ITZ tension debonding behavior. The specimens with a strength ratio of 1.0 (A2 series) exhibited a combination of the two failure behaviors.

The initial cracking was observed visually, from digital recordings. It was observed that regardless of the strength ratios and the volume fraction, cracking was always initiated in the mortar matrix (Fig. 6a and 6b). In A1 series specimen with a strength ratio of 0.8, it was observed that the cracks rapidly proliferated vertically and passed through the inclusion. In A3 to A5 series specimens with strength ratios greater than unity, it was found that the cracks propagated in a straight line and deviated into the interface in tension. In A2 series specimen with a strength ratio of 1.0, an amalgamation of behavior was noted. This particular case was distinguished by an almost identical compressive strength between the mortar matrix and the inclusion.

Since all cracks were initiated in the mortar, it can be concluded that a good bond within the interface is present. This leading to the assumption correctness that the test specimens were a composite material. Also, this finding contradicts the research on diorite inclusions with identical volume fraction [5] where the crack was found always to initiate at the ITZ. Compared to aggregate inclusions, a better bond between mortar inclusions and the surrounding mortar exist.



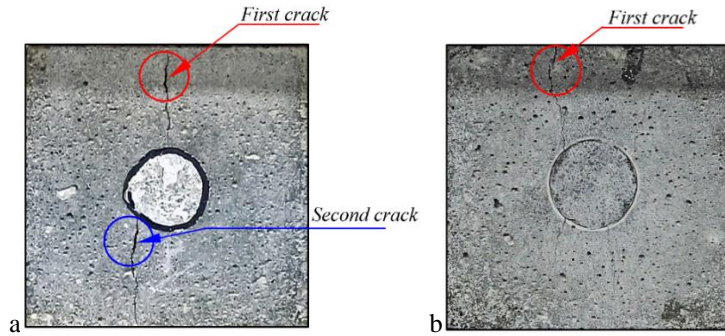


Fig. 6. (a) Initial cracking for strength ratio of 0.8; (b) Initial cracking for strength ratios larger than 0.8

### 3.3. Initial stiffness modulus

Fig. 7 illustrates the predicted initial stiffness moduli as derived from the Counto equation, plotted together with the observed values determined from the specimen’s stress-strain relationship. The Young’s modulus of the mortar matrix and inclusions were determined from the cylinder compressive strength in accordance with the *fib* Model Code 2010 [12]. The experimental data are in good agreement with the values as predicted by the Counto equation.

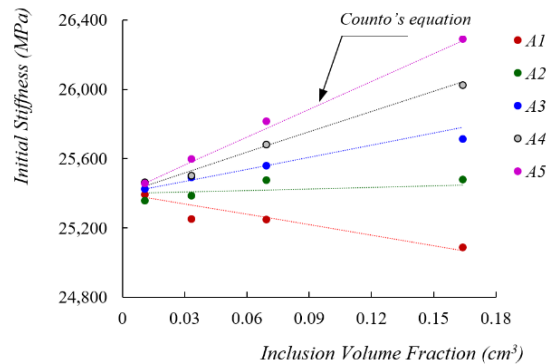


Fig. 7. Initial Stiffness modulus as a function of Volume fraction

## 4. Analysis and Discussions

### 4.1. Compressive strength

The reduction in compressive strength with increasing inclusion volume fraction for all strength ratios is thought to originate from the presence of the ITZ. The initial cracking in the mortar suggests that the tensile strength of the interface exceeded the mortar’s tensile capacity, yet a perfectly full-bond was not achieved. This conclusion is supported by the 6% to 30% load carrying capacity reduction between the mortar only specimen and the specimen incorporating inclusion with similar strength (1.0 strength ratio). The higher the inclusion volume fraction, the larger the strength reduction. The stresses induced by the load were not uniformly distributed between the mortar matrix and inclusions due to the imperfect ITZ bond. The width of the mortar-strip adjacent to the inclusion is heavily influenced the resulting maximum stresses. These high-stress concentrations, in turn, led to premature cracking of mortar. The result of finite element analysis comparing the stresses in a mortar strip specimen nearby a hole (weak inclusion), inclusion with a perfect bond and no inclusion are shown in Fig 7. The stresses in the direction of the z-z axis are plotted against the nodal coordinates of the mortar strip. In the analysis simulating the effect of inclusion, it



was assumed that the strength ratio is 1.6, and the inclusion is perfectly bonded to the mortar. A similar approach was conducted by [13], validating the finite element results to the iBEM readings.

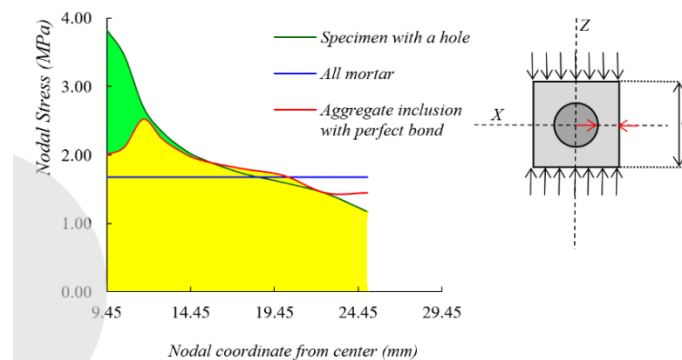


Fig. 6. Stress concentration in the ITZ

The blue line shows the theoretical stresses for the mortar only specimen, the green line stands for the specimen with a hole and the red line represents the analysis case with an inclusion perfectly bonded to the surrounding matrix. The analysis results show that when an inclusion with a perfect bond is present, the stress concentrations in the vicinity of the ITZ are drastically reduced. If the volume fraction increases, the remaining mortar strip will decrease, resulting in a significant escalation in stresses. The true behavior would lay between the two lines, explaining the better load carrying capacity for the inclusion with relatively higher strength ratios. This analysis also supports the fact that for a constant inclusion volume fraction, the higher stress ratios resulted in a better performance in compression. Figure 6 also implies that for high volume fractions, eq. larger sized inclusions, the low strength ratio has a more pronounced effect on the load carrying capacity. For the larger inclusion volume fraction, the ITZ surface area also increases, resulting in an additional negative effect on the overall specimen behavior.

#### 4.2. Cracking behavior and initial stiffness modulus

The crack propagation is strongly affected by the inclusion strength ratio, but is less influenced by the volume fraction. When the strength ratio is smaller than 1.0, the crack propagation will follow a pattern as if the specimen was homogeneous. No deviation from the columnar path was detected. For a strength ratio larger than 1.0, the cracks propagated through the ITZ in tension, following an en-echelon shear flow. For a strength ratio equal 1.0, a combination of both failure modes occur. When the inclusions have a stronger bond in tension to the surrounding mortar than the mortar matrix tensile capacity, the crack will initiate in the mortar matrix. For aggregate inclusions, the ITZ bond is weaker, first cracking always takes place in the ITZ. However, even for mortar inclusions, the ITZ bond is imperfect, concluded from the reduction in compression strength between the mortar only specimen and the specimen with an equal strength inclusion (strength ratio = 1.0). The finite element models constructed by Wu and Wong [8] using low and high strength inclusions, and the study of iron inclusions [6] underlined these findings.

The evaluation on the initial stiffness revealed that for specimens with an inclusion strength ratio lower than 1.0, the stiffness decreases with increasing inclusion volume fraction. For a 1.0 ratio, the path follows an almost horizontal line, while for ratios larger than 1.0, an enhancement in stiffness is observed. While an increase in inclusion volume fraction always decreases the compressive strength, it may increase the initial stiffness as in a case when the strength ratio is larger than 1.0. The initial stiffness ratio directly related to the compressive strength by the *fib* and the majority of standards is, therefore, incorrect. The approach of Counto provides a better illustration of the stiffness behavior of an inclusion specimen. These findings were also underlined by previous studies [1, 14, 15]. The study of Le Roy et al. [14] investigated the inclusion size effect in lightweight concretes. Their research work

suggested to assess a physical model rather than an empirical one through, for example, using the Hashin-Shtrikman bounds to approximate the Young's modulus.

## 5. Conclusions

In a nutshell, it is concluded that a lower inclusion volume fraction, thus smaller inclusions, will lead to a better load carrying capacity regardless of the quality of inclusions. When dealing with larger volume of inclusions, a better performance will be obtained when the inclusions are stronger than the surrounding mortar matrix. When calculating the initial stiffness, the laboratory results obtained support the notion that the stiffness is not only related to the compressive strength. The mathematical models proposed by Counto and Hashin-Shtrikman were proven to provide more accurate predictions of the Young's modulus of concrete.

## References

- [1] H. Beushausen, T. Dittmer, The influence of aggregate type on the strength and elastic modulus of high strength concrete, *Construction and Building Materials*, 74, (2015), 132-139.
- [2] A. L. Han, B. S. Gan, R. Yuniarto, A. Yesica, R. N. Editia, Inclusion-to-specimen volume ratio Influence on the Strength and Stiffness Behaviors of Concrete: an Experimental Study, in press, *Applied Mechanics and Material*, Trans Tech Publications, 845, (2016), 113-118.
- [3] A.L. Han, B. S. Gan, and Y. Setiawan, The Aggregate Multi-inclusion Interaction and Interface Influence on the Compression Behavior of Concrete, in: S. Saha, Y. X. Zhang (Eds), *Implementing Innovative Ideas in Structural Engineering and Project Management*, ISEC Press, 2015. 695-700.
- [4] A. L. Han, I. Nurhuda, Y. Setiawan, The Effect of Aggregate Shape and Configuration to the Concrete Behavior", *Smart Science*, Taylor and Francis online, 2-2, (2014a), 85-90.
- [5] A. L. Han, B. S. Gan, Y. Setiawan, The influence of single inclusions to the crack initiation, propagation and compression strength of mortar, *Procedia Engineering*, 95,(2014b), 376-385.
- [6] Y. Kan, K. Pei, C. Chang, 2004, Strength and Fracture Toughness of Heavy Concrete with Various Iron Aggregate Inclusions, *Nuclear Engineering and Design*, 228-1-3, (2004), 119-127.
- [7] G. van Lysebetten , A. Vervoort, J. Maertens, N. Huybrechts, Discrete element modeling for the study of the effect of soft inclusions on the behavior of soil mix material, *Computers and Geotechnics*, 55, (2014), 342-351.
- [8] Z. Wu, L. N. Y. Wong, Modeling cracking behavior of rock mass containing inclusions using the enriched numerical manifold method, *Engineering Geology*, 162, (2013), 1-13.
- [9] J. Lv, T. Zhou, Q. Du, H. Wu, Effects of rubber particles on mechanical properties of lightweight aggregate concrete, *Construction and Building Materials*, 91, (2015), 145-149.
- [10] U. J. Counto, The effect of the elastic modulus of the aggregate on the elastic modulus, creep and creep recovery of concrete, *Magazine of Concrete Research*, 16-48, (1964), 129-138.
- [11] J.G.M. van Mier, Failure of concrete under uniaxial compression: an overview, in: H. Mihashi, K. Rokugo (Eds.), *Fracture Mechanics of Concrete Structures 3*, AEDIFICATIO, Freiburg, 1998, pp. 1169–1182.
- [12] *fib Model Code for Concrete Structures 2010*, Ernst & Sohn, Berlin, 2013.
- [13] G. Song, L. Wang, L. Deng, H. M. Yin, Mechanical characterization and inclusion based boundary element modeling of lightweight concrete containing foam particles, *Mechanics of Materials*, 91-1, (2015), 208-225.
- [14] R. Le Roy, E. Parant, C. Boulay, Taking into account the inclusions' size in lightweight concrete compressive strength prediction, *Cement and Concrete Research*, 35-4, (2005), 770-775.
- [15] E. J. Garboczi, J. G. Berryman, Elastic Moduli of Material Containing Composite Inclusions: Effective Medium Theory and Finite Element Computations, *Mechanics of Materials*, 33-3, (2001), 455-470.



Sustainable Civil Engineering Structures and Construction Materials, SCESCM 2016

## Thermal conductivity and compressive strength of lightweight mortar utilizing pumice breccia as fine aggregate

Slamet Widodo<sup>a</sup>, Faqih Ma'arif<sup>a</sup>, Buntara Sthenly Gan<sup>b\*</sup>

<sup>a</sup>Faculty of Engineering, Yogyakarta State University, Karangmalang, Yogyakarta 55281, Indonesia

<sup>b</sup>Department of Architecture, College of Engineering, Nihon University, Koriyama 963-8642, Japan

---

### Abstract

Pumice Breccia is a natural material which is available in a vast deposit of volume in Indonesia, especially in Yogyakarta area. The main characteristics of this type of rock are lightweight and having low thermal conductivity. Pumice breccia utilization is expected to support the implementation of green building concept by minimizing electrical power needs that may be required for setting the room temperature (air conditioning system). The aim of this study is to evaluate the effect of pumice breccia utilization as fine aggregate in various compositions on the thermal conductivity and compressive strength of the mortar. This study conducted using the experimental method to determine the thermal conductivity and compressive strength of each variation of the mortar. Two (2) types of mortar were investigated in this research. The first type is normal mortar using sand as the fine aggregate with mixture compositions variations of 1 Pc (Portland Cement):4 Ns (Sand), 1 Pc:6 Ns, and 1 Pc:8 Ns, which are labeled as MN1, MN2, and MN3. The second type of mortar is pumice breccia mortar that utilizing pumice breccia material as fine aggregate with mixture compositions variations of 1 Pc (Portland Cement):4 Pb (Pumice Breccia), 1 Pc:6 Pb and 1 Pc:8 Pb, named as MP1, MP2, and MP3. All composition of mortar mixtures is prepared based on the volume ratio. Test results show by using the Pumice Breccia as fine aggregate in the mortar mixtures, the thermal conductivity of the normal mortar can be reduced nearly considerably. Even though, the reduction in compressive strength is observed in all the compositions of mortar mixtures, based on SNI 03-6882-2002, still the Pumice Breccia based mortar can be classified into the type-O mortar that can be used for partition walls, protective and decorative purposes.

© 2017 The Authors. Published by Elsevier Ltd.

Peer-review under responsibility of the organizing committee of SCESCM 2016.

*Keywords:* Compressive strength, Mortar, Pumice Breccia, Thermal conductivity

---

---

\* Corresponding author. Tel.: +6281567966990; fax: +62274554692.

E-mail address: [swidodo@uny.ac.id](mailto:swidodo@uny.ac.id)

## 1. Introduction

The increase of human population led to the rapid development of the construction industry. The existence of a business center buildings, offices, education and housing become a necessity that cannot be avoided. In accordance to the development of construction technology, the need of complementary infrastructure inside the building is also increasing. One of building fixtures which is largely use is air conditioning system (Air Conditioner). It is widely used for almost every type of buildings, starting from skyscraper, educational buildings to housing. The use of AC (Air Conditioner) has given rise to negative effects such as global warming.

One of the main triggers of global warming caused by the use of AC is that Chlorofluorocarbons (CFCs) gas which is resulted from the cooling process. Increased use of AC in the building is very risky to accelerate the depletion of the ozone layer of the earth. It will lead to global warming acceleration. Any reduction of temperature in the air-conditioned room will always be followed by the increase of outdoor temperature. In addition, the use of air conditioning system in the building also spent large energy consumption. It encourages governments in various countries to pursue policies for energy saving, especially associated with the electricity consumption for lighting and air conditioning. For each additional one degree Celsius of thermostat, it will be able to save 3-5% of the air conditioning cost [1].

In order to minimize the negative impact of the use of air conditioning system in the building, it has developed the concept of environmentally friendly building (green building) by minimizing the need for air conditioning system. To minimize the need for air conditioning system, it is necessary to develop the wall material becomes capable to reduce the propagation of heat from the outdoors that will fit into the room. To develop a heat-absorbing wall material, it is necessary to develop such kind of materials that have quite small thermal conductivity. In general, building materials that save a lot of pores and has low specific gravity will have a lower thermal conductivity or better thermal insulating capability.

Experimental research on foamed concrete (FC) exhibits that thermal conductivity increases with increasing density, as expected. For the low density specimen of FC, more foam is incorporated in the concrete, and, as a result, a high amount of air pores are formed inside. As air is a good insulator, the thermal conductivity of FC was found to be lower than that of lightweight concrete. The thermal conductivity of FC and lightweight concrete is lower than that of normal weight concrete, conventional block and brick, which are conventionally used in construction field [2].

Pumice breccia is a type of coarse grained pyroclastic rocks with its breccia fragments dominated by pumice with highly variable shape and size, white-gray color, and its matrix consisting of limestone with amorphous silica. Pumice breccia is formed by the volcanism activity. Therefore, it can be found abundantly along the volcanic line in Indonesia. The location that had been identified as the largest pumice breccia deposit area is Semilir Formation. The Semilir Formation is typically originated from products of a very explosive volcanic activity. It is a widespread mountainous area at the southern part of Java Island. The formation is widely distributed from the west side at Pleret and Piyungan areas in Bantul Regency, Special Province of Yogyakarta until Eromoko area in Wonogiri Regency, Central Java Province in the east [3]. Based on the official data which is released by the center of investigation resources development in the Indonesian Ministry of Public Works, the Special Province of Yogyakarta has 2.50 billion m<sup>3</sup> deposit of pumice breccia which is located in Bantul, Gunung Kidul and Sleman region [4]. Pumice breccia having relatively low density therefore it is met the requirements to be used as lightweight aggregate [5].

In this research, pumice breccia which can be found abundantly in Indonesia proposed to be utilized as the fine aggregate for the development of insulating mortar. The main objectives of this research are: (1) evaluating the effect of pumice breccia utilization as fine aggregate in various compositions on the thermal conductivity, and (2) examining compressive strength of several mortar types which are using pumice breccia as fine aggregate.

## 2. Material and Methods

The mixtures were prepared with blended cement which satisfies to the requirements in the Indonesian National Standards [6]. The detail of its chemical compounds is presented in Table 1.

Table 1: Chemical composition of Portland cement

Chemical Compounds	SiO <sub>2</sub>	Al <sub>2</sub> O <sub>3</sub>	Fe <sub>2</sub> O <sub>3</sub>	CaO	MgO	SO <sub>3</sub>	LoI
Mass (%)	23.13	8.76	4.62	58.66	0.90	2.18	1.69

The coarse aggregate of all concrete mixtures utilize continuously graded crushed lightweight pumice breccia from Bawuran Mountain, Bantul District in the Special Province of Yogyakarta which is one of the largest pumice breccia deposits in Indonesia. This pumice breccia has dry-loose bulk density of 760 kg/m<sup>3</sup> with particle density of 1620 kg/m<sup>3</sup> which is satisfied to the technical specification of lightweight aggregate. Therefore, it is proposed to be utilized as coarse aggregate in the mixtures. The fine aggregate prepared using pumice breccia with maximum size of 4.8 mm, and in air-dried condition before mixing process. Detail of mixes proportion between Portland cement (Pc), natural sand (Ns), and pumice breccia (Pb) in this research can be found in the following Table 2.

Table 2: Mixture proportion of nine (9) series of mortar mixtures

No	Samples type	Volume ratio
1	MN1	1Pc : 4Ns
2	MN2	1Pc : 6Ns
3	MN3	1Pc : 8Ns
4	MNP1	1Pc : 2Ns : 2Pb
5	MNP2	1Pc : 3Ns : 3Pb
6	MNP3	1Pc : 4Ns : 4Pb
7	MP1	1Pc : 4Pb
8	MP2	1Pc : 6Pb
9	MP3	1Pc : 8Pb

### 3. Experimental Works

Hardened properties of mortar mixes were evaluated based on its thermal conductivity and compressive strength after 28 days of mortar age. Thermal conductivity evaluation was conducted for all the mortar variants using cylinders with 40 mm in diameter and 5 mm height. Compressive strength examination for all variants was done on standard cubes with 50 mm x 50 mm x 50 mm dimension. The thermal conductivity and compressive strength of the mortars was determined as the average of those five specimens for each variant. The experimental setting for thermal conductivity and compressive strength test can be observed in figure 1.



a. Thermal conductivity measuring apparatus



b. Compressive strength test

Figure 1: Experimental setting

For determination of thermal conductivity of each sample, the calculation was carried out using standard formula as follows:

$$\Delta t_R = \frac{\Delta t_{1,2} + \Delta t_{2,3} + \Delta t_{3,4} + \Delta t_{7,8} + \Delta t_{8,9} + \Delta t_{9,10}}{6} \text{ (}^\circ\text{C)} \tag{1}$$

$$\lambda'_a = \frac{\Delta t_R}{\Delta t_a} \times \frac{L_a}{L_R} \lambda_R \text{ (W/m.}^\circ\text{C)} \tag{2}$$

$$\lambda'_b = \frac{\Delta t_R}{\Delta t_b} \times \frac{L_b}{L_R} \lambda_R \text{ (W/m.}^\circ\text{C)} \tag{3}$$

$$\lambda = \frac{\frac{L_b - L_a}{\lambda'_b} - \frac{L_b - L_a}{\lambda'_a}}{\frac{L_b - L_a}{\lambda'_b} - \frac{L_b - L_a}{\lambda'_a}} \text{ (W/m.}^\circ\text{C)} \tag{4}$$

where

- $\Delta t_{1,2}$  : temperature change between first and second node
- $\Delta t_a$  : temperature change of sample “a”
- $\Delta t_b$  : temperature change of sample “b”
- $\Delta t_R$  : average of temperature change
- $L_a$  : height of sample “a” (5 mm)
- $L_b$  : height of sample “b” (10 mm)
- $L_R$  : 30 mm
- $\lambda$  : thermal conductivity
- $\lambda'_a$  : thermal conductivity of sample “a”
- $\lambda'_b$  : thermal conductivity of sample “b”
- $\lambda_R$  : thermal conductivity of copper rod (372.16 W/m. °C)

While following formula was used to determine the compressive strength of each mortar sample

$$f_{ck} = \frac{P}{A} \tag{5}$$

where

- $f_{ck}$  : compressive strength of cube (MPa)
- $P$  : compression load (N)
- $A$  : area (mm<sup>2</sup>)

## 4. Results and discussion

Experimental results of nine types of mortar which were evaluated to determine the thermal conductivity and compressive strength can be observed in Table 3 as follows.

Table 3: Thermal conductivity and compressive strength of nine (9) series of mortar mixtures

No	Samples type	Average thermal conductivity (W/m.°C)	Average compressive strength (MPa)	Mortar type based on SNI: 03-6882-2002
1	MN1	0.63	5.21	N
2	MN2	0.61	3.45	O
3	MN3	0.53	1.66	-
4	MNP1	0.50	3.33	O
5	MNP2	0.49	2.91	O
6	MNP3	0.40	2.17	-
7	MP1	0.37	3.99	O
8	MP2	0.35	2.55	O
9	MP3	0.29	0.46	-

Test results show by using the Pumice Breccia as fine aggregate in the mortar mixtures, the thermal conductivity of the normal mortar can be reduced nearly considerably. It can be observed that thermal conductivity decreases in accordance with the decrease of mortar compressive strength, as expected. For the low compressive strength of mortar, more air pores are formed inside. As air is a good insulator, the thermal conductivity of mortar was found to be lower than that of normal mortar. The thermal conductivity of lightweight mortar that utilizing pumice breccia as fine aggregate is lower than that of normal weight mortar which is conventionally used in construction field

Even though, the reduction in compressive strength is observed in all the compositions of mortar mixtures, based on the Indonesia National Standard of mortar specification for construction works; SNI: 03-6882-2002, still the Pumice Breccia based mortar can be classified into the type-O mortar that can be used for partition walls, protective and decorative purposes [7].

Simple steady state heat transfer analysis also performed to get an initial information regarding the effectiveness of the use of mortar utilizing pumice breccia as fine aggregate in decreasing the inside room temperature buildings in the Indonesian coastal region with assuming that outdoor temperatures is around 36 °C. The numerical analysis was conducted using Strand7 software. The model will only assign convection coefficients, and assumed that there is no radiative heat transfer, as it is not significant over the range of temperatures considered. Analysis result shows that using Class-O pumice breccia mortar the indoor temperature will be 23.1 °C and when using normal mortar the indoor temperature will be 24.5 °C. The finite element model of heat transfer analysis can be found in Figure 2 as follows.

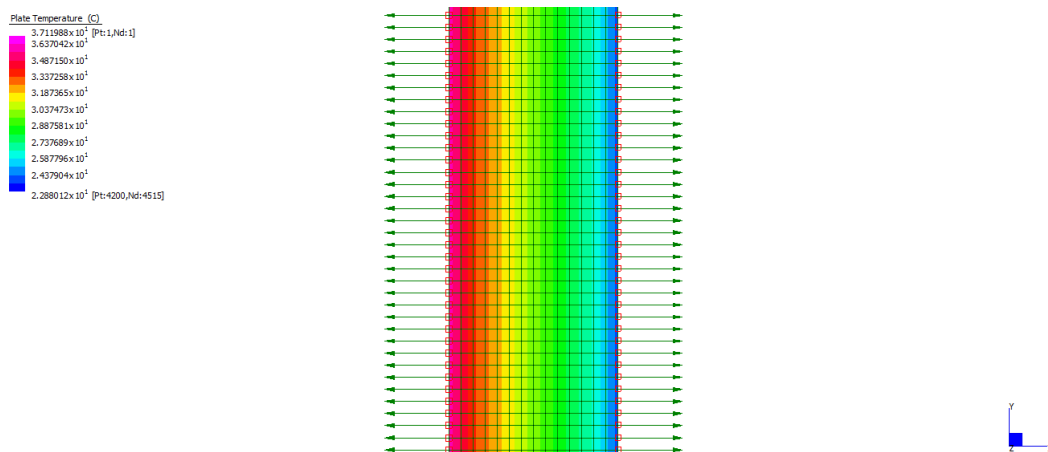


Figure 2: Finite element model of steady state heat transfer analysis in building wall using Strand7

## 5. Conclusions

Based on the tests results of the hardened properties of pumice breccia lightweight concrete, the following conclusions can be drawn:

- (1) Utilization of pumice breccia as fine aggregate in the mortar mixtures will effect to the thermal conductivity reduction significantly. The thermal conductivity can be reduced nearly 40%.
- (2) Thermal conductivity of mortar specimens can be reduced in accordance with the decrease of mortar compressive strength. Based on the Indonesia National Standard of mortar specification for construction works; SNI: 03-6882-2002, still the Pumice Breccia based mortar can be classified into the type-O mortar that can be used for partition walls, protective and decorative purposes.



## Acknowledgements

The authors highly appreciate the financial support from the Ministry of Research, Technology and Higher Education. The support of the Building Material Laboratory staffs at the Faculty of Engineering, Universitas Negeri Yogyakarta for their assistance in conducting the experimental works are also gratefully acknowledged.

## References

- [1] R. Cluett, Small actions that add up to large energy savings for Earth Day, 2014 (April 22), retrieved from: <http://aceee.org/blog/2014/04/small-actions-add-large-energy-saving>.
- [2] U.J. Alengaram, B.A. Al Muhit, M.Z. bin Jumaat, M.L.Y. Jing, A comparison of the thermal conductivity of oil palm shell foamed concrete with conventional materials, *Materials and Design* 51, (2013), 522–529.
- [3] S. Bronto, S. Mulyaningsih, G. Hartono, and B. Astuti, “Waduk Parangjoho dan Songputri: Alternatif Sumber Erupsi Formasi Semilir di daerah Eromoko, Kabupaten Wonogiri, Jawa Tengah,” *Jurnal Geologi Indonesia*, Vol. 4 No. 2, pp. 79-92, 2009. (In Indonesian).
- [4] Pusat Pembinaan Sumber Daya Investasi, Sistem informasi Sumber Daya Investasi: Potensi Material Konstruksi Propinsi DI Yogyakarta, Kementerian Pekerjaan Umum, 2013 (September 14), retrieved from: [http://www.pusbinsdi.net/main.php?page=potensi\\_material&type=&op=detail&id\\_prop=12](http://www.pusbinsdi.net/main.php?page=potensi_material&type=&op=detail&id_prop=12). (In Indonesian).
- [5] S. Widodo, I. Satyarno, S. Tudjono, Experimental study on the potential use of pumice breccia as coarse aggregate in structural lightweight concrete, *International Journal of Sustainable Construction Engineering & Technology* (ISSN: 2180-3242) Vol 5, No 1, 2014, 1-8.
- [6] Badan Standarisasi Nasional, SNI: 15-0302-2004: Pozzolan Portland Cement, BSN, 2004. (In Indonesian).
- [7] Badan Standarisasi Nasional, SNI: 03-6882-2002: Spesifikasi Mortar untuk Pekerjaan Pasangan, BSN, 2002. (In Indonesian).



Sustainable Civil Engineering Structures and Construction Materials, SCESCM 2016

## Effect of the fibre geometry on pull-out behaviour of HVFA mortar containing nanosilica

Y Shafaei<sup>a</sup>, F.U.A Shaikh<sup>a</sup>, P.K. Sarker<sup>a</sup>

<sup>a</sup> *Department of civil engineering, Curtin University, Perth, Australia.*

---

### Abstract

It is essential to understand the single fibre pull-out response in order to understand and predict the behavior of fibre reinforced composites. Hook geometry can largely affect the post-crack behaviour of fibres in structural elements. There is limited data available on newly developed multi hooked end steel fibers. This paper presents results of single fibre pull-out tests of three types of hooked end steel fibres embedded in high volume fly ash (HVFA) mortar. Steel fibres were defined as double, triple or quadruple hooked based on their geometry. The results of this study indicates that the pull-out load of the steel fibres was increased with the increase of the number of bends at the ends. It was also observed that the extra hooks resulted in some plastic deformation of the fibres. The average pull-out load of the quadruple hooked fibre was 1.4 times higher than that of the average pull-out load of the double hooked fibre. Pull out strength was increased with the increase of the matrix strength. The compressive strength of the mortar was increased by 18% with the addition of 2% nanosilica (NS) and 10% microsilia (MS). Inclusion of these fine particles improved the bond between fibres and the mortar which consequently increased the pull-out load. The double hooked end fibre exhibited the smallest pull-out load among the three types of fibre studied. It was also observed that the pull-out load of all types of fibres increased with the reduction of fly ash (FA) content. Furthermore, results also demonstrate that the addition of MS and NS increased the pull-out load of steel fibres in HVFA mortar up to 31%.

© 2017 The Authors. Published by Elsevier Ltd.

Peer-review under responsibility of the organizing committee of SCESCM 2016.

*Keywords:* Hooked-end steel fibre, PVA fibre, High volume fly ash mortar, Pull-out test

---

## 1. Introduction

Despite all the benefits of cement based mortar and concrete, they are identified as brittle construction materials with a low tensile strength which makes them prone to cracking. For decades, the addition of fibres to these materials have been a common practice to improve the mechanical behaviour, and delay propagation of cracks while saving the costs of excessive reinforcement. An additional mechanical component is obtained when straight fibres are deformed, which produces anchorage effect. In case of smooth fibres the only mechanism preventing slippage are adherence and friction. However, in case of deformed fibre particular geometry such as hooked end or twists will provide additional bonding force. Mechanical anchorage is the key parameter affecting toughness and energy absorption capacity and is caused mainly by deformations or hooks in fibres.

It is important to study the bond between fibre-matrix interface characteristics in order to understand the behaviour of any composite material produced with fibres. The fibre-matrix interface bond has been studied in recent years [1]. Numerical models have been developed based on geometry and strength of fibres with focus on fibre inclination [2-4]. Some of the parameters affecting the bond are known as length of the fibres ( $L$ ), diameter ( $d$ ), embedment length ( $L_b$ ), Aspect ratio ( $L/d$ ), fibre orientation angle ( $\theta$ ) and the tensile strength of fibres [5]. Analytical models have been developed to predict the pull-out load by other researchers [6-8]. Alwan et al. [9] investigated various parameters such as fibre diameter, length and aspect ratio.

The fiber–matrix interface bond is usually determined by a single fiber pull-out test. Pull-out behaviour depends on both the matrix and the fibre characteristics. An ideal pull-out test has two main components: sliding and mechanical anchorage. The embedment length of smooth and hooked-end fibres have been studied by researchers [10-12]. Tuyan and Yazici [10] showed that the peak pull-out load of hooked steel fibres was significantly higher than smooth steel fibres. By implementing microstructural study, it has been observed that the transition zone in mature traditional cementitious composite is quite porous which is filled with CH gel where it is also in direct contact with fibres [13]. The density of the interfacial transition zone can be increased by addition of supplementary cementitious materials (SCM) [14-20]. Shannag et al. [11] studied the embedment length of fibres, it has been observed that embedment length affects both the peak pull-out load and pull-out work. Silva et al. [21] reported that fibre morphology plays an important role in the bond strength of the fibre-matrix. Lee et al. [22] observed that highest peak load for fibre during the pull-out test occurs with angle of  $30^\circ$  and  $45^\circ$ .

A series of experimental pull-out tests of different fibres from various types of matrix have been investigated in this paper. Limited studies are available on the effects of fibre geometry, matrix type and combined actions of the above parameters. The effect of end condition of steel fibres on the fibre-matrix bond characteristics is investigated here. Based on the results, the pull-out behaviour has been analysed and mechanisms affecting the pull-out load and post peak behaviour are explained.

## 2. Experimental program

### 2.1. Materials and specimen preparation

Ordinary Portland cement (OPC), Class F fly ash, microsilica (MS) and nanosilica (NS) with the properties given in Table 1 were used in all the mortar mixtures. The properties of the fibres used in this study are given in Table 2. The fibres were of a smooth surface with the ends bent in three different configurations, as shown in Fig. 1.

Table 1-Chemical composition and physical properties of cementitious materials

Chemical analysis	Cement (wt%)	Fly ash (wt%)	Microsilica (wt%)	Nanosilica (wt%)
SiO <sub>2</sub>	21.1	63.13	89.6	99
Al <sub>2</sub> O <sub>3</sub>	5.24	24.88	-	-
Fe <sub>2</sub> O <sub>3</sub>	3.1	3.07	-	-
CaO	64.39	2.58	-	-
MgO	1.1	0.61	-	-
K <sub>2</sub> O	0.57	2.01	0.225	-
Na <sub>2</sub> O	0.23	0.71	0.11	-
SO <sub>3</sub>	2.52	0.18	-	-
LOI	1.22	1.45	3.8	-
Particle size	-	73% < 45 μm	95% < 1 μm	25 nm
Specific gravity	3.17	2.65	0.625	2.2-2.6
BET Surface area (m <sup>2</sup> /g)	-	1.53	15-30	160

Table 2-Properties of fibres

Type	Geometry	Length (mm)	Diameter (mm)	Aspect ratio	Modulus (GPa)	Tensile strength (MPa)
Steel	Hooked end	60	0.90	65	210	1345

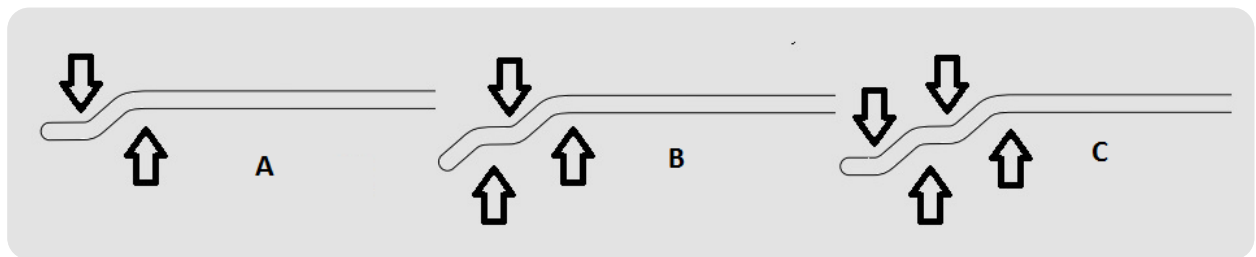


Figure 1- Configuration of fibres used in this study: (A) doubled bend ; (B) triple bend ; (C) quadruple bend.(bends numbering is based on number of bends shown by the arrows).

The mixtures were mixed in a Hobart mixer. A constant water/ binder ratio of 0.4 and sand/binder ratio of 2 was used to prepare all the mortars. In this study, seven types of mortars were prepared and cast in plastic moulds. The first series was control mortar that consisted of OPC only as the binder. After casting, the specimens were kept for 24h in  $20 \pm 2$  °C and then were demolded and cured for a testing period of 7 and 28 days.

The second, third and fourth series were HVFA mortars containing 40%, 50% and 60% (by wt) fly ash as partial replacement of the OPC, respectively. The fifth, sixth and seventh series contained 2% NS, 10% MS and combined 2% NS + 10% MS, respectively, with fly ash. The specimens were prepared in a plastic mould with a size of  $12 \times 24 \times 42$  mm. Cube specimens of 50 mm size were cast for compressive strength tests at 28 days.

## 2.2. Test procedure

In order to determine the fibre-matrix characteristics, a single fibre pull-out test was carried out which is a common method for pull-out test used by other researchers [20]. A stiff steel frame was used during the pull-out test. The fibre was embedded half way through the matrix ( $L_b=0.5 \times l_f$ ) during casting. The fibre orientation is in the same direction as that of the pull-out force. The specimen was mounted in a steel supporting system with a hole located on the top, through which the fibre was clamped to the upper jaw of a universal testing machine, while a long screw bolt which is connected to the bottom of the tube was clamped by the lower jaw of the machine. The test set up is shown in Fig 2. By using this setup it was assured that the specimens were only under pull-out load and no other lateral confining pressure existed. The upper jaw was connected to a load cell with a capacity of 5 kN and a loading rate of 1 mm/min was used in the test. The pull-out load vs displacement data were recorded for each specimen. The maximum pull-out load was determined from the load displacement curve.



Figure 2-Apparatus of pull-out test

## 3. Results and discussion

The 28-day compressive strengths of the mortars containing fly ash, microsilica and nanosilica with no fibres are presented in Fig. 3. As expected, compressive strength of mortars decreased with the increase of fly ash replacing cement. It can be seen that 2% NS, 10% MS or 2% NS and 10% MS increased compressive strength as compared to the mortar containing 40% fly ash. The compressive strength of the mortar containing 10% MS and 2% NS was closest to that of the control mortar mix.

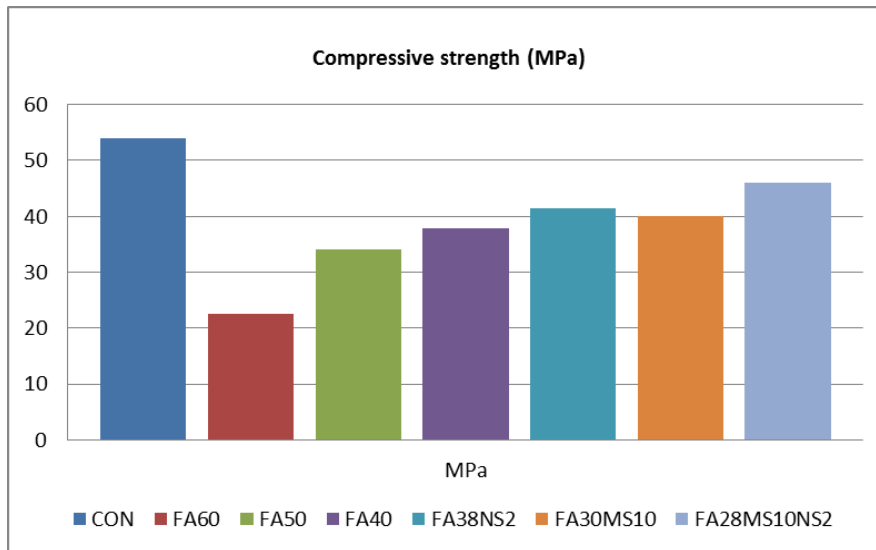


Figure 3-compressive strength of mortars at 28 days

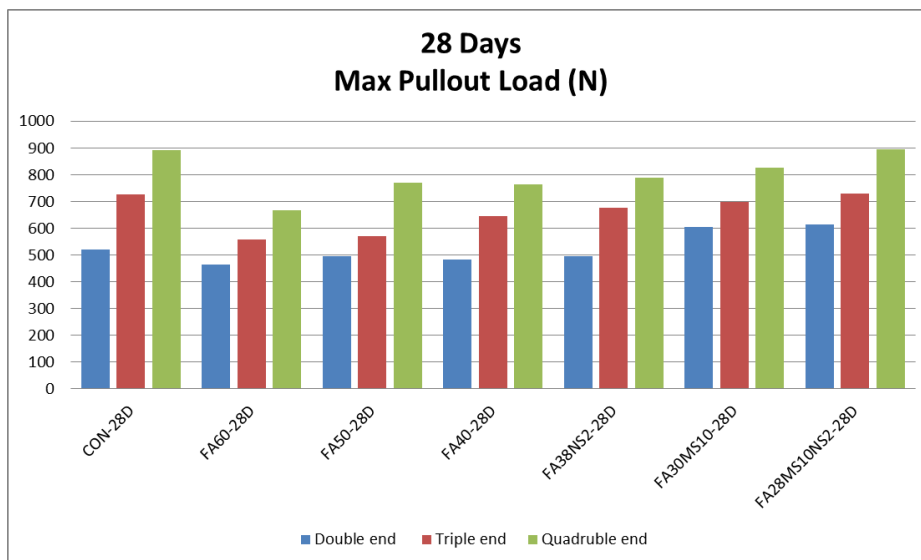


Figure 4-Peak pull-out load at 28 days curing

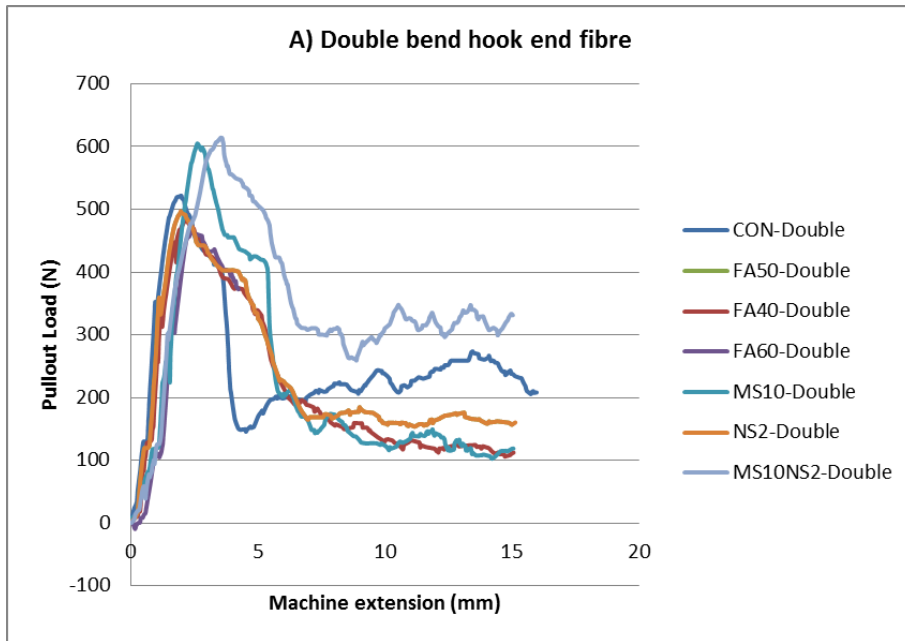


Figure 5-Pull-out vs displacement of the double-bend fibres

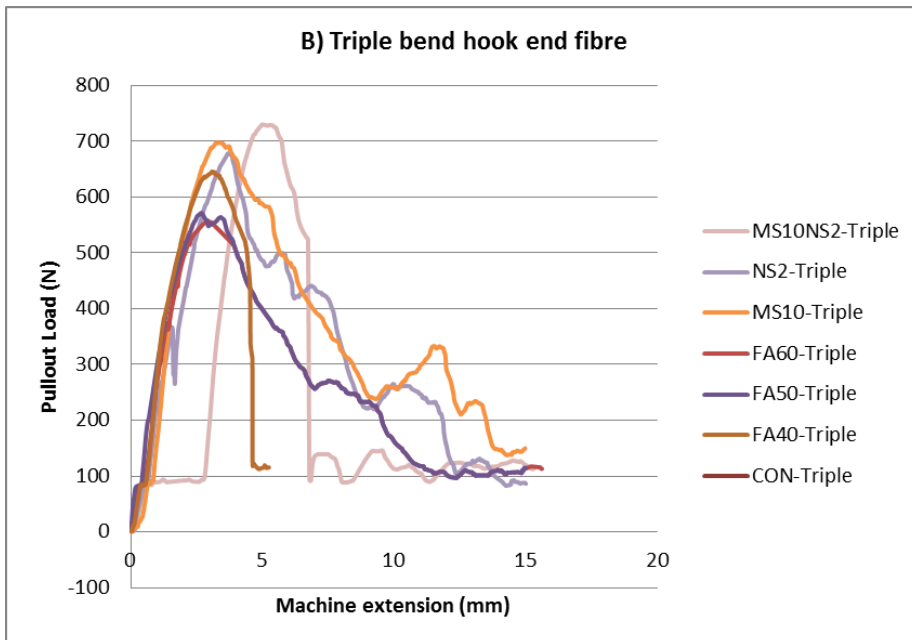


Figure 6- Pull-out load vs displacement of the triple-bend fibres



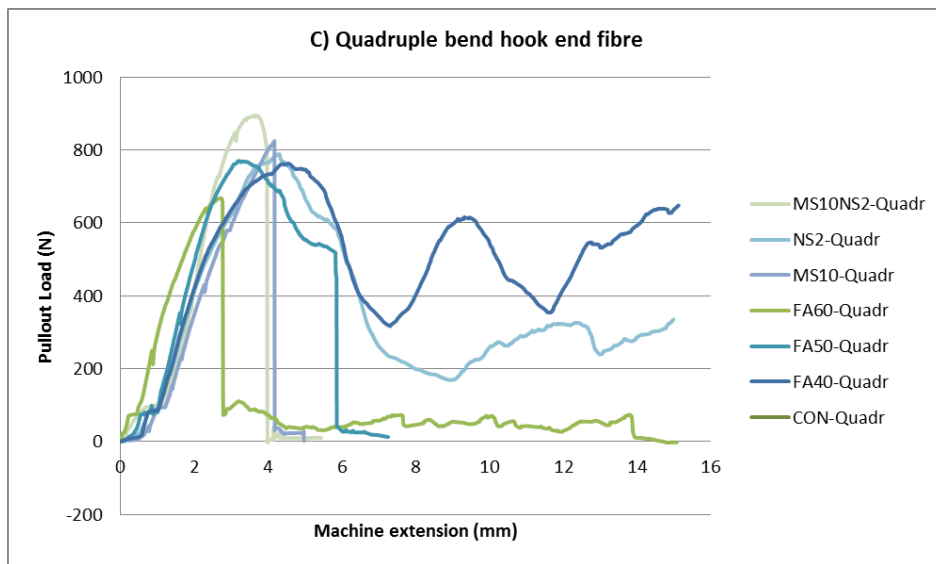


Figure 7-Pull-out vs displacment of the quadruple-bend fibres

### 3.1. Effect of fibre geometry on the pull-out behaviour

The maximum values of the pull-out load of the fibres in different matrices are shown in Fig.4. It can be seen that the maximum pull-out load of the fibre in each type of matrix was increased with the increase in the number of bends in the fibre. The pull out load was decreased by the replacement of cement by fly ash. However, it can be seen that the pull-out load gradually increased by the addition of microsilica and nanosilica. The decrease of the pull-out load is attributed to the decrease of the compressive strength by fly ash. The maximum pull-out load of the fibres in the matrix containing 28% fly ash, 10% MS and 2% NS were almost same as those of the fibres in the control matrix. The trends of the maximum pull-out load of a particular type of fibre in different matrices is seen to be similar to that of the compressive strength of the mortars shown in Fig. 3.

The effects of different fly ash contents, 2% NS, 10% MS and combinations of both (2NS%+10MS%) on the bond behavior of three types of hook-end steel fibres in HVFA mortar are presented in Figs. 5, 6 and 7. By investigating the failure modes of fibres in this study, it was observed that the fibres were pulled out with some plastic deformation. It can be observed from results that pull-out load displacement curves present characteristics mainly based on fibre geometry and matrix properties. A variability of experimental results were observed by considering a single matrix on various fibre types. This is attributed to fibre geometry. Quadruple fibre has shown superior peak loads in all mixes as compared to the triple bend and double bend fibres. This can be due to the effectiveness of hook geometry and better mechanical interlock of bends.

Zile et al. [23] identified the overall pull-out load ( $P$ ) of steel fibres into two main resisting elements; the first component is the load associated with geometric deformation under plastic bending force ( $P_{pl}$ ) and the second is the load corresponding to the frictional force ( $P_{fric}$ ), as described by Eq. 1

$$P = P_{pl} + P_{fric} \quad (\text{Eq. 1})$$

$P_{pl}$  is a result of bending or unbending of fibers. A similar amount of load is required to bend a straight fibre during the production of a hooked fibre, and is known as plastic bending force. This load will be released when fibres are under debonding process and while the geometric deformation happens during the pull-out. The cementitious matrix is assumed as a curve duct where fibres are positioned inside it. Frictional force ( $P_{fric}$ ) is another resisting element

which is a result of the friction between steel fibre and the matrix duct. The frictional force is affected by the parameters such as friction shearing stress, embedded length and the fibre slip.

By observing Fig. 5, it can be said that, addition of combined MS+NS resulted in highest peak load and the best post peak behaviour in case of double bend fibres. A very similar effect was observed in Fig. 6 in case of triple bend fibres and in Fig. 7 for quadruple bend fibres.

By comparing Figs. 5, 6 and 7, the effect of different fibre geometry can be observed. The repetitive bending and unbending required to smoothen the quadruple fibres has increased the plastic deformation. Furthermore, extra bending of this fibre in comparison to the triple bend fibre has increased the frictional force by increasing the anchorage which have been in a direct contact with the matrix during the bending. Better post-peak behaviour was observed due to the greater mechanical interlock of bends with quadruple and triple bend fibres.

The principal failure mode observed in case of double, triple and quadruple end steel fibres was plastic deformation followed by pull-out. The reason for fluctuation after peak load can be due to fractures of matrix in micro-level while fibres go through an elasto-plastic phase. As it can be observed in Fig 5, 6 and 7 the slope of the load vs displacement graph of these type of fibres has been close to linear to the point of peak load. The first stage of pull-out of the fibres occurred when the maximum load was reached. The second stage of pull-out begun after peak load, when the fibre went through the curved matrix and debonding resulted. The debonding happened either in a hardening behaviour such as the double bend fibre in the matrix of FA28MS10NS2 or with a drastic drop in the load such as the triple bend fibre in in the matrix of FA28MS10NS2.

#### 4. Conclusion

In this study a sustainable mortar containing a high volume of fly ash as a partial replacement of cement was used to characterize the bond slip behaviour of three types of hooked end steel fibres. A displacement controlled pull-out test was conducted. The results are discussed based on compressive strength of the matrix and the pull-out load vs displacement graphs. The main findings of this study can be summarized as follows:

1. The addition of 2% NS and 10% MS increased the compressive strength of flu ash mortar by 18%. By implementing a relatively low w/c ratio besides the addition of these SCMs, the amorphous content of the matrix has been increased. Due to the addition of SCM materials, the formation of additional calcium silicate hydrate (C-S-H) gel improved the bonding. All these resulted in the production of a sustainable matrix with a dense microstructure which improved the frictional force ( $P_{fric}$ ). The stiffness of the matrix played an important role both in failure modes and in post peak behavior of the fibre pull-out.
2. The fibre geometry has affected both peak load and post peak behavior. The average pull-out load of the quadruple hooked fibre was 1.4 times higher than that of the average pull-out load of double hooked fibre. An elasto-plastic semi-hardening behaviour has been observed in most mixes which is result of debonding and sliding in the fibre-matrix interface. The pull-out peak load and the debonding toughness increased with increase in number of bends, this corresponds to increase in plastic bending force ( $P_{pl}$ ) and increased mechanical interlock caused by the bends at the ends.

#### References

- [1] M. Maage Interaction between steel fibers and cement based matrixes *Mater Struct*, 10 (5) (1977), pp. 297–301
- [2] K. Georgiadi-Stefanidi, E. Mistakidis, D. Pantousa, M. Zygomalas Numerical modeling of the pull-out of hooked steel fibers from high-strength cementitious matrix, supplemented by experimental results *Constr Build Mater*, 24 (12) (2010), pp. 2489–2506
- [3] F. Laranjeira, C. Molins, A. Aguado Predicting the pullout response of inclined hooked steel fibers *Cem Concr Res*, 40 (10) (2010), pp. 1471–1487
- [4] F. Laranjeira, C. Molins, A. Aguado Predicting the pullout response of inclined straight steel fibers *Mater Struct*, 43 (6) (2010), pp. 875–895
- [5] P. Robins, S. Austin, P. Jones Pull-out behavior of hooked steel fibers *Mater Struct*, 35 (7) (2002), pp. 434–442
- [6] S. Hamoush, T. Abu-Lebdeh, T. Cummins, B. Zornig Pullout characterizations of various steel fibers embedded in very high-strength concrete *Am J Eng Appl Sci*, 3 (2) (2010), pp. 418–426
- [7] B. Banholzer, W. Brameshuber, W. Jung Analytical simulation of pull-out tests-the direct problem *Cem Concr Compos*, 27 (1) (2005), pp. 93–101
- [8] B. Banholzer, W. Brameshuber, W. Jung Analytical simulation of pull-out tests-the direct problem *Cem Concr Compos*, 28 (6) (2006), pp. 564–571

- [9] J.M. Alwan, A.E. Naaman, W. Hansen Pull-out work of steel fibers from cementitious composites: analytical investigation *Cem Concr Compos*, 13 (4) (1991), pp. 247–255
- [10] M. Tuyan, H. Yazici Pullout behavior of single steel fiber from SIFCON matrix *Constr Build Mater*, 35 (2012), pp. 571–577
- [11] M.J. Shannag, R. Brincker, W. Hansen Pullout behavior of steel fibers from cement-based composites *Cem Concr Res*, 27 (1997), pp. 925–936
- [12] J.J. Kim, D.J. Kim, S.T. Kang, J.H. Lee Influence of sand to coarse aggregate ratio on the interfacial bond strength of steel fibers in concrete for nuclear power plant *Nucl Eng Des*, 252 (2012), pp. 1–10
- [13] Bentur A, Diamond S, Mindess S. The microstructure of the steel fibre–cement. *J Mater Sci* 1985;20(10):3610–20.
- [14] Neville AM. Properties of concrete. New York: John Wiley & Sons; 1973.
- [15] Bentur A, Wu ST, Banthia N, Baggott R, Hansen W, Katz A, et al. Fibre–matrix interfaces. In: High performance fibre reinforced cementitious composites. London: Chapman and Hall; 1995.
- [16] Banthia N, Bentur A, Mufti A. Fiber reinforced concrete: present and future. The Canadian Society for Civil Engineering; 1998.
- [17] Chan YW, Li VC. Effects of transition zone densification on fiber/cement paste bond strength improvement. *Adv Cem Based Mater* 1997;5(1):8–17.
- [18] Kayali OA. Effect on high volume fly ash on mechanical properties of fiber reinforced concrete. *Mater Struct* 2004;37(5):318–27.
- [19] Chan YW, Chu SH. Effect of silica fume on steel fiber bond characteristics in reactive powder concrete. *Cem Concr Res* 2004;34(7):1167–72.
- [20] Tuyan M, Yazıcı H. Pull-out behavior of single steel fiber from SIFCON matrix. *Constr Build Mater* 2012;35:571–7.
- [21] Silva FA, Mobasher B, Soranakom C, Filho RDT. Effect of fiber shape and morphology on interfacial bond and cracking behaviors of sisal fiber cement based composites. *Cem Concr Compos* 2011;33(8):814–23.
- [22] Zile E, Zile O. Effect of the fiber geometry on the pull-out response of mechanically deformed steel fibers. *Cem Concr Res* 2013;44:18–24.